LIGAND DESIGN FOR GOLD CATALYSIS

KARIM MURATOV

Thesis submitted to the University of Ottawa
in partial Fulfillment of the requirements for the
Doctorate in Philosophy degree in Chemistry

Department of Chemistry and Biomolecular Sciences
Faculty of Science
University of Ottawa

© Karim Muratov, Ottawa, Canada, 2024

Abstract

The field of gold catalysis has undergone significant development over the past two decades. Once considered largely inert with limited applications in catalysis, the discovery of π-activation with Au(I) cations revolutionized the field, revealing gold's unique reactivity and potential applications. However, the linear geometry of Au(I) species presents a challenge in developing new complexes for Au(I) catalysis, as it is difficult to translate steric information from a ligand on one side of the Au(I) atom to the reaction site on the opposite side. One strategy to induce selectivity in gold-catalyzed reactions is the encapsulation of a gold atom in a sterically demanding area. However, previously developed confined complexes are often supramolecular compounds and suffer from lengthy synthesis.

The first part of this thesis is dedicated to the synthesis of a new type of confined Au(I)-cationic catalysts. Upon comparing the performance of our complexes with the traditional Au(I) catalyst, it was discovered that the confinement and steric loading around the reactive site of the designed catalyst enabled us to alter and reverse the selectivity observed in standard benchmark Au(I) catalyzed cycloisomerization reactions. The new complexes were tested across a range of cycloisomerization reactions, where they demonstrated high selectivity between exo/endo and *E/Z* products. Furthermore, the synthesized catalysts displayed a high degree of substrate selectivity, reacting exclusively with one isomer of a compound, a characteristic reminiscent of enzymes. It was also demonstrated that the new complexes could catalyze the regioselective hydration of alkynes, offering superior selectivity compared to traditional phosphine-based Au(I) complexes. These findings were corroborated through X-ray studies and the calculation of various steric parameters, which revealed that the developed complexes exhibit a high degree of steric loading around the reaction site.

The second part of the thesis discusses the work on understanding Au(I)/Au(III) catalytic processes and the subsequent development of a new family of potent and highly tunable hemilabile (P^N) catalysts. Less than a decade ago, the field of external oxidant-free Au(I)/Au(III) chemistry started to develop rapidly due to the discovery that properly designed hemilabile ligands can greatly facilitate the challenging oxidative addition step in the Au(I)/Au(III) catalytic cycle. However, the advancement of this field is severely hindered by the dependency on a limited number of reliable Au(I)/Au(III) catalysts, highlighting a requirement for deeper understanding on key parameters. This understanding could facilitate the development of new catalysts and broaden the horizons for their future applications.

The study began with an investigation into the mechanism of Au(I)/Au(III)-catalyzed alkoxycyclization, which subsequently led to the elucidation and exploration of the so-called “silver effect” in such reactions. The mechanism and rate-limiting steps were determined, and the findings were supported through experimental and Density Functional Theory (DFT) studies. This understanding paved the way for the design of a new family of highly tunable Au(I)/Au(III) catalysts, whose efficacy was demonstrated in various reactions.

Subsequently, a novel C–S coupling reaction was developed using readily available thiotosylate reagents and an Au(I)/Au(III) catalyst to prepare the corresponding ArSTs compounds. The reaction was validated with over 40 examples, and the versatility of this substrate class in a range of modifications was demonstarted. Importantly, this is the first instance of accessing this class of compounds using readily available reagents. It was also found that Pd(0)/Pd(II) is not an effective catalyst in this reaction. The mechanism of this reaction was studied both experimentally and via DFT.

In summary, the research presented in this thesis introduces novel classes of potent catalysts for both Au(I) and Au(I)/Au(III) catalytic processes. It was demonstrated that the distinct properties

of Au-complexes can be meticulously adjusted through thoughtful ligand design. Furthermore, we conducted an in-depth examination of the Au(I)/Au(III) catalytic cycles, providing valuable insights that could guide future studies in this field.

Acknowledgments

I would like to express my deepest gratitude to my supervisor, Professor Fabien Gagosz, whose guidance, support, and invaluable expertise have profoundly influenced my PhD journey. Professor Gagosz's mentorship has been the keystone of not only my academic development but also my personal growth. He has taught me the necessary skills and raised my confidence to conduct research. His readiness to engage in discussions, share insights and ideas, and offer support in all aspects of life, not just research, has been immensely encouraging. Prof. Gagosz's passion for chemistry has been particularly inspiring, and his willingness to share knowledge has been a cornerstone in shaping my work and expanding my knowledge and experience.

I would also like to thank all the members of the Gagosz group. Dr. David Fabian León Rayo taught me a lot and was always there to answer my numerous questions. Dominic Campeau has been a constant source of support, always willing to discuss chemistry together and to help me find equipment in the lab. Ali Mansour was always there to share the fascinating chemical moments together and discuss various great food recipes. Alice Pommainville's impressive work, dedication and exceptionall skils in making presentations served as a significant source of inspiration for me. Additionally, I thank our present and past undergraduate students—Jessica, Mila, Elyssa, Dante, Liam, Unteni, Ayoung, and particularly Samuel, the first undergraduate student with whom I had the opportunity to collaborate on a research project.

Big thanks to everyone in the Barriault group for all the chemistry talk and support, especially when it came to feedback on my thesis and other projects. A special thanks to Tegan O'Brien and Avery Morris for being my go-to people for all the writing, feedback, and just generally providing me moral support throughout my whole PhD journey.

I also want to give a huge thanks to the whole University of Ottawa and Department of Chemistry and Biomolecular Sciences for creating such a great place to learn and research. A special thanks to Dr. Peter Pallister and Dr. Patrick Szell from the NMR facility, and Dr. Jeff Ovens from the X-Ray facility for troubleshooting the vital equipment and always keeping it running smoothly.

I owe a profound debt of gratitude to my parents, Ramilya and Marat Muratov, whose unwavering support and sacrifices have made all of this feasible. Their constant presence and effort to ensure I received a quality education and a promising future have been the cornerstone of my life. Without their love, support, and guidance, none of this would have been attainable. I am forever grateful and indebted for their role in shaping my life and supporting every decision I've made.

I extend my sincere gratitude to Prof. Tito Scaiano and Dr. Yu for their generosity in providing scholarships that have enabled my studies. Their support has been crucial in allowing me to study here and achieve my academic goals.

Statement of Contributions

The research efforts summarized in this work represent primarily my individual contributions, which are carefully supervised by Prof. Fabien Gagosz. Additionally, important collaborative efforts have enriched the scope and impact of this work. Undergraduate researchers Samuel Karki and Elyssa Caron made valuable contributions to the studies described in **Chapters 2** and **3**, respectively. Samuel Karki synthesized the tri-(*N*-phenyl-triazolyl)phosphine ligand—originally described by Fossey and colleagues—as well as its AuCl complex, and attempted a series of catalytic tests. Attempts to catalyze the coupling of thiotosylate **3-41** with *p*-fluoroiodobenzene **3-42a** under Pd(0)/Pd(II) catalysis were performed by Elyssa Caron.

For structural characterization, I carried out and analyzed the X-ray crystallography studies, under close guidance of Dr. Jeffrey Ovens from the University of Ottawa X-ray Core Facility. High-Resolution Mass Spectrometry were carried out in collaboration with the laboratory of Prof. Maxim Berezovski. Emil Zaripov, a PhD candidate in the laboratory of Prof. Berezovski, performed the HRMS evaluations for both reaction mixtures and our novel gold complexes.

Although the Density Functional Theory analyses were not carried out by me, they are an essential part of this dissertation. Prof. Fabien Gagosz conducted these crucial computational studies and provided invaluable mechanistic perspectives that significantly improve our understanding of the novel transformations described here.

List of Schemes

Scheme 1.1-1. Lewis theory and DCD model.....2

Scheme 1.2-1. Relativistic effect.....2

Scheme 1.3.1-1. General approaches to synthesis of NHC- and phosphine-ligated Au(I) complexes.....5

Scheme 1.3.1-2. Examples of NHC and phosphine ligands.....5

Scheme 1.3.1-3. Ligand descriptors and the respective values for selected ligands.....6

Scheme 1.3.2-1. General mechanism of Au(I) catalyzed nucleophilic addition.....7

Scheme 1.3.2-2. Ligand effect of the Au(I) catalyzed nucleophilic addition.....8

Scheme 1.3.3-1. General mechanism of Au(I)/Au(III) catalyzed cross-coupling reactions.....9

Scheme 1.3.3-2. Hemilabile ligand.....9

Scheme 1.3.4-1. Carbene-like and carbocation-like resonance forms of a gold complex.....10

Scheme 1.3.4-2. Examples of Au(I)-complexes with high carbenoid character.....11

Scheme 1.3.5-1. Ligand effect in cyclization of *N*-tosylanilines.....12

Scheme 1.3.5-2. Chemoselectivity in cyclization of alkynones.....13

Scheme 1.3.5-3. Synergistic metal-ligand cooperation.....14

Scheme 1.3.5-4. Influence of the steric effects on the outcome of the reaction.....14

Scheme 1.4-1. O-H insertion vs C-H functionalization.....15

Scheme 1.4-2. C2 vs C3 arylation.....16

Scheme 1.4-3. Au vs Pt catalysis.....16

Scheme 1.4-4. Au vs Rh catalysis.....17

Scheme 1.5-1. Synthesis of (±)-Brevianamide A.....18

Scheme 1.5-2. Synthesis of (±)-Salvinorin A.....19

Scheme 1.5-3. Some of the examples of natural products synthesized using Au(I)-catalysis.....19

Scheme 1.6-1. Examples of highly efficient homogeneous Au(I)-catalysis.....21

Scheme 1.6-2. Examples of exceptionally low catalyst loading.....21

Scheme 2.2.1-1. Cycloisomerization of 1,6-enynes.....34

Scheme 2.2.2-1. 8-membered NHC ligands.....35

Scheme 2.2.2-2. NHC-capped cyclodextrins.....36

Scheme 2.2.2-3. Enantioselectivity and substrate selectivity.....38

Scheme 2.2.2-4. Bulky carbene ligands.....39

Scheme 2.2.3-1. Bulky phosphine ligands.....41

Scheme 2.2.3-2. Hollow-shaped phosphines.....42

Scheme 2.2.3-3. Cavitand-based phosphines.....43

Scheme 2.2.4-1. Bulky phosphite ligand.....44

Scheme 2.3-1. Selectivity control with bulky tris-(o-biphenyl)phosphine ligands.....45

Scheme 2.3-2. Synthesis of tri-(*ortho*-biaryl)phosphine ligands and the corresponding Au(I) complexes.....46

Scheme 2.3-3. Steric details.....47

Scheme 2.3-4. Comparative analysis of steric parameters and SCXRD structures.....48

Scheme 2.3-5. Cycloisomerization of propargyl malonate **2.3-17**.....51

Scheme 2.3-6. Cycloisomerization of various diethyl propargylmalonates.....52

Scheme 2.3-7. Cycloisomerization of *N*-propargyltosylamide derivatives.....53

Scheme 2.3-8. Cycloisomerization crotyl and prenyl derivatives.....54

Scheme 2.3-9. Interrupted cycloisomerizations.....55

Scheme 2.3-10. Carbene trapping experiments.....56

Scheme 2.3-11. Substrate selection in the cyclization of 1,7-enynes.....57

Scheme 2.3-12. (*E*,*Z*)-Stereoselectivity in the cycloisomerization of 1,6-enyne.....59

Scheme 2.3-13. Regioselectivity in the hydration reactions.....60

Scheme 2.3-14. Substrate selection in the hydration reactions.....62

Scheme 3.2.1-1. Chelation-assisted oxidative addition.....102

Scheme 3.2.1-2. Oxidative addition into C-C and C-I bonds.....103

Scheme 3.2.1-3. Stoichometric Negishi cross-coupling.....104

Scheme 3.2.1-4. Chelation-assisted gold-catalyzed C-X bond formation……104

Scheme 3.2.2.1-1. Gold-catalyzed cross-coupling……106

Scheme 3.2.2.1-2. Heteroarylation of alkenes……107

Scheme 3.2.2.1-3. Mechanism of heteroarylation of alkenes……108

Scheme 3.2.2.1-4. Gold-catalyzed diarylation of alkenes……109

Scheme 3.2.2.1-5. Allylation of indole……109

Scheme 3.2.2.1-6. Gold-catalyzed Heck and interrupted-relay Heck reactions……110

Scheme 3.2.2.1-7. Mechanism of gold-catalyzed Heck and interrupted-relay Heck reactions……111

Scheme 3.2.2.2-1. Formation of C-N bonds……113

Scheme 3.2.2.2-2. Formation of C-O bonds……114

Scheme 3.2.2.2-3. Formation of C-S bonds……114

Scheme 3.2.2.2-4. Reactivity of arylsulfonyl hydrazides……115

Scheme 3.2.2.3-1. Reactivity of alkynes under Au(I)/Au(III) catalysis……116

Scheme 3.2.2.4-1. Chiral ligands……117

Scheme 3.2.2.5-1. MIC^N ligands……118

Scheme 3.2.2.5-2. Heterobidentate (N^C) ligand……119

Scheme 3.2.2.6-1. Stoichometric oxidation……120

Scheme 3.2.2.6-2. Comparison of (P^N) and (C^N) hemilabile ligands……120

Scheme 3.2.2.6-3. Oxidation with *o*-benzoquinones. ……121

Scheme 3.2.2.6-4. Applications of arylgold(III) fluoride complexes and CO insertion……122

Scheme 3.3-1. Design and strategy for the development of new (P^N) ligands……123

Scheme 3.3-2. Strategy of synthesis of new (P^N) AuCl complexes and their RedOx activity……124

Scheme 3.3-3. Synthesis and structure of new (P^N) AuCl complexes……126

Scheme 3.3-4. Initial catalytic tests……127

Scheme 3.3-5. Catalytic tests……128

Scheme 3.3-6. Transmetallation tests……129

Scheme 3.3-6. DFT-guided ligand optimization……131

Scheme 3.3-7. Synthesis of (P^N) ligands KArPhos (**3.3-30**$_H$) and ClKarPhos (**3.3-30**$_{Cl}$) and the corresponding AuCl complexes……132

Scheme 3.3-8. Catalytic tests of complexes **3.3-31**……133

Scheme 3.3-9. Thiosulfonylation of aryl iodides……134

Scheme 3.3-10. Initial results and optimization……137

Scheme 3.3-11. Scope of the Au-catalyzed cross-coupling reaction of aryl iodides with ammonium thiotosylate……138

Scheme 3.3-12. Structural diversification *via* post-transformations on arylthiotosylate **3.3-43a**……139

Scheme 3.3-13. Mechanistic studies and proposed catalytic cycle for the Au(I)/Au(III)-mediated thiosulfonylation of aryl iodides……141

Scheme 3.3-14. Studies on reaction kinetics……142

Scheme 4-1. Possible modifications, inspired by the work of Zhang & Qian……197

Scheme 4-2. Example of stabilization of reactive species……197

Scheme 4-3. Flexible structure……198

Scheme 4-4. Gold-catalyzed C(sp2)-O cross-coupling……200

List of Figures

Figure 6.1-1. ^{1}H NMR spectra @t= 0 and t= 0.5h for [Au] = **2.3-22**.....203

Figure 6.1-2. ^{1}H NMR spectra @t= 0 and t= 2h for [Au] = **2.3-20**.....204

Figure 6.1-3. ^{1}H NMR spectra @t= 0 and t= 5min for [Au] = **2.3-20**.....205

Figure 6.1-4. ^{1}H NMR spectra @t= 0 and t= 5min for [Au] = **2.3-6$_{H}$**.....206

Figure 6.1-5. ^{1}H NMR spectra @t= 0 and t= 5min for [Au] = **2.3-6$_{H}$**.....207

Figure 6.1-6. ^{1}H NMR spectra @t= 0 and t= 3h for [Au] = **2.3-22**.....208

Figure 6.1-7. ^{1}H NMR spectra @t= 0 and t= 15min for [Au] = **2.3-22**.....209

Figure 6.1-8. ^{1}H NMR spectra @t= 0 and t= 15min for [Au] = **2.3-21**.....210

Figure 6.1-9. ^{1}H NMR spectra @t= 0 and t= 15min for [Au] = **2.3-6$_{pnPe}$**.....211

Figure 6.1-10. ^{1}H NMR spectra @t= 0 and t= 12h for [Au] = **2.3-21**.....212

Figure 6.1-11. ^{1}H NMR spectra @t= 0 and t= 30min for [Au] = **2.3-21**.....213

Figure 6.1-12. ^{1}H NMR spectra @t= 0 and t= 30min for [Au] = **2.3-23**.....214

Figure 6.1-13. ^{1}H NMR spectra @t= 0 and t= 30min for [Au] = **2.3-21**.....215

Figure 6.1-14. ^{1}H NMR spectra @t= 0 and t= 24h for [Au] = **2.3-19**.....216

Figure 6.1-15. ^{1}H NMR spectra @t= 0 and t= 24h for [Au] = **2.3-6$_{H}$**.....217

Figure 6.1-16. ^{1}H NMR spectra @t= 0 and t= 24h for [Au] = **2.3-6$_{H}$**.....218

Figure 6.1-17. ^{1}H NMR spectra @t= 0 and t= 24h for [Au] = **2.3-7**.....219

Figure 6.1-18. ^{1}H NMR spectra @t= 0 and t= 6h for **L** = JohnPhos.....220

Figure 6.1-19. ^{1}H NMR spectra @t= 0 and t= 1h for **L** = IPr.....221

Figure 6.1-20. ^{1}H NMR spectra @t= 0 and t= 20min for **L** = IPr.....222

Figure 6.1-21. ^{1}H NMR spectra @t= 0 and t= 3h for **L** = **2.3-4$_{H}$**.....223

Figure 6.2-1. First set of pyridine-based ligands tested.....237

Figure 6.2-2. A representative ^{1}H NMR spectra @t= 0 and t= 16h with complex **3.3-31$_{Cl}$**.....238

Figure 6.2-3. A representative ^{1}H NMR spectra @t= 0 and t= 16h with complex **3.3-31$_{Cl}$**.....239

Figure 6.2-4. A representative ^{1}H NMR spectra @t= 0 and t= 2h with ligand **3.3-18** (MeDalPhos).....240

Figure 6.2-5. A representative ^{1}H NMR spectra @t= 0 and t= 2h with ligand **3.3-18** (MeDalPhos) and *base* = **pyridine**……241

Figure 6.2-6. A representative ^{1}H NMR spectra @t= 0 and t= 12h with ligand **3.3-18** (MeDalPhos)……241

Figure 6.2-7. A representative ^{1}H NMR spectra @t= 0 and t= 6h with ligand **3.3-15$_{H}$**……242

Figure 6.2-8. A representative ^{1}H NMR spectra @t= 0 and t= 16h with complex **3.3-31$_{Cl}$**……243

Figure 6.2-9. A representative ^{1}H NMR spectra @t= 0 and t= 2h with complex **3.3-31$_{Cl}$**……244

Figure 6.2-10. A representative ^{1}H NMR spectra @t= 0 and t= 2h with complex **3.3-31$_{Cl}$**……245

Figure 6.2-11. ^{1}H NMR analysis of the crude reaction mixture with *S*-(4-fluorophenyl) 4-methylbenzenesulfonothioate **3.3-43a**……246

Figure 6.2-12. ^{19}F NMR analysis of the crude reaction mixture with 1-(4-fluorophenyl)-2-phenyldisulfane **3.3-44a**……247

Figure 6.2-13. ^{19}F NMR analysis of the crude reaction mixture with 4-((4-fluorophenyl)thio)morpholine **3.3-44b**……248

Figure 6.2-14. ^{1}H NMR analysis of the crude reaction mixture with S-(4-fluorophenyl) diphenylphosphinothioate **3.3-44c**……249

Figure 6.2-15. ^{19}F NMR analysis of the crude reaction mixture with chlorotetrafluoro(4-fluorophenyl)-λ^{6}-sulfane **3.3-44d**……250

Figure 6.2-16. ^{19}F NMR analysis of the crude reaction mixture with (4-fluorophenyl)(trifluoromethyl)sulfane **3.3-44e**……251

Figure 6.2-17. ^{19}F NMR analysis of the crude reaction mixture with 4-((4-fluorophenyl)thio)phenol **3.3-44f**……252

Figure 6.2-18. ^{19}F NMR analysis of the crude reaction mixture with (4-fluorophenyl)(phenylethynyl)sulfane **3.3-44g**……253

Figure 6.2-19. ^{1}H NMR analysis of the crude reaction mixture with 1-fluoro-4-thiocyanatobenzene **3.3-45**……254

Figure 6.2-20. ^{31}P NMR spectra @t= 5, 10, 20 and 30 min……255

Figure 6.2-21. HRMS of the reaction mixture……256

Figure 6.2-22-1. H NMR spectra @t= 0 and t= 18h for additive = $AgSbF_6$……256

Figure 6.2-22-2. ^{19}F NMR spectra @t= 18h……257

Figure 6.2-23-1. ^{1}H NMR spectra @t= 0 and t= 90min……257

Figure 6.2-23-2. Stacked ^{19}F NMR spectra @t= 0-90min……258

Figure 6.2-23-3. Stacked ^{31}P NMR spectra @t= 0-90min……258

Figure 6.2-23-4. Yields of product **3.3-43a**……259

Figure 6.2-24. ^{1}H NMR spectra @t= 0, 14 d and 14+7 d……259

Abbreviations

$\%V_{bur}$ – percentage of buried volume

@ – at

[Au] – gold complex

°C – degrees Celsius

2,6-DMP – 2,6-dimethoxyphenyl

Å – angstrom

Ac – acetyl

acac – acetylacetonate anion

Ad – adamantyl

Ag – silver

aq – solution in water

Ar – generic aromatic group

atm – atmosphere

Au – gold

BArF – tetrakis(3,5-bis(trifluoromethyl)phenyl)borate

BINAP – 2,2'-bis(diphenylphosphino)-1,1'-binaphthyl

BINOL – 1,1'-Bi-2-naphthol

biPy – bipyridine

Bn – benzyl

Boc – tert-butyloxycarbonyl

Br – bromine

bs – broad singlet.

Bz – benzoyl

C – carbon

CAAC – (alkyl)(amino)carbenes

Cbz – benzyloxycarbonyl

CCDC – Cambridge crystallographic data centre

CD – cyclodextrin

Cl – chlorine

cm – centimeter

Cs – caesium

Cu – copper

Cy – cyclohexyl

D – deuterium

d – doublet

dba – dibenzylideneacetone

DCB – 1,2-dichlorobenzene

DCD – Dewar-Chatt-Duncanson

DCE – 1,2-dichloroethane

DCM – dichloromethane

dd – doublet of doublets

ddd – doublet of doublet of doublets

ddt – doublet of doublet of triplets

DFT – density functional theory

Dipp – 2,6-diisopropylphenyl

DMF – dimethylformamide

DMSO – dimethyl sulfoxide

DPPF – 1,1'-Bis(diphenylphosphino)ferrocene

dppm – 1,1-Bis(diphenylphosphino)methane

dt – doublet of triplets

DTBP – Di-tert-butyl peroxide

E – entgegen (opposite, trans)

E^0 – oxidation/reduction potential

ECA – equivalent cone angle

ECP – effective core potential

EDG – electron-donating group

ee – enantiomeric excess

EI – electronic impact

equiv. – stoichiometric equivalent

ESI – electrospray ionization

Et – ethyl

EWG – electron-withdrawing group

F – fluorine

FG – functional group

g – gram

Ga – gallium

h – hour

H – hydrogen

HetAr – generic heteroaromatic

HFIP – Hexafluoro-2-propanol

Hg – mercury

HOMO – highest occupied molecular orbital

HRMS – high-resolution mass spectrometry

Hz – hertz

I – iodine

i.e. – id est (Latin for "that is")

*i*Pr – *i*-propyl

Ir – iridium

IRC – intrinsic reaction coordinate

J – coupling constant

K – potassium

kcal – kilocalories

KHMDS – potassium bis(trimethylsilyl)amide

L – ligand

LA – Lewis acid

LB – Lewis base

LE – ligand exchange

LG – leaving group

LUMO – lowest unoccupied molecular orbital

M – generic metal

M – molar

m – multiplet

m/z – mass-to-charge ratio

Me – methyl

Mes – mesityl

Mg – magnesium

mg – milligram

MHz – megahertz

MIC – mesoionic carbene

min – minute

mL – milliliter

mmol – millimole

MS – molecular sieves

N – nitrogen

Na – sodium

NBS – *N*-bromosuccinimide

*n*Bu – *n*-butyl

NCS – *N*-chlorosuccinimide

NHC – *N*-heterocyclic carbene

*n*Hex – *n*-hexyl

Ni – nickel

NIS – *N*-iodosuccinimide

NMR – nuclear magnetic resonance

NTf_2 – bistriflimide

Nu or Nuc – nucleophile

o – ortho

O – oxygen

OA or Ox. Add. – oxidative addition

OAc – acetoxy

ORTEP – Oak Ridge thermal ellipsoid plot

OTf – trifluoromethanesulfonate

p – para

P – phosphorus

Pd – palladium

Pent – pentyl

Ph – phenyl

phen – 1,10-phenanthroline

Pin – pinacolato

Piv – pivaloyl

pKa – the negative base-10 logarithm of the acid dissociation constant

ppm – parts per million

p-Tol or Tol – para-toluene

py – pyridine

q – charge on the atom

q – quartet

quant. – quantitative

R – generic group

RE or Red. Elim. – reductive elimination

RedOx – oxidation-reduction

Rh – rhodium

rpm – revolutions per minute

rt – room temperature

s – singlet

S – sulfur

SASP – solid angle spherical projections

Sb – antimony

SCXRD – single crystal X-ray diffraction

Se – selenium

Si – silicon

t◦ – temperature

t – triplet

TBA – tetra-*n*-butylammonium

TBAC – tetra-*n*-butylammonium chloride

*t*Bu – *t*-butyl

TCICA – trichloroisocyanuric acid

Tf – trifluoromethanesulfonyl

TFA – trifluoroacetic acid

THF – tetrahydrofuran

tht – tetrahydrothiophene

TIPS – triisopropylsilyl

TLC – thin-layer chromatography

TMS – trimethylsilyl

TOF – turnover frequency

TON – turnover number

Ts – para-toluenesulfonyl

TS – transition state

TSM – topographic steric map

tt – triplet of triplets

UV – ultraviolet

wt. – weight

Z – zusammen (same side, cis)

Zn – zinc

δ – chemical shift in parts per million

ΔG – Gibbs free energy change

µL – microliter

µmol – micromole

Table of Contents

Abstract i

Acknowledgments iv

Statement of Contributions v

List of Schemes vi

List of Figures x

Abbreviations xiii

1. Chapter 1: Introduction 1

1.1. Lewis acid-base theory 1

1.2. Relativistic effects 2

1.3. Ligand effects 3

1.3.1. Properties of the ligands 4

1.3.2. Ligand effects in Au(I) catalysis 6

1.3.3. Ligand effects in Au(I)/Au(III) catalysis 8

1.3.4. Ligand effects in stabilization of intermediates 10

1.3.5. Ligand effects and selectivity in catalytic transformations 12

1.4. Gold vs other metals 15

1.5. Au(I)-catalysis in the synthesis of natural compounds 17

1.6. Industrial applications and difficulties 20

1.7. Summary and outlook 21

1.8. Research goals 22

1.9. List of references 24

2. Chapter 2. Confinement-Induced Selectivities in Gold(I) Catalysis—The Benefit of Using Bulky Tri-(*ortho*-biaryl)phosphine Ligands 32

2.1. Abstract 32

2.2. Introduction 32

2.2.1. Cycloisomerization 33

2.2.2. NHC-based complexes 35

2.2.3. Phosphines 40

2.2.4. Phosphites 44

2.3. Results and Discussion 44

2.3.1. Synthesis of gold complexes 45

2.3.2. Structural analyses 46

2.3.3. Steric properties 47
2.3.4. Product selectivity 49
2.3.5. Substrate selection in the cycloisomerization reaction 56
2.3.6. Stereoselectivity 58
2.3.7. Regioselectivity 59
2.3.8. Substrate selection in hydration reaction 61
2.4. Conclusion 62
2.5. Experimental procedures 63
2.5.1. General information 63
2.5.2. Synthesis of *tris*-(*ortho*-biaryl)phosphine ligands 2.3-24, ligand 2.3-18 and Au(I) complexes 2.3-6 & 2.3-7 63
2.5.3. Catalytic studies 78
2.6. List of references 90
3. Chapter 3. DFT-guided Development of New Hemilabile (P^N) Ligands for Gold-(I/III) RedOx Catalysis : Application to the Thiotosylation of Aryl Iodides 100
3.1. Abstract 100
3.2. Introduction 100
3.2.1. Chelation-assisted strategy 101
3.2.2. Hemilabile ligands 105
3.3. Results and discussion 122
3.3.1. Synthesis, analysis, and reactivity of pyridine-based (P^N) Au(I) complexes 122
3.3.2. Catalytic reactivity 126
3.3.3. Computational study and ligand optimization 129
3.3.4. Exploring the catalytic potential of new (P^N) Au(I) complexes in C-S bond formation processes 133
3.3.5. Reaction scope and applications 137
3.3.6. Mechanistic investigations 140
3.4. Conclusion 142
3.5. Experimental procedures 143
3.5.1. General information 143
3.5.2. Synthesis of ligands 3.3-15 & 3.3-26, Au(I) & Au(III) complexes 3.3-11 – 3-13, 3.3-31 144
3.5.3. Initial studies 153
3.5.4. Attempts with Pd(0)/Pd(II) catalysis 158
3.5.5. Cross-coupling reaction of aryl iodides with ammonium thiotosylate 158

3.5.6. Structural diversifications of thiotosylate 3.3-43a 177
3.5.7. Synthesis of cross-coupling product 3.3-45 181
3.5.8. Other data and experiments 181
3.6. List of references 185
4. Chapter 4. Conclusion and outlook 196
4.1. Claims to Original Research 200
4.2. List of references 201
5. Publications and presentations 202
5.1. Publications of work in this thesis 202
5.2. Publications not presented in this thesis 202
5.3. Presentations of work in this thesis 202
6. Appendix 203
6.1. Appendix for Chapter 2 203
6.1.1. Cycloisomerization of enyne 2.3-17 (Chapter 2, Scheme 2.3-5) 203
6.1.2. Cycloisomerization of enyne 2.3-24 (Chapter 2, Scheme 2.3-6, A) 204
6.1.3. Cycloisomerization of enyne 2.3-25 (Chapter 2, Scheme 2.3-6, B) 204
6.1.4. Cycloisomerization of enyne 2.3-26 (Chapter 2, Scheme 2.3-6, C) 205
6.1.5. Cycloisomerization of enyne 2.3-27 (Chapter 2, Scheme 2.3-6, D) 206
6.1.6. Cycloisomerization of enyne 2.3-28 (Chapter 2, Scheme 2.3-7, A) 207
6.1.7. Cycloisomerization of enyne 2.3-29 (Chapter 2, Scheme 2.3-7, B) 208
6.1.8. Cycloisomerization of enyne 2.3-30 (Chapter 2, Scheme 2.3-8, A) 209
6.1.9. Cycloisomerization of enyne 2.3-31 (Chapter 2, Scheme 2.3-8, B) 210
6.1.10. Interrupted cycloisomerization of enyne 2.3-24 with styrene (Chapter 2, Scheme 2.3-9) 211
6.1.11. Interrupted cycloisomerization of enyne 2.3-24 with 1,3-dimethoxybenzene (Chapter 2, Scheme 2.3-9) 212
6.1.12. Interrupted cycloisomerization of N-cinnamyl-4-methyl-N-(prop-2-yn-1-yl)benzenesulfonamide 2.3-33 with indole (Chapter 2, Scheme 2.3-10, A) 213
6.1.13. Interrupted cycloisomerization of ethyl 2-diazo-2-phenylacetate 2.3-34 with styrene (Chapter 2, Scheme 2.3-10, B) 214
6.1.14. Cycloisomerization of enyne 2.3-35 (Chapter 2, Scheme 2.3-11, A) 215
6.1.15. Cycloisomerization of enyne 2.3-36 (Chapter 2, Scheme 2.3-11, A) 216
6.1.16. Competetive cycloisomerization of enynes 2.3-35 and 2.3-36 (Chapter 2, Scheme 2.3-11, B) 217
6.1.17. Cycloisomerization of enyne 2.3-37 (Chapter 2, Scheme 2.3-12) 218

6.1.18. Hydration of alkyne 2.3-38 (Chapter 2, Scheme 2.3-13, A) 219
6.1.19. Hydration of alkyne 2.3-39 (Chapter 2, Scheme 2.3-13, B) 220
6.1.20. Competetive hydration of alkynes 2.3-38 and 2.3-39 (Chapter 2, Scheme 2.3-14, A) 221
6.1.21. Competetive hydration of alkynes 2.3-40 and 2.3-41 (Chapter 2, Scheme 2.3-14, B) 222
6.1.22. SCXRD analysis and data 223
6.1.23. Calculation of percent buried volumes (V_{Bur}%) and generation of topographic steric maps (TSM) 228
6.1.23. Calculation of G_{Au} parameters, equivalent cone angles (ECA) and generation of solid angle spherical projections (SASP) 231
6.1.24. List of references 235
6.2. Appendix for Chapter 3 236
6.2.1. First set of pyridine-based ligands tested 236
6.2.2. Alkoxyarylation with pent-4-en-1-ol 3.3-16a (Chapter 3, Scheme 3.3-4, A) 237
6.2.3. Amidoarylation with *N*-tosyl aminopentene 3.3-16b (Chapter 3, Scheme 3.3-4, A) 238
6.2.4. Amination with 2-nitroaniline 3.3-24 (Chapter 3, Scheme 3.3-5) 239
6.2.5. Heck reaction with hex-1-ene (Chapter 3, Scheme 3.3-5) 240
6.2.6. Transmetallation with tributyl(thiophen-2-yl)stannane 3.3-27a (Chapter 3, Scheme 3.3-6, A) 241
6.2.7. Transmetallation with silver reagent 3.3-27b (Chapter 3, Scheme 3.3-6, A) 242
6.2.8. Alkoxyarylation with hex-5-en-1-ol 3.3-16c (Chapter 3, Scheme 3.3-8) 242
6.2.9. Alkoxyarylation with (*E*)-(2-iodovinyl)benzene and pent-4-en-1-ol 3.3-16a (Chapter 3, Scheme 3.3-8) 243
6.2.10. Amidoarylation with (*E*)-(2-iodovinyl)benzene and *N*-tosyl aminopentene 3.3-16b (Chapter 3, Scheme 3.3-8) 244
6.2.11. General procedure for the calculation of yield of cross-coupling products 3.3-43 (Chapter 3, Scheme 3.3-11) 245
6.2.12. Calculation of yield of diversification product 3.3-44a (Chapter 3, Scheme 3.3-12) 246
6.2.13. Calculation of yield of diversification product 3.3-44b (Chapter 3, Scheme 3.3-12) 247
6.2.14. Calculation of yield of diversification product 3.3-44c (Chapter 3, Scheme 3.3-12) 248
6.2.15. Calculation of yield of diversification product 3.3-44d (Chapter 3, Scheme 3.3-12) 249
6.2.16. Calculation of yield of diversification product 3.3-44e (Chapter 3, Scheme 3.3-12) 250
6.2.17. Calculation of yield of diversification product 3.3-44f (Chapter 3, Scheme 3.3-12) 251
6.2.18. Calculation of yield of diversification product 3.3-44g (Chapter 3, Scheme 3.3-12) 252
6.2.19. Synthesis of cross-coupling product 3.3-45 (Chapter 3, Equation 3) 253

6.2.20. Role of Ag^+ in Au(I)/Au(III) redox catalysis (alkene/ArI exchange) (Chapter 3, Scheme 3.3-13, A) 254
6.2.21. Thiotosylate Au(I) complex 3.3-$35_{STs\text{-}Cl}$ as the resting state in the cross-coupling reaction (Chapter 3, Scheme 3.3-12, A) 255
6.2.22. Importance of Ag^+ salt on the course of the cross-coupling reaction (Chapter 3, Scheme 3.3-12, B) 256
6.2.23. Ag^+ is not required to induce the cross coupling reaction from Au(III) oxidative complex 3.3-49 (Chapter 3, Scheme 3.3-13, B) 257
6.2.24. Robustness of Au(I) complex 3.3-11_H (Chapter 3) 259
6.2.25. SCXRD analysis and data 259
6.2.26. DFT calculations 262
6.2.27. List of references 275
7. Collective NMR data 278
7.1. NMR data for Chapter 2. 278
7.2. NMR data for Chapter 3. 325

1. Chapter 1: Introduction

In this section, we will discuss the underlying concepts and intrinsic properties that make gold an interesting and important element in the field of catalysis. We will provide an introduction to the unique properties of gold that characterize its reactivity and catalytic potential. In addition, the crucial role of ligands in gold catalysis is briefly discussed. To facilitate this discussion, we will present the key descriptors essential for evaluating ligand properties in the context of gold catalysis.

We will also briefly discuss the impact of ligands on stabilizing gold intermediates and show how this influences the efficacy and selectivity of reaction outcomes. Furthermore, we will present an examples of ligand-dependent gold catalysis, discussing the divergent reaction pathways and products when using gold catalysis or other metals. Additionally, we will offer a brief overview of diverse applications of gold, spanning from its use in the total synthesis of natural products to its emerging potential in industrial applications.

1.1. Lewis acid-base theory

The concept of a "Lewis acid," originally introduced by the eminent chemist Prof. Gilbert N. Lewis (1875-1946), revolutionized our understanding of chemical reactivity. G. N. Lewis postulated that any entity with a vacant orbital could qualify as an acid, while those with an electron pair could be seen as a base. Consequently, the combination of these two entities leads to a Lewis acid-base adduct (**Scheme 1.1-1, A**).

The Dewar-Chatt-Duncanson (DCD) model, introduced in the early 1950s, expanded upon this concept and its application to metal-catalyzed processes. The proposed model advanced the understanding of chemical interactions, especially in the context of transition metal complexes.[1,2] The DCD model, a cornerstone of organometallic chemistry, describes the bonding between a transition metal and an unsaturated organic ligand – such as an olefin or alkyne – through a combination of σ-donation and π-backdonation interactions.

In the Dewar-Chatt-Duncanson model, the ligand donates a pair of electrons from its Highest Occupied Molecular Orbital (HOMO) into an empty *d*-orbital of the metal, forming a σ-bond (**Scheme 1.1-1, B**). Simultaneously, the metal accepts electron density from the π-antibonding orbital of the ligand into metal's Lowest Unoccupied Molecular Orbital (LUMO), making a π-bond. This synergistic interaction not only strengthens the metal-ligand bond but also modifies the electronic and steric properties of the complex. This model has proven valuable in understanding the reactivity and catalytic potential of various transition metal complexes, including those involving gold in catalysis.

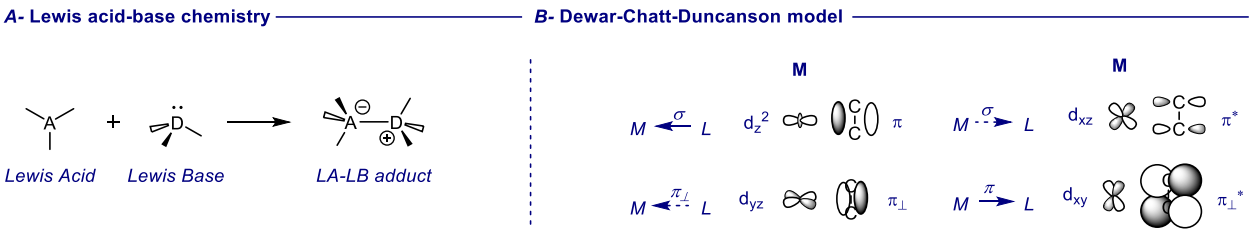

Scheme 1.1-1. Lewis theory and DCD model.

Furthermore, the concepts of hard and soft interactions[3–5] are invaluable in categorizing the propensities of Lewis acids towards different electron donors or Lewis bases. Hard Lewis acids exhibit strong positive charge, condensed dimensions, and elevated electronegativity, predisposing them to bond with hard Lewis bases that possess dense electron concentration and more confined dimensions, such as hydroxide or fluoride ions. Conversely, soft Lewis acids, characterized by a dispersed positive charge, expanded dimensions, and reduced electronegativity, display an affinity towards soft Lewis bases with lower electron density and larger size, including entities like CO, phosphines, alkenes, aromatics, and amines. It is noteworthy that soft Lewis acids often manifest in transition metal complexes and heavy metal ions. This distinction not only enhances the individuality of soft Lewis acids but also contributes to their special role in various chemical reactions.

1.2. Relativistic effects

To better understand the soft Lewis acidic nature of Au(I) species it is crucial to consider relativistic effects.[6–9] Essentially, the observed effects illustrate the differences between values calculated by theoretical models that incorporate relativistic principles and those that omit them. Heavier elements like gold experience these effects more strongly. With an increase in atomic nuclear charge, the velocity of *s*-electrons and mass increase, leading to a contraction of the *s*-orbitals beyond non-relativistic predictions. Consequently, the *s*-electrons bind more tightly to the nucleus, effectively shielding its charge from the outer *d*- and *f*-electrons. The decreased binding in *d*- and *f*-electrons leads to an expansion and increased diffuseness of these orbitals (**Scheme 1.2-1**). As gold occupies the terminal position in the *5d* orbital filling sequence, followed by *4f* filling, it experiences the maximum impact of relativistic effects.

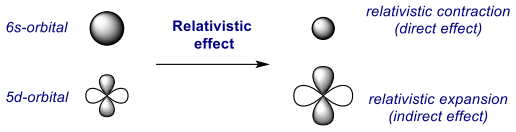

Scheme 1.2-1. Relativistic effect.

These relativistic phenomena manifest in several notable ways. First, characteristic yellow color of gold originates from the transition between the *5d* electrons' higher energy levels and the Fermi level, primarily displaying *6s* character. Second, gold's renowned resistance to oxidation

can be traced back to the robust bonding of the *6s* electrons, resulting in a relatively large first ionization potential necessary to detach the *s*-electron from the *6s* orbital. Lastly, the relativistic effects contribute to a shorter Au(I)-L bond length. In comparison to copper and other Group 11 metals, Au(I) exhibits diminished nucleophilicity, classifying it as a softer Lewis acid.[9] This trait can be linked to the relativistic contraction of the valence *s*-orbital, yielding a lower energy level for the LUMO. These factors not only render Au(I) less nucleophilic compared to copper but also underscore its distinctive status as a softer Lewis acid among Group 11 metals. Additionally, considering the extensive and diffuse cationic nature of Au(I), it is rational to conclude that orbital interactions govern its binding affinity to a π-system.

In summary, the relativistic effects, especially as they apply to gold, provide profound insights into the unique physical and chemical properties of the element. They facilitate a deeper understanding of the appearance of gold, reactivity, and its distinctive role as a soft Lewis acid in various chemical contexts.

1.3. Ligand effects

The evolving role of gold in catalysis is characterized by a multifaceted shift in understanding and application. Gold catalysts, initially viewed as expensive, are now considered economically viable alternatives to commonly utilized palladium (Pd), rhodium (Rh), and iridium (Ir) complexes. Several factors contribute to this perception. Firstly, Au(I) catalysis usually lacks redox chemistry, simplifying the recovery process and reducing associated costs[10]. Gold complexes also display remarkable air and moisture stability, eliminating the need for strict inert conditions, and showcase selectivity towards C-C π-systems, enhancing reaction efficiency. Together, these attributes have broadened gold's application beyond niche domains.

An essential aspect of gold catalysis lies in the activation of linear dicoordinated gold-complexes [(L)AuCl], which are usually unreactive in their precatalytic state. Activation typically requires chloride abstraction to form a cationic $[(L)Au]^+$, often using silver salts. It is worth noting that the use of silver salt can influence the outcome of the reaction in some cases, which is known as the "silver effect" and has been thoroughly studied. However, in most cases, silver salts are considered inert throughout the reaction profile[11].

Interestingly, in addition to the "silver effect", the reactivity of a gold-catalyst is markedly influenced by the counterion used.[12,13] Weakly coordinated counterions such as SbF_6^-, BF_4^-, and $BArF^-$ tend to increase catalytic activity by facilitating substrate binding. Conversely, more strongly coordinated and electrophilic counterions like NTf_2^- or OTf^- may decrease activity by competing with substrates for coordination sites on the catalyst. Additionally, counterions can alter product selectivity by changing the geometry of transition states or offering extra stabilization through the formation of hydrogen bonds.

However, the major role in tuning the reactivity of a gold center is played by ligands. The choice of ligand can significantly influence the stability, electronic properties, and steric environment of the gold catalyst and thus control the course of the reaction. Ligands can modulate the electronic properties of the gold center. Electron-donating ligands can enhance the nucleophilicity of the gold, while electron-withdrawing ligands can increase its electrophilicity. The steric bulk of ligands can influence the accessibility of substrates and reagents to the active catalytic center. Steric considerations are also crucial in determining the regio- and stereoselectivity of gold-catalyzed reactions. In addition, ligands can stabilize the active gold species, increasing their stability and preventing degradation. Some ligands can actively participate in the catalytic cycle, facilitating substrate activation or stabilization of reaction intermediates. In addition, in redox-active catalysis, ligands can also participate in the redox process by stabilizing high oxidation states of gold. The design and selection of appropriate ligands is therefore a cornerstone in the advancement of gold catalysis and enables the fine-tuning of catalytic systems to achieve the desired reactivity and selectivity profile.

1.3.1. Properties of the ligands

In the field of gold catalysis, phosphines and N-heterocyclic carbene ligands are predominantly used. Both of these ligand classes form stable Au-L bonds, with NHCs generally acting as stronger electron donors than phosphines. Despite their differences, both types of ligands can be described as σ-donor/π-acceptor structures. The relative contributions of these bonding interactions can vary, dependent on the specific structural features of the ligand and the nature of the metal center involved.[14,15]

Two key approaches have emerged for the synthesis of NHC-ligated Au(I) complexes.[16] Historically, silver oxide was used to form a silver complex by reacting with an N-heterocyclic carbene precursor (**Scheme 1.3.1-1, A**). Transmetallation was then carried out with Au(I) chloride or thioether complexes.[17] N-heterocyclic carbene copper(I) chloride complexes have also been successfully applied in this transmetallation processes.[18] However, there were some concerns with the transmetalation method. Notably, the atom economy was reduced by using equal amounts of silver and the Au(I) complexes were exposed to the risk of contamination by metals such as silver or copper, which was particularly undesirable in catalysis. As a result, researchers began to favor direct methods. Gimeno[19] and Nolan[20] indepently made a significant advance when they reported an effective method for the synthesis of NHC-ligated Au(I) complexes. The researchers used K_2CO_3 in solvents such as DCM or acetone to react $AuCl{\cdot}SMe_2$ with N-heterocyclic carbene precursors (**Scheme 1.3.1-1, B**). Additionally, $NBu_4(acac)$[21] or strong bases such as KHMDS[21] or a combination of NaH/KO*t*Bu[22] have found use in certain situations.

The preparation of phosphine-bound Au(I) complexes is characterized by its simplicity and efficiency. Typically, the synthesis is achieved by the coordination of free phosphine ligands with a Au(I) complex that has a weakly coordinating ligand such as a thioether (**Scheme 1.3.1-1, C**).[23]

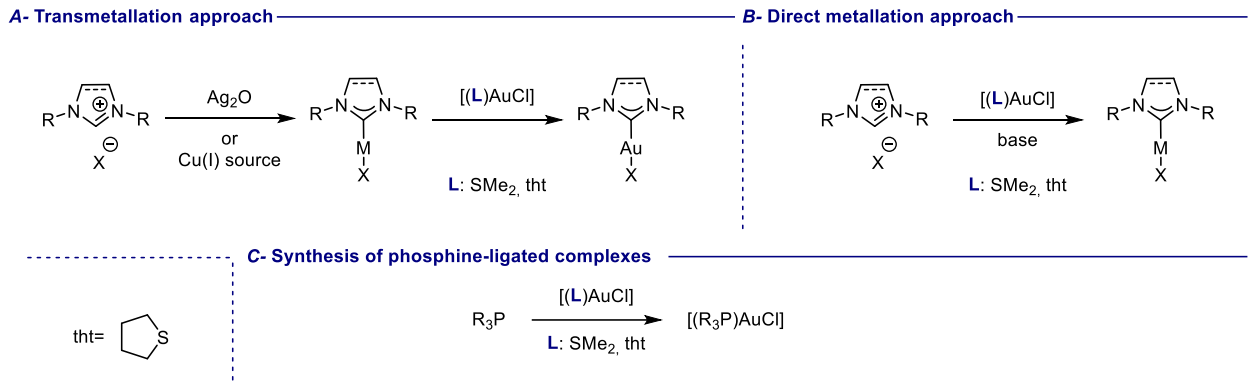

Scheme 1.3.1-1. General approaches to synthesis of NHC- and phosphine-ligated Au(I) complexes.

Due to their ease of synthesis and facile tuning of their steric and electronic properties, N-heterocyclic carbenes and phosphines have become the most commonly used ligands in gold chemistry. They maintain their status as "blockbuster" ligand classes and below are the selected examples of ligands developed in these categories (**Scheme 1.3.1-2**).

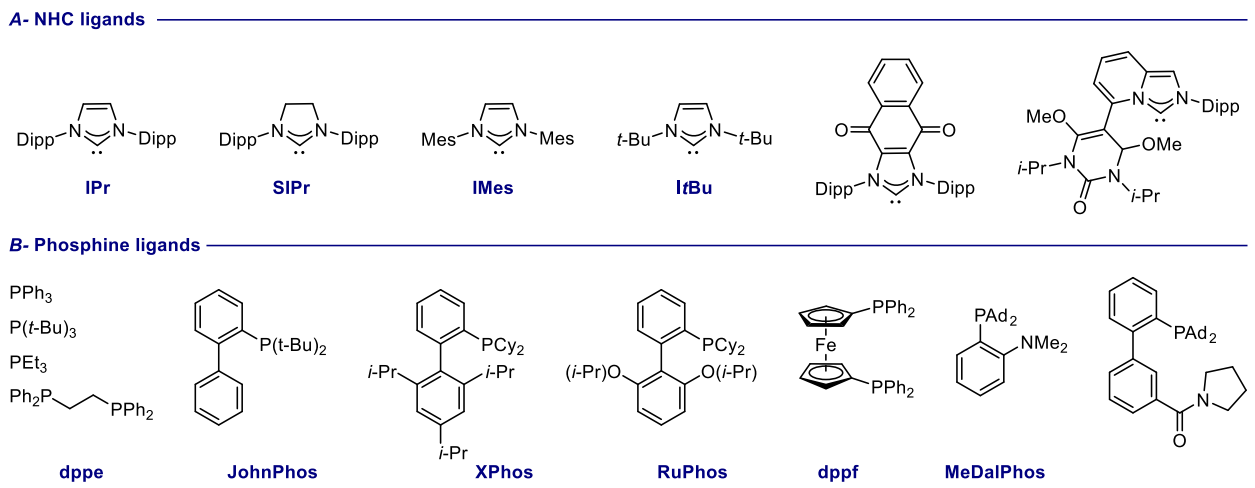

Scheme 1.3.1-2. Examples of NHC and phosphine ligands.

These ligands are notable for their modifiable stereoelectronic attributes, which play a crucial role in tuning the behavior of the corresponding catalytic systems.[24,25] Extensive research has been conducted to determine the steric and electronic characteristics of these ligands, aiming to gain deeper insights into the factors governing the ligand influence by establishing various descriptors.[26–29] Among them, the Tolman cone angle and the percentage of buried volume (%V_{bur}), are used for steric analysis, and the Tolman electronic parameter describes electronic properties.

The Tolman cone angle, defined as the angle formed at the metal center by a cone enclosing the outermost atoms of the ligand, serves as a quantitative measure of the steric bulkiness of the ligand (**Scheme 1.3.1-3, A**).[25] Such steric considerations are crucial because they can modulate

the steric congestion at the metal center, which can have a significant impact on the accessibility of the substrate and the course of the catalytic cycle.

On the other hand, the $\%V_{bur}$ is calculated by evaluating the volume of space occupied by a ligand in the coordination sphere and expressing it as a percentage of the total volume of the coordination sphere (**Scheme 1.3.1-3, B**).[30,31] This parameter allows a more nuanced understanding of the steric properties of ligands compared to the Tolman cone angle, as it takes into account the three-dimensional spatial population of the ligand around the metal center.

The Tolman electronic parameter is a crucial measure for determining the ability of ligands to donate electrons (**Scheme 1.3.1-3, C**).[25] This parameter is measured in carbonyl complexes by assessing the ν(CO) stretching frequency, which provides insight into the electron density at the metal center.[25] After coordination of CO to the metal, the ν(CO) normally decreases from the 2143 cm^{-1} observed for free CO. This shift in ν(CO) can be explained by π-backbonding, in which the metal forms a π-bond with the carbonyl ligand by giving electrons from its *d*-orbitals into the empty antibonding π* orbitals on CO. A lower vibration frequency results from the fact that this interaction strengthens the metal-carbon bond while weakening the bond between carbon and oxygen. Additional ligands that increase the π electron density of the metal weaken the C-O bond and reduce ν(CO) even more. Conversely, if the additional ligand competes with CO for π-backdonation, an increase in ν(CO) occurs.

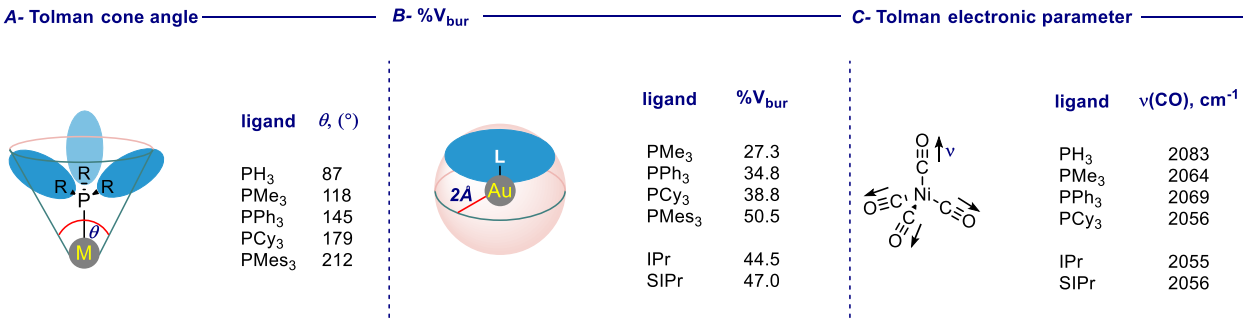

Scheme 1.3.1-3. Ligand descriptors and the respective values for selected ligands.[25,27,32,33]

1.3.2. Ligand effects in Au(I) catalysis

It is well accepted that the general catalytic cycle for the Au(I)-catalyzed nucleophilic functionalization of π-systems in the mechanistic pathway (**Scheme 1.3.2-1**) begins with the coordination of the Lewis acidic Au(I) species to a π-system.[34] This coordination polarizes the π-bond, making it more electrophilic. Next, a nucleophilic attack occurs across the triple bond in a trans orientation, forming an intermediate **1.3.2-1**. Finally, with the aid of a proton source, protodeauration occurs, leading to the formation of the final product **1.3.2-2** and regenerating the catalyst. Additionally, the catalytically active Au(I) can suffer modifications, yielding catalytically inactive Au(0) and bis-ligated Au(I) species.

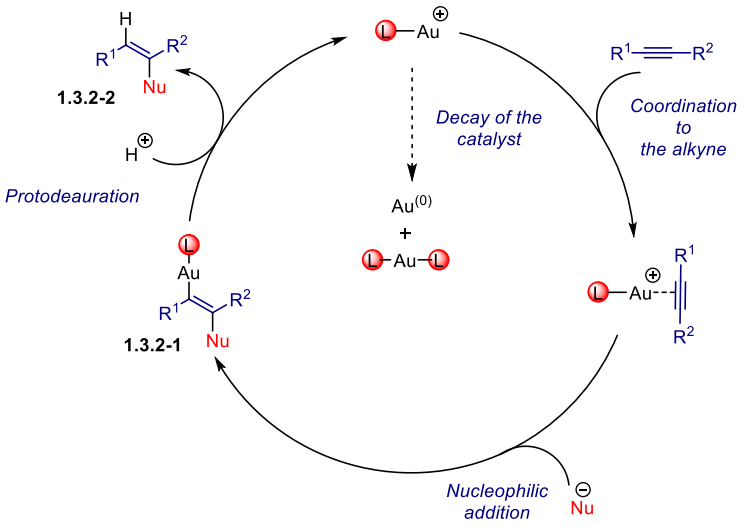

Scheme 1.3.2-1. General mechanism of Au(I) catalyzed nucleophilic addition.

The influence of ligands on different stages of a catalytic process was studied in detail by the group of Xu in 2012.[35] The researchers found that the protodeauration of **1.3.2-3** was noticeably accelerated by electron-donating ligands (**Scheme 1.3.2-2, A**). Notably, the Buchwald-type ligand JohnPhos accelerated the reaction, possibly through η2-interaction from the ortho-substituted phenyl ring, which stabilized the cationic gold complex. The researchers stated that the alkyne coordination step was fast, negating the possibility of it being the rate-determining step. The following nucleophilic addition to form compound **1.3.2-4** was accelerated by using electron-deficient ligands (**Scheme 1.3.2-2, B**). Due to the inherent rapidity of this step, it was necessary to specifically slow down the reaction by adding excess of benzotriazole, which can reversibly and competitively bind to the gold cation.

Assessing the decay profile of the catalyst, they found that the conventional cationic gold complex [(Ph_3P)AuOTf] exhibited excellent stability in solution. However, when a reductive substrate such as an alkyne **1.3.2-5** was introduced, rapid decay of the gold complex was observed. Remarkably, the electronic properties of the ligands did not have a significant impact on the stability of the cationic gold. Both electron-rich and electron-poor ligands accelerated the decay. However, Au(I) complexes with the Buchwald-type ligand showed increased stability (**Scheme 1.3.2-2, C**). This could possibly be attributed to the stabilizing η2-interaction observed in biphenyl gold(I) complexes.

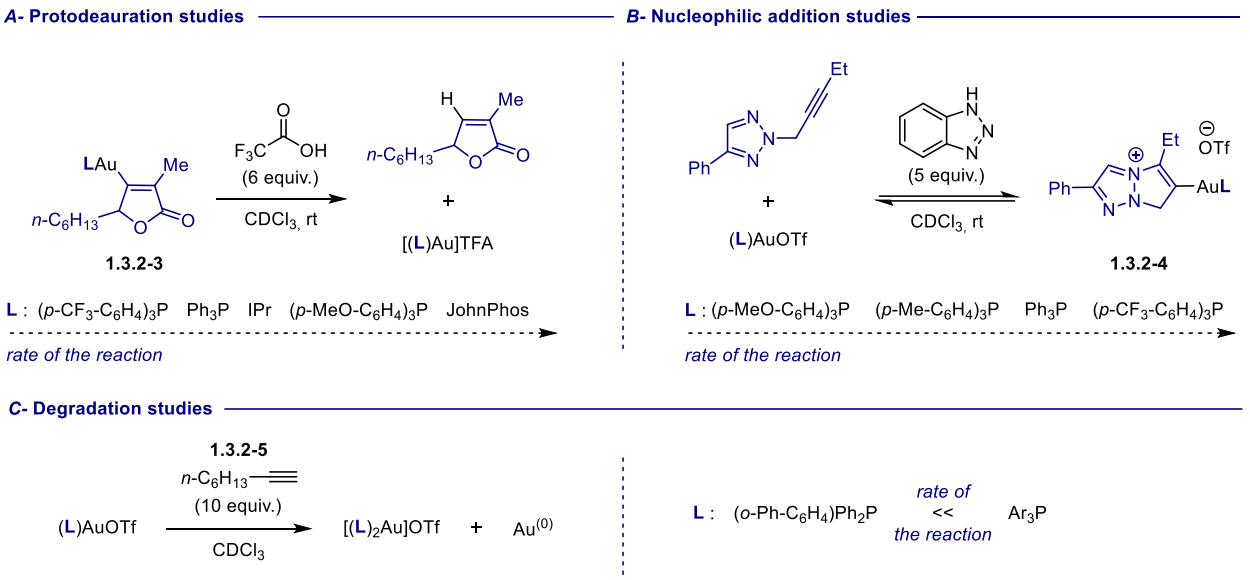

Scheme 1.3.2-2. Ligand effect of the Au(I) catalyzed nucleophilic addition.

1.3.3. Ligand effect in Au(I)/Au(III) catalysis

One of the main characteristics of gold catalysis is its resistance to cycle between Au(I) and Au(III), which is essential for the oxidative addition step, a typical entry point in catalytic cross-coupling cycles. Although this resistance facilitated the utilization of functional groups, which are typically incompatible with commonly employed transition metals, it considerably limited the range of possible transformations. Apparently, the oxidative addition step proved to be a bottleneck to achieve and develop Au-catalyzed cross-coupling reactions with common electrophiles such as aryl halides.

Initial efforts to address this challenge were based on the utilization of stoichiometric amounts of strong external oxidants, such as hypervalent iodine or electrophilic fluorination reagents to facilitate the transition to the Au(III) oxidation state.[36–44] Alternatively, another approach involved the use of photochemical conditions to stimulate the oxidative addition to Au(I) complexes,[45–49] or the application of diazonium under either photochemical or thermal conditions.[50–55] These strategies were used to promote the formation of crucial Au(III) intermediate **1.3.3-1** via a 2-electron oxidation pathway, thereby providing a way to promote the Au(I)/Au(III) catalytic cycle.

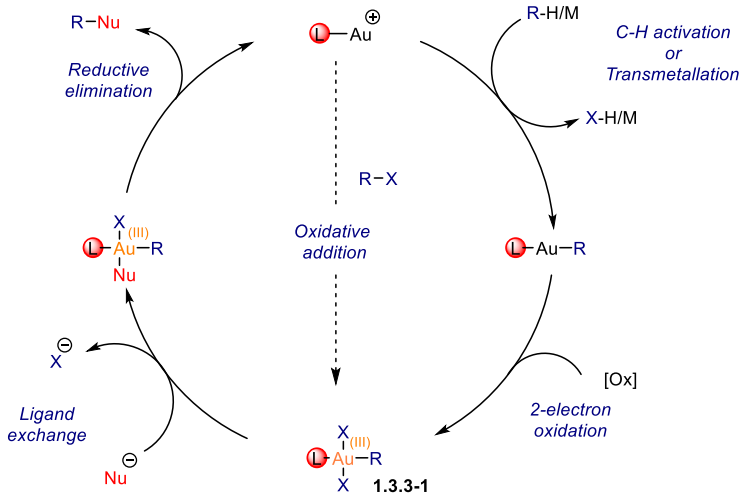

Scheme 1.3.3-1. General mechanism of Au(I)/Au(III) catalyzed cross-coupling reactions.

A significant paradigm shift occurred with the introduction of the ligand-assisted approach. With this novel method, the access to the Au(III) intermediate **1.3.3-1** is significantly facilitated by using specifically designed hemilabile ligands. This ligand-centered approach deviates from traditional methodology and seeks to exploit the inherent electronic and steric properties of ligands to modulate the redox behavior of gold, thereby opening the way to a more controlled and effective catalytic process.

Hemilabile ligands, which possess both strong and weak coordinating sites, can dynamically modulate their coordination behavior in response to the changing needs of the catalytic cycle (**Scheme 1.3.3-2, A**). This unique characteristic allows for the stabilization of both the Au(I) and Au(III) oxidation states within the same catalytic cycle, that is challenging to achieve with traditional chelating ligands due to the distinct geometric and electronic preferences of these two oxidation states. The use of hemilabile ligands is particularly promising as it offers the opportunity for more controlled reactions and a wider range of applications.

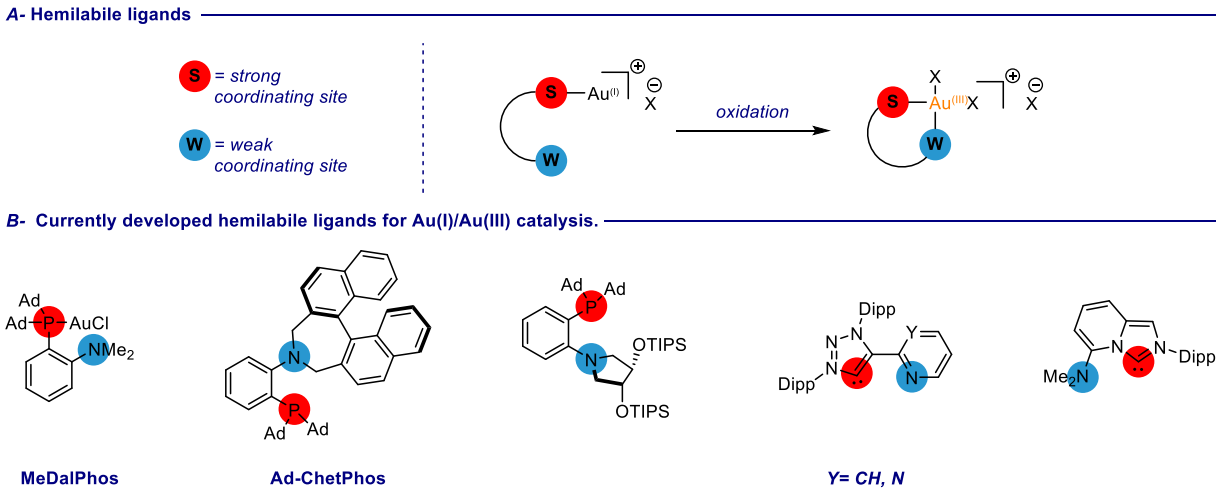

Scheme 1.3.3-2. Hemilabile ligands.

However, this area is still in its infancy. A critical and ongoing challenge is the lack of comprehensive understanding of the crucial ligand parameters that are essential for catalyst design. This knowledge gap hinders the further development of the field and the repertoire of suitable ligand complexes remains significantly limited, as only a handful of successful examples have been described to date (**Scheme 1.3.3-2, B**).[56–61] The interactions between ligands and gold and their subsequent influence on the oxidative addition step and the overall mechanism require thorough elucidation.

1.3.4. Ligand effect in stabilization of intermediates

The choice of ligands has a major impact on the stability of intermediates in gold catalysis, and this is particularly important in carbene transfer reactions. It is important to understand the variables that influence the stability and reactivity of this species. The bonding in cationic gold complexes involves two key interactions: formation of a σ-bond between the lone pair of electrons on the carbon moiety and an orbital of appropriate symmetry on the gold results in a structure **1.3.4-1b** resembling a carbocation, while a π-backbonding from the *d*-orbital of the gold to an empty *p*-orbital on the carbon atom results in a singlet carbene form **1.3.4-1a** (**Scheme 1.3.4-1**).

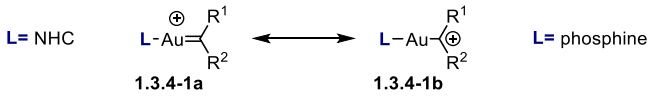

Scheme 1.3.4-1. Carbene-like and carbocation-like resonance forms of a gold complex.

The stability of carbene-like structures in Au(I) catalysis is related to the π-backbonding of the gold atom. The degree of gold-coordinated carbocation **1.3.4-1b** and gold-stabilized singlet carbene **1.3.4-1a** character in gold carbene intermediates is determined by the balance between σ and π bonding, which is influenced by the substituents on the ligand. By controlling π-backbonding, the auxiliary ligand modulates the stability of the complex by stabilizing the carbene. Due to the competition for electron density from the metal by two π-bonding moieties, ligands with higher π-acidity typically favor the carbocation-like properties of the intermediates. Conversely, ligands with stronger electron-donating abilities enhance carbene-like reactivity.

This concept was nicely applied by Straub and coworkers in 2014 (**Scheme 1.3.4-2, A**).[62] Using Au(I) complex **1.3.4-2** containing a bulky ligand and a sterically demanding diazomethane substrate Mes_2CN_2, the researchers succeeded in synthesizing and isolating a non-heteroatom-stabilized gold complex **1.3.4-2a** that is characterized by high carbenoid character. Impressively, the synthesized complex exhibited remarkable stability to air, water, and heat. The authors proposed that the extreme steric shielding of the resulting carbene center is a key to this remarkable stability.

Later, Bourissou and collegues employed a different ligand-based approach to synthesize the Au(I) complex **1.3.4-3a** with high carbenoid character (**Scheme 1.3.4-2, B**).[63] The key to this synthesis was the use of *o*-carborane diphosphine as the ligand in a bent Au(I) complex **1.3.4-3**. The researchers postulated that the unique bent structure of the complex enhances π back-donation, which helps stabilize the complex. It is proposed that the bending of the $[PAuP]^+$ fragment and a three-coordinate gold environment increase the energy level of the occupied d_{xz} orbital on gold and strengthen its interaction with the empty π* CO orbital. This complex has been reported to be stable up to 158 degrees Celsius before decomposition occurs.

On the other hand, in the same year, Widenhoefer and Harris synthesized a Au(I) complex with pronounced carbocation character (**Scheme 1.3.4-2, C**).[64] It was shown that the phosphine-bound Au(I) complex **1.3.4-4** upon reaction with $[Ph_3C][BF_4]$ is giving the desired complex **1.3.4-4a** in 52% yield. The researchers hypothesized that the stabilization of this complex is facilitated by π-delocalization, leading to the formation of a cationic tropylium structure.

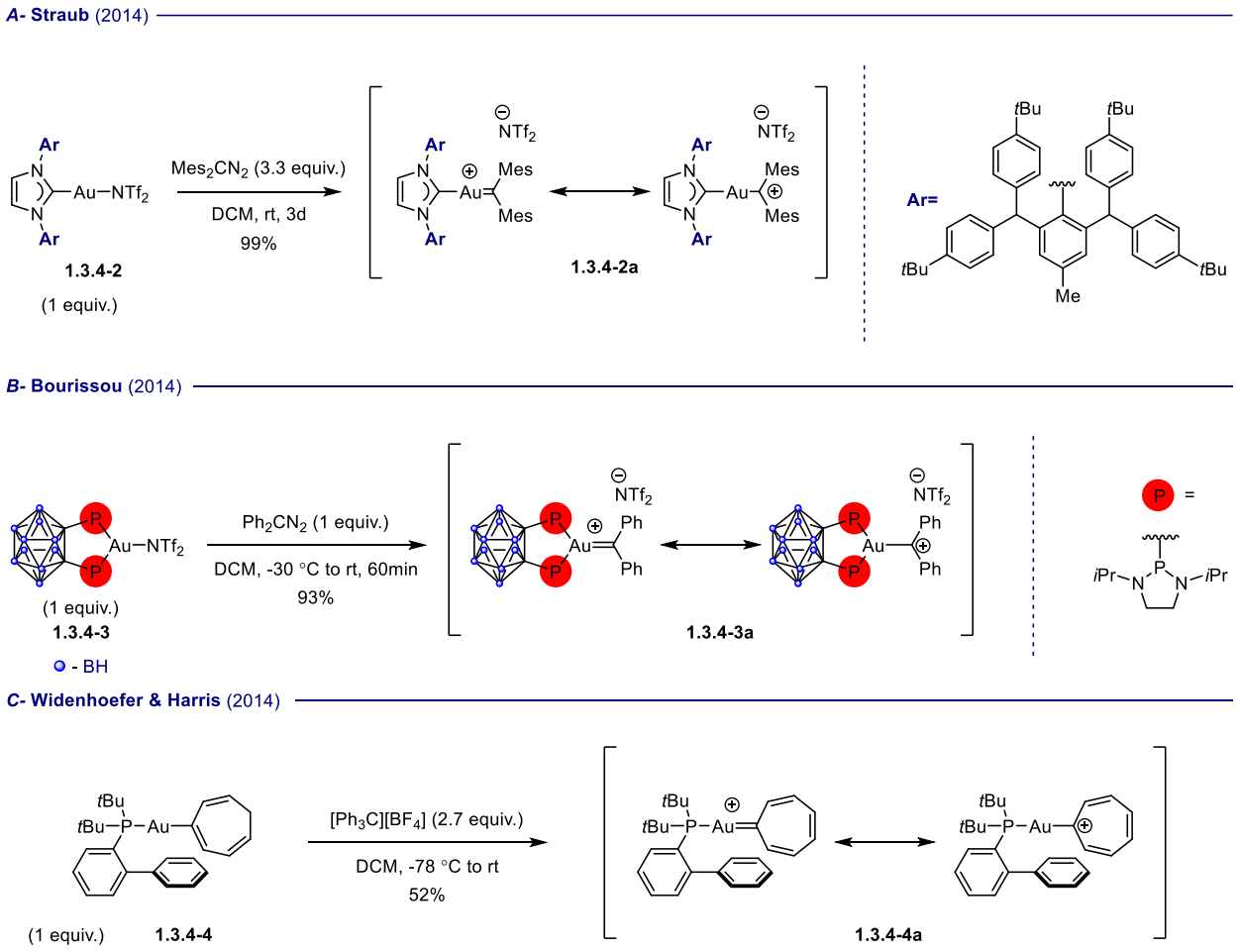

Scheme 1.3.4-2. Examples of Au(I)-complexes with high carbenoid character.

These studies illustrate the complexity of ligand design in gold catalysis. The stabilization of reactive intermediates can be achieved by various methods. By carefully manipulating the

electronic and steric properties of gold complexes, it is possible to tailor the reactivity and stability to specific targets. This versatility not only highlights the potential of gold in catalysis, but also highlights the crucial role of ligand architecture in controlling the behavior of catalytic species. Such advances contribute significantly to a more comprehensive understanding of catalytic processes and to the development of more efficient and selective catalytic systems.

1.3.5. Ligand effects and selectivity in catalytic transformations

Ligand-dependent divergent gold catalysis represents a significant influence of ligand effects on the results of chemical reactions. Depending on the type of ligand that coordinates to the gold center, it is possible to generate different products from common substrates. Because of this dependence on ligand properties, it provides a flexible platform to control reaction pathways and product profiles. The intricate interplay between the ligand and the gold catalyst is instrumental in determining the selectivity and efficiency of the catalytic process, making ligand-dependent divergent gold catalysis a promising area of study to explore the potential of gold in catalytic transformations.[65,66]

The group of González in 2011 provided an example of how the electron density in the ligand of a Au(I) complex can play a crucial role in determining the reaction outcome.[67] When a Au(I) complex with a phosphite ligand is employed in cyclization of *N*-tosylanilines **1.3.5-1**, the reaction affords 4-iodo substituted quinolone **1.3.5-1a** as a main product (**Scheme 1.3.5-1**). On the other hand, a significant change in the reaction pathway occurs when a more electron-donating ligand such as IPr is employed. By forming Au(I) vinylidene intermediate **1.3.5-1i** via 1,2-iodide shift before the cyclization step, this reaction affords the 3-iodo substituted quinolone **1.3.5-1b**. This example shows how important the electron density of the ligand is in controlling the reaction mechanism and the composition of the final product.

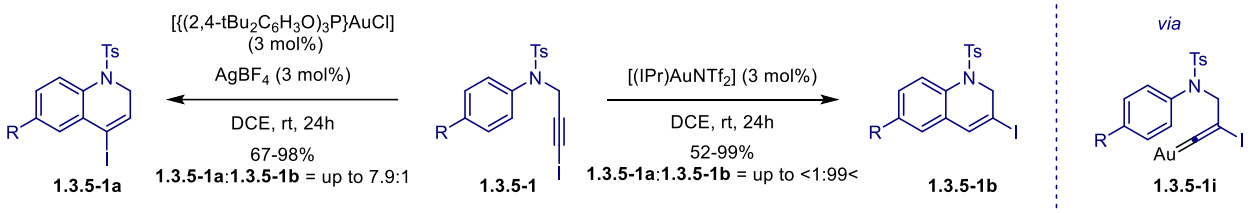

Scheme 1.3.5-1. Ligand effect in cyclization of *N*-tosylanilines.

Another illustrative example of the influence of electronic properties of the ligand on chemical reactions was presented in a 2013 study by the research group of Hashmi.[68] In their publication, the researchers observed the chemoselectivity in the Au(I)-catalyzed cyclization of alkynones **1.3.5-2** (**Scheme 1.3.5-2**). It was proposed that this selectivity is a consequence of the electronic characteristics of the ligand attached to the Au(I) complex. Variations in the electronic properties of these ligands significantly modify the electrophilic properties of the corresponding Au(I) species, thus affecting the reaction pathway. Specifically, an electron-donating IPr ligand

effectively facilitate the conversion of alkynones **1.3.5-2** into **1.3.5-2b**. On the other hand, the less electron-donating PPh_3 ligand predominantly yields product **1.3.5-2a**.

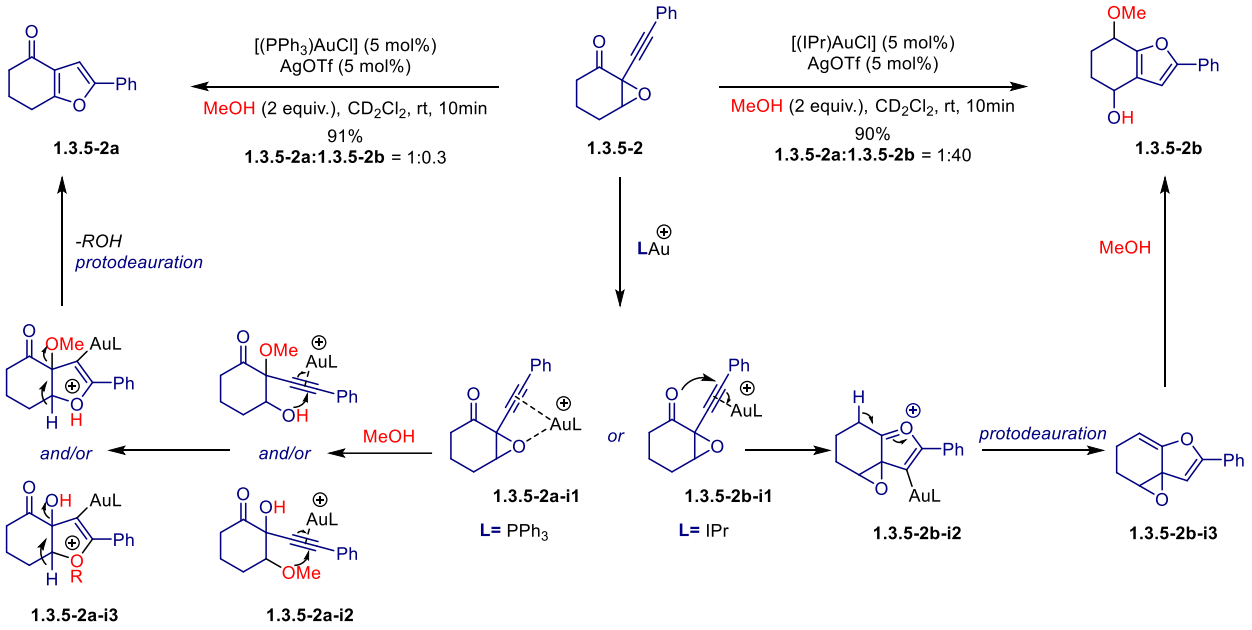

Scheme 1.3.5-2. Chemoselectivity in cyclization of alkynones.

From a mechanistic perspective, it is hypothesized that electron-withdrawing ligands reduce the electron density at the Au(I) center, thereby making it a harder Lewis acid, which prefers to open the epoxide moiety, rather than activating the alkyne part of the molecule. The intermediate **1.3.5-2a-i1** is then subject to nucleophilic attack by methanol, leading to the formation of isomers **1.3.5-2a-i2**. These isomers are can further undergo a 5-endo-dig cyclization to form **1.3.5-2a-i3**, followed by elimination and protodeauration to afford the final product **1.3.5-2a**.

Conversely, a more electron-donating IPr ligand is proposed to reduce the electrophilicity at the Au(I) center, making it a softer Lewis acid. This modified reactivity profile allows the Au(I) species to preferentially activate the triple bond of the alkyne rather than the epoxide. The subsequent nucleophilic attack by a carbonyl group yields an intermediate **1.3.5-2b-i2**, which can undergo protodeauration and afford subsequent intermediate **1.3.5-2b-i3**. The formed **1.3.5-2b-i3** species can then be attacked by a methanol molecule, facilitating the opening of the epoxide and yielding product **1.3.5-2b**.

Notably, the ligand itself can play an important role over the course of the reaction and thus influence its outcome. One of the most recent examples of such an approach was demonstrated by the group of Zhang in 2022.[69]. The researchers developed an enantioselective dearomatization process of **1.3.5-3** facilitated by synergistic metal-ligand cooperation (**Scheme 1.3.5-3**). Crucial to this methodology was the interaction between the basic group of the ligand and the reaction substrate which is a critical factor for the progression of the reaction. Notably, this reaction was found to be unfeasible with conventional phosphines like JohnPhos, highlighting the unique role

of the specifically designed ligand **1.3.5-4**. The mechanism is hypothesized to involve a transition state **1.3.5-3t** in which hydrogen bonding between the substrate and the basic group of the ligand promotes metal-ligand cooperation, which significantly accelerates the enantioselective cyclization process. This mechanistic proposal was further supported by DFT calculations.

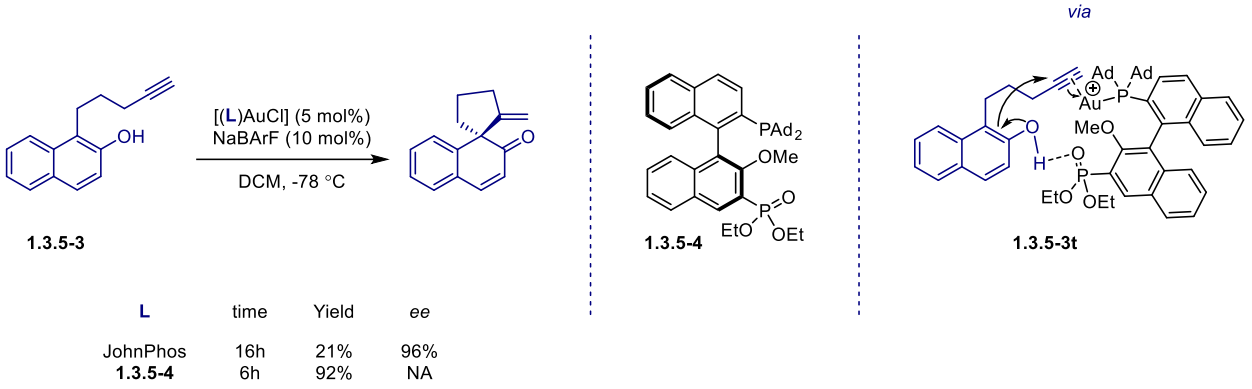

L	time	Yield	*ee*
JohnPhos	16h	21%	96%
1.3.5-4	6h	92%	NA

Scheme 1.3.5-3. Synergistic metal-ligand cooperation.

An example of steric effects on the outcome of the reaction was demonstrated in the synthesis of *E*- or *Z*-α-haloenones from propargylic acetates (**Scheme 1.3.5-4**). Zhang and colleagues in 2007 reported an interesting strategy to synthesize *Z*-α-iodoenones with good yields by the reaction of **1.3.5-5** with N-iodosuccinimide (NIS) catalyzed by $[(Ph_3P)AuNTf_2]$.[70] According to the proposed mechanism, an initially formed allene acetate **1.3.5-5i** reacts with Au(I) species to form in the *Z*-selective vinylgold(I) intermediate **1.3.5-5v** which gives *Z*-α-iodoenones after halogenation and hydrolysis. On the other hand, in 2010, Shi and colleagues demonstrated the synthesis of various *E*-α-iodoenones using the same starting material.[71] The use of a triazole-based Au(I) catalyst **1.3.5-6** was crucial for the preparation of α-iodoenones with reversed stereoselectivity. The proposed mechanism involves the same allene intermediate **1.3.5-5i**, but instead of forming a vinylgold(I) intermediate **1.3.5-5i-a**, it is reacting with NIS directly to form the product **1.3.5-5b**.

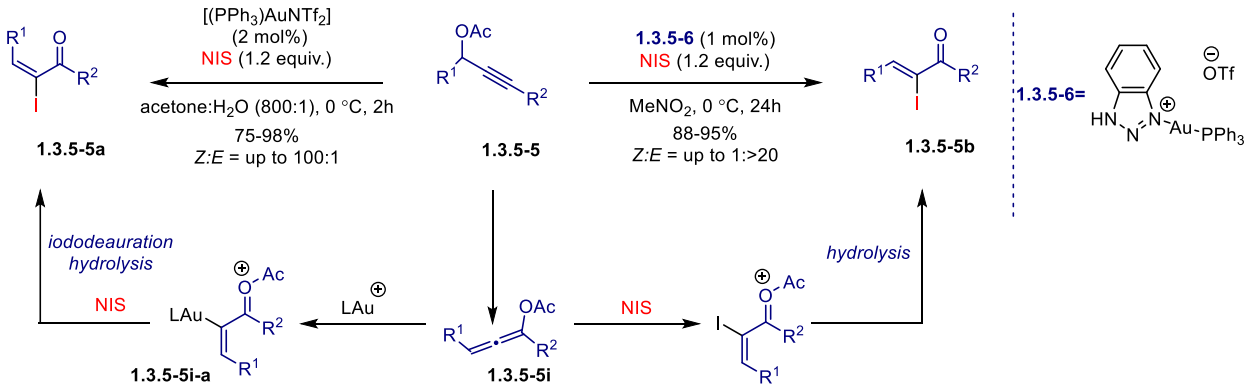

Scheme 1.3.5-4. Influence of the steric effects on the outcome of the reaction.

The role of sterically demanding ligands in catalytic reactions, with particular emphasis on their confinement effects, will be examined and explained in more detail in **Chapter 2**. This detailed

investigation includes an assessment of how the spatial arrangement of ligands influences the reaction pathways and impacts both the efficiency and selectivity of the catalytic processes.

1.4. Gold vs other metals

Gold catalysis occupies a distinct role within the field of transition metal catalysis. It serves as a complementary alternative to the traditional metals like palladium, platinum, rhodium and others. Gold catalysis is distinguished by its ability to facilitate novel chemical transformations that are unattainable with other transition metals, or to significantly alter the selectivity of reactions in comparison to conventional transition metal catalysts.

In the field of C−H functionalization via transition metal-catalyzed carbene transfer reactions using diazo compounds, gold distinguishes itself by demonstrating reactivities that are different from other metals, such as commonly employed palladium (**Scheme 1.4-1**). A report by Zhang and Liu in 2014 underscored this divergence, showing how Au(I) catalysis leads to the para-C−H functionalization of phenols with aryl diazoesters **1.4-1** to afford products **1.4-1a** with high selectivity.[72] It should also be mentioned that the developed protocol is extremely mild and the reaction finishes after just 1 minute of stirring at room temperature. In contrast, the use of palladium as a catalyst in similar conditions, as reported by Zhou and Zhu, led primarily to O−H bond insertion in the phenols to give **1.4-1b**.[73]

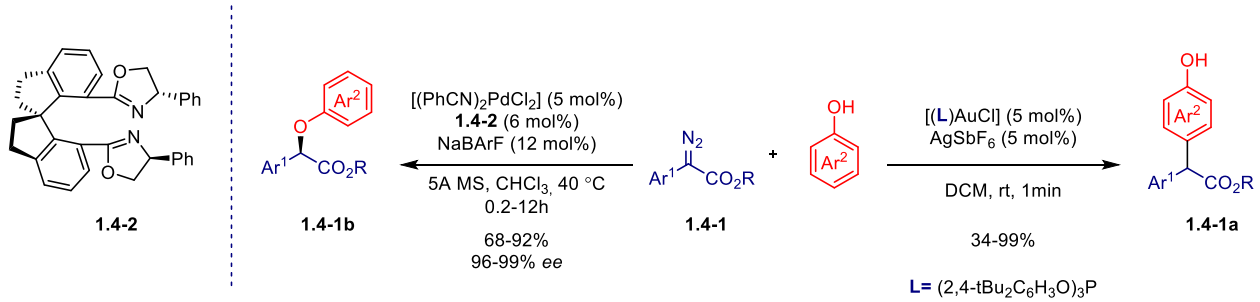

Scheme 1.4-1. O-H insertion vs C-H functionalization.

Another interesting example of divergent reactivity between gold and palladium can be seen in the arylation of N-substituted pyrrole **1.4-3** (**Scheme 1.4-2**). Recently the group of Bourissou demonstrated that under Au(I)/Au(III) RedOx catalysis using hemilabile MeDalPhos ligand the arylation of pyrrole **1.4-3** predominantly affords the C3-arylation product **1.4-3a**.[56] Alternatively, it has been shown by the group of Yamaguchi and Itami in 2014 that the similar palladium catalyzed cross-coupling affords the C2-arylation product **1.4-3b** with high selectivity.[74] Notably, the gold-catalyzed version of this reaction is characterized by milder conditions and proceeds at a faster rate, underscoring the distinct advantages and specificities of gold catalysis.

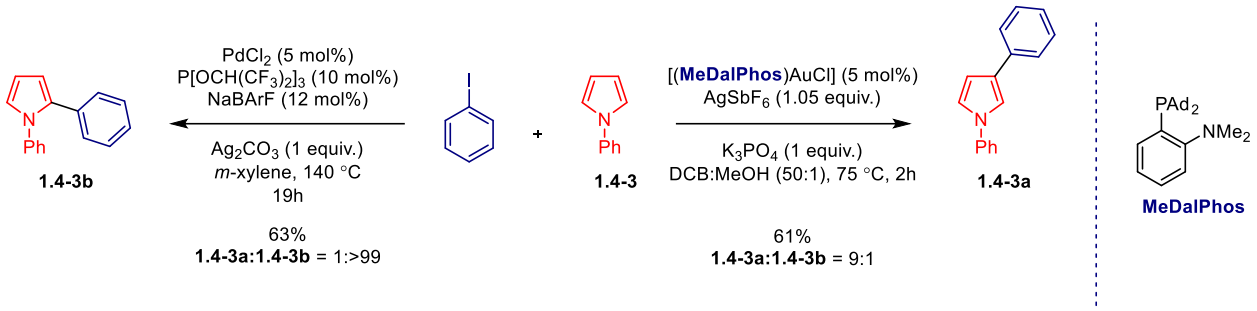

Scheme 1.4-2. C2 vs C3 arylation.

An example of product divergence between gold and platinum has been elegantly demonstrated by the group of Ma in 2014 (**Scheme 1.4-3**).[75] The researchers showed that treating the substrate **1.4-4** with Au(I)-catalyst predominantly affords a carbazole derivative **1.4-4a**. However, when the same substrate was treated with $PtCl_4$, a different regioselectivity was noticed, leading to an alternative isomeric carbazole derivative **1.4-4b**. The proposed mechanism for both reactions begins with a 6-endo-dig cyclization, followed by a series of steps including rearomatization and water elimination, forming an intermediate **1.4-4i**. This intermediate can be viewed either as a carbocationic form **1.4-4i-a** or its vinylic carbene resonance form **1.4-4i-b**. In the Au(I)-catalyzed reaction, a 1,2-methyl shift from the cationic form **1.4-4i-a** is predominant, yielding the respective carbazole derivative **1.4-4a**. Meanwhile, with platinum catalysis, the reaction pathway favors a 1,2-methyl shift from the carbene intermediate **1.4-4i-b**, ultimately leading to a different carbazole derivative **1.4-4b**.

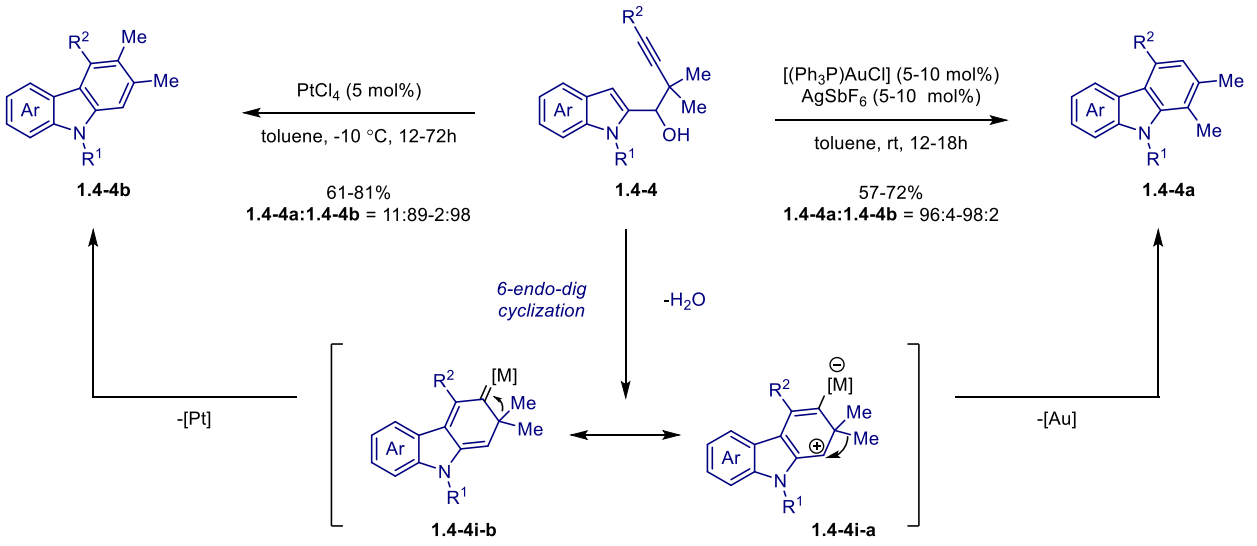

Scheme 1.4-3. Au vs Pt catalysis.

In 2016, Patil and colleagues developed an interesting C-H alkynylation of isoquinolines **1.4-5**, wherein the choice of metal catalyst played a critical role in determining the selectivity of the reaction (**Scheme 1.4-4**).[76] The use of a Au(I) catalyst led to the selective formation of the C4-alkynylation product **1.4-5a**, while, in contrast, employing a rhodium catalyst shifted the

selectivity towards C8-alkynylated product **1.4-5b**. It is suggested that the pronounced alkynophilicity of the gold catalyst enables it to activate the triple bond in TIPS-EBX, facilitating a nucleophilic attack from the C4 position of the isoquinoline, which would lead to an intermediate **1.4-5i-a**. This intermediate likely undergoes α/β−elimination to yield the targeted product **1.4-5a**. Conversely, the use of rhodium promotes directed C−H activation at the C8 position of the isoquinoline, resulting in intermediate **1.4-5i-b1**. After that the intermediate **1.4-5i-b1** would undergo an oxidative insertion of TIPS-EBX to form intermediate **1.4-5i-b2**, which eventually undergoes reductive elimination to afford the C8-alkynylated product **1.4-5b**.

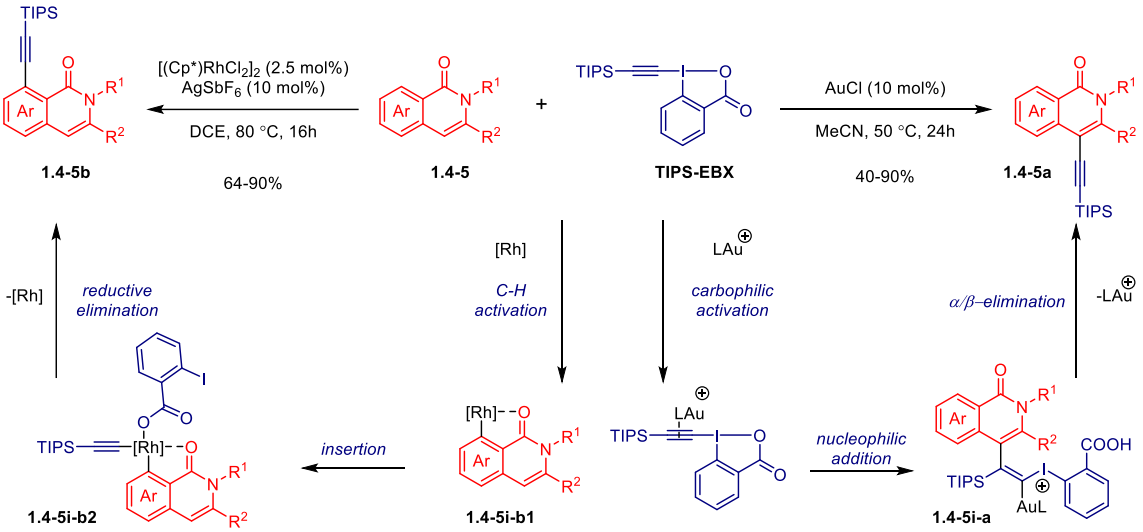

Scheme 1.4-4. Au vs Rh catalysis.

The examples shown here serve to show the unique and interesting aspect of gold catalysis, in relation to other transition metals. It considerably broadens the toolbox of organic chemistry and underscores the capacity of gold catalysis to open new pathways in chemical synthesis, thereby enriching the field with innovative methodologies and outcomes.

1.5. Au(I)-catalysis in the synthesis of natural compounds

Gold catalysis has become a cornerstone in the total synthesis of complex natural products, offering an array of sophisticated methodologies to construct intricate molecular architectures. The unique ability of gold catalysts to facilitate diverse transformations, particularly through cascade reactions and carbocyclizations, has substantially advanced the synthesis of complex natural products.[77–80] These methodologies not only exemplify the versatility of gold catalysis but also underscore its critical role in the development of new synthetic routes for natural product synthesis.

In a recent contribution from our group, we achieved the concise total synthesis of (±)-Brevianamide A using an available amino acid **1.5-1**.[81] Key to this approach was the use of a Au(I)-

catalyzed cascade process. This step readily constructs the pseudoindoxyl motif of the natural product while simultaneously establishing two adjacent quaternary centers (**Scheme 1.5-1**). The proposed mechanism begins with the activation of the alkyne moiety in the substrate **1.5-2**, leading to a 5-endo-dig cyclization that forms intermediate **1.5-2a**. This intermediate **1.5-2a** is proposed to undergo nitrogen gas elimination to form intermediate **1.5-2b**. This species, in turn, can react with alcohol **1.5-3**, forming another intermediate **1.5-2c**, which subsequently undergoes a [3,3]-sigmatropic rearrangement to yield the final product **1.5-4**. This synthesis not only demonstrates the structural complexity attainable through gold catalysis but also highlights its potential for efficient and high-yield synthesis of complex molecules like (±)-brevianamide.

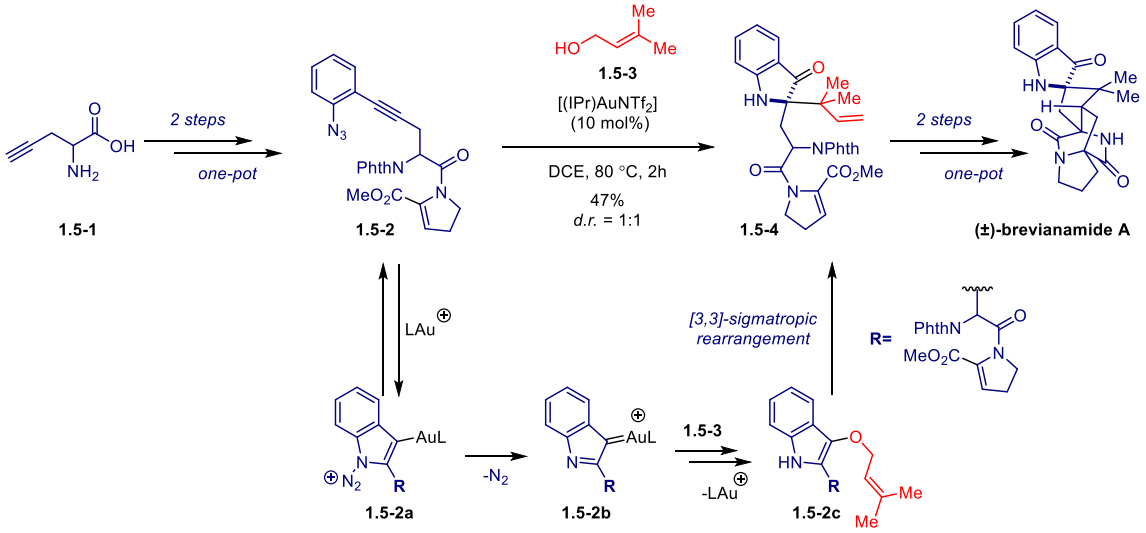

Scheme 1.5-1. Synthesis of (±)-Brevianamide A.

Another recent example from our department was demonstrated by the Barriault group in 2023 in the formal synthesis of (±)-Salvinorin A.[82] The demonstrated approach is especially interesting for employing two distinct Au(I)-catalyzed steps. Initially, to construct the second ring of Salvinorin A, the researchers utilized Au(I)-catalyzed selective 6-endo-dig carbocyclization of a **1.5-5**, which successfully yielded the cyclized product **1.5-5a** in good yield (**Scheme 1.5-2, A**). Following this, the team accessed the decalin **1.5-5c** through a 5-exo-trig radical cyclization of **1.5-5b**, which afforded the desired compound with excellent yield (**Scheme 1.5-2, B**). This evidence of two distinct protocols utilizing Au(I)-catalysis proves the versatility and efficacy of Au(I) catalysts in modern organic synthesis.

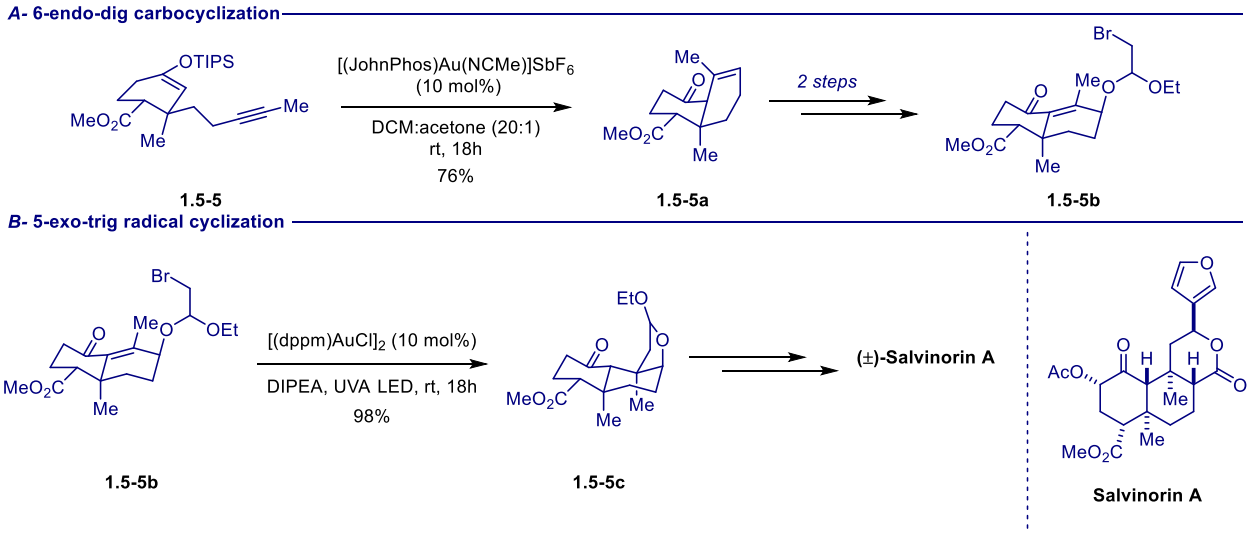

Scheme 1.5-2. Synthesis of (±)-Salvinorin A.

The examples discussed herein serve to provide a quick look of the vast potential of Au(I)-catalysis in natural product synthesis. The versatility and synthetic prowess of Au(I)-catalyzed reactions have been further demonstrated in the synthesis of a diverse array of complex natural products. Some of the notable examples include the synthesis of hyperforin and papuaforins A-C,[83] (+)-lycopladine A,[84] (+)-fawcettimine,[85] (±)-gomerone C[86], ventricosene,[87] platencin[88] and daphenylline (**Scheme 1.5-3**).[89] These achievements underscore the increasing role of Au(I)-catalyzed reactions in modern synthetic chemistry, providing a powerful approach to build complex molecular architectures and access compounds of substantial interest.

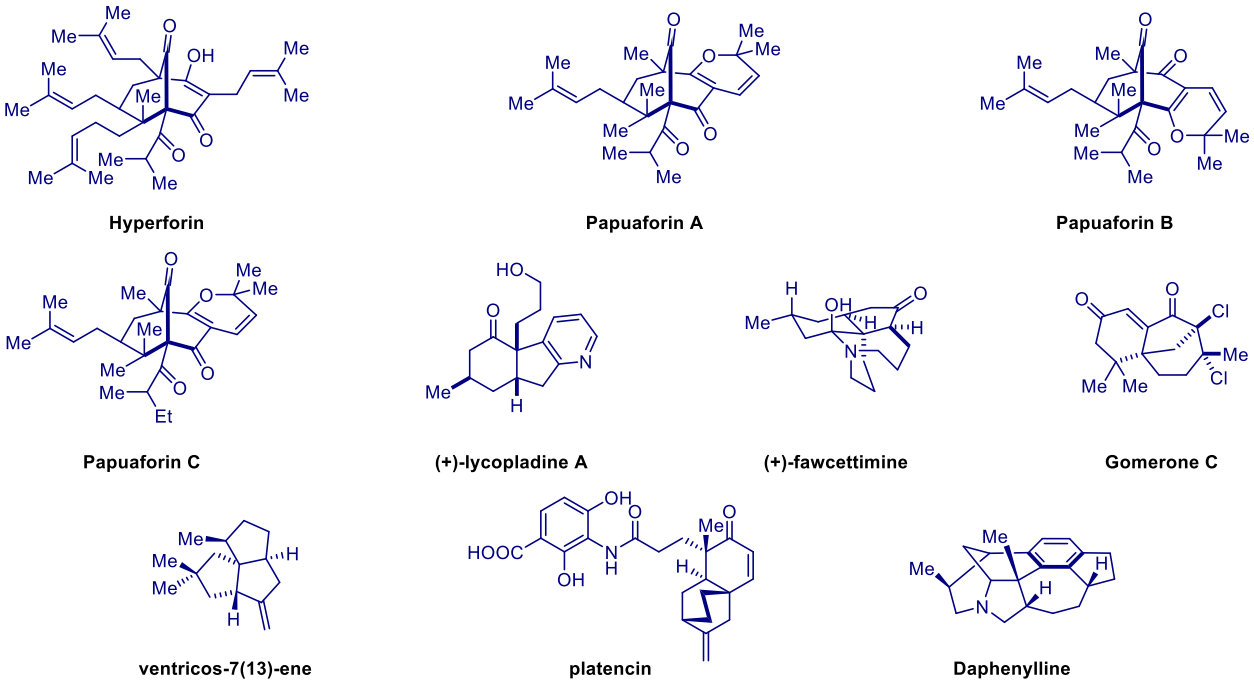

Scheme 1.5-3. Some of the examples of natural products synthesized using Au(I)-catalysis.

1.6. Industrial applications and difficulties

Although gold is widely used in industrial synthesis to produce bulk chemicals,[90–92] it is surprisingly underutilized in the synthesis of fine chemicals or active pharmaceutical ingredients. This is particularly interesting because the relatively low toxicity of gold compared to other platinum group metals makes it ideal for these types of applications. However, gold has not become a dominant force in the pharmaceutical industry, despite strict regulations requiring very low residual levels of palladium or platinum in active ingredients. The significant cost of gold, the difficulty of extracting it from solutions, and the unavoidable loss of catalyst of the process are the reasons for this reluctance to exploit the potential of this metal. These factors have limited the large-scale implementation of homogeneous gold catalysis on an industrial scale, despite the fact that a variety of reactions catalyzed by gold complexes have been observed in academic circles. Additionally, many gold-catalyzed reactions suffer from low turnover numbers (TON) due to catalyst deactivation, a process significantly influenced by counterions and additives. Although the detailed mechanism of the deactivation process remains undefined, certain reactions like alkyne hydration demonstrate high TON or require low gold loading, achievable at parts-per-million levels. In contrast, reactions such as cycloisomerization consistently demonstrate lower TONs, highlighting the need for further optimization and development in Au catalysis.

However, there are some examples of research dedicated to the industrial use of Au-catalysis. In particular, a 1997 study by BASF researchers showed that Au(I) complexes can efficiently catalyze the addition of alcohols to alkynes under mild conditions, achieving an impressive TON of 100,000 and a high turnover frequency (TOF) of 5400 h^{-1}. This discovery demonstrated the ability of gold catalysis to promote efficient reactions. Despite these remarkable catalytic successes, the process has not met with commercial success, highlighting the difficulties in combining academic research and industrial application.[93] An interesting example of the complementary effects of both homogeneous and heterogeneous catalysis was demonstrated in the work of Somorjai and Toste in 2012.[94] According to their findings, catalytic reactivity can be precisely tuned by incorporating Au nanoclusters into dendrimers. This method, achieved by modulating the properties of the dendrimer, is comparable to changing the catalytic properties by tuning the ligand.

Nolan and colleagues in 2008 achieved a remarkable breakthrough in gold catalysis through the highly efficient hydration of alkynes.[95] Using as low as 10 ppm of [(IPr)AuCl], the researchers were able to achieve a 84% yield of product **1.6-1** (**Scheme 1.6-1, A**). In 2013, Zhang and Li presented another example of creative ligand design in order to achieve a highly efficient Au(I)-catalysis.[96] By using a ligand **1.6-2** based on a biphenyl skeleton with an amido group at the 3' position, the researchers were able to achieve a TON of up to 99,000 (**Scheme 1.6-1, B**). The researchers proposed that the amido group acted as an important directing element for incoming nucleophiles and contributed to the high activity of the catalyst.

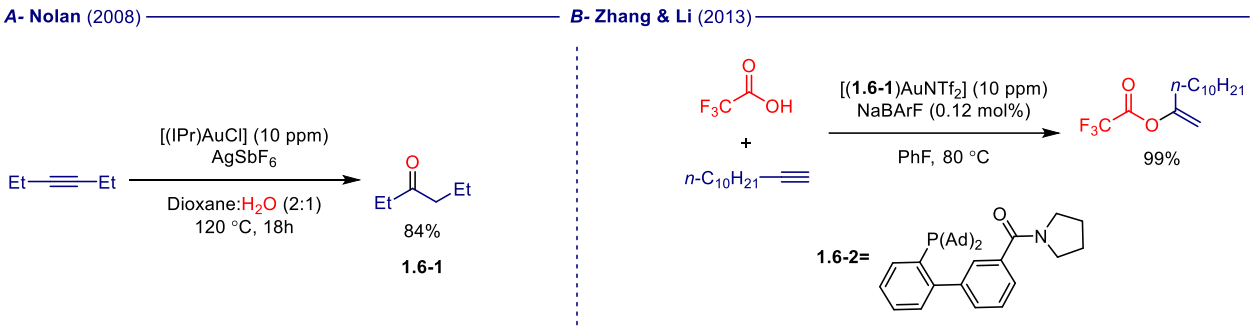

Scheme 1.6-1. Examples of highly efficient homogeneous Au(I)-catalysis.

The importance of ligand design in achieving high TONs and exceptionally low catalyst loadings with silsesquioxane-substituted catalysts **1.6-3** was further demonstrated by the work of Hashmi and colleagues in 2013.[97] The researchers achieved a remarkable 33% conversion of the starting material **1.6-4** into intramolecular hydroalkoxylation products **1.6-4a** using only 0.01 ppm of the catalyst (**Scheme 1.6-1, C**). Later studies by the same group suggested that the long lifetime of the catalytic species – which is protected from degradation by bulky ligands – could be responsible for the high catalytic activity. [98] This highlights the crucial influence of the ligand structure on the effectiveness and stability of gold catalysts.

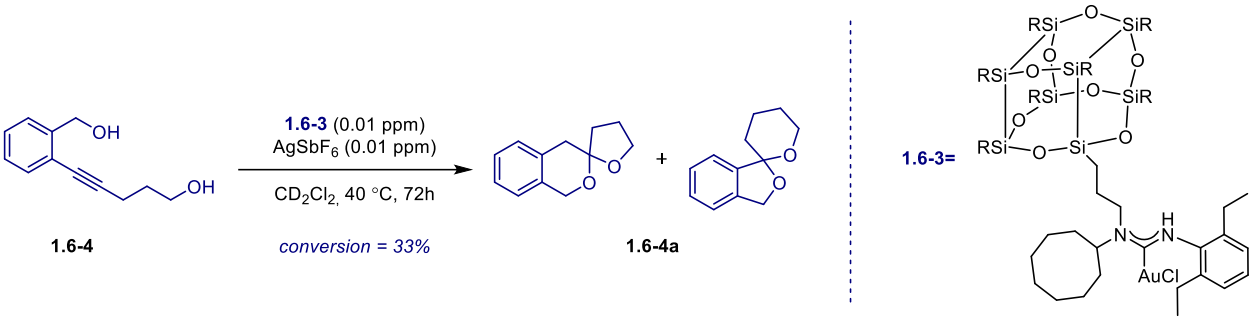

Scheme 1.6-2. Examples of exceptionally low catalyst loading.

The examples presented here underscore the growing potential of homogeneous gold catalysis in industrial applications. While the costs associated with gold and certain operational challenges are notable, appropriate ligand design can significantly increase the catalytic efficiency of gold species. Such advances promise greater integration of gold catalysis into industrial processes. Ongoing research in this area is crucial to expanding the scope and efficiency of gold catalysis in various industrial sectors. A deeper understanding of the catalyst deactivation pathway could enable more rational catalyst design, potentially enhancing TON in Au-catalyzed processes.

1.7. Summary and outlook

In this section we described some examples of the use of two primary classes of ligands in Au(I) catalysis: phosphines and N-heterocyclic carbenes. Archetypical examples of these categories

include PPh_3 and IPr, which are often the first choices in gold-promoted transformations due to their availability and ability to stabilize $[Au\text{-}L]^+$ fragments. These ligands demonstrate wide applicability across various gold-catalyzed transformations and are often used as representatives of their respective ligand classes.

The properties of the ligands significantly influence not only the final yields but also the reaction rates and selectivity. Optimizing protocols, reducing catalyst loadings, and performing challenging transformations require a detailed understanding of the electronic and steric properties of the ancillary ligands. Such understanding is essential to differentiate between catalysts with low turnover frequencies and those that are superior.

Another major milestone in the catalysis with gold complexes is the understanding of Au(I)/Au(III) RedOx chemistry, which has emerged as a field with promising prospects and challenges for future exploration. Discovering the factors that favor the key steps in metal-promoted coupling reactions, such as oxidation addition to Au(I) to form Au(III) species and reductive elimination, would extend our knowledge in Au(I)/Au(III) RedOx processes and might broaden the toolbox for conduction cross-coupling reactions.

The introduction section of **Chapter 2** will present an overview of the critical role that the steric properties of ligands play in Au(I) catalysis. We will examine how variations in steric bulk of ligands can significantly influence the course of Au(I)-catalyzed reactions. This section aims to offer insight into the design of ligands for optimizing Au(I)-catalyzed reactions and provide a necessary context before we start to present our work in this field.

The introduction section of **Chapter 3** will focus on the recent advancements in external oxidant-free Au(I)/Au(III) RedOx chemistry. We will particularly highlight the role of specially designed hemilabile ligands in facilitating these RedOx processes. In this section we will discuss the significant studies made in this area, showing how these ligands have revolutionized the field of Au(I)/Au(III) RedOx reactions. With this discourse we aim to provide the basis for the experimental studies described in the following parts of this work.

1.8. Research goals

The research study discussed in **Chapter 2** aims to investigate the influence of sterically hindered catalysts on Au(I)-catalyzed reactions, with a particular focus on how the confinement effects influence the outcome of the reactions. This research includes understanding the interplay between steric hindrance and reactivity and selectivity in Au(I)-catalyzed processes. We will present a thorough assessment of how steric parameters, particularly percent buried volume ($\%V_{bur}$), influence the catalytic effectiveness of Au(I) complexes.

We will also provide an analysis of the performance of newly synthesized sterically demanding ligands in Au(I) catalysis and provide a comparison with commonly used ligands in this field. This comparison includes both phosphine and N-heterocyclic carbene complexes and focused on the

steric properties and its influence on the activity of Au(I) catalysts. We will use a set of Au(I)-catalyzed transformations, including but not limited to cycloisomerization, to evaluate and quantify the influence of steric hindrance of the ligand on product selectivity and reaction efficiency in Au(I)-catalysis.

Chapter 3 of this thesis is dedicated to the development of ligand structures tailored for Au(I)/Au(III) catalysis. The initial focus will be on the design and synthesis of ligands capable of stabilizing both Au(I) and Au(III) oxidation states, searching for a ligand framework that is flexible enough to accommodate the distinct characteristics of each state. After that, we will present a thorough mechanistic study, which includes kinetic studies and the characterization of intermediates. We will follow it with providing a comparative analysis of these novel ligands with traditional ones in standard Au(I)/Au(III) catalyzed reactions. This study is essential to delineate the influence of these ligands within the catalytic cycle and to assess their impact on reactivity and selectivity.

Utilizing the optimized ligand systems, we will continue the story with the development of novel Au(I)/Au(III) C-S cross-coupling reactions. This reaction will serve as a practical demonstration of the effectiveness of the newly developed ligands. We will also provide an assessment of the synthetic utility of the obtained products to underscore their potential in subsequent organic transformations as a viable sulfur-contained building blocks.

The results of presented research cover several key areas in the field of gold catalysis. First, we provide a deeper understanding of the influence of steric effects in Au(I) catalysis with particular focus on how these effects can be manipulated to improve the efficiency and selectivity of reactions. This study includes the investigation of the steric parameters of various ligands and their resulting effects on the catalytic activity of Au(I) species.

Furthermore, the development of novel ligand architectures for Au(I)/Au(III) RedOx catalysis is another important outcome. These new ligands are can stabilize both Au(I) and Au(III) species, enabling a broader range of gold-catalyzed reactions. Evaluating these ligands in benchmark reactions provides insights into their effectiveness in terms of reaction efficiency, selectivity, and scope.

A particularly exciting aspect of this research is the development of a new C-S cross-coupling reaction using Au(I)/Au(III) catalyzed cross-coupling reaction. This development includes not only the discovery of new chemical transformations, but also the optimization of reaction conditions and a thorough mechanistic investigation, as well as exploration of the synthetic potential of the resulting species. This protocol could open new avenues in organic synthesis.

Finally, the broader impact of this research include providing valuable insights into the design and optimization of catalysts for specific reactions. These insights have implications for future research and applications in various areas, such as the synthesis of pharmaceuticals and fine chemicals.

1.9. List of references

(1) Chatt, J.; Duncanson, L. A. 586. Olefin Co-Ordination Compounds. Part III. Infra-Red Spectra and Structure: Attempted Preparation of Acetylene Complexes. *J. Chem. Soc.* **1953**, No. 0, 2939–2947. https://doi.org/10.1039/JR9530002939.

(2) Chatt, J.; Duncanson, L. A.; Venanzi, L. M. Directing Effects in Inorganic Substitution Reactions. Part I. A Hypothesis to Explain the Trans-Effect. *J. Chem. Soc.* **1955**, No. 0, 4456–4460. https://doi.org/10.1039/JR9550004456.

(3) Pearson, R. G. Hard and Soft Acids and Bases. *J. Am. Chem. Soc.* **1963**, *85* (22), 3533–3539. https://doi.org/10.1021/ja00905a001.

(4) Pearson, R. G. Hard and Soft Acids and Bases, HSAB, Part 1: Fundamental Principles. *J. Chem. Educ.* **1968**, *45* (9), 581. https://doi.org/10.1021/ED045P581.

(5) Pearson, R. G. Hard and Soft Acids and Bases, HSAB, Part II: Underlying Theories. *J. Chem. Educ.* **1968**, *45* (10), 643. https://doi.org/10.1021/ed045p643.

(6) Pyykko, P.; Desclaux, J. P. Relativity and the Periodic System of Elements. *Acc. Chem. Res.* **1979**, *12* (8), 276–281. https://doi.org/10.1021/ar50140a002.

(7) Bartlett, N. Relativistic Effects and the Chemistry of Gold. *Gold Bull.* **1998**, *31* (1), 22–25. https://doi.org/10.1007/BF03215471.

(8) Schwerdtfeger, P. Relativistic Effects in Properties of Gold. *Heteroat. Chem.* **2002**, *13* (6), 578–584. https://doi.org/10.1002/hc.10093.

(9) Gorin, D. J.; Toste, F. D. Relativistic Effects in Homogeneous Gold Catalysis. *Nature* **2007**, *446* (7134), 395–403. https://doi.org/10.1038/nature05592.

(10) Syed, S. Recovery of Gold from Secondary Sources—A Review. *Hydrometallurgy* **2012**, *115–116*, 30–51. https://doi.org/10.1016/j.hydromet.2011.12.012.

(11) Wang, D.; Cai, R.; Sharma, S.; Jirak, J.; Thummanapelli, S. K.; Akhmedov, N. G.; Zhang, H.; Liu, X.; Petersen, J. L.; Shi, X. "Silver Effect" in Gold(I) Catalysis: An Overlooked Important Factor. *J. Am. Chem. Soc.* **2012**, *134* (21), 9012–9019. https://doi.org/10.1021/ja303862z.

(12) Jia, M.; Bandini, M. Counterion Effects in Homogeneous Gold Catalysis. *ACS Catal.* **2015**, *5* (3), 1638–1652. https://doi.org/10.1021/cs501902v.

(13) Lu, Z.; Li, T.; Mudshinge, S. R.; Xu, B.; Hammond, G. B. Optimization of Catalysts and Conditions in Gold(I) Catalysis—Counterion and Additive Effects. *Chem. Rev.* **2021**, *121* (14), 8452–8477. https://doi.org/10.1021/acs.chemrev.0c00713.

(14) Marchione, D.; Belpassi, L.; Bistoni, G.; Macchioni, A.; Tarantelli, F.; Zuccaccia, D. The Chemical Bond in Gold(I) Complexes with N-Heterocyclic Carbenes. *Organometallics* **2014**, *33* (16), 4200–4208. https://doi.org/10.1021/om5003667.

(15) Jacobsen, H.; Correa, A.; Costabile, C.; Cavallo, L. π-Acidity and π-Basicity of N-Heterocyclic Carbene Ligands. A Computational Assessment. *J. Organomet. Chem.* **2006**,

691 (21), 4350–4358. https://doi.org/10.1016/j.jorganchem.2006.01.026.

(16) Michalak, M.; Kośnik, W. Chiral N-Heterocyclic Carbene Gold Complexes: Synthesis and Applications in Catalysis. *Catalysts*. 2019. https://doi.org/10.3390/catal9110890.

(17) Wang, H. M. J.; Lin, I. J. B. Facile Synthesis of Silver(I)−Carbene Complexes. Useful Carbene Transfer Agents. *Organometallics* **1998**, *17* (5), 972–975. https://doi.org/10.1021/om9709704.

(18) Furst, M. R. L.; Cazin, C. S. J. Copper N-Heterocyclic Carbene (NHC) Complexes as Carbene Transfer Reagents. *Chem. Commun.* **2010**, *46* (37), 6924–6925. https://doi.org/10.1039/C0CC02308F.

(19) Visbal, R.; Laguna, A.; Gimeno, M. C. Simple and Efficient Synthesis of [MCI(NHC)] (M = Au, Ag) Complexes. *Chem. Commun.* **2013**, *49* (50), 5642–5644. https://doi.org/10.1039/C3CC42919A.

(20) Collado, A.; Gómez-Suárez, A.; Martin, A. R.; Slawin, A. M. Z.; Nolan, S. P. Straightforward Synthesis of [Au(NHC)X] (NHC = N-Heterocyclic Carbene, X = Cl, Br, I) Complexes. *Chem. Commun.* **2013**, *49* (49), 5541–5543. https://doi.org/10.1039/C3CC43076F.

(21) Johnson, A.; Gimeno, M. C. An Efficient and Sustainable Synthesis of NHC Gold Complexes. *Chem. Commun.* **2016**, *52* (62), 9664–9667. https://doi.org/10.1039/C6CC05190A.

(22) Gaillard, S.; Slawin, A. M. Z.; Bonura, A. T.; Stevens, E. D.; Nolan, S. P. Synthetic and Structural Studies of [$AuCl_3$(NHC)] Complexes. *Organometallics* **2010**, *29* (2), 394–402. https://doi.org/10.1021/om900814e.

(23) Michalska, M.; Songis, O.; Taillier, C.; Bew, S. P.; Dalla, V. Synergistic Gold(I)/Trimethylsilyl Catalysis: Efficient Alkynylation of N,O-Acetals and Related Pro-Electrophiles. *Adv. Synth. Catal.* **2014**, *356* (9), 2040–2050. https://doi.org/10.1002/adsc.201400169.

(24) Klahn, P.; Kirsch, S. F. Electronic Fine-Tuning of Carbene Ligands and Its Impact on Gold Catalysis. *ChemCatChem* **2011**, *3* (4), 649–652. https://doi.org/10.1002/cctc.201000366.

(25) Tolman, C. A. Steric Effects of Phosphorus Ligands in Organometallic Chemistry and Homogeneous Catalysis. *Chem. Rev.* **1977**, *77* (3), 313–348. https://doi.org/10.1021/cr60307a002.

(26) Nelson, D. J.; Nolan, S. P. Quantifying and Understanding the Electronic Properties of N-Heterocyclic Carbenes. *Chem. Soc. Rev.* **2013**, *42* (16), 6723–6753. https://doi.org/10.1039/C3CS60146C.

(27) Huynh, H. V. Electronic Properties of N-Heterocyclic Carbenes and Their Experimental Determination. *Chem. Rev.* **2018**, *118* (19), 9457–9492. https://doi.org/10.1021/acs.chemrev.8b00067.

(28) Gaggioli, C. A.; Bistoni, G.; Ciancaleoni, G.; Tarantelli, F.; Belpassi, L.; Belanzoni, P. Modulating the Bonding Properties of N-Heterocyclic Carbenes (NHCs): A Systematic

Charge-Displacement Analysis. *Chem. – A Eur. J.* **2017**, *23* (31), 7558–7569. https://doi.org/10.1002/chem.201700638.

(29) Durand, D. J.; Fey, N. Computational Ligand Descriptors for Catalyst Design. *Chem. Rev.* **2019**, *119* (11), 6561–6594. https://doi.org/10.1021/acs.chemrev.8b00588.

(30) Falivene, L.; Credendino, R.; Poater, A.; Petta, A.; Serra, L.; Oliva, R.; Scarano, V.; Cavallo, L. SambVca 2. A Web Tool for Analyzing Catalytic Pockets with Topographic Steric Maps. *Organometallics* **2016**, *35* (13), 2286–2293. https://doi.org/10.1021/acs.organomet.6b00371.

(31) Falivene, L.; Cao, Z.; Petta, A.; Serra, L.; Poater, A.; Oliva, R.; Scarano, V.; Cavallo, L. Towards the Online Computer-Aided Design of Catalytic Pockets. *Nat. Chem.* **2019**, *11* (10), 872–879. https://doi.org/10.1038/s41557-019-0319-5.

(32) Tolman, C. A. Phosphorus Ligand Exchange Equilibriums on Zerovalent Nickel. Dominant Role for Steric Effects. *J. Am. Chem. Soc.* **1970**, *92* (10), 2956–2965. https://doi.org/10.1021/ja00713a007.

(33) Clavier, H.; Nolan, S. P. Percent Buried Volume for Phosphine and N-Heterocyclic Carbene Ligands: Steric Properties in Organometallic Chemistry. *Chem. Commun.* **2010**, *46* (6), 841–861. https://doi.org/10.1039/B922984A.

(34) Hashmi, A. S. K. Homogeneous Gold Catalysis Beyond Assumptions and Proposals—Characterized Intermediates. *Angew. Chemie Int. Ed.* **2010**, *49* (31), 5232–5241. hhttps://doi.org/10.1002/anie.200907078.

(35) Wang, W.; Hammond, G. B.; Xu, B. Ligand Effects and Ligand Design in Homogeneous Gold(I) Catalysis. *J. Am. Chem. Soc.* **2012**, *134* (12), 5697–5705. https://doi.org/10.1021/ja3011397.

(36) Nevado, C. Gold Catalysis: Recent Developments and Future Trends. *Chimia (Aarau).* **2010**, *64* (4 SE-Scientific Articles), 247. https://doi.org/10.2533/chimia.2010.247.

(37) Garcia, P.; Malacria, M.; Aubert, C.; Gandon, V.; Fensterbank, L. Gold-Catalyzed Cross-Couplings: New Opportunities for C-C Bond Formation. *ChemCatChem* **2010**, *2* (5), 493–497. https://doi.org/10.1002/cctc.200900319.

(38) Hopkinson, M. N.; Gee, A. D.; Gouverneur, V. Au^{I}/Au^{III} Catalysis: An Alternative Approach for C-C Oxidative Coupling. *Chem. – A Eur. J.* **2011**, *17* (30), 8248–8262. https://doi.org/10.1002/chem.201100736.

(39) Wegner, H. A.; Auzias, M. Gold for C-C Coupling Reactions: A Swiss-Army-Knife Catalyst? *Angew. Chemie Int. Ed.* **2011**, *50* (36), 8236–8247. https://doi.org/10.1002/anie.201101603.

(40) Kar, A.; Mangu, N.; Kaiser, H. M.; Beller, M.; Tse, M. K. A General Gold-Catalyzed Direct Oxidative Coupling of Non-Activated Arenes. *Chem. Commun.* **2008**, No. 3, 386–388. https://doi.org/10.1039/B714928J.

(41) Cui, L.; Zhang, G.; Zhang, L. Homogeneous Gold-Catalyzed Efficient Oxidative Dimerization of Propargylic Acetates. *Bioorg. Med. Chem. Lett.* **2009**, *19* (14), 3884–3887. https://doi.org/10.1016/j.bmcl.2009.03.127.

(42) Zhang, G.; Peng, Y.; Cui, L.; Zhang, L. Gold-Catalyzed Homogeneous Oxidative Cross-Coupling Reactions. *Angew. Chemie Int. Ed.* **2009**, *48* (17), 3112–3115. https://doi.org/10.1002/anie.200900585.

(43) Ball, L. T.; Green, M.; Lloyd-Jones, G. C.; Russell, C. A. Arylsilanes: Application to Gold-Catalyzed Oxyarylation of Alkenes. *Org. Lett.* **2010**, *12* (21), 4724–4727. https://doi.org/10.1021/ol1019162.

(44) Brenzovich, W. E. J.; Brazeau, J.-F.; Toste, F. D. Gold-Catalyzed Oxidative Coupling Reactions with Aryltrimethylsilanes. *Org. Lett.* **2010**, *12* (21), 4728–4731. https://doi.org/10.1021/ol102194c.

(45) Winston, M. S.; Wolf, W. J.; Toste, F. D. Photoinitiated Oxidative Addition of CF_3I to Gold(I) and Facile Aryl-CF_3 Reductive Elimination. *J. Am. Chem. Soc.* **2014**, *136* (21), 7777–7782. https://doi.org/10.1021/ja503974x.

(46) Liu, S.; Kang, K.; Liu, S.; Wang, D.; Wei, P.; Lan, Y.; Shen, Q. The Difluoromethylated Organogold(III) Complex Cis-[$Au(PCy_3)(4\text{-}F\text{-}C_6H_4)(CF_2H)(Cl)$]: Preparation, Characterization, and Its $C(sp^2)$–CF_2H Reductive Elimination. *Organometallics* **2018**, *37* (21), 3901–3908. https://doi.org/10.1021/acs.organomet.8b00579.

(47) Sahoo, B.; Hopkinson, M. N.; Glorius, F. Combining Gold and Photoredox Catalysis: Visible Light-Mediated Oxy- and Aminoarylation of Alkenes. *J. Am. Chem. Soc.* **2013**, *135* (15), 5505–5508. https://doi.org/10.1021/ja400311h.

(48) Shu, X.; Zhang, M.; He, Y.; Frei, H.; Toste, F. D. Dual Visible Light Photoredox and Gold-Catalyzed Arylative Ring Expansion. *J. Am. Chem. Soc.* **2014**, *136* (16), 5844–5847. https://doi.org/10.1021/ja500716j.

(49) Hopkinson, M. N.; Tlahuext-Aca, A.; Glorius, F. Merging Visible Light Photoredox and Gold Catalysis. *Acc. Chem. Res.* **2016**, *49* (10), 2261–2272. https://doi.org/10.1021/acs.accounts.6b00351.

(50) Huang, L.; Rudolph, M.; Rominger, F.; Hashmi, A. S. K. Photosensitizer-Free Visible-Light-Mediated Gold-Catalyzed 1,2-Difunctionalization of Alkynes. *Angew. Chemie Int. Ed.* **2016**, *55* (15), 4808–4813. https://doi.org/10.1002/anie.201511487.

(51) Deng, J.-R.; Chan, W.-C.; Chun-Him Lai, N.; Yang, B.; Tsang, C.-S.; Chi-Bun Ko, B.; Lai-Fung Chan, S.; Wong, M.-K. Photosensitizer-Free Visible Light-Mediated Gold-Catalysed Cis-Difunctionalization of Silyl-Substituted Alkynes. *Chem. Sci.* **2017**, *8* (11), 7537–7544. https://doi.org/10.1039/C7SC02294H.

(52) Xie, J.; Sekine, K.; Witzel, S.; Krämer, P.; Rudolph, M.; Rominger, F.; Hashmi, A. S. K. Light-Induced Gold-Catalyzed Hiyama Arylation: A Coupling Access to Biarylboronates. *Angew. Chemie Int. Ed.* **2018**, *57* (51), 16648–16653. https://doi.org/10.1002/anie.201806427.

(53) Taschinski, S.; Döpp, R.; Ackermann, M.; Rominger, F.; de Vries, F.; Menger, M. F. S. J.; Rudolph, M.; Hashmi, A. S. K.; Klein, J. E. M. N. Light-Induced Mechanistic Divergence in Gold(I) Catalysis: Revisiting the Reactivity of Diazonium Salts. *Angew. Chemie Int. Ed.* **2019**, *58* (47), 16988–16993. https://doi.org/10.1002/anie.201908268.

(54) Dong, B.; Peng, H.; Motika, S. E.; Shi, X. Gold Redox Catalysis through Base-Initiated Diazonium Decomposition toward Alkene, Alkyne, and Allene Activation. *Chem. – A Eur. J.* **2017**, *23* (46), 11093–11099. https://doi.org/10.1002/chem.201701970.

(55) Witzel, S.; Xie, J.; Rudolph, M.; Hashmi, A. S. K. Photosensitizer-Free, Gold-Catalyzed C–C Cross-Coupling of Boronic Acids and Diazonium Salts Enabled by Visible Light. *Adv. Synth. Catal.* **2017**, *359* (9), 1522–1528. https://doi.org/10.1002/adsc.201700121.

(56) Zeineddine, A.; Estévez, L.; Mallet-Ladeira, S.; Miqueu, K.; Amgoune, A.; Bourissou, D. Rational Development of Catalytic Au(I)/Au(III) Arylation Involving Mild Oxidative Addition of Aryl Halides. *Nat. Commun.* **2017**, *8* (1), 565. https://doi.org/10.1038/s41467-017-00672-8.

(57) Ye, X.; Wang, C.; Zhang, S.; Tang, Q.; Wojtas, L.; Li, M.; Shi, X. Chiral Hemilabile P,N-Ligand-Assisted Gold Redox Catalysis for Enantioselective Alkene Aminoarylation. *Chem. – A Eur. J.* **2022**, *28* (34), e202201018. https://doi.org/10.1002/chem.202201018.

(58) Chintawar, C. C.; Bhoyare, V. W.; Mane, M. V; Patil, N. T. Enantioselective Au(I)/Au(III) Redox Catalysis Enabled by Chiral (P,N)-Ligands. *J. Am. Chem. Soc.* **2022**, *144* (16), 7089–7095. https://doi.org/10.1021/jacs.2c02799.

(59) Font, P.; Valdés, H.; Guisado-Barrios, G.; Ribas, X. Hemilabile MIC^N Ligands Allow Oxidant-Free Au(I)/Au(III) Arylation-Lactonization of γ-Alkenoic Acids. *Chem. Sci.* **2022**, *13* (32), 9351–9360. https://doi.org/10.1039/D2SC01966C.

(60) Gao, P.; Xu, J.; Zhou, T.; Liu, Y.; Bisz, E.; Dziuk, B.; Lalancette, R.; Szostak, R.; Zhang, D.; Szostak, M. L-Shaped Heterobidentate Imidazo[1,5-a]Pyridin-3-Ylidene (N,C)-Ligands for Oxidant-Free Au^{I}/Au^{III} Catalysis. *Angew. Chemie Int. Ed.* **2023**, *62* (12), e202218427. https://doi.org/10.1002/anie.202218427.

(61) Scott, S. C.; Cadge, J. A.; Boden, G. K.; Bower, J. F.; Russell, C. A. A Hemilabile NHC-Gold Complex and Its Application to the Redox Neutral 1,2-Oxyarylation of Feedstock Alkenes. *Angew. Chemie Int. Ed.* **2023**, *62* (23), e202301526. https://doi.org/10.1002/anie.202301526.

(62) Hussong, M. W.; Rominger, F.; Krämer, P.; Straub, B. F. Isolation of a Non-Heteroatom-Stabilized Gold–Carbene Complex. *Angew. Chemie Int. Ed.* **2014**, *53* (35), 9372–9375. https://doi.org/10.1002/anie.201404032.

(63) Joost, M.; Estévez, L.; Mallet-Ladeira, S.; Miqueu, K.; Amgoune, A.; Bourissou, D. Enhanced π-Backdonation from Gold(I): Isolation of Original Carbonyl and Carbene Complexes. *Angew. Chemie Int. Ed.* **2014**, *53* (52), 14512–14516. https://doi.org/10.1002/anie.201407684.

(64) Harris, R. J.; Widenhoefer, R. A. Synthesis, Structure, and Reactivity of a Gold Carbenoid Complex That Lacks Heteroatom Stabilization. https://doi.org/10.1002/ange.201404882.

(65) Chintawar, C. C.; Yadav, A. K.; Kumar, A.; Sancheti, S. P.; Patil, N. T. Divergent Gold Catalysis: Unlocking Molecular Diversity through Catalyst Control. *Chem. Rev.* **2021**, *121* (14), 8478–8558. https://doi.org/10.1021/acs.chemrev.0c00903.

(66) Stylianakis, I.; Kolocouris, A. Comprehensive Overview of Homogeneous Gold-Catalyzed Transformations of π-Systems for Application Scientists. *Catalysts*. 2023. https://doi.org/10.3390/catal13060921.

(67) Morán-Poladura, P.; Suárez-Pantiga, S.; Piedrafita, M.; Rubio, E.; González, J. M. Regiocontrolled Gold(I)-Catalyzed Cyclization Reactions of N-(3-Iodoprop-2-Ynyl)-N-Tosylanilines. *J. Organomet. Chem.* **2011**, *696* (1), 12–15. https://doi.org/10.1016/j.jorganchem.2010.09.014.

(68) Wang, T.; Shi, S.; Vilhelmsen, M. H.; Zhang, T.; Rudolph, M.; Rominger, F.; Hashmi, A. S. K. Chemoselectivity Control: Gold(I)-Catalyzed Synthesis of 6,7-Dihydrobenzofuran-4(5H)-Ones and Benzofurans from 1-(Alkynyl)-7-Oxabicyclo[4.1.0]Heptan-2-Ones. *Chem. – A Eur. J.* **2013**, *19* (37), 12512–12516. https://doi.org/10.1002/chem.201301698.

(69) Zhao, K.; Kohnke, P.; Yang, Z.; Cheng, X.; You, S.-L.; Zhang, L. Enantioselective Dearomative Cyclization Enabled by Asymmetric Cooperative Gold Catalysis. *Angew. Chemie Int. Ed.* **2022**, *61* (37), e202207518. https://doi.org/10.1002/anie.202207518.

(70) Yu, M.; Zhang, G.; Zhang, L. Gold-Catalyzed Efficient Preparation of Linear α-Iodoenones from Propargylic Acetates. *Org. Lett.* **2007**, *9* (11), 2147–2150. https://doi.org/10.1021/ol070637o.

(71) Wang, D.; Ye, X.; Shi, X. Efficient Synthesis of E-α-Haloenones Through Chemoselective Alkyne Activation Over Allene with Triazole−Au Catalysts. *Org. Lett.* **2010**, *12* (9), 2088–2091. https://doi.org/10.1021/ol100576m.

(72) Yu, Z.; Ma, B.; Chen, M.; Wu, H.-H.; Liu, L.; Zhang, J. Highly Site-Selective Direct C–H Bond Functionalization of Phenols with α-Aryl-α-Diazoacetates and Diazooxindoles via Gold Catalysis. *J. Am. Chem. Soc.* **2014**, *136* (19), 6904–6907. https://doi.org/10.1021/ja503163k.

(73) Xie, X.-L.; Zhu, S.-F.; Guo, J.-X.; Cai, Y.; Zhou, Q.-L. Enantioselective Palladium-Catalyzed Insertion of α-Aryl-α-Diazoacetates into the O-H Bonds of Phenols. *Angew. Chemie Int. Ed.* **2014**, *53* (11), 2978–2981. https://doi.org/10.1002/anie.201309820.

(74) Ueda, K.; Amaike, K.; Maceiczyk, R. M.; Itami, K.; Yamaguchi, J. β-Selective C–H Arylation of Pyrroles Leading to Concise Syntheses of Lamellarins C and I. *J. Am. Chem. Soc.* **2014**, *136* (38), 13226–13232. https://doi.org/10.1021/ja508449y.

(75) Qiu, Y.; Ma, D.; Kong, W.; Fu, C.; Ma, S. Regiocontrolled 1,2-Migration in Cyclization of 1-(Indol-2-yl)-3-Alkyn-1-Ols: $(Ph_3P)Au^+$vs. $PtCl_4$. *Org. Chem. Front.* **2014**, *1* (1), 62–67. https://doi.org/10.1039/C3QO00006K.

(76) Shaikh, A. C.; Shinde, D. R.; Patil, N. T. Gold vs Rhodium Catalysis: Tuning Reactivity through Catalyst Control in the C–H Alkynylation of Isoquinolones. *Org. Lett.* **2016**, *18* (5), 1056–1059. https://doi.org/10.1021/acs.orglett.6b00175.

(77) Zhang, Y.; Luo, T.; Yang, Z. Strategic Innovation in the Total Synthesis of Complex Natural Products Using Gold Catalysis. *Nat. Prod. Rep.* **2014**, *31* (4), 489–503. https://doi.org/10.1039/C3NP70075E.

(78) De, S.; Dan, A. K.; Sahu, R.; Parida, S.; Das, D. Total Synthesis of Natural Products Using Gold Catalysis. *Chem. – An Asian J.* **2022**, *17* (24), e202200896. https://doi.org/10.1002/asia.202200896.

(79) Fürstner, A. From Understanding to Prediction: Gold- and Platinum-Based π-Acid Catalysis for Target Oriented Synthesis. *Acc. Chem. Res.* **2014**, *47* (3), 925–938. https://doi.org/10.1021/ar4001789.

(80) Rudolph, M.; Hashmi, A. S. K. Gold Catalysis in Total Synthesis—an Update. *Chem. Soc. Rev.* **2012**, *41* (6), 2448–2462. https://doi.org/10.1039/C1CS15279C.

(81) Mansour, A.; Gagosz, F. Expedited Total Synthesis of (±)-Brevianamide A via the Strategic Use of Gold(I) Catalysis. *Org. Lett.* **2022**, *24* (39), 7200–7204. https://doi.org/10.1021/acs.orglett.2c02971.

(82) Tran, H.; McGee, P.; Barriault, L. Formal Synthesis of (±)-Salvinorin A via Gold(I) Catalysis. *Chem. – A Eur. J.* **2023**, *29* (49), e202301640. https://doi.org/10.1002/chem.202301640.

(83) Bellavance, G.; Barriault, L. Total Syntheses of Hyperforin and Papuaforins A–C, and Formal Synthesis of Nemorosone through a Gold(I)-Catalyzed Carbocyclization. *Angew. Chemie Int. Ed.* **2014**, *53* (26), 6701–6704. https://doi.org/10.1002/anie.201403939.

(84) Staben, S. T.; Kennedy-Smith, J. J.; Huang, D.; Corkey, B. K.; LaLonde, R. L.; Toste, F. D. Gold(I)-Catalyzed Cyclizations of Silyl Enol Ethers: Application to the Synthesis of (+)-Lycopladine A. *Angew. Chemie Int. Ed.* **2006**, *45* (36), 5991–5994. https://doi.org/10.1002/anie.200602035.

(85) Linghu, X.; Kennedy-Smith, J. J.; Toste, F. D. Total Synthesis of (+)-Fawcettimine. *Angew. Chemie Int. Ed.* **2007**, *46* (40), 7671–7673. https://doi.org/10.1002/anie.200702695.

(86) Huwyler, N.; Carreira, E. M. Total Synthesis and Stereochemical Revision of the Chlorinated Sesquiterpene (±)-Gomerone C. *Angew. Chemie Int. Ed.* **2012**, *51* (52), 13066–13069. https://doi.org/10.1002/anie.201207203.

(87) Sethofer, S. G.; Staben, S. T.; Hung, O. Y.; Toste, F. D. Au(I)-Catalyzed Ring Expanding Cycloisomerizations: Total Synthesis of Ventricosene. *Org. Lett.* **2008**, *10* (19), 4315–4318. https://doi.org/10.1021/ol801760w.

(88) Nicolaou, K. C.; Tria, G. S.; Edmonds, D. J. Total Synthesis of Platencin. *Angew. Chemie Int. Ed.* **2008**, *47* (9), 1780–1783. https://doi.org/https://doi.org/10.1002/anie.200800066.

(89) Lu, Z.; Li, Y.; Deng, J.; Li, A. Total Synthesis of the Daphniphyllum Alkaloid Daphenylline.

Nat. Chem. **2013**, *5* (8), 679–684. https://doi.org/10.1038/nchem.1694.

(90) Ciriminna, R.; Falletta, E.; Della Pina, C.; Teles, J. H.; Pagliaro, M. Industrial Applications of Gold Catalysis. *Angew. Chemie Int. Ed.* **2016**, *55* (46), 14210–14217. https://doi.org/https://doi.org/10.1002/anie.201604656.

(91) Price, C. A. H.; Pastor-Pérez, L.; Ivanova, S.; Reina, T. R.; Liu, J. The Success Story of Gold-Based Catalysts for Gas- and Liquid-Phase Reactions: A Brief Perspective and Beyond. *Frontiers in Chemistry*. **2019**, *7.* https://doi.org/10.3389/fchem.2019.00691

(92) Alshammari, A. S. Heterogeneous Gold Catalysis: From Discovery to Applications. *Catalysts*. 2019. https://doi.org/10.3390/catal9050402.

(93) M. Schulz, J. H. T. No Title. *WO 97/21648* **1997**.

(94) Gross, E.; Liu, J. H.-C.; Toste, F. D.; Somorjai, G. A. Control of Selectivity in Heterogeneous Catalysis by Tuning Nanoparticle Properties and Reactor Residence Time. *Nat. Chem.* **2012**, *4* (11), 947–952. https://doi.org/10.1038/nchem.1465.

(95) Marion, N.; Ramón, R. S.; Nolan, S. P. [(NHC)AuI]-Catalyzed Acid-Free Alkyne Hydration at Part-per-Million Catalyst Loadings. *J. Am. Chem. Soc.* **2009**, *131* (2), 448–449. https://doi.org/10.1021/ja809403e.

(96) Wang, Y.; Wang, Z.; Li, Y.; Wu, G.; Cao, Z.; Zhang, L. A General Ligand Design for Gold Catalysis Allowing Ligand-Directed Anti-Nucleophilic Attack of Alkynes. *Nat. Commun.* **2014**, *5* (1), 3470. https://doi.org/10.1038/ncomms4470.

(97) Blanco Jaimes, M. C.; Böhling, C. R. N.; Serrano-Becerra, J. M.; Hashmi, A. S. K. Highly Active Mononuclear NAC–Gold(I) Catalysts. *Angew. Chemie Int. Ed.* **2013**, *52* (31), 7963–7966. https://doi.org/https://doi.org/10.1002/anie.201210351.

(98) Blanco Jaimes, M. C.; Rominger, F.; Pereira, M. M.; Carrilho, R. M. B.; Carabineiro, S. A. C.; Hashmi, A. S. K. Highly Active Phosphite Gold(i) Catalysts for Intramolecular Hydroalkoxylation, Enyne Cyclization and Furanyne Cyclization. *Chem. Commun.* **2014**, *50* (38), 4937–4940. https://doi.org/10.1039/C4CC00839A.

2. Chapter 2. Confinement-Induced Selectivities in Gold(I) Catalysis—The Benefit of Using Bulky Tri-(*ortho*-biaryl)phosphine Ligands

Muratov, K.; Gagosz, F. Confinement-Induced Selectivities in Gold(I) Catalysis—The Benefit of Using Bulky Tri-(*ortho*-biaryl)phosphine Ligands. *Angew. Chem., Int. Ed.,* **2022**, *61* (28), e202203452, https://doi.org/10.1002/anie.202203452

2.1. Abstract

The confinement of a catalytic site is an efficient strategy to control a reaction and modulate its selectivity. In the present work, a new class of structurally simple and easily accessible bulky tri-(*ortho*-biaryl)phosphine ligands were accessed, and their gold(I) complexes synthesized. Their X-ray diffraction analysis and the comparative evaluation of their V_{Bur}% and *G* steric parameters against a series of gold complexes commonly employed in catalysis demonstrated their confined nature. Despite their notable steric congestion, these complexes exhibited remarkable catalytic activities and unusual selectivities, both in nature and level, that make them unique in the field of synthetic homogeneous gold catalysis.

2.2. Introduction

In the early years of gold catalysis, Au(I)-catalysts were initially used as chloride salts. However, researchers soon recognized the influence of ligands in tuning the reactivity of Au(I)-species. This understanding has been vital in customizing the attributes of Au(I)-complexes, allowing for a proper control of specific properties. For example, complexes incorporating N-heterocyclic carbenes, known for their donating nature, generally exhibit reduced electrophilicity compared to those with phosphine ligands[1]. On the other hand, the use of less donating phosphite ligands or similar species has led to the emergence of highly electrophilic catalysts. The impact of ligands is of particular significance in the research work described in the present thesis, as they have a profound effect on the properties of Au(I) complexes.

One of the most studied and explored areas of gold-catalysis is the nucleophilic addition to a π-system. Traditional approaches, such as Brønsted acid-catalyzed nucleophilic additions to alkenes or alkynes, often necessitate harsh reaction conditions, leading to non-selective outcomes due to the formation of carbocation intermediates. To address this challenge, classical methodologies have employed Hg(II) catalysts, which are isolobal to protons,[2] capitalizing on the soft character of Hg(II) to enhance affinity for π-bonds. This strategy employs milder reaction conditions and

improves selectivity but introduces a complication; the resulting C(sp^3)-Hg bond exhibits considerable stability, requiring a subsequent step for its cleavage to liberate the final product.

Contrastingly, gold salts have emerged as an innovative and effective alternative to this approach. Not only are these salts considered non-toxic, but they also display pronounced affinity towards π-systems, a property that correlates with their intrinsic soft Lewis acid character. A salient feature that differentiates gold catalysis from the above mentioned Hg(II) catalysts is the formation of Au(I)-carbon bonds, which are characterized by their susceptibility to cleavage. This attribute not only expedites the release of the final product but also contributes to the superior catalytic turnover of gold complexes.[3–5]

In recent years, gold-catalyzed cycloisomerization reactions have emerged as a powerful tool for constructing cyclic architectures. The mild reaction conditions typically associated with gold catalysis as well as its compatibility with a wide range of functional groups make it an attractive choice for the synthesis of complex molecules. Furthermore, the exploration of chiral gold catalysts has opened the door to enantioselective cycloisomerizations and further expanded the synthetic utility of this method. Mechanistic understanding has also evolved, shedding light on the role of auxiliary ligands in modulating the reactivity and selectivity of the catalytic cycle.

In this section, we will explore the use of monometalated Au(I) complexes with covalently bound bulky ligands. In particular, we will discuss how the structural arrangement of the complex, and most importantly its confinement, can alter reaction pathways and affect the specific outcomes of certain chemical reactions. A literature review of the studies conducted prior to our work in this field (*Angew. Chem. Int. Ed.* ***2022****, 134,* e202203452) will be provided, referencing the relevant sources.

2.2.1. Cycloisomerization

The cycloisomerization of 1,6-enynes stands as the most extensively studied example of Au(I)-catalyzed cycloisomerization reactions and is frequently used as a benchmark reaction for catalyst assessment. The pioneering work on the 6-endo-dig skeletal rearrangement of 1,6-enynes **2.2.1-1** with Au(I) complexes was first published by Echavarren and colleagues in 2004.[6] Utilizing a simple [(PPh_3)AuCl]/$AgSbF_6$ system, they provided an alkynophilic catalyst that proved highly effective for both exo- and endo-cyclization of enynes (**Scheme 2.2.1-1, A**).

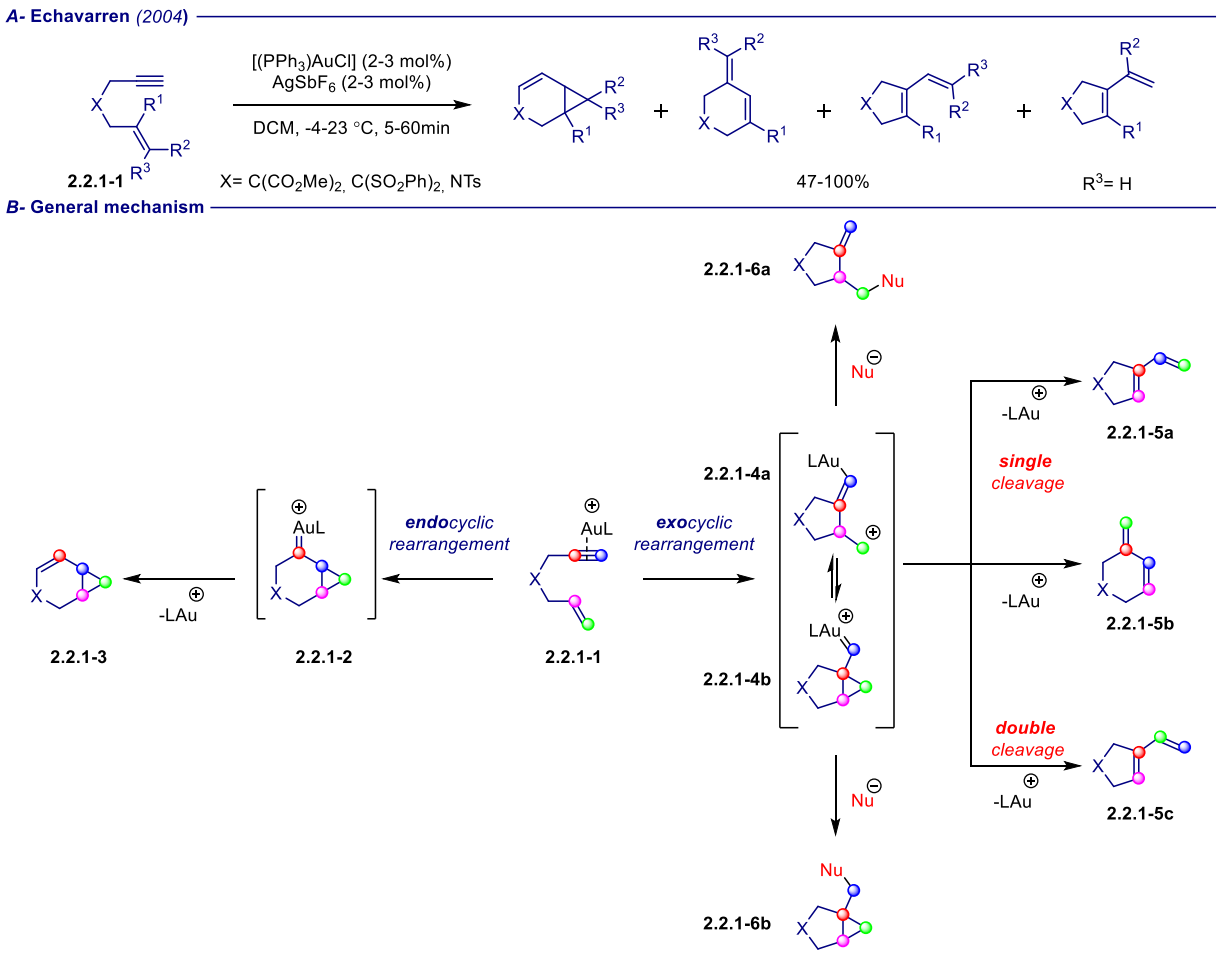

Scheme 2.2.1-1. Cycloisomerization of 1,6-enynes.

This reaction exhibits a complex mechanism with diverse possible pathways (**Scheme 2.2.1-1, B**). Initially, the activated alkyne **2.2.1-1** can undergo endo cyclization, leading to the formation of intermediate **2.2.1-2**, which subsequently proceeds to yield product **2.2.1-3** through hydride shift and protodeauration. Alternatively, the initially activated alkyne may undergo exocyclization, generating **2.2.1-4,** which can be described either as a carbocationic alkenyl intermediate **2.2.1-4a** or its carbenoid form **2.2.1-4b.** From here, intermediate **2.2.1-4a** can undergo either a single-cleavage skeletal rearrangement via a formal 1,3-migration of the terminal carbon of the alkene, resulting in the formation of product **2.2.1-5a** upon protodeauration,[7] or an endo-fashion single-cleavage process, where the internal carbon of the double bond migrates towards the terminal carbon of the alkyne, giving rise to product **2.2.1-5b** after protodeauration.[8] On the other hand, intermediate **2.2.1-4a** can engage in a double-cleavage rearrangement, involving the formal insertion of the terminal carbon of the alkene into the alkyne triple bond, resulting in the generation of product **2.2.1-5c** upon protodeauration.[9–13] Additionally, when external nucleophiles are present, various outcomes can be expected. The nucleophile can attack the carbocationic center, leading to the formation of product **2.2.1-6a**. Conversely, an attack on the carbene center would result in the formation of **2.2.1-6b.**[14]

The question of selectivity naturally emerges from this context, presenting an intricate problem to be addressed. One of the strategies to deal with this challenge involves the utilization of specially designed ligands, characterized by their bulky, sterically demanding nature. Such ligands can alter the steric environment within the metal's primary coordination sphere, thereby favoring the formation of specific products. However, this method of manipulating catalyst properties through steric modification of the ligand encounters limitations, particularly with Au(I) catalysts. This restriction is primarily attributed to the preferred linear coordination geometry of Au(I), which poses constraints on how steric effects can be employed to control selectivity.

2.2.2. NHC-based complexes

In a recent study, Hashmi and colleagues explored the use of 8-membered NHC ligands **2.2.2-1** in the cycloisomerization of 1,6-enynes (**Scheme 2.2.2-1**).[15] The application of complex **2.2.2-1a** yielded compound **2.2.2-2a** as the primary product, aligning with the standard exo-type mechanism and proceeding through the single cleavage of the gold-intermediate. However, when employing cationic complexes **2.2.2-1b** or **2.2.2-1c**, a decline in selectivity was observed, thus emphasizing the susceptibility of the reaction to the specific nature of the catalyst. A striking deviation was seen with the use of **2.2.2-1d** with a substrate bearing a NTs linker, which led to the formation of the endo-type product **2.2.2-2c**, illustrating the marked influence of catalyst choice on reaction outcomes. Additionally, when complex **2.2.2-1d** was employed with substrates having $C(CO_2Me)_2$ or $C(SO_2Ph)_2$ linkers, the absence of the endo-product highlighted the role of steric hindrance in determining the course of the reaction.

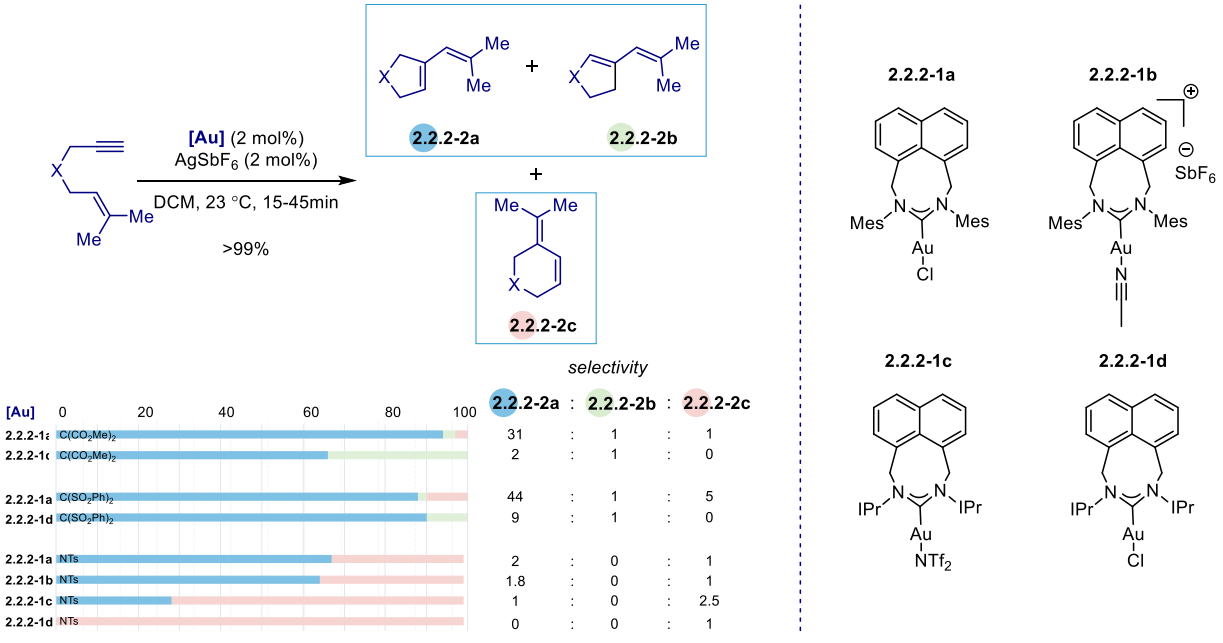

Scheme 2.2.2-1. 8-membered NHC ligands.

A novel approach to encapsulate gold was introduced by Sollogoub and co-workers,[16,17] who were inspired by the structure of metalloenzymes. They designed a family of cyclodextrins (CDs) with an internal N-heterocyclic carbene gold complex, anchored to the smaller rim, effectively burying the gold atom deep within the cavity. The researchers explored how this unique confinement influenced the Au(I)-catalyzed cycloisomerization of compound **2.2.2-3** (**Scheme 2.2.2-2, A**). Utilizing the widely used carbene-based catalyst [(IPr)AuCl], products **2.2.2-3a** and **2.2.2-3b** were obtained at a ratio of 1.5:1. Interestingly, while the selectivity was similar with the smaller **2.2.2-4-α**, the slightly larger **2.2.2-4-β** shifted the product ratio, resulting in the absence of **2.2.2-3b**, minimal formation of **2.2.2-3a**, and dominant 6-membered ring compound **2.2.2-3c**. The use of **2.2.2-4-γ** also modified the product distribution but to a lesser extent.

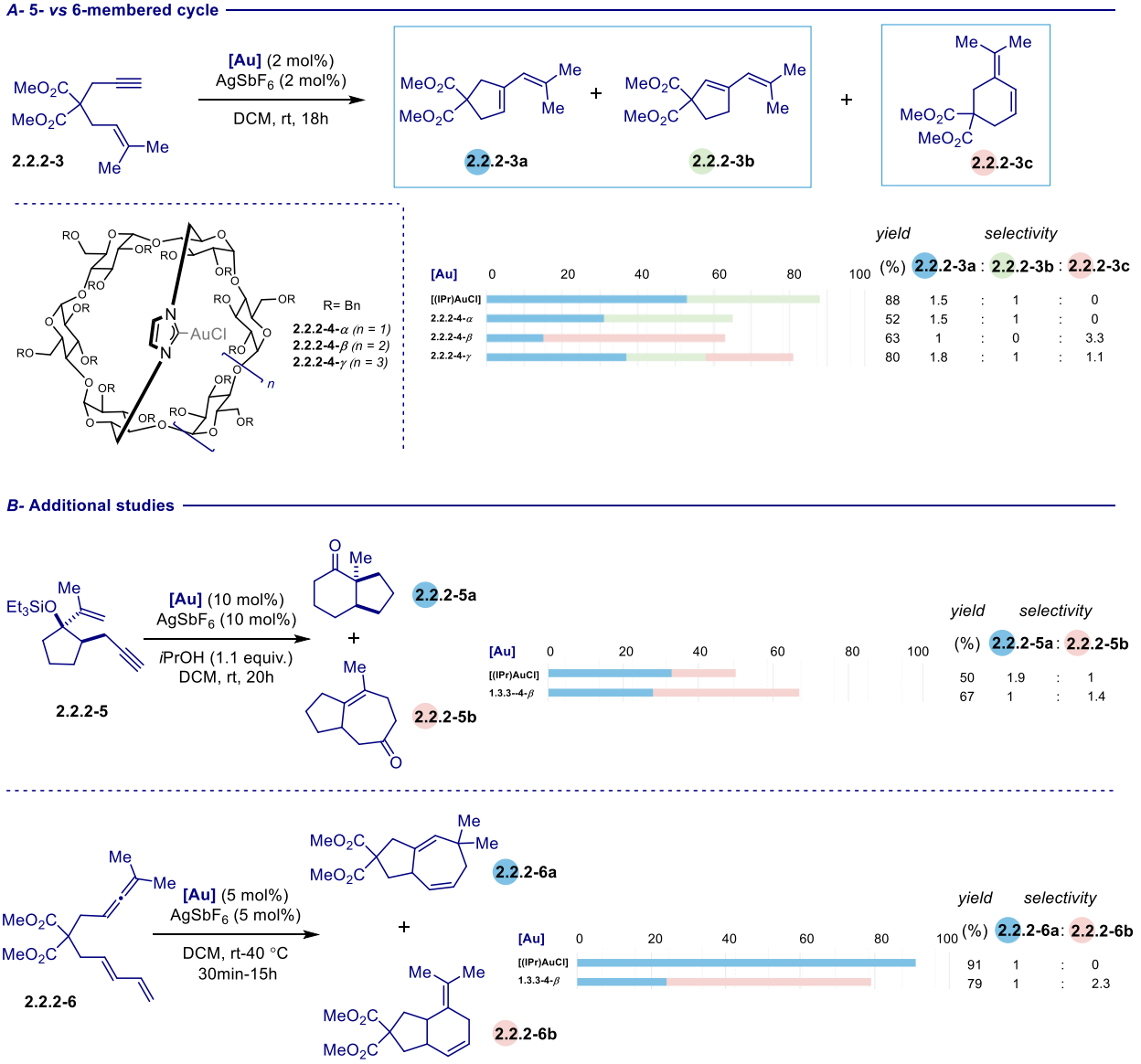

Scheme 2.2.2-2. NHC-capped cyclodextrins.

To further prove the impact of confinement within a ligand's cavity, two separate cycloisomerization reactions were studied by the researchers (**Scheme 2.2.2-2, B**).[18] With the classical carbene-based complex [(IPr)AuCl], the formation of product **2.2.2-3a** was found to be favored. On the other hand, employing the complex with **2.2.2-4-β** led to a reversal in reaction selectivity, predominantly generating product **2.2.2-3b**. Additionally, a marked contrast in selectivity was observed in the cyclization process of allenediene **2.2.2-6**. The [(IPr)AuCl] complex primarily yielded **2.2.2-6a**, while the complex **2.2.2-4-β** resulted in a 2.3:1 ratio of **2.2.2-6a** to **2.2.2-6b**.

The cyclodextrins were also found to confer substantial enantioselectivity (up to 80% *ee*), with the β-CD-based ligand showing better enantioselective control than its α-CD counterpart. It is important to note that reactions are generally slower with α-CD catalysts than β-CD ones, requiring higher temperatures to attain similar reaction rates (**Scheme 2.2.2-3, A**). A high degree of enantioselectivity (up to 94%) was demonstrated in alkoxycyclization of substrates **2.2.2-7** in MeOH:DCM mixture.[18] In a subsequent study it was shown that the gold-catalyzed cycloisomerization and hydroxycyclization reactions could also be performed with high enantioselectivity in pure water by utilizing water-soluble cyclodextrin complexes **2.2.2-8**, derived from permethylated α- or β-CD (**Scheme 2.2.2-3, B**).[19] The nature of the cavity in hydroxycyclization reactions was found to significantly impact both reactivity and enantioselectivity. When **2.2.2-8-α** was employed with enyne **2.2.2-3** at 50°C without silver salts, the reaction showed almost no progress. However, adding silver salts ($AgSbF_6$) led to the formation of cyclized product **2.2.2-3e**, with a 74% conversion after 18 hours and an enantioselectivity of 54% ee. On the other hand, catalyst **2.2.2-4-β** allowed the conversion of **2.2.2-3** into **2.2.2-3e** at 50°C without silver salts, achieving a yield of 74%. Impressively, this method afforded a high enantioselectivity of 96%. When conducted at a reduced temperature of 20°C, the enantioselectivity further increased to 98%, although this was accompanied by a decrease in yield.

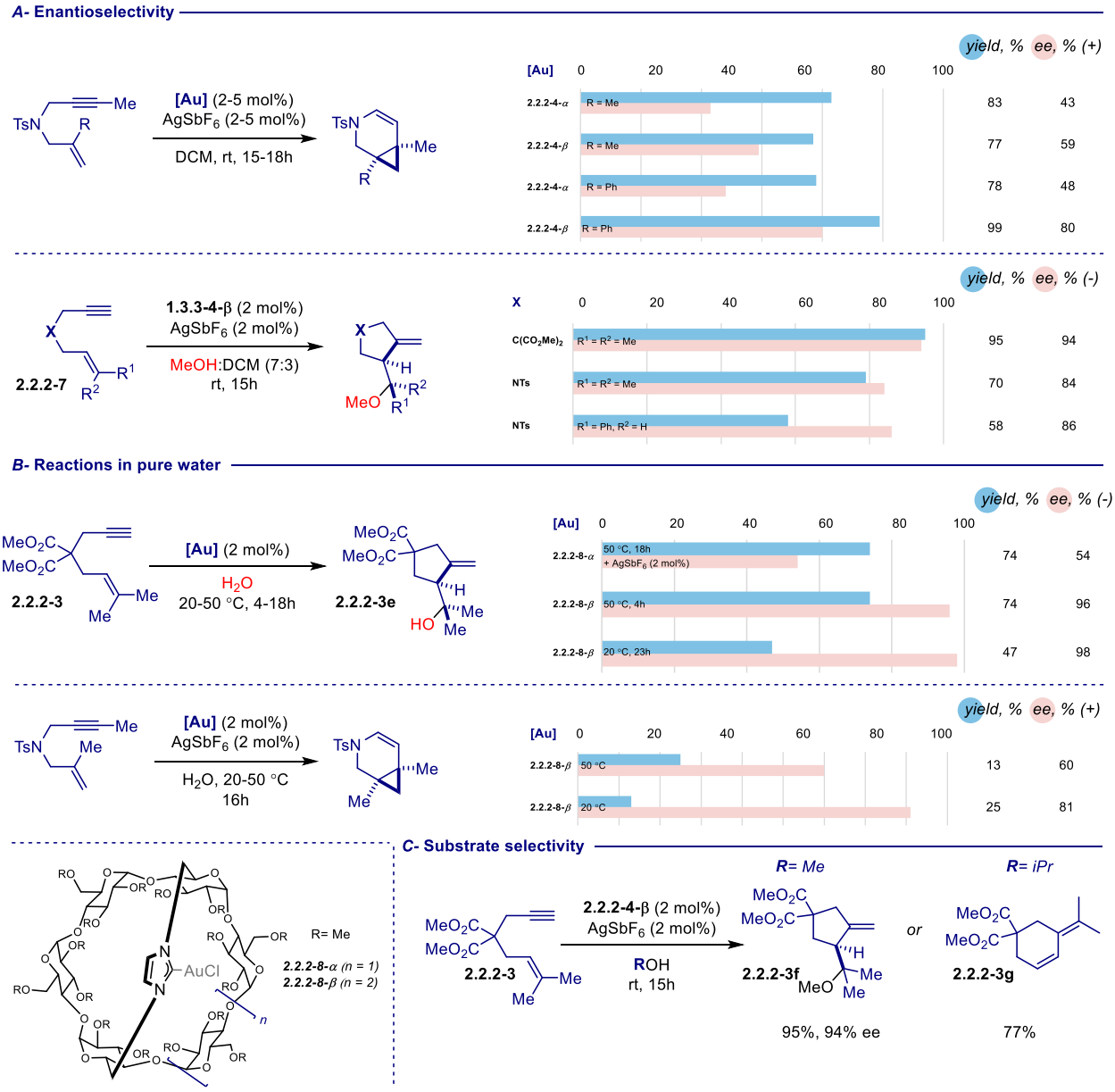

Scheme 2.2.2-3. Enantioselectivity and substrate selectivity.

The impact of the alcohol's size on the reaction pathway was also investigated.[18] Specifically, it was found that smaller alcohol nucleophiles, such as MeOH, primarily engaged in an alkoxycyclization reaction with **2.2.2-3** to form **2.2.2-3f** (**Scheme 2.2.2-3, C**). However, when the size of the alcohol was increased with the use of larger molecules such as *i*PrOH, a competitive enyne cyclization product **2.2.2-3g** was predominantly formed, excluding the involvement of the alcohol. This outcome underscores the significance of the confined environment within the cavity of β-CD-derived ligands, which noticeably influences the reaction based on the size of the nucleophilic agent involved.

In 2010, the research group of Hong investigated the influence of a newly developed bulky acyclic diaminocarbene complex **2.2.2-9** on the Au(I)-catalyzed cyclization/hydroarylation of 1,6-enyne **2.2.2-12** with indole (**Scheme 2.2.2-4, A**).[20] Their results showed that the selectivity of the reaction was substantially determined by the steric environment at the catalytic center. While the conventional IPr-based gold complex predominantly produced **2.2.2-12b**, the newly developed complex completely changed the selectivity, affording **2.2.2-12a** as the primary product. This change was attributed to the steric factors of the ligand. Subsequently, in 2017, Matt, Brenner, and Blanc developed a bulky bis-*N,N'*-(9-alkylfluorenyl) heterocyclic carbene complex **2.2.2-10**.[21] However, while this complex provided **2.2.2-12a** with exceptional selectivity, the yield was reduced slightly. The group of Slaughter continued exploring this topic and showed in 2021 that they could obtain **2.2.2-12a** in good yield and remarkable selectivity using the novel bulky acyclic diaminocarbene complex **2.2.2-11**.[22]

In a 2018 report, Blanc and Pale further exploited the steric properties of **2.2.2-10** to develop a regioselective method for the synthesis of 1,3-indenes from 3-aryl propargylic gem-dipivalates (**Scheme 2.2.2-4, B**).[23] Upon examining different carbene ligands, they found that the use of the complex **2.2.2-10** gave **2.2.2-13a** in high yield and high selectivity. Conversely, application of a traditional NHC ligand resulted in a mixture of species, highlighting the specific properties of the **2.2.2-10** complex.

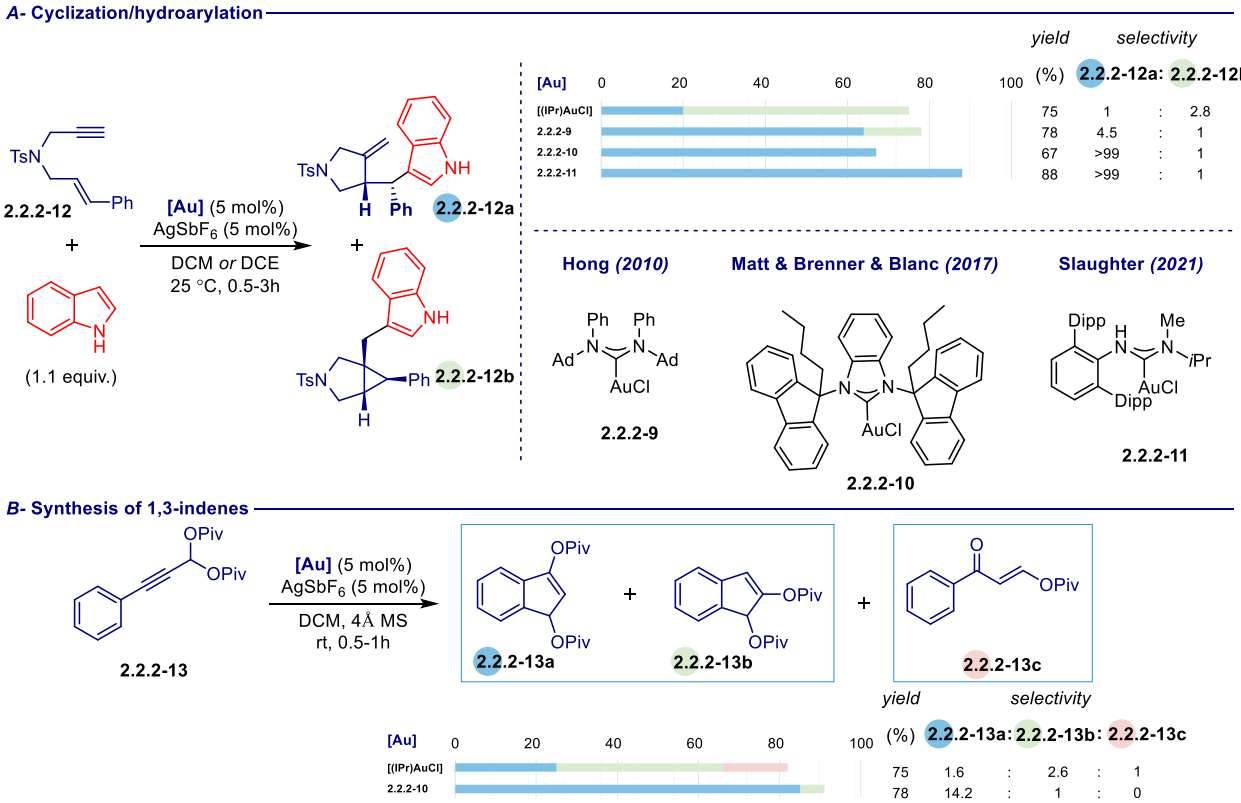

Scheme 2.2.2-4. Bulky carbene ligands.

2.2.3. Phosphines

In Au(I) chemistry, phosphines are recognized as key ligands and have a distinguished role. Well-known phosphine ligands such as triphenylphosphine facilitate various reactions and synthetic methodologies. Yet, scientists continue to explore broader chemical landscapes, seeking to uncover more effective ligands and tailor catalysts to achieve specific reaction outcomes.

In 2016, Knight and Doherty analyzed ligands featuring 12-phenyl-9,10-dihydro-9,10-ethenoanthracene (KITPHOS) ligand and examined how these influenced the Au(I)-catalyzed cyclization of 2-alkynylbenzoic acids **2.2.3-1**.[24] An intriguing observation was made with regard to selectivity. Whereas the AuCl-catalyzed lactonization of **2.2.3-1** predominantly yielded the 5-exo-dig cyclization product **2.2.3-1a**, the introduction of a KITPHOS-based complex led to a dramatic shift in product distribution. The 6-endo-dig regioisomer **2.2.3-1b** was produced exclusively, with excellent yield achieved in just 15 minutes at room temperature (**Scheme 2.2.3-1, A**).

Another report on the use of sterically bulky phosphines came in 2019 from Fossey and co-workers (**Scheme 2.2.3-1, B**).[25] The researchers synthesized a series of 1,2,3-triazoles, each bearing 1-aryl and 5-phosphino functionalities. Within this series, the phosphorus atom was attached to one, two, or three triazole units, allowing for a systematic investigation of how the number of appended triazoles influenced the chemical properties. These novel phosphines were then compared with tricyclohexylphosphine and triphenylphosphine to evaluate how the triazole modification impacted the catalytic activity. To probe the effect of these structural variations, the gold complexes were tested in a model hydration reaction of alkyne **2.2.3-2**. The reaction's typical outcome is the Markovnikov addition at the benzylic position of the alkyne to give product **2.2.3-2a**, while the anti-Markovnikov addition at the alternate alkyne position to afford ketone **2.2.3-2b** presents a greater challenge. Complete conversion was achieved in all cases except for the tris-triazole complex. Interestingly, while all the complexes showed a preference for Markovnikov addition, the phosphines bearing a single triazole ring demonstrated an enhanced ability to produce the challenging anti-Markovnikov product **2.2.3-2b**, even though **2.2.3-2a** remained the main product.

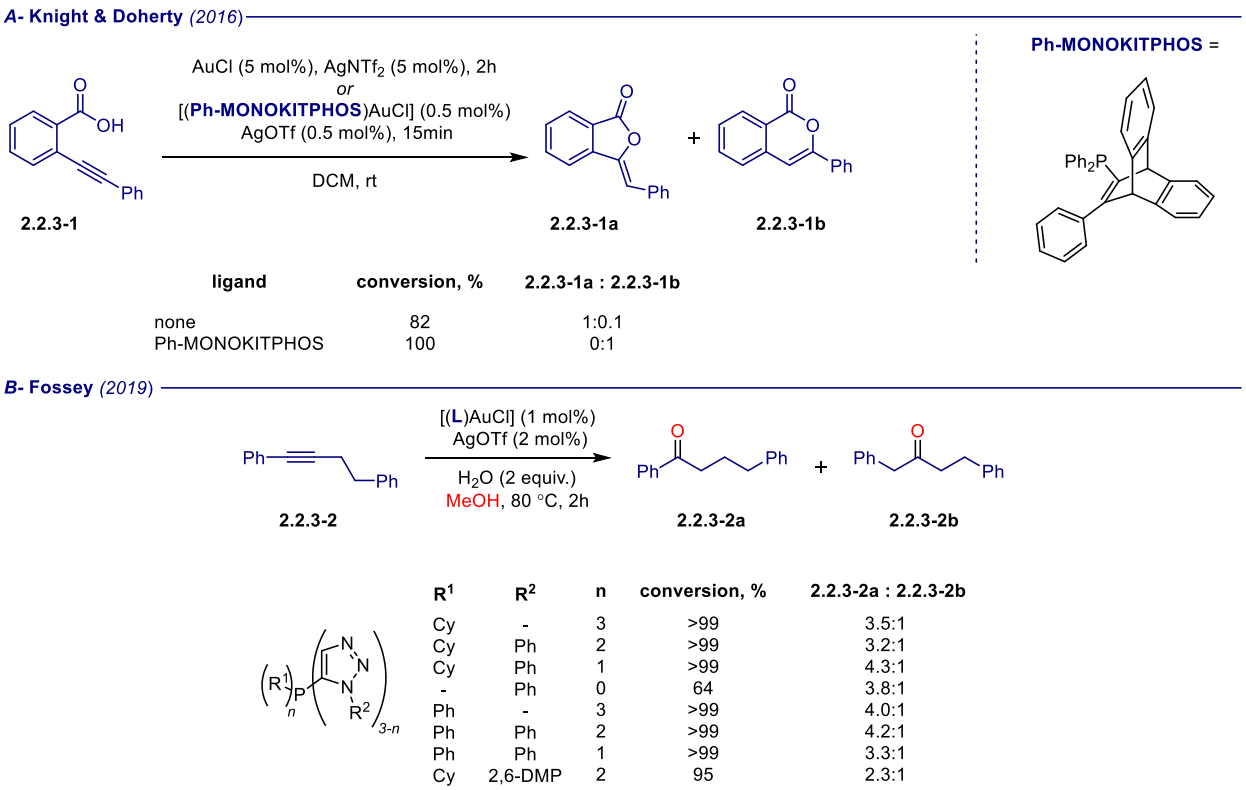

Scheme 2.2.3-1. Bulky phosphine ligands.

Sawamura and co-workers introduced a novel strategy to encapsulate gold in a confined environment using the hollow-shaped phosphine **2.2.3-3a** and studied the corresponding complex in the cyclization of **2.2.3-4** (**Scheme 2.2.3-2, A**). [26] Compared to conventional XPhos and IPr ligands, the use of **2.2.3-3a** increased the selectivity towards the product **2.2.3-4a**, mainly favoring the formation of the *E* isomer, while the conventional ligands gave a 1:1 mixture of *E* and *Z* isomers. In a subsequent study, researchers extended the use of this architectural concept to the cycloisomerization reaction of enynes.[27] They found that in addition to forming the cyclobutene fused product **2.2.3-5**, the complexes **2.2.3-3a** and **2.2.3-3b** produced the diene products **2.2.3-5b** and **2.2.3-5c**. Such products were absent when using the XPhos ligand (**Scheme 2.2.3-2, B**). Interestingly, the corresponding XPhos-based complex failed to generate eight-membered ring products in the cycloisomerization of 1,9-enyne **2.2.3-6** (**Scheme 2.2.3-2, C**), and only partial substrate consumption was observed. In contrast, complexes **2.2.3-3a** and **2.2.3-3b** allowed the formation of the corresponding products **2.2.3-6a-c** in good to excellent yields.

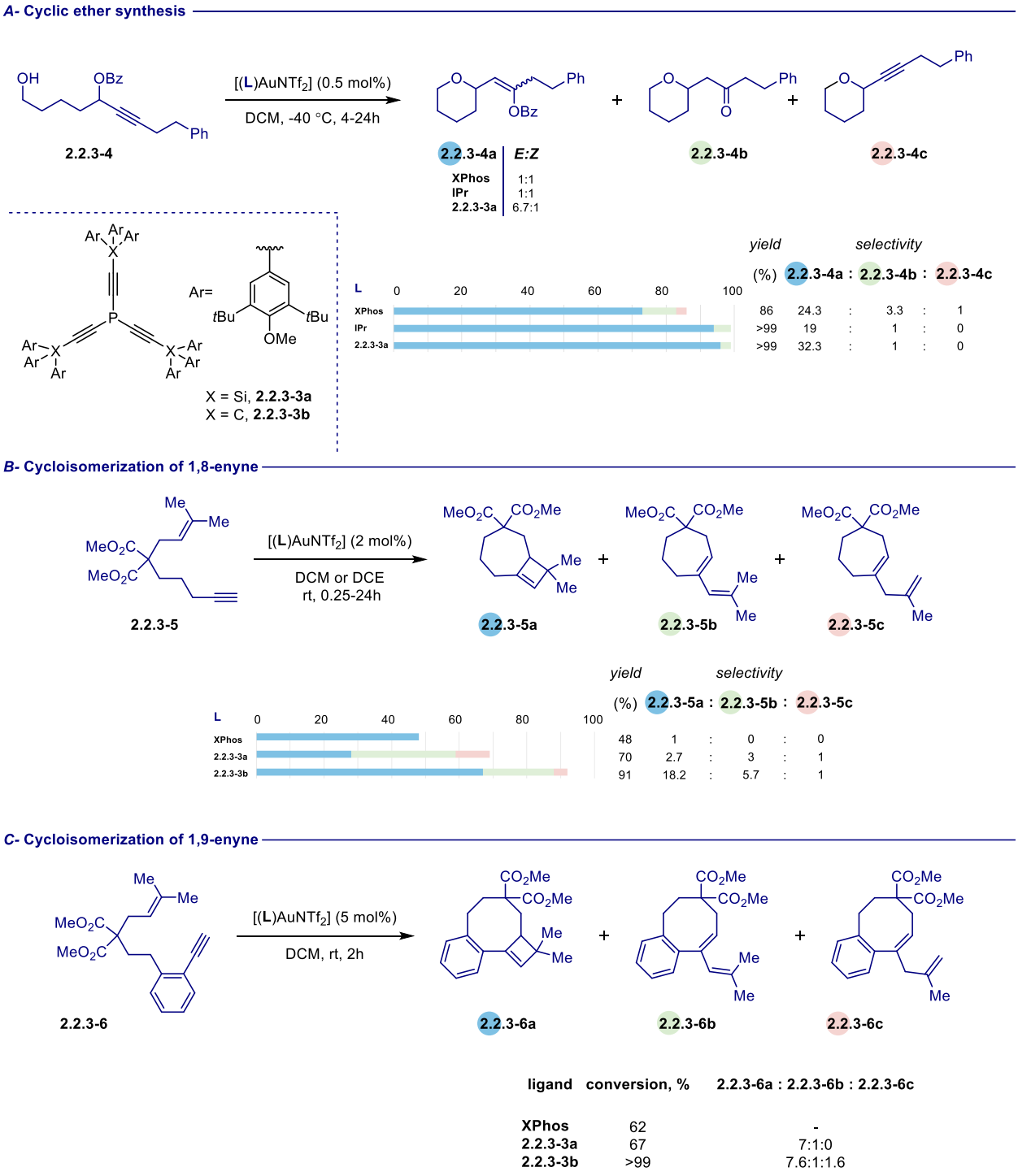

Scheme 2.2.3-2. Hollow-shaped phosphines.

Iwasawa and coworkers reported the use of a supramolecular gold complex **2.2.3-7a** based on a resorcin[4]arene cavitand (**Scheme 2.2.3-3, A**).[28] This cavitand, carrying an incorporated phosphorus atom, operates as a ligand, securing a metal ion at its center. Intriguingly, the phosphorus atom's lone pair is aligned towards the cavity space, compelling the coordinated

metal ion to project into the cavity and confront three walls formed by the ligand. Researchers also suggested that the presence of a Lewis basic P=O moiety in the complex could act as a hydrogen bond acceptor and actively direct an incoming water molecule. This concept was tested in the hydration reaction of the alkyne **2.2.3-8**. The results showed that the newly developed complex **2.2.3-7a** provided the desired product **2.2.3-8b** with high selectivity and excellent yield. In contrast, complexes based on IPr and PPh_3 led to inferior selectivity and yield. Further investigations involved a related complex, **2.2.3-7b**, which lacked the P=O moiety, and it was observed that the hydration reaction was severely hampered under the same conditions. Attempts to enhance the reaction by employing Ph_3PO with IPr- or PPh_3-coordinated complexes did not lead to significant improvements, which demonstrates the unique potency of the original **2.2.3-7a** complex in this particular reaction.

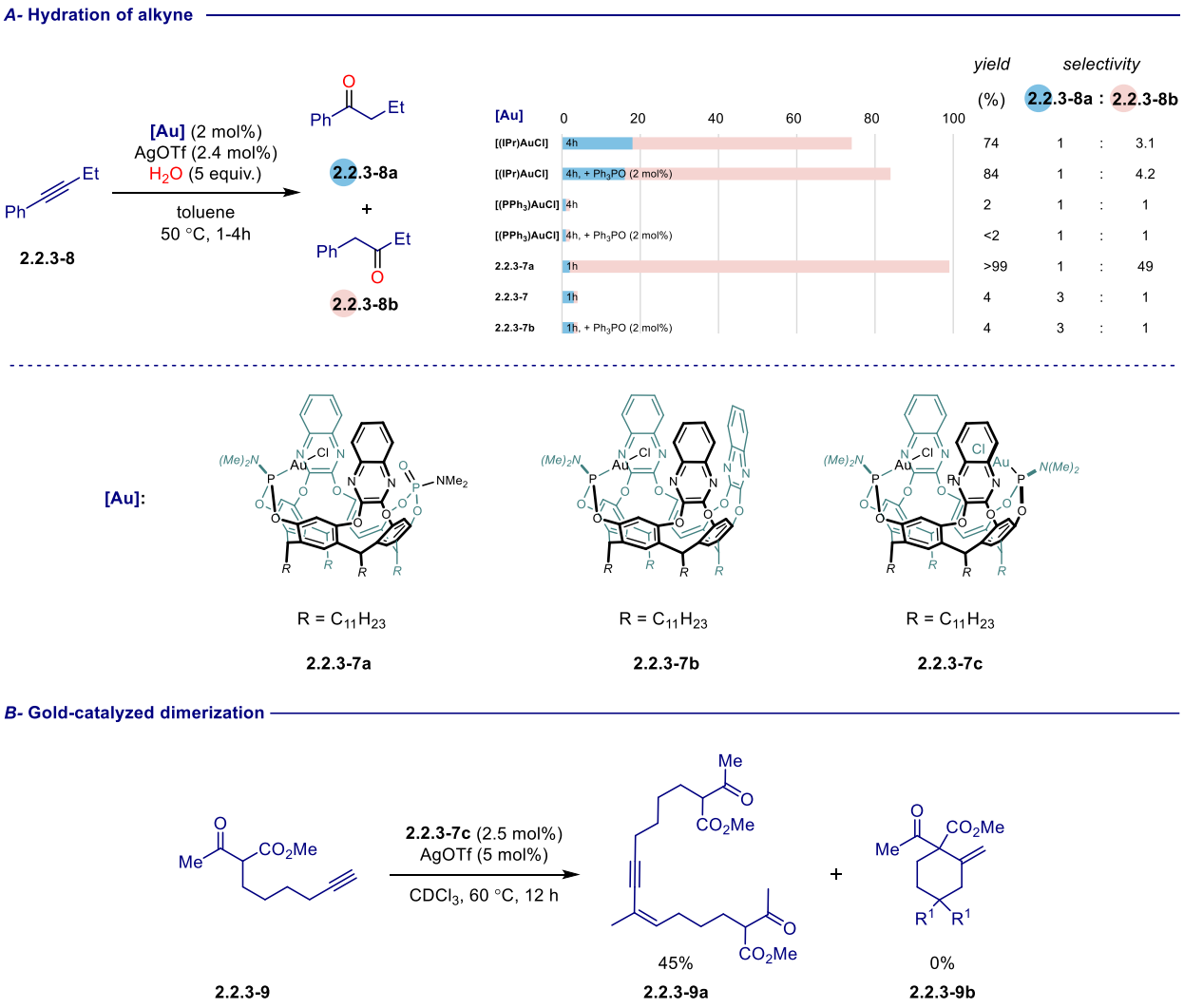

Scheme 2.2.3-3. Cavitand-based phosphines.

Subsequent research by the same group examined the binuclear version of the complex, with two gold atoms positioned opposite each other.[29–31] This unique dinuclear Au(I) catalyst **2.2.3-7c**

demonstrated the ability to catalyze the dimerization of terminal alkyne **2.2.3-9**, leading to the formation of conjugated enyne **2.2.3-9a** (**Scheme 2.2.3-3, B**). This specific reaction was not observed using the mononuclear cavitand-bases Au(I) complex. Interestingly, the expected Conia-ene product **2.2.3-9b**, which is often a typical result of such reactions, was not detected in this case. Instead, the dinuclear Au(I) catalyst exclusively enabled the synthesis of a dimerization product.

2.2.4. Phosphites

Phosphites, as phosphorus-based ligands, generally exhibit less electron-rich characteristics compared to phosphines, attributed to their enhanced π-accepting nature[32]. This difference could make the corresponding gold complexes more prone to electrophilic behavior, which may in turn accelerate those catalytic processes where the rate-determining step involves a nucleophilic attack.[33]

In 2014, Hashmi and colleagues synthesized a bulky phosphite ligand **2.2.4-1** and compared its performance to that of triphenyl and triadamantyl phosphites in a model reaction (**Scheme 2.2.4-1**).[34] This ligand, derived from the highly sterically hindered BINAP derivative, showed both a favorable yield and a slightly improved selectivity over the tested $P(OPh)_3$ in the cycloisomerization of the 1,6-enyne **2.2.4-2**.

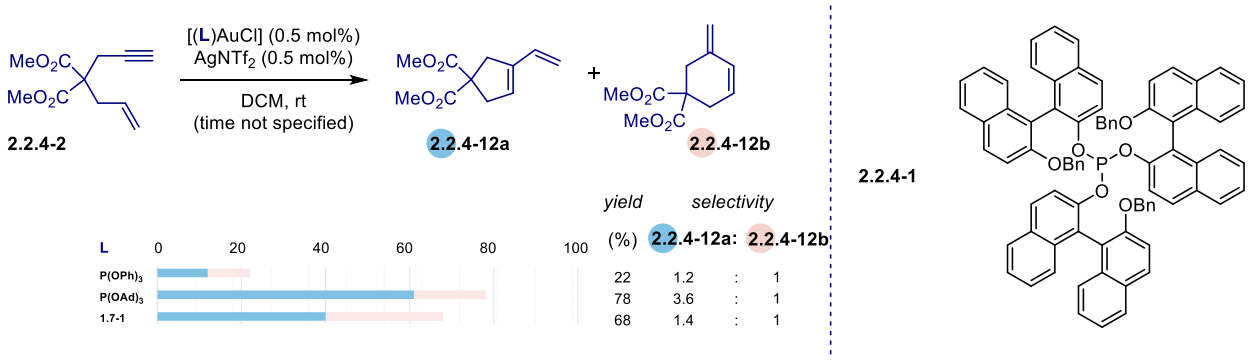

Scheme 2.2.4-1. Bulky phosphite ligand.

2.3. Results and Discussion

The confinement of a reactive site is an attractive approach for controlling a reaction and inducing selectivities that could be hardly achieved if the catalytic environment would be free of geometrical constraints. By contrast with the continuous efforts devoted to the development of new gold catalytic systems and despite their promises for controlling selectivities, small-molecule confined catalysts remain very limited.[15,21,35] In this context, we were intrigued by the possibility that similar confinement effects could be observed with phosphine ligands of simpler architecture. We considered that the completely open catalytic site of the popular

triphenylphosphine gold complex **2.3-1** could be confined by introducing a substituent at the *ortho* position of each phenyl group (**Scheme 2.3-1**). Our attention was brought to gold complex of type **2.3-2** which feature a tri-(*ortho*-biaryl)phosphine ligand. While the catalytic site in **2.3-2** might appear somewhat limited in space, the use of the *ortho*-biaryl motif, reminiscent of Buchwald type ligands, had previously been shown to positively affect the reactivity or the stability of gold(I) complexes.[33,36–39]

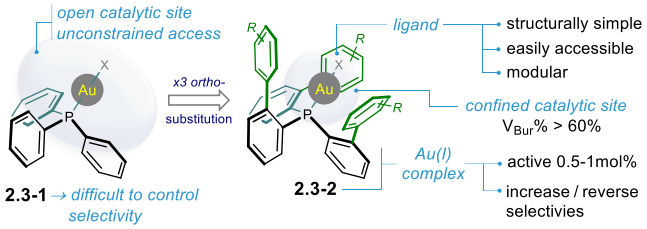

Scheme 2.3-1. Selectivity control with bulky tris-(o-biphenyl)phosphine ligands.

Tri-(*ortho*-biaryl)phosphine ligands could also be accessed with substitutions on both aryl rings,[40] thus offering the potential to modulate their electronic properties and the possibility to further develop (poly)functionalized catalysts. Interestingly, the simplest representative of gold complex **5** (R=H, X= Cl) has been mentioned in a report by Hammond and Xu, but was shown to be poorly reactive in the hydroamination reaction they studied.[37] Structurally related systems involving a tri-KITPHOS[24] or *tri*-(*N*-phenyltriazolyl) phosphine[25] were also reported, but they demonstrated no significant catalytic activity and no specific selectivity. In this chapter we report the synthesis of a series of tri-(*ortho*-biaryl)phosphine Au(I) complexes **2.3-2**, their structural analysis and selected applications in catalysis. Preliminary results presented herein demonstrate that these complexes possess a confined reactive site allowing for various types of selectivities and should therefore be considered as valuable tools in synthetic organic chemistry.

2.3.1. Synthesis of gold complexes.

We began our investigations with the synthesis of biaryl ligands **2.3-4** (**Scheme 2.3-2, A**). They were easily accessed from the corresponding bromo *ortho*-biaryl derivatives **2.3-3** in 21-88% yield by treatment with *n* or *t*BuLi followed by addition of 1/3 equivalent of PCl_3. The *ortho*-phenyl group in **2.3-4$_H$** is replaced by a 2-naphthyl motif in **2.3-4$_{2Nap}$**. The reaction of ligands **2.3-4** with 1 equiv. of AuCl•SMe_2 delivered the corresponding complexes **2.3-5** (**Scheme 2.3-2, B**, 62-98% yield) which were then treated with $AgSbF_6$ in acetonitrile to provide the active gold complexes **2.3-6** (73-88% yield). The triflimide gold complex **2.3-7** possessing ligand **2.3-4** was also synthesized in 67% yield.

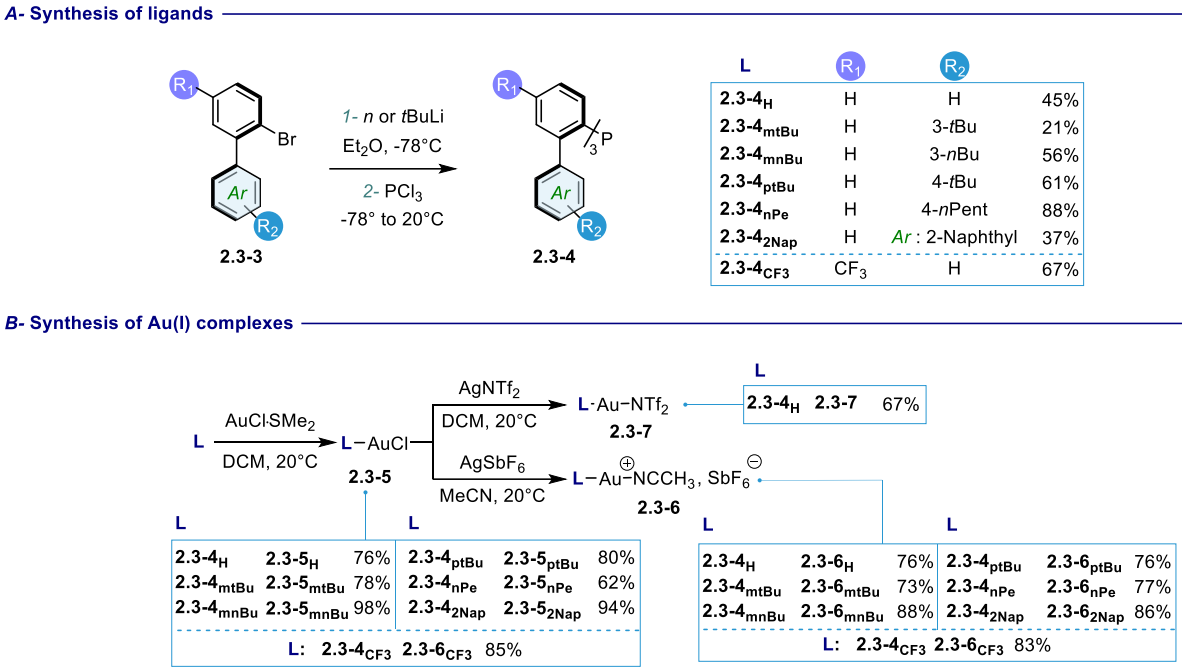

Scheme 2.3-2. Synthesis of tri-(*ortho*-biaryl)phosphine ligands and the corresponding Au(I) complexes.

2.3.2. Structural analyses

All complexes were obtained as solids and crystals suitable for SCXRD analyses could be obtained for representative AuCl complexes **2.3-5$_{H}$**, **2.3-5$_{nPe}$** and **2.3-5$_{mtBu}$**. These complexes display a three-blade propeller type arrangement of the phenyl groups attached to the P atom, similarly to what is observed for AuCl complex **2.3-8** (**Scheme 2.3-4, B**).[41] The three *ortho*-aryl moieties point in the same direction as the P-AuCl bond. The helical organization of the phenyl groups is transmitted to the *ortho*-aryl moieties with biaryl motifs displaying an average torsion angle of 67° for **2.3-5$_{H}$**, 69° for **2.3-5$_{nPe}$** and 62° for **2.3-5$_{mtBu}$**. For the three complexes **2.3-5$_{H}$**, **2.3-5$_{mtBu}$** and **2.3-5$_{nPe}$**, the gold atom was found to be confined inside the structures, capped, and surrounded by the three *ortho*-aryl units of the ligand with a classical P-Au distance of 2.23 Å. The average distance [d] from the *ortho*-aryl centroids to the Au atom was calculated to be 3.48 Å for complex **2.3-5$_{H}$**. This value is very similar for **2.3-5$_{mtBu}$** (3.47 Å), but slightly longer for **2.3-5$_{nPe}$** (3.58 Å). Complex **2.3-5$_{H}$** could be schematically represented as an empty cone shaped structure with an upper opening diameter of the cavity of approximately 8.0 Å, and a gold atom inserted 1.9 Å inside. While the cavity in **2.3-5$_{H}$** is as deep as that of trialkynylphosphine gold complexes **2.3-16**[42] (**Scheme 2.3-4, A**), its opening diameter is comparatively reduced (13-18 Å for **2.3-16**).

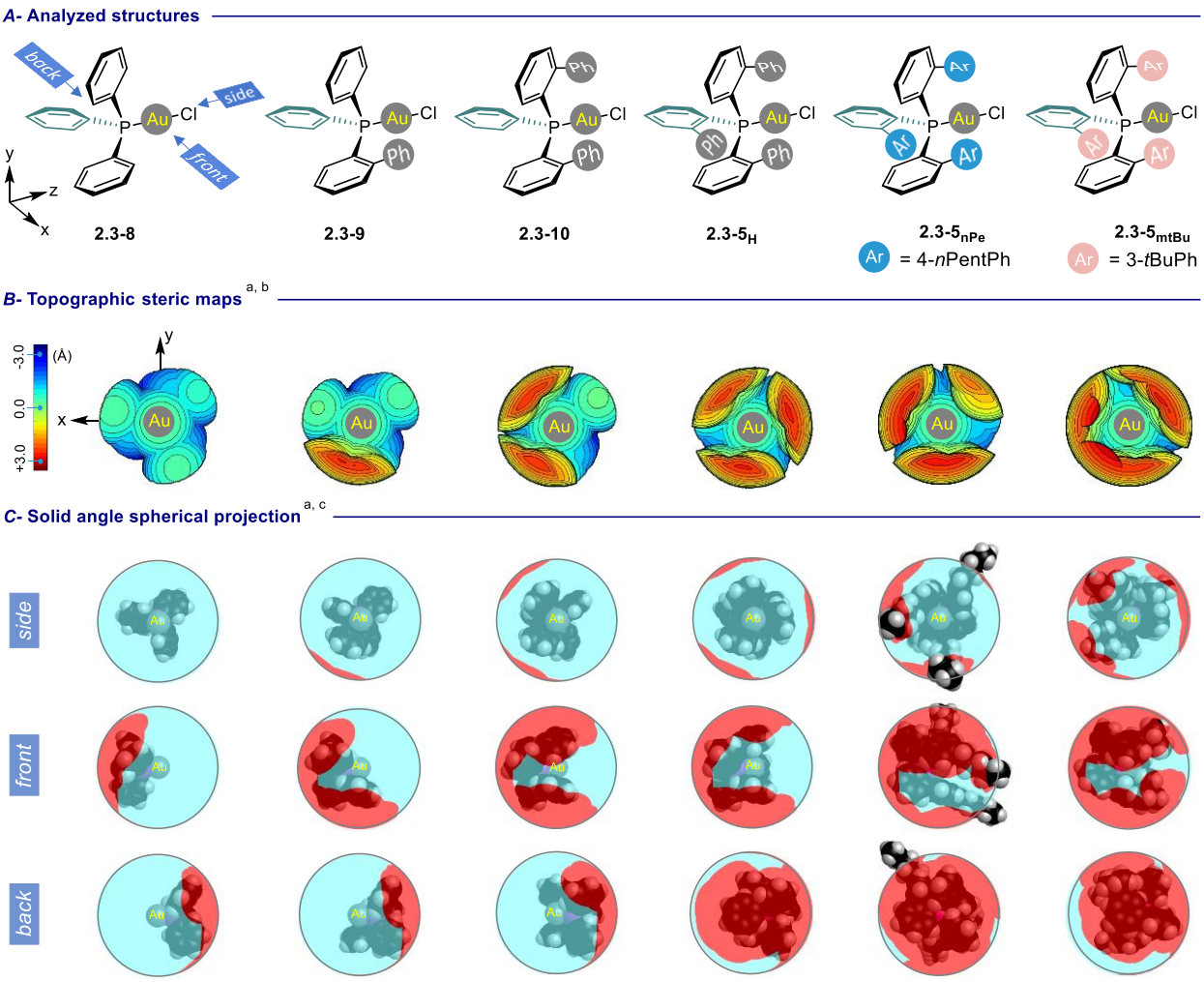

Scheme 2.3-3. Steric details. [a] Results by Prof. Fabien Gagosz. [b] Topographic steric maps and $V_{Bur\%}$ were calculated using SambVca 2.1. [c] Solid angles projections (coloured in red) were obtained using SolidAngleGL. GAu and EDA were calculated using Solid-G.

2.3.3. Steric properties

To get a deeper look into the steric properties of the newly synthesized gold complexes, the topographic steric maps (TSM) and the percent buried volumes (V_{Bur}%)[43–47] of gold complexes **2.3-5$_H$**, **2.3-5$_{mtBu}$** and **2.3-5$_{nPe}$** were calculated using SambVca 2.1, and compared to those of triphenylphosphine AuCl complex **2.3-8**,[41] and complexes **2.3-9**[48] and **2.3-10**[38] which possess only one and two biphenyl units, respectively (**Scheme 2.3-3, A** and **Scheme 2.3-4, A**). When visually comparing the TSM of **2.3-8**, **2.3-9**, **2.3-10** and **2.3-5$_H$** shown in Part A, it is apparent that the steric hindrance around the metal center regularly increases when replacing the phenyl rings in **2.3-8** by biphenyl units (with intervals of ≈ 11%). The V_{Bur}% of **2.3-5$_H$**, [43–47]was calculated to be 64.5%, a value that exceeds those of commonly employed gold complexes JohnPhosAuCl **2.3-11** (50.7%),[49] XPhosAuCl **2.3-12** (53.4%)[50] and IPrAuCl **2.3-13** (46.3%)[51] (**Scheme 2.3-4, A**). Complexes **2.3-5$_{mtBu}$**

and **2.3-5$_{nPe}$** possess V_{Bur}% similar to **2.3-5$_{H}$**. The more sterically demanding *t*Bu groups in **2.3-5$_{nPe}$** are likely to account for the relative V_{Bur}% increase. Interestingly, a confined semi-hollow shaped complex **2.3-14**[52,53] and cavitand complex **2.3-15**[54] have comparatively low V_{Bur}% (32.1% and 37.6%, respectively), thus reflecting the limited steric hindrance in the Au coordination sphere. To account for the steric effect of the confining ligand in **2.3-15** and **2.3-16**, their G_{Au} parameter[55] which quantifies *the fraction of the Au coordination sphere shielded by the ligand* were calculated using the Solid-G software (**Scheme 2.3-4, A**).

***A*- Steric descriptors** [a]

	2.3-8	2.3-9	2.3-10	2.3-5$_{H}$	2.3-5$_{nPe}$	2.3-5$_{mtBu}$	2.3-11	2.3-12	2.3-13	2.3-14	2.3-15
V_{Bur} (%) [b]	30.8	42.4	53.6	64.5	63.5	67.5	50.7	53.4	46.3	32.1	37.6
G_{Au} (%) [c]	28.5	39.8	50.9	61.8	67.5	74.0	47.3	56.1	47.6	55.1	65.4
ECA (deg) [c]	128.5	156.6	182.0	207.3	216.5	237.4	173.7	194.1	174.5	181.6	216.0

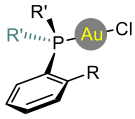

2.3-11 JohnPhosAuCl, R= Ph, R'= *t*Bu

2.3-12 XPhosAuCl, R= 2,4,6-*i*Pr$_3$C$_6$H$_2$, R'= *t*Bu

2.3-13 IPrAuCl

2.3-14

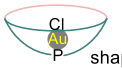

Sawamura *semi-hollow* shaped complex

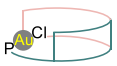

Iwasawa *cavitand* complex

2.3-15

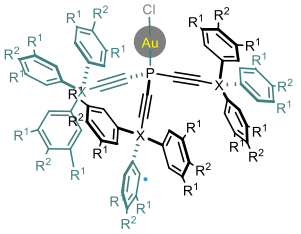

2.3-14 X= Si, R^1= SiMe$_3$, R^2= H

2.3-16 X= C, Si; R^1= *t*Bu, R^2= OMe

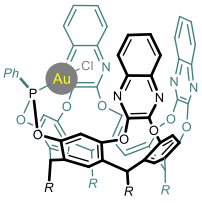

R = $C_{11}H_{23}$

2.3-15

***B*- XRD structures** [d]

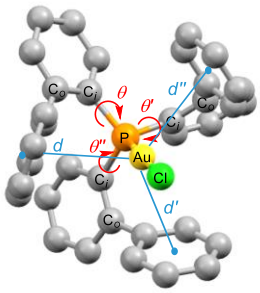

2.3-5$_{H}$

P-Au = 2.231 Å

[d] = 3.48 Å

[θ] = 35.7°

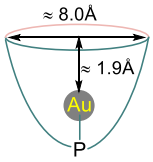

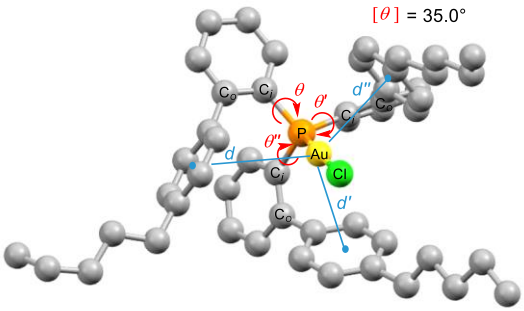

2.3-5$_{nPe}$ P-Au = 2.230 Å [d] = 3.58 Å [θ] = 35.0°

C_i : carbon *ipso* C_o : carbon *ortho*

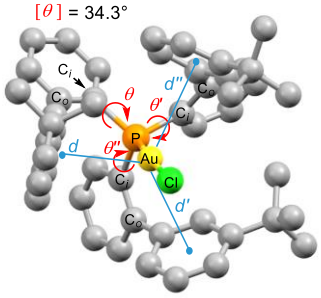

2.3-5$_{mtBu}$ P-Au = 2.231 Å [d] = 3.47 Å [θ] = 34.3°

Scheme 2.3-4. Comparative analysis of steric parameters and SCXRD structures. [a] Results by Prof. Fabien Gagosz. [b] Topographic steric maps and VBur% were calculated using SambVca 2.1. [c] Solid angles projections (coloured in red) were obtained using SolidAngleGL. GAu and EDA were calculated using Solid-G. [d] Ball-and-stick representations of tri-(ortho-biaryl)phosphine AuI complexes **2.3-5** (H-atoms omitted for clarity, rendered in PovRay). d, d' and d'' are distances from the gold atom to the o-aryl centroid and [d] is the average distance value. θ, θ' and θ'' are Au-P-Ci -Co torsion angles as shown on the structural representations and [θ] is the average value.

This steric parameter "measures the probability of an incoming reagent not accessing the metal center" and can therefore be used to evaluate remote sterics. As expected, **2.3-15** and **2.3-16** have high G_{Au} values of 55.1% and 65.4%, respectively, which reflect the cavity shaped by the ligand around the metal center. In contrast, the difference between the V_{Bur}% and G_{Au} values are not as pronounced for complexes **2.3-5$_H$**, **2.3-5$_{mtBu}$** and **2.3-5$_{nPe}$** thus showing that, in these cases, the ligand sterics mainly affect the first Au coordination sphere. For complexes **2.3-5$_H$**, **2.3-5$_{mtBu}$** and **2.3-5$_{nPe}$** the size of the substituents on the *ortho*-aryl moiety of the ligand are shown to have a direct effect on their G_{Au} value. The ECA (Equivalent Cone Angle) values of the ligands were derived from the G_{Au} parameters (**Scheme 2.3-4, A**). Large values varying between 207° and 237° were obtained for complexes **2.3-5$_H$**, **2.3-5$_{mtBu}$** and **2.3-5$_{nPe}$**. Solid angle spherical projections, which are 3D representations of the ligand shielding around the metal center, could also be generated for complexes **2.3-5$_H$**, **2.3-5$_{mtBu}$**, **2.3-5$_{nPe}$** and **2.3-8**, **2.3-9, 2.3-10** using the SolidAngleGL software (**Scheme 2.3-4, B**). The red-coloured projections, visualized from three directions (front, side and back views), allow for a rapid and qualitative comparison of the reactive site accessibility. The completely open catalytic site observed in the projections of triphenylphosphine AuCl complex **2.3-8** appears to be gradually shuttered by converting phenyl groups into biphenyl ones (compare front and back views for **2.3-8, 2.3-9, 2.3-10** and **2.3-5$_H$**). The capping of the gold center by the three *ortho*-biphenyl units in complex **2.3-5$_H$** can be clearly seen, the side view direction appearing to be a privileged access path for potential incoming substrates. Despite the clear utility of the V_{Bur}% and G_{Au} steric parameters for appreciating, rationalizing, or predicting catalytic activities, the values remain calculated from SCXRD data. They do not account for the dynamics of metal ligand complexes in solution and can therefore only partially reflect their behaviour.

With the structural analyses of representative complexes **2.3-5$_H$**, **2.3-5$_{mtBu}$** and **2.3-5$_{nPe}$** having shown that these species could potentially behave as confined catalysts, we then focused our attention on evaluating the catalytic activity of the newly synthesized complexes **2.3-5**.

2.3.4. Product selectivity

The prototypical cycloisomerization of propargyl malonate **2.3-17** was first examined (**Scheme 2.3-5**). Under homogeneous Au-catalysis, **2.3-17** is known to produce an intermediate **2.3-17i**[56] which can subsequently evolve into either **2.3-17a** or **2.3-17b** following an *exo*- or *endo*cyclic skeletal rearrangement, respectively.[8,11,13,57] A mixture of **2.3-17a** and **2.3-17b** is generally obtained with classical phosphine or NHC based Au(I) complexes, with the formation of the 6-

membered cycle **2.3-17** being favoured.[6,8,13,34,58,59] However, DFT calculations performed by the group of Echavarren on model 1,6-enynes showed that the TS leading to **2.3-17a**[8] has a comparatively more compact geometrical arrangement around the metal center than that leading to **2.3-17b**.[57]

We therefore considered that in the presence of a more geometrically constrained catalytic environment, as should be the case for Au(I) complexes **2.3-6**, a change in product selectivity could potentially be observed. To properly evaluate the catalytic activity of complexes **2.3-6**, the reaction was performed in parallel and under the same experimental conditions (1 mol% of catalyst, CD_2Cl_2 [0.2M], 20°C) with a selection of commonly employed gold complexes (**2.3-20 – 2.3-23**). All reactions were monitored by ^{1}H NMR spectroscopy and the yields determined relative to an internal standard (see **Appendix** for more details). In agreement with the literature,[6,8,13,34,58,59] the use of complexes **2.3-20 – 2.3-23** led to the formation of **2.3-17a** and **2.3-17b** in moderate to high yields (63-99%) and in mixtures varying from 1:1.8 to 1:4.7 in favor of **2.3-17b**. In sharp contrast, complexes **2.3-6** uniformly exhibit the opposite selectivity. In these cases, compound **2.3-17a** was not only produced with selectivity greater than 8:1, but also in high yields (> 92%). Notably, the substitution on the *ortho*-aryl moiety of the ligand had little influence on the outcome of the reaction. The use of ligand **2.3-4$_{mnBu}$** required a slightly longer time to reach completion (1 h versus 0.5 h). Most importantly, an almost quantitative yield and nearly perfect selectivity (>30:1) could be obtained when **2.3-6$_H$** possessing the simplest tri-(*ortho*-biphenyl)phosphine ligand **2.3-4$_H$** was employed. The nature of the counteranion did not greatly affect the outcome of the reaction (compare **2.3-4$_H$** and **2.3-7**). To the best of our knowledge, such a selectivity (in nature and level) and efficiency have rarely been achieved.[37,60–63] To point out the importance of the biaryl units on the ligand, the reaction was also performed with complex **2.3-19** which possesses only two *ortho*-biphenyl motifs in its ligand structure **2.3-18** and is therefore lacking the confined catalytic pocket observed for complexes **2.3-6** (see representations of AuCl complex **2.3-10** in **Scheme 2.3-3**). Consistent with our proposal, complex **2-19** was shown to behave as **2.3-20 – 2.3-23** producing **2.3-17b** with a similar 2.5:1 selectivity.

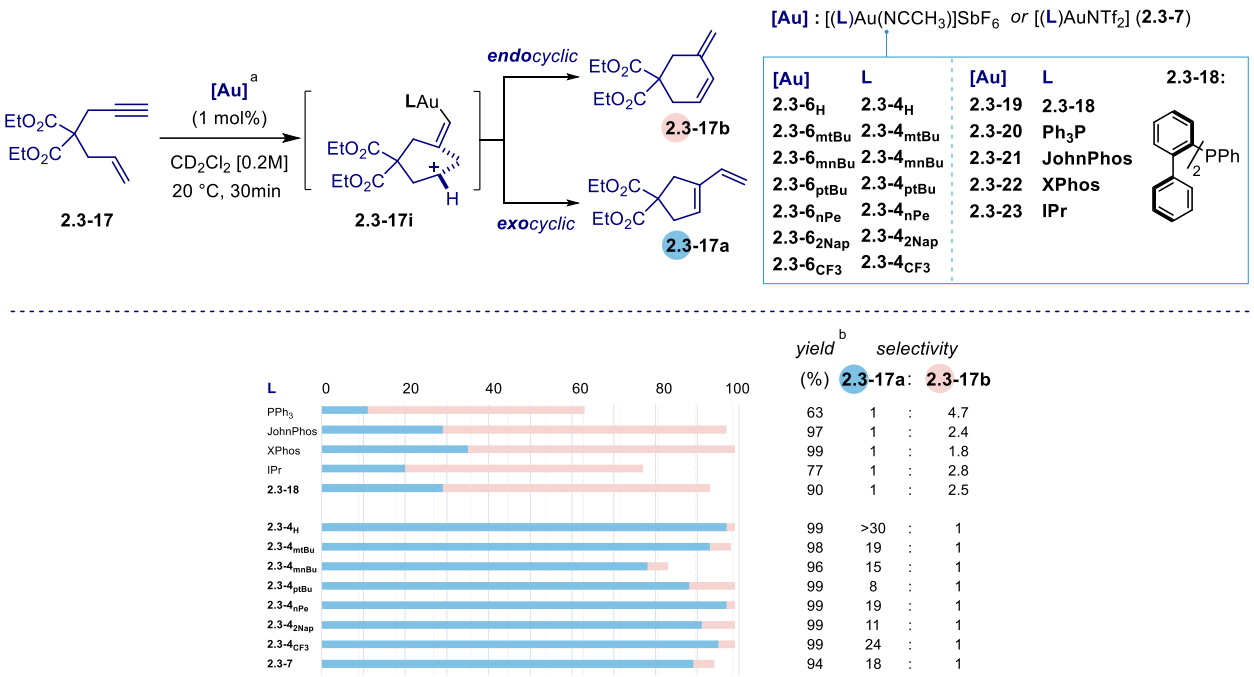

Scheme 2.3-5. Cycloisomerization of propargyl malonate **2.3-17**. [a] Reactions performed at 0.08-0.1 mmol scale using NMR tubes. [b] Yield determined by ^{1}H NMR spectroscopy analysis of the crude reaction mixture using mesitylene as an internal standard.

The selectivity towards the formation of the 5-membered cycle seen with substrate **2.3-17** was also observed with propargylmalonates **2.3-24** and **2.3-25** (**Scheme 2.3-6**). For cinnamyl derivative **2.3-24** (**Scheme 2.3-6, A**),[13,64–68] no trace of compound **2.3-24b** could be observed, and **2.3-24a** was produced in high yield with either catalyst **2.3-6$_H$** (90%) or **2.3-6$_{mtBu}$** (95%) used at a 0.5 mol% loading. These results contrast once again with the completely unselective reaction obtained with complexes **2.3-19 – 2.3-23**(**2.3-24b**:**2.3-24a**≈1.2:1). Interestingly, the IPr ligand was found to have a similar effect to **2.3-4$_H$** and **2.3-4$_{nPe}$** on the outcome of this reaction.[68] While methallyl derivative **2.3-25** was shown to be converted into **2.3-25a** with moderate to high selectivity in the presence of classical catalysts (**Scheme 2.3-6, B**),[6,13,62,69,70]complexes **2.3-6$_H$** and **2.3-6$_{nPe}$** proved to be not only completely selective but highly efficient (>95% yield). Very similar results were obtained in the case of *trans*-crotyl and prenyl substrates **2.3-26** (**Scheme 2.3-6, C**) and **2.3-27** (**Scheme 2.3-6, D**).[6,13]

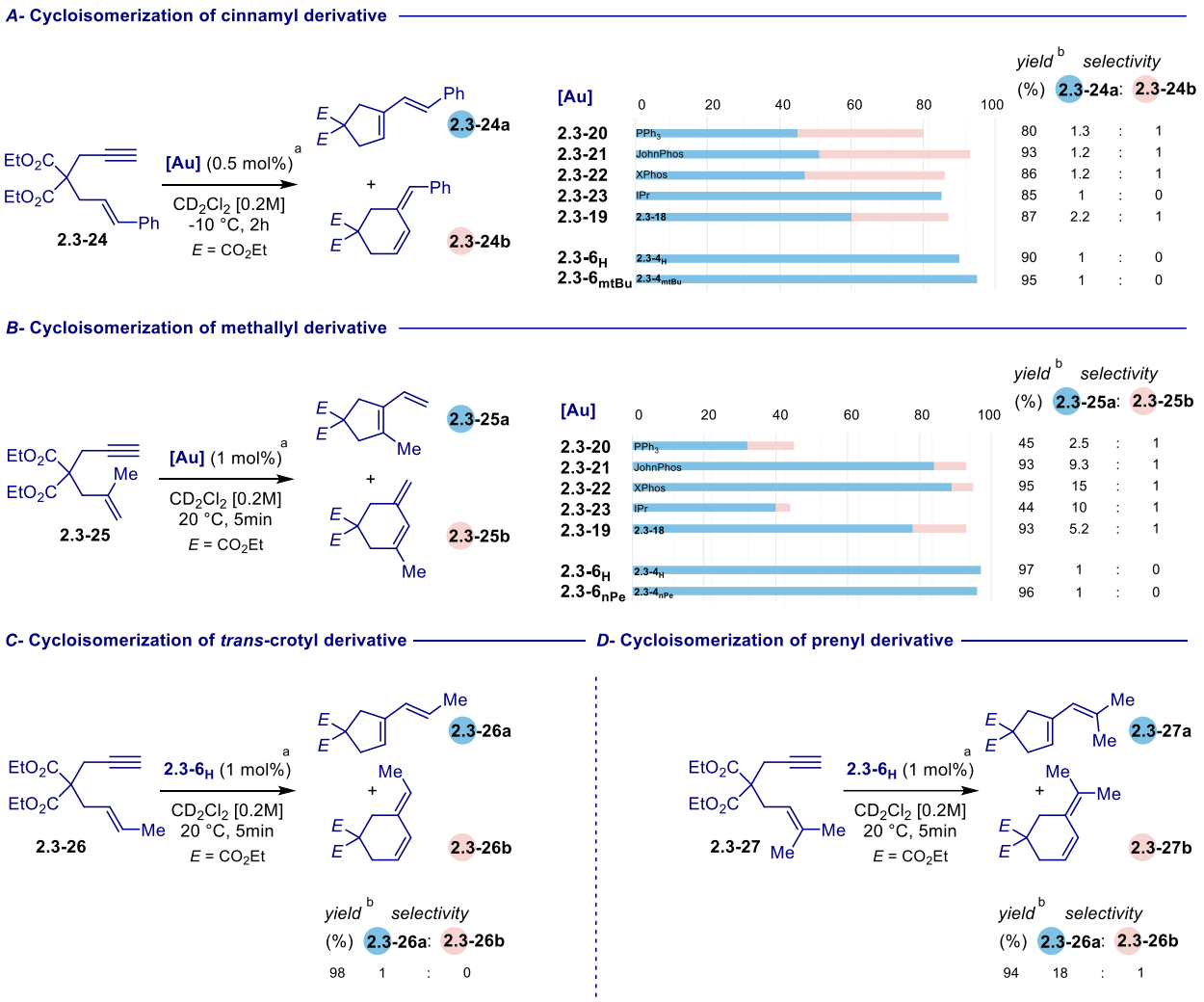

Scheme 2.3-6. Cycloisomerization of various diethyl propargylmalonates. [a] Reactions performed at 0.08-0.1 mmol scale using NMR tubes. [b] Yield determined by ^{1}H NMR spectroscopy analysis of the crude reaction mixture using mesitylene as an internal standard.

The catalytic activity of complexes **2.3-4$_H$** and **2.3-4$_{mtBu}$** was also evaluated in the cycloisomerization reaction of 1,6-enynes bearing a tosylamide linker (**Scheme 2.3-7**). For allyl derivative **2.3-28** (**Scheme 2.3-7, A**), both **2.3-4$_H$** and **2.3-4$_{mtBu}$** were very active (< 0.25h), efficient (> 95%) and selective towards the formation of the 6-*endo*-dig cyclization product **2.3-28c** (up to 30:1). By comparison, catalysts **2.3-19 – 2.3-23** generally delivered a mixture of the three products **2.3-28a**, **2.3-28b** and **2.3-28c** in moderate yield (40% in average) and low *endo*/*exo* selectivity. While catalysts **2.3-19 – 2.3-23** were more efficient in cyclizing methallyl tosylamide **2.3-29** than **2.3-28** (**Scheme 2.3-7, B**), their selectivity did not compete with that observed when **2.3-4$_{mtBu}$** was employed (> 30:1). Remarkably, while these two cycloisomerization reactions can potentially furnish three products, complex **2.3-4$_{mtBu}$** not only delivers the 6-*endo-dig* product **2.3-29c** very selectively, but no trace of the *endo*-skeletal rearrangement product **2.3-29b** could be observed.

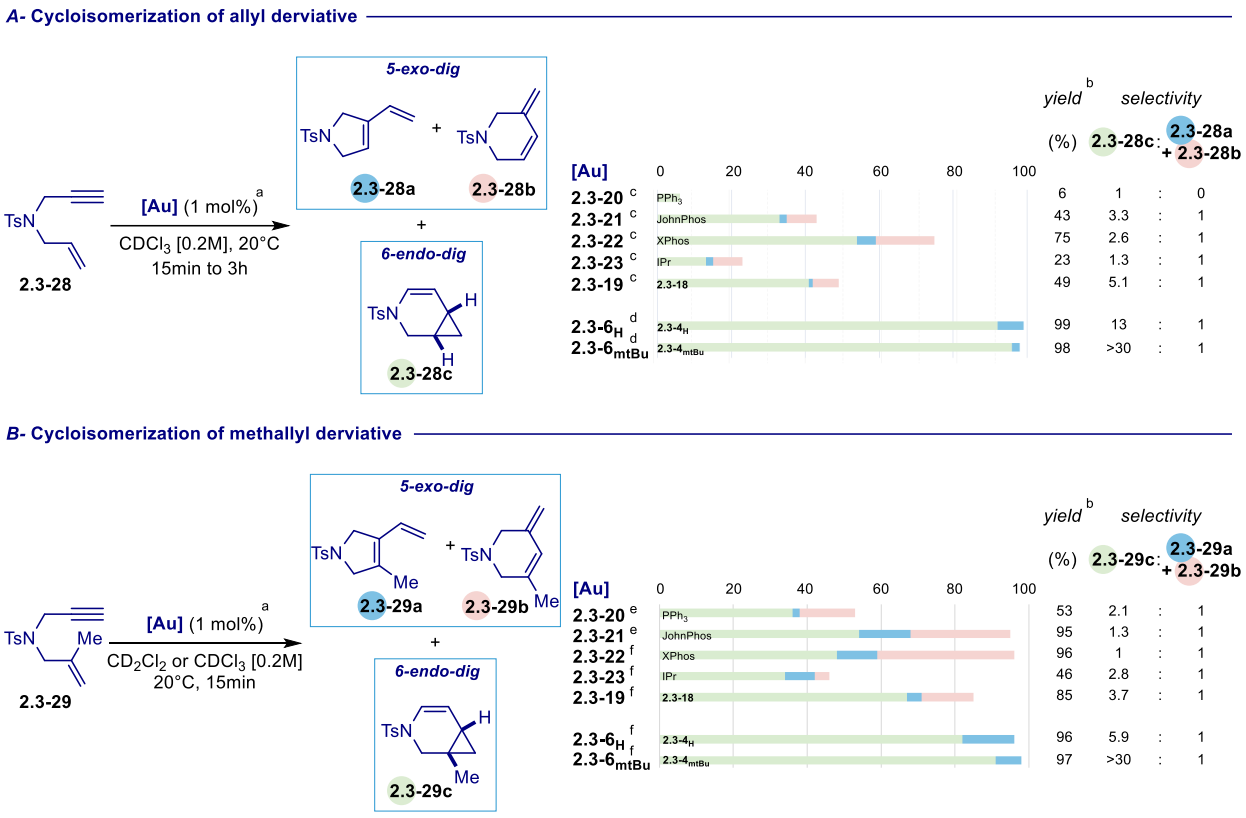

Scheme 2.3-7. Cycloisomerization of *N*-propargyltosylamide derivatives. [a] Reactions performed at 0.08-0.1 mmol scale using NMR tubes. [b] Yield determined by ^{1}H NMR spectroscopy analysis of the crude reaction mixture using mesitylene as an internal standard. [c] Run for 3h. [d] Run for 15min. [e] Run in $CDCl_3$. [f] Run in CD_2Cl_2.

In our study of cyclization reactions, we found that substrates **2.3-30** and **2.3-31** demonstrated a bias toward the formation of 5-exo-dig cyclization products.[15] However, using the developed catalysts **2.3-6**, we were able to override this intrinsic selectivity for compound **2.3-30**, resulting in the preferential formation of the 6-endo-dig product **2.3-30c** (**Scheme 2.3-8, A**). In contrast, the inherent selectivity of compound **2.3-31** was not entirely overridden by the **2.3-6** series catalysts, although we observed the formation of a detectable amount of the 6-endo-dig product **2.3-31c** (**Scheme 2.3-8, B**). Interestingly, the more sterically hindered catalyst **2.3-6$_{nPe}$**, demonstrated a slightly better performance over the simple **2.3-6$_H$**. It should be noted that attempts to use the cinnamyl derivative **2.3-33** did not provide a reliable result due to the rapid decomposition of cycloisomerization products.

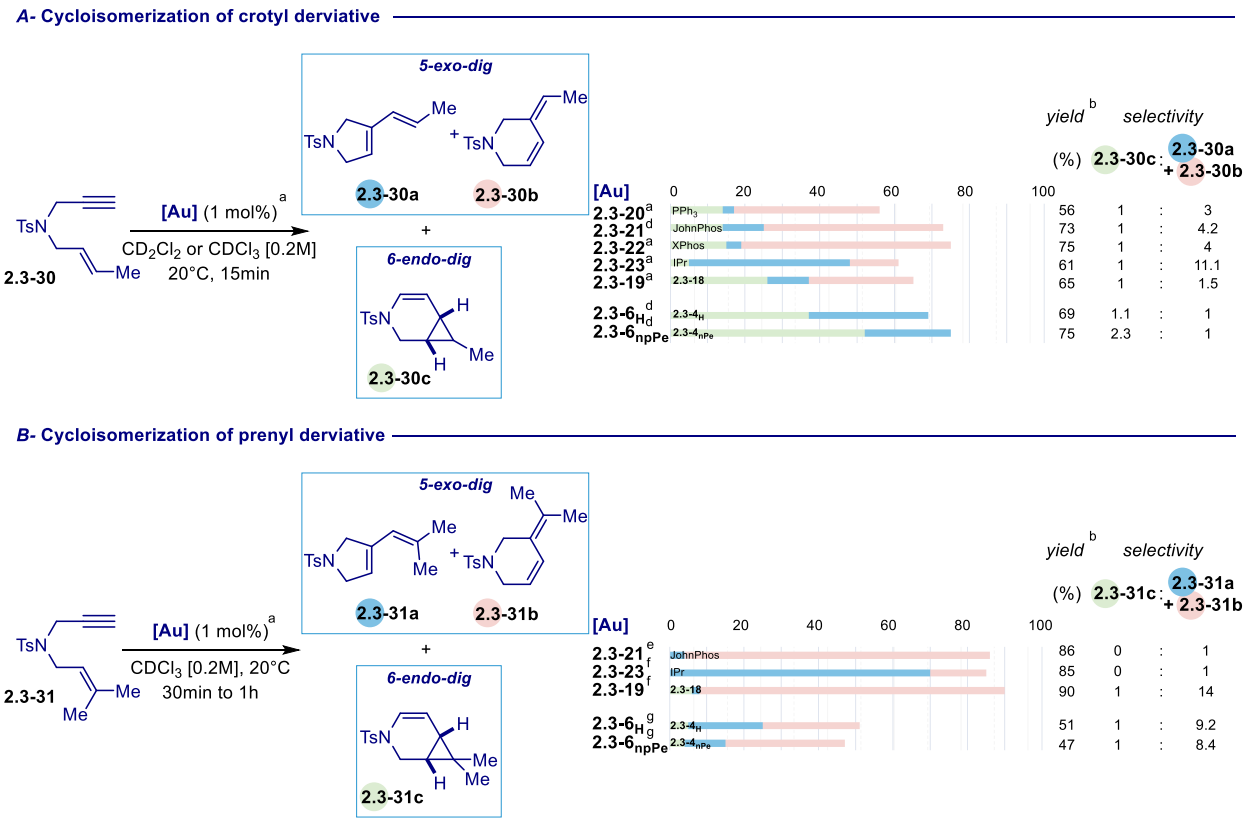

Scheme 2.3-8. Cycloisomerization crotyl and prenyl derivatives. [a] Reactions performed at 0.08-0.1 mmol scale using NMR tubes. [b] Yield determined by ^{1}H NMR spectroscopy analysis of the crude reaction mixture using mesitylene as an internal standard. [c] Run in $CDCl_3$. [d] Run in CD_2Cl_2. [e] Run for 15min. [f] Run for 30min. [g] Run for 1h.

Interestingly, *bis*-cyclopropane **2.3-32a**, the sole product formed when malonate **2.3-24** is treated at low temperature with an excess of styrene in the presence of [(JohnPhos)Au(NCMe)]SbF_6 (**2.3-21**) (**Scheme 2.3-9**),[66] was not observed when **2.3-6$_H$** was employed as the catalyst. Such an orthogonal reactivity can be rationalized by the difficulty for the styrene to access the reactive Au-*C* center in intermediate **2.3-24i** when the bulky tri-(*ortho*-biphenyl)phosphine **2.3-4$_H$** is employed as the ligand. In this case, the cycloisomerization sequence proceeds to yield **2.3-24b**, analogously to what has been observed in the absence of styrene (**Scheme 2.3-6, A**).[71] A similar observation was made when an excess of 1,3-dimethoxybenzene was used (**Scheme 2.3-9**).[14,65] Catalyst **2.3-21** delivered a mixture of three products, among which **2.3-32b**, resulting from the trapping of intermediate **2.3-24i** by the arene, was predominant (47% yield). In contrast, complex **2.3-6$_H$** favored a selective intramolecular reaction (81% yield) with little trapping product being formed. Such reactivity may have some applications in synthesis since the steric protection of reactive intermediates could prevent side-product formation in the presence of external nucleophiles.

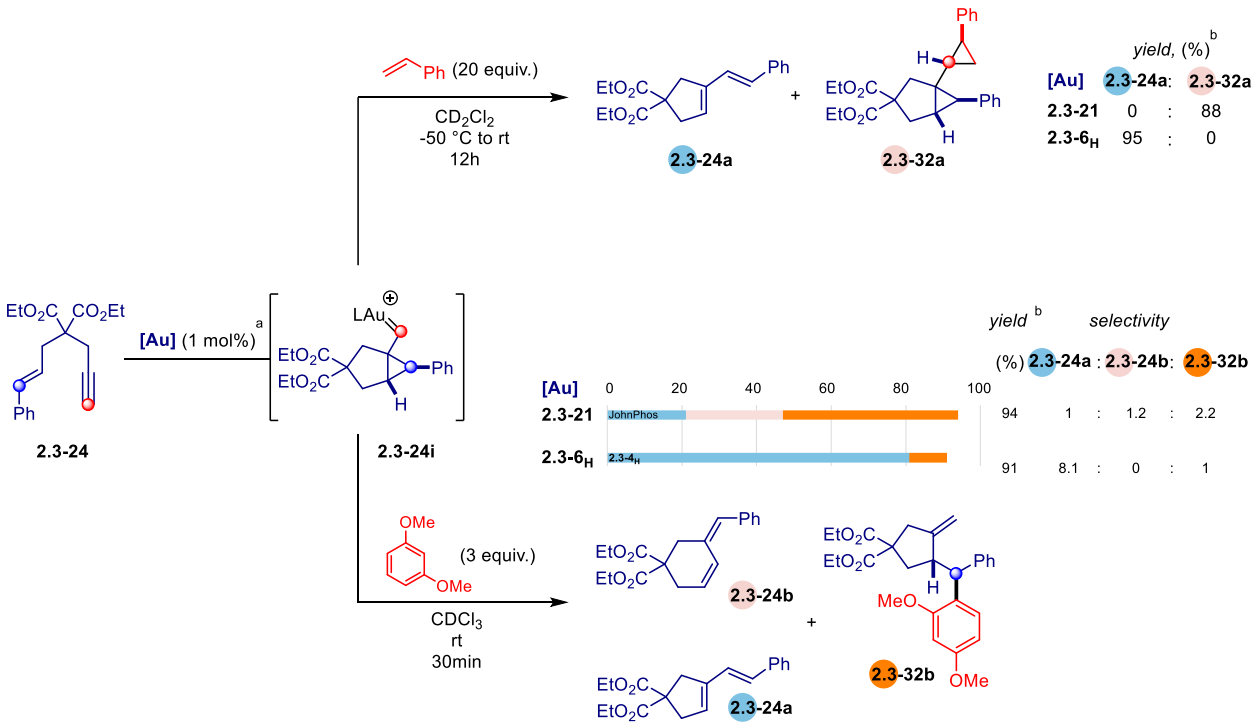

Scheme 2.3-9. Interrupted cycloisomerizations. [a] Reactions performed at 0.1 mmol scale using NMR tubes. [b] Yield determined by ^{1}H NMR spectroscopy analysis of the crude reaction mixture using mesitylene as an internal standard.

To further investigate this finding, we extended our studies to a trapping experiment using indole and a 1,6-enyne substrate **2.3-33**, which has a tosylamide linker and a cinnamyl group (**Scheme 2.3-10, A**).[20,22,72,73] When catalysts **2.3-21** and **2.3-23** were employed, we observed the formation of a mixture of trapping products **2.3-30a** and **2.3-30b**. Notably, product **.32-33b**, formed by the trapping of intermediate **2.3-33i** at the carbene position by indole, was the predominant species and accounted for a 57% yield using catalyst **2.3-21**. In contrast, the use of catalyst **2.3-6$_H$** resulted in selective trapping at the benzylic position of intermediate **2.3-37i** in 81% yield, while the formation of product **2.3-33b** was completely suppressed. This particular selectivity can be explained in a similar way by taking steric hindrance into account, when the bulky tri-(ortho-biphenyl)phosphine ligand **2.3-4$_H$** hinders the indoles' ability to access the carbene center in intermediate **2.3-33i**.

To further substantiate the lack of reactivity at the carbene center, we performed a carbene trapping experiment using styrene as a trapping agent (**Scheme 2.3-10, B**) and compound **2.3-34** as the carbene precursor.[74] The use of catalyst **2.3-21** led to the formation of product **2.3-35** in 86% yield, highlighting the reactivity of the carbene centers. On the other hand, no product was detected when catalyst **2.3-6$_H$** was used. Interestingly, the reaction mixture initially showed a bright yellow color, suggesting the possible formation of a Au–carbene complex. Despite this colorimetric evidence, our efforts to synthesize and isolate this putative Au-carbene complex

were unsuccessful. These observations support the hypothesis that steric hindrance in catalyst **2.3-6$_H$** effectively inhibits reactivity at the carbene center.

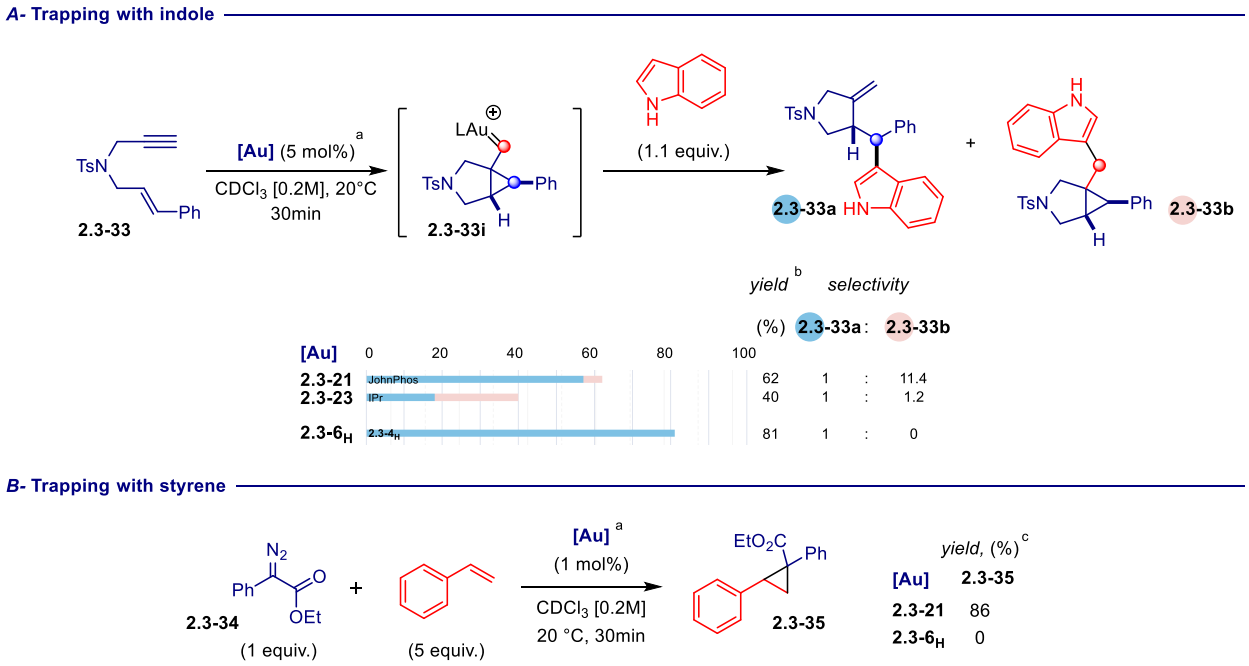

Scheme 2.3-10. Carbene trapping experiments. [a] Reactions performed at 0.1 mmol scale using NMR tubes. [b] Yield determined by ^{1}H NMR spectroscopy analysis of the crude reaction mixture using mesitylene as an internal standard. [c] DCE was used as an internal standard.

2.3.5. Substrate selection in the cycloisomerization reaction

We continued our investigations by studying if the geometrically constrained catalytic environment of the newly synthesized gold complexes could be advantageously exploited to discriminate between substrates of similar structure. Our attention was focused on comparing the cycloisomerization reactions of 1,7-enynes **2.3-35** and **2.3-36**, substrates that differ by the position of the malonate unit in the ene-yne linker (**Scheme 2.3-11**).[75]

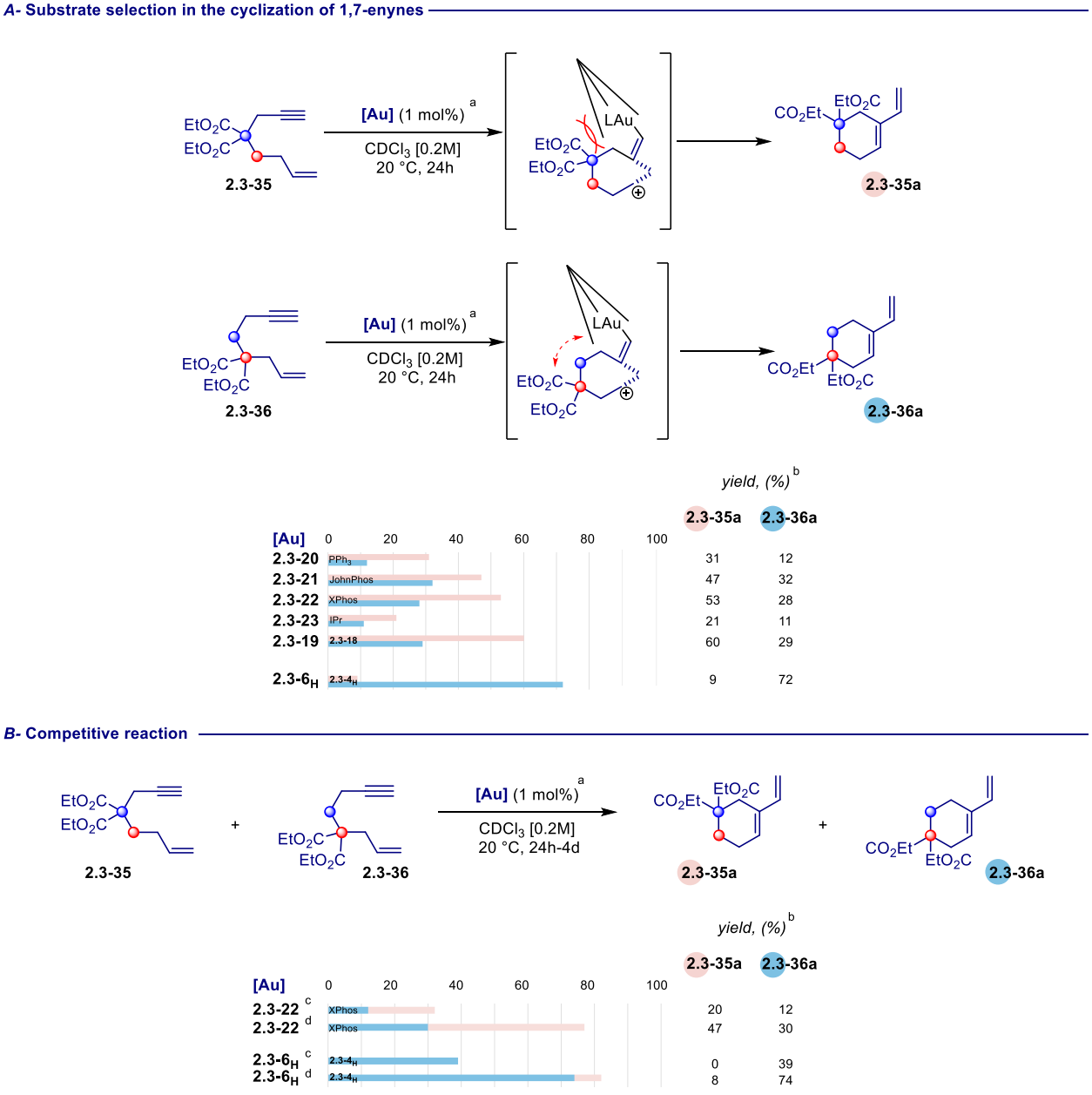

Scheme 2.3-11. Substrate selection in the cyclization of 1,7-enynes. [a] Reactions performed at 0.1 mmol scale using NMR tubes. [b] Yield determined by ^{1}H NMR spectroscopy analysis of the crude reaction mixture using mesitylene as an internal standard. [c] Run for 24h. [d] Run for 4d.

We considered that the closer in proximity to the alkyne (and therefore to the gold atom) the sterically demanding malonate moiety, the less easily it could be accommodated in the catalytic pocket. Following this hypothesis, a more remote malonate moiety as featured in enyne **2.3-36** would lead to a more effective transformation with tri-(*ortho*-biaryl)phosphine ligands and a selection could potentially be achieved between substrates **2.3-35** and **2.3-36**. To evaluate such a possibility, the reactions of enynes **2.3-35** and **2.3-36** were first run in parallel under the same conditions and the outcomes analyzed using ^{1}H NMR spectroscopy. As seen in the graph depicted

in **Scheme 2.3-11, A,** classical catalysts **2.3-20 – 2.3-23** as well as bis-(*ortho*-biphenyl)phosphine based complex **2.3-19** favor both the conversion of **2.3-35** and the corresponding formation of **2.3-35a**. Highest yields of **2.3-35a** and apparent selectivity for the conversion of **2.3-35** was obtained with XPhos and the bis-(*ortho*-biphenyl)phosphine ligand **2.3-18** (complexes **2.3-22** and **2.3-19**, respectively). In contrast, when complex **2.3-6$_H$** was employed, minimum conversion of substrate **2.3-35** was observed, while a remarkably efficient transformation of **2.3-36** into **2.3-36a** took place. Compound **2.3-36a** was formed in 72% yield, a value at least two-fold greater than those obtained with catalysts **2.3-20 – 2.3-23** (<32%). This selectivity was confirmed when an equimolar mixture of **2.3-35** and **2.3-36** was treated with 1 mol% of **2.3-6$_H$** under the same conditions (**Scheme 2.3-11, B**). After 24h, substrate **2.3-35** was hardly consumed and only traces of compound **2.3-35a** were observed. Conversely, cyclohexene **2.3-36a** was produced in 39% yield. The lower conversion of **2.3-36** observed when **2.3-35** is also present in the reaction medium (42% versus 73%) can be attributed to the competitive binding of **2.3-35** to the gold center. After 4 days, a substrate selectivity higher than 9:1 was found in favor of enyne **2.3-36**, and **2.3-36a** was produced in 74% yield. In sharp contrast, the competitive reaction in the presence of complex **2.3-22** led to a poor 1.6:1 selectivity in favor of the other enyne **2.3-35**. These results represent a fascinating example of substrate selection and reaction rate enhancement enabled by a sterically constrained catalytic environment.

2.3.6. Stereoselectivity

Another manifestation of the confinement effect exerted by the tri-(*ortho*-biaryl)phosphine ligands was observed in the cycloisomerization of 1,6-enyne **2.3-37** (**Scheme 2.3-12**).[8,11,57] In this transformation, a double cleavage of the enyne takes place to initially produce a gold carbene intermediate **2.3-37i**. Cyclopentene derivative **2.3-38** is subsequently produced following a proton loss/demetallation sequence. The reaction was run for 24h at 20°C for complexes **2.3-19 – 2.3-22**. For the (IPr)Au complex **2.3-23** heating to 40 °C was required to observe a similar level of reactivity.

Consistent with previous reports,[8,11,57]catalysts **2.3-19 – 2.3-23** efficiently produced cyclopentene derivative **2.3-38** (74-87%) as a *E*:*Z* mixture of stereoisomers largely in favour of the *trans* isomer (*E*:*Z* > 8.7:1). In sharp contrast, the use of complexes **2.3-6H** and **2.3-7** delivered **2.3-38** with a complete reversal in selectivity, which in the case of **2.3-6H**, was found to be as high as *E*:*Z*= 1:4.4. Similarly to complex **2.3-23**, gold complexes **2v-6H** and **2.3-7** were less active and gently heating the reaction mixture to 40 °C was required to achieve a similar conversion to that observed at 20 °C with **2.3-19 – 2.3-22**. Alternatively, increasing the loading of **2.3-7** to 5 mol% while running the reaction at 20 °C, allowed for the same level of efficiency and selectivity (82% yield, *E*:*Z*=1:4.9). Control experiments showed that the *E*:*Z* ratio remained constant over the course of the reaction. Treatment of the *E* isomer with complex **2.3-6** under the same experimental conditions did not provide the *Z* isomer. Such a reversal in stereoselectivity can be tentatively explained by considering the two conformers **2.3-37i$_{cis}$** and **2.3-37i$_{trans}$** leading to **2.3-38*E*** and **2.3-38*Z***,

respectively. When tri-(*ortho*-biphenyl)phosphine **2.3-4H** is employed as the ligand (*i.e.* for catalysts **2.3-6H** and **2.3-7**), the cyclopentenyl unit would most probably prefer to be positioned *trans* to the AuL fragment as shown in conformer **2.3-37i*trans*** to limit its steric interaction with the bulky ligand. In the case of the far less sterically demanding ligands **2.3-19 – 2.3-23**, the cyclopentenyl motif could be more easily accommodated around the metal center thus allowing the formation of the more stable **2.3-38*E*** isomer. This result is a remarkable illustration of how the confinement of a reactive site can profoundly alter the stereochemical outcome of a reaction.

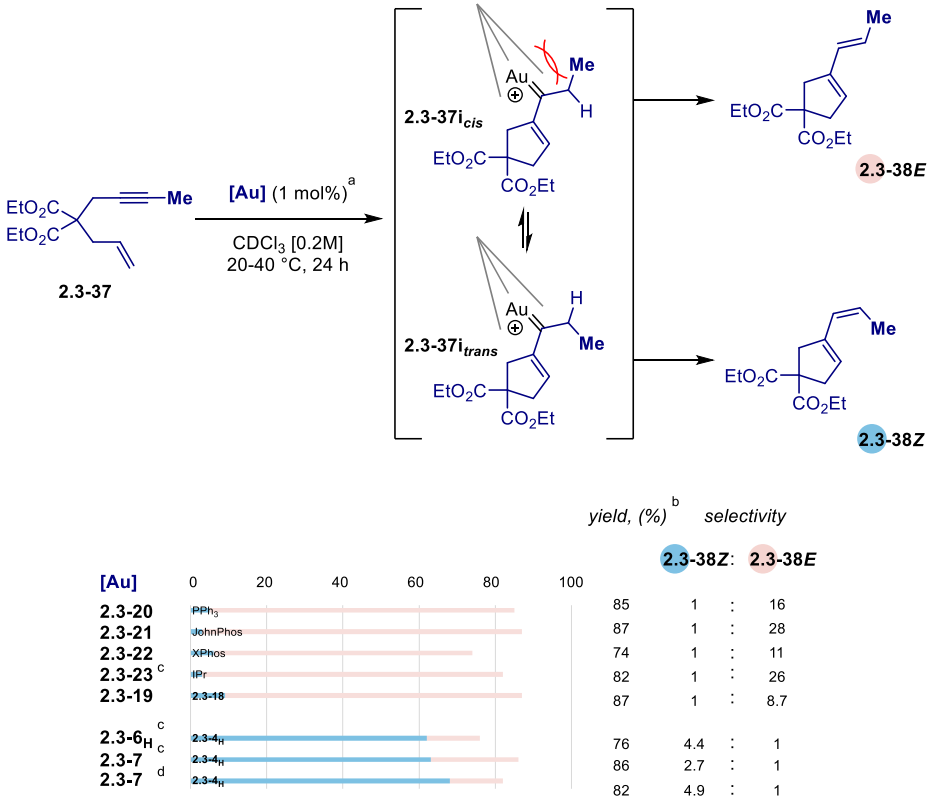

Scheme 2.3-12. (*E*,*Z*)-Stereoselectivity in the cycloisomerization of 1,6-enyne. [a] Reactions performed at 0.1 mmol scale using screw-cap NMR tubes and an oil bath with temperature regulation. [b] Yield determined by ^{1}H NMR spectroscopy analysis of the crude reaction mixture using mesitylene as an internal standard. [c] run at 40 °C. [d] run with 5 mol% of catalyst.

2.3.7. Regioselectivity

We continued our studies by considering the possibility to employ the confined tri-(*ortho*-biaryl)phosphine Au(I) complexes to induce regioselectivity in the nucleophilic intermolecular functionalization of alkynes. The prototypical hydration reaction of phenylpropyne **2.3-36** was used for this purpose.[28,76–78] As seen in **Scheme 2.3-13, A**, the use of the classical ligands Ph_3P, JohnPhos, XPhos and IPr along with bis-(*ortho*-biphenyl)phosphine ligand **2.3-18** delivered a

mixture of ketones **2.3-38a** and **2.3-38b** in high yields (78-99%), but with very low selectivity. Consistent with literature precedents,[43,44] the best selectivity was obtained with the IPr ligand (2.7:1). When ligand **2.3-4$_H$** was employed, a dramatic increase in regioselectivity (9.3:1) was observed and ketone **2.3-38a**, which results from an *anti*-Markovnikov nucleophilic addition to the alkyne, was predominantly formed. A longer reaction time (6h versus 1h for classical ligands and **2.3-18**) was, however, required.

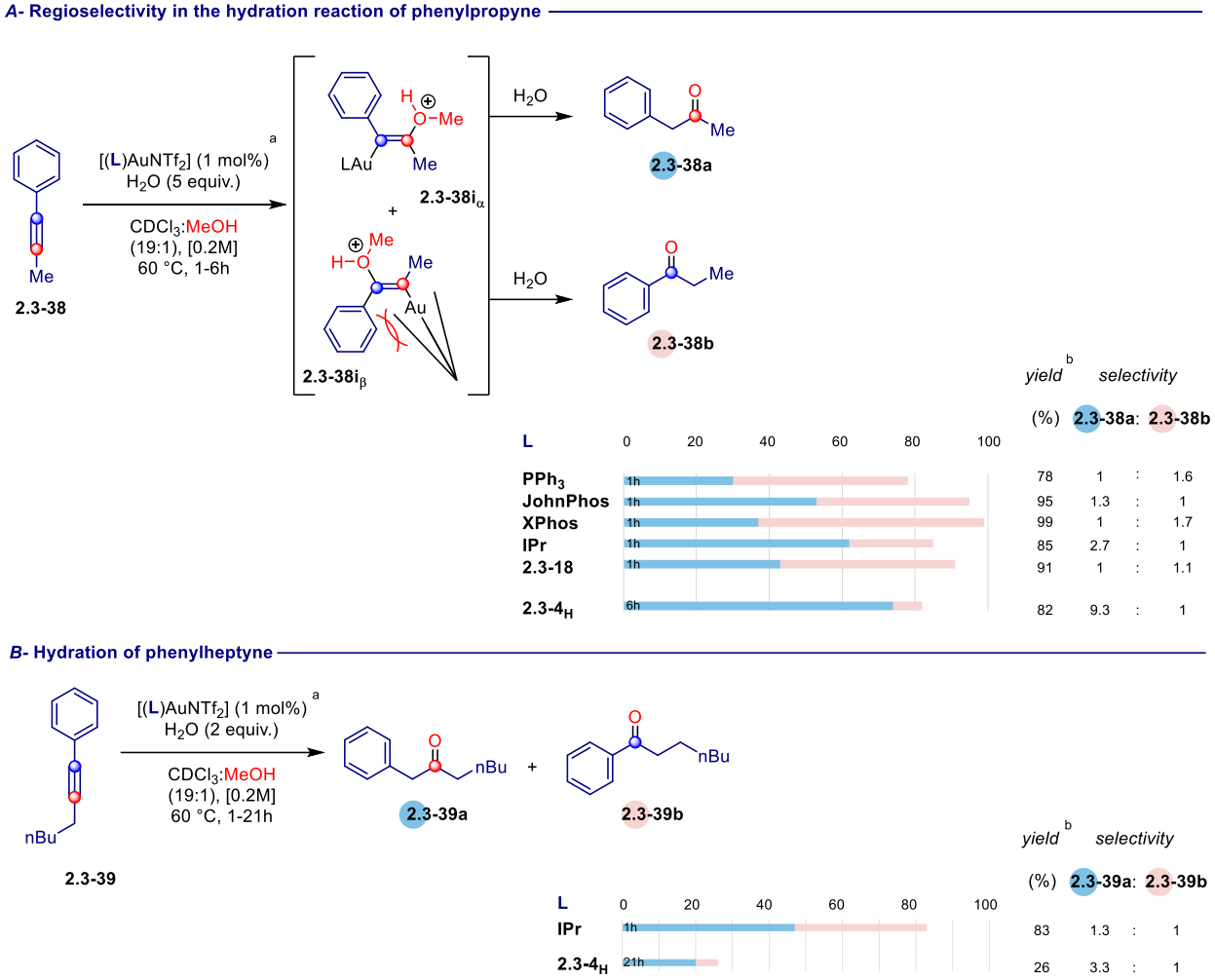

Scheme 2.3-13. Regioselectivity in the hydration reactions. [a] Reactions performed at 0.1 mmol scale using screw-cap NMR tubes and an oil bath with temperature regulation. [b] Yield determined by ^{1}H NMR spectroscopy analysis of the crude reaction mixture using mesitylene as an internal standard.

The origin of the high regioselectivity observed may be the greater steric repulsion between the phenyl moiety of the substrate and the *ortho*-phenyl rings of the ligand **2.3-4$_H$** in the TS leading to intermediate **2.3-38iβ**. A reaction *via* **2.3-38iα** would be more favourable since, in this case, the phenyl group would be pointing away from the coordination sphere. Similar levels of regioselectivity were recently reported for the hydration of alkylarylacetylenes using a 7-membered NHC as the ligand.[79]

Interestingly, when alkyne **2.3-39** with an extended alkyl chain was employed, the use of ligand **2.3-4$_H$** led to a marked deceleration in the reaction rate (26% yield after 21h). In contrast, the IPr ligand showed robust performance, achieving 83% yield after one hour (**Scheme 2.3-13, B**). Despite its slower kinetics, the **2.3-4$_H$** ligand outperformed IPr in selectivity, providing a ratio of 3.3:1, while IPr only achieved an approximately 1:1 product mixture. This disparity in reaction rates can be explained by the steric demands imposed by the longer alkyl chain. In particular, the extended chain hinders the access of the substrate to the catalytic center when bulkier **2.3-4$_H$** ligand was used, thereby slowing down the reaction.

2.3.8. Substrate selection in hydration reaction

Given the intriguing observations on substrate selectivity, we conducted a hydration of internal aliphatic alkynes. We performed an experiment with an equimolar mixture of alkynes **2.3-38** and **2.3-39** using both IPr and **2.3-4$_H$** ligands under identical reaction conditions (**Scheme 2.3-13, A**). Remarkably, we found that the IPr ligand enabled efficient reactivity for both substrates and showed little discrimination. In contrast, the use of the **2.3-4$_H$** ligand resulted in a pronounced selectivity in favor of substrate **2.3-38**. To corroborate these results, we performed hydration reactions on internal aliphatic alkynes (**Scheme 2.3-13, B**). Consistent with our previous observations, we found that the sterically demanding alkyne **2.3-41** showed limited reactivity in the presence of the **2.3-4$_H$** ligand. However, when the IPr ligand was used, both alkynes reacted rapidly and showed comparable reaction rates even at a temperature of 40 °C.

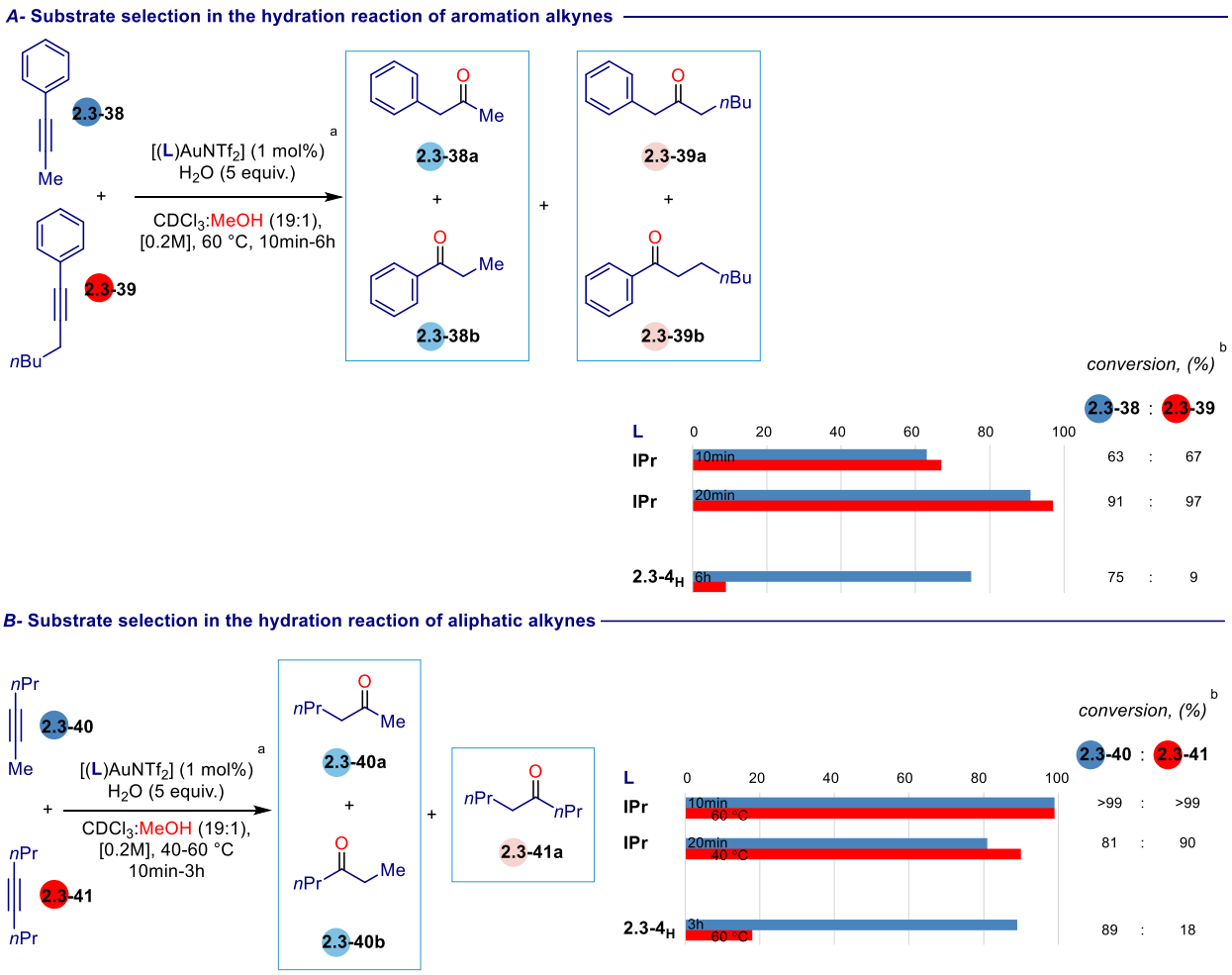

Scheme 2.3-14. Substrate selection in the hydration reactions. [a] Reactions performed at 0.1 mmol scale using screw-cap NMR tubes and an oil bath with temperature regulation. [b] Conversion determined by ^{1}H NMR spectroscopy analysis of the crude reaction mixture using mesitylene as an internal standard.

2.4. Conclusion

A series of tri-(*ortho*-biaryl)phosphine ligands could be readily synthesized and the corresponding AuCl complexes accessed. Their SCXRD analyses showed the Au atom to be confined inside the structures, capped, and surrounded by the three *ortho*-aryl units of the ligand. The sterically constrained nature of these complexes is reflected by their high V_{Bur}% and ECA values which have been calculated to be up to 67% and 237° respectively. Despite their notable steric congestion, these complexes exhibited remarkable catalytic activities thus showing their value as synthetic tools in organic chemistry. The limited accessible space in the coordination sphere of the metal could be advantageously exploited in a series of prototypical catalytic transformations showing the possibility to 1-increase and/or reverse product selectivity, 2- perform substrate selection, 3-accelerate substrate conversion, 4- reverse stereoselectivity and 5- enhance regioselectivity. Exchanging the *ortho*-aryl moiety of the phosphine ligand by a more flexible and appropriately

functionalized structural motif could allow the synthesis of gold complexes with a less congested and geometrically more adaptable catalytic pocket potentially amenable for specific transformations.

2.5. Experimental procedures

2.5.1. General information

Commercially available reagents were purchased from Sigma-Aldrich, Alfa-Aesar, Oakwood Chemicals, TCI America, Fluorochem Chemical or Combi-Blocks suppliers and were used as delivered without further purification unless otherwise noted. Dichloromethane stock was dried with 4Å MS. Reactions carried out under inert atmosphere were performed under nitrogen gas. Thin layer chromatography was performed on TLC Silicagel 60 F254 plates. Flash column chromatography was carried out on silica gel using a forced flow of eluents. NMR spectra were recorded at room temperature in the given deuterated solvent on a Bruker Avance II 400, Bruker Avance II 300 or Bruker Avance 300 instrument operating at the indicated frequency. Chemical shifts (δ) are given in parts per million (ppm) using CD_2Cl_2 and $CDCl_3$ solvent peaks as the reference for ^{1}H-NMR and ^{13}C-NMR spectra, respectively. Signal multiplicities are depicted using the following abbreviations: s = singlet, d = doublet, t = triplet, q = quartet, m = multiplet, dd = doublet of doublet, dt = doublet of triplet, tt = triplet of triplet, dq = doublet of quartet, ddd = doublet of doublet of doublet, ddt = doublet of doublet of triplet, bs = broad singlet. Proton decoupling was employed for all ^{13}C and ^{31}P spectra. High-resolution mass spectrometry by electron impact (HRMS-EI) was performed on a JEOL JMCGCmate II mass spectrometer, and high-resolution mass spectrometry by electrospray ionization (HRMS-ESI) was performed on a Micromass Q-TOF II Mass Spectrometer or ESI-MS (orbitrap Velos Pro). Molecular ion and/or fragment signals were given in mass per charge number (m/z).

2.5.2. Synthesis of *tris*-(*ortho*-biaryl)phosphine ligands 2.3-24, ligand 2.3-18 and Au(I) complexes 2.3-6 & 2.3-7

2.5.2.1. Synthesis of *tris*-(*ortho*-biaryl)phosphine ligands 2.3-4

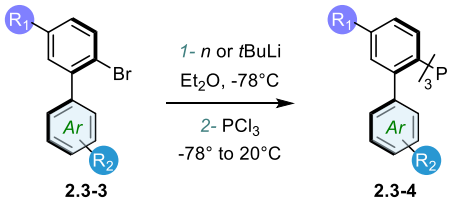

2.3-3 2.3-4

L	R_1	R_2	
2.3-4$_{H}$	H	H	45%
2.3-4$_{mtBu}$	H	3-*t*Bu	21%
2.3-4$_{mnBu}$	H	3-*n*Bu	56%
2.3-4$_{ptBu}$	H	4-*t*Bu	61%
2.3-4$_{nPe}$	H	4-*n*Pent	88%
2.3-4$_{2Nap}$	H	*Ar* : 2-Naphthyl	37%
2.3-4$_{CF3}$	CF_3	H	67%

General procedure 2-1:

The following procedure was repeated for the series of ligands **2.3-4**. A flame dried flask under nitrogen was charged with bromobiaryl (1 equiv.) and dry Et_2O [0.4 M]. The solution was cooled down to -78 °C before a solution of *n*BuLi in hexane (1.1 equiv.) or *t*BuLi in pentane (2 equiv.) was added dropwise. The mixture was stirred at -78 °C for 1h, and PCl_3 (0.25 eq.) was then added dropwise. At the end of the addition, the mixture was slowly warmed to room temperature and stirred overnight. The reaction mixture was quenched by addition of a saturated aqueous NH_4Cl solution and extracted with Et_2O. The combined organic layers were washed with brine and dried over anhydrous $MgSO_4$. The solvent was evaporated, and the product was purified by crystallization in acetone or EtOH, or by flash column chromatography.

tris([1,1'-biphenyl]-2-yl)phosphane (2.3-4_H)

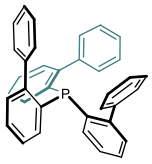

Prepared from 2-bromo-1,1'-biphenyl (1.1 mL, 1.5 g, 6.44 mmol), 2.5 M solution of *n*BuLi in hexane (2.8 mL, 7.08 mmol) and PCl_3 (168 µL, 264.4 mg, 1.93 mmol) according to the general procedure **2-1**.

Purification by crystallization in acetone.

2.3-4_H was obtained as a white solid: 427 mg, 45% yield.

^{1}H NMR (300 MHz, $CDCl_3$): δ(ppm) 7.31 (td, J = 7.4, 1.5 Hz, 1H), 7.22 (td, J = 7.5, 1.5 Hz, 1H), 7.18 – 7.06 (m, 4H), 7.00 (m, 1H), 6.77 (m, 2H).

^{13}C NMR (75 MHz, $CDCl_3$): δ(ppm) 148.0 (d, J = 30.1 Hz), 141.7 (d, J = 6.1 Hz), 136.5 (d, J = 19.2 Hz), 134.9, 129.8, 129.7, 128.3, 127.3, 127.2, 126.6.

^{31}P NMR (121 MHz, $CDCl_3$): δ(ppm) -28.6.

HRMS (ESI) Calculated for $C_{36}H_{28}P$ $[M+H]^+$: 491.1923; found: *m/z* 491.1929.

tris(3'-(tert-butyl)-[1,1'-biphenyl]-2-yl)phosphane (2.3-4_{mtBu})

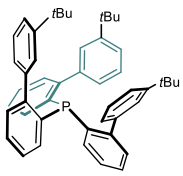

Prepared from 2-bromo-3'-(*tert*-butyl)-1,1'-biphenyl (277 mg, 0.96 mmol), 1.7 M solution of *t*BuLi in pentane (1.06 mL, 1.80 mmol) and PCl_3 (21.0 µL, 33.0 mg, 0.24 mmol) according to the general procedure **2-1**.

Purification by crystallization in ethanol.

2.3-4$_{mtBu}$ was obtained as a white solid: 34 mg, 21% yield.

^{1}H NMR (300 MHz, $CDCl_3$): δ(ppm) 7.34 (td, J = 7.4, 1.5 Hz, 1H), 7.30 – 7.21 (m, 2H), 7.19 – 7.13 (m, 1H), 7.08 (t, J = 7.7 Hz, 1H), 7.02 – 6.97 (m, 1H), 6.84 (bs, 1H), 6.67 – 6.61 (m, 1H), 1.13 (s, 9H).

^{13}C NMR (75 MHz, $CDCl_3$): δ(ppm) 149.8, 148.5 (d, J = 29.7 Hz), 141.3 (d, J = 6.2 Hz), 136.8 (d, J = 19.7 Hz), 134.8, 129.6 (d, J = 4.3 Hz), 128.2, 127.1, 127.0 (d, J = 3.9 Hz), 126.9, 126.8 (d, J = 4.4 Hz), 123.6, 34.5, 31.3.

^{31}P NMR (121 MHz, $CDCl_3$): δ(ppm) -26.3.

HRMS (ESI) Calculated for $C_{48}H_{52}P$ $[M+H]^+$: 659.3801; found: *m/z* 659.3824.

tris(3'-butyl-[1,1'-biphenyl]-2-yl)phosphane (2.3-4$_{mnBu}$)

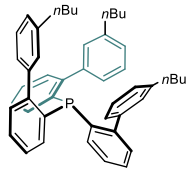

Prepared from 2-bromo-3'-(*n*-butyl)-1,1'-biphenyl (170 mg, 0.59 mmol), 1.7 M solution of *t*BuLi in pentane (0.7 mL, 1.17 mmol) and PCl_3 (15.4 µL, 24.2 mg, 0.18 mmol) according to the general procedure **2-1**.

Purification by flash column chromatography (Hexane:EtOAC = 98:2).

2.3-4$_{mnBu}$ was obtained as a yellowish solid: 65 mg, 56% yield.

^{1}H NMR (300 MHz, $CDCl_3$): δ(ppm) 7.30 (td, J = 7.4, 1.5 Hz, 3H), 7.22 (td, J = 7.5, 1.6 Hz, 3H), 7.18 – 7.07 (m, 3H), 7.05 – 6.92 (m, 9H), 6.58 (s, 6H), 2.48 – 2.30 (m, 6H), 1.49 – 1.29 (m, 6H), 1.28 – 1.18 (m, 6H), 0.87 (t, J = 7.1 Hz, 9H).

^{13}C NMR (75 MHz, $CDCl_3$): All peaks are listed due to being unable to determine coupling patterns. δ(ppm) 148.5, 148.1, 141.6, 141.6, 141.6, 136.9, 136.7, 134.9, 130.1, 130.0, 129.5, 129.5, 128.2, 127.1, 127.0, 126.9, 126.7, 35.7, 33.5, 22.6, 14.1.

^{31}P NMR (121 MHz, $CDCl_3$): δ(ppm) - 28.1.

HRMS (ESI) Calculated for $C_{48}H_{52}P$ $[M+H]^+$: 659.3801; found: *m/z* 659.3794.

tris(4'-(*tert*-butyl)-[1,1'-biphenyl]-2-yl)phosphane (2.3-4$_{ptBu}$)

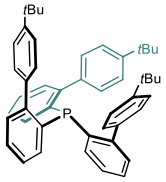

Prepared from 2-bromo-4'-(tert-butyl)-1,1'-biphenyl (552 mg, 1.91 mmol), 1.7 M solution of *t*BuLi in pentane (2.2 mL, 3.82 mmol) and PCl_3 (41.8 µL, 69.7 mg, 0.5 mmol) according to the general procedure **2-1**.

Purification by crystallization in acetone.

2.3-4$_{ptBu}$ was obtained as a white solid: 164 mg, 61% yield.

^{1}H NMR (300 MHz, $CDCl_3$): δ(ppm) 7.30 (td, J = 7.4, 1.3 Hz, 3H), 7.24 – 7.12 (m, 6H), 7.09 (d, J = 8.3 Hz, 6H), 6.98 (d, J = 7.6 Hz, 3H), 6.66 (d, J = 8.2 Hz, 6H), 1.31 (s, 27H).

^{13}C NMR (75 MHz, $CDCl_3$): δ(ppm) 149.2, 148.0 (d, J = 31.1 Hz), 138.9 (d, J = 6.6 Hz), 137.0 (d, J = 19.4 Hz), 135.0, 129.5 (d, J = 4.6 Hz), 129.4 (d, J = 4.8 Hz), 128.2, 127.0, 124.0, 34.5, 31.6.

^{31}P NMR (121 MHz, $CDCl_3$): δ(ppm) -33.8.

HRMS (ESI) Calculated for $C_{48}H_{52}P$ $[M+H]^+$: 659.3801, found: *m/z* 659.3784.

tris(4'-pentyl-[1,1'-biphenyl]-2-yl)phosphane (2.3-4$_{nPe}$)

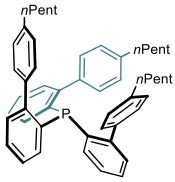

Prepared from 2-bromo-4'-pentyl-1,1'-biphenyl (314 mg, 1.04 mmol), 1.7 M solution of *t*BuLi in pentane (1.2 mL, 2.08 mmol) and PCl_3 (22.7 µL, 35.8 mg, 0.26 mmol) according to the general procedure **2-1**.

Purification by flash column chromatography (Hexane).

2.3-4$_{pnPe}$ was obtained as a white solid: 160 mg, 88% yield.

^{1}H NMR (300 MHz, $CDCl_3$): δ(ppm) 7.32 (td, J = 7.4, 1.4 Hz, 3H), 7.25 – 7.22 (m, 3H), 7.22 – 7.12 (m, 3H), 7.03 – 6.99 (m, 3H), 6.95 (d, J = 8.0 Hz, 6H), 6.79 – 6.69 (m, 6H), 2.66 – 2.55 (m, 6H), 1.68 – 1.63 (m, 6H), 1.39 – 1.28 (d, J = 3.5 Hz, 12H), 0.96 (s, 9H).

^{13}C NMR (76 MHz, $CDCl_3$): δ(ppm) 148.1 (d, J = 30.2 Hz), 141.1, 139.1 (d, J = 6.6 Hz), 136.7 (d, J = 19.1 Hz), 134.9, 129.7 (d, J = 3.4 Hz), 129.6 (d, J = 4.5 Hz), 128.2, 127.2, 127.0, 35.8, 31.7, 31.4, 22.8, 14.2.

^{31}P NMR (121 MHz, $CDCl_3$): δ(ppm) -31.8.

HRMS (ESI) Calculated for $C_{51}H_{58}P$ $[M+H]^+$: 701.4271; found: *m/z* 701.4270.

tris(2-(naphthalen-2-yl)phenyl)phosphane (2.3-4$_{2Nap}$)

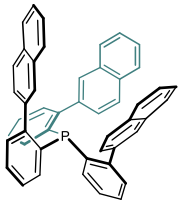

Prepared from 2-(2-bromophenyl)naphthalene (957 mg, 3.4 mmol), 1.7 M solution of *t*BuLi in pentane (4 mL, 6.8 mmol) and PCl_3 (73 µL, 115.4 mg, 0.84 mmol) according to the general procedure **2-1**.

Purification by crystallization in acetone.

2.3-4$_{2Nap}$ was obtained as a white solid: 143 mg, 37% yield.

^{1}H NMR (300 MHz, $CDCl_3$): δ(ppm) 7.74 (d, J = 8.0 Hz, 3H), 7.49 – 7.30 (m, 15H), 7.23 – 7.12 (m, 9H), 6.90 (s, 3H), 6.62 (d, J = 8.4 Hz, 3H).

^{13}C NMR (75 MHz, $CDCl_3$): All peaks are listed due to being unable to determine coupling patterns. δ(ppm) 148.2, 147.8, 139.0, 138.9, 135.1, 132.7, 132.2, 129.8, 129.7, 128.7, 128.6, 128.5, 128.3, 127.9, 127.9, 127.5, 127.4, 126.6, 125.7, 125.7.

^{31}P NMR (121 MHz, $CDCl_3$): δ(ppm) -32.3.

HRMS (ESI) Calculated for $C_{48}H_{34}P$ $[M+H]^+$: 641.2393; found: *m/z* 641.2372.

tris(5-(trifluoromethyl)-[1,1'-biphenyl]-2-yl)phosphane (2.3-4$_{CF3}$)

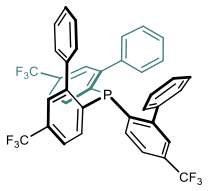

Prepared from -bromo-5-(trifluoromethyl)-1,1'-biphenyl (800 mg, 2.66 mmol), 2.5 M solution of *n*BuLi in hexane (1.2 mL, 2.8 mmol) and PCl_3 (69.6 µL, 109.6 mg, 0.80 mmol) according to the general procedure **2-1**.

Purification by crystallization in ethanol.

2.3-4$_{CF3}$ was obtained as a white solid: 370 mg, 67% yield.

^{1}H NMR (300 MHz, $CDCl_3$): δ(ppm) 7.55 (dd, J = 8.1, 1.9 Hz, 3H), 7.46 (d, J = 4.3 Hz, 3H), 7.34 – 7.25 (m, 3H), 7.23 – 7.16 (m, 6H), 7.09 (dd, J = 8.0, 2.4 Hz, 3H), 6.83 – 6.74 (m, 6H).

^{13}C NMR (76 MHz, $CDCl_3$): δ(ppm) All peaks are listed due to being unable to determine coupling patterns. 149.0, 148.6, 140.1, 139.9, 139.8, 135.0, 131.24 (q, J = 32.5 Hz), 129.5, 129.4, 127.8, 127.7, 126.6 (p, J = 3.7 Hz), 125.9, 124.1 (q, J = 3.7 Hz), 122.2, 118.6.

^{31}P NMR (121 MHz, $CDCl_3$): δ(ppm) -25.7 – -34.8 (m).

^{19}F NMR (283 MHz, $CDCl_3$): δ(ppm) -62.8.

HRMS (ESI) Calculated for $C_{39}H_{25}F_9P$ $[M+H]^+$: 695.1545; found: *m/z* 695.6301.

2.5.2.2. Synthesis of tris-(ortho-biaryl)phosphine Au(I) complexes 2.3-5

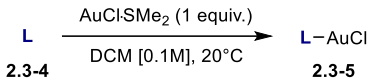

General procedure 2-2:

The following procedure was repeated for the series of gold complexes **2.3-5**. A flame dried flask was charged with the phosphine ligand **2.3-4** (1 equiv.) and AuCl•SMe_2 (1 equiv.). Dry DCM [0.1M] was added, and the reaction mixture was stirred at 20 ◦C for 1h. The reaction mixture was then filtered through a short pad of celite that was rinsed with dry DCM. The solvent was evaporated in vacuo and the residue was dried under reduced pressure to afford the corresponding gold chloride complex **2.3-5**.

Gold chloride complex 2.3-5_H

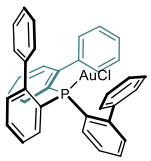

Prepared from ligand **2.3-4_H** (93.8 mg, 0.19 mmol) and AuCl•SMe_2 (56.4 mg, 0.19 mmol) according to the general procedure **2-2**.

2.3-5_H was obtained as a white solid: 104 mg, 76% yield.

^{1}H NMR (400 MHz, $CDCl_3$): δ(ppm) 7.61 (tt, J = 7.5, 1.5 Hz, 3H), 7.48 (tt, J = 7.5, 1.5 Hz, 3H), 7.44 – 7.34 (m, 6H), 7.31 – 7.25 (m, 3H), 7.16 – 7.04 (m, 6H), 6.67 (bs, 6H).

^{13}C NMR (75 MHz, $CDCl_3$): δ(ppm) 147.8 (d, J = 16.5 Hz), 140.2 (d, J = 7.6 Hz), 135.3 (d, J = 5.5 Hz), 132.5 (d, J = 8.2 Hz), 131.0 (d, J = 2.3 Hz), 130.2, 129.4, 129.2, 128.2, 128.1 (bs), 127.5 (d, J = 8.3 Hz).

^{31}P NMR (121 MHz, $CDCl_3$): δ(ppm) 8.1.

NMR data match those reported in the literature.[37]

Gold chloride complex 2.3-5$_{mtBu}$

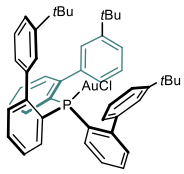

Prepared from ligand **2.3-4$_{mtBu}$** (117 mg, 0.18 mmol) and AuCl•SMe_2 (52.3 mg, 0.18 mmol) according to the general procedure **2-2**.

2.3-5$_{mtBu}$ was obtained as a white solid: 123 mg, 78 % yield.

^{1}H NMR (300 MHz, CD_2Cl_2): δ(ppm) 7.58 (tt, J = 7.5, 1.6 Hz, 3H), 7.45 (tt, J = 7.5, 1.6 Hz, 3H), 7.40 – 7.30 (m, 6H), 7.25 – 7.21 (m, 3H), 7.03 (bs, 3H), 6.74 – 6.47 (br m, 6H), 1.01 (s, 27H).

^{13}C NMR (75 MHz, CD_2Cl_2): δ(ppm) 150.4 (bs), 148.3 (d, J = 16.4 Hz), 140.0 (d, J = 7.1 Hz), 135.6 (d, J = 4.5 Hz), 132.9 (d, J = 8.3 Hz), 130.9 (d, J = 2.2 Hz), 130.0 (br d, J = 63.8 Hz), 127.9 (bs), 127.5 (d, J = 8.2 Hz), 126.5, 126.3, 125.1, 34.3, 30.9.

^{31}P NMR (121 MHz, $CDCl_3$): δ(ppm) 9.2.

HRMS (ESI) Calculated for $C_{48}H_{51}AuClNaP^+$ $[M+Na]^+$: 913.2975; found: *m/z* 913.2987.

Gold chloride complex 2.3-5$_{mnBu}$

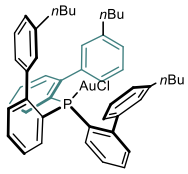

Prepared from ligand **2.3-4$_{mnBu}$** (40 mg, 0.06 mmol) and AuCl•SMe_2 (17.9 mg, 0.06 mmol) according to the general procedure **2-2**.

2.3-5$_{mnBu}$ was obtained as a yellow oil that solidifies upon standing: 53 mg, 98% yield.

^{1}H NMR (300 MHz, $CDCl_3$): δ(ppm) 7.65 – 7.55 (m, 3H), 7.53 – 7.36 (m, 9H), 7.07 (bs, 6H), 6.61 (bs, 3H), 6.33 (bs, 3H), 2.29 (bs, 6H), 1.24 (bs, 12H), 0.84 (t, J = 7.0 Hz, 9H).

^{13}C NMR (75 MHz, CD_2Cl_2): δ(ppm) 148.2 (d, J = 16.5 Hz), 142.1 (bs), 140.1 (d, J = 7.3 Hz), 135.6 (d, J = 5.4 Hz), 132.5 (d, J = 8.2 Hz), 130.9 (d, J = 2.2 Hz), 130.4 (d, J = 60.4 Hz), 129.6, 128.6 (bs), 128.3, 127.4 (d, J = 8.2 Hz), 126.5, 35.6, 33.0, 22.7, 14.1.

^{31}P NMR (121 MHz, $CDCl_3$): δ(ppm) 9.7.

HRMS (ESI) Calculated for $C_{48}H_{51}AuP^+$ $[M\text{-}Cl]^+$: 855.3388; found: *m/z* 855.3394.

Gold chloride complex 2.3-5$_{ptBu}$

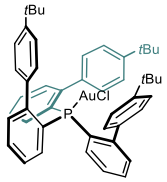

Prepared ligand **2.3-4$_{ptBu}$** (164 mg, 0.25 mmol) and AuCl•SMe_2 (73.4 mg, 0.25 mmol) according to the general procedure **2-2**.

2.3-5$_{ptBu}$ was obtained as a white solid: 178 mg, 80% yield.

^{1}H NMR (300 MHz, $CDCl_3$): δ(ppm) 7.60 – 7.51 (m, 3H), 7.43 – 7.30 (m, 9H), 7.09 (d, J = 8.6 Hz, 6H), 6.62 (d, J = 7.8 Hz, 6H), 1.29 (s, 27H).

^{13}C NMR (75 MHz, $CDCl_3$): All peaks are listed due to being unable to determine coupling patterns. δ(ppm) 151.1, 148.1, 147.9, 137.4, 137.3, 135.4, 135.3, 132.3, 132.2, 130.8, 130.7, 130.7, 130.0, 128.9, 127.3, 127.2, 125.3, 34.6, 31.5.

^{31}P NMR (121 MHz, $CDCl_3$): δ(ppm) 6.5.

HRMS (ESI) Calculated for $C_{48}H_{51}AuP^+$ $[M\text{-}Cl]^+$: 855.3388; found: *m/z* 855.3359.

Gold chloride complex 2.3-5$_{nPe}$

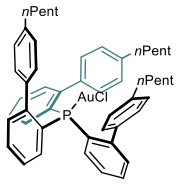

Prepared from ligand **2.3-4$_{nPe}$** (160 mg, 0.23 mmol) and AuCl•SMe_2 (67.2 mg, 0.23 mmol) according to the general procedure **2-2**.

2.3-5$_{pnPe}$ was obtained as a white solid: 132 mg, 62% yield.

^{1}H NMR (300 MHz, $CDCl_3$): δ(ppm) 7.55 (tt, J = 7.5, 1.5 Hz, 3H), 7.43 – 7.29 (m, 9H), 6.90 (d, J = 7.8 Hz, 6H), 6.60 (d, J = 7.6 Hz, 6H), 2.58 – 2.46 (t, J = 7.5, 6H), 1.67 – 1.55 (m, 6H), 1.41 – 1.20 (m, 12H), 0.89 (t, J = 6.8, 9H).

^{13}C NMR (75 MHz, $CDCl_3$): All peaks are listed due to being unable to determine coupling patterns. δ(ppm) 148.2, 148.0, 143.2, 137.5, 137.4, 135.4, 135.3, 132.5, 132.4, 130.8, 130.7, 130.5, 129.7, 129.2, 128.2, 127.3, 127.2, 35.8, 31.8, 31.2, 22.7, 14.3.

^{31}P NMR (121 MHz, $CDCl_3$): δ(ppm) 9.1.

HRMS (ESI) Calculated for $C_{51}H_{57}AuP^+$ $[M\text{-}Cl]^+$: 897.3858; found: *m/z* 897.3815.

Gold chloride complex 2.3-5$_{2Nap}$

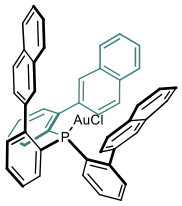

Prepared from ligand **2.3-4$_{2Nap}$** (92.4 mg, 0.14 mmol) and AuCl•SMe_2 (42.5 mg, 0.14 mmol) according to the general procedure **2-2**.

2.3-5$_{2Nap}$ was obtained as a white solid: 118 mg, 94% yield.

^{1}H NMR (300 MHz, $CDCl_3$): δ(ppm) 7.75 – 7.48 (m, 15H), 7.49 – 7.31 (m, 9H), 7.12 (d, J = 7.7 Hz, 3H), 6.74 (bs, 3H), 6.69 (d, J = 8.3 Hz, 3H).

^{13}C NMR (75 MHz, $CDCl_3$): All peaks are listed due to being unable to determine coupling patterns. δ(ppm) 148.0, 147.8, 137.3, 137.2, 135.7, 135.6, 132.8, 132.5, 132.4, 132.0, 130.8, 130.8, 130.8, 130.0, 128.8, 128.6, 127.9, 127.7, 127.5, 127.4, 126.7, 126.1, 126.0.

^{31}P NMR (121 MHz, $CDCl_3$): δ(ppm) 7.7.

HRMS (ESI) Calculated for $C_{48}H_{33}AuClNaP^+$ $[M+Na]^+$: 895.1561; found: *m/z* 895.1584.

Gold chloride complex 2.3-5$_{CF3}$

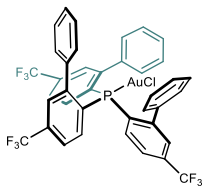

Prepared from ligand **2.3-4$_{CF3}$** (100 mg, 0.14 mmol) and AuCl•SMe_2 (42.5 mg, 0.14 mmol) according to the general procedure **2-2**.

2.3-5$_{CF3}$ was obtained as a white solid: 114 mg, 85% yield.

^{1}H NMR (300 MHz, $CDCl_3$): δ(ppm) 7.85 – 7.72 (m, 3H), 7.68 (dd, J = 4.6, 1.9 Hz, 3H), 7.51 – 7.43 (m, 3H), 7.36 (tt, J = 7.6, 1.2 Hz, 3H), 7.17 (t, J = 7.6 Hz, 6H), 6.66 (bs, 6H).

^{13}C NMR (151 MHz, CD_2Cl_2): δ(ppm) 148.6 (d, J = 17.5 Hz), 138.7 (d, J = 7.1 Hz), 135.8 (d, J = 5.8 Hz), 133.3 (qd, J = 33.0, 2.3 Hz), 132.9 (d, J = 58.9 Hz), 129.5 (dq, J = 7.7, 3.6 Hz), 129.1, 128.9, 128.5, 124.5 (dq, J = 7.6, 3.6 Hz), 123.5 (q, J = 272.9 Hz).

^{31}P NMR (122 MHz, $CDCl_3$): δ(ppm) 8.6.

19F NMR (283 MHz, $CDCl_3$) δ(ppm) -63.1.

HRMS (ESI) Calculated for $C_{39}H_{24}AuClF_9NaP$ $[M+Na]^+$: 949.0713; found: *m/z* 949.07328.

2.5.2.3. Synthesis of *tris*-(*ortho*-biaryl)phosphine Au(I) complexes 2.3-6

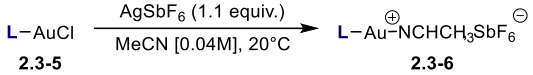

General procedure 2-3:

The following procedure was repeated for the series of gold complexes **2.3-6**. A flame dried flask was charged with the gold chloride complex **2.3-5** (1 equiv.) under nitrogen atmosphere. Dry Me_3CN [0.04M] and $AgSbF_6$ (1.1 equiv.) were then sequentially added, and the reaction mixture was stirred at room temperature overnight. The solvent was removed under reduced pressure, dry DCM was added, and the resulting mixture was filtrated through a short pad of celite. The solvents were evaporated, and the residue was dried under reduced pressure to afford the corresponding gold complex **2.3-6**.

Gold complex 2.3-6$_H$

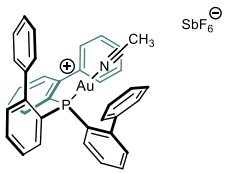

Prepared from **2.3-5$_H$** (104 mg, 0.14 mmol) and $AgSbF_6$ (55.3 mg, 0.16 mmol) according to the general procedure **2-3**.

2.3-6$_H$ was obtained as a white solid: 106 mg, 76% yield.

^{1}H NMR (400 MHz, $CDCl_3$): δ(ppm) 7.70 (tt, J = 7.5, 1.5 Hz, 1H), 7.56 (tt, J = 7.5, 1.7 Hz, 1H), 7.49 – 7.38 (m, 2H), 7.32 (t, J = 7.5 Hz, 1H), 7.15 (s, 2H), 6.61 (s, 2H), 2.30 (s, 1H).

^{13}C NMR (75 MHz, $CDCl_3$): All peaks are listed due to being unable to determine coupling patterns. δ(ppm) 147.3, 147.1, 140.4, 140.3, 135.4, 135.3, 132.7, 132.6, 132.2 (bs), 129.4, 129.4 (bs), 128.6, 128.4 (bs), 128.3, 128.2, 127.9, 127.0, 1.9.

^{31}P NMR (122 MHz, $CDCl_3$): δ(ppm) 0.6.

HRMS (ESI) Calculated for $C_{38}H_{30}AuNP^+$ $[M\text{-}SbF_6]^+$: 728.1776; found: *m/z* 728.1776.

Gold complex 2.3-6$_{mtBu}$

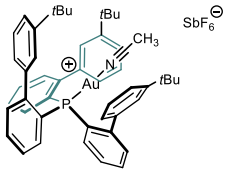

Prepared from **2.3-5$_{mtBu}$** (24.7 mg, 0.03 mmol) and $AgSbF_6$ (10.5 mg, 0.03 mmol) according to the general procedure **2-3**.

2.3-6$_{mtBu}$ was obtained as a white solid: 23 mg, 73% yield.

^{1}H NMR (300 MHz, $CDCl_3$): All peaks were extremely broadened. δ(ppm) 7.68 (t, J = 8.3 Hz, 3H), 7.62 – 7.50 (m, 3H), 7.45 – 7.32 (m, 6H), 7.12 (bs, 12H), 2.29 (bs, 3H), 1.01 (bs, 27H).

^{13}C NMR (75 MHz, CD_2Cl_2): All peaks were extremely broadened. They are listed due to being unable to determine coupling patterns. δ(ppm) 151.1 (bs), 147.5 (bs), 140.1 (bs), 135.4 (bs), 133.0, 132.8, 132.0, 128.2, 128.1, 126.4 (bs), 125.3, 125.0 (bs), 34.3, 30.8, 2.1.

^{31}P NMR (121 MHz, $CDCl_3$): δ(ppm) 3.1.

HRMS (ESI) Calculated for $C_{50}H_{54}AuNP^+$ $[M\text{-}SbF_6]^+$: 896.3654; found: *m/z* 896.3615.

Gold complex 2.3-6$_{mnBu}$

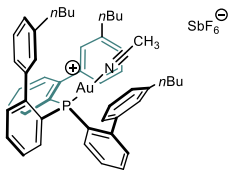

Prepared from **2.3-5$_{mnBu}$** (33.0 mg, 0.04 mmol) and $AgSbF_6$ (14.4 mg, 0.04 mmol) according to the general procedure **2-3**.

2.3-6$_{mnBu}$ was obtained as a light brown oil that solidifies upon standing: 40 mg, 88% yield.

^{1}H NMR (300 MHz, CD_2Cl_2): δ(ppm) 7.70 (tt, J = 7.5, 1.6 Hz, 3H), 7.63 – 7.42 (m, 9H), 7.07 (bs, 6H), 6.55 (bs, 3H), 6.33 (bs, 3H), 2.41 – 2.26 (m, 6H), 2.24 (bs, 3H), 1.25 (bs, 12H), 0.87 (t, J = 7.1 Hz, 9H).

^{13}C NMR (76 MHz, $CDCl_3$): All peaks are listed due to being unable to determine coupling patterns. δ(ppm) 147.4, 147.1, 142.9, 141.0, 140.6, 140.5, 135.74, 135.7, 132.6, 132.5, 132.1, 132.1, 129.8, 128.3, 128.2, 127.2, 126.6, 35.5, 33.3, 22.5, 13.8, 2.0.

^{31}P NMR (122 MHz, $CDCl_3$): δ(ppm) 3.6.

HRMS (ESI) Calculated $C_{50}H_{54}AuNP^+$ [M-SbF_6]$^+$: 896.3654; found: *m/z* 896.3634.

Gold complex 2.3-6$_{ptBu}$

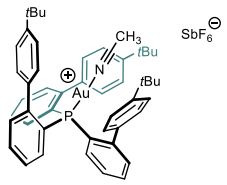

Prepared from **2.3-5$_{ptBu}$** (104 mg, 0.14 mmol) and $AgSbF_6$ (55.3 mg, 0.16 mmol) according to the general procedure **2-3**.

2.3-6$_{ptBu}$ was obtained as a white solid: 106 mg, 76% yield.

^{1}H NMR (400 MHz, $CDCl_3$): δ(ppm) 7.70 (t, J = 7.5 Hz, 3H), 7.56 (t, J = 7.6 Hz, 3H), 7.51 – 7.41 (m, 6H), 7.17 – 7.06 (m, 6H), 6.53 (bs, 6H), 2.25 (s, 3H), 1.26 (s, 27H).

^{13}C NMR (75 MHz, $CDCl_3$): δ(ppm) 151.8, 147.1 (d, J = 15.9 Hz), 137.6 (d, J = 8.2 Hz), 135.5 (d, J = 6.2 Hz), 132.7 (d, J = 8.4 Hz), 132.3 (d, J = 2.0 Hz), 129.2, 128.2 (d, J = 9.1 Hz), 127.7 (d, J = 67.6 Hz), 125.1, 34.7, 31.4, 2.5.

^{31}P NMR (122 MHz, $CDCl_3$): δ(ppm) 3.4.

HRMS (ESI) Calculated for $C_{50}H_{54}AuNP^+$ [M-SbF_6]$^+$: 896.3654; found: *m/z* 896.3638.

Gold complex 2.3-6$_{nPe}$

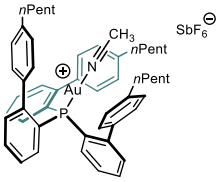

Prepared from **2.3-5$_{nPe}$** (95 mg, 0.10 mmol) and $AgSbF_6$ (38.4 mg, 0.11 mmol) according to the general procedure **2-3**.

2.3-6$_{pnPe}$ was obtained as a white solid: 91 mg, 77% yield.

^{1}H NMR (400 MHz, CD_2Cl_2): δ(ppm) 7.69 (t, J = 7.5 Hz, 3H), 7.54 (t, J = 7.6 Hz, 3H), 7.49 – 7.40 (m, 6H), 6.97 – 6.86 (m, 6H), 6.53 (very bs, 2H), 2.55 – 2.39 (m, 6H), 2.19 (s, 3H), 1.49 – 1.22 (m, 18H), 0.91 (t, J = 6.8 Hz, 9H).

^{13}C NMR (76 MHz, CD_2Cl_2): All peaks are listed due to being unable to determine coupling patterns. δ(ppm) 147.1, 146.9, 143.3, 138.1, 138.0, 135.6, 135.5, 132.6, 132.5, 132.1, 132.1, 129.4, 128.2, 128.1, 127.9, 127.0, 35.6, 31.7, 31.5, 22.7, 13.9, 1.8.

^{31}P NMR (122 MHz, $CDCl_3$): δ(ppm) 0.9.

HRMS (ESI) Calculated for $C_{53}H_{60}AuNP^+$ $[M\text{-}SbF_6]^+$: 938.4123; found: *m/z* 938.4134.

Gold complex 2.3-6$_{2Nap}$

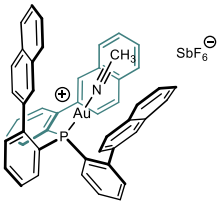

Prepared from **2.3-5$_{2Nap}$** (100 mg, 0.11 mmol) and $AgSbF_6$ (43.3 mg, 0.13 mmol) according to the general procedure **2-3**.

2.3-6$_{2Nap}$ was obtained as a white solid: 110 mg, 86% yield.

^{1}H NMR (300 MHz, $CDCl_3$): δ(ppm) 7.91 – 7.37 (m, 24H), 7.18 br (s, 3H), 6.65 (bs, 6H), 2.49 (bs, 3H).

^{13}C NMR (76 MHz, $CDCl_3$): All peaks are listed due to being unable to determine coupling patterns. The primary CH_3 carbon of the acetonitrile moiety is not visible, probably due to significant broadening of the signal. δ(ppm) 147.3, 147.1, 138.0 (bs), 135.5 (bs), 132.7, 132.6, 132.5, 132.3 (bs), 128.6 (bs), 128.5, 127.9 (bs), 127.0 (bs).

^{31}P NMR (122 MHz, $CDCl_3$): δ(ppm) 0.2 (bs).

HRMS (ESI) Calculated for $C_{50}H_{36}AuNP^+$ $[M\text{-}SbF_6]^+$: 878.2245; found: *m/z* 878.2254.

Gold complex 2.3-6_{CF3}

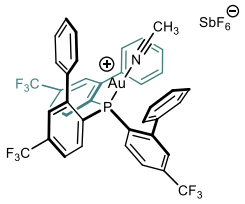

Prepared from **2.3-5_{CF3}** (40 mg, 0.041 mmol) and $AgSbF_6$ (15.5 mg, 0.045 mmol) according to the general procedure **2-3**.

2.3-6_{CF3} was obtained as a white solid: 39.7 mg, 83% yield.

^{1}H NMR (600 MHz, CD_2Cl_2): δ(ppm) 7.96 (d, J = 8.2 Hz, 3H), 7.86 (ddd, J = 4.8, 1.4, 0.7 Hz, 3H), 7.66 (dd, J = 11.1, 8.2 Hz, 3H), 7.52 – 7.41 (m, 3H), 7.31 (bs, 6H), 6.71 (bs, 6H), 2.39 (s, 3H).

^{13}C NMR (151 MHz, CD_2Cl_2): δ(ppm) 148.1 (d, J = 17.0 Hz), 138.8 (d, J = 8.0 Hz), 135.9 (d, J = 6.2 Hz), 134.4 (q, J = 33.0 Hz), 130.4 (d, J = 66.3 Hz), 129.6 (dt, J = 7.6, 3.7 Hz), 129.3, 129.3, 128.9, 125.3 (dd, J = 9.3, 3.9 Hz), 123.2 (q, J = 273.3 Hz), 2.0.

^{31}P NMR (122 MHz, $CDCl_3$): δ(ppm) 0.6.

^{19}F NMR (283 MHz, $CDCl_3$) δ(ppm) -63.1.

HRMS (ESI) Calculated for $C_{41}H_{27}AuF_9NP$ $[M\text{-}Cl]^+$: 932.1397 found: *m/z* 932.13596.

2.5.2.4. Synthesis of *tris*-(*ortho*-biphenyl)phosphine Au(I) complexes 2.3-7 & 2.3-42

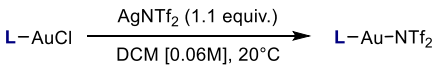

General procedure 2-4:

A flame dried flask was charged with the corresponding gold chloride complex (1 equiv.) under nitrogen atmosphere. Dry DCM [0.06M] and $AgNTf_2$ (1.1 equiv.) were then sequentially added, and the reaction mixture was stirred at room temperature for 1 hour. The resulting mixture was filtrated through a short pad of Celite that was rinsed with CH_2Cl_2. The solvent was then evaporated, and the residue was dried under reduced pressure to afford the corresponding gold complex.

Gold complex 2.3-7

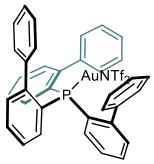

Prepared from the corresponding gold chloride complex (41.7 mg, 0.06 mmol) and $AgNTf_2$ (24.6 mg, 0.06 mmol) according to the general procedure **2-4**.

2.3-7 was obtained as a white solid: 37.4 mg, 67% yield.

^{1}H NMR (300 MHz, $CDCl_3$): δ(ppm) 7.80 – 7.67 (m, 3H), 7.65 – 7.52 (m, 3H), 7.56 – 7.45 (m, 6H), 7.49 – 7.36 (m, 3H), 7.09 (bs, 12H).

^{13}C NMR (75 MHz, CD_2Cl_2): All peaks are listed due to being unable to determine coupling patterns. δ(ppm) 146.2, 146.0, 142.2, 142.1, 135.8, 135.8, 133.0, 132.8, 132.5, 132.5, 129.4, 128.8, 128.7, 128.5, 127.6, 126.4.

^{31}P NMR (121 MHz, CD_2Cl_2): δ(ppm) 3.2

HRMS (ESI) Calculated for $C_{36}H_{27}AuP^+$ $[M\text{-}NTf_2]^+$: 687.1510; found: *m/z* 687.1509.

Gold complex 2.3-42

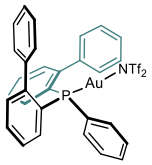

Prepared from the corresponding gold chloride complex (70.0 mg, 0.11 mmol) and $AgNTf_2$ (46.3 mg, 0.12 mmol) according to the general procedure **2-4**.

2.3-42 was obtained as a light brown solid: 80 mg, 84% yield.

^{1}H NMR (300 MHz, $CDCl_3$): δ(ppm) 7.70 – 7.49 (m, 7H), 7.43 – 7.28 (m, 5H), 7.24 – 7.07 (m, 6H), 6.85 (d, J = 7.4 Hz, 4H), 6.69 (bs, 1H).

^{13}C NMR (75 MHz, $CDCl_3$): All peaks are listed due to being unable to determine coupling patterns. δ(ppm) 147.6, 147.5, 139.6 (bs), 139.5 (bs), 135.4, 135.2, 134.2, 134.1, 132.6, 132.5 (bs), 131.8, 129.7, 129.5, 129.4, 128.7, 128.3, 127.8, 127.7, 127.2, 126.3, 121.7, 117.4.

^{31}P NMR (121 MHz, $CDCl_3$): δ(ppm) 11.5.

2.5.2.5. Synthesis of Au(I) complex 2.3-19

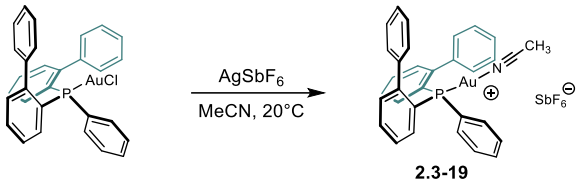

2.3-19

Prepared from the corresponding gold chloride complex (93.0 mg, 0.14 mmol) and $AgSbF_6$ (54.4 mg, 0.16 mmol) according to the general procedure **2-3**.

2.3-19 was obtained as a light brown solid: 118 mg, 92% yield.

^{1}H NMR (300 MHz, CD_2Cl_2): δ(ppm) 7.81 – 7.46 (m, 11H), 7.45 – 7.37 (m, 2H), 7.34 – 7.20 (m, 6H), 6.85 (d, J = 7.4 Hz, 4H), 2.37 (s, 3H).

^{13}C NMR (76 MHz, $CDCl_3$): All peaks are listed due to being unable to determine coupling patterns. δ(ppm) 147.4, 147.2, 140.4, 140.3, 134.8, 134.6, 134.5, 134.4, 132.8, 132.8, 132.5, 132.4, 132.3, 132.2, 129.9, 129.8, 129.7, 128.6, 128.3, 128.2, 127.0, 126.1, 119.2, 2.1.

^{31}P NMR (121 MHz, $CDCl_3$): δ(ppm) 8.2.

HRMS (ESI) Calculated $C_{32}H_{26}AuNP^+$ $[M\text{-}SbF_6]^+$: 652.1463; found: *m/z* 652.1443.

2.5.3. Catalytic studies

2.5.3.1. Cycloisomerization of enyne 2.3-17

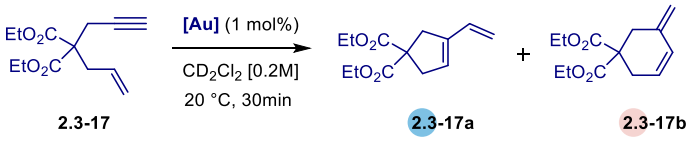

2.3-17 **2.3-17a** **2.3-17b**

The following procedure was repeated for the series of gold complexes **2.3-6** and **2.3-19 – 2.3-23**: Into an NMR tube were sequentially added substrate **2.3-17** (1 equiv.) and dry CD_2Cl_2 [0.2M]. A few µL of 1,3,5-trimethylbenzene, used as an internal standard for NMR analysis and monitoring, was then added. The NMR tube was capped and vigorously shaken before a ^{1}H NMR spectrum of the mixture was recorded (t=0). The gold complex [Au] (1 mol%) was added to the NMR tube and the reaction mixture was vigorously shaken. After 0.5h of reaction, another ^{1}H NMR spectrum was recorded. The overall yield (**2.3-17a**+**2.3-17b**) and the **2.3-17a**: **2.3-17b** ratio were assessed by comparing the relative integration of the internal standard peaks with those of products **2.3-17a**[80] and **2.3-17b**[81] (see **Appendix Figure 6.1-1** for representative example).

2.5.3.2. Cycloisomerization of enyne 2.3-24

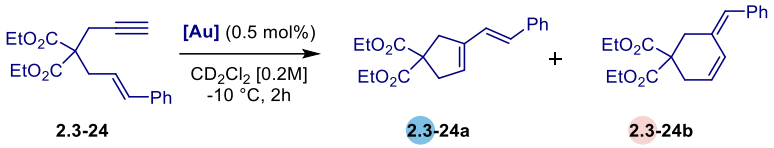

2.3-24 — 2.3-24a — 2.3-24b

The following procedure was repeated for the series of gold complexes **2.3-6** and **2.3-19 – 2.3-23**: Into an NMR tube were sequentially added substrate **2.3-24** (1 equiv.), 10 mol% of diethyl 2-(prop-2-yn-1-yl)malonate[1] and dry CD_2Cl_2 [0.2M]. A few µL of 1,3,5-trimethylbenzene, used as an internal standard for NMR analysis and monitoring, was then added. The NMR tube was capped and vigorously shaken before a ^1H NMR spectrum of the mixture was recorded (t=0). The gold complex [Au] (0.5 mol%) was added to the NMR tube and the reaction mixture was vigorously shaken. After 2h of reaction, another ^1H NMR spectrum was recorded. The overall yield (**2.3-24a**+**2.3-24b**) and the **2.3-24a**:**2v-24b** ratio were assessed by comparing the relative integration of the internal standard peaks with those of products **2.3-24a**[82] and **2.3-24b**[83] (see **Appendix Figure 6.1-2** for representative example).

2.5.3.3. Cycloisomerization of enyne 2.3-25

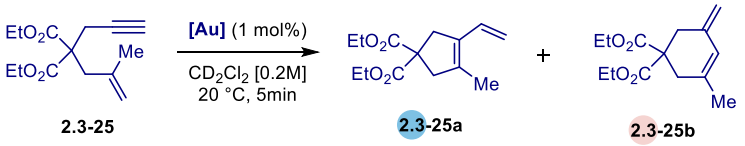

2.3-25 — 2.3-25a — 2.3-25b

The following procedure was repeated for the series of gold complexes **2.3-6** and **2.3-19 – 2.3-23**: an NMR tube were sequentially added substrate **2v-25** (1 equiv.) and dry CD_2Cl_2 [0.2M]. A few µL of 1,3,5-trimethylbenzene, used as an internal standard for NMR analysis and monitoring, was then added. The NMR tube was capped and vigorously shaken before a ^1H NMR spectrum of the mixture was recorded (t=0). The gold complex [Au] (1 mol%) was added to the NMR tube and the reaction mixture was vigorously shaken. After 5 min of reaction, another ^1H NMR spectrum was recorded. The overall yield (**2.3-25a**+**2.3-25b**) and the **2.3-25a**:**2.3-25b** ratio were assessed by comparing the relative integration of the internal standard peaks with those of products **2.3-25a**[82] and **2.3-25b**[84] (see **Appendix Figure 6.1-3** for representative example).

2.5.3.4. Cycloisomerization of enyne 2.3-26

[1] The cyclopentene product **2.3-24a** was found to rapidly degrade under the reaction conditions whatever the nature of the catalyst and the temperature employed, thus biasing the **2.3-24a**:**2.3-24b** ratio and rendering the analysis of ligand effect complicated. After several experiments, it was found that the use of 10 mol% of diethyl 2-(prop-2-yn-1-yl)malonate prevented the degradation of **2.3-24a**. It has been hypothesized that this alkyne, which is not consumed under the reaction conditions, prevents the deleterious electrophilic activation to the diene unit in **2.3-24** by the Au(I) complex by competitively coordinating to this complex.

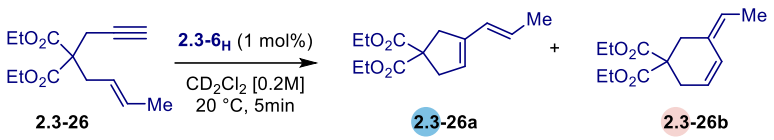

Into an NMR tube were sequentially added substrate **2.3-26** (1 equiv., used as a 4.4:1 *E*:*Z* mixture of alkenes) and dry CD_2Cl_2 [0.2M]. A few µL of 1,3,5-trimethylbenzene, used as an internal standard for NMR analysis and monitoring, was then added. The NMR tube was capped and vigorously shaken before a ^{1}H NMR spectrum of the mixture was recorded (t=0). The gold complex **2.3-6$_H$** (1 mol%) was added to the NMR tube and the reaction mixture was vigorously shaken. After 5 min of reaction, another ^{1}H NMR spectrum was recorded. For convenience, due to the low amount of *Z* isomer in substrate **2.3-26**, only the conversion of the *E* isomer was considered. Sole the formation of product **2.3-26a**[82] could be observed (see **Appendix Figure 6.1-4**).

2.5.3.5. Cycloisomerization of enyne 2.3-27

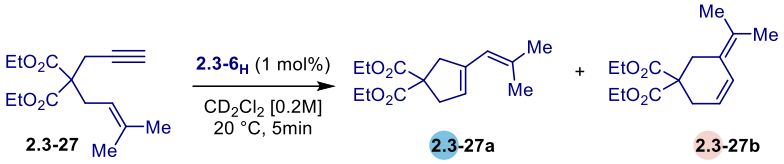

Into an NMR tube were sequentially added substrate **2.3-27** (1 equiv.) and dry CD_2Cl_2 [0.2M]. A few µL of 1,3,5-trimethylbenzene, used as an internal standard for NMR analysis and monitoring, was then added. The NMR tube was capped and vigorously shaken before a ^{1}H NMR spectrum of the mixture was recorded (t=0). The gold complex **2.3-6$_H$** (1 mol%) was added to the NMR tube and the reaction mixture was vigorously shaken. After 5min of reaction, another ^{1}H NMR spectrum was recorded. The overall yield (**2.3-27a**+**2.3-27b**) and the **2.3-27a**:**2.3-27b** ratio were assessed by comparing the relative integration of the internal standard peaks with those of products **2.3-27a**[70] and **2.3-27b**[70] (see **Appendix Figure 6.1-5**).

2.5.3.6. Cycloisomerization of enyne 2.3-28

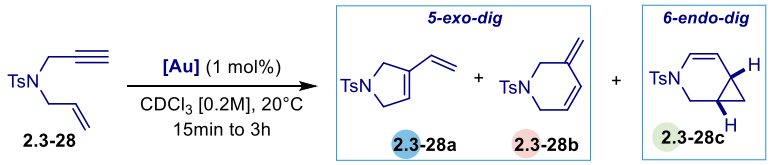

The following procedure was repeated for the series of gold complexes **2.3-6** and **2.3-19 – 2.3-23**: Into an NMR tube were sequentially added substrate **2.3-28** (1 equiv.) and $CDCl_3$ [0.2M]. A few µL of 1,3,5-trimethylbenzene, used as an internal standard for NMR analysis and monitoring, was then added. The NMR tube was capped and vigorously shaken before a ^{1}H NMR spectrum of the mixture was recorded (t=0). The gold complex [Au] (1 mol%) was added to the NMR tube and the

reaction mixture was vigorously shaken. After the specified reaction time, another ^{1}H NMR spectrum was recorded. The overall yield (**2.3-28a**+**2.3-28b**+**2.3-28c**) and the (**2.3-28a+2-28b**):**2.3-28c** ratio were assessed by comparing the relative integration of the internal standard peaks with those of products **2.3-28a**[85], **2.3-28b**[85] and **2.3-28c**[86] (see **Appendix Figure 6.1-6** for representative example).

2.5.3.7. Cycloisomerization of enyne 2.3-29

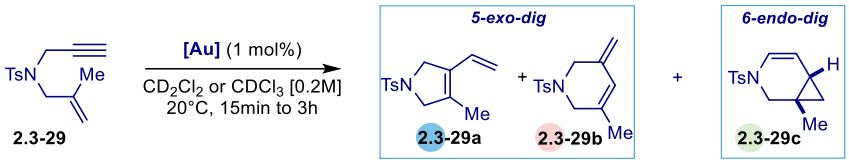

The following procedure was repeated for the series of gold complexes **2.3-6** and **2.3-19 – 2.3-23**: Into an NMR tube were sequentially added substrate **2.3-29** (1 equiv.) and CD_2Cl_2 (or $CDCl_3$)[2] [0.2M]. A few µL of 1,3,5-trimethylbenzene, used as an internal standard for NMR analysis and monitoring, was then added. The NMR tube was capped and vigorously shaken before a ^{1}H NMR spectrum of the mixture was recorded (t=0). The gold complex [Au] (1 mol%) was added to the NMR tube and the reaction mixture was vigorously shaken. After 15min of reaction, another ^{1}H NMR spectrum was recorded. The overall yield (**2.3-29a**+**2.3-29b**+**2.3-29c**) and the (**2.3-29a+2.3-29b**):**2.3-29c** ratio were assessed by comparing the relative integration of the internal standard peaks with those of products **2.3-29a**[85], **2.3-29b**[85] and **2.3-29c**[85] (see **Appendix Figure 6.1-7** for representative example).

2.5.3.8. Cycloisomerization of enyne 2.3-30

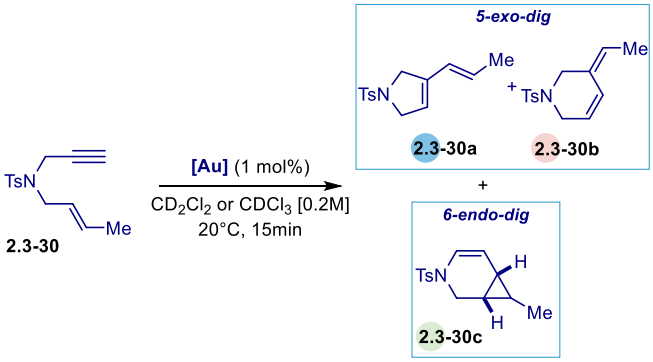

The following procedure was repeated for the series of gold complexes **2.3-6** and **2.3-19 – 2.3-23**: Into an NMR tube were sequentially added substrate **2.3-30** (1 equiv., used as a 3.7:1 *E*:*Z* mixture of alkenes) and CD_2Cl_2 (or $CDCl_3$)[2] [0.2M]. A few µL of 1,3,5-trimethylbenzene, used as an internal

[2] The study was started using CD_2Cl_2 as the solvent but due to shortage and lack of supply, it was completed for complexes with $CDCl_3$. It is believed that the difference between these two solvents would not remarkably impact the course of the reaction and the observed selectivity.

standard for NMR analysis and monitoring, was then added. The NMR tube was capped and vigorously shaken before a ^{1}H NMR spectrum of the mixture was recorded (t=0). The gold complex [Au] (1 mol%) was added to the NMR tube and the reaction mixture was vigorously shaken. After 15min of reaction, another ^{1}H NMR spectrum was recorded. For convenience, due to the low amount of *Z* isomer in substrate **2.3-30**, only the conversion of the *E* isomer was considered. The overall yield (**2.3-30a**+**2.3-30b**+**2.3-30c**) and the (**2.3-30a+2.3-30b**):**2.3-30c** ratio were assessed by comparing the relative integration of the internal standard peaks with those of products **2.3-30a**[13], **2.3-30b**[13] and **2.3-30c**[13] (see **Appendix Figure 6.1-8** for representative example).

2.5.3.9. Cycloisomerization of enyne 2.3-31

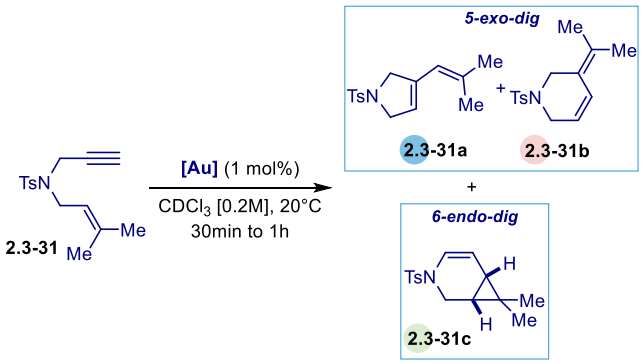

The following procedure was repeated for the series of gold complexes **2.3-6** and **2.3-19, 2.3-21, 2.3-23**: Into an NMR tube were sequentially added substrate **2.3-31** (1 equiv.) and CD_2Cl_2 (or $CDCl_3$)2 [0.2M]. A few µL of 1,3,5-trimethylbenzene, used as an internal standard for NMR analysis and monitoring, was then added. The NMR tube was capped and vigorously shaken before a ^{1}H NMR spectrum of the mixture was recorded (t=0). The gold complex [Au] (1 mol%) was added to the NMR tube and the reaction mixture was vigorously shaken. After the specified reaction time, another ^{1}H NMR spectrum was recorded. The overall yield (**2.3-31a**+**2.3-31b**+**2.3-31c**) and the (**2.3-31a+2.3-31b**):**2.3-31c** ratio were assessed by comparing the relative integration of the internal standard peaks with those of products **2.3-31a**[87], **2.3-31b**[13] and **2.3-31c**[86] (see **Appendix Figure 6.1-9** for representative example).

2.5.3.10. Interrupted cycloisomerization: reaction enyne 2.3-24 with styrene

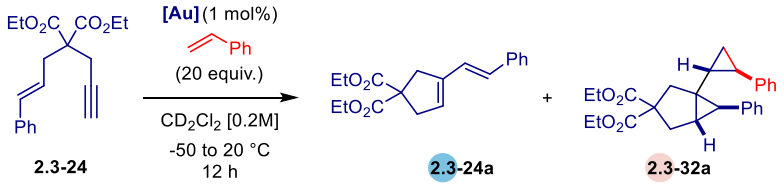

The following procedure was repeated for the of gold complexes [Au] = **2.3-6$_H$**, **2.3-21**: Into an NMR tube were sequentially added substrate **2.3-24** (1 equiv.), styrene (20 equiv.) and CD_2Cl_2 [0.2M]. A few µL of 1,3,5-trimethylbenzene, used as an internal standard for NMR analysis and

monitoring, was then added. The NMR tube was capped and vigorously shaken before a ^{1}H NMR spectrum of the mixture was recorded (t=0). Then it was placed in a -50 °C cooling bath and the gold complex [Au] (1 mol%) was added to the NMR tube and the reaction mixture was vigorously shaken. After 12h of reaction, another ^{1}H NMR spectrum was recorded. The overall conversion and the yield of the corresponding product were assessed by comparing the relative integration of the internal standard peaks with those of products **2.3-24a**[82] and **2.3-32** (see **Appendix Figure 6.1-10** for representative example).

Diethyl 6-phenyl-1-(2-phenylcyclopropyl)bicyclo[3.1.0]hexane-3,3-dicarboxylate 2.3-32a

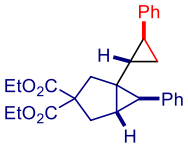

Synthesized from malonate **2.3-24** (31.4 mg, 0.1 mmol) and styrene (229.6 µL, 2 mmol) and obtained as a colourless oil. Stereochemistry was given by analogy with the results reported by Echavarren and coworkers.[66]

^{1}H NMR (300 MHz, $CDCl_3$): δ(ppm) 7.26 – 7.04 (m, 8H), 6.94 – 6.86 (m, 2H), 4.32 – 4.06 (m, 4H), 2.84 (d, J = 14.0 Hz, 1H), 2.71 – 2.65 (m, 2H), 2.54 (d, J = 14.0 Hz, 1H), 1.92 (d, J = 4.2 Hz, 1H), 1.80 – 1.65 (m, 2H), 1.27 (td, J = 7.1, 2.5 Hz, 6H), 1.10 – 1.00 (m, 1H), 0.69 – 0.56 (m, 2H).

^{13}C NMR (75 MHz, $CDCl_3$): δ(ppm) 172.8, 172.2, 143.2, 138.6, 129.3, 128.2, 128.0, 125.9, 125.8, 125.4, 61.9, 61.7, 61.1, 42.3, 38.0, 37.2, 33.4, 27.3, 23.7, 22.2, 16.6, 14.2.

HRMS (ESI) Calculated for $C_{27}H_{30}NaO_4^+$ $[M+Na]^+$: 441.2036; found: *m/z* 441.2072

2.5.3.11. Interrupted cycloisomerization: reaction enyne 2.3-24 with 1,3-dimethoxybenzene

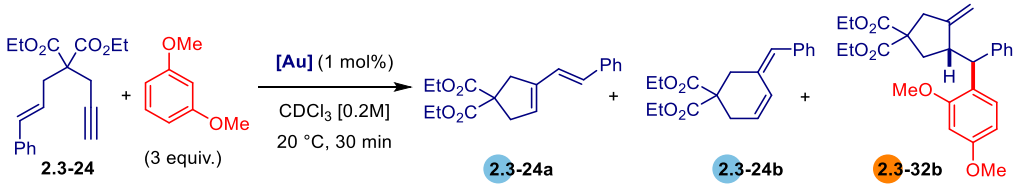

The following procedure was repeated for the of gold complexes [Au] = **2.3-6$_H$**, **2.3-21**: Into an NMR tube were sequentially added substrate **2.3-24** (1 equiv.), 1,3-dimethoxybenzene (3 equiv.) and $CDCl_3$ [0.2M]. A few µL of 1,3,5-trimethylbenzene, used as an internal standard for NMR analysis and monitoring, was then added. The NMR tube was capped and vigorously shaken before a ^{1}H NMR spectrum of the mixture was recorded (t=0). The gold complex [Au] (1 mol%) was added to the NMR tube and the reaction mixture was vigorously shaken. After 30min of reaction, another ^{1}H NMR spectrum was recorded. The overall yield (**2.3-24a**+**2.3-24b**+**2.3-33**)

and the (**2.3-24a**+**2.3-24b**):**2.3-33** ratio were assessed by comparing the relative integration of the internal standard peaks with those of products **2.3-24a**[82], **2.3-24b**[83] and **2.3-33** (see **Appendix Figure 6.1-11** for representative example).

Diethyl 3-((2,4-dimethoxyphenyl)(phenyl)methyl)-4-methylenecyclopentane-1,1-dicarboxylate 2.3-32b

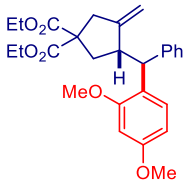

Synthesized from malonate **2.3-24** (62.8 mg, 0.2 mmol) and 1,3-dimethoxybenzene (78.6 µL, 82.9 mg, 0.6 mmol) and obtained as a colourless oil.

^{1}H NMR (300 MHz, $CDCl_3$): δ(ppm) 7.39 – 7.20 (m, 5H), 7.18 – 7.11 (m, 1H), 6.50 (dd, J = 8.4, 2.5 Hz, 1H), 6.42 (d, J = 2.5 Hz, 1H), 4.75 (bs, 1H), 4.30 – 4.05 (m, 6H), 3.80 (s, 6H), 3.65 – 3.51 (m, 1H), 3.22 – 3.08 (m, 1H), 2.93 (dd, J = 16.0, 1.6 Hz, 3H), 2.57 (ddd, J = 13.4, 7.7, 1.6 Hz, 1H), 1.75 (dd, J = 13.4, 9.3 Hz, 1H), 1.27 (t, J = 7.1 Hz, 3H), 1.23 (t, J = 7.1 Hz, 3H).

^{13}C NMR (75 MHz, $CDCl_3$): δ(ppm) 172.0, 171.8, 159.1, 158.0, 149.7, 144.5, 128.7, 128.1, 125.9, 125.2, 109.5, 104.4, 98.8, 61.5, 58.2, 55.5, 55.4, 48.3, 45.3, 41.8, 39.9, 14.2, 14.1.

HRMS (ESI) Calculated for $C_{27}H_{32}NaO_6^+$ $[M+Na]^+$: 475.2091; found: *m/z* 475.2108.

2.5.3.12. Interrupted cycloisomerization: reaction enyne 2.3-33 with indole

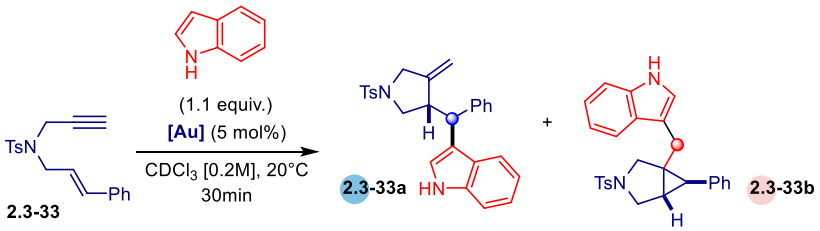

The following procedure was repeated for the gold complexes [Au] = **2.3-6$_H$**, **2.3-21** and **2.3-23**: Into an NMR tube were sequentially added substrate **2.3-33** (1 equiv.), indole (1.1 equiv.) and $CDCl_3$ [0.2M]. A few µL of 1,3,5-trimethylbenzene, used as an internal standard for NMR analysis and monitoring, was then added. The NMR tube was capped and vigorously shaken before a ^{1}H NMR spectrum of the mixture was recorded (t=0). The gold complex [Au] (5 mol%) was added to the NMR tube and the reaction mixture was vigorously shaken. After 30min of reaction, another ^{1}H NMR spectrum was recorded. The overall conversion and the yield of the corresponding products were assessed by comparing the relative integration of the internal standard peaks with

those of products **2.3-33a**[21] and **2.3-33b**[14] (see **Appendix Figure 6.1-12** for representative example).

2.5.3.13. Trapping reaction of ethyl 2-diazo-2-phenylacetate 2.3-34 with styrene

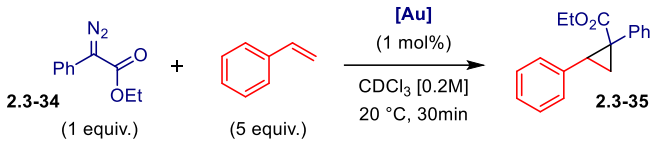

The following procedure was repeated for the gold complexes [Au] = **2.3-6$_H$**, **2.3-21**: Into an NMR tube were sequentially added substrate **2.3-34** (1 equiv.), styrene (5 equiv.) and $CDCl_3$ [0.2M]. A few µL of DCE, used as an internal standard for NMR analysis and monitoring, was then added. The NMR tube was capped and vigorously shaken before a ^{1}H NMR spectrum of the mixture was recorded (t=0). The gold complex [Au] (1 mol%) was added to the NMR tube and the reaction mixture was vigorously shaken. After 30min of reaction, another ^{1}H NMR spectrum was recorded. The overall conversion and the yield of the corresponding product were assessed by comparing the relative integration of the internal standard peaks with those of product **2.3-35a**[88] (see **Appendix Figure 6.1-13** for representative example).

2.5.3.14. Cycloisomerization of enyne 2.3-35

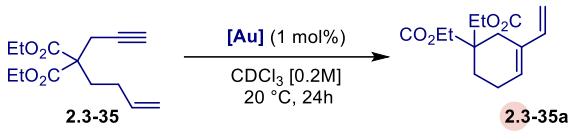

The following procedure was repeated for the gold complexes [Au] = **2.3-6$_H$**, **2.3-19 – 2.3-23**: Into an NMR tube were sequentially added substrate **2.3-35** (1 equiv.) and $CDCl_3$ [0.2M]. A few µL of 1,3,5-trimethylbenzene, used as an internal standard for NMR analysis and monitoring, was then added. The NMR tube was capped and vigorously shaken before a ^{1}H NMR spectrum of the mixture was recorded (t=0). The gold complex [Au] (1 mol%) was added to the NMR tube and the reaction mixture was vigorously shaken. After 24h of reaction, another ^{1}H NMR spectrum was recorded. The conversion and the yield of **2.3-35a** were assessed by comparing the relative integration of the internal standard peaks with those of product **2.3-35a**[89] (see **Appendix Figure 6.1-14** for representative example).

2.5.3.15. Cycloisomerization of enyne 2.3-36

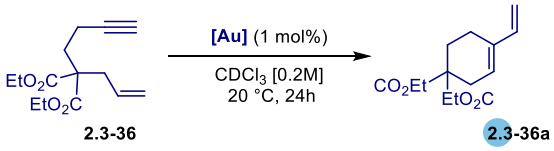

The following procedure was repeated for the gold complexes [Au] = **2.3-6$_H$**, **2.3-19 – 2.3-23**: Into an NMR tube were sequentially added substrate **2.3-36** (1 equiv.) and $CDCl_3$ [0.2M]. A few µL of 1,3,5-trimethylbenzene, used as an internal standard for NMR analysis and monitoring, was then added. The NMR tube was capped and vigorously shaken before a ^{1}H NMR spectrum of the mixture was recorded (t=0). The gold complex [Au] (1 mol%) was added to the NMR tube and the reaction mixture was vigorously shaken. After 24h of reaction, another ^{1}H NMR spectrum was recorded. The conversion and the yield of **2.3-36a** were assessed by comparing the relative integration of the internal standard peaks with those of product **2.3-36a** (see **Appendix Figure 6.1-15** for representative example).

Diethyl 4-vinylcyclohex-3-ene-1,1-dicarboxylate (2.3-36a)

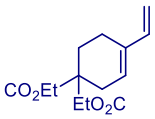

Synthesized from malonate **2.3-36** (25.2 mg, 0.1 mmol).

^{1}H NMR (300 MHz, $CDCl_3$): δ(ppm) 6.41 – 6.23 (m, 1H), 5.75 – 5.65 (m, 1H), 5.04 (d, J = 17.4 Hz, 1H), 4.92 (d, J = 10.8 Hz, 1H), 4.24 – 4.10 (m, 4H), 2.67 (bs, 2H), 2.20 (s, 4H), 1.23 (t, J = 7.1 Hz, 6H).

^{13}C NMR (76 MHz, $CDCl_3$): δ(ppm) 171.5, 139.1, 135.0, 125.9, 111.0, 61.5, 53.2, 31.1, 27.4, 21.1, 14.1.

HRMS (ESI) Calculated for $C_{14}H_{20}NaO_4$ $[M+Na]^+$: 275.1219; found: *m/z* 275.1240.

2.5.3.16. Competetive cycloisomerization of enynes 2.3-35 and 2.3-36

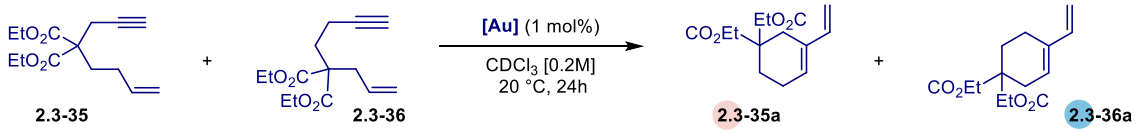

The following procedure was repeated for the gold complexes [Au] = **2.3-6$_H$**, **2.3-19**: Into an NMR tube were sequentially added substrate **2.3-35** (1 equiv.), substrate **2.3-36** (1 equiv.) and $CDCl_3$ [0.2M]. A few µL of 1,3,5-trimethylbenzene (2 µl), used as an internal standard for NMR analysis and monitoring, was then added. The NMR tube was capped and vigorously shaken before a ^{1}H NMR spectrum of the mixture was recorded (t=0). The gold complex [Au] (1 mol%) was added to the NMR tube and the reaction mixture was vigorously shaken. After 24h of reaction, another ^{1}H NMR spectrum was recorded. The overall conversion and the yield of the corresponding products were assessed by comparing the relative integration of the internal standard peaks with those of products **2.3-35a**[89] and **2.3-36a**. To circumvent the challenge associated with overlapping of the signals, the ratio of **2.3-35a**:**2.3-36a** ratio was determined by evaluating the conversion of the corresponding substrates **2.3-35** and **2.3-36**. (see **Appendix Figure 6.1-16** for representative example).

2.5.3.17. Cycloisomerization of enyne 2.3-37

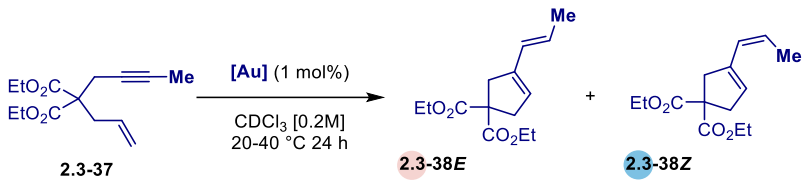

The following procedure was repeated for the series of gold complexes [Au] = **2.3-6$_H$, 2.3-7, 2.3-29 – 2.3-23**: Into an NMR tube were sequentially added substrate **2.3-37** (1 equiv.) and $CDCl_3$ [0.2M]. A few µL of 1,3,5-trimethylbenzene, used as an internal standard for NMR analysis and monitoring, was then added. The NMR tube was capped and vigorously shaken before a ^{1}H NMR spectrum of the mixture was recorded (t=0). The gold complex [Au] (1 - 5 mol%) was added to the NMR tube and the reaction mixture was vigorously shaken. After 24h of reaction at the corresponding temperature, another ^{1}H NMR spectrum was recorded. The overall yield (**2.3-38*E*** + **2.3-38*Z***) and the **2.3-38*E***:**2.3-38*Z*** ratio were assessed by comparing the relative integration of the internal standard peaks with those of products **2.3-38*E*** and **2.3-38*Z*** (see **Appendix Figure 6.1-17** for representative example).

2.5.3.18. Hydration of alkyne 2.3-38

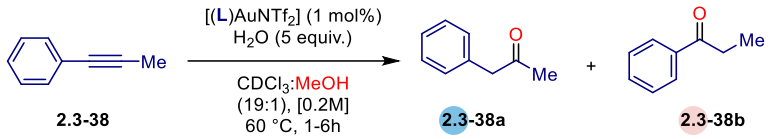

The following procedure was repeated for the series of gold complexes [(**L**)AuNTf$_2$]: Into an NMR tube were sequentially added substrate **2.3-38** (1 equiv.), methanol and $CDCl_3$ (19:1, 0.2M). Water (5 equiv.) and a few µL of 1,3,5-trimethylbenzene, used as an internal standard for NMR analysis and monitoring, were then added. The NMR tube was fitted with a plastic cap and vigorously shaken before a ^{1}H NMR spectrum of the mixture was recorded (t=0). The gold complex [Au] (1 mol%) was added to the NMR tube and the reaction mixture was vigorously shaken and placed in a preheated oil bath at 60 °C. After 6h of reaction, another ^{1}H NMR spectrum was recorded. The overall yield (**2.3-38a**+**2.3-38b**) and the **2.3-38a**:**2.3-38b** ratio were assessed by comparing the relative integration of the internal standard peaks with those of products **2.3-38a**[90] and **2.3-38b**[91] (see **Appendix Figure 6.1-18** for representative example).

2.5.3.19. Hydration of alkyne 2.3-39

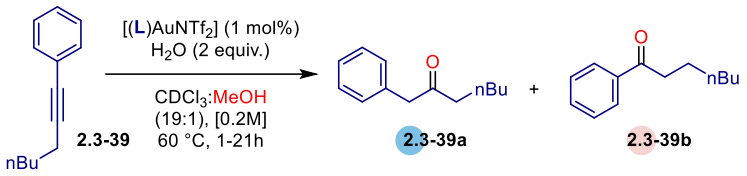

The following procedure was repeated for the series of gold complexes [(**L**)AuNTf$_2$]: Into an NMR tube were sequentially added substrate **2.3-39** (1 equiv.), methanol and $CDCl_3$ (19:1, 0.2M). Water (5 equiv.) and a few µL of 1,3,5-trimethylbenzene, used as an internal standard for NMR analysis and monitoring, were then added. The NMR tube was fitted with a plastic cap and vigorously shaken before a ^{1}H NMR spectrum of the mixture was recorded (t=0). The gold complex [Au] (1 mol%) was added to the NMR tube and the reaction mixture was vigorously shaken and placed in a preheated oil bath at 60 °C. After the corresponding time of the reaction of reaction, another ^{1}H NMR spectrum was recorded. The overall yield (**2.3-39a**+**2.3-39b**) and the **2.3-39a**:**2.3-39b** ratio were assessed by comparing the relative integration of the internal standard peaks with those of products **2.3-39a**[92] and **2.3-39b**[93] (see **Appendix Figure 6.1-19** for representative example).

2.5.3.20. Competitive hydration of alkynes 2.3-38 and 2.3-39

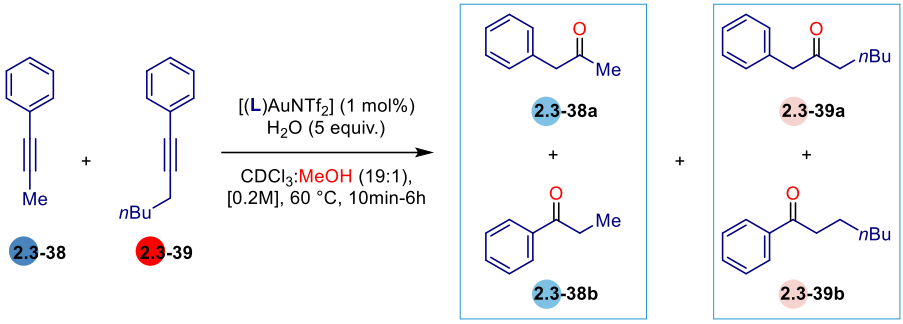

The following procedure was repeated for the series of gold complexes [(**L**)AuNTf$_2$]: Into an NMR tube were sequentially added substrate **2.3-38** (1 equiv.), substrate **2.3-39** (1 equiv.), methanol and $CDCl_3$ (19:1, 0.2M). Water (5 equiv.) and a few µL of 1,3,5-trimethylbenzene, used as an internal standard for NMR analysis and monitoring, were then added. The NMR tube was fitted with a plastic cap and vigorously shaken before a ^{1}H NMR spectrum of the mixture was recorded (t=0). The gold complex [Au] (1 mol%) was added to the NMR tube and the reaction mixture was vigorously shaken and placed in a preheated oil bath at 60 °C. After the corresponding time of the reaction of reaction, another ^{1}H NMR spectrum was recorded. The conversion of the substrates was assessed by comparing the relative integration of the internal standard peaks with those of substrates **2.3-38**[94] and **2.3-39**[94] (see **Appendix Figure 6.1-20** for representative example).

2.5.3.21. Competitive hydration of alkynes 2.3-40 and 2.3-41

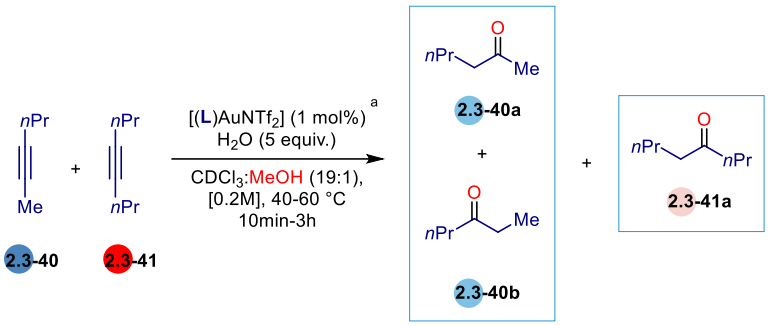

The following procedure was repeated for the series of gold complexes [(**L**)AuNTf$_2$]: Into an NMR tube were sequentially added substrate **2.3-40** (1 equiv.), substrate **2.3-41** (1 equiv.), methanol and $CDCl_3$ (19:1, 0.2M). Water (5 equiv.) and a few µL of 1,3,5-trimethylbenzene, used as an internal standard for NMR analysis and monitoring, were then added. The NMR tube was fitted with a plastic cap and vigorously shaken before a ^{1}H NMR spectrum of the mixture was recorded (t=0). The gold complex [Au] (1 mol%) was added to the NMR tube and the reaction mixture was vigorously shaken and placed in a preheated oil bath at 60 °C. After the corresponding time of the reaction of reaction, another ^{1}H NMR spectrum was recorded. The conversion of the substrates was assessed by comparing the relative integration of the internal standard peaks with those of substrates **2.3-40**[95], **2.3-41**[96] and products **2.3-40a**[97], **2.3-40b**[98] and **2.3-41a**[99] (see **Appendix Figure 6.1-21** for representative example).

2.6. List of references

(1) Jiménez-Núñez, E.; Echavarren, A. M. Gold-Catalyzed Cycloisomerizations of Enynes: A Mechanistic Perspective. *Chem. Rev.* **2008**, *108* (8), 3326–3350. https://doi.org/10.1021/cr0684319.

(2) Hoffmann, R. Building Bridges Between Inorganic and Organic Chemistry (Nobel Lecture). *Angew. Chemie Int. Ed. English* **1982**, *21* (10), 711–724. https://doi.org/10.1002/ANIE.198207113.

(3) Fukuda, Y.; Utimoto, K. Effective Transformation of Unactivated Alkynes into Ketones or Acetals with a Gold(III) Catalyst. *J. Org. Chem.* **1991**, *56* (11), 3729–3731. https://doi.org/10.1021/jo00011a058.

(4) Mizushima, E.; Sato, K.; Hayashi, T.; Tanaka, M. Highly Efficient Au^{I}-Catalyzed Hydration of Alkynes. *Angew. Chemie Int. Ed.* **2002**, *41* (23), 4563–4565. https://doi.org/10.1002/1521-3773(20021202)41:23<4563::AID-ANIE4563>3.0.CO;2-U.

(5) Inamdar, S. M.; Patil, N. T. Engineering Ligands on the Au Center: Discovering Broadly Applicable Gold Catalysis with High Turnover Numbers. *Org. Chem. Front.* **2015**, *2* (8), 995–998. https://doi.org/10.1039/C5QO00162E.

(6) Nieto-Oberhuber, C.; Muñoz, M. P.; Buñuel, E.; Nevado, C.; Cárdenas, D. J.; Echavarren, A. M. Cationic Gold(I) Complexes: Highly Alkynophilic Catalysts for the Exo- and Endo-Cyclization of Enynes. *Angew. Chemie Int. Ed.* **2004**, *43* (18), 2402–2406. https://doi.org/10.1002/anie.200353207.

(7) Escribano-Cuesta, A.; Pérez-Galán, P.; Herrero-Gómez, E.; Sekine, M.; Braga, A. A. C.; Maseras, F.; Echavarren, A. M. The Role of Cyclobutenes in Gold(I)-Catalysed Skeletal Rearrangement of 1,6-Enynes. *Org. Biomol. Chem.* **2012**, *10* (30), 6105–6111. https://doi.org/10.1039/C2OB25419K.

(8) Cabello, N.; Jiménez-Núñez, E.; Buñuel, E.; Cárdenas, D. J.; Echavarren, A. M. On the Mechanism of the Puzzling "Endocyclic" Skeletal Rearrangement of 1,6-Enynes. *European J. Org. Chem.* **2007**, *2007* (25), 4217–4223. https://doi.org/10.1002/ejoc.200700402.

(9) Nieto-Oberhuber, C.; López, S.; Muñoz, M. P.; Jiménez-Núñez, E.; Buñuel, E.; Cárdenas, D. J.; Echavarren, A. M. Gold(I)-Catalyzed Intramolecular Cyclopropanation of Dienynes. *Chem. – A Eur. J.* **2006**, *12* (6), 1694–1702. https://doi.org/10.1002/chem.200501089.

(10) Nieto-Oberhuber, C.; Pérez-Galán, P.; Herrero-Gómez, E.; Lauterbach, T.; Rodríguez, C.; López, S.; Bour, C.; Rosellón, A.; Cárdenas, D. J.; Echavarren, A. M. Gold(I)-Catalyzed Intramolecular [4+2] Cycloadditions of Arylalkynes or 1,3-Enynes with Alkenes: Scope and Mechanism. *J. Am. Chem. Soc.* **2008**, *130* (1), 269–279. https://doi.org/10.1021/ja075794x.

(11) Nieto-Oberhuber, C.; López, S.; Jiménez-Núñez, E.; Echavarren, A. M. The Mechanistic Puzzle of Transition-Metal-Catalyzed Skeletal Rearrangements of Enynes. *Chem. – A Eur. J.* **2006**, *12* (23), 5916–5923. https://doi.org/10.1002/chem.200600174.

(12) Lee, S. I.; Kim, S. M.; Choi, M. R.; Kim, S. Y.; Chung, Y. K.; Han, W.-S.; Kang, S. O. Au(I)-Catalyzed Cyclization of Enynes Bearing an Olefinic Cycle. *J. Org. Chem.* **2006**, *71* (25), 9366–9372. https://doi.org/10.1021/jo061254r.

(13) Nieto-Oberhuber, C.; Muñoz, M. P.; López, S.; Jiménez-Núñez, E.; Nevado, C.; Herrero-Gómez, E.; Raducan, M.; Echavarren, A. M. Gold(I)-Catalyzed Cyclizations of 1,6-Enynes: Alkoxycyclizations and Exo/Endo Skeletal Rearrangements. *Chem. – A Eur. J.* **2006**, *12* (6), 1677–1693. https://doi.org/10.1002/chem.200501088.

(14) Amijs, C. H. M.; Ferrer, C.; Echavarren, A. M. Gold(I)-Catalysed Arylation of 1,6-Enynes: Different Site Reactivity of Cyclopropyl Gold Carbenes. *Chem. Commun.* **2007**, No. 7, 698–700. https://doi.org/10.1039/B615335F.

(15) Cervantes-Reyes, A.; Rominger, F.; Rudolph, M.; Hashmi, A. S. K. Gold(I) Complexes with Eight-Membered NHC Ligands: Synthesis, Structures and Catalytic Activity. *Adv. Synth. Catal.* **2020**, *362* (12), 2523–2533. https://doi.org/10.1002/adsc.202000281.

(16) Guitet, M.; Zhang, P.; Marcelo, F.; Tugny, C.; Jiménez-Barbero, J.; Buriez, O.; Amatore, C.; Mouriès-Mansuy, V.; Goddard, J.-P.; Fensterbank, L.; Zhang, Y.; Roland, S.; Ménand, M.; Sollogoub, M. NHC-Capped Cyclodextrins (ICyDs): Insulated Metal Complexes, Commutable Multicoordination Sphere, and Cavity-Dependent Catalysis. *Angew. Chemie Int. Ed.* **2013**, *52* (28), 7213–7218. https://doi.org/10.1002/anie.201301225.

(17) Zhang, P.; Tugny, C.; Meijide Suárez, J.; Guitet, M.; Derat, E.; Vanthuyne, N.; Zhang, Y.; Bistri, O.; Mouriès-Mansuy, V.; Ménand, M.; Roland, S.; Fensterbank, L.; Sollogoub, M. Artificial Chiral Metallo-Pockets Including a Single Metal Serving as Structural Probe and Catalytic Center. *Chem* **2017**, *3* (1), 174–191. https://doi.org/10.1016/j.chempr.2017.05.009.

(18) Tugny, C.; del Rio, N.; Koohgard, M.; Vanthuyne, N.; Lesage, D.; Bijouard, K.; Zhang, P.; Meijide Suárez, J.; Roland, S.; Derat, E.; Bistri-Aslanoff, O.; Sollogoub, M.; Fensterbank, L.; Mouriès-Mansuy, V. β-Cyclodextrin–NHC–Gold(I) Complex (β-ICyD)AuCl: A Chiral Nanoreactor for Enantioselective and Substrate-Selective Alkoxycyclization Reactions. *ACS Catal.* **2020**, *10* (11), 5964–5972. https://doi.org/10.1021/acscatal.0c00127.

(19) Zhu, X.; Xu, G.; Chamoreau, L.-M.; Zhang, Y.; Mouriès-Mansuy, V.; Fensterbank, L.; Bistri-Aslanoff, O.; Roland, S.; Sollogoub, M. Permethylated NHC-Capped α- and β-Cyclodextrins (ICyDMe) Regioselective and Enantioselective Gold-Catalysis in Pure Water. *Chem. – A Eur. J.* **2020**, *26* (68), 15901–15909. https://doi.org/10.1002/chem.202001990.

(20) Seo, H.; Roberts, B. P.; Abboud, K. A.; Merz, K. M. J.; Hong, S. Novel Acyclic Diaminocarbene Ligands with Increased Steric Demand and Their Application in Gold Catalysis. *Org. Lett.* **2010**, *12* (21), 4860–4863. https://doi.org/10.1021/ol102018z.

(21) Teci, M.; Hueber, D.; Pale, P.; Toupet, L.; Blanc, A.; Brenner, E.; Matt, D. Metal Confinement through N-(9-Alkyl)Fluorenyl-Substituted N-Heterocyclic Carbenes and Its Consequences in Gold-Catalysed Reactions Involving Enynes. *Chem. – A Eur. J.* **2017**, *23* (32), 7809–7818. https://doi.org/10.1002/chem.201701129.

(22) Ruch, A. A.; Ellison, M. C.; Nguyen, J. K.; Kong, F.; Handa, S.; Nesterov, V. N.; Slaughter, L. M. Highly Sterically Encumbered Gold Acyclic Diaminocarbene Complexes: Overriding Electronic Control in Regiodivergent Gold Catalysis. *Organometallics* **2021**, *40* (10), 1416–1433. https://doi.org/10.1021/acs.organomet.0c00776.

(23) Hueber, D.; Teci, M.; Brenner, E.; Matt, D.; Weibel, J.-M.; Pale, P.; Blanc, A. Regioselective Synthesis of Indene from 3-Aryl Propargylic Gem-Dipivalates Catalyzed by N-Heterocyclic Carbene Gold(I) Complexes. *Adv. Synth. Catal.* **2018**, *360* (13), 2453–2459. https://doi.org/10.1002/adsc.201800305.

(24) Doherty, S.; Knight, J. G.; Perry, D. O.; Ward, N. A. B.; Bittner, D. M.; McFarlane, W.; Wills, C.; Probert, M. R. Triaryl-Like MONO-, BIS-, and TRISKITPHOS Phosphines: Synthesis, Solution NMR Studies, and a Comparison in Gold-Catalyzed Carbon–Heteroatom Bond Forming 5-Exo-Dig and 6-Endo-Dig Cyclizations. *Organometallics* **2016**, *35* (9), 1265–1278. https://doi.org/10.1021/acs.organomet.6b00146.

(25) Zhao, Y.; Wakeling, M. G.; Meloni, F.; Sum, T. J.; van Nguyen, H.; Buckley, B. R.; Davies, P. W.; Fossey, J. S. Balancing Bulkiness in Gold(I) Phosphino-Triazole Catalysis. *European J. Org. Chem.* **2019**, *2019* (31–32), 5540–5548. https://doi.org/https://doi.org/10.1002/ejoc.201900850.

(26) Ito, H.; Harada, A.; Ohmiya, H.; Sawamura, M. Use of a Semihollow-Shaped Triethynylphosphane Ligand for Efficient Formation of Six- and Seven-Membered Ring Ethers through Gold(I)-Catalyzed Cyclization of Hydroxy-Tethered Propargylic Esters. *Adv. Synth. Catal.* **2013**, *355* (4), 647–652. https://doi.org/10.1002/adsc.201200949.

(27) Iwai, T.; Ueno, M.; Okochi, H.; Sawamura, M. Synthesis of Cyclobutene-Fused Eight-Membered Carbocycles through Gold-Catalyzed Intramolecular Enyne [2+2] Cycloaddition. *Adv. Synth. Catal.* **2018**, *360* (4), 670–675. https://doi.org/10.1002/adsc.201701193.

(28) Endo, N.; Inoue, M.; Iwasawa, T. Rational Design of a Metallocatalytic Cavitand for Regioselective Hydration of Specific Alkynes. *European J. Org. Chem.* **2018**, *2018* (9), 1136–1140. https://doi.org/10.1002/ejoc.201701613.

(29) Endo, N.; Kanaura, M.; Schramm, M. P.; Iwasawa, T. An Introverted Bis-Au Cavitand and Its Catalytic Dimerization of Terminal Alkynes. *European J. Org. Chem.* **2016**, *2016* (14), 2514–2521. https://doi.org/10.1002/ejoc.201600362.

(30) Endo, N.; Kanaura, M.; Schramm, M. P.; Iwasawa, T. Evaluation of Tuned Phosphorus Cavitands on Catalytic Cross-Dimerization of Terminal Alkynes. *Tetrahedron Lett.* **2016**, *57* (42), 4754–4757. https://doi.org/10.1016/j.tetlet.2016.09.039.

(31) Kanaura, M.; Endo, N.; Schramm, M. P.; Iwasawa, T. Evaluation of the Reactivity of Metallocatalytic Cavities in the Dimerization of Terminal Alkynes. *European J. Org. Chem.* **2016**, *2016* (29), 4970–4975. https://doi.org/10.1002/ejoc.201601070.

(32) Tolman, C. A. Steric Effects of Phosphorus Ligands in Organometallic Chemistry and

Homogeneous Catalysis. *Chem. Rev.* **1977**, *77* (3), 313–348. https://doi.org/10.1021/cr60307a002.

(33) Wang, W.; Hammond, G. B.; Xu, B. Ligand Effects and Ligand Design in Homogeneous Gold(I) Catalysis. *J. Am. Chem. Soc.* **2012**, *134* (12), 5697–5705. https://doi.org/10.1021/ja3011397.

(34) Blanco Jaimes, M. C.; Rominger, F.; Pereira, M. M.; Carrilho, R. M. B.; Carabineiro, S. A. C.; Hashmi, A. S. K. Highly Active Phosphite Gold(I) Catalysts for Intramolecular Hydroalkoxylation, Enyne Cyclization and Furanyne Cyclization. *Chem. Commun.* **2014**, *50* (38), 4937–4940. https://doi.org/10.1039/C4CC00839A.

(35) Gómez-Suárez, A.; Ramón, R. S.; Songis, O.; Slawin, A. M. Z.; Cazin, C. S. J.; Nolan, S. P. Influence of a Very Bulky N-Heterocyclic Carbene in Gold-Mediated Catalysis. *Organometallics* **2011**, *30* (20), 5463–5470. https://doi.org/10.1021/om200705y.

(36) Herrero-Gómez, E.; Nieto-Oberhuber, C.; López, S.; Benet-Buchholz, J.; Echavarren, A. M. Cationic η^1/η^2-Gold(I) Complexes of Simple Arenes. *Angew. Chemie Int. Ed.* **2006**, *45* (33), 5455–5459. https://doi.org/10.1002/anie.200601688.

(37) Malhotra, D.; Mashuta, M. S.; Hammond, G. B.; Xu, B. A Highly Efficient and Broadly Applicable Cationic Gold Catalyst. *Angew. Chemie Int. Ed.* **2014**, *53* (17), 4456–4459. https://doi.org/10.1002/anie.201310239.

(38) Griebel, C.; Hodges, D. D.; Yager, B. R.; Liu, F. L.; Zhou, W.; Makaravage, K. J.; Zhu, Y.; Norman, S. G.; Lan, R.; Day, C. S.; et al. Bisbiphenyl Phosphines: Structure and Synthesis of Gold(I) Alkene π-Complexes with Variable Phosphine Donicity and Enhanced Stability. *Organometallics* **2020**, *39* (14), 2665–2671. https://doi.org/10.1021/acs.organomet.0c00278.

(39) Navarro, M.; Miranda-Pizarro, J.; Moreno, J. J.; Navarro-Gilabert, C.; Fernández, I.; Campos, J. A Dicoordinate Gold(I)–Ethylene Complex. *Chem. Commun.* **2021**, *57* (73), 9280–9283. https://doi.org/10.1039/D1CC02769G.

(40) Worrall, D. E. Studies in the Biphenyl Series. IV. Some 0-Biphenyl Derivatives of Phosphorus, Arsenic and Antimony. *J. Am. Chem. Soc.* **1940**, *62* (9), 2514–2515. https://doi.org/10.1021/ja01866a068.

(41) Dunstan, S. P. C.; Healy, P. C.; Sobolev, A. N.; Tiekink, E. R. T.; White, A. H.; Williams, M. L. Isomorphism in the Structural Chemistry of Two-Coordinate Adducts of Diphenyl(2-Formylphenyl)Phosphine and Triphenylphosphine with Gold(I) Halides. *J. Mol. Struct.* **2014**, *1072* (1), 253–259. https://doi.org/10.1016/J.MOLSTRUC.2014.05.020.

(42) Iwai, T.; Okochi, H.; Ito, H.; Sawamura, M. Construction of Eight-Membered Carbocycles through Gold Catalysis with Acetylene-Tethered Silyl Enol Ethers. *Angew. Chemie Int. Ed.* **2013**, *52* (15), 4239–4242. https://doi.org/10.1002/anie.201300265.

(43) Gómez-Suárez, A.; Nelson, D. J.; Nolan, S. P. Quantifying and Understanding the Steric Properties of N-Heterocyclic Carbenes. *Chem. Commun.* **2017**, *53* (18), 2650–2660.

https://doi.org/10.1039/C7CC00255F.

(44) Clavier, H.; Nolan, S. P. Percent Buried Volume for Phosphine and N-Heterocyclic Carbene Ligands: Steric Properties in Organometallic Chemistry. *Chem. Commun.* **2010**, *46* (6), 841–861. https://doi.org/10.1039/B922984A.

(45) Hillier, A. C.; Sommer, W. J.; Yong, B. S.; Petersen, J. L.; Cavallo, L.; Nolan, S. P. A Combined Experimental and Theoretical Study Examining the Binding of N-Heterocyclic Carbenes (NHC) to the Cp*RuCl (Cp* = H_5-C_5Me_5) Moiety: Insight into Stereoelectronic Differences between Unsaturated and Saturated NHC Ligands. *Organometallics* **2003**, *22* (21), 4322–4326. https://doi.org/10.1021/om034016k.

(46) Falivene, L.; Credendino, R.; Poater, A.; Petta, A.; Serra, L.; Oliva, R.; Scarano, V.; Cavallo, L. SambVca 2. A Web Tool for Analyzing Catalytic Pockets with Topographic Steric Maps. *Organometallics* **2016**, *35* (13), 2286–2293. https://doi.org/10.1021/acs.organomet.6b00371.

(47) Falivene, L.; Cao, Z.; Petta, A.; Serra, L.; Poater, A.; Oliva, R.; Scarano, V.; Cavallo, L. Towards the Online Computer-Aided Design of Catalytic Pockets. *Nat. Chem.* **2019**, *11* (10), 872–879. https://doi.org/10.1038/s41557-019-0319-5.

(48) Barnes, N. A.; Flower, K. R.; Fyyaz, S. A.; Godfrey, S. M.; McGown, A. T.; Miles, P. J.; Pritchard, R. G.; Warren, J. E. Can the Solid State Structures of the Dihalogen Adducts R_3EX_2 (E = P, As; R = Alkyl, Aryl; X = Br, I) with the Molecular Spoke Geometry Be Considered Good Mimics of the Gold(I) Systems [(R_3E)AuX] (E = As, P; R = Alkyl, Aryl; X = Cl, Br, I)? *CrystEngComm* **2010**, *12* (3), 784–794. https://doi.org/10.1039/B917245A.

(49) Grirrane, A.; Álvarez, E.; García, H.; Corma, A. Deactivation of Cationic Cu^{I} and Au^{I} Catalysts for A^3 Coupling by CH_2Cl_2: Mechanistic Implications of the Formation of Neutral Cu^{I} and Au^{I} Chlorides. *Angew. Chemie Int. Ed.* **2014**, *53* (28), 7253–7258. https://doi.org/10.1002/anie.201403973.

(50) Touil, M.; Bechem, B.; Hashmi, A. S. K.; Engels, B.; Omary, M. A.; Rabaâ, H. Theoretical Study of Weak CC Double Bond Coordination in a Gold (I) Catalyst Precursor. *J. Mol. Struct. THEOCHEM* **2010**, *957* (1), 21–25. https://doi.org/10.1016/j.theochem.2010.06.030.

(51) de Frémont, P.; Scott, N. M.; Stevens, E. D.; Nolan, S. P. Synthesis and Structural Characterization of N-Heterocyclic Carbene Gold(I) Complexes. *Organometallics* **2005**, *24* (10), 2411–2418. https://doi.org/10.1021/om050111c.

(52) Ochida, A.; Ito, H.; Sawamura, M. Using Triethynylphosphine Ligands Bearing Bulky End Caps To Create a Holey Catalytic Environment: Application to Gold(I)-Catalyzed Alkyne Cyclizations. *J. Am. Chem. Soc.* **2006**, *128* (51), 16486–16487. https://doi.org/10.1021/ja066800c.

(53) Ochida, A.; Sawamura, M. Phosphorus Ligands with a Large Cavity: Synthesis of Triethynylphosphines with Bulky End Caps and Application to the Rhodium-Catalyzed

Hydrosilylation of Ketones. *Chem. – An Asian J.* **2007**, *2* (5), 609–618. https://doi.org/10.1002/asia.200700006.

(54) Martín-Torres, I.; Ogalla, G.; Yang, J.-M.; Rinaldi, A.; Echavarren, A. M. Enantioselective Alkoxycyclization of 1,6-Enynes with Gold(I)-Cavitands: Total Synthesis of Mafaicheenamine C. *Angew. Chemie Int. Ed.* **2021**, *60* (17), 9339–9344. https://doi.org/10.1002/anie.202017035.

(55) Guzei, I. A.; Wendt, M. An Improved Method for the Computation of Ligand Steric Effects Based on Solid Angles. *Dalt. Trans.* **2006**, No. 33, 3991–3999. https://doi.org/10.1039/B605102B.

(56) Escofet, I.; Armengol-Relats, H.; Bruss, H.; Besora, M.; Echavarren, A. M. On the Structure of Intermediates in Enyne Gold(I)-Catalyzed Cyclizations: Formation of Trans-Fused Bicyclo[5.1.0]Octanes as a Case Study. *Chem. – A Eur. J.* **2020**, *26* (67), 15738–15745. https://doi.org/10.1002/chem.202004237.

(57) Nieto-Oberhuber, C.; López, S.; Muñoz, M. P.; Cárdenas, D. J.; Buñuel, E.; Nevado, C.; Echavarren, A. M. Divergent Mechanisms for the Skeletal Rearrangement and [2+2] Cycloaddition of Enynes Catalyzed by Gold. *Angew. Chemie Int. Ed.* **2005**, *44* (38), 6146–6148. https://doi.org/10.1002/anie.200501937.

(58) Inagaki, F.; Matsumoto, C.; Okada, Y.; Maruyama, N.; Mukai, C. Air-Stable Cationic Gold(I) Catalyst Featuring a Z-Type Ligand: Promoting Enyne Cyclizations. *Angew. Chemie Int. Ed.* **2015**, *54* (3), 818–822. https://doi.org/10.1002/anie.201408037.

(59) Schelwies, M.; Moser, R.; Dempwolff, A. L.; Rominger, F.; Helmchen, G. Gold-Catalyzed Intermolecular Addition of Carbonyl Compounds to 1,6-Enynes: Reactivity, Scope, and Mechanistic Aspects. *Chem. – A Eur. J.* **2009**, *15* (41), 10888–10900. https://doi.org/10.1002/chem.200901614.

(60) Ito, S.; Kusano, S.; Morita, N.; Mikami, K.; Yoshifuji, M. Ligand Effect of Bulky 2,2-Dialkyl-1-Phosphaethenes on Au-Catalyzed Cycloisomerization of 1,6-Enynes and Lactonization of Pent-4-Ynoic Acids. *J. Organomet. Chem.* **2010**, *695* (2), 291–296. https://doi.org/10.1016/j.jorganchem.2009.09.040.

(61) Tang, D.; Chen, Z.; Tang, Y.; Zhang, J.; Xu, Z.; Zhang, J. Investigation of the Cycloisomerization of 1,6-Enynes Catalyzed by Gold Nanoparticles with First-Principles Calculations: Mechanism and Selectivity. *J. Phys. Chem. C* **2014**, *118* (32), 18510–18520. https://doi.org/10.1021/jp503721q.

(62) Gryparis, C.; Efe, C.; Raptis, C.; Lykakis, I. N.; Stratakis, M. Cyclization of 1,6-Enynes Catalyzed by Gold Nanoparticles Supported on TiO2: Significant Changes in Selectivity and Mechanism, as Compared to Homogeneous Au-Catalysis. *Org. Lett.* **2012**, *14* (12), 2956–2959. https://doi.org/10.1021/ol301212j.

(63) Nasrallah, H. O.; Min, Y.; Lerayer, E.; Nguyen, T.-A.; Poinsot, D.; Roger, J.; Brandès, S.; Heintz, O.; Roblin, P.; Jolibois, F.; Poteau, R.; Coppel, Y.; Kahn, M. L.; Gerber, I. C.; Axet, M.

R.; Serp, P.; Hierso, J.-C. Nanocatalysts for High Selectivity Enyne Cyclization: Oxidative Surface Reorganization of Gold Sub-2-nm Nanoparticle Networks. *JACS Au* **2021**, *1* (2), 187–200. https://doi.org/10.1021/jacsau.0c00062.

(64) Leenders, S. H. A. M.; Dürr, M.; Ivanović-Burmazović, I.; Reek, J. N. H. Gold Functionalized Platinum $M_{12}L_{24}$-Nanospheres and Their Application in Cyclization Reactions. *Adv. Synth. Catal.* **2016**, *358* (9), 1509–1518. https://doi.org/10.1002/adsc.201600071.

(65) Toullec, P. Y.; Genin, E.; Leseurre, L.; Genêt, J.-P.; Michelet, V. Room-Temperature Au^{I}-Catalyzed C-C Bond Formation through a Tandem Friedel–Crafts-Type Addition/Carbocyclization Reaction. *Angew. Chemie Int. Ed.* **2006**, *45* (44), 7427–7430. https://doi.org/10.1002/anie.200601980.

(66) López, S.; Herrero-Gómez, E.; Pérez-Galán, P.; Nieto-Oberhuber, C.; Echavarren, A. M. Gold(I)-Catalyzed Intermolecular Cyclopropanation of Enynes with Alkenes: Trapping of Two Different Gold Carbenes. *Angew. Chemie Int. Ed.* **2006**, *45* (36), 6029–6032. https://doi.org/10.1002/anie.200602448.

(67) Leseurre, L.; Toullec, P. Y.; Genêt, J.-P.; Michelet, V. Gold-Catalyzed Hydroamination/Cycloisomerization Reaction of 1,6-Enynes. *Org. Lett.* **2007**, *9* (20), 4049–4052. https://doi.org/10.1021/ol7017483.

(68) Frutos, M.; Avello, M. G.; Viso, A.; Fernández de la Pradilla, R.; de la Torre, M. C.; Sierra, M. A.; Gornitzka, H.; Hemmert, C. Gold Sulfinyl Mesoionic Carbenes: Synthesis, Structure, and Catalytic Activity. *Org. Lett.* **2016**, *18* (15), 3570–3573. https://doi.org/10.1021/acs.orglett.6b01555.

(69) Guérinot, A.; Fang, W.; Sircoglou, M.; Bour, C.; Bezzenine-Lafollée, S.; Gandon, V. Copper Salts as Additives in Gold(I)-Catalyzed Reactions. *Angew. Chemie Int. Ed.* **2013**, *52* (22), 5848–5852. https://doi.org/10.1002/anie.201300600.

(70) Mahamulkar, S. G.; Císařová, I.; Jahn, U. New Phosphine Ligand Architectures Lead to Efficient Gold Catalysts for Cycloisomerization Reactions at Very Low Loading. *Adv. Synth. Catal.* **2018**, *360* (21), 4215–4224. https://doi.org/10.1002/adsc.201800938.

(71) Witham, C. A.; Mauleón, P.; Shapiro, N. D.; Sherry, B. D.; Toste, F. D. Gold(I)-Catalyzed Oxidative Rearrangements. *J. Am. Chem. Soc.* **2007**, *129* (18), 5838–5839. https://doi.org/10.1021/ja071231+.

(72) Carreras, J.; Pereira, A.; Zanini, M.; Echavarren, A. M. Variations on the Theme of JohnPhos Gold(I) Catalysts: Arsine and Carbene Complexes with Similar Architectures. *Organometallics* **2018**, *37* (20), 3588–3597. https://doi.org/10.1021/acs.organomet.8b00276.

(73) de Frémont, P.; Clavier, H.; Rosa, V.; Avilés, T.; Braunstein, P. Synthesis, Characterization, and Reactivity of Cationic Gold(I) α-Diimine Complexes. *Organometallics* **2011**, *30* (8), 2241–2251. https://doi.org/10.1021/om2000426.

(74) Zeineddine, A.; Rekhroukh, F.; Sosa Carrizo, E. D.; Mallet-Ladeira, S.; Miqueu, K.;

Amgoune, A.; Bourissou, D. Isolation of a Reactive Tricoordinate α-Oxo Gold Carbene Complex. *Angew. Chemie Int. Ed.* **2018**, *57* (5), 1306–1310. https://doi.org/10.1002/anie.201711647.

(75) Nieto-Oberhuber, C.; Paz Muñoz, M.; Buñuel, E.; Nevado, C.; Cárdenas, D. J.; Echavarren, A. M.;Cyclization Reactions Cationic Gold(I) Complexes: Highly Alkynophilic Catalysts for the Exo-and Endo-Cyclization of Enynes. *Angew. Chem. Int. Ed* **2004**, *43*, 2402–2406. https://doi.org/10.1002/anie.200353207.

(76) Leyva, A.; Corma, A. Isolable Gold(I) Complexes Having One Low-Coordinating Ligand as Catalysts for the Selective Hydration of Substituted Alkynes at Room Temperature without Acidic Promoters. *J. Org. Chem.* **2009**, *74* (5), 2067–2074. https://doi.org/10.1021/jo802558e.

(77) Marion, N.; Ramón, R. S.; Nolan, S. P. [(NHC)Au^{I}]-Catalyzed Acid-Free Alkyne Hydration at Part-per-Million Catalyst Loadings. *J. Am. Chem. Soc.* **2009**, *131* (2), 448–449. https://doi.org/10.1021/ja809403e.

(78) Inoue, M.; Ugawa, K.; Maruyama, T.; Iwasawa, T. Selective Catalytic Hydration of Alkynes in the Presence of Au-Cavitands: A Study in Structure–Activity Relationships. *European J. Org. Chem.* **2018**, *2018* (38), 5304–5311. https://doi.org/10.1002/ejoc.201800948.

(79) Rzhevskiy, S. A.; Philippova, A. N.; Chesnokov, G. A.; Ageshina, A. A.; Minaeva, L. I.; Topchiy, M. A.; Nechaev, M. S.; Asachenko, A. F. Ring Size and Nothing Else Matters: Unusual Regioselectivity of Alkyne Hydration by NHC Gold(I) Complexes. *Chem. Commun.* **2021**, *57* (46), 5686–5689. https://doi.org/10.1039/D1CC01837J.

(80) Zhou, J.; Litle, E. D.; Gabbaï, F. P. Isolation and Reactivity of a Gold(i) Hydroxytrifluoroborate Complex Stabilized by Anion- π^{+} Interactions. *Chem. Commun.* **2021**, *57* (79), 10154–10157. https://doi.org/10.1039/D1CC04105C.

(81) Nečas, D.; Kotora, M. Ring Opening of Methylenecycloalkenes via the C−C Bond Cleavage. *Org. Lett.* **2008**, *10* (22), 5261–5263. https://doi.org/10.1021/ol801728f.

(82) Hasegawa, M.; Kurahashi, T.; Matsubara, S. Rhodium(III) Porphyrin-Catalyzed Reactions via Activation of Alkynes. *Chem. Lett.* **2014**, *43* (12), 1937–1939. https://doi.org/10.1246/cl.140810.

(83) Nakai, Y.; Kimura, T.; Uozumi, Y. Alkylative Cyclization of 1,6-Enynes in Water with an Amphiphilic Resin-Supported Palladium Catalyst. *Synlett* **2006**, *2006* (18), 3065–3068. https://doi.org/10.1055/S-2006-951498/ID/4/BIB.

(84) Lee, Y.-J.; Schrock, R. R.; Hoveyda, A. H. Endo-Selective Enyne Ring-Closing Metathesis Promoted by Stereogenic-at-Mo Monoalkoxide and Monoaryloxide Complexes. Efficient Synthesis of Cyclic Dienes Not Accessible through Reactions with Ru Carbenes. *J. Am. Chem. Soc.* **2009**, *131* (30), 10652–10661. https://doi.org/10.1021/ja904098h.

(85) Nguyen, T.-A.; Roger, J.; Nasrallah, H.; Rampazzi, V.; Fournier, S.; Cattey, H.; Sosa Carrizo, E. D.; Fleurat-Lessard, P.; Devillers, C. H.; Pirio, N.; Lucas, D.; Hierso, J.-C. Gold(I)

Complexes Nuclearity in Constrained Ferrocenyl Diphosphines: Dramatic Effect in Gold-Catalyzed Enyne Cycloisomerization. *Chem. – An Asian J.* **2020**, *15* (18), 2879–2885. https://doi.org/10.1002/asia.202000579.

(86) Johnson, J. A.; Petersen, B. M.; Kormos, A.; Echeverría, E.; Chen, Y.-S.; Zhang, J. A New Approach to Non-Coordinating Anions: Lewis Acid Enhancement of Porphyrin Metal Centers in a Zwitterionic Metal–Organic Framework. *J. Am. Chem. Soc.* **2016**, *138* (32), 10293–10298. https://doi.org/10.1021/jacs.6b05626.

(87) Broggi, J.; Urbina-Blanco, C. A.; Clavier, H.; Leitgeb, A.; Slugovc, C.; Slawin, A. M. Z.; Nolan, S. P. The Influence of Phosphane Ligands on the Versatility of Ruthenium–Indenylidene Complexes in Metathesis. *Chem. – A Eur. J.* **2010**, *16* (30), 9215–9225. https://doi.org/10.1002/chem.201000659.

(88) Pizarro, J. D.; Molina, F.; Fructos, M. R.; Pérez, P. J. Alkoxydiaminophosphine Ligands as Surrogates of NHCs in Copper Catalysis. *Chem. – A Eur. J.* **2020**, *26* (45), 10330–10335. https://doi.org/10.1002/chem.202001517.

(89) Vasil'ev, A. A.; Engman, L.; Serebryakov, E. P. Intramolecular Alkene–Alkyne Metathesis and 1,4-Cis-Hydrogenation as a Stereocontrolled Route to Compounds with Exocyclic Double Bonds. *Russ. Chem. Bull.* **2020**, *69* (1), 169–171. https://doi.org/10.1007/s11172-020-2739-1.

(90) Swamy, P.; Reddy, M. M.; Naresh, M.; Kumar, M. A.; Srujana, K.; Durgaiah, C.; Narender, N. Very Important Publication: Hypoiodite-Catalyzed Regioselective Oxidation of Alkenes: An Expeditious Access to Aldehydes in Aqueous Micellar Media. *Adv. Synth. Catal.* **2015**, *357* (6), 1125–1130. https://doi.org/10.1002/adsc.201400986.

(91) Chang, X.; Cheng, X.; Liu, X.-T.; Fu, C.; Wang, W.-Y.; Wang, C.-J. Stereodivergent Construction of 1,4-Nonadjacent Stereocenters via Hydroalkylation of Racemic Allylic Alcohols Enabled by Copper/Ruthenium Relay Catalysis. *Angew. Chemie Int. Ed.* **2022**, *61* (36), e202206517. https://doi.org/10.1002/anie.202206517.

(92) Griffiths, O. M.; Esteves, H. A.; Chen, Y.; Sowa, K.; May, O. S.; Morse, P.; Blakemore, D. C.; Ley, S. V. Photoredox-Catalyzed Dehydrogenative Csp^3–Csp^2 Cross-Coupling of Alkylarenes to Aldehydes in Flow. *J. Org. Chem.* **2021**, *86* (19), 13559–13571. https://doi.org/10.1021/acs.joc.1c01621.

(93) Hayashi, R.; Ando, K.; Udagawa, T.; Sai, M. β-Functionalized and α,β-Difunctionalized Ketones from 1-Arylallylic Alcohols via Dipotassio α,β-Dianion Intermediates. *Adv. Synth. Catal.* **2023**, *365* (6), 826–833. https://doi.org/10.1002/adsc.202201047.

(94) Shabalin, D. A.; Kazak, M. K.; Ushakov, I. A.; Vashchenko, A. V; Schmidt, E. Y. Synthesis of Pyrrolo[2,1-a]Isoquinolinium Salts from 1-Pyrrolines and Alkynes via Rhodium-Catalyzed C–H Functionalization/N-Annulation Tandem Reaction. *J. Org. Chem.* **2022**, *87* (10), 6860–6869. https://doi.org/10.1021/acs.joc.2c00555.

(95) Makioka, Y.; Taniguchi, Y.; Kitamura, T.; Fujiwara, Y.; Saiki, A.; Takaki, K. Isomerization of

Terminal Alkynes Catalyzed by Ytterbium(II)-Aromatic Imine Complexes. *Bull. Soc. Chim. Fr.* **1997**, *134* (3–4), 349–355.

(96) Ghiringhelli, F.; Nattmann, L.; Bognar, S.; van Gemmeren, M. The Direct Conversion of α-Hydroxyketones to Alkynes. *J. Org. Chem.* **2019**, *84* (2), 983–993. https://doi.org/10.1021/acs.joc.8b02941.

(97) León Sandoval, A.; Doherty, K. E.; Wadey, G. P.; Schroeder, C. M.; Leadbeater, N. E. Fast, Easy Oxidation of Alcohols Using an Oxoammonium Salt Bearing the Nitrate Anion. *Tetrahedron Lett.* **2023**, *116*, 154332. https://doi.org/10.1016/j.tetlet.2022.154332.

(98) Gatto, M.; Del Zotto, A.; Segato, J.; Zuccaccia, D. Hydration of Alkynes Catalyzed by L–Au–X under Solvent- and Acid-Free Conditions: New Insights into an Efficient, General, and Green Methodology. *Organometallics* **2018**, *37* (24), 4685–4691. https://doi.org/10.1021/acs.organomet.8b00689.

(99) Huang, Q.; Li, Y.-W.; Ning, X.-S.; Jiang, G.-Q.; Zhang, X.-W.; Qu, J.-P.; Kang, Y.-B. Regioselective Wacker-Type Oxidation of Internal Olefins in TBuOH Using Oxygen as the Sole Oxidant and TBuONO as the Organic Redox Cocatalyst. *Org. Lett.* **2020**, *22* (3), 965–969. https://doi.org/10.1021/acs.orglett.9b04503.

3. Chapter 3. DFT-guided Development of New Hemilabile (P^N) Ligands for Gold-(I/III) RedOx Catalysis : Application to the Thiotosylation of Aryl Iodides

Muratov, K.; Zaripov, E.; Berezovski, M. V.; Gagosz, F. DFT-guided Development of New Hemilabile (P^N) Ligands for Gold-(I/III) RedOx Catalysis : Application to the Thiotosylation of Aryl Iodides, *Submitted*

3.1. Abstract

Ligand-enabled oxidative addition of C(sp^2)-X bonds to Au(I) centers has recently appeared as a valuable strategy for the development of catalytic RedOx processes**.** Several cross-coupling reactions that were previously considered difficult to achieve were reported lately, thus expanding the synthetic potential of Au(I) complexes beyond the traditional nucleophilic functionalization of π-systems. MeDalPhos has played an important role in this development and, despite several studies on alternative structures, remains so far, the only general ligand for such process. We report herein the discovery and the DFT-guided structural optimization of a new family of hemilabile (P^N) ligands that can promote oxidative addition of aryl iodides to Au(I). These flexible ligands, which possess a common 2-methylamino heteroaromatic *N*-donor motif, are structurally and electronically tunable, beyond being easily accessible and affordable. The corresponding Au(I) complexes were shown to outperform the reactivity of (MeDalPhos)Au(I) in a series of alkoxy- and amidoarylation of alkenes. Their synthetic potential and comparatively higher reactivity were further highlighted in the thiotosylation of aryl iodides, a challenging unreported C-S cross-coupling reaction that could not be achieved under classical Pd(0)/Pd(II) catalysis and that allows a general and divergent access to aryl sulfur derivatives.

3.2. Introduction

The exploration of Au(I) chemistry has revealed intriguing patterns of reactivity and paved the way for diverse catalytic applications. As research advances, attention is also turning to Au(I)/Au(III)) RedOx chemistry, an area that presents unique opportunities and challenges and promises to advance our understanding of gold catalysis to a different field of study.

Cross-coupling reactions driven by transition metal catalysts typically rely on catalytic cycles that involve the interconversion between different oxidation states of the metal atom. This fluctuation is usually accomplished via 2-electron RedOx steps, specifically oxidative addition and reductive elimination. Traditionally, palladium has emerged as the preferred metal for employment in a plethora of cross-coupling reactions.[1–4]

However, the Au(I)/Au(III) redox pair stands as a distinctive case. This is primarily because it exhibits an exceptionally high RedOx potential (E^0=1.41 V versus the Standard Hydrogen Electrode in water) compared to the isoelectronic Pd(0)/Pd(II) pair (E^0=0.92 V).[5] Initial investigations into this phenomenon adopted the strategy of using stoichiometric amounts of external oxidants[6–14], photochemical conditions[15–19] or diazonium salts[20–25] to design Au(I)/Au(III) catalytic cycles via 2-electron oxidation to generate the key Au(III) intermediates. While these advancements have proven effective, they are not without their limitations and restrictions, which could potentially hinder their broader utilization.

In view of these challenges, alternative approaches are explored, such as the chelate-assisted strategy and the application of hemilabile ligands. The chelation-assisted method focuses on the generation of a Au(I) complex coordinated with a ligand that places a functional group close to the metal center. This proximity increases the susceptibility to oxidative addition to the gold atom. Conversely, the use of hemilabile ligands is particularly promising as it offers the opportunity for more controlled reactions and a wider range of applications. These hemilabile ligands can be crucial in the stabilization of Au(III) species by acting as a chelate upon coordination to the metal center, which offers an exciting direction for the development of novel catalytic systems.

In this section, the discussion will be focused on Au(I)/Au(III) catalysis without the use of external oxidants and an up-to-date summary of research progress in this area willl be provided. Particular attention will be paid to the use of hemilabile ligands to promote the Au(I)/Au(III) catalytic cycle with a discussion of recent research breakthroughs in this area.

3.2.1. Chelation-assisted strategy

Bourissou and Amgoune in 2014 described the pioneering use of chelation assisted oxidative addition of C(sp^2)-X (X - I, Br) to a Au(I), resulting in the formation of P,C-chelated Au(III) complex **3.2.1-3** (**Scheme 3.2.1-1, A**).[26] This complex is traditionally difficult to obtain via the classical C-H activation pathway due to the propensity of phosphines to be oxidized by Au(III). In their experimental design, the researchers utilized 8-halo naphthyl phosphines **3.2.1-1** as ligands, resulting in the generation of Au(I) complexes **3.2.1-2**. Notably, when X was iodine, the oxidative addition proceeded at room temperature, yielding Au(III)-complex in high efficiency. Conversely, when X was bromine, the oxidative addition from Au(I) necessitated heating for an extended period at 130 °C. Notably, no oxidative addition occurred when X was a chloride.

Building on this approach, subsequent studies introduced secondary phosphine oxide complexes **3.2.1-4a**, a novel agent in Au(III) chemistry (**Scheme 3.2.1-1, B**).[27] However, contrasting with the related phosphines, this reaction necessitated a base to proceed cleanly, yielding the corresponding (P=O,C)-cyclometalated complexes. A further intriguing finding was the behavior of amino-phosphine **3.2.1-4b**, which readily underwent oxidative addition at room temperature, demonstrating the potential versatility of phosphine derivatives in this field.

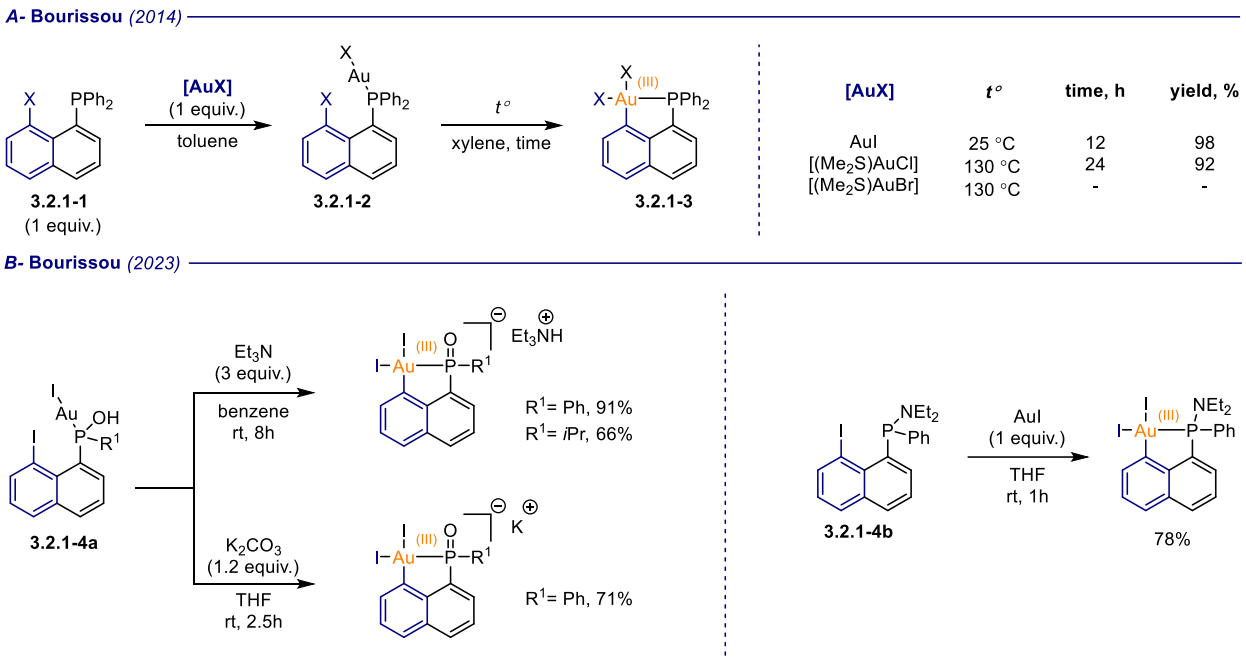

Scheme 3.2.1-1. Chelation-assisted oxidative addition.

Using a different approach, Nevado's group in 2021 reported a new type of chelation-assisted oxidative addition of Au(I) into C-C bonds (**Scheme 3.2.1-2, A**).[28] The focus of their study lay in understanding the influence of neighboring chelating groups on the insertion of the strained C-C bond of biphenylene. After a series of steps, the Au(I) complex **3.2.1-5** underwent the ring-opening of the biphenylene system and the researchers were able to isolate a monocyclometalated (P^C) Au(III) complex **3.2.1-6**. It was hypothesized that the unexpected presence of water might be responsible for the formation of this complex. Confirmation of the C-C activation was further established through the analysis of product **3.2.17**. This product was formed via reductive elimination at the gold(III) center, following the exchange of the BF_4^- counter-anion with the weakly coordinating sodium tetrakis[3,5-bis(trifluoromethyl)phenyl]borate (NaBArF). Furthermore, it is significant to note a divergence in reactivity when comparing the pyridine-substituted biphenylene with the P-coordinated gold(I) complex **3.2.1-8**. In contrast to the **3.2.1-5**, the latter failed to yield similar cyclometalated products despite being subjected to extended heating, and instead afforded (N^C^C)-complex **3.2.1-9** in 60% yield. Their work also underlined the importance of finely tuning the chelating group, as evidenced by the formation of cationic dimeric species when the biphenylene and phosphine were connected by a shorter linker.

In 2014, the research group led by Bourissou reported the ability of a bisphosphine-ligated Au(I)-complex **3.2.1-10** to undergo oxidative addition of aryl iodides (**Scheme 3.2.1-2, B**) to give Au(III) complex **3.2.1-11**.[29] Their approach involved careful manipulation of the Au(I)-complex structure to elevate its energy state, effectively predisposing it to adopt the square-planar geometry of the forming Au(III)-product after oxidative addition. This marked a significant deviation from the typically two-coordinate linear geometry favored by Au(I), which typically forms dinuclear

complexes with the majority of bidentate ligands.[30,31] Nevertheless, the researchers capitalized on the prior work of Laguna and Jones,[32] integrating a carborane-based three-coordinate Au(I)-complex into their research. They discovered that this particular complex was capable of undergoing oxidative addition of aryl iodides under relatively mild conditions. In a subsequent publication,[33] the researchers demonstrated that the (diphosphinocarborane) gold(I) complexes can also participate in the addition into strained C-C bonds of biphenylene to give complex **3.2.1-12**.

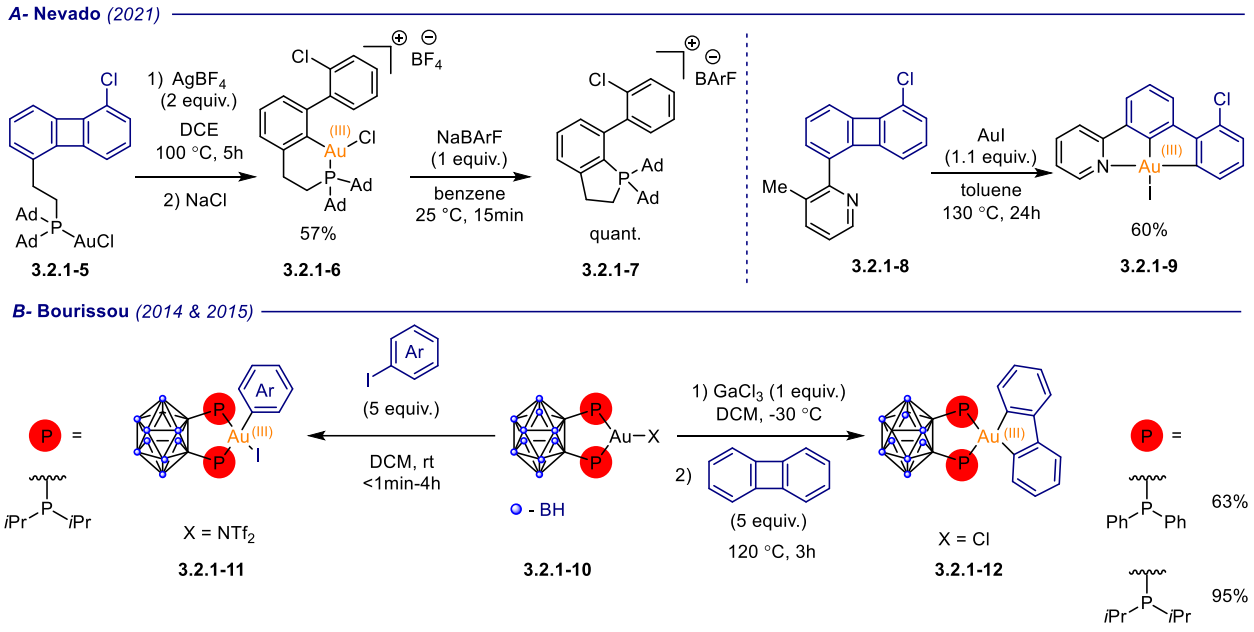

Scheme 3.2.1-2. Oxidative addition into C-C and C-I bonds.

Utilizing an analogous strategy, Russel and co-workers synthesized a tricoordinate bipyridyl gold complex **3.2.1-13** (**Scheme 3.2.1-3**).[34] This species has shown the ability to participate in an oxidative addition with aryl iodides, thus generating the Au(III) oxidative addition complex **3.2.1-14a**. The produced complex intriguingly forms a dynamic equilibrium with ethylene, requiring a static vacuum for a complete conversion. This reaction is marked by its reversibility, as re-introducing 1 bar of ethylene induces over 95% reconversion to the initial Au(I) complex **3.2.1-13** in just an hour. In subsequent investigations, the team expanded their study to understand the mechanism of the oxidative addition to gold and the subsequent reductive elimination.[35] They were also successful in extending the range of the oxidative addition to include vinyl and alkynyl iodides.[36] An interesting discovery was that the application of alkynyl iodides resulted in a bimetallic complex **3.2.1-14b**, with one Au-center participating in the oxidative addition and the other in π-bonding to the alkynyl unit. Interestingly, the employment of 4-CF_3 and 4-OMe substituted alkynes led to unexpected reactions, as only monometallic complexes **3.2.1-14a** were formed, bypassing the formation of bimetallic complexes. Another significant finding was that introducing an organozinc reagent to the Au(III) complex **3.2.1-14a** led to a coupling product,

marking the first instance of Negishi cross-coupling at gold, although it occurred under stoichiometric conditions.

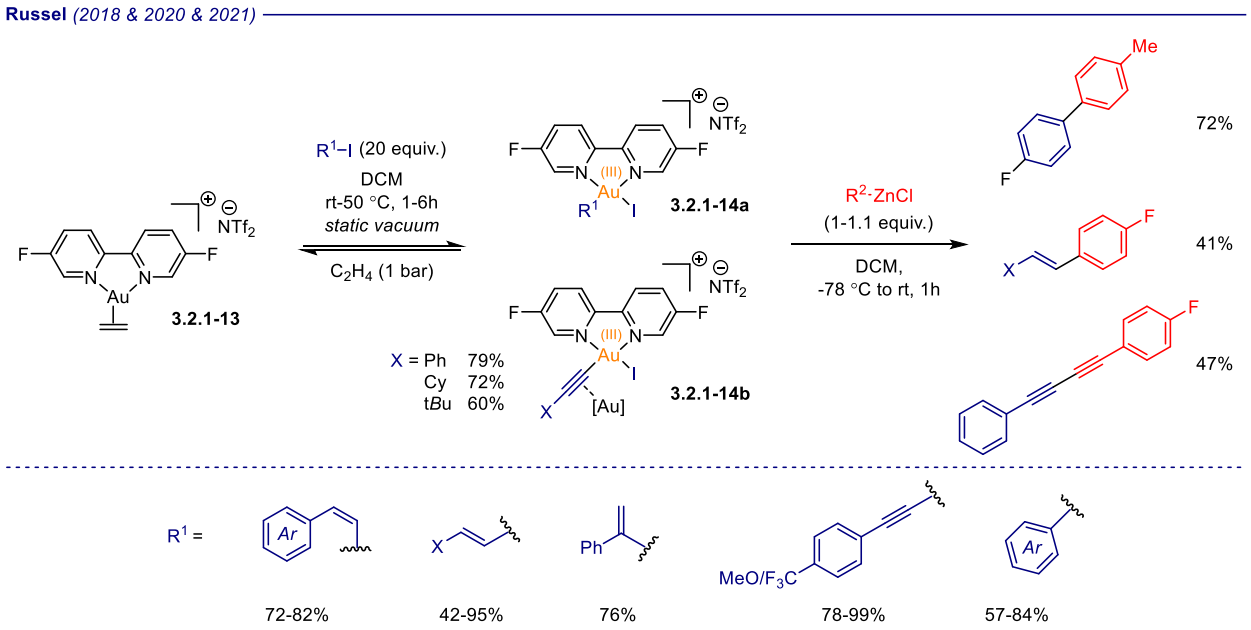

Scheme 3.2.1-3. Stoichometric Negishi cross-coupling.

Ribas and collegues presented an interesting publication in 2015, showing that a chelation-assisted strategy allows for an oxidant-free Au(I)/Au(III)-catalyzed C-X coupling reaction (**Scheme 3.2.1-4, A**).[37] The researchers successfully conducted halide exchange and C(sp^2)-O bond formation reactions with Au(I) complexes and aryl halide triazomacrocyclic substrates **3.2.1-15**.

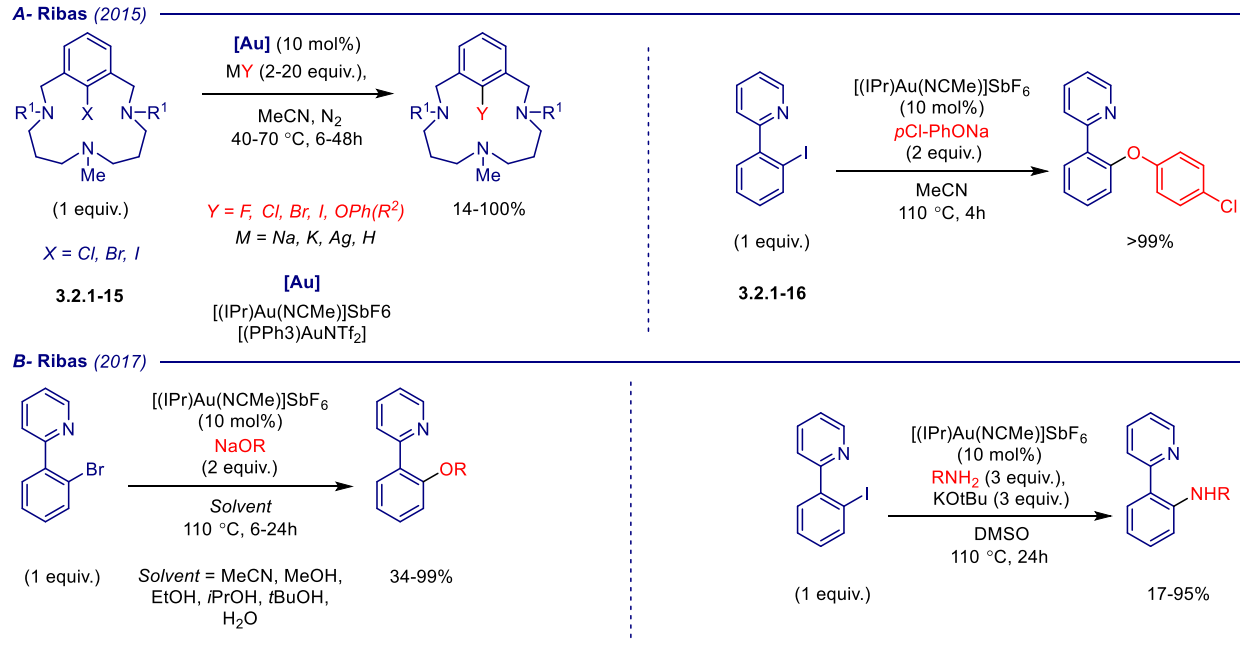

Scheme 3.2.1-4. Chelation-assisted gold-catalyzed C-X bond formation.

Notably, they demonstrated the applicability of this methodology to more readily available substrates, specifically 2-(2-halophenyl)pyridines **3.2.1-16**, characterized by a single chelating group. In their follow-up publication (**Scheme 3.2.1-4, B**),[38] the researchers explored the reaction mechanism in greater depth. They broadened the spectrum of employed nucleophiles from halides and phenols to amines and amides, which marked the first instance of an Au(I)/Au(III)-catalyzed C-N bond formation.

3.2.2. Hemilabile ligands

Recently the use of hemilabile ligands in Au(I)/Au(III) chemistry has emerged as a powerful strategy, offering several advantages over the traditional approaches. The dynamic nature of hemilabile ligands allows for the fine-tuning of the steric and electronic environment around the gold center, thereby enabling the control of regioselectivity and enantioselectivity in gold-catalyzed reactions. This is a significant advantage over the chelation-assisted strategy, which often requires the design of new chelating species for each specific transformation.

3.2.2.1. Formation of C-C bonds

A groundbreaking discovery in this field came in 2017 when Bourissou and Amgoune made a remarkable advancement in the field of Au(I)/Au(III) catalysis.[39] They demonstrated an innovative application of a simple (P^N) ligand, known as MeDalPhos,[40] enabling an efficient, oxidant-free Au(I)/Au(III) catalytic cycle. The key to their discovery resided in the capacity of this ancillary ligand to facilitate the typically demanding oxidative addition of aryl iodides and bromides under mild conditions (**Scheme 3.2.2.1-1, A**). The crucial role of the hemilabile amino group in this transformation was confirmed through DFT calculations. Upon oxidative addition to the **3.2.2.1-1**, the auxiliary amine group would subsequently coordinate with the resultant harder Au(III)-center, thus tempering its reactivity and yielding Au(III) complex **3.2.2.1-2**. Another intriguing discovery was the impact of the counter-anion on the reaction rate. For instance, when utilizing SbF_6^-, which exhibits less coordinating properties than NTf_2^-, the oxidative addition of PhI was found to be spontaneous, occurring within the mixing duration at ambient temperature. They undertook an assessment of various aryl halides in the oxidative addition reaction, noting that the electron-rich substrates were more reactive than electron-poor ones, which contrasted with palladium's increased reactivity towards electron-poor compounds, and they also found that aryl iodides reacted more readily than aryl bromides. Further, the researchers examined a gold-catalyzed arylation process involving 1,3,5-trimethoxybenzene and aryl iodides to give cross-coupling products **3.2.2.1-3**. The reaction was rapid and achieved good yields, ranging from 65% to 99%. This research marked a critical turning point in the field of oxidant-free Au(I)/Au(III) catalysis. The [(MeDalPhos)AuCl] complex quickly found a common use in the aftermath of these studies. The exceptional performance of the MeDalphos ligand in stabilizing Au(III) intermediates

unlocked new possibilities for future Au(I)/Au(III) catalytic transformations using simple [(MeDalphos)AuCl] complex.

In 2019, another important example was reported by the Bourissou research team, who uncovered the potential for regioselective C3 arylation of indoles to give products **3.2.2.1-4** (**Scheme 3.2.2.1-1, B**).[41] Such a transformation is rarely encountered in other forms of transition metal-mediated catalysis. Notably, this reaction demonstrated significant tolerance for a variety of functional groups within both aryl iodide and indole partners.

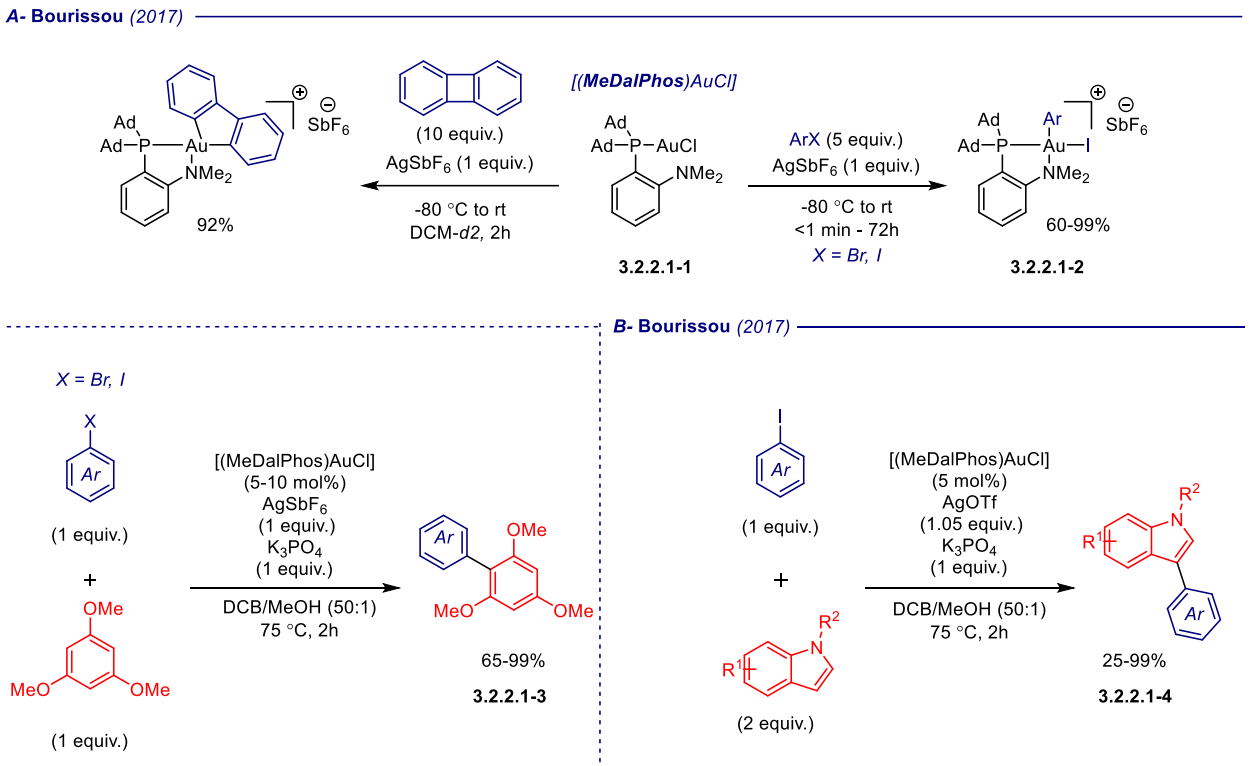

Scheme 3.2.2.1-1. Gold-catalyzed cross-coupling.

In 2020, the groups of Bourissou,[42] Patil,[43] and Shi[44] independently published a similar methodology aimed at the heteroarylation of alkenes. Interestingly, in each of these studies the researchers discovered that the cyclization reaction occurs with full selectivity, and exclusively follows a 5-exo fashion. This strategy has exhibited adaptability in synthesizing products **3.2.2.1-5** with 5-, 6, and 7-membered rings, and also allows amido-arylation reactions to proceed under the developed conditions (**Scheme 3.2.2.1-2, A**). An extension of this methodology was explored by the groups led by Patil (**Scheme 3.2.2.1-2, B**) and Shi (**Scheme 3.2.2.1-2, C**), where they successfully demonstrated that a three-component oxyarylation reaction to yield product **3.2.2.1-6** could be performed. The researchers managed to vary the nucleophilic coupling partner, employing compounds such as ethanol, isopropanol, cyclohexanol, and even water. The result was the generation of the respective oxyarylated products with moderate to excellent yields. The group of Shi further investigated the reaction using internal alkenes, which required harsher conditions (**Scheme 3.2.2.1-2, C**). Experimentation with alternative external nucleophiles was

limited in success, with 4-nitroaniline or 1,3,5-dimethoxybenzene being among the few that reacted favorably. The latter provided only a moderate yield, attributed to substantial C-C bond cross-coupling byproducts. A noteworthy contribution by the team of Shi was their development of a procedure to easily replace the OMe group with various nucleophiles (such as N, C, S), producing the desired functionalized products **3.2.2.1-8** in satisfactory yields.

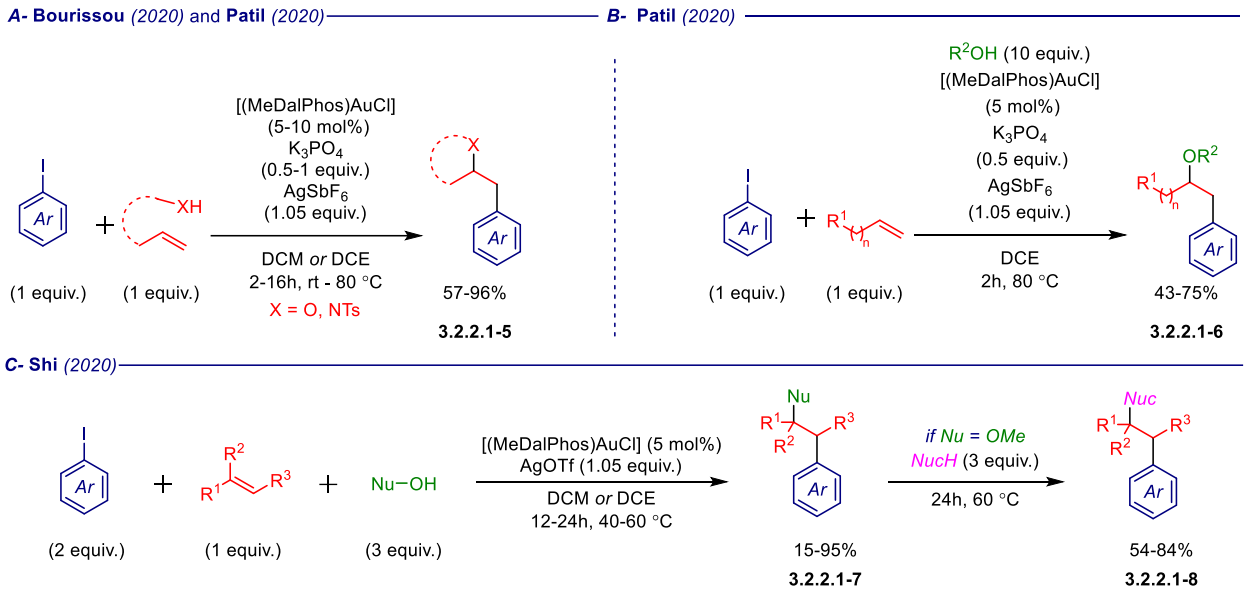

Scheme 3.2.2.1-2. Heteroarylation of alkenes.

From a mechanistic perspective, the reactions are proposed to proceed through a Au(I)/Au(III) catalytic cycle, starting from the [(MeDalPhos)AuCl] complex (**Scheme 3.2.2.1-3**). The cycle initiates with the aryl iodide's oxidative addition to gold to provide Au(III) complex **3.2.2.1-9**, which is facilitated by the presence of the (P,N) ligand. Subsequent iodide abstraction and coordination of the alkene to Au(III) forms complex **3.2.2.1-10** and stimulates cyclization by the nucleophilic addition from the adjacent alcohol or amide to give complex **3.2.2.1-11**. The catalytic cycle finishes with a reductive elimination at the gold center, making a $C(sp^2)$-$C(sp^3)$ bond and regenerating the active [(MeDalPhos)Au^+] species.

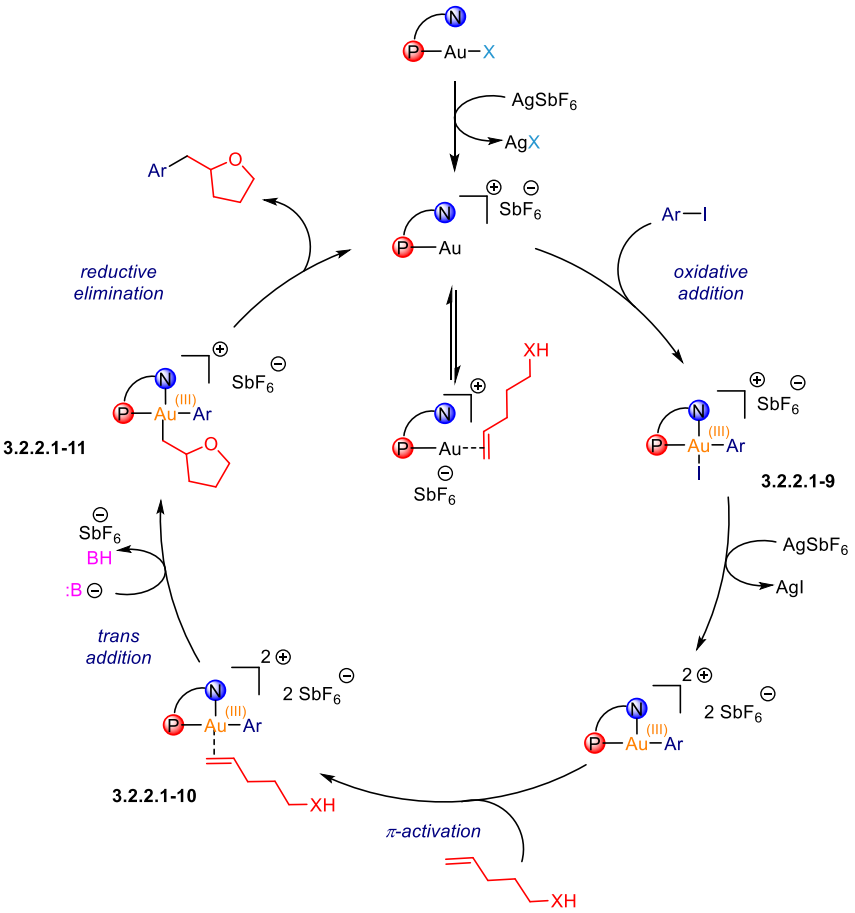

Scheme 3.2.2.1-3. Mechanism of heteroarylation of alkenes.

In 2020, Patil and colleagues expanded this approach and published a novel gold-catalyzed 1,2-diarylation method for alkenes (**Scheme 3.2.2.1-4**) to obtain products **3.2.2.1-12**.[45] This methodology evades the potential formation of unwanted direct Ar-Ar' coupling byproducts. The developed reaction was found to be tolerant to a variety of aryl iodide and alkene partners, although a slight drop in yields was noted with electron-deficient aryl iodides. This reduction in the yield is possibly due to challenges in participating in the key oxidative addition step. The researchers successfully broadened the reaction's scope to synthesize 9,10-dihydrophenanthrenes **3.2.2.1-13** by engaging 2-allyl-1,1'-biphenyl with appropriate aryl iodides. Additionally, they applied the approach to reactions involving iodoaryl alkenes and indoles, producing the 6-membered products **3.2.2.1-14** in yields ranging from moderate to excellent.

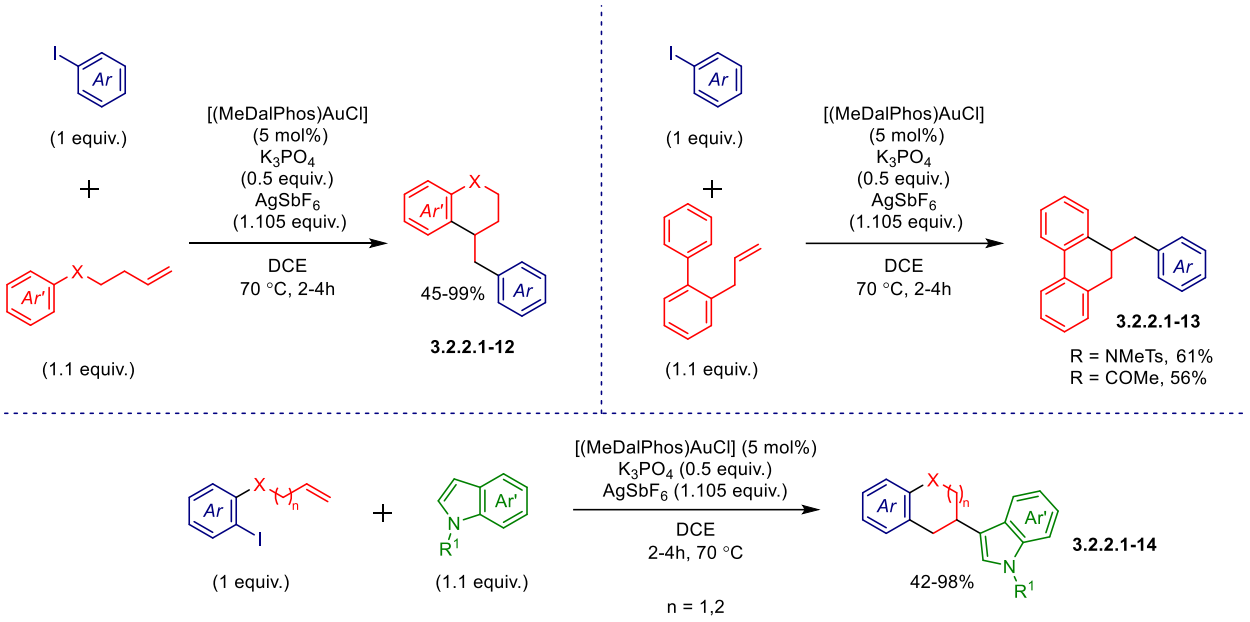

Scheme 3.2.2.1-4. Gold-catalyzed diarylation of alkenes.

In 2022, Bourissou and collegues made notable progress in gold redox catalysis, reporting the use of both α- and γ-allyl substrates in a Au(I)/(III)-catalyzed indole allylation that selectively generated C3-allylated derivatives **3.2.2.1-15** (**Scheme 3.2.2.1-5, A**).[46] The researchers proposed that this C(sp^2)-C(sp^3) coupling reaction utilizes a key intermediate, a dicationic π-allyl Au(III) complex **3.2.2.1-16**. It is noteworthy that the synthesis and verification of the first gold π -allyl complexes were only accomplished in 2020, via separate research by Tilset[47] (**Scheme 3.2.2.1-5, B**) and Bourissou (**Scheme 3.2.2.1-5, C**).[48]

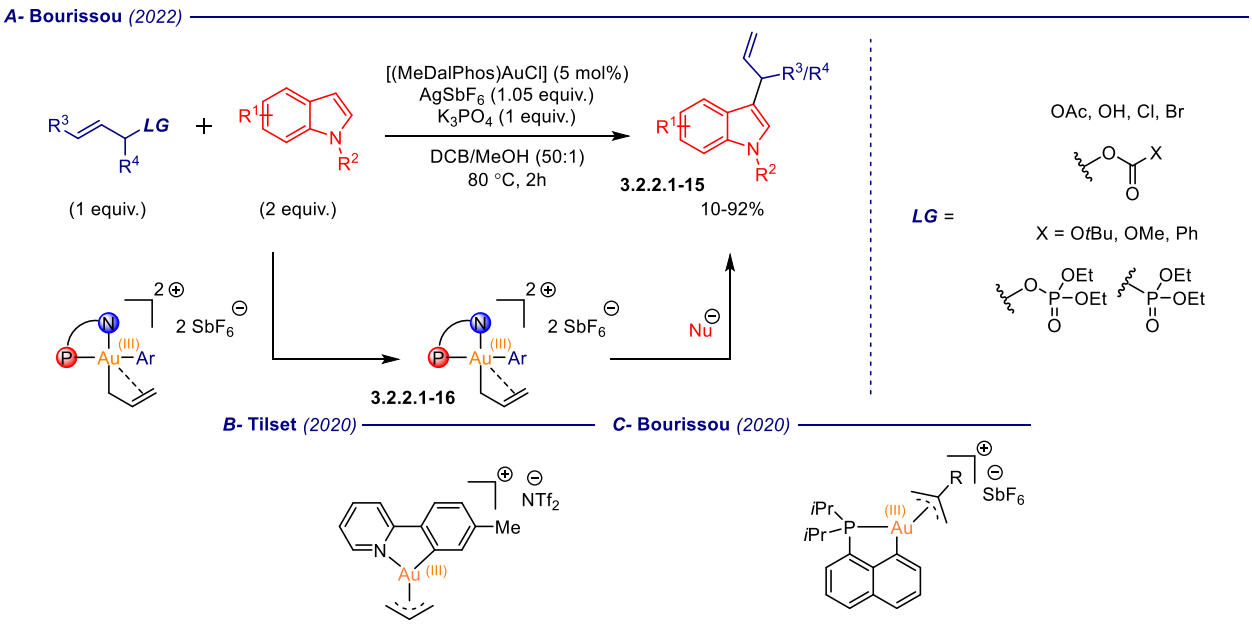

Scheme 3.2.2.1-5. Allylation of indole.

Interestingly, the method they developed accommodates a range of leaving groups on the allyl substrates, including simple groups such as OH or Cl, which shows the wide applicability and adaptability of the gold-catalyzed allylation protocol.

Patil and coworkers recently introduced a groundbreaking report that shows the use of a gold-catalyzed Heck reaction for the first time through Au(I)/Au(III) redox catalysis (**Scheme 3.2.2.1-6, A**).[49] This work represents a pioneering achievement in gold chemistry, executing in catalytic manner the key organometallic steps, such as migratory insertion and β-hydride elimination. It also offers a solution to some limitations found in earlier transition metal-catalyzed Heck reactions by offering complementary regioselectivity. Various alkenes were tested and found to be suitable for the reaction, mainly yielding the *E*-isomers **3.2.2.1-17** with good efficiency. The research team further explored a gold-catalyzed interrupted relay Heck reaction, marking the first successful implementation of a chain-walking process in gold catalysis (**Scheme 3.2.2.1-6, B**).[50] This innovative reaction combines three distinct chemical processes: Heck reaction, chain-walking, and anti-addition through π-activation to afford substrates **3.2.2.1-18**. The intrinsic π-activation ability of gold catalyst plays a crucial role by interrupting the chain-walking procedure, consequently activating alkenes and enabling nucleophilic attack by an adjacent aryl ring. This distinctive feature elevates this gold-catalyzed reaction above other methodologies that employ transition metals for chain-walking or related relay Heck reactions. The research team also demonstrated the reaction's versatility in the development of 1,3-diarylation to give products **3.2.2.1-19** and the intriguing 1,n-hydroarylation of alkenes, which yields compounds **3.2.2.1-20.**

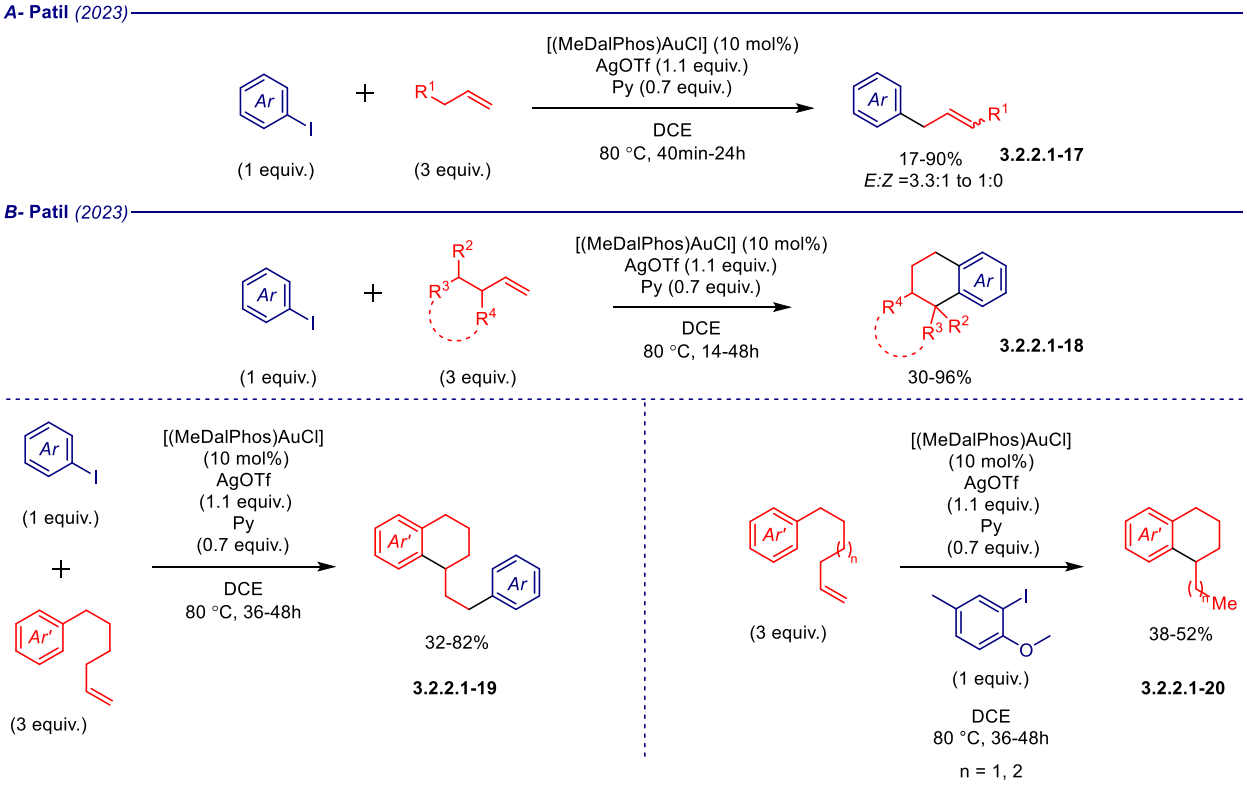

Scheme 3.2.2.1-6. Gold-catalyzed Heck and interrupted-relay Heck reactions.

From a mechanistic point of view, the authors proposed that both the Heck and interrupted-relay Heck reactions start via a similar mechanism, with the complex **3.2.2.1-22** acting as a common intermediate (**Scheme 3.2.2.1-7**). They proposed a process starting with oxidative addition, followed by migratory insertion into the double bond to give intermediate **3.2.2.1-21**. After that, β-hydrogen elimination can occur to form π-complex **3.2.2.1-22**, which can release the Heck product and give Au(III) species **3.2.2.1-23**. The latter might undergo N-H reductive elimination to afford a N-protonated Au(I) complex **3.2.2.1-24**, which, upon deprotonation, regenerates the active catalytic species. Conversely, the π-complex **3.2.2.1-22** might proceed with alkene insertion into the Au-H bond to give intermediate **3.2.2.1-25**, followed by another β-H elimination, which would result in a compound **3.2.2.1-26.** Subsequent hydroarylation would give intermediate **3.2.2.1-27**, which then can undergo reductive elimination to give final product **3.2.2.1-18** and regenerate the catalytic species. The researchers supported the proposed mechanism with both empirical findings and DFT studies.

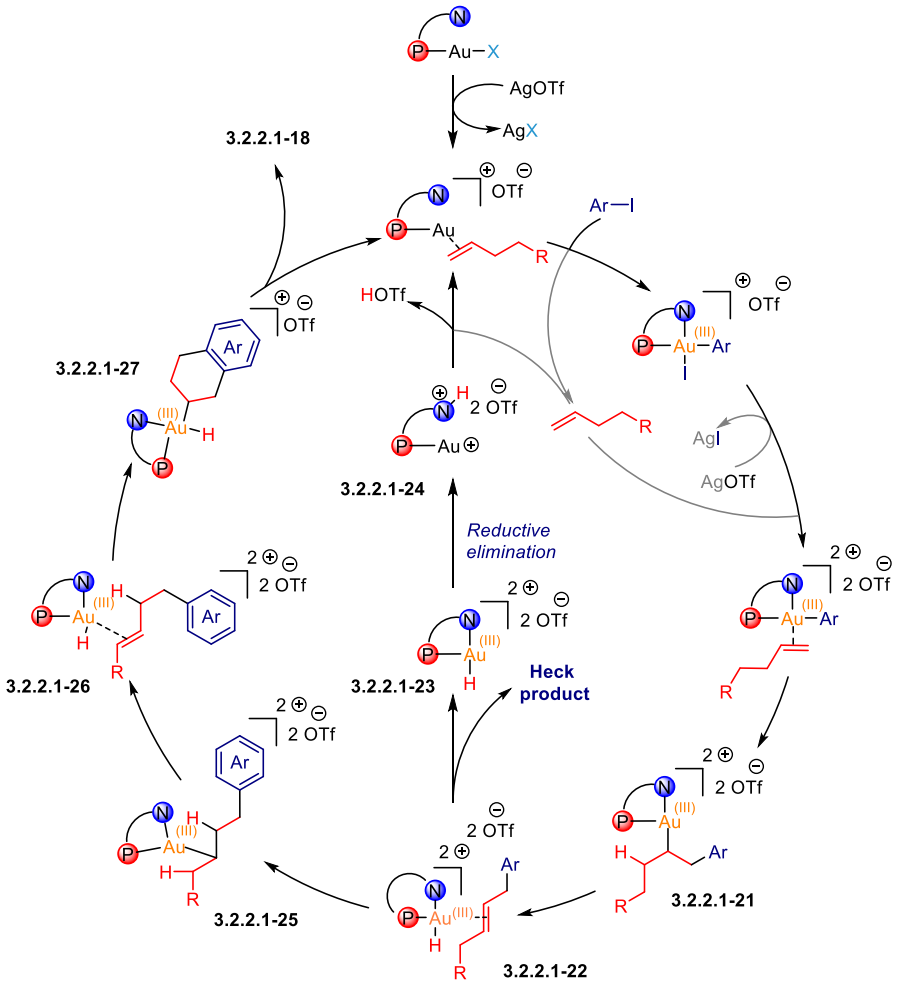

Scheme 3.2.2.1-7. Mechanism of gold-catalyzed Heck and interrupted-relay Heck reactions.

3.2.2.2. Formation of C-X bonds

In 2019, the research groups of Patil and Bourissou independently described a series of C(sp^2)-N coupling reactions.[51,52] In a significant divergence from conventional transition metal-catalyzed C-N coupling reactions, Patil's study demonstrated that the reaction could proceed even in the absence of a base (**Scheme 3.2.2.2-1, A**). Both research groups noted a preferential reactivity with electron-poor amines, while the reactions involving electron-rich anilines resulted in significantly reduced yields (7%). Additionally, they demonstrated the ability to synthesize protected primary anilines by utilizing tert-butyl carbamate (Boc) and benzyl carbamate (Cbz), achieving the desired cross-coupling products **3.2.2.2-1** in nearly quantitative yields (**Scheme 3.2.2.2-1, B**). An intriguing aspect of their discovery was the complete selectivity for the activation of the C–I bond in the presence of other functional groups such as C–Br, C–OTf, and C–Bpin. This finding emphasizes the orthogonal characteristics and potential synergies between gold and palladium catalysis. Patil also extended this approach to obtain carbazoles **3.2.2.2-2** directly from 1,2-di-iodobenzene in a tandem manner. Interestingly, in the paper published by Patil, the significance of incorporating sterically bulky and electron-rich adamantyl (−Ad) and hemilabile−NMe_2 groups in a gold-catalyst was highlighted. This specific design was found to be crucial in achieving optimal performance, as other gold catalysts (**3.2.2.2-3a** to **3.2.2.2-3d**) that did not feature these groups delivered markedly lower yields.

In a related advancement, in 2021 the group of Patil reported an innovative approach for 1,2-aminoarylation of alkenes to give products **3.2.2.2-4** by employing an external amine coupling partner, exploiting the unique reactivity of gold to prevent the formation of direct C-N coupled products (**Scheme 3.2.2.2-1, C**).[53] Their hypothesis centered around the idea that, following oxidative addition, the Au(III) intermediate would be selectively trapped with the alkene instead of performing ligand exchange with aniline. This would avoid the formation of a C-N cross-coupling product, guiding the reaction towards the desired outcome. The researchers observed an intriguing dependency of the reaction on the concentration of K_3PO_4. When they used 1 equivalent of K_3PO_4, they observed a large amount of the C−N cross-coupled product **3.2.2.2-4a**. In contrast, reducing the base to 0.3 equivalents enhanced the yield of the desired product, while minimizing the formation of byproduct **3.2.2.2-4a**. This suggested that a higher base concentration encourages the formation of the C−N cross-coupled product by aiding the coordination of the amine with the generated Au(III) species.

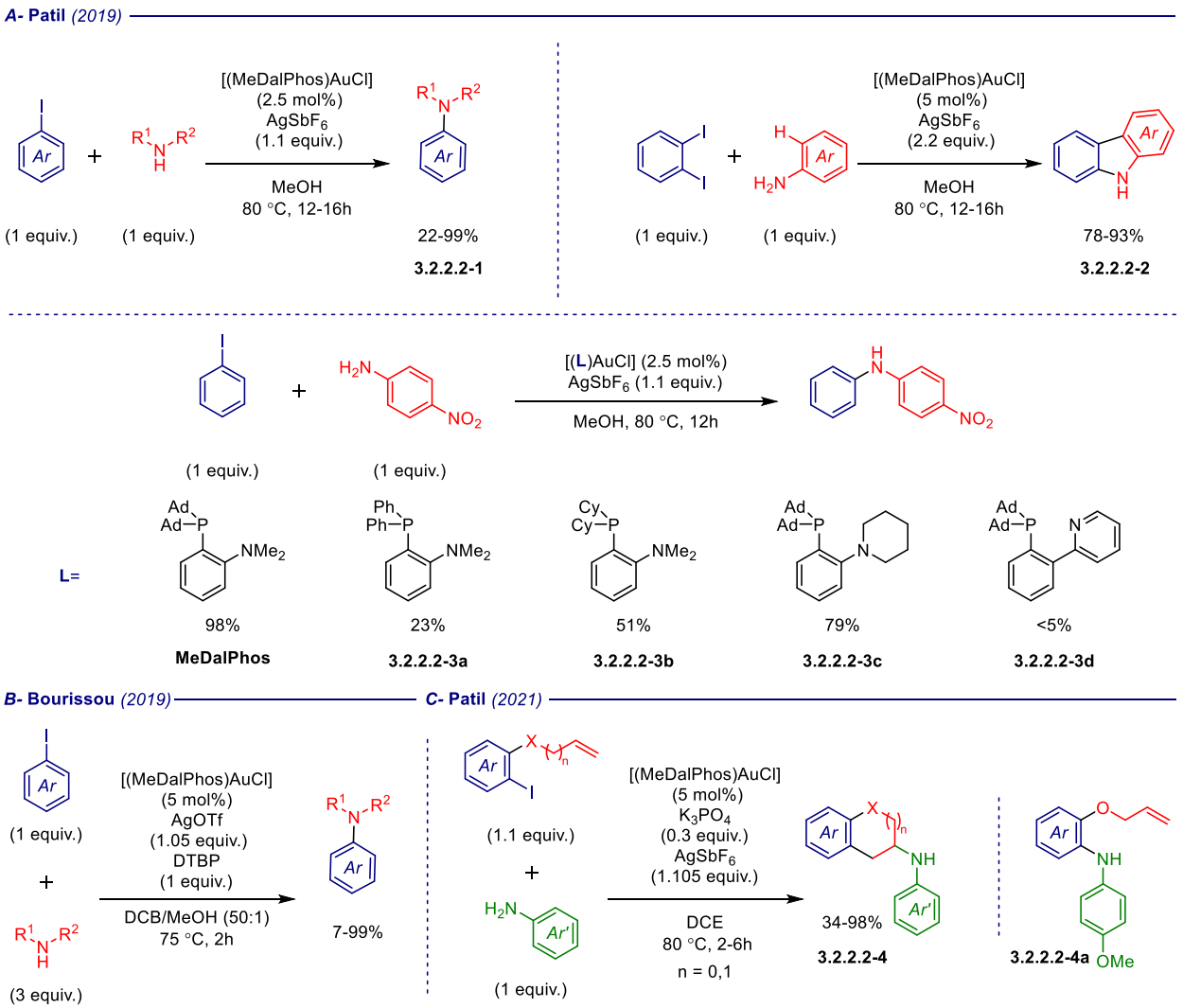

Scheme 3.2.2.2-1. Formation of C-N bonds.

The groups of Xu[54] and Patil[55] independently investigated C-O cross-coupling reactions, catalyzed by a Au(I)/Au(III) system, involving aryl iodides and alcohols. In the work of Xu (**Scheme 3.2.2.2-2, A**), the yield of the reaction was found to improve with the use of $TBACO_2CF_3$, likely through the acceleration of the nucleophilic substitution process.[56] In contrast, the team of Patil (**Scheme 3.2.2.2-2, B**) encountered an unusual requirement for an electronically poor iodoarene to facilitate reductive elimination from electron-rich organogold(III) alkoxide complexes. This requirement diverged from the usual preference for electron-rich iodoarenes in cross-coupling reactions facilitated by Au(I)/Au(III) catalysis. Interestingly, both research groups discovered the necessity of employing alcohol in significant excess to achieve good yields.

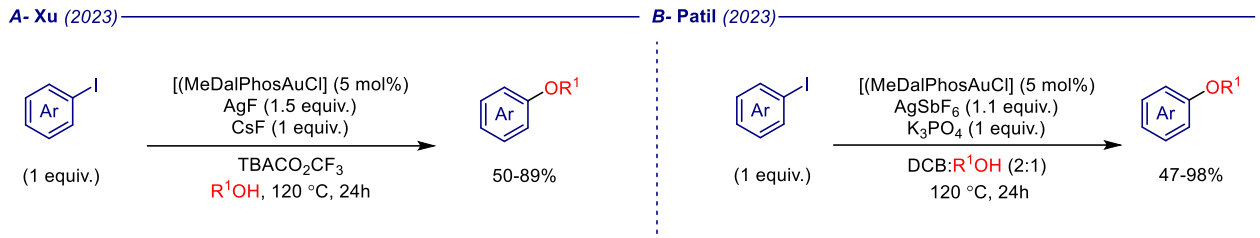

Scheme 3.2.2.2-2. Formation of C-O bonds.

Gold mediated formation of C-S bonds using MeDalPhos-ligated arylgold(III) complexes was exploited by Spokoyny and co-workers for the structural modification of proteins and sugars using thiols.[57–60] However, the recent work of Lu and Hammond reported the first use of [(MeDalPhos)AuCl] in order to make various trifluoromethylthio- and selenoethers (**Scheme 3.2.2.2-3**).[61] It should be noted that their protocol allows use of other nucleophilic SCF_3 or $SeCF_3$ reagents like the tetramethylammonium salts of the corresponding nucleophiles. Notably, their protocols also allow access to not only aryl, but alkenyl **3.2.2.2-5** and even alkynyl **3.2.2.2-6** trifluoromethylthio- and selenoethers.

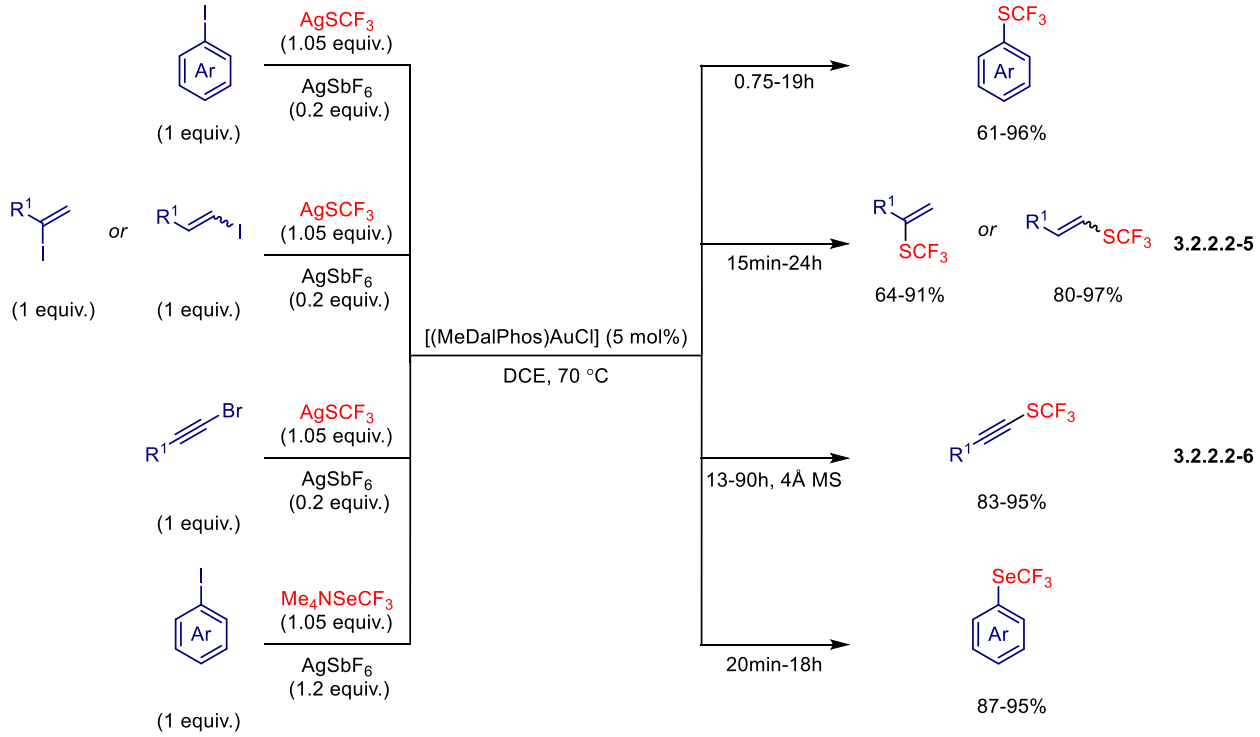

Scheme 3.2.2.2-3. Formation of C-S bonds.

Another report on forming C-S bonds was published by Patil, who utilized aryl iodides and arylsulfonyl hydrazides as reactants to synthesize biaryl sulfones **3.2.2.2-7** (**Scheme 3.2.2.2-4**).[62] It is noteworthy that the reaction didn't produce any direct C–N cross-coupled products. The proposed reaction mechanism starts with an oxidative addition to form an arylgold(III) intermediate **3.2.2.2-8**. Following iodide abstraction, this intermediate can react with arylsulfonyl

hydrazide, leading to another Au(III) complex **3.2.2.2-9**. The sequential release of N_2 and H_2 from this complex yields a further Au(III) species **3.2.2.2-10**, from which the final product is formed through reductive elimination. Alternatively, this process can involve an aryl sulfinate salt intermediate **3.2.2.2-11** that produces biaryl sulfone product **3.2.2.2-7** via the same reductive elimination from a Au(III) complex **3.2.2.2-10**.

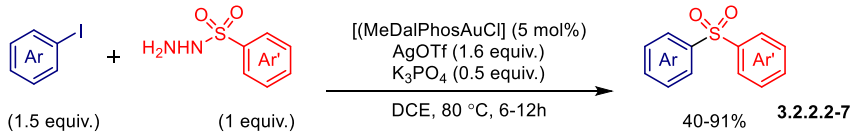

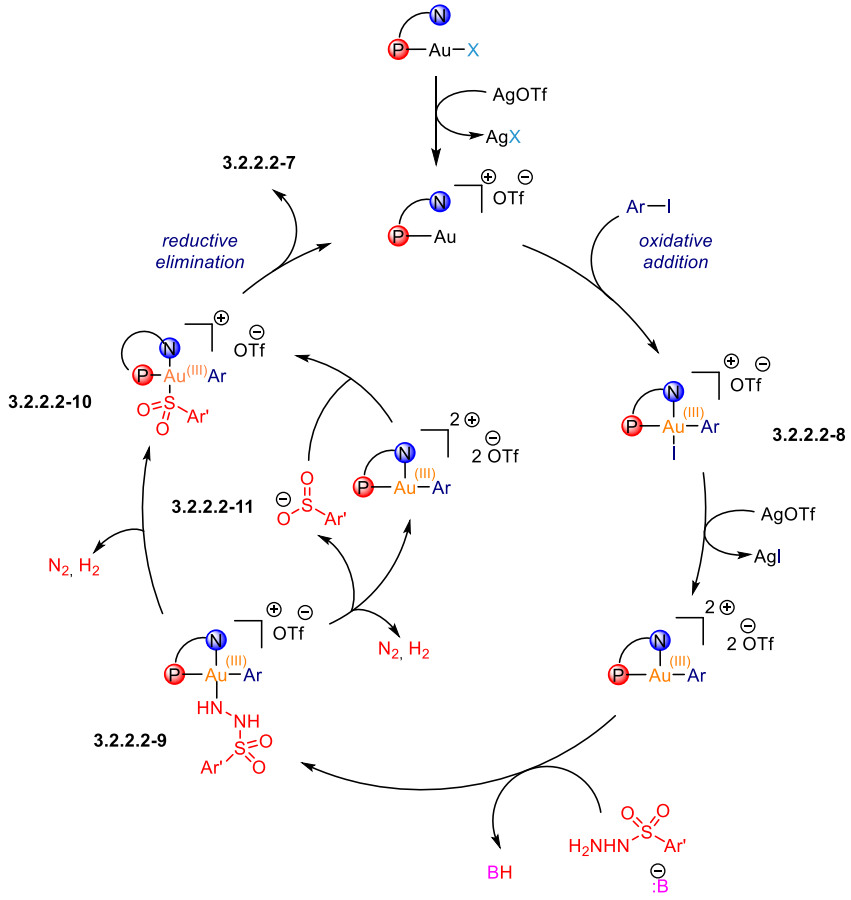

Scheme 3.2.2.2-4. Reactivity of arylsulfonyl hydrazides.

3.2.2.3. Alkynes in Au(I)/Au(III) catalysis

The application of alkynes in Au(I)/Au(III) catalysis has been challenging, facing difficulties such as the formation of stable vinyl-Au(I) species, facile Au(I)- and Ag-catalyzed hydroarylation, direct cross-coupling reactions, and issues concerning regioselectivity. The group of Patil recently advanced this field by introducing a novel 1,2-dicarbofunctionalization reaction of alkynes,

utilizing aryl halides, and also applying this method to the oxyarylation of alkynes (**Scheme 3.2.2.3-1**).[63] The newly developed protocol is versatile, accommodating various coupling partners like vinyl iodides and bromoalkyne, and extending to the oxyarylation of alkynes using either external aryl iodide or alcohol as an external nucleophile. In terms of mechanism, the reaction employs an oxidative addition/π-activation pathway, in contrast to the more conventional migratory insertion/cis-trans isomerization seen with other transition metals. This unique pathway facilitates the anti-selective incorporation of functional groups, showcasing a significant advancement in gold-catalyzed reactions.

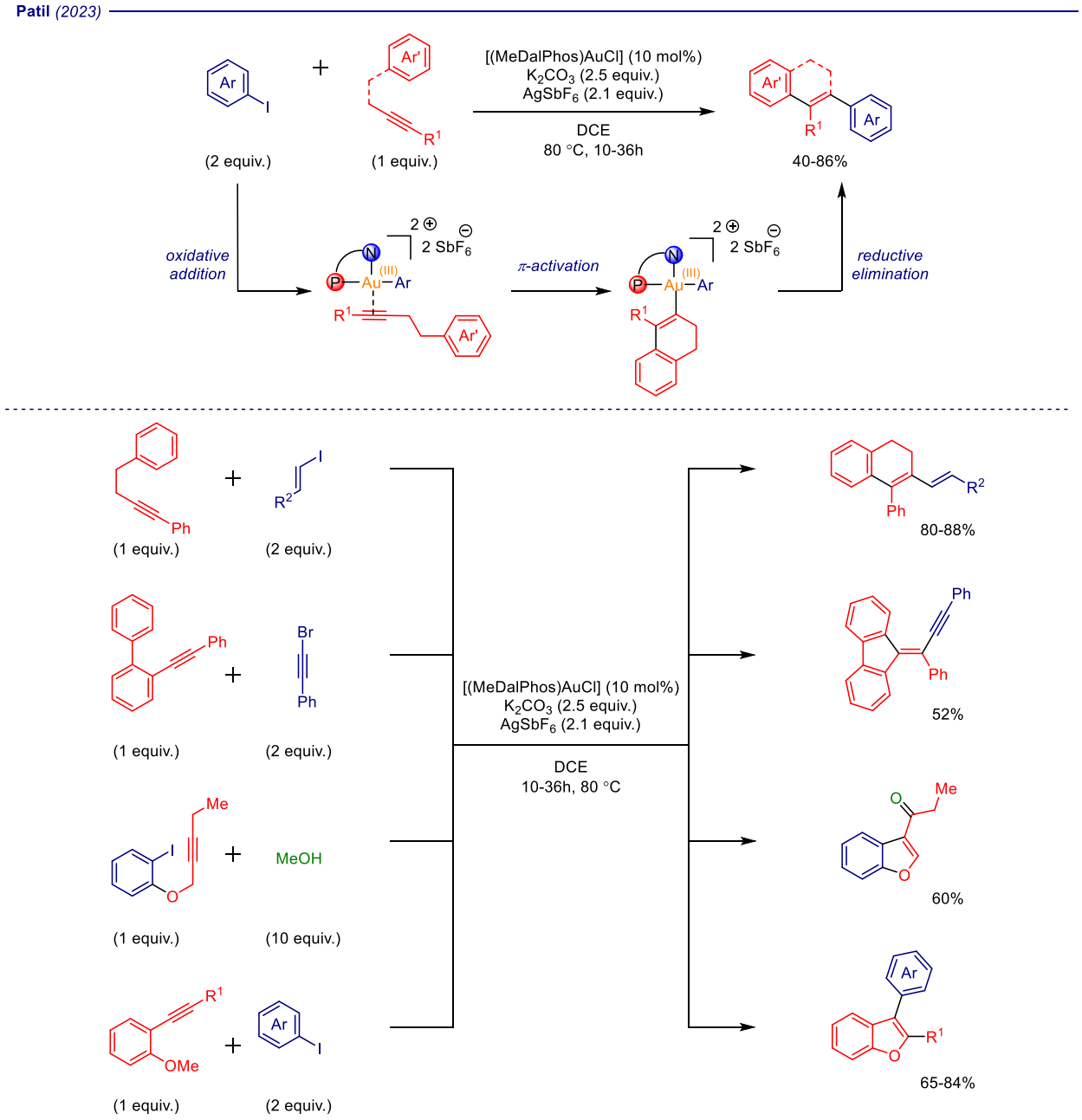

Scheme 3.2.2.3-1. Reactivity of alkynes under Au(I)/Au(III) catalysis.

3.2.2.4. Enantioselective Au(I)/Au(III) catalysis

Significant advancements in the development of MeDalPhos-derived catalysts for enantioselective Au(I)/Au(III) catalysis have been made by two independent research groups led by Shi and Li,[64] and Patil.[65] Notably, the design of enantioselective Au(I)/Au(III) redox catalysis is a formidable task due to the distinct geometric limitations and coordination properties of Au(I) and Au(III) species. Enantioselective transformations involving Au(I) are hard to achieve due to its linear geometry, which complicates the ability of a chiral ligand to effectively manage spatial control. Meanwhile, establishing square planar Au(III) complexes poses a challenge due to the necessity to stabilize the Au(III) state, with very few existing examples of complexes capable of doing so. The need to control the four coordination sites of an emergent Au(III) intermediate with a single adjusting ligand, in conjunction with the structural adaptability of the tetracoordinated Au(III) intermediate, makes the enantioinduction process especially challenging.

The approach taken by the groups of Shi and Li involved using a hemilabile (P,N) ligand that contains a pyrrolidine ring **3.2.2.4-1** (**Scheme 3.2.2.4-1, A**). This facilitated an aminoarylation reaction, producing compounds **3.2.2.4-2** in good yields and excellent enantioselectivity. Interestingly, the method was successful only with anilines that had strong electron-withdrawing groups, with electron-rich anilines being unreactive. This phenomenon was thought to be the result of strong Au-aniline coordination. The group of Patil, on the other hand, induced chirality by utilizing BINOL-based substituents to develop an AdChetPhos-ligated Au(I) complex (**Scheme 3.2.2.4-1, B**). This method led to the successful development of 1,2-oxy- and 1,2-aminoarylation reactions, which resulted in high enantioselectivity and good yields, producing the corresponding 3-oxy- and 3-aminochromanes **3.2.2.4-3**.

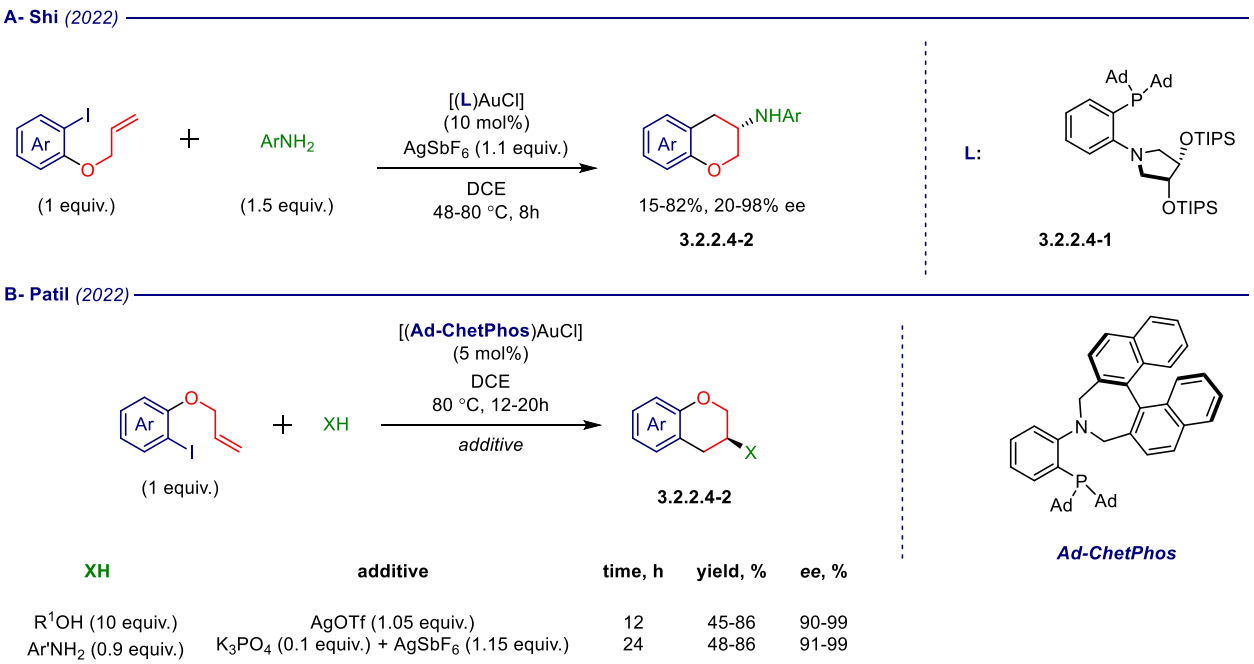

XH	additive	time, h	yield, %	ee, %
R^1OH (10 equiv.)	AgOTf (1.05 equiv.)	12	45-86	90-99
$Ar'NH_2$ (0.9 equiv.)	K_3PO_4 (0.1 equiv.) + $AgSbF_6$ (1.15 equiv.)	24	48-86	91-99

Scheme 3.2.2.4-1. Chiral ligands.

3.2.2.5. Other architectures

In a recent 2022 publication, Ribas and collegues introduced a new family of MIC^N (MIC = mesoionic carbene) Au(I)/Au(III) catalysts **3.2.2.5-1**, featuring bidentate hemilabile ligands.[66] The hemilabile N-ligand, upon coordinating with the metal center, forms a five-membered ring chelate that stabilizes the Au(III) species (**Scheme 3.2.2.5-1**). The formation of these Au(III) complexes can be achieved in two ways: either through strong external oxidants like $PhIX_2$ (X= Cl or Ac) to give complexes **3.2.2.5-2** or via oxidative addition involving strained biphenylene C–C bonds, which would afford Au(III) complex **3.2.2.5-3**. By utilizing these newly developed complexes, the authors were able to create an innovative synthetic approach for γ-substituted γ-butyrolactones **3.2.2.5-4**. This approach, based on the arylation-lactonization reaction of γ-alkenoic acid, necessitates the oxidative addition of the aryl iodide, which is made possible by the distinctive hemilabile nature of the MIC^N ligand.

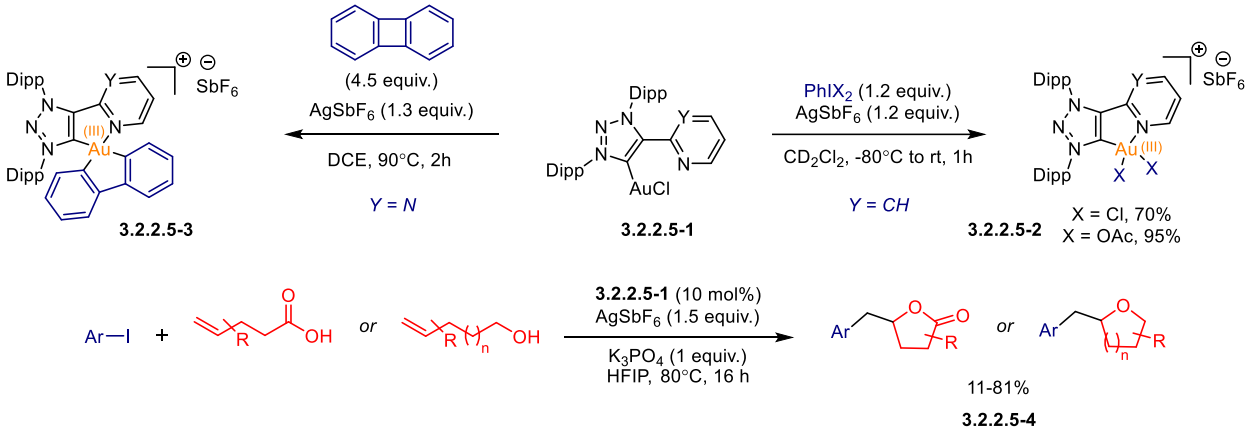

Scheme 3.2.2.5-1. MIC^N ligands.

Two independent research groups, led by Szostac and Zhang[67] and Russel and Bower,[68] have recently introduced a new hemilabile carbene complex **3.2.2.5-5**. This complex, characterized by an L-shaped heterobidentate (N^C) ligand configuration, combines the flexible character of an amino group with the powerful σ-donation ability of a carbene center. This design is further stabilized by a specifically imposed rigid conformation within the ligand structure. The group of Szostac and Zhang applied this complex in the Au(I)/Au(III) C-H arylation (**Scheme 3.2.2.5-2, A**). Their work illustrated the capabilities of their complex in effectively catalyzing this specific transformation, shedding light on a promising new catalyst structure. On the other hand, the team led by Russel and Bower focused on investigating the arylgold(III) complexes **3.2.2.5-6** formed after oxidative addition to the initial complex **3.2.2.5-5** (**Scheme 3.2.2.5-2, B**). The researchers successfully isolated these complexes in good yield, making a curious observation that the initially formed Au(III)-iodide complex underwent a straightforward halide exchange, yielding a more stable Au(III)-chloride form. Furthermore, Russel and Bower developed a method for 1,2-oxyarylations of common alkenes such as ethylene and propylene. This innovative approach presents a rare catalytic difunctionalization technique for these crucial industrial

building blocks to afford products **3.2.2.5-7**. They also demonstrated that their gold-catalyzed approach facilitated ArI oxidative addition without being hindered by the competitive β-hydride elimination pathways often encountered in Pd(0) catalysis.

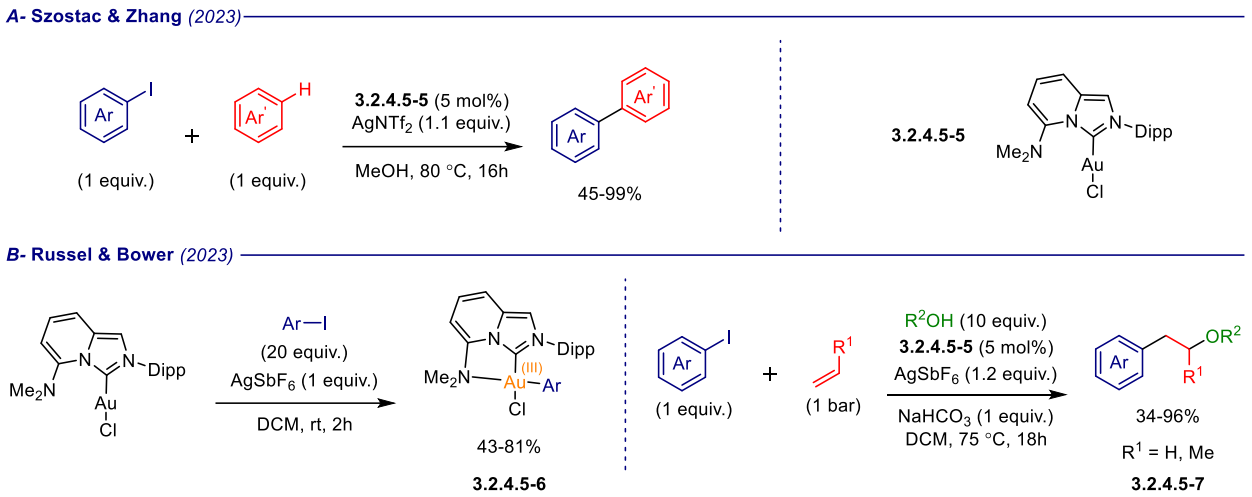

Scheme 3.2.2.5-2. Heterobidentate (N^C) ligand.

3.2.2.6. Stoichometric reactions with hemilabile complexes

In 2016, Bertrand and coworkers used hemilabile bidentate cyclic (alkyl)(amino)carbenes (CAACs) **3.2.2.6-1** with an attached pendant imine moiety (**Scheme 3.2.2.6-1, A**).[69] Their research showed that this particular imine functional group could effectively stabilize the Au(III) oxidation state, thereby aiding the oxidative addition of the C-C bond of biphenylene to the corresponding Au(I)-complex. Notably, the absence of imine functional groups on the side chain prevented the oxidative addition from occurring in (CAAC)AuCl complexes, even when subjected to heat at 80°C in the presence of $KB(C_6F_5)_4$.

In 2021, Fiksdahl and Erdélyi conducted an interesting study into the use of the external two-electron oxidant $PhICl_2$ to transform (P^N)-chelated Au(I) complexes into their corresponding Au(III) species **3.2.2.62** (**Scheme 3.2.2.6-1, B**).[70] Their research focused on the synthesis, characterization, and catalytic properties of Au(III) complexes utilizing (P^N) ligands, a challenging and seldom-encountered aspect in Au(III) chemistry. This is primarily due to the propensity of phosphorus to be easily oxidized by Au(III). In addressing this challenge, the authors developed an innovative method that allowed them to prevent ligand oxidation.

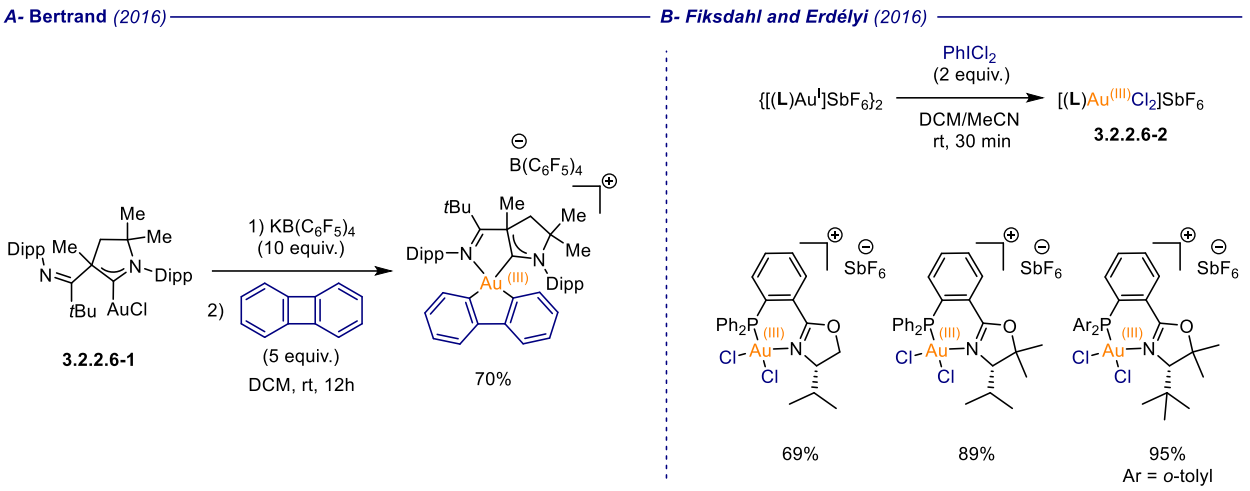

Scheme 3.2.2.6-1. Stoichometric oxidation.

The research group of Bourissou, in a study published in 2021, further studied this approach[71]. They particularly studied the complex [(MeDalPhos)AuCl], revealing that its geometry was suitable for facilitating the synthesis of (P^N)-chelated cationic Au(III) species **3.2.2.6-3** (**Scheme 3.2.2.6-2, A**). These species, however, were found to be unstable and underwent slow degradation in solution. To overcome this issue, the researchers conducted an anion metathesis, forming a more stable BArF derivative of the Au(III) species. Moreover, the use of a **3.2.2.6-4** species, which have (C^N) hemilabile ligand (**Scheme 3.2.2.6-2, B**), resulted in the neutral compound [(MIC-pyridine)$AuCl_3$] **3.2.2.6-5**. This outcome was linked to a lesser extent of preorganization required for successful chelation, compared to the (P^N) ligand. Interestingly, the researchers were able to induce pyridine chelation by cationizing the Au(III) complex **3.2.2.6-5** using a chloride-abstracting agent.

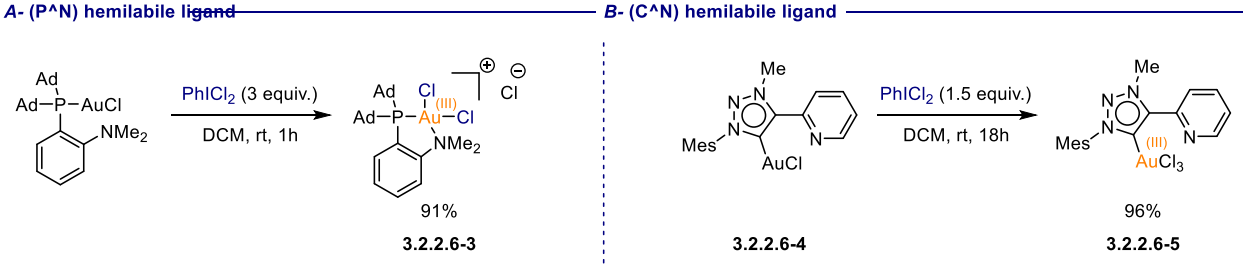

Scheme 3.2.2.6-2. Comparison of (P^N) and (C^N) hemilabile ligands.

The same group recently expanded on their research by introducing a novel approach to the stoichiometric oxidation of gold complexes with hemilabile ligands.[72] In this method, they utilized chelating P^P and hemilabile P^N ligands to induce the oxidation of Au(I) complexes by o-benzoquinones to form the corresponding Au(III) catecholate complexes **3.2.2.6-6** and **3.2.2.6-7** (**Scheme 3.2.2.6-3**). An intriguing aspect of this research is the demonstrated reversibility of the transformation. Through reactivity studies, the group of Bourissou found that the addition of

competing ligands like chloride and alkenes could reverse the process, reverting the Au(III) complex **3.2.2.6-7** back to Au(I), and simultaneously liberating the o-quinone.

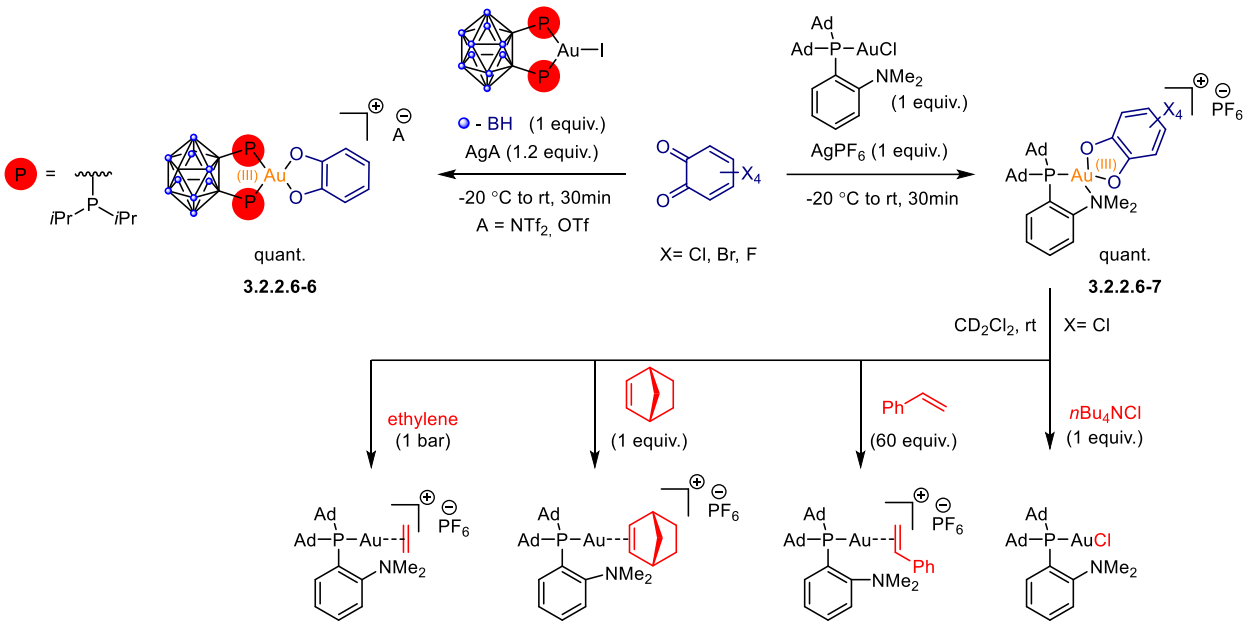

Scheme 3.2.2.6-3. Oxidation with *o*-benzoquinones.

In a 2020 publication, Nevado and coworkers introduced a new approach to the synthesis of stable bidentate arylgold(III) fluoride complexes featuring (P^N) coordination **3.2.2.6-8** (**Scheme 3.2.2.6-4, A**).[73] The synthesis of these arylgold(III) fluoride complexes was achieved from known MeDalPhos-ligated Au(III) complexes, utilizing a straightforward I/F ligand exchange method with AgF in dichloromethane and the corresponding products **3.2.2.6-8** were obtained in remarkable yields. Utilizing these complexes, the researchers explored the mechanism of C(sp^2)-C(sp) reductive elimination in Au(III) catalysis. Specifically, when the reaction was conducted with TMSCN, a Au(III) cyanide **3.2.2.6-8i** intermediate was identified, which then underwent reductive elimination to yield the final cross-coupling products **3.2.2.6-9**. Furthermore, when subjected to reaction with alkynes, these arylgold(III) fluoride complexes afforded the corresponding products **3.2.2.6-10** in moderate to excellent yields.

Russel and Bower recently explored the interaction between a MeDalPhos-ligated Au(III) metallafluorene complex and carbon monoxide (CO) through an extensive study employing both experimental and computational techniques (**Scheme 3.2.2.6-4, B**).[74] Their investigation revealed a reaction pathway involving a formal migratory insertion that transits through an intermediate acyl-Au complex **3.2.2.6-11**. The presence of the hemilabile MeDalPhos ligand was found to be pivotal in enabling CO binding. This specific ligand was shown to significantly lower the energy barrier for insertion when compared to other related systems. Interestingly, the researchers were able to synthesize a 9-fluorenone product **3.2.2.6-12** from [(MeDalPhos)AuCl] by employing a two-step telescoped procedure. Attempting to introduce CO at the start of the reaction did not result in the desired product, leading the researchers to postulate that CO may interfere with the

C–C oxidative addition of biphenylene. This interference could be attributed to the competing formation of inactive Au–CO species.

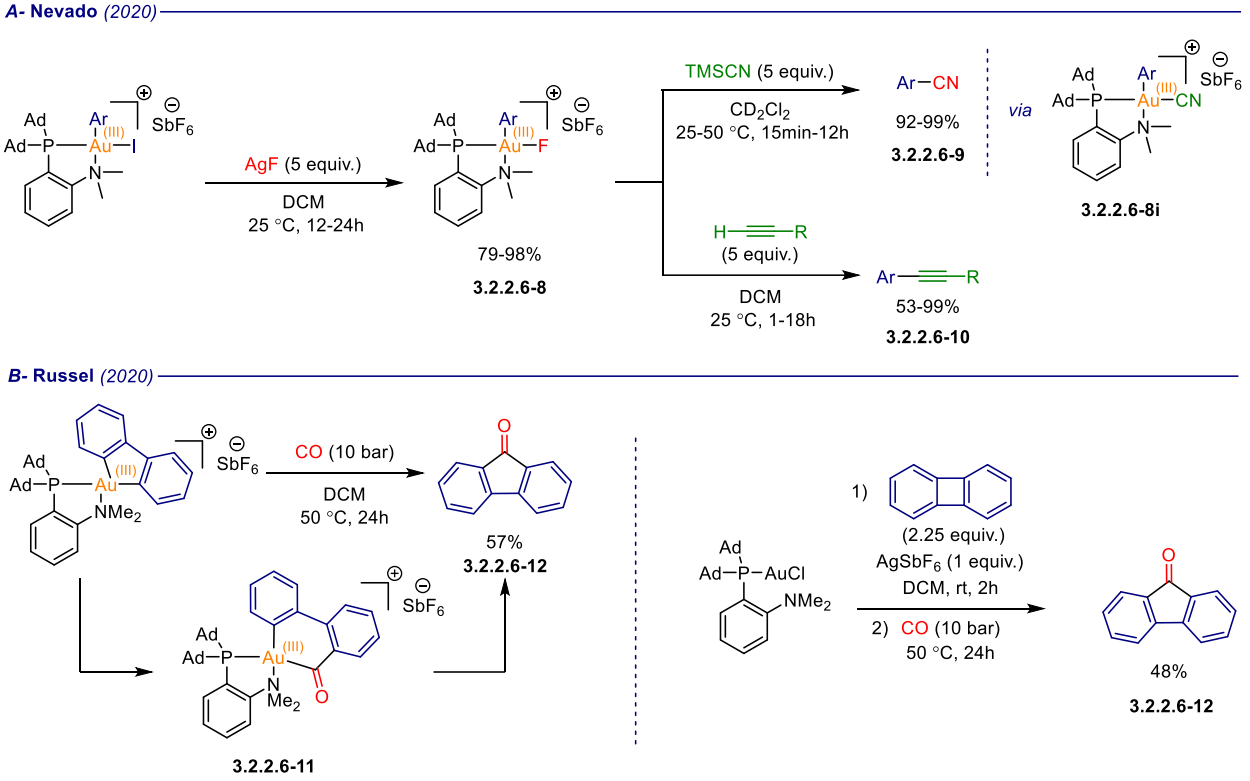

Scheme 3.2.2.6-4. Applications of arylgold(III) fluoride complexes and CO insertion.

3.3. Results and discussion

3.3.1. Synthesis, analysis, and reactivity of pyridine-based (P^N) Au(I) complexes.

Despite being a privileged ligand, MeDalPhos possesses a very rigid and compact structure with limited possibility to efficiently tune the electronics (**Scheme 3.3-1, A**). This is more especially true for the N-donor atom, given the orthogonality between the lone pair of electrons and the aromatic π-system, that would likely limit the effect of aromatic substitution. According to the study on C-N cross-coupling reactions by Patil,[51] electron rich and sterically demanding adamantyl groups on the P atom are also essential for the catalytic activity. Their replacement by either Cy or Ph groups led to a ≈ 50% and ≈ 75% reduced catalytic efficiency, respectively. The same modifications even led to a complete loss of activity in their study on the alkoxyarylation of alkenes.[75] In this context, we considered developing new (P^N) ligands that would allow more structural variation and an easier modulation of their electronics. Our strategy, described in **Scheme 3.3-1, A**, relies on the replacement of the dimethylaniline moiety by a pyridine N-donor[37,38,66,71] that would be linked to the phosphanyl moiety by a one-atom X tether. As such the possibility to produce a 5-membered chelate would be retained. Compared to MeDalPhos, such

a ligand would be less rigid. Its hemilability would be increased thanks to the introduction of the C-X σ-bond, and the inclusion of the N-atom donor in the heteroaromatic ring would reduce the steric constraints around the metal center. More importantly, the structural changes would allow a facile modulation of the ligand electronics by direct substitution at the pyridine ring or by modification of the X tether.

We report herein the results of our investigations (**Scheme 3.3-1, B**) which have led to the development of a new family of (P^N) ligand for Au(I)/Au(III) RedOx catalysis. A DFT-guided optimization of the initially designed ligands **3.3-1** allowed for the discovery of highly efficient catalysts **3.3-2** whose activity surpasses that of the [(MeDalPhos)AuCl] standard for a series of alkoxy- and amidoarylation of alkenes. To further demonstrate the potential of these new catalysts, a gold-catalyzed thiotosylation of aryl iodides (**3.3-3**→**3.3-4**) was developed that allows a general and divergent access to arylsulfur derivatives **3.3-5**. Strikingly, this unknown cross-coupling could not be achieved via Pd(0)/Pd(II) catalysis. The work was concluded by a computational and experimental study supporting the key role played by silver salts in this challenging catalytic C-S cross coupling.

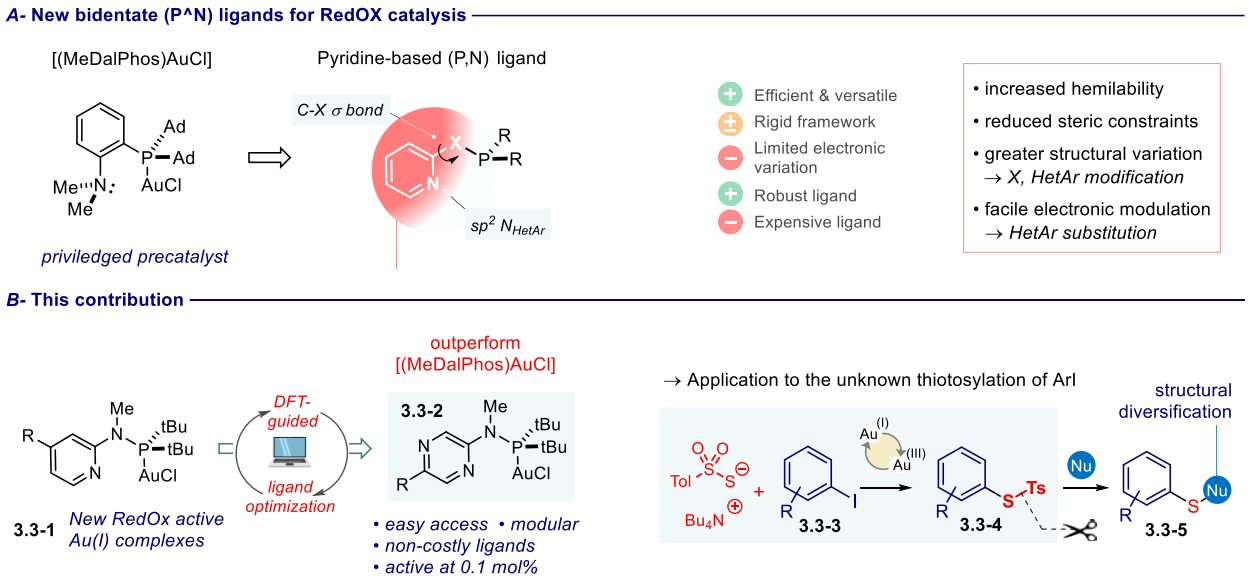

Scheme 3.3-1. Design and strategy for the development of new (P^N) ligands.

We started our investigations with the synthesis of the targeted bidentate (P^N) ligands and the corresponding AuCl complexes. Our methodology is presented in **Scheme 3.3-2, A**. Among the various structural variations that could be considered, N and O linkers between the pyridine core and the phosphanyl moiety were selected since they would be easy to install from readily available starting materials (2-hydroxy/amino pyridines **3.3-6** & chlorophosphines **3.3-7**). This choice was made despite the potential lability of resulting P-O and P-N bonds but expecting the accessibility to the P center to be reduced in the metallic complexes **3.3-8**.[76] Position C4 of the pyridine was considered for substitution as it would allow a modulation of its electronics (and consequently its interaction with the Au center) without introducing steric constraints. The

expensive Ad_2P fragment found in MeDalPhos was disregarded, and the more accessible and convenient to introduce $PtBu_2$, PCy_2 and PPh_2 groups selected for evaluation. To assess the potential ability of the corresponding (P^N) AuCl complexes **3.3-8** to be used as catalysts in RedOx processes, a set of two stoichiometric experiments were employed: the oxidative addition of **3.3-8** into the C-I bond of *p*F-iodobenzene to produce aryl-Au(III) complex **3.3-9**,[39] and the oxidation of **3.3-8** into the $Au(III)Cl_2$ complex **3.3-10** by treatment with $PhICl_2$ (**Scheme 3.3-2, A**).[70,71] These reactions could be easily monitored and/or analyzed using ^{31}P, ^{19}F and ^{1}H NMR spectroscopy. Among the series of pyridine-based (P^N) AuCl complexes that were synthesized and tested (8) (see **Appendix Figure 6.2-1** for details), we were very pleased to discover that complexes **3.3-11** possessing the MeN-$PtBu_2$ subunit could be converted into the corresponding Au(III) complexes **3.3-12** and **3.3-13** in a very efficient manner (**Scheme 3.3-2, B**). The presence of this structural motif was found to be crucial. Exchanging the NMe fragment for a simple O atom or replacing the Me group by a H or a longer *n*Bu alkyl chain led to a complete loss of reactivity or to a very unselective reaction (see **Appendix Figure 6.2-1** for details). Similarly, no activity was observed when the $PtBu_2$ group was altered.

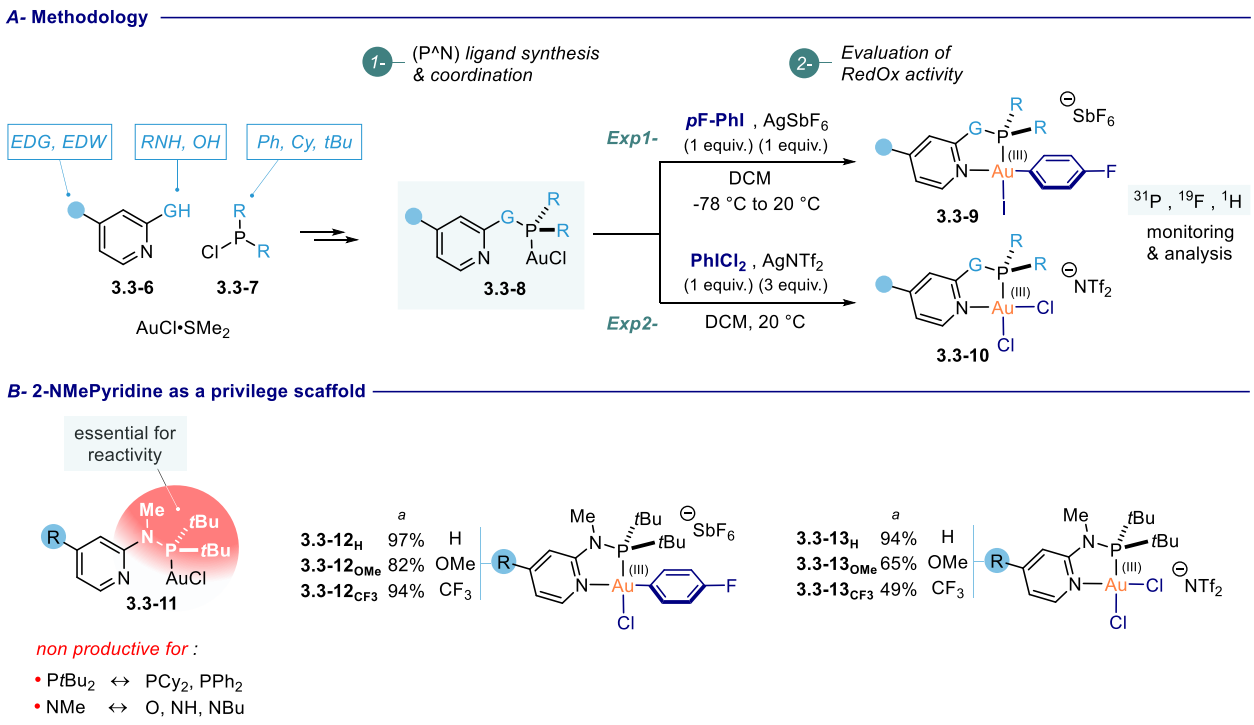

Scheme 3.3-2. Strategy of synthesis of new (P^N) AuCl complexes and their RedOx activity. [a] Isolated yields.

From a synthetic point of view, the three AuCl complexes **3.3-11$_{H,OMe,CF3}$** were easily obtained in a 2-step sequence starting from the corresponding 2-NMe pyridine **3-14** (**Scheme 3.3-3, A**). This route is not only rapid but, amenable to gram scale synthesis and rather cheap. It also allows for a rapid structural diversification since 2-NMe pyridines **3.3-14** are either commercially available or easily accessible from < $2/g building blocks. The potential lability of the ligand P-N bond was

evaluated by studying the stability of the AuCl complex **3.3-11$_H$** in MeOH. No decomposition was observed by ^{31}P NMR spectroscopy analysis after 2 weeks at 20 °C and only 10% of degradation could be detected after 7 days at 60 °C, thus demonstrating the robustness of the ligand structure (see **Appendix Figure 6.2-24** for details). As for the oxidative addition reaction with 4-F-iodobenzene, isolated yields ranging from 82 to 97% were obtained (**Scheme 3.3-3, B**). Complexes **3.3-12$_{H,OMe,CF3}$** were formed and isolated as chloride derivatives, which is the likely result of a thermodynamically driven salt metathesis event between the AgCl by-product and the initially produced iodo-Au(III) oxidative addition complex. Similar observations were previously made using either MeDalPhos, biPy or an NHC ligand.[36,39,68] Complexes **3.3-12$_{H,OMe,CF3}$** were found to be very stable at room temperature, easy to handle and manipulate. Comparatively, Au(III)Cl_2 complexes **3.3-13$_{H,OMe,CF3}$** appeared to be more sensitive and were obtained in moderate to excellent yields (49-94%). The use of the NTf_2^- counteranion was crucial for preventing in situ degradation and make their isolation possible, in stark contrast to the use of the SbF_6^- counteranion, which resulted in degradation. The structural changes induced by the oxidative processes on the (P^N)Au subunit could be directly observed by NMR spectroscopy analysis. As seen in **Scheme 3.3-3, B** for the oxidation of Au(I) complex **3.3-11$_H$** to the (P^N) Au(III) complexes **3.3-12$_H$** and **3.3-13$_H$**, the ^{1}H chemical shifts of the pyridine hydrogen atoms increase upon oxidation at the Au center as the result of coordination of the N_{pyr} atom to gold. As expected, the effect was far more pronounced for the *ortho* and *para* positions to N, the Δδ of the H_{ortho} being approximately twice that of H_{para}. The shift was also more significant for **3.3-13$_H$** ($\Delta\delta_{Hortho}$=1.46 ppm) than for **3.3-12$_H$** ($\Delta\delta_{Hortho}$=1.19 ppm) most probably due to the higher electropositivity of the Au center in **3.3-13$_H$**. Notably, this variation in chemical shift was dependent on the nature of the substituent at position C4 of the pyridine, with a maximum of $\Delta\delta_{Hortho}$=1.55 ppm reached with the formation of **3.3-13$_{CF3}$.** The ^{31}P NMR chemical shifts were also affected by the oxidation of the gold center. The signal observed for the Au(I) complex **3.3-11$_H$** at 125.3 ppm raises up up to 156.4 ppm for Au(III) complex **3.3-13$_H$**. For comparison, $\delta(^{31}P)$ [(MeDalPhos)Au(III)Cl_2](PF_6) was observed at 109.8 ppm. The structures of Au(III) complexes **3.3-12$_H$** and **3.3-13$_H$** were confirmed by SCXRD analysis showing a slightly distorted square planar environment around the Au center, and an aryl moiety positioned *trans* to the N atom. Selected measurements are given in **Scheme 3.3-3, B**. The structures were similar to those previously reported with the MeDalPhos ligand.[71,73]Interestingly, the P-Au bond is slightly longer (2.308 Å vs 2.270 Å) and the P-N bond shorter (2.114 Å vs 2.137 Å) for the pyridine-based ligand **3.3-11$_H$**, which also exhibits a smaller N-Au-P bite angles (83° vs 87°). The V_{Bur}%[77] of **3.3-11$_H$** is 45.8%, as calculated from the X-ray crystal structure utilizing the publicly accessible SambVca 2.1 software, which is below that of MeDalPhos (49.6%). This reduction may be the result of the planarity of the pyridine N donor and could potentially translate into a more favorable access to the Au(III) center.

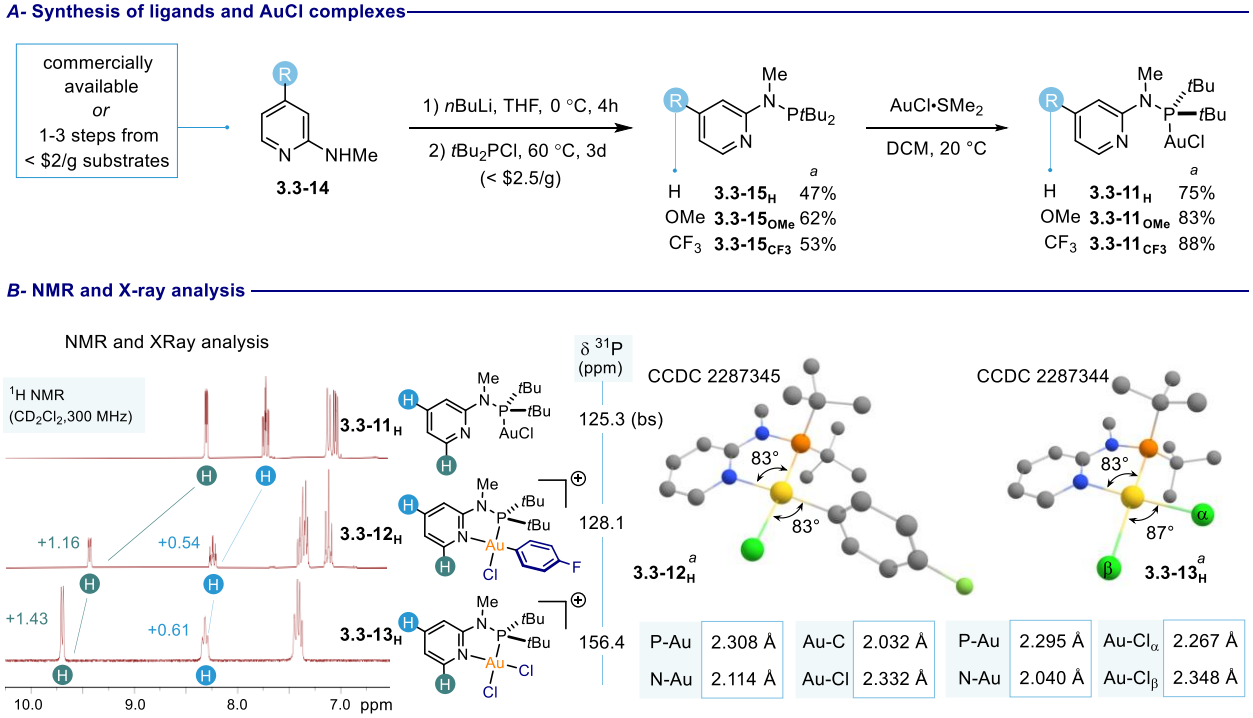

Scheme 3.3-3. Synthesis and structures of new (P^N) AuCl complexes. [a] H atoms and counteranions (SbF_6^- for **3.3-12$_H$** and Tf_2N^- for **3.3-13$_H$**) omitted for clarity.

3.3.2. Catalytic reactivity

The catalytic reactivity of the new pyridine-based (P^N) $Au^{(I)}Cl$ complexes **3.3-11** was then evaluated. To this purpose, the intramolecular alkoxy- and amidoarylation of alkenes, previously reported independently by the groups of Bourissou and Patil were chosen as model reactions (**Scheme 3.3-4, A**).[42,43] The reason for such a choice stands in the specificity of the transformation which capitalizes both on the RedOx properties of Au(I) complexes for the activation of Ar-I bonds and on the Lewis acid reactivity of Au(III) species for the nucleophilic functionalization of π-systems. The mechanism proposed for this transformation is shown in **Scheme 3.3-4, B**.[39,78] In addition, a large reaction scope has been reported with the [(MeDalPhos)AuCl] complex that would allow for an appropriate comparative evaluation of the catalytic potential of the new (P^N) AuCl complexes **3.3-11**. Experimental conditions from the literature[42,43] were directly employed in an attempt to accessing furan derivative **3.3-17a** and pyrrolidine derivative **3.3-17b**. When MeDalPhos was used as the ligand, yields similar to those reported in the literature were obtained (**Scheme 3.3-4, A**). [42,43] We were pleased to see that **3.3-17a** and **3.3-17b** could also be produced when ligands **3.3-15** were employed but the efficiency of the transformations was largely dependent on the nature of the substitution on the pyridine moiety.

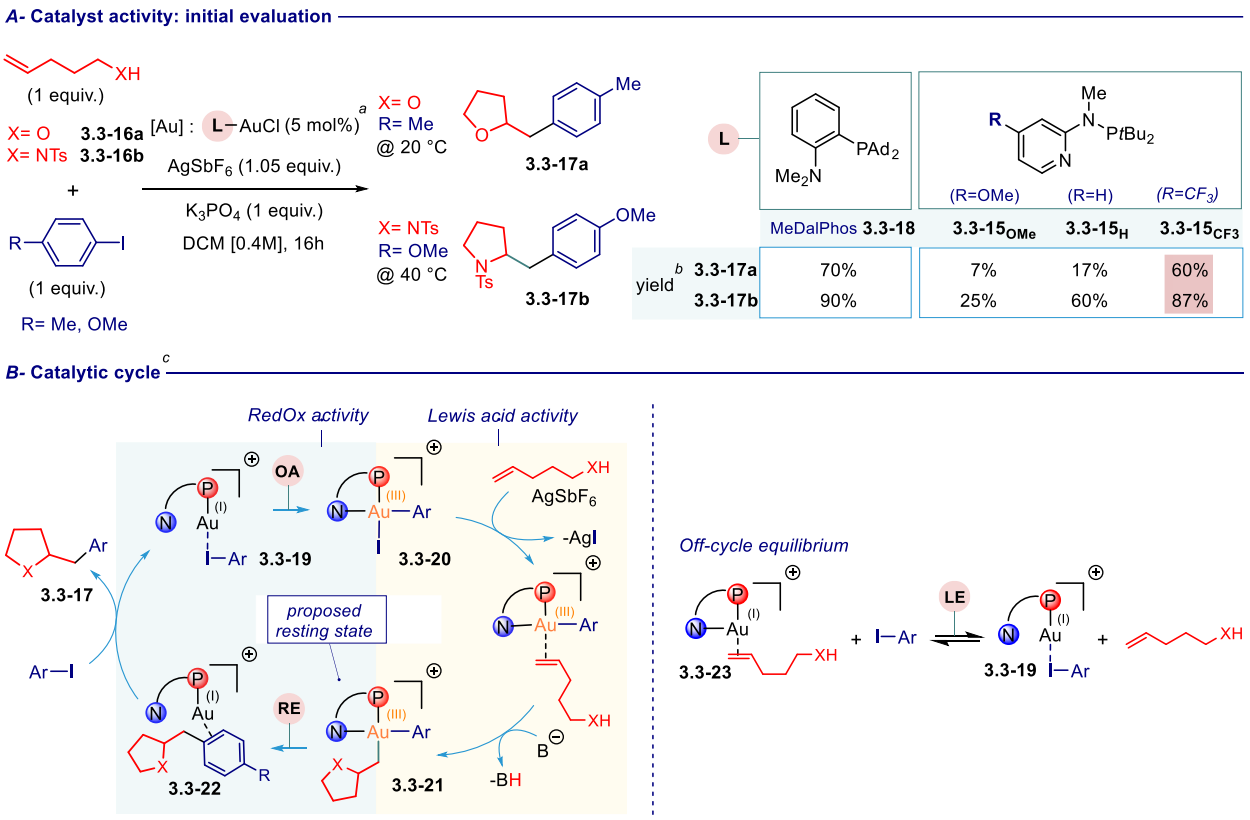

Scheme 3.3-4. Initial catalytic tests. [a] Reactions performed at 0.05-0.1 mmol scale using screw-cap vials and an oil bath with temperature regulation. [b] Yield determined by ^{1}H NMR spectroscopy analysis of the crude reaction mixture using mesitylene as an internal standard. [c] see ref 78.

The use of ligands **3.3-15$_H$** and **3.3-15$_{OMe}$** with respectively no substitution or with a OMe group at position C4 led to the inefficient formation of **3.3-17a** (7% and 17%, respectively). In contrast, ligand **3.3-15$_{CF3}$** with a *p*-CF_3 substituent allowed for a largely improved reactivity (**3.3-17a**: 60% yield) that is comparable to that observed when MeDalPhos is employed (70%). The same trend was observed for the synthesis of pyrrolidine **3.3-17b**. In this case, very comparable yields were obtained when **3.3-15$_{CF3}$** (87%) and MeDalPhos (90%) were used, while **3.3-15$_H$** allowed for the production of **3.3-17b** with a more moderate efficiency (60%). These seminal results were found promising in light of the very limited number of ligands available for Au(I)/Au(III) RedOx catalysis and the modulation of reactivity that could be easily achieved by simply modifying the substitution pattern of the pyridine moiety. An obvious trend emerged from analyzing the results of these preliminary catalytic tests: the more electron poor the pyridine moiety, the better the yield. The presence of substituents on the pyridine will affect its Lewis basicity and therefore the way it will interact with the gold center, which will ultimately impact the stability of the catalytic species along the reaction pathway. According to DFT calculations by Miqueu and Bourissou using MeDalPhos as the ligand, **3.3-16a** and PhI as substrates,[78] the portion of the transformation relying on the Lewis acid reactivity of the catalyst (**3.3-20**→**3.3-21**) (**Scheme 3-4, B**) is highly exergonic and exhibits a low activation energy ($\Delta G^{\neq}$ cyclization < 3 kcal/mol). The oxidative

addition (OA) was also calculated to be largely accessible ($\Delta G^{\neq}_{\mathbf{3.3\text{-}19}\rightarrow\mathbf{3.3\text{-}20}}$= 11.2 kcal/mol), while the reductive elimination step (RE) was proposed to be rate determining ($\Delta G^{\neq}_{\mathbf{3.3\text{-}21}\rightarrow\mathbf{3.3\text{-}22}}$= 17.9 kcal/mol). These computational and analytical data are in line with the substitution effect observed when the catalytic activity of complexes **3.3-11$_{H,OMe,CF3}$** were assessed. Provided that it does not severely impact the other steps of the reaction, the use of a more electron poor ligand (like **3.3-15$_{CF3}$**) would be beneficial as it would lower the energy barrier of the RE step.

Following the promising results obtained with complex **3.3-11$_{CF3}$**, we decided to assess its applicability in other known Au(I)/Au(III) catalytic processes. Specifically, we attempted a C(sp2)-N coupling reaction using a previously reported procedure (**Scheme 3.3-5, A**).[51] Disappointingly, the yield was markedly reduced, affording only 10%, compared to the 50% yield achieved when utilizing MeDalPhos as the ligand. We hypothesized that this diminished yield may be attributable to competitive binding of the gold center by the starting aniline substrate **3.3-24** instead of the pyridine moiety of the ligand, which would inhibit the catalytic process.

This effect is especially pronounced during comparative studies on gold-catalyzed Heck reaction (**Scheme 3.3-5, B**).[49,50] When pyridine was used as a base, we saw the absence of product using ligand **3.3-15$_{CF3}$**, while the use of MeDalPhos afforded an excellent yield of 95%. However, when non-binding sodium carbonate was employed as the base, ligand **3.3-15$_{CF3}$** afforded a yield of 37%, whereas MeDalPhos delivered a significantly reduced yield of 46%.

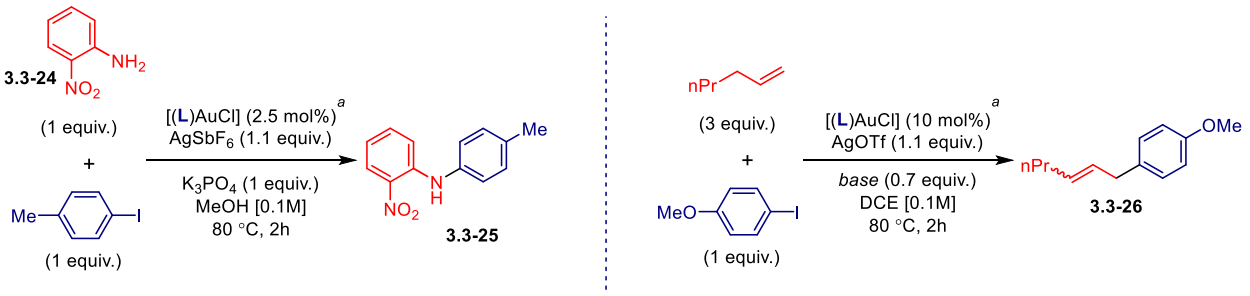

		MeDalPhos 3.3-18	3.3-15$_{CF3}$
yield [b]	3.3-25	50%	10%
	3.3-26 [c]	95%	0%
	3.3-26 [d]	46%	37%

Scheme 3.3-5. Catalytic tests. [a] Reactions performed at 0.025-0.05 mmol scale using screw-cap vials and an oil bath with temperature regulation. [b] Yield determined by ^{1}H NMR spectroscopy analysis of the crude reaction mixture using mesitylene as an internal standard. [c] pyridine was used as a base. [d] sodium carbonate was used as a base.

To further elucidate the influence of electron-deficient ligands on the reaction mechanism, we investigated transmetalation and subsequent reductive elimination in the Stille coupling with a stannyl reagent **3.3-27a** (**Scheme 3.3-6, A**). We were pleased to find that all of the developed ligands exhibited superior reactivity compared to the traditional MeDalPhos. This improvement in reactivity can be attributed to the increased electron deficiency of new ligands compared to

MeDalPhos. A clear illustration of this trend is seen when comparing the performance of MeDalPhos with the ligand **3.3-15$_{CF3}$**, where the product **3.3-28a** was obtained in yields of 17% and 52%, respectively. In addition, we extended our tests to include a more relevant transmetallation step using a silver reagent **3.3-27b** and were pleased to observe a similar trend in the formation of product **3.3-28b**.

Despite our efforts to synthesize metallocycle **3.3-29**, the reaction proved unsuccessful and resulted only in the degradation of the starting materials (**Scheme 3.3-6, B**). We hypothesize that the instability of complex **3.3-29** may be due to the presence of a strong electron-withdrawing ligand that promotes reductive elimination. We attempted to increase the stability of this complex by replacing the counterion from SbF_6^- to NTf_2^-. Although this strategy of counterion switching was found to be effective in stabilizing complexes **3.3-13**, it was ineffective in the present case.

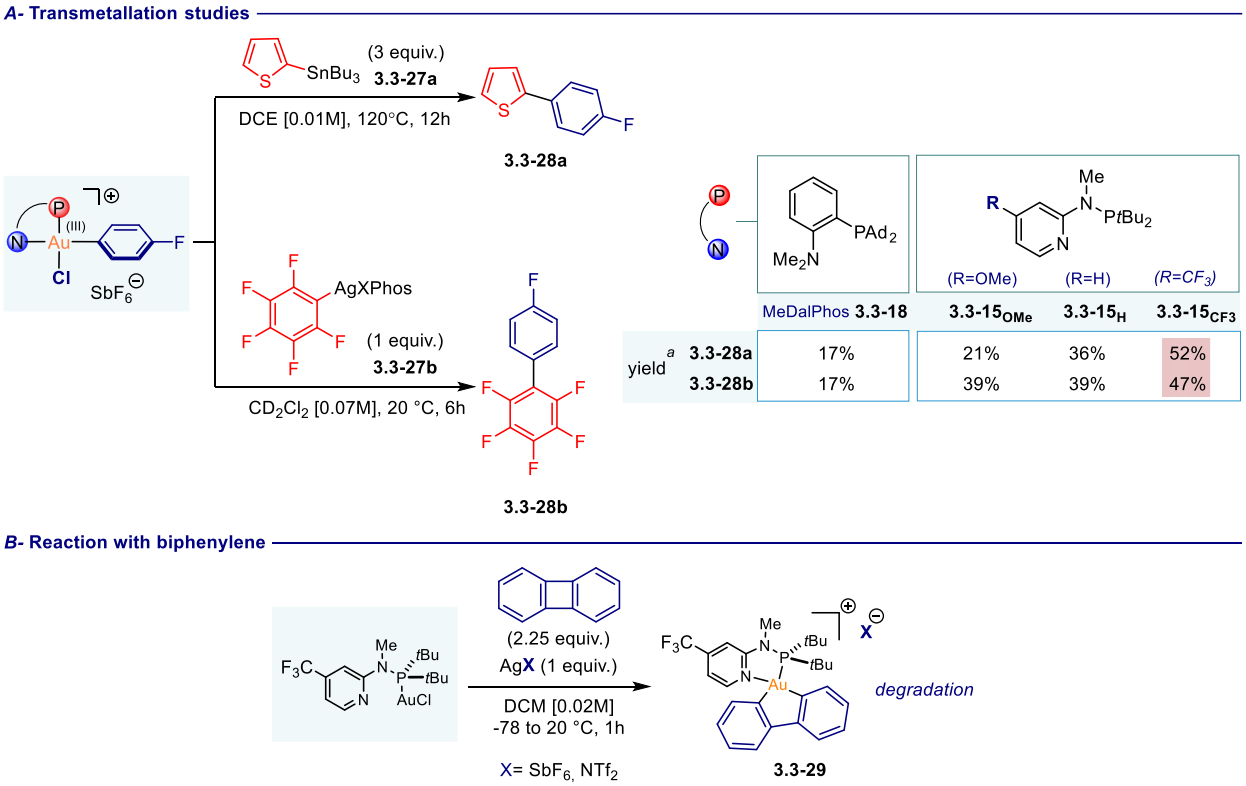

Scheme 3.3-6. Transmetallation tests. [a] Yield determined by ^{1}H NMR spectroscopy analysis of the crude reaction mixture using $PhCF_3$ as an internal standard.

3.3.3. Computational study and ligand optimization

To get more insight into how the substitution of the pyridine moiety in ligands **3.3-15** can affect the reaction, and with the goal of developing more efficient catalytic systems, a computational study was performed (**Scheme 3.3-6**). The reaction between pentenol **3.3-16a** and PhI was

examined and, to have a broader view on the ligand substitution effect, three steps were considered: the reductive elimination (RE, see **3.3-21**→**3.3-22**, **Scheme 3.3-6**), the oxidative addition (OA, see **3.3-19**→**3.3-20**, **Scheme 3.3-6**), and the pentenol to PhI ligand exchange at the Au(I) center (LE, see **3.3-19**→**3.3-23**, **Scheme 3.3-6**). This exchange, which is an off-cycle equilibrium, was considered to possibly affect the reaction depending on the experimental conditions employed.[79,80] Calculations were conducted with ORCA 5.0.2[81,82] at the PWPB95-D4/def2-TZVPP + CPCM(CH_2Cl_2)//R2SCAN-3c level of theory, which, following recent papers on the subject,[83–85] was considered to be a good compromise between computational effort and accuracy. Dispersion (D4) and solvent effects (CH_2Cl_2) were taken into account.

The same series of calculations ($\Delta G^{\neq}$ and ΔG for RE and OA, ΔG for LE) were performed using either MeDalPhos, **3.3-15$_{OMe}$**, **3.3-15$_{H}$** or **3.3-15$_{CF3}$** as the ligand and the data were compared (**Scheme 3.3-6**, **Tab1**). With MeDalPhos, energy values in agreement with those previously reported were obtained, thus validating the method employed. For instance, the ($\Delta G^{\neq}$, ΔG) set of energies for the RE step was calculated to be (17.4, -25.4 kcal/mol), in good agreement with the data reported by Miqueu and Bourissou (17.9, -24.7 kcal/mol).[78] As expected, the RE activation barrier gradually decreases (while the exergonicity increased) when the pyridine moiety becomes more electron poor (**Scheme 3.3-6**, **Tab1**). A $\Delta\Delta G^{\neq}$= 2.4 kcal/mol was found when comparing the data for the disparate **3.3-15$_{OMe}$** and **3.3-15$_{CF3}$** ligands. This value may account for the difference of reactivity observed during the catalytic tests (**Scheme 3.3-7**). Logically, the opposite effect was observed for the OA step, that was calculated to be both more accessible and more exergonic when making the pyridine core more electron rich. Notably, the electronic effect induced by the substitution appeared to be less pronounced for the OA than for the RE ($\Delta\Delta G^{\neq}$= 1.0 kcal/mol, $\Delta G^{\neq}$(**3.3-15$_{OMe}$**) versus $\Delta G^{\neq}$(**3.3-15$_{CF3}$**)). As for the LE step, the stability of the Au(I)-pentenol complex **3.3-23** decreases with ligands possessing a more electron poor pyridine moiety. This evolution reflects the involvement of the pyridine N atom in the stabilization of the π-complex **3.3-23** by coordination,[79,80] an effect not in play for complex **3.3-19**. While **3.3-15$_{CF3}$** led to a promising result during the catalytic tests (**Scheme 3.3-6**), these DFT calculations also demonstrate that, when compared to the series of ligands **3.3-15**, the use of MeDalPhos allows for the lower RE and OA energy barriers, and the least unfavorable LE equilibrium.

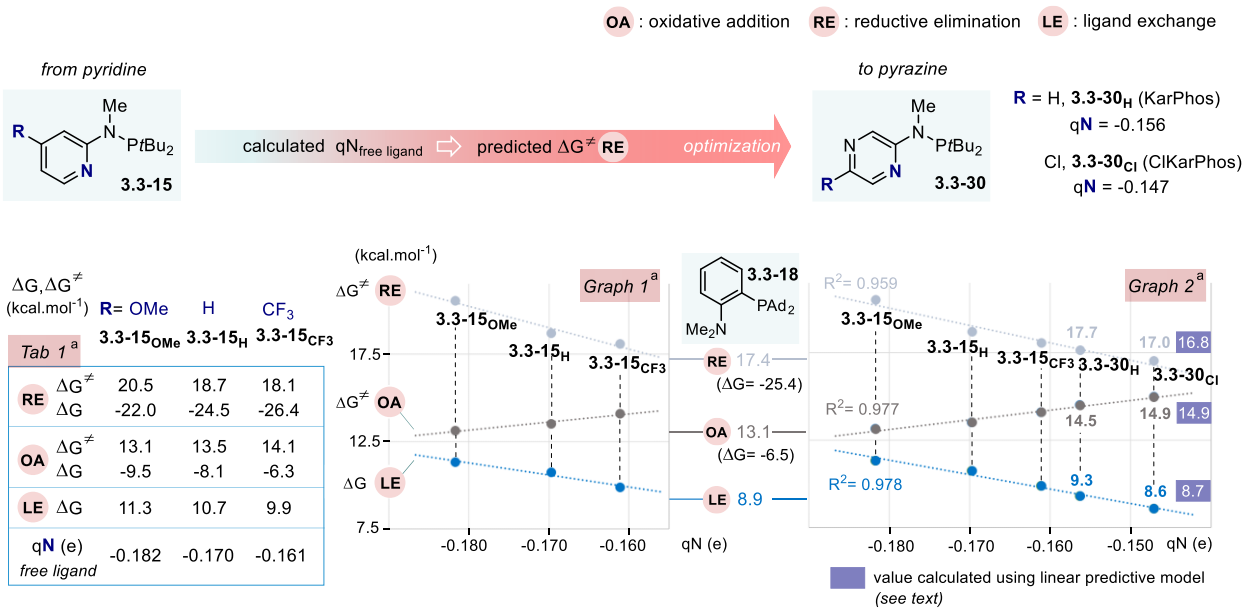

ΔG, ΔG≠ (kcal.mol-1)	R= OMe	H	CF3
	3.3-15OMe	3.3-15H	3.3-15CF3
RE ΔG≠	20.5	18.7	18.1
RE ΔG	-22.0	-24.5	-26.4
OA ΔG≠	13.1	13.5	14.1
OA ΔG	-9.5	-8.1	-6.3
LE ΔG	11.3	10.7	9.9
qN (e) free ligand	-0.182	-0.170	-0.161

Scheme 3.3-6. DFT-guided ligand optimization. [a] Results by Prof. Fabien Gagosz.

In an effort to correlate the calculated variation in energy (ΔG≠, ΔG for RE, OA and LE) with the nature of the substituents on the pyridine moiety, we looked for a parameter that could reflect the change in the pyridine electronics and its resulting modified interaction with the gold center. Since the pyridine moiety coordinates to Au *via* the N atom, we hypothesized that the charge on this atom (qN) could be a suitable descriptor of the substituent effect and ideally an appropriate predictor of the reaction barrier heights and energies. To this end, the structures of the free ligands **3.3-15$_{OMe}$**, **3.3-15$_{H}$** or **3.3-15$_{CF3}$** were optimized and the Hirshfeld charge at the N_{pyr} atom (qN) calculated for each of them. These data are compiled in **Tab1** of **Scheme 3.3-6**. Interestingly, when plotting the ΔG≠ of the OA and RE steps, and the ΔG of the LE step as a function of qN, some linear correlations were found (**Scheme 3.3-6, Graph1**). Similar correlations (not shown in **Graph1**) were obtained for the ΔG of the OA and RE steps. Given the minimal set of data, and with the idea to design new and more efficient catalysts, we decide to confront this emerging model with additional data calculated for a new ligand. The unreported pyrazine-based (P^N) ligand **3.3-30$_{H}$** (KarPhos) was considered an appropriate candidate. By comparing the pKa values of 4-CF_3-pyridine (2.8) and pyrazine (0.6), we conclude that pyrazine should have weaker coordination abilities compared to its 4-CF_3-pyridine counterpart, what should translate in a lower ΔG≠ for the RE step. The structure of KarPhos (**3.3-30$_{H}$**) was optimized and the Hirshfeld charge at the N atom calculated, providing indeed a lower value than for **3.3-15$_{CF3}$** (**Scheme 3.3-6**). Then, the barrier heights and energies for the RE, OA and LE steps were calculated, and the values plotted along with those previously obtained for the pyridine-based (P^N) ligands **3.3-15**. Gratifyingly, we found the new set of data to reinforce the suspected correlation and therefore the possibility to use the qN Hirshfeld charge as an efficient predictor (**Scheme 3.3-6, Graph2**). The model build with the 4-point data set was tested with an additional ligand, ClKarPhos (**3.3-30$_{Cl}$**) considering that the chlorine atom introduced on the pyrazine moiety would make the RE

even more favorable. A similar in silico process was employed to determine after structural optimization that the qN value was the lowest calculated so far (qN= -0.147 e, **Scheme 3.3-6**). This value was employed to predict the barrier heights and energy of the reaction using the linear model derived from the 4-point data set (**Scheme 3.3-6, Graph2**). Remarkably, these predicted values were found to deviate by less than 2% from the values calculated by DFT, a process that was obviously far more demanding in time and resources. From a reactivity point of view, the DFT-guided designed ligands KarPhos (**3.3-30$_H$**) and ClKarphos (**3.3-30$_{Cl}$**) should, according to the calculations, be at least competitive to MeDalPhos for the model reactions studied. ClKarPhos even provided the lowest $\Delta G^{\neq}$ for the key RE step (17.0 kcal/mol). The minimization of this barrier height could be made in exchange to a more energy demanding OA, which remains however comparatively lower (14.9 kcal/mol). To validate our optimization approach and the data produced in silico, ligands **3.3-30$_H$** and **3.3-30$_{Cl}$** were synthesized following a route analogous to that previously employed for the pyridine-based ligands **3.3-15** (**Scheme 3.3-3**). The process was efficient and amenable to multigram scale synthesis starting from readily available pyrazine building blocks (**Scheme 3.3-7**). The corresponding AuCl complexes were produced in very good yield from **3.3-30$_H$** and **3.3-30$_{Cl}$**.

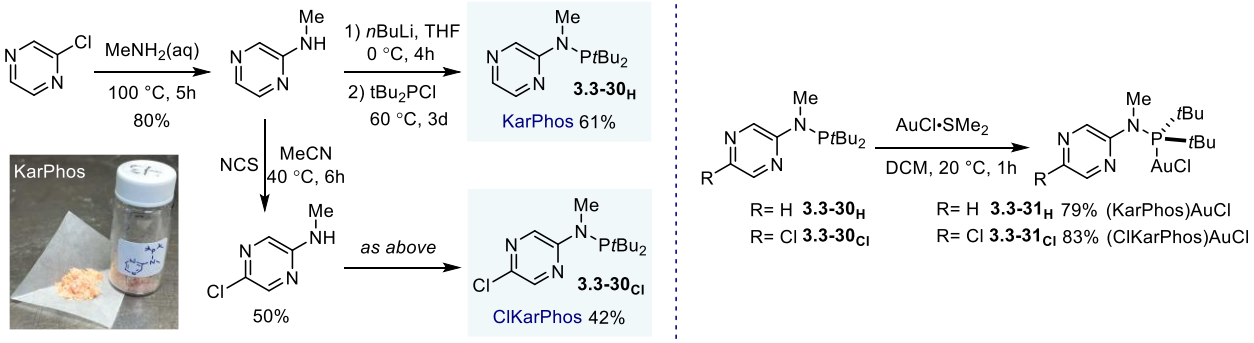

Scheme 3.3-7. Synthesis of (P^N) ligands KArPhos (**3.3-30$_H$**) and ClKarPhos (**3.3-30$_{Cl}$**) and the corresponding AuCl complexes.

The catalytic activity of complexes **3.3-31$_H$** and **3.3-31$_{Cl}$** was first assessed in the model reactions leading to **3.3-17a** and **3.3-17b**. The results of these experiments are provided in **Scheme 3.3-8**. Not only were these DFT-guided designed complexes shown to be more efficient precatalysts than those based on the use of pyridine-based ligands, but they also equaled or outperformed [(MeDalPhos)AuCl]. Furan **3.3-17a,** whose formation served as a model for the ligand optimization, was produced in an improved 84% yield in the presence of [(ClKarPhos)AuCl] (**3.3-31$_{Cl}$**), (+14%) while the formation of pyrrolidine **3.3-17b** was almost quantitative (98%). The same trend was observed over three additional examples of alkoxy or amidoarylation of alkenes (**3.3-17c-e**) thus demonstrating the catalytic potential of **3.3-27$_H$** and **3.3-27$_{Cl}$** for such reactions.

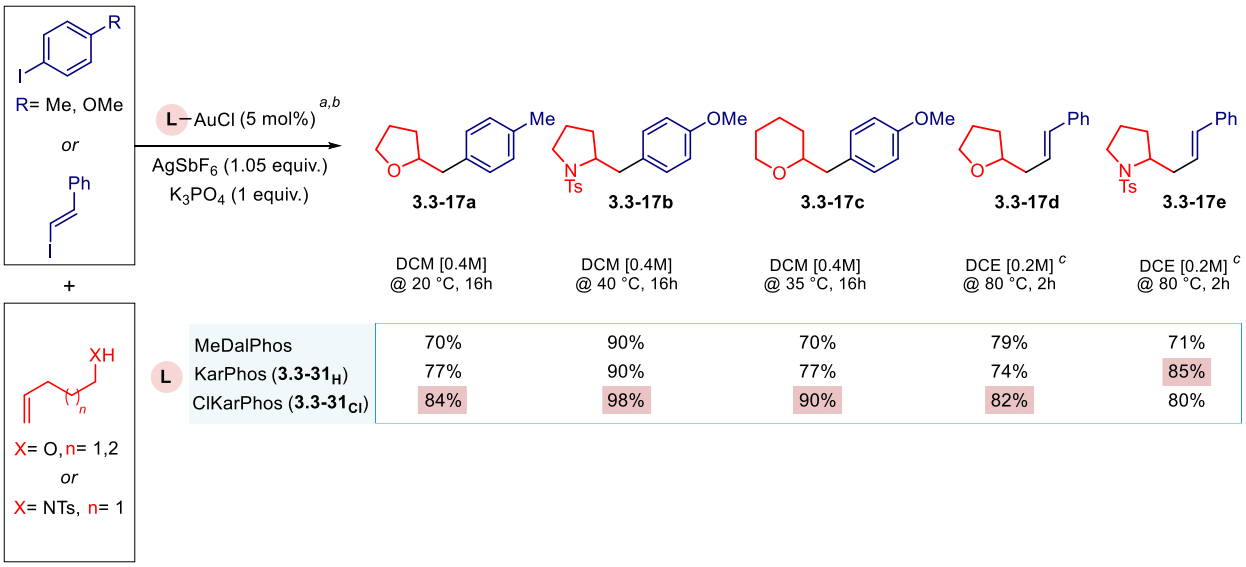

Scheme 3.3-8. Catalytic tests of complexes **3.3-31**. [a] Reactions performed at 0.05-0.1 mmol scale using screw-cap vials and an oil bath with temperature regulation. [b] Yield determined by ^{1}H NMR spectroscopy analysis of the crude reaction mixture using mesitylene as an internal standard. [c] AgOTf was employed.

It is interesting to note that, according to the predictive model (**Scheme 3.3-6, Graph2**), the $\Delta G^{\neq}$ of the RE step could still be reduced provided that an appropriate heteroaromatic motif allowing a lower qN of the ligand could be found. However, this optimization has some limit which should be reached when the $\Delta G^{\neq}$ of the OA step would equal that of the RE step. An optimum value of $\Delta G^{\neq}$= 15.6 kcal/mol for qN= -0.135 e is proposed by the model.

3.3.4. Exploring the catalytic potential of new (P^N) Au(I) complexes in C-S bond formation processes

Given the remarkable efficiency demonstrated by complexes **3.3-31$_H$** and **3.3-31$_{Cl}$** in the alkoxy- and amidoarylation of alkenes, it was decided to further explore their potential as catalysts to achieve more challenging transformations. We turned our attention to the catalytic formation of C-S bonds by cross-coupling of aryl iodides with sulfur derivatives. The stoichiometric reaction between cyclometalated Au(III) complexes and thiols was initially described by Leung and Wong in the context of cysteine residues bioconjugation.[86] The concept was further developed and exploited by Spokoyny and collaborators for the chemoselective structural modification of proteins and sugars with aryl gold(III) complexes bearing bidentate (P^N) ligands.[57–59] The group of Bochmann also reported the stoichiometric reaction of (C^N^C)Au(III) pincer complexes with adamantly thiol, showing the capacity of the resulting Au(III) thiolates to generate C-S bonds by reductive elimination.[87] The first instance of C-S bond formation under catalytic conditions was reported by Shi and coworkers using aryldiazonium salts and a cysteine derivative as reactions partners in the presence of [(Ph_3P)AuCl].[88,89] Lu and Hammond recently reported that less hazardous and structurally more varied aryl iodides could be employed as substrates in the

catalytic formation of aryl trifluoromethylthioethers **3.3-32** (**Scheme 3.3-9, A**).[61] The comparatively more energy demanding C-I bond oxidative addition step could be achieved using MeDalPhos as the ligand. However, the rather mild experimental conditions employed in this transformation appear to be specific to the formation of C-SCF_3 bonds. The cross-coupling with a simple alkyl thiol was attempted by Xu and coworkers and was shown to require more forcing conditions (additives, 140 °C, 24h, see **Scheme 3.3-9, A**).[54] Despite its moderate efficiency (60%), the formation of **3.3-33** remains to date, the only example of a gold-catalyzed cross-coupling of an aryl halide with an alkylthiol.

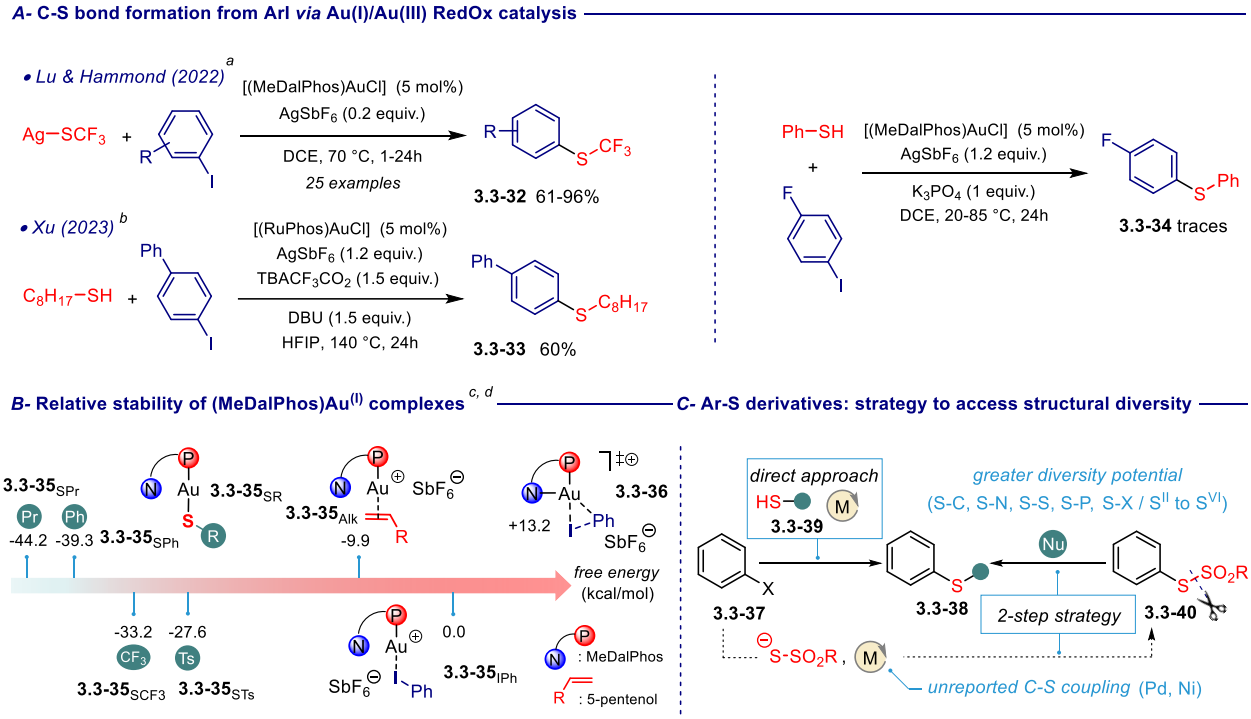

Scheme 3.3-9. Thiosulfonylation of aryl iodides. [a] see ref [61]. [b] see ref [54]. [c] DFT calculations performed at the PWPB95-D4/def2-TZVPP + CPCM(CH_2Cl_2)//R2SCAN-3c level of theory. [d] Results by Prof. Fabien Gagosz.

Our attempts to produce **3.3-34** by reaction between thiophenol and 4-fluoroiodobenzene using experimental conditions commonly employed in Au(I)/Au(III) RedOx catalysis failed (**Scheme 3.3-9, A**).[44] The difficulty to form C-S bonds under Au(I)/Au(III) redox catalysis using thiols as reaction partners could be associated with the high thiophilicity of gold species and the resulting stability of thiolate-Au(I) complexes.[90] During a catalytic process, the formation of such complexes would compete with the coordination of the Au(I) catalyst to the aryliodide, a requisite event prior to the oxidative addition step.

To evaluate such a possibility, the free energies of a series of MeDalPhos-Au(I) complexes **3.3-35** bearing various ligands were calculated (**Scheme 3.3-9, B**). The PhI-coordinated Au(I) complex **3.3-35**$_{PhI}$ was chosen as the reference and the relative stabilities of the other complexes **3.3-35** were assessed by calculating ΔG of the corresponding ligand exchange reactions. Notably, thiolate

complexes **3.3-35**$_{SPh}$ and **3.3-35**$_{SPr}$ were found to be more stable than **3.3-35**$_{PhI}$ by ≈40 kcal/mol, thus rendering the direct ligand exchange between thiolates and phenyl iodide inaccessible. Comparatively, the pentenol/Au(I) π-complex **3.3-35**$_{Alk}$ was calculated to be only 9.9 kcal/mol lower in energy than **3.3-35**$_{PhI}$, thus allowing the ligand exchange and subsequent oxidative addition step to take place at room temperature (overall $\Delta G^{\neq}$= 23.1 kcal/mol).This value agrees with the experimental evidence reported by Bourissou and coworkers that oxidative addition slowly proceeded (days) when (MeDalPhos)Au(I)-octene complex was reacted at 20 °C with a stoechiometric amount of PhI.[42] We found that this reaction could be largely accelerated (> 90% conversion after 0.5h) when 1 equiv. of $AgSbF_6$ was added to the mixture (see **Appendix Figure 6.2-20** for more details). This silver effect, which can be attributed to the competitive coordination of Ag^+ to the alkene, should also be in play in the trifluoromethylthiolation of aryl iodides (**Scheme 3.3-9, A**), as suggested by Lu and Hammond.[61] Despite the significant difference in thermodynamic stability between Au(I)-SCF_3 complex **3.3-35**$_{SCF3}$ and **3.3-35**$_{PhI}$ (≈33 kcal/mol, see **Scheme 3.3-9, B**), the oxidative addition step could remain accessible in the presence of excess Ag+ salts since these ones could compete with the gold(I) complex for coordination to the SCF_3 moiety. DFT calculations support this hypothesis (**equation 1**): in the presence of $AgSbF_6$, the thiolate/PhI exchange was found to be thermodynamically less unfavorable (≈11.7 kcal/mol) (see section on mechanistic investigations for additional information).

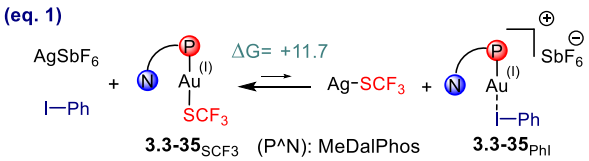

In this context and following the above considerations, we design a new approach to the synthesis of aryl sulfur derivatives **3.3-38** (**Scheme 3.3-9, C**). These important structural motifs are commonly produced by C-S bond forming process *via* a direct metal-catalyzed cross-coupling between an activated aryl derivative **3.3-37** and the corresponding sulfide reaction partner **3.3-39**.[91] Such an approach has several significant limitations mostly associated with the use of **3.3-39**. First, the number of commercially available R-SH building blocks is limited, which may require their synthesis prior to the coupling and second, they are notoriously malodorous in their great majority, thus making their use on large scale unpractical. In addition, thiols can be readily oxidized into disulfides and are therefore air-sensitive compounds. Finally, the method is generally restricted to the use of RSH coupling partner where R is a carbon-based substituent, which limits the structural motifs that can be accessed. Our strategy to access aryl sulfur derivatives **3.3-38** (**Scheme 3.3-9, C**) is based on a two-step sequence that involves 1- an initial cross-coupling of an Ar-I with an amphiphilic thiosulfonate derivative RSO_2S^-, followed by 2- a functionalization of the resulting arylthiosulfonate intermediate **3.3-40** by umpolung at the S center. While being less straightforward, this approach could allow for a greater structural diversity with the possibility to employ a variety of nucleophilic partners during the functionalization step.

The formation of *S*-arylthiosulfonate of type **3.3-40** by C-S bond formation is an unclassical approach and very limited work has been done in this area.[92,93] Very surprisingly, and to the best of our knowledge, the coupling of an aryl halide with a thiosulfonate has never been explored. Boehringer Ingelheim Pharmaceuticals researchers reported in 2014 a Cu(I)-catalyzed cross-coupling of aryl iodides with sodium thiosulfate to produce $ArSSO_2Na$ Bunte salts, which represents to date the only example of metal-mediated coupling with a thiosulfonyl moiety (**equation 2**).[94] While efficient, the method requires high loading of catalyst (10 mol%), had limited exemplification and the Bunte salts $Ar\text{-}S_2O_3Na$ could only be obtained in 50-70 wt.% purity as the result of the isolation protocol.

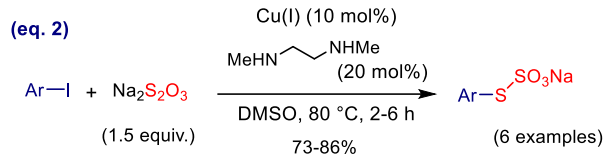

We considered that a thiotosylate anion could be an appropriate coupling partner for our approach. This choice was motivated by the ease of access to such species and the calculated greater lability of the TsS moiety in the corresponding [(MeDalPhos)AuSTs] complex **3.3-35**$_{STs}$ as compared to other thiolate Au-(I) complexes **3.3-35**$_{SR}$ (**Scheme 3.3-9, B**). More specifically, the STs complex **3.3-35**$_{STs}$ was found 5.6 kcal/mol less stable than the SCF_3 one (**3.3-35**$_{SCF3}$) which was considered as a favorable factor for the targeted cross-coupling reaction. The tetrabutylammonium thiotosylate salt **3.3-41** (Bu_4NSTs) could be easily produced in a 2-step sequence using inexpensive starting materials ($TsSO_2Na$, S_8 and TBAC) (**Scheme 3.3-10, A**). The sequence was efficient (85% overall yield), could be performed on a multigram scale and **3.3-41** appeared to be a bench stable solid with low hygroscopicity. The cross-coupling was attempted using stoichiometric amounts of **3.3-41** and 4-F-iodobenzene **3.3-42a**, 1.2 equiv. of $AgSbF_6$ as halide scavenger and ligand exchange facilitator, in DCE at 80 °C. When 2.5 mol% of [(MeDalPhos)AuCl] complex was employed as pre-catalyst, we were pleased to observe that the desired aryl thiotosylate **3.3-43a** was produced in 86% yield after 3h of reaction (**Scheme 3.3-10, A**). Gratifyingly, the use of the KarPhos ligand (**3.3-30**$_H$) led to a similar outcome (**3.3-43a**: 85%). When the catalyst loading was reduced to 1 mol%, a slightly better result was obtained with **3.3-30**$_H$ (61% versus 54%). However, ClKarPhos (**3.3-30**$_{Cl}$) was found to be an optimum ligand for this transformation, allowing the formation of **3.3-43a** in a largely improved 83% yield. This remarkable result, which was confirmed by triplicate experiments, attests to the potential of the newly designed (P^N)-Au(I) complexes for RedOx catalysis. The success encountered with the use of the ClKarPhos allowed for a reduction of the catalyst loading to 0.3 mol% without noticeable loss of efficiency (81% yield, 24h). At 0.1 mol%, 310 TON could be obtained, what, to the best of our knowledge, represents the highest value for a such a type of Au-mediated RedOx process. For comparison, at lower loading than 5 mol% of [(MeDalPhos)AuCl], the trifluoromethylthiolation reported by Hammond and Lu (**Scheme 3.3-9, A**) was far less efficient (32%, 2 mol%).[61]

Finally, we rapidly evaluate the possibility to perform the reaction using Pd-catalysis. Similarly, to what was previously reported by Schoenebeck and coworkers for the cross-coupling of aryl iodides with phosphorothiolate **3.3-44** (**Scheme 3.3-10, B**),[95] the reaction could not be performed under Pd(0)/Pd(II) catalysis using classical experimental conditions. This result highlights the singular catalytic potential of Au(I) complexes in such transformation.

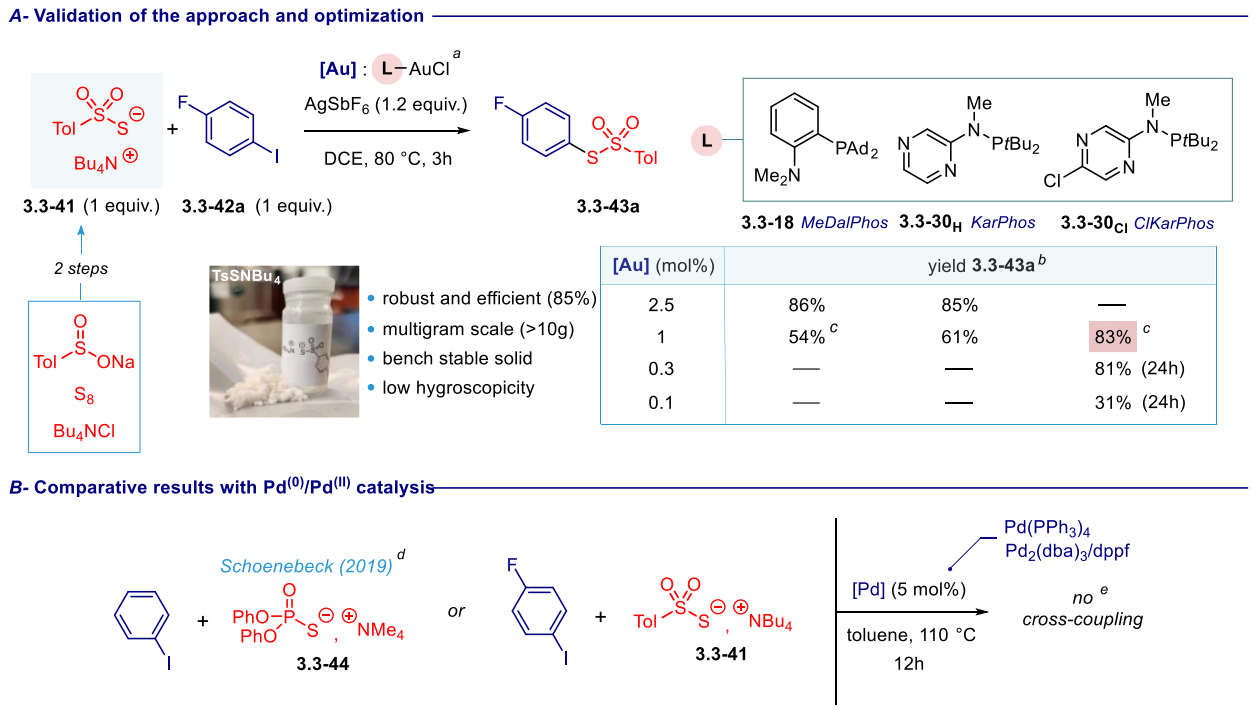

Scheme 3.3-10. Initial results and optimization. [a] Reactions performed with screw-cap vials using an oil bath with temperature regulation and >700rpm stirring. [b] Yield determined by ^{1}H NMR spectroscopy analysis of the crude reaction mixture using mesitylene as an internal standard. [c] average yield for a triplicate experiment. [d] see ref [95] . [e] Results by Elyssa Caron.

3.3.5. Reaction scope and applications

The scope of the transformation was then evaluated (**Scheme 3.3-11**). A variety of aryl iodides (48 representative examples) were treated under the optimized conditions using generally 1-2 mol% of complex **3.3-31$_{Cl}$**. Alkyl, halogen, EDG and EWG substituents were well tolerated. Yields were found to be largely independent of the nature of the substituent (81% average yield). Multiple substitution was tolerated at any position of the aromatic (ortho, meta, para) but a limit in reactivity was reached for di-*ortho*-substituted aryl iodide bearing sterically demanding group/atoms. (see for instance **3.3-43k** and **3.3-43z** versus **3.3-43y**). A remarkable chemoselectivity was observed for aryl iodides possessing different halogen atoms (F, Cl, Br). The cases of aryl iodides **3.3-43aa** and **3.3-43ab**, which possess 3 and 4 different halogens respectively, are particularly representative. Thiotosylates **3.3-43aa** and **3.3-43ab** resulting from

an exclusive cross-coupling at the C-I position were formed in excellent yield (91% and 88%, respectively). As for EWGs, ester, aldehyde, ketone, cyano, nitro and trifluoromethyl substituents were all tolerated. A 2 mol% catalyst loading was generally required to achieve high conversion of the substrates. The reaction was easier to perform in the case of aryl iodide possessing EDGs: 1 mol% of **3.3-31$_{Cl}$** and 3h of reaction allowed for yields in cross-coupling products higher than 80%. While the reaction could not be performed on pyridines (see **3.3-43ar** and **3.3-43as**), it was efficient with thiophenes (see **3.3-43ap** and **3.3-43aq**). Multiple cross-couplings could be realized on poly-iodo derivatives as attested by the formation of compounds **3.3-43n** and **3.3-43aq**. Finally, the reaction of β-iodostyrene **3.3-43at**, which delivered compound **3.3-43at** in an efficient, stereoselective and rapid manner (85%, *E* isomer, 0.5h), attests that the cross-coupling has the potential for functionalization of other C(sp^2)-I bonds.

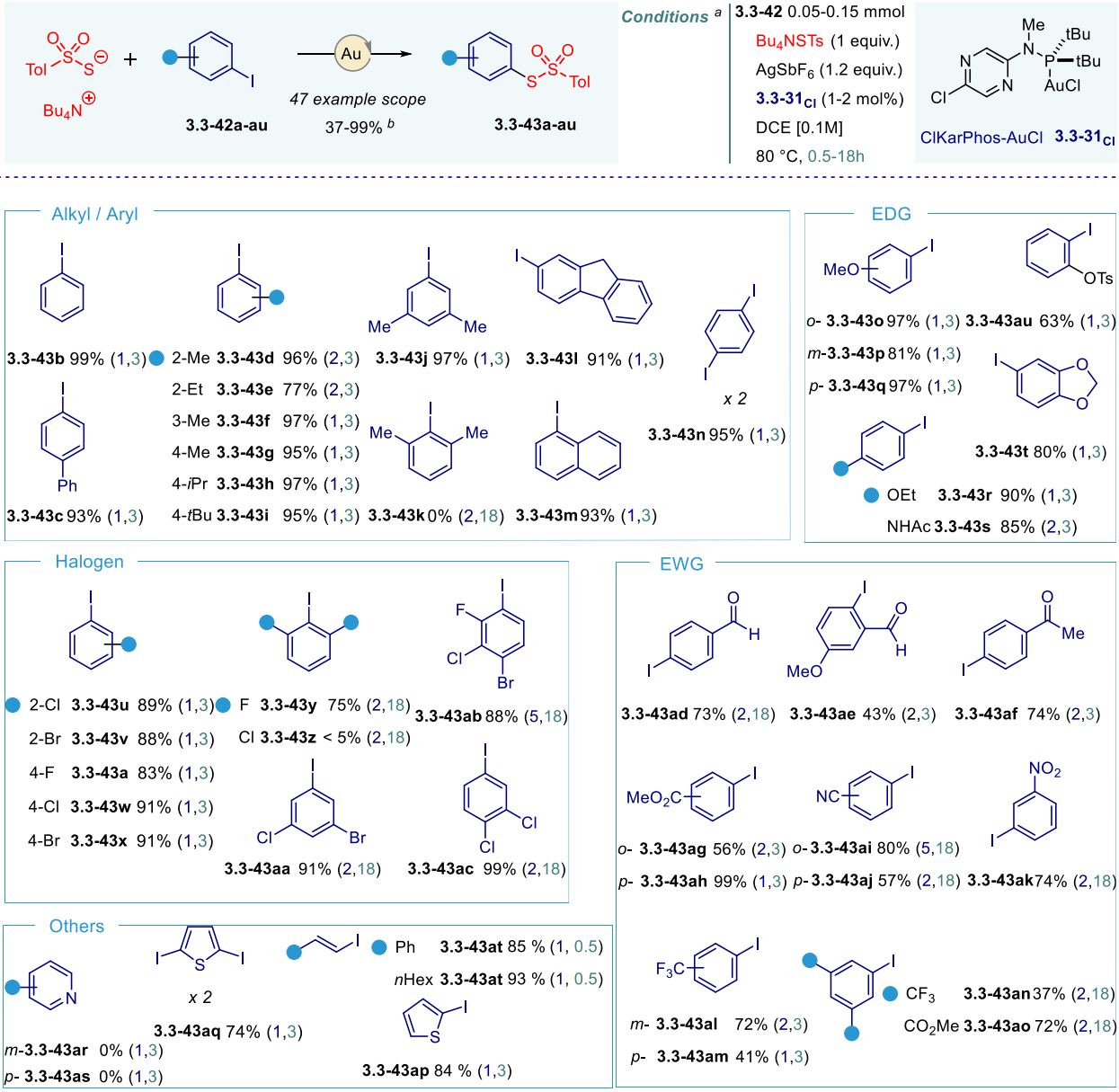

Scheme 3.3-11. Scope of the Au-catalyzed cross-coupling reaction of aryl iodides with ammonium thiotosylate. [a] Reactions were performed with screw-cap vials using an oil bath with temperature regulation and >700rpm stirring. For each substrate the catalyst loading (mol%), and the reaction time (h) are sequentially provided between brackets. [b] Yields were determined by ^{1}H NMR spectroscopy analysis of the crude reaction mixture using mesitylene as an internal standard.

To conclude with our 2-step strategy, thiotosylate **3.3-43a** was transformed under a variety of conditions allowing the cleavage of the S-Ts bond with concomitant functionalization at the S center (**Scheme 3.3-12**). A small library of products could be generated by directly using procedures from the literature or by adapting reported protocols (see **Appendix** for more details). New S-C(sp^3), -C(sp^2) and –C(sp) bonds could be formed by addition of organometallics, Ni-catalyzed cross-coupling or by simple nucleophilic substitution (see **3.3-44e-g**). S-Heteroatom bond formation was also amenable as attested by the production of disulfide **3.3-44a** (72%), sulfenylamine **3.3-44b** (62%) and thiophosphinate **3.3-44c** (95%). Finally, the valuable SF_4Cl derivatives **3.3-44d** was produced in 80% by adapting a procedure reported by the Cornella group for the conversion of somewhat related aryl phosphorothiolate substrates (see **Appendix** for more details). Notably, among the derivatization products obtained, a large number could not be directly produced by metal-catalyzed cross coupling reaction of an aryl halide with the corresponding R-SH derivative.

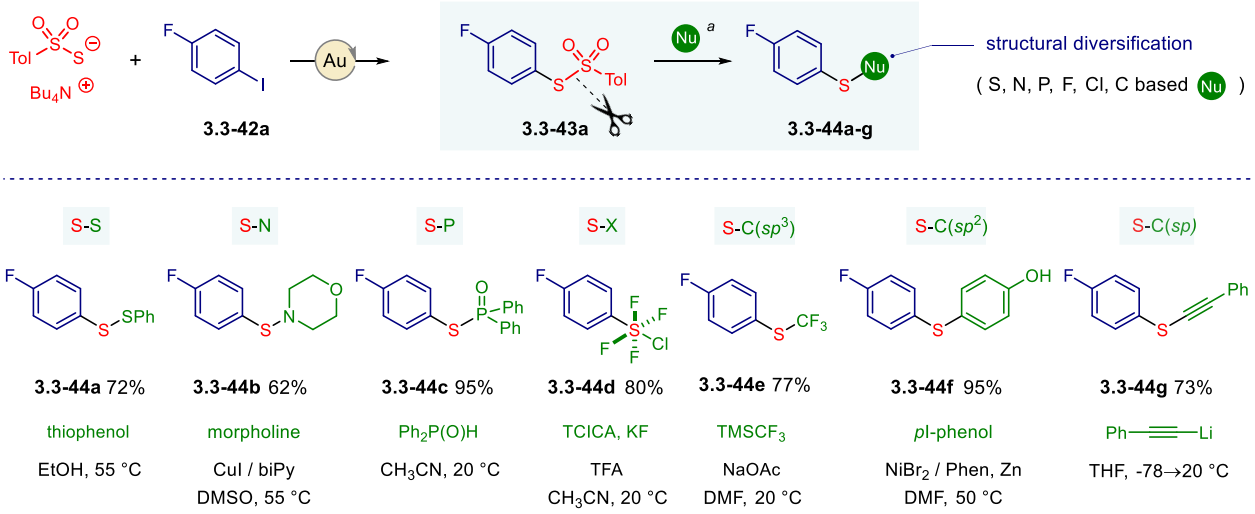

Scheme 3.3-12. Structural diversification *via* post-transformations on arylthiotosylate **3.3-43a**.

After successful development of the thiotosylation protocol, we decided to extend its applicability by employing another sulfur nucleophile: ammonium thiocyanate, with the intention of introducing an SCN moiety (**equation 3**). Unfortunately, the reaction performance was not optimal under analogous conditions and yielded only 10% of the desired product **3.3-45**. Increasing the reaction time to 24 hours improved the yield to 37%. We speculate that the reduced reactivity is due to the lower solubility of the resulting AgSCN salt compared to the corresponding AgSTs salt. This solubility difference likely affected the reaction kinetics and required a longer reaction time to achieve a modest yield.

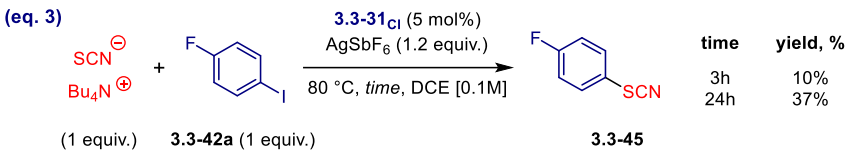

3.3.6. Mechanistic investigations

To get more insight into the mechanism of the reaction, a series of computational and experimental studies were conducted. The results of these investigations are summarized in **Scheme 3.3-13**. DFT calculations were performed with ORCA 5.0.2 at the PWPB95-D4/def2-TZVPP + CPCM(1,2-dichloroethane)//R2SCAN-3c level of theory, using ClKarPhos as the ligand and Et_4N^+ as a model for Bu_4N^+.[81–85]

The oxidative addition step (**3.3-35**$_{PhI}$→**3.3-46**) was found to have a moderate energy of activation ($\Delta G^{\neq}$= +15.8 kcal/mol) and to be slightly exergonic (ΔG= -5.0 kcal/mol) (**Scheme 3.3-13, A**). The subsequent I to STs ligand exchange by reaction of **3.3-46** with AgSTs was calculated to be favorable by 3.1 kcal/mol. It was considered that the thiophilic $AgSbF_6$ species would easily react with Et_4NSTs, to produce AgSTs and Et_4NSbF_6, an assumption that is supported by calculation (ΔG= -25.7 kcal/mol). The reductive elimination step (**3.3-47**→**3.3-48**) was slightly more energy demanding ($\Delta G^{\neq}$= +18.0 kcal/mol) than the oxidation step but far more exergonic (ΔG= -25.3 kcal/mol). The catalytic cycle could be closed by TsS-Ph to PhI ligand exchange at the Au(I) center (**3.3-48**→**3.3-35**$_{PhI}$), a step that was found to be uphill (ΔG= +6.6 kcal/mol). Alternatively, Au(I) species **3.3-48** most likely reacts with AgSTs to produce the Au(I)-thiotosylate complex **3.3-35**$_{STs}$.[96] Intermediate **3.3-35**$_{STs}$ appears to be a thermodynamic sink – 26.2 kcal/mol more stable than **3.3-35**$_{PhI}$, a value comparable to that calculated for the (MeDalPhos)Au(I) complex (see **Scheme 3.3-9, B**) and was detected by ESI-HRMS analysis of a running reaction as the catalyst resting state. The Ag^+ mediated off-cycle equilibrium between **3.3-35**$_{STs}$ and **3.3-35**$_{PhI}$ appears to be essential to the success of the cross-coupling reaction. $AgSbF_6$ has a dual role in the transformation: not only it is acting as an iodide scavenger, but also reducing the energy required to access **3.3-35**$_{PhI}$. As a consequence, $AgSbF_6$ has to be used in slight excess (1.2 equiv.) to ensure that it is not initially fully converted into AgSTs since "free" Ag^+ is required for the TsS to PhI exchange at the Au(I) center (**3.3-35**$_{STs}$→**3.3-35**$_{PhI}$). At the beginning of the reaction, the ≈ 0.2 equiv. of Ag^+ salt not complexed to TsS^- would most probably be in solution as κ-IArAg(I) complexes. When the reaction progresses, κ-S coordination to the ArSTs might become prevalent. "Free" Ag^+ salt refers to Ag^+ not being consumed (to produce AgI) and present as complexes with a lower binding affinity ligand (ArI, ArSTs) than TsS^-. The role of the silver salt was confirmed by a stoichiometric reaction in which Au(I)-STs complex **3.3-35**$_{STs}$ was treated with an excess of 4-fluoro iodobenzene (**Scheme 3.3-13, B**). In the absence of $AgSbF_6$, the catalytic cycle could not be initiated, whatever the temperature and reaction time, as the result of the difficulty to perform the required STs to PhI exchange. The same reaction performed with 1 equiv. of $AgSbF_6$ led to the quantitative formation of the Ar-STs cross-coupling product **3.3-43a** after only 1 h at 20 °C. A control experiment showed

that the Ag^+ salt was key to achieve such a reactivity as $TBAPF_6$ could not trigger the RedOx process. It was also demonstrated that the role played by $AgSbF_6$ in the off-cycle equilibrium is more important than its activity as iodide scavenger. In the absence of $AgSbF_6$, the Au(III) complex **3.3-49** could still react with Bu_4NSTs to ultimately produce the Ar-STs cross-coupling product **3.3-43a** (**Scheme 3.3-13, B**). The reaction was perfomed with MeDalPhos as the ligand due to the instability of the corresponding Au(III) complex when AuClKarPhos is employed. This reaction was found to follow zero-order kinetics, the rate determining step being the reductive elimination of **3.3-47** into **3.3-48**. ^{31}P NMR monitoring of the reaction showed that a fast equilibrium takes place between **3.3-46** and **3.3-47**, as attested by the broadening of the P ligand signal and its slight shifting over the course of the reaction. A similar equilibrium should also be in play between the (P^N)Au(I)-I by-product of the reaction and the corrresponding (P^N)Au(I)-STs (**3.3-35**$_{STs}$).

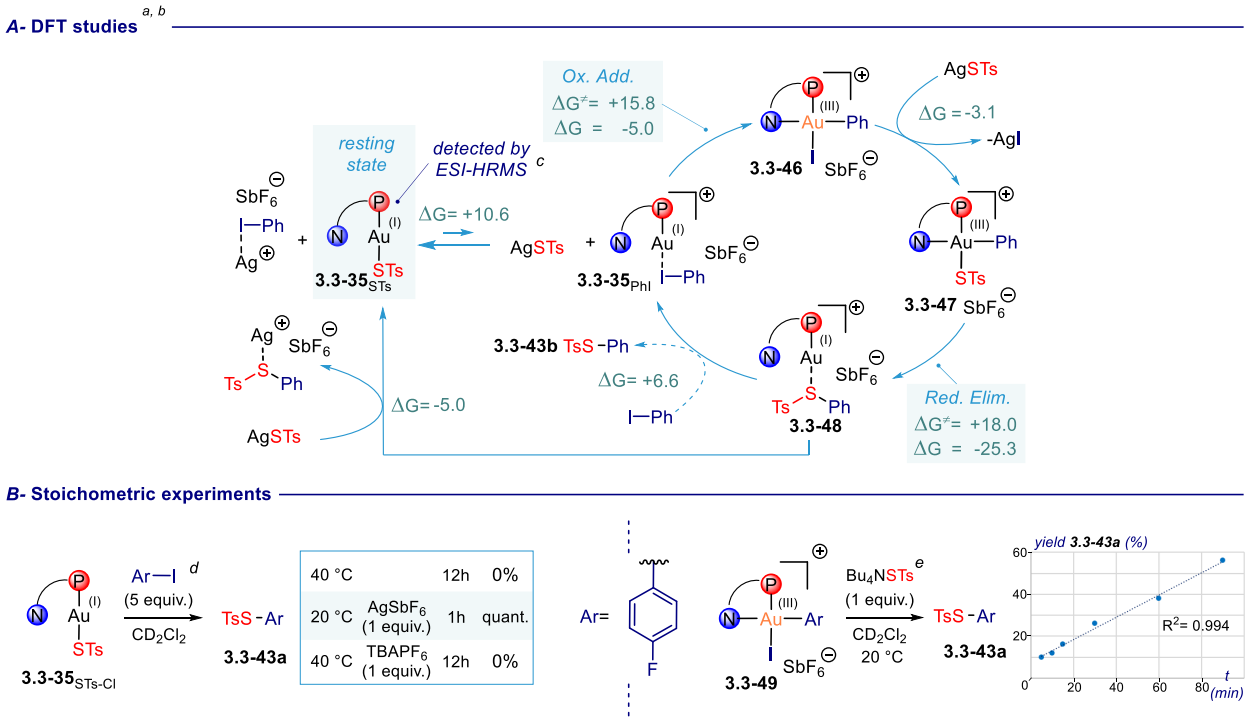

Scheme 3.3-13. Mechanistic studies and proposed catalytic cycle for the Au(I)/Au(III)-mediated thiosulfonylation of aryl iodides. [a] Results by Prof. Fabien Gagosz. [b] DFT calculations performed at the PWPB95-D4/def2-TZVPP + CPCM(1,2-dichloroethane)//R2SCAN-3c level of theory. (P^N)= ClKarPhos. [c] Result by Emil Zaripov [d] Reaction monitored by ^1H, ^{31}P and ^{19}F NMR analysis; (P^N)= ClKarPhos. [e] Reaction monitored by ^1H, ^{31}P and ^{19}F NMR analysis; (P^N)= MeDalPhos.

In summary, the kinetics and the overall efficiency of the transformation seem to be dictated by the off-cycle equilibrium between complexes **3.3-35**$_{STs}$ and **3.3-35**$_{PhI}$. Superstoichiometric amounts of the silver salt and aryl iodide would be beneficial, while excess of the thiotosylate coupling partner would be detrimental. The observed higher catalyst loadings and longer reaction times required to convert aryl iodides possessing EWGs (**Scheme 3.3-11**) could be linked to the lower stability of the corresponding κ-IAr-Au(I) complex as compared to **3.3-35**$_{PhI}$. In aryl iodides

with EWGs, electronic density on the iodine atom would be diminished, reducing its Lewis basicity. As a consequence, weaker binding to the Au(I) center should be anticipated, resulting in an elevated ΔG for the off-cycle equilibrium. Preliminary results from DFT calculations show that these values vary by less than 2 kcal/mol when comparing the effects of a *para*-OMe substituent versus a *para*-CF_3 substituent. The conclusions of this study with regard to the dual role of the silver salt and the parameters affecting the kinetics and efficiency of the reaction, are important points to be considered in the design of gold-catalyzed RedOx transformations, more especially when one or several of the reactants can strongly bind to the cationic LAu(I) complex.

To further prove the influence of the off-cycle equilibrium on the reaction kinetics, catalytic tests were carried out in which the stoichiometry of pent-4-en-1-ol, silver salt, and aryl iodide was systematically varied. Our results indicate a remarkable dependence of the reaction rate on the reagent ratios. When pent-4-en-1-ol was used in excess (**Scheme 3.3-14, entry 3**), a substantial slowdown of the reaction was observed. Conversely, an excess of aryl iodide led to a slight acceleration of the reaction compared to equimolar amounts of ArI (**Scheme 3.3-14, entries 1** and **2,** respectively). Interestingly, the deleterious effect of non-productive alkene binding to the Au(I) complex could be significantly attenuated by using an excess of silver salt (**Scheme 3.3-14, entry 4**).

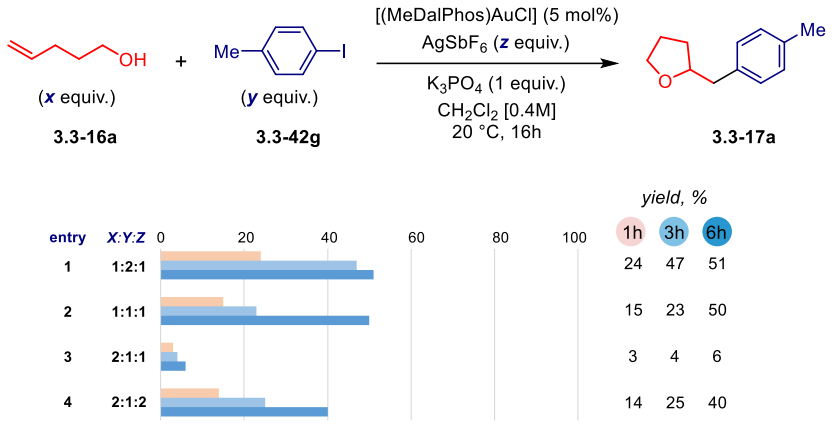

Scheme 3.3-14. Studies on reaction kinetic.

This observation is consistent with the idea that the silver salt may bind competitively to the alkene, thereby weakening its nonproductive interaction with the Au(I) complex. These results empirically support our original hypothesis that unproductive alkene binding to the Au(I) complex competes with the formation of the κ-IAr-Au(I) complex, a key intermediate in the reaction mechanism.

3.4. Conclusion

During our investigations, a new family of hemilabile bidendate (P^N) ligands possessing a distinct structure than MeDalPhos was discovered to enable the oxidative addition of C(sp^2)-I to Au(I)

centers. The initial design which consisted of replacing the Me_2NPh fragment of MeDalPhos by a 2-NMe-pyridine motif to increase ligand hemilability, structural and electronic modulation capacity was found successful. The first set of ligands, which exhibited promising RedOx activity in the model alkoxy- and amidoarylation of alkenes, were refined and optimized using DFT computational studies. The Hirshfeld charge at the coordinating N_{py} atom, calculated on the free ligand, was shown to be an appropriate predictor of the $\Delta G^{‡}$ of the rate determining reductive elimination step. Two pyrazine-based ligands, KarPhos and ClKarPhos, suggested by the in silico study to possess improved reactivity, were indeed shown to match or outperform MeDalPhos in the model reactions and a series of related alkene arylations.

Notably, these ligands can be obtained at the gram scale in a straightforward manner and from relatively inexpensive building blocks. The synthetic potential and comparatively higher reactivity of these new ligands was further highlighted in the thiotosylation of aryl iodides, a challenging unreported metal-catalyzed C-S cross-coupling reaction. Remarkably, while this transformation could not be achieved under Pd(0)/Pd(II) catalysis and was moderately efficient at 2 mol% catalyst loading using MeDalPhos, high yields in cross coupling product were achieved at just 0.3 mol% with ClKarPhos. Ultimately, this reactivity allowed us to develop a general divergent 2-step strategy to access various aryl sulfur derivatives. An additional computational and experimental study dedicated to determining the mechanism and the energetics of the transformation, highlighted the key role played by the silver salts in an off-cycle equilibrium. Fundamentally, this study demonstrated the potential of (P^N) ligands for gold RedOx catalysis and the particular interest of the 2-NMe heteroaromatic fragment as the N-donor motif. We believe that structural and electronic variation on this platform will allow us to easily and effectively tune the stability of the Au(III) intermediates and the barrier heights of the key OA and RE steps depending on their prevalence in a RedOx process. The study also highlights the value of predictive DFT calculations in the optimization of gold catalytic systems. The implementation of AI and machine learning in this process would most probably speed up the discovery of ligands, allowing improved reactivity and specificity.

3.5. Experimental procedures

3.5.1. General information

Commercially available reagents were purchased from Sigma-Aldrich, Alfa-Aesar, Oakwood Chemicals, TCI America, Fluorochem Chemical, Aarom Chemicals, AmBeed or Combi-Blocks suppliers and were used as delivered without further purification unless otherwise noted. Dichloromethane stock was dried with 4Å MS. Reactions carried out under inert atmosphere were performed under nitrogen gas. Thin layer chromatography was performed on TLC Silicagel 60 F254 plates. Flash column chromatography was carried out on silica gel using a forced flow of eluents. NMR spectra were recorded at room temperature in the given deuterated solvent on a Bruker Avance III 600, Bruker Avance II 400, Bruker Avance II 300 or Bruker Avance 300 instrument

operating at the indicated frequency. Chemical shifts (δ) are given in parts per million (ppm) using CD_2Cl_2, $CDCl_3$ and $(CD_3)_2CO$ solvent peaks as the reference for ^{1}H-NMR and ^{13}C-NMR spectra, respectively. Signal multiplicities are depicted using the following abbreviations: s = singlet, d = doublet, t = triplet, q = quartet, m = multiplet, dd = doublet of doublet, dt = doublet of triplet, tt = triplet of triplet, dq = doublet of quartet, ddd = doublet of doublet of doublet, ddt = doublet of doublet of triplet, bs = broad singlet. Proton decoupling was employed for all ^{13}C and ^{31}P spectra. High-resolution mass spectrometry by electron impact (HRMS-EI) was performed on a JEOL JMCGCmate II mass spectrometer, and high-resolution mass spectrometry by electrospray ionization (HRMS-ESI) was performed on a Micromass Q-TOF II Mass Spectrometer, ESI-MS (orbitrap Velos Pro) or SYNAPT G2 (for the determination of reaction resting states). Molecular ion and/or fragment signals were given in mass per charge number (*m/z*).

3.5.2. Synthesis of ligands 3.3-15 & 3.3-26, Au(I) & Au(III) complexes 3.3-11 – 3-13, 3.3-31

3.5.2.1. Synthesis of ligands 3.3-15$_H$, 3.3-15$_{OMe}$, 3.3-15$_{CF3}$, 3.3-30$_H$ and 3.3-30$_{Cl}$

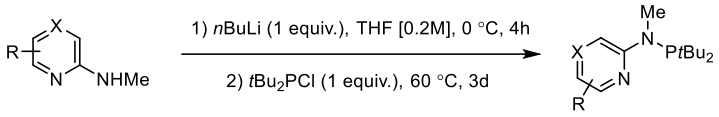

General procedure 3-1:

The following general procedure was employed for the synthesis of ligands **3.3-15$_H$, 3.3-15$_{OMe}$, 3.3-15$_{CF3}$, 3.3-30$_H$** and **3.3-30$_{Cl}$**. A flame dried Schlenk flask was charged with the amine (1 equiv.) and dry THF [0.2M] under a nitrogen atmosphere. The resulting solution was cooled down to 0 °C before a solution of *n*BuLi in hexane (1 equiv.) was added dropwise. The reaction mixture was allowed to reach room temperature and was then stirred for 4h before *t*Bu$_2$PCl (1 equiv.) was added dropwise. At the end of the addition, the temperature was raised to 60 °C and the reaction mixture was stirred for 3 days. The solvent was then evaporated, and the crude residue was purified by flash column chromatography.

***N*-(di-tert-butylphosphaneyl)-N-methylpyridin-2-amine 3.3-15$_H$**

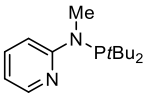

Prepared from *N*-methylpyridin-2-amine (372 mg, 3.44 mmol), 2.5M solution of *n*BuLi in hexane (1.4 mL, 3.44 mmol) and *t*Bu$_2$PCl (652 µL, 620 mg, 3.44 mmol) according to the general procedure **3-1**. Purification by flash column chromatography in Hexane:EtOAc:Et$_3$N = 4:1:0.005.

3.3-15$_H$ was obtained as a white solid: 405 mg, 47% yield.

^{1}H NMR (300 MHz, $CDCl_3$) δ(ppm) δ 8.12 (dd, *J* = 5.0, 1.9 Hz, 1H), 7.63 (dd, *J* = 8.8, 4.5 Hz, 1H), 7.42 – 7.20 (m, 1H), 6.67 – 6.40 (m, 1H), 3.23 (s, 3H), 1.18 (d, *J* = 12.6 Hz, 18H).

^{13}C NMR (75 MHz, $CDCl_3$) δ(ppm) 162.9 (d, *J* = 27.3 Hz), 146.9 (d, *J* = 1.7 Hz), 135.9 (d, *J* = 3.9 Hz), 113.4 (d, *J* = 1.8 Hz), 111.7 (d, *J* = 30.2 Hz), 36.8 (d, *J* = 8.3 Hz), 35.9 (d, *J* = 27.9 Hz), 29.8 (d, *J* = 17.0 Hz).

^{31}P NMR (122 MHz, $CDCl_3$) δ(ppm) 85.1.

HRMS (ESI) Calculated for $C_{14}H_{26}N_2P^+$ $[M+H]^+$: 253.1828; found: *m/z* 253.1808.

N-(di-tert-butylphosphaneyl)-4-methoxy-N-methylpyridin-2-amine 3.3-15$_{OMe}$

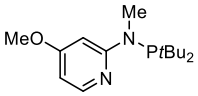

Prepared from 4-methoxy-*N*-methylpyridin-2-amine (170 mg, 1.23 mmol), 2.5M solution of *n*BuLi in hexane (0.49 mL, 1.23 mmol) and *t*Bu$_2$PCl (233 µL, 221.6 mg, 1.23 mmol) according to the general procedure **3-1**. Purification by flash column chromatography in Hexane:EtOAC:Et_3N = 4:1:0.005.

3.3-15$_{OMe}$ was obtained as a yellowish solid: 214.8 mg, 62% yield.

^{1}H NMR (300 MHz, $CDCl_3$) δ(ppm) 8.01 (d, *J* = 5.8 Hz, 1H), 7.22 (dd, *J* = 5.7, 2.2 Hz, 1H), 6.26 (dd, *J* = 5.8, 2.3 Hz, 1H), 3.79 (s, 3H), 3.27 (s, 3H), 1.24 (d, *J* = 12.5 Hz, 18H).

^{13}C NMR (76 MHz, $CDCl_3$) δ(ppm) 166.0 (d, *J* = 3.3 Hz), 165.0 (d, *J* = 27.3 Hz), 148.0 (d, *J* = 2.2 Hz), 102.5, 95.6 (d, *J* = 32.0 Hz), 55.0, 37.2 (d, *J* = 8.6 Hz), 36.0 (d, *J* = 28.3 Hz), 29.9 (d, *J* = 17.0 Hz).

^{31}P NMR (122 MHz, $CDCl_3$) δ(ppm) 84.5.

HRMS (ESI) Calculated for $C_{15}H_{28}N_2OP^+$ $[M+H]^+$: 283.1934; found: *m/z* 283.1960.

N-(di-tert-butylphosphaneyl)-N-methyl-4-(trifluoromethyl)pyridin-2-amine 3.3-15$_{CF3}$

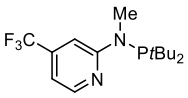

Prepared from *N*-methyl-4-(trifluoromethyl)pyridin-2-amine (176 mg, 1 mmol), 2.5M solution of *n*BuLi in hexane (0.40 mL, 1 mmol) and *t*Bu$_2$PCl (189 µL, 179.7 mg, 1 mmol) according to the general procedure **3-1**. Purification by flash column chromatography in Hexane:EtOAC = 10:1.

3.3-15$_{CF3}$ was obtained as a yellowish solid: 121 mg, 38% yield.

^{1}H NMR (300 MHz, $CDCl_3$) δ(ppm) 8.30 (d, J = 5.2 Hz, 1H), 7.98 (d, J = 5.5 Hz, 1H), 6.79 (dd, J = 5.2, 1.3 Hz, 1H), 3.30 (s, 3H), 1.25 (d, J = 12.7 Hz, 18H).

^{13}C NMR (76 MHz, $CDCl_3$) δ(ppm) 163.6 (d, J = 27.8 Hz), 148.3 (d, J = 1.8 Hz), 140.4 – 136.9 (m), 123.5 (q, J = 273.0 Hz), 108.7 (d, J = 3.5 Hz), 107.7 (dq, J = 33.0, 4.4 Hz), 37.3 (d, J = 8.1 Hz), 36.1 (d, J = 27.8 Hz), 29.8 (d, J = 16.8 Hz).

^{31}P NMR (122 MHz, $CDCl_3$) δ(ppm) 85.9.

^{19}F NMR (283 MHz, $CDCl_3$) δ(ppm) -64.8.

HRMS (ESI) Calculated for $C_{15}H_{25}F_3N_2P^+$ $[M+H]^+$: 321.1702; found: *m/z* 321.1696.

N-(di-tert-butylphosphaneyl)-N-methylpyrazin-2-amine 3.3-30$_H$

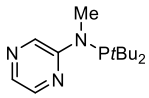

Prepared from *N*-methylpyrazin-2-amine (151.5 mg, 1.39 mmol), 2.5M solution of *n*BuLi in hexane (0.56 mL, 1.39 mmol) and tBu_2PCl (263 µL, 250.1 mg, 1.23 mmol) according to the general procedure **3-1**. Purification by flash column chromatography in Hexane:EtOAC = 2:1

3.3-30$_H$ was obtained as a yellowish solid: 140 mg, 40% yield.

^{1}H NMR (300 MHz, $CDCl_3$) δ(ppm) δ 9.15 (d, J = 4.5 Hz, 1H), 8.11 – 8.03 (m, 1H), 7.90 – 7.84 (m, 1H), 3.27 (s, 3H), 1.26 (d, J = 12.7 Hz, 18H).

^{13}C NMR (76 MHz, $CDCl_3$) δ(ppm) 159.2 (d, J = 24.1 Hz), 140.7, 136.0 (d, J = 36.1 Hz), 132.9 (d, J = 2.1 Hz), 36.7 (d, J = 7.6 Hz), 36.0 (d, J = 28.0 Hz), 29.7 (d, J = 16.8 Hz).

^{31}P NMR (122 MHz, $CDCl_3$) δ(ppm) 86.2.

HRMS (ESI) Calculated for $C_{13}H_{25}N_3P^+$ $[M+H]^+$: 254.1781; found: *m/z* 254.1795.

N-(di-tert-butylphosphaneyl)-N-methylpyrazin-2-amine 3.3-30$_{Cl}$

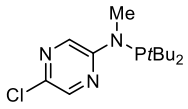

Prepared from 5-chloro-N-methylpyrazin-2-amine (65.3 mg, 0.45 mmol), 2.5M solution of *n*BuLi in hexane (0.18 mL, 0.45 mmol) and tBu_2PCl (86.4 µL, 90.8 mg, 0.45 mmol) according to the general procedure **3-1**. Purification by flash column chromatography in Hexane:EtOAC = 10:1

3.3-30$_{Cl}$ was obtained as orange solid: 55 mg, 42% yield.

^{1}H NMR (300 MHz, $CDCl_3$) δ(ppm) 8.89 (dd, J = 4.5, 1.5 Hz, 1H), 8.05 (dd, J = 1.5, 0.7 Hz, 1H), 3.24 (s, 3H), 1.25 (d, J = 12.8, 18H).

^{13}C NMR (75 MHz, $CDCl_3$) δ(ppm) 158.1 (d, J = 24.7 Hz), 139.9, 136.8 (d, J = 2.7 Hz), 134.6 (d, J = 36.9 Hz), 37.2 (d, J = 7.4 Hz), 36.2 (d, J = 27.8 Hz), 29.8 (d, J = 16.7 Hz).

^{31}P NMR (122 MHz, $CDCl_3$) δ(ppm) 85.0

HRMS (ESI) Calculated for $C_{13}H_{24}ClN_3P^+$ $[M+H]^+$: 288.1391; found: *m/z* 288.1378.

3.5.2.2. Synthesis of AuCl complexes 3.3-11$_H$, 3.3-11$_{OMe}$, 3.3-11$_{CF3}$, 3.3-31$_H$ and 3.3-31$_{Cl}$

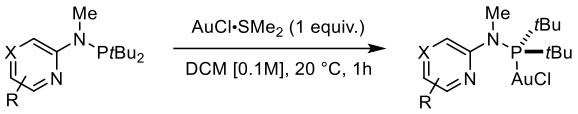

General procedure 3-2:

The following general procedure was employed for the synthesis of gold complexes **3.3-11$_H$**, **3.3-11$_{OMe}$**, **3.3-11$_{CF3}$**, **3.3-31$_H$** and **3.3-31$_{Cl}$**. A flame dried flask was charged with the phosphine ligand (1 equiv.) and AuCl•SMe_2 (1 equiv.). Dry DCM [0.1M] was added, and the reaction mixture was stirred at 20 °C for 1h. The reaction mixture was then filtered through a short pad of celite that was rinsed with dry DCM. The solvent was evaporated in vacuo and the residue was dried under reduced pressure to afford the corresponding gold chloride complex**.**

Gold (I) complex 3.3-11$_H$

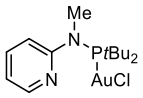

Prepared from ligand **3.3-15$_H$** (70 mg, 0.28 mmol) and AuCl•SMe_2 (81.8 mg, 0.28 mmol) according to the general procedure **3-2**.

3.3-11$_H$ was obtained as a white solid: 102.2 mg, 75% yield.

^{1}H NMR (300 MHz, $CDCl_3$) δ(ppm) 8.29 – 8.20 (m, 1H), 7.71 – 7.58 (m, 1H), 7.04 (d, *J* = 8.1 Hz, 1H), 7.02 – 6.91 (m, 1H), 3.58 (d, *J* = 9.1 Hz, 3H), 1.48 (d, *J* = 16.9 Hz, 18H).

^{13}C NMR (76 MHz, $CDCl_3$) δ(ppm) 158.9, 146.9, 138.5, 118.3, 112.9, 43.8 (d, *J* = 13.6 Hz), 41.6 (d, *J* = 25.2 Hz), 30.5 (d, *J* = 7.9 Hz).

^{31}P NMR (122 MHz, $CDCl_3$) δ(ppm) 124.8 (bs).

HRMS (ESI) Calculated $C_{14}H_{25}AuN_2P^+$ [M-Cl]$^+$: 449.1415; found: *m/z* 449.1599.

Gold (I) complex 3.3-11$_{OMe}$

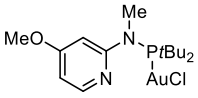

Prepared from ligand **3.3-15$_{OMe}$** (50 mg, 0.18 mmol) and AuCl•SMe_2 (52 mg, 0.18 mmol) according to the general procedure **3-2**.

3.3-11$_{OMe}$ was obtained as a white solid: 75.6 mg, 83% yield.

^{1}H NMR (300 MHz, $CDCl_3$) δ(ppm) 8.03 (d, *J* = 5.7 Hz, 1H), 6.63 – 6.47 (m, 2H), 3.86 (s, 3H), 3.53 (d, *J* = 8.9 Hz, 3H), 1.46 (d, *J* = 16.9 Hz, 18H).

^{13}C NMR (76 MHz, $CDCl_3$) δ(ppm) 167.7, 160.5, 147.6, 105.6, 98.8 (bs), 55.5, 43.5 (bs), 41.6 (d, *J* = 25.1 Hz), 30.4 (d, *J* = 8.2 Hz).

^{31}P NMR (122 MHz, $CDCl_3$) δ(ppm) 122.0 (bs).

HRMS (ESI) Calculated $C_{15}H_{27}AuN_2OP^+$ [M-Cl]$^+$: 479.1521; found: *m/z* 479.1576.

Gold (I) complex 3.3-11$_{CF3}$

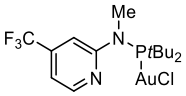

Prepared from ligand **3.3-15$_{CF3}$** (50 mg, 0.16 mmol) and AuCl•SMe_2 (46 mg, 0.16 mmol) according to the general procedure **3-2**.

3.3-15$_{CF3}$ was obtained as a white solid: 75.7 mg, 88% yield.

^{1}H NMR (300 MHz, $CDCl_3$) δ(ppm) 8.39 (d, J = 5.0 Hz, 1H), 7.14 (d, J = 5.0 Hz, 1H), 7.08 (bs, 1H), 3.60 (d, J = 8.5 Hz, 3H), 1.46 (d, J = 17.0 Hz, 18H).

^{13}C NMR (76 MHz, $CDCl_3$) δ(ppm) 159.2, 148.0, 140.8 (q, J = 34.0 Hz), 122.7z (q, J = 273.7 Hz), 113.4 (d, J = 3.4 Hz), 107.1, 43.8 (bs), 41.7 (d, J = 23.7 Hz), 30.5 (d, J = 8.2 Hz)

^{31}P NMR (122 MHz, $CDCl_3$) δ(ppm) 136.9 (bs).

^{19}F NMR (283 MHz, $CDCl_3$) δ(ppm) -64.8.

HRMS (ESI) Calculated $C_{15}H_{25}AuClF_3N_2P^+$ [M+H]$^+$: 553.1056; found: *m/z* 553.1113.

Gold (I) complex 3.3-31$_H$

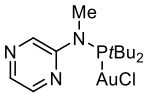

Prepared from ligand **3.3-30$_H$** (50 mg, 0.2 mmol) and AuCl•SMe_2 (58 mg, 0.2 mmol) according to the general procedure **3-2**.

3.3-31$_H$ was obtained as a white solid: 57 mg, 59% yield.

^{1}H NMR (300 MHz, $CDCl_3$) δ(ppm) 8.47 (bs, 1H), 8.25 (bs, 1H), 8.21 (bs, 1H), 3.61 (d, J = 8.3 Hz, 3H), 1.48 (d, J = 16.9 Hz, 18H).

^{13}C NMR (151 MHz, CD_2Cl_2) δ(ppm) 155.9, 140.6, 138.6, 136.2, 42.1 (bs), 41.3 (d, J = 24.5 Hz), 30.0 (d, J = 7.8 Hz).

^{31}P NMR (122 MHz, $CDCl_3$) δ(ppm) 125.0 (bs).

HRMS (ESI) Calculated $C_{13}H_{24}AuN_3P^+$ [M-Cl]$^+$: 450.1368; found: *m/z* 450.1519.

Gold (I) complex 3.3-31$_{Cl}$

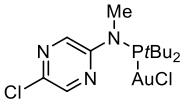

Prepared from ligand **3.3-30$_{Cl}$** (30 mg, 0.1 mmol) and AuCl•SMe_2 (30.7 mg, 0.1 mmol) according to the general procedure **3-2**.

3.3-31$_{Cl}$ was obtained as a white solid: 44.9 mg, 83% yield.

^{1}H NMR (300 MHz, $CDCl_3$) δ(ppm) 8.27 (s, 2H), 3.63 (d, J = 7.9 Hz, 3H), 1.53 (d, J = 17.0 Hz, 18H).

^{13}C NMR (151 MHz, $CDCl_3$) δ(ppm) 154.2, 142.2, 140.3, 134.0, 42.5 (bs), 41.5 (d, J = 23.7 Hz), 30.2 (d, J = 8.0 Hz).

^{31}P NMR (122 MHz, $CDCl_3$) δ(ppm) 116.7 (bs)

HRMS (ESI) Calculated $C_{13}H_{23}AuClN_3P^+$ [M-Cl]$^+$: 484.0978; found: *m/z* 484.1183.

3.5.2.3. Synthesis of AuCl complexes 3.3-12$_H$, 3.3-12$_{OMe}$, 3.3-12$_{CF3}$

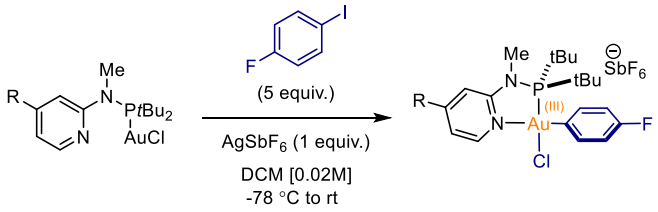

General procedure 3-3:

The following general procedure was employed for the synthesis of Au(III) complexes **3.3-12$_H$, 3.3-12$_{OMe}$** and **3.3-12$_{CF3}$**. Inside a glovebox, a vial was charged with $AgSbF_6$ (1 equiv.) and a stir bar. The vial was capped and removed from the glovebox. Outside a glovebox, the corresponding Au(I) complex (1 equiv.) was weighted and solubilized in dry DCM [0.02M] before 4-fluoroiodobenzene (5 equiv.) was added. This solution was charged in a syringe and added slowly into the vial that was precooled at -78 °C. Once the addition was complete, the mixture was stirred for approximately 10s before the cooling bath was removed to allow the solution to warm up to room temperature. After stirring for an additional 20 min, the reaction mixture was filtered through celite. The solvent was evaporated and the residue was washed three times with dry Et_2O and three times with pentane to provide the desired Au(III) complex.

Gold (III) complex 3.3-12$_H$

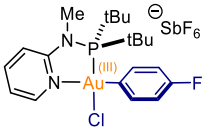

Prepared from complex **3.3-11$_H$** (30 mg, 0.062 mmol) and 4-fluoroiodobenzene (36 µL, 69.3 mg, 0.31 mmol) according to the general procedure **3-3**.

3.3-12$_H$ was obtained as a white solid: 41.1 mg, 97% yield.

^{1}H NMR (300 MHz, CD_2Cl_2) δ(ppm) 9.48 – 9.38 (m, 1H), 8.30 – 8.17 (m, 1H), 7.44 – 7.29 (m, 4H), 7.17 – 7.04 (m, 2H), 3.54 (d, J = 5.8 Hz, 3H), 1.55 (d, J = 18.5 Hz, 18H).

^{13}C NMR (76 MHz, CD_2Cl_2) δ(ppm) 163.9, 160.7 (d, J = 2.9 Hz), 145.9, 145.0, 135.1 (d, J = 7.2 Hz), 120.6, 119.6, 117.2 (d, J = 21.4 Hz), 112.0 (d, J = 4.3 Hz), 45.6 (d, J = 17.1 Hz), 39.2 (d, J = 3.0 Hz), 29.5 (d, J = 3.3 Hz).

^{31}P NMR (122 MHz, CD_2Cl_2) δ(ppm) 128.4.

^{19}F NMR (283 MHz, CD_2Cl_2) δ(ppm) -115.4.

HRMS (ESI) Calculated $C_{20}H_{29}AuClFN_2P^+$ $[M\text{-}SbF_6]^+$: 579.1401; found: *m/z* 579.1590.

Gold (III) complex 3.3-12$_{OMe}$

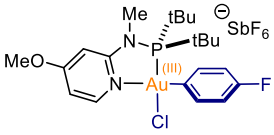

Prepared from complex **3.3-11$_{OMe}$** (30 mg, 0.058 mmol) and 4-fluoroiodobenzene (33.6 µL, 64.7 mg, 0.29 mmol) according to the general procedure **3-3**.

3.3-12$_{OMe}$ was obtained as an orange solid: 34.1 mg, 82% yield.

^{1}H NMR (300 MHz, $(CD_3)_2CO$) δ(ppm) 9.21 (d, J = 7.0 Hz, 1H), 7.62 (dd, J = 8.7, 5.6 Hz, 2H), 7.25 – 7.07 (m, 3H), 6.97 (d, J = 2.5 Hz, 1H), 4.14 (s, 3H), 3.77 (d, J = 5.9 Hz, 3H), 1.67 (d, J = 18.4 Hz, 18H).

^{13}C NMR (76 MHz, $(CD_3)_2CO$) δ(ppm) 172.1, 163.9 (d, *J* = 3.9 Hz), 163.0 (d, *J* = 244.8 Hz), 147.6, 136.9 (dd, J = 7.1, 1.5 Hz), 122.8, 117.2 (d, *J* = 21.3 Hz), 107.8, 97.3 (d, *J* = 4.9 Hz), 57.6, 46.4, 43.6, 39.7 (d, *J* = 2.8 Hz).

^{31}P NMR (122 MHz, $(CD_3)_2CO$) δ(ppm) 128.0.

^{19}F NMR (283 MHz, $(CD_3)_2CO$) δ(ppm) -117.8.

HRMS (ESI) Calculated $C_{21}H_{31}AuClFN_2OP^+$ [M-SbF_6]$^+$: 609.1507; found: *m/z* 609.1574.

Gold (III) complex 3.3-12$_{CF3}$

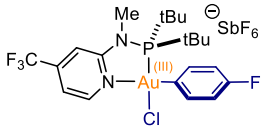

Prepared from complex **3.3-11$_{CF3}$** (30 mg, 0.054 mmol) and 4-fluoroiodobenzene (31.4 µL, 60.4 mg, 0.27 mmol) according to the general procedure **3-3**.

3.3-12$_{CF3}$ was obtained as a yellowish solid: 38.1 mg, 94% yield.

^{1}H NMR (600 MHz, $(CD_3)_2CO$) δ(ppm) 9.70 (d, J = 6.3 Hz, 1H), 7.98 (s, 1H), 7.88 (dd, J = 6.3, 1.7 Hz, 1H), 7.72 – 7.64 (m, 2H), 7.25 (t, J = 8.9 Hz, 2H), 3.99 (d, J = 5.8 Hz, 3H), 1.77 (d, J = 18.6 Hz, 18H).

^{13}C NMR (151 MHz, $(CD_3)_2CO$) δ(ppm) 163.5 (d, *J* = 3.6 Hz), 163.2 (d, *J* = 245.3 Hz), 148.6, 144.7 (*J* = 34.9 Hz), 136.7 (dd, *J* = 7.2, 1.3 Hz), 123.1 (q, *J* = 274.0 Hz), 121.8, 117.6 (d, *J* = 21.5 Hz), 115.4 (q, *J* = 3.3 Hz), 111.0 (p, *J* = 4.1 Hz), 55.0, 46.8 (d, *J* = 16.4 Hz), 40.4 (d, *J* = 2.8 Hz).

^{31}P NMR (122 MHz, $(CD_3)_2CO$) δ(ppm) 129.5.

^{19}F NMR (283 MHz, $(CD_3)_2CO$) δ(ppm) -65.9, -117.4.

HRMS (ESI) Calculated $C_{21}H_{28}AuClF_4N_2P^+$ [M-SbF_6]$^+$: 647.1275; found: *m/z* 647.1227.

3.5.2.4. Synthesis of AuCl complexes 3.3-13$_H$, 3.3-13$_{OMe}$, 3.3-13$_{CF3}$

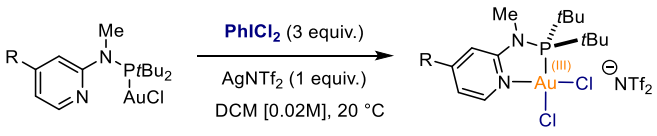

General procedure 3-4:

The following general procedure was employed for the synthesis of Au(III) complexes **3.3-13$_H$**, **3.3-13$_{OMe}$** and **3.3-13$_{CF3}$**. Inside a glovebox, a vial was charged with $AgNTf_2$ (1 equiv.) and a stir bar.

The vial was capped and removed from the glovebox. Outside a glovebox, the corresponding Au(I) complex (1 equiv.) was weighted and solubilized in dry DCM [0.02M]. This solution was charged in a syringe and added into the vial at room temperature. Once the addition was complete, the mixture was stirred for approximately 10s before $PhICl_2$ (3 equiv.) was added. The vial was protected from light and the solution was stirred for 1h before being filtered through celite. The solvent was evaporated and the residue was washed five times with dry Et_2O to provide the desired Au(III) complex.

Gold (III) complex 3.3-13$_H$

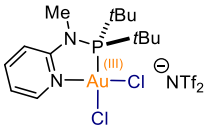

Prepared from complex **3.3-11$_H$** (15 mg, 0.03 mmol) and $PhICl_2$ (25.2 mg, 0.09 mmol) according to the general procedure **3-4**.

3.3-13$_H$ was obtained as a white solid: 16.2 mg, 94% yield.

^{1}H NMR (300 MHz, CD_2Cl_2) δ(ppm) 9.70 (d, J = 6.6 Hz, 1H), 8.32 (t, J = 7.8 Hz, 1H), 7.57 – 7.32 (m, 2H), 3.61 (d, J = 6.1 Hz, 3H), 1.77 (d, J = 19.4 Hz, 18H).

^{13}C NMR (300 MHz, CD_2Cl_2) δ(ppm) 162.5, 147.3, 146.8, 120.6, 119.9 (q, J = 321.3 Hz), 114.1 (d, J = 5.0 Hz), 48.3 (d, J = 11.8 Hz), 40.1 (d, J = 3.0 Hz), 29.7 (d, J = 2.4 Hz).

^{31}P NMR (122 MHz, CD_2Cl_2) δ(ppm) 156.4.

HRMS (ESI) Calculated $C_{16}H_{25}AuClF_6N_3O_4PS_2^+$ [M-Cl]$^+$: 764.0277; found: *m/z* 764.5037.

Gold (III) complex 3.3-13$_{OMe}$

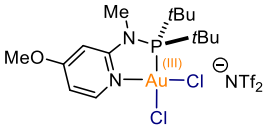

Prepared from complex **3.3-11$_{OMe}$** (10 mg, 0.019 mmol) and $PhICl_2$ (16.2 mg, 0.058 mmol) according to the general procedure **3-4**.

3.3-13$_{OMe}$ was obtained as a white solid: 10.4 mg, 65% yield.

^{1}H NMR (300 MHz, $CDCl_3$) δ(ppm) 9.39 (d, J = 7.3 Hz, 1H), 6.91 – 6.66 (m, 2H), 4.14 (s, 3H), 3.65 (bs, 3H), 1.77 (d, J = 19.2 Hz, 18H).

^{13}C NMR (151 MHz, $CDCl_3$) δ(ppm) 172.3, 164.5 (d, J = 3.3 Hz), 147.3, 119.9 (q, J = 321.5 Hz), 109.8, 96.6 (d, J = 5.9 Hz), 58.3, 48.2 (d, J = 12.8 Hz), 40.3, 30.0 (d, J = 2.5 Hz).

^{31}P NMR (122 MHz, $CDCl_3$) δ(ppm) 153.4.

HRMS (ESI) Calculated $C_{15}H_{27}AuCl_2N_2OP^+$ [M-NTf_2]$^+$: 549.0898; found: *m/z* 549.0981.

Gold (III) complex 3.3-13$_{CF3}$

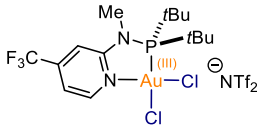

Prepared from complex **3.3-11$_{CF3}$** (7.7 mg, 0.014 mmol) and $PhICl_2$ (11.5 mg, 0.042 mmol) according to the general procedure **3-4**.

3.3-13$_{CF3}$ was obtained as a white solid: 6.1 mg, 49% yield.

^{1}H NMR (300 MHz, CD_2Cl_2) δ(ppm) 9.94 (d, J = 6.6 Hz, 1H), 7.65 – 7.46 (m, 2H), 3.71 (d, J = 5.9 Hz, 3H), 1.80 (d, J = 19.7 Hz, 18H).

^{13}C NMR (151 MHz, CD_2Cl_2) δ(ppm) 163.4, 149.2, 146.6 (q, J = 36.7 Hz), 121.0 (q, J = 274.6 Hz), 119.8 (q, J = 321.2 Hz), 116.3, 111.1, 48.7 (d, J = 10.1 Hz), 40.6, 29.8 (d, J = 2.5 Hz).

^{31}P NMR (122 MHz, CD_2Cl_2) δ(ppm) 157.4.

^{19}F NMR (283 MHz, CD_2Cl_2) δ(ppm) -65.9, -79.5.

HRMS (ESI) Calculated $C_{17}H_{24}AuClF_9N_3O_4PS_2^+$ [M-Cl]$^+$: 832.0151; found: *m/z* 832.0490.

3.5.3. Initial studies

3.5.3.1. Alkoxyarylation with pent-4-en-1-ol 3.3-16a

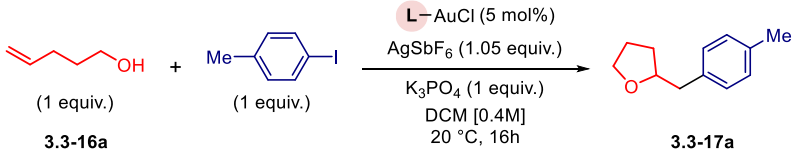

A stock solution composed of an equimolar amount of 1-iodo-4-methylbenzene and pent-4-en-1-ol in dry DCM [0.4M] was prepared. A few µL of 1,3,5-trimethylbenzene, used as an internal standard, were added to this solution. An aliquot of this solution was diluted with $CDCl_3$ and a ^{1}H NMR spectrum of the mixture was recorded (t=0) to assess the relative concentration of the reactants versus the standard. Inside a nitrogen-filled glovebox, an amber 1-dram vial containing a stir bar was charged with $AgSbF_6$ (1.05 equiv.) and K_3PO_4 (1 equiv.). The appropriate amount of the stock solution corresponding to 1 equiv. of 1-iodo-4-methylbenzene and 1 equiv. of pent-4-en-1-ol was added to a vial containing the corresponding gold(I) complex (5 mol%). The resulting mixture was charged in a septum-capped syringe that was transferred inside the glovebox. The

solution contained in the syringe was then added to the vial containing $AgSbF_6$ and K_3PO_4. The vial was vigorously shaken, capped, isolated with parafilm and removed from the glovebox. After stirring at 20 °C for 16h, the reaction mixture was passed through a plug of celite. $CDCl_3$ was used to rinse the pad and dilute the filtrate. The resulting solution was then analyzed by ^1H NMR spectroscopy. The yield was calculated by comparing the relative integration of the internal standard peaks with those of the product (see **Appendix Figure 6.2-2** for representative example). NMR data were compared to those reported in the literature.[97]

3.5.3.1. Amidoarylation with *N*-tosyl aminopentene 3.3-16b

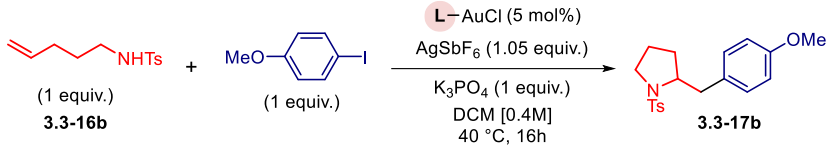

A stock solution composed of an equimolar amount of 1-iodo-4-methoxybenzene and *N*-tosyl aminopentene in dry DCM [0.4M] was prepared. A few µL of 1,3,5-trimethylbenzene, used as an internal standard, were added to this solution. An aliquot of this solution was diluted with $CDCl_3$ and a ^1H NMR spectrum of the mixture was recorded (t=0) to assess the relative concentration of the reactants versus the standard. Inside a nitrogen-filled glovebox, an amber 1-dram vial containing a stir bar was charged with $AgSbF_6$ (1.05 equiv.) and K_3PO_4 (1 equiv.). The appropriate amount of the stock solution corresponding to 1 equiv. of 1-iodo-4-methoxybenzene and 1 equiv. of *N*-tosyl aminopentene was added to a vial containing the corresponding gold(I) complex (5 mol%). The resulting mixture was charged in a septum-capped syringe that was transferred inside the glovebox. The solution contained in the syringe was then added to the vial containing $AgSbF_6$ and K_3PO_4. The vial was vigorously shaken, capped, isolated with parafilm and removed from the glovebox. After stirring at 40 °C for 16h, the reaction mixture was passed through a plug of celite. $CDCl_3$ was used to rinse the pad and dilute the filtrate. The resulting solution was then analyzed by ^1H NMR spectroscopy. The yield was calculated by comparing the relative integration of the internal standard peaks with those of the product (see **Appendix Figure 6.2-3** for representative example). NMR data were compared to those reported in the literature.[98]

3.5.3.2. Amination with 2-nitroaniline 3.3-24

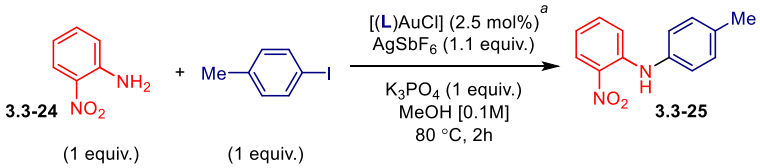

A stock solution composed of an equimolar amount of 1-iodo-4-methylbenzene and 2-nitroaniline in MeOH [0.1M] was prepared. A few µL of 1,3,5-trimethylbenzene, used as an internal standard, were added to this solution. An aliquot of this solution was diluted with $CDCl_3$ and a ^1H NMR

spectrum of the mixture was recorded (t=0) to assess the relative concentration of the reactants versus the standard. Inside a nitrogen-filled glovebox, an amber 1-dram vial containing a stir bar was charged with $AgSbF_6$ (1.1 equiv.) and K_3PO_4 (1 equiv.). The appropriate amount of the stock solution corresponding to 1 equiv. of 1-iodo-4-methylbenzene and 1 equiv. of 2-nitroaniline was added to a vial containing the corresponding gold(I) complex (2.5 mol%). The resulting mixture was charged in a septum-capped syringe that was transferred inside the glovebox. The solution contained in the syringe was then added to the vial containing $AgSbF_6$ and K_3PO_4. The vial was vigorously shaken, capped, isolated with parafilm and removed from the glovebox. After stirring at 80 °C for 2h, the reaction mixture was passed through a plug of celite. $CDCl_3$ was used to rinse the pad and dilute the filtrate. The resulting solution was then analyzed by ^1H NMR spectroscopy. The yield was calculated by comparing the relative integration of the internal standard peaks with those of the product (see **Appendix Figure 6.2-4** for representative example). NMR data were compared to those reported in the literature.[99]

3.5.3.3. Heck reaction with hex-1-ene

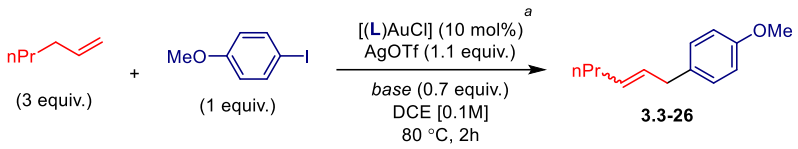

A stock solution composed of the 1-iodo-4-methoxybenzene (1 equiv.), hex-1-ene (3 equiv.) and base (if liquid, 0.07 equiv.) in DCE [0.1M] was prepared. A few μL of 1,3,5-trimethylbenzene, used as an internal standard, were added to this solution. An aliquot of this solution was diluted with $CDCl_3$ and a ^1H NMR spectrum of the mixture was recorded (t=0) to assess the relative concentration of the reactants versus the standard. Inside a nitrogen-filled glovebox, an amber 1-dram vial containing a stir bar was charged with $AgSbF_6$ (1.1 equiv.) and base (if solid, 0.7 equiv.). The appropriate amount of the stock solution corresponding to 1 equiv. of 1-iodo-4-methoxybenzene and 3 equiv. of hex-1-ene was added to a vial containing the corresponding gold(I) complex (10 mol%). The resulting mixture was charged in a septum-capped syringe that was transferred inside the glovebox. The solution contained in the syringe was then added to the vial containing $AgSbF_6$ and base. The vial was vigorously shaken, capped, isolated with parafilm and removed from the glovebox. After stirring at 80 °C for 2h, the reaction mixture was passed through a plug of celite. $CDCl_3$ was used to rinse the pad and dilute the filtrate. The resulting solution was then analyzed by ^1H NMR spectroscopy. The yield was calculated by comparing the relative integration of the internal standard peaks with those of the product (see **Appendix Figure 6.2-5** for representative example). NMR data were compared to those reported in the literature.[49]

3.5.3.4. Transmetallation with tributyl(thiophen-2-yl)stannane 3.3-27a

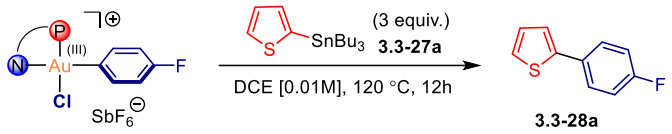

A microwave 2 mL tube was charged with a solution of corresponding Au(III) complex (1 equiv.) and tributyl(thiophen-2-yl)stannane (3 equiv.) in DCE [0.01M]. After stirring at 120 °C for 12h, the reaction mixture was evaporated and dissolved in $CDCl_3$. Trifluorotoluene (1 mg), used as an internal standard, was added to the filtrate and the resulting solution was then analyzed by ^{19}F NMR spectroscopy. The yield of the product **3.3-28a** was calculated by comparing the relative integration of the internal standard peaks with those of the product (see **Appendix Figure 6.2-6** for representative example). NMR data were compared to those reported in the literature.[100]

3.5.3.5. Transmetallation with silver reagent 3.3-27b

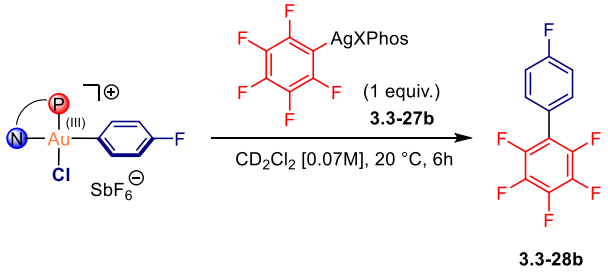

A srew-cap NMR tube was charged with a solution of corresponding Au(III) complex (1 equiv.) in CD_2Cl_2 [0.07M]. A 1 µL of $PhCF_3$, used as an internal standard for NMR analysis and monitoring, was then added. The NMR tube was capped and vigorously shaken before a ^{19}F NMR spectrum of the mixture was recorded (t=0). The silver complex **3.3-27b** (1 equiv.) was added to the NMR tube and the reaction mixture was run for 6h. The yield of the product **3.3-28b** was calculated by comparing the relative integration of the internal standard peaks with those of the product (see **Appendix Figure 6.2-7** for representative example). NMR data were compared to those reported in the literature.[101]

3.5.3.6. Alkoxyarylation with hex-5-en-1-ol 3.3-16c

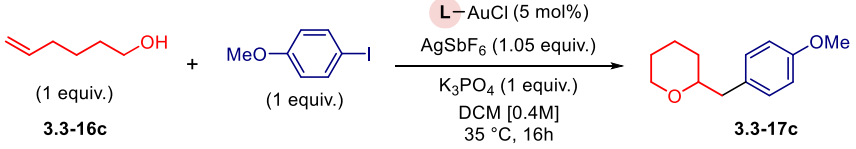

A stock solution composed of an equimolar amount of 1-iodo-4-methoxybenzene and hex-5-en-1-ol in dry DCM [0.4M] was prepared. A few µL of 1,3,5-trimethylbenzene, used as an internal standard, were added to this solution. An aliquot of this solution was diluted with $CDCl_3$ and a ^1H NMR spectrum of the mixture was recorded (t=0) to assess the relative concentration of the reactants versus the standard. Inside a nitrogen-filled glovebox, an amber 1-dram vial containing a stir bar was charged with $AgSbF_6$ (1.05 equiv.) and K_3PO_4 (1 equiv.). The appropriate amount of the stock solution corresponding to 1 equiv. of 1-iodo-4-methoxybenzene and 1 equiv. of hex-5-en-1-ol was added to a vial containing the corresponding gold(I) complex (5 mol%). The resulting mixture was charged in a septum-capped syringe that was transferred inside the glovebox. The solution contained in the syringe was then added to the vial containing $AgSbF_6$ and K_3PO_4. The vial was vigorously shaken, capped, isolated with parafilm and removed from the glovebox. After stirring at 35 °C for 16h, the reaction mixture was passed through a plug of celite. $CDCl_3$ was used to rinse the pad and dilute the filtrate. The resulting solution was then analyzed by ^1H NMR spectroscopy. The yield was calculated by comparing the relative integration of the internal standard peaks with those of the product (see **Appendix Figure 6.2-8** for representative example). NMR data were compared to those reported in the literature.[102]

3.5.3.7. Alkoxyarylation with (*E*)-(2-iodovinyl)benzene and pent-4-en-1-ol 3.3-16a

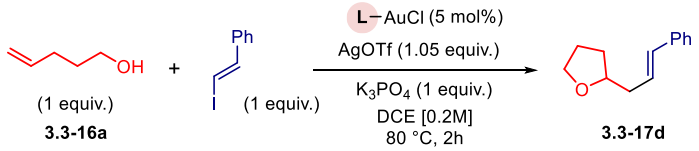

A stock solution composed of an equimolar amount of (*E*)-(2-iodovinyl)benzene and pent-4-en-1-ol in dry DCE [0.4M] was prepared. A few µL of 1,3,5-trimethylbenzene, used as an internal standard, were added to this solution. An aliquot of this solution was diluted with $CDCl_3$ and a ^1H NMR spectrum of the mixture was recorded (t=0) to assess the relative concentration of the reactants versus the standard. Inside a nitrogen-filled glovebox, an amber 1-dram vial containing a stir bar was charged with $AgSbF_6$ (1.05 equiv.) and K_3PO_4 (1 equiv.). The appropriate amount of the stock solution corresponding to 1 equiv. of (*E*)-(2-iodovinyl)benzene and 1 equiv. of pent-4-en-1-ol was added to a vial containing the corresponding gold(I) complex (5 mol%). The resulting mixture was charged in a septum-capped syringe that was transferred inside the glovebox. The solution contained in the syringe was then added to the vial containing $AgSbF_6$ and K_3PO_4. The vial was vigorously shaken, capped, isolated with parafilm and removed from the glovebox. After stirring at 80 °C for 2h, the reaction mixture was passed through a plug of celite. $CDCl_3$ was used to rinse the pad and dilute the filtrate. The resulting solution was then analyzed by ^1H NMR spectroscopy. The yield was calculated by comparing the relative integration of the internal standard peaks with those of the product (see **Appendix Figure 6.2-9** for representative example). NMR data were compared to those reported in the literature.[103]

3.5.3.8. Amidoarylation with (*E*)-(2-iodovinyl)benzene and *N*-tosyl aminopentene 3.3-16b

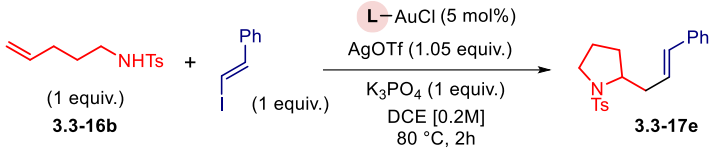

A stock solution composed of an equimolar amount of (*E*)-(2-iodovinyl)benzene and *N*-tosyl aminopentene in dry DCE [0.4M] was prepared. A few µL of 1,3,5-trimethylbenzene, used as an internal standard, were added to this solution. An aliquot of this solution was diluted with $CDCl_3$ and a ^1H NMR spectrum of the mixture was recorded (t=0) to assess the relative concentration of the reactants versus the standard. Inside a nitrogen-filled glovebox, an amber 1-dram vial containing a stir bar was charged with $AgSbF_6$ (1.05 equiv.) and K_3PO_4 (1 equiv.). The appropriate amount of the stock solution corresponding to 1 equiv. of (*E*)-(2-iodovinyl)benzene and 1 equiv. of *N*-tosyl aminopentene was added to a vial containing the corresponding gold(I) complex (5 mol%). The resulting mixture was charged in a septum-capped syringe that was transferred inside the glovebox. The solution contained in the syringe was then added to the vial containing $AgSbF_6$ and K_3PO_4. The vial was vigorously shaken, capped, isolated with parafilm and removed from the glovebox. After stirring at 80 °C for 2 h, the reaction mixture was passed through a plug of celite. $CDCl_3$ was used to rinse the pad and dilute the filtrate. The resulting solution was then analyzed by ^1H NMR spectroscopy. The yield was calculated by comparing the relative integration of the internal standard peaks with those of the product (see **Appendix Figure 6.2-10** for representative example). NMR data were compared to those reported in the literature.[104]

3.5.4. Attempts with Pd(0)/Pd(II) catalysis

Attempts to catalyze the coupling of thiotosylate **3.3-41**, 0.1 mmol of *p*-fluoroiodobenzene **3.3-42a** under Pd(0)/Pd(II) catalysis were performed as previously described by Schoenbeck and coworkers in their attempt to cross couple aryl iodides with phosphorothiolates (scale 0.15 mmol).[95]

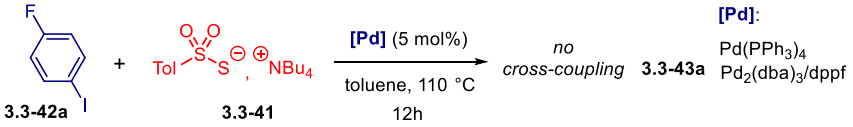

To a vial containing a stir bar, *p*-fluoroiodobenzene **3.3-42a** (1 equiv.) and thiotosylate **3.3-41** (1 equiv.) was added the palladium catalyst ($Pd(PPh_3)_4$ 5 mol% or $Pd_2(dba)_3$/dppf 5 mol%). Dry toluene [0.1M] was then added, and the vial was capped and isolated with parafilm. The reaction mixture was stirred at 100 °C for 12h, then cooled down to room temp and evaporated under reduced pressure. The residue was dissolved in $CDCl_3$ and analyzed by ^1H NMR spectroscopy to detect the presence of the cross coupling product **3.3-43a**. No trace of **3.3-43a** could be observed.

3.5.5. Cross-coupling reaction of aryl iodides with ammonium thiotosylate

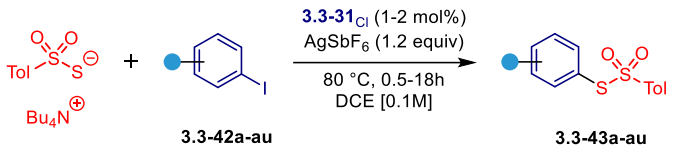

General procedure 3-5:

Inside a nitrogen-filled glovebox, a 1-dram vial containing a stir bar was charged with $AgSbF_6$ (1.2 equiv.), capped and then removed from the glovebox. A separate vial was charged with gold complex **3.3-31$_{Cl}$** (1-5 mol%, see **Scheme 3.3-11**), the aryl iodide **3.3-42a-au** (1 equiv.) and tetrabutylammonium thiotosylate (1 equiv.) (scale: 0.05-0.15 mmol). DCE [0.1M] was added and the resulting mixture was charged in a syringe. The solution contained in the syringe was quickly added to the vial containing $AgSbF_6$. The vial with the mixture was capped, vigorously shaken and isolated with parafilm. After stirring the mixture at 80 °C for the required time (0.5 – 18h, see **Scheme 3.3-11**), the reaction mixture was passed through a plug of celite. A small amount of $CDCl_3$ was used to rinse the pad and dilute the filtrate. A few µL of 1,3,5-trimethylbenzene, used as an internal standard, were added to this solution. The resulting solution was then analyzed by ^1H NMR spectroscopy. The yield was calculated by comparing the relative integration of the internal standard peaks with those of the product (see **Appendix Figure 6.2-11** for representative example). NMR data were compared to those reported in the literature when available to confirm the nature of the product. In the case of unreported products, the solvent was evaporated in vacuo after the NMR analysis and the residue was purified by flash column chromatography**.**

3.5.5.1. Cross-coupling products

S-(4-fluorophenyl) 4-methylbenzenesulfonothioate 3.3-43a

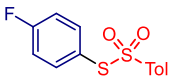

The reaction was conducted according to the general procedure **3-5** using *p*-fluoroiodobenzene (5.8 µL, 11 mg, 0.05 mmol), tetrabutylammonium thiotosylate (21.5 mg, 0.05 mmol), $AgSbF_6$ (20.6 mg, 0.06 mmol), gold complex **3.3-31$_{Cl}$** (0.26 mg, 0.5 µmol) and DCE (0.5 mL). Yield calculated by comparing the relative integration of the internal standard peaks with those of product (83%). NMR data match those reported in the literature.[105]

S-phenyl 4-methylbenzenesulfonothioate 3.3-43b

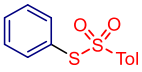

The reaction was conducted according to the general **3-5** using iodobenzene (5.6 µL, 10.2 mg, 0.05 mmol), tetrabutylammonium thiotosylate (21.5 mg, 0.05 mmol), $AgSbF_6$ (20.6 mg, 0.06 mmol), gold complex **3.3-31$_{Cl}$** (0.26 mg, 0.5 µmol) and DCE (0.5 mL). Yield calculated by comparing the relative integration of the internal standard peaks with those of product (99%). NMR data match those reported in the literature.[106]

S-([1,1'-biphenyl]-4-yl) 4-methylbenzenesulfonothioate 3.3-43c

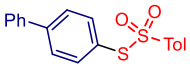

The reaction was conducted according to the general procedure **3-5** using iodobenzene (42 mg, 0.15 mmol), tetrabutylammonium thiotosylate (64.5 mg, 0.15 mmol), $AgSbF_6$ (61.8 mg, 0.18 mmol), gold complex **3.3-31$_{Cl}$** (0.78 mg, 1.5 µmol) and DCE (1.5 mL). Yield calculated by comparing the relative integration of the internal standard peaks with those of product (93%).

Purification by flash column chromatography (Hexane:EtOAc = 10:1).

3.3-43c was obtained as a white solid: 37.2 mg, 73% yield.

^{1}H NMR (300 MHz, $CDCl_3$): δ(ppm) 7.68 – 7.56 (m, 4H), 7.59 – 7.39 (m, 7H), 7.26 (d, J = 7.9 Hz, 2H), 2.46 (s, 3H).

^{13}C NMR (151 MHz, $CDCl_3$): δ(ppm) 144.9, 144.3, 140.5, 139.6, 137.1, 129.6, 129.1, 128.4, 128.1, 127.8, 127.3, 126.8, 21.8.

HRMS (ESI) Calculated for $C_{19}H_{16}NaO_2S_2$ $[M+Na]^+$: 363.0484; found: *m* 363.0392.

S-(o-tolyl) 4-methylbenzenesulfonothioate 3.3-43d

The reaction was conducted according to the general procedure **3-5** using 1-iodo-2-methylbenzene (6.4 µL, 10.9 mg, 0.05 mmol), tetrabutylammonium thiotosylate (21.5 mg, 0.05 mmol), $AgSbF_6$ (20.6 mg, 0.06 mmol), gold complex **3.3-31$_{Cl}$** (0.52 mg, 1.0 µmol) and DCE (0.5 mL). Yield calculated by comparing the relative integration of the internal standard peaks with those of product (96%). NMR data match those reported in the literature.[105]

S-(2-ethylphenyl) 4-methylbenzenesulfonothioate 3.3-43e

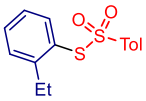

The reaction was conducted according to the general procedure **3-5** using 1-ethyl-2-iodobenzene (7.2 µL, 11.6 mg, 0.05 mmol), tetrabutylammonium thiotosylate (21.5 mg, 0.05 mmol), $AgSbF_6$ (20.6 mg, 0.06 mmol), gold complex **3.3-31$_{Cl}$** (0.52 mg, 1.0 µmol) and DCE (0.5 mL). Yield calculated by comparing the relative integration of the internal standard peaks with those of product (77%).

Purification by flash column chromatography (Hexane:EtOAc = 10:1).

3.3-43e was obtained as a white solid: 11.0 mg, 75% yield.

^{1}H NMR (300 MHz, $CDCl_3$): δ(ppm) 7.46 – 7.34 (m, 4H), 7.28 – 7.13 (m, 4H), 2.52 (q, J = 7.5 Hz, 2H), 2.42 (s, 3H), 1.03 (t, J = 7.6 Hz, 3H).

^{13}C NMR (151 MHz, $CDCl_3$): δ(ppm) 149.9, 144.8, 140.7, 138.5, 132.1, 129.6, 129.5, 127.7, 126.9, 126.9, 26.9, 21.8, 15.3.

HRMS (EI) Calculated for $C_{15}H_{16}O_2S_2$: 292.0592; found: *m* 292.0573.

S-(m-tolyl) 4-methylbenzenesulfonothioate 3.3-43f

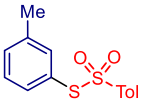

The reaction was conducted according to the general procedure **3-5** using 1-iodo-3-methylbenzene (6.2 µL, 10.9 mg, 0.05 mmol), tetrabutylammonium thiotosylate (21.5 mg, 0.05 mmol), $AgSbF_6$ (20.6 mg, 0.06 mmol), gold complex **3.3-31$_{Cl}$** (0.26 mg, 0.5 µmol) and DCE (0.5 mL). Yield calculated by comparing the relative integration of the internal standard peaks with those of product (97%). NMR data match those reported in the literature.[105]

S-(p-tolyl) 4-methylbenzenesulfonothioate 3.3-43g

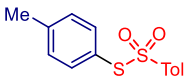

The reaction was conducted according to the general procedure **3-5** using 1-iodo-4-methylbenzene (10.9 mg, 0.05 mmol), tetrabutylammonium thiotosylate (21.5 mg, 0.05 mmol), $AgSbF_6$ (20.6 mg, 0.06 mmol), gold complex **3.3-31$_{Cl}$** (0.26 mg, 0.5 µmol) and DCE (0.5 mL). Yield calculated by comparing the relative integration of the internal standard peaks with those of product (95%). NMR data match those reported in the literature.[105]

S-(4-isopropylphenyl) 4-methylbenzenesulfonothioate 3.3-43h

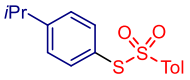

The reaction was conducted according to the general procedure **3-5** using 1-iodo-4-isopropylbenzene (8.1 µL, 12.3 mg, 0.05 mmol), tetrabutylammonium thiotosylate (21.5 mg, 0.05 mmol), $AgSbF_6$ (20.6 mg, 0.06 mmol), gold complex **3.3-31$_{Cl}$** (0.26 mg, 0.5 µmol) and DCE (0.5 mL). Yield calculated by comparing the relative integration of the internal standard peaks with those of product (97%).

Purification by flash column chromatography (Hexane:EtOAc = 10:1).

3.3-43h was obtained as a white solid: 13.5 mg, 88% yield.

^{1}H NMR (300 MHz, $CDCl_3$): δ(ppm) 7.48 (d, J = 8.3 Hz, 2H), 7.36 – 7.27 (m, 1H), 7.29 – 7.18 (m, 4H), 2.96 (p, J = 6.9 Hz, 1H), 2.46 (s, 3H), 1.28 (d, J = 6.9 Hz, 46H).

^{13}C NMR (151 MHz, $CDCl_3$): δ(ppm) 152.9, 144.7, 140.6, 136.8, 129.5, 127.7, 125.0, 34.2, 23.9, 21.8.

HRMS (ESI) Calculated $C_{16}H_{18}F_2NaO_2S_2^+$ $[M+Na]^+$: 329.0640; found: *m/z* 329.0646.

S-(4-(tert-butyl)phenyl) 4-methylbenzenesulfonothioate 3.3-43i

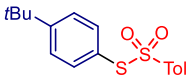

The reaction was conducted according to the general procedure **3-5** using 1-(*tert*-butyl)-4-iodobenzene (8.9 µL, 13.0 mg, 0.05 mmol), tetrabutylammonium thiotosylate (21.5 mg, 0.05 mmol), $AgSbF_6$ (20.6 mg, 0.06 mmol), gold complex **3.3-31$_{Cl}$** (0.26 mg, 0.5 µmol) and DCE (0.5 mL). Yield calculated by comparing the relative integration of the internal standard peaks with those of product (95%). NMR data match those reported in the literature.[107]

S-(3,5-dimethylphenyl) 4-methylbenzenesulfonothioate 3.3-43j

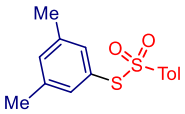

The reaction was conducted according to the general procedure **3-5** using 1-iodo-3,5-dimethylbenzene (7.2 µL, 11.6 mg, 0.05 mmol), tetrabutylammonium thiotosylate (21.5 mg, 0.05 mmol), $AgSbF_6$ (20.6 mg, 0.06 mmol), gold complex **3.3-31$_{Cl}$** (0.26 mg, 0.5 µmol) and DCE (0.5 mL).

Yield calculated by comparing the relative integration of the internal standard peaks with those of product (97%).

Purification by flash column chromatography (Hexane:EtOAc = 10:1).

3.3-43j was obtained as a white solid: 12.5 mg, 86% yield.

^{1}H NMR (300 MHz, $CDCl_3$): δ(ppm) 7.47 (d, J = 8.4 Hz, 2H), 7.22 (d, J = 7.9 Hz, 2H), 7.08 (s, 1H), 6.94 (s, 2H), 2.43 (s, 3H), 2.24 (s, 6H).

^{13}C NMR (151 MHz, $CDCl_3$): δ(ppm) 144.7, 140.4, 139.2, 134.3, 133.2, 129.3, 128.0, 127.4, 21.8, 21.2.

HRMS (EI) Calculated for $C_{15}H_{16}O_2S_2$: 292.0592; found: *m* 292.0571.

S-(9H-fluoren-2-yl) 4-methylbenzenesulfonothioate 3.3-43l

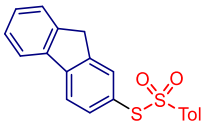

The reaction was conducted according to the general procedure **3-5** using 2-iodo-9H-fluorene (14.6 mg, 0.05 mmol), tetrabutylammonium thiotosylate (21.5 mg, 0.05 mmol), $AgSbF_6$ (20.6 mg, 0.06 mmol), gold complex **3.3-31$_{Cl}$** (0.26 mg, 0.5 µmol) and DCE (0.5 mL). Yield calculated by comparing the relative integration of the internal standard peaks with those of product (91%).

Purification by flash column chromatography (Hexane:EtOAc = 10:1).

3.3-43l was obtained as a white solid: 15.6 mg, 88% yield.

^{1}H NMR (300 MHz, $CDCl_3$): δ(ppm) 7.83 – 7.79 (m, 1H), 7.71 (d, J = 8.0 Hz, 1H), 7.62 – 7.55 (m, 2H), 7.46 (d, J = 8.4 Hz, 2H), 7.46 – 7.35 (m, 2H), 7.34 – 7.29 (m, 1H), 7.20 (d, J = 8.0 Hz, 2H), 3.88 (s, 2H), 2.42 (s, 3H).

^{13}C NMR (151 MHz, $CDCl_3$): δ(ppm) 145.0, 144.7, 144.3, 144.0, 140.4, 140.4, 135.5, 133.5, 129.5, 128.2, 127.8, 127.3, 125.6, 125.4, 120.8, 120.6, 36.9, 21.8.

HRMS (EI) Calculated for $C_{20}H_{16}O_2S_2$: 352.0592; found: *m* 352.0605.

S-(naphthalen-1-yl) 4-methylbenzenesulfonothioate 3.3-43m

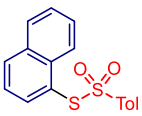

The reaction was conducted according to the general procedure **3-5** using 1-iodonaphthalene (7.3 µL, 12.7 mg, 0.05 mmol), tetrabutylammonium thiotosylate (21.5 mg, 0.05 mmol), $AgSbF_6$ (20.6 mg, 0.06 mmol), gold complex **3.3-31$_{Cl}$** (0.26 mg, 0.5 µmol) and DCE (0.5 mL). Yield calculated by comparing the relative integration of the internal standard peaks with those of product (93%).

Purification by flash column chromatography (Hexane:EtOAc = 10:1).

3.3-43m was obtained as a white solid: 14.0 mg, 89% yield.

^{1}H NMR (300 MHz, $CDCl_3$): δ(ppm) 8.14 – 7.97 (m, 2H), 7.87 (d, J = 8.1 Hz, 1H), 7.71 (dd, J = 7.2, 1.3 Hz, 1H), 7.58 – 7.32 (m, 5H), 7.08 (d, J = 8.0 Hz, 2H), 2.37 (s, 3H).

^{13}C NMR (151 MHz, $CDCl_3$): δ(ppm) 144.8, 140.2, 138.1, 134.7, 134.2, 132.8, 129.4, 128.5, 127.7, 127.5, 126.7, 125.7, 125.6, 125.6, 21.7.

HRMS (ESI) Calculated for $C_{17}H_{14}NaO_2S_2^+$ $[M+Na]^+$: 337.0327; found: *m/z* 337.0333.

S,S'-(1,4-phenylene) bis(4-methylbenzenesulfonothioate) 3.3-43n

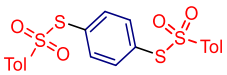

The reaction was conducted according to the general procedure **3-5** using 1,4-diiodobenzene (16.5 mg, 0.05 mmol), tetrabutylammonium thiotosylate (43.0 mg, 0.10 mmol), $AgSbF_6$ (37.8 mg, 0.11 mmol), gold complex **3.3-31$_{Cl}$** (0.52 mg, 1.0 µmol) and DCE (0.5 mL). Yield calculated by comparing the relative integration of the internal standard peaks with those of product (95%).

Purification by preparative TLC (Hexane:EtOAc = 10:1).

3.3-43n was obtained as a white solid: 13.0 mg, 58% yield.

^{1}H NMR (300 MHz, $CDCl_3$): δ(ppm) 7.46 (d, J = 8.4 Hz, 4H), 7.35 (s, 4H), 7.28 – 7.24 (m, 4H), 2.44 (s, 6H).

^{13}C NMR (151 MHz, $CDCl_3$): δ(ppm) 145.4, 140.4, 137.1, 132.0, 129.8, 127.7, 21.9.

HRMS (EI) Calculated for $C_{20}H_{18}O_4S_4$: 450.0088; found: *m* 450.0091.

S-(2-methoxyphenyl) 4-methylbenzenesulfonothioate 3.3-43o

The reaction was conducted according to the general procedure **3-5** using 1-iodo-2-methoxybenzene (6.5 µL, 11.7 mg, 0.05 mmol), tetrabutylammonium thiotosylate (21.5 mg, 0.05

mmol), $AgSbF_6$ (20.6 mg, 0.06 mmol), gold complex **3.3-31$_{Cl}$** (0.26 mg, 0.5 µmol) and DCE (0.5 mL). Yield calculated by comparing the relative integration of the internal standard peaks with those of product (97%). NMR data match those reported in the literature.[108]

S-(3-methoxyphenyl) 4-methylbenzenesulfonothioate 3.3-43p

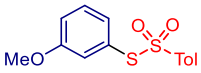

The reaction was conducted according to the general procedure **3-5** using 1-iodo-3-methoxybenzene (6.0 µL, 11.7 mg, 0.05 mmol), tetrabutylammonium thiotosylate (21.5 mg, 0.05 mmol), $AgSbF_6$ (20.6 mg, 0.06 mmol), gold complex **3.3-31$_{Cl}$** (0.26 mg, 0.5 µmol) and DCE (0.5 mL). Yield calculated by comparing the relative integration of the internal standard peaks with those of product (81%). NMR data match those reported in the literature.[106]

S-(4-methoxyphenyl) 4-methylbenzenesulfonothioate 3.3-43q

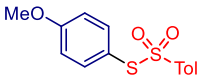

The reaction was conducted according to the general procedure **3-5** using 1-iodo-4-methoxybenzene (11.7 mg, 0.05 mmol), tetrabutylammonium thiotosylate (21.5 mg, 0.05 mmol), $AgSbF_6$ (20.6 mg, 0.06 mmol), gold complex **3.3-31$_{Cl}$** (0.26 mg, 0.5 µmol) and DCE (0.5 mL). Yield calculated by comparing the relative integration of the internal standard peaks with those of product (97%). NMR data match those reported in the literature.[105]

S-(4-ethoxyphenyl) 4-methylbenzenesulfonothioate 3.3-43r

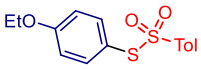

The reaction was conducted according to the general procedure **3-5** using 1-ethoxy-4-iodobenzene (7.7 µL, 12.4 mg, 0.05 mmol), tetrabutylammonium thiotosylate (21.5 mg, 0.05 mmol), $AgSbF_6$ (20.6 mg, 0.06 mmol), gold complex **3.3-31$_{Cl}$** (0.26 mg, 0.5 µmol) and DCE (0.5 mL). Yield calculated by comparing the relative integration of the internal standard peaks with those of product (90%).

Purification by flash column chromatography (Hexane:EtOAc = 10:1).

3.3-43r was obtained as a white solid: 13.0 mg, 84% yield.

^{1}H NMR (300 MHz, $CDCl_3$): δ(ppm) 7.45 (d, J = 8.3 Hz, 2H), 7.30 – 7.18 (m, 4H), 6.82 (d, J = 8.8 Hz, 2H), 4.05 (q, J = 7.0 Hz, 2H), 2.42 (s, 3H), 1.43 (t, J = 7.0 Hz, 3H).

^{13}C NMR (151 MHz, $CDCl_3$): δ(ppm) 161.8, 144.6, 140.5, 138.5, 129.5, 127.8, 118.6, 115.5, 63.9, 21.8, 14.8.

HRMS (EI) Calculated for $C_{15}H_{16}O_3S_2$: 308.0541; found: *m* 308.0639.

S-(4-acetamidophenyl) 4-methylbenzenesulfonothioate 3.3-43s

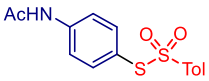

The reaction was conducted according to the general procedure **3-5** using *N*-(4-iodophenyl)acetamide (13.1 mg, 0.05 mmol), tetrabutylammonium thiotosylate (21.5 mg, 0.05 mmol), $AgSbF_6$ (20.6 mg, 0.06 mmol), gold complex **3.3-31$_{Cl}$** (0.52 mg, 1.0 µmol) and DCE (0.5 mL). Yield calculated by comparing the relative integration of the internal standard peaks with those of product (85%).

Purification by flash column chromatography (Hexane:EtOAc = 1:1).

3.3-43s was obtained as a white solid: 12.4 mg, 77% yield.

^{1}H NMR (600 MHz, $CDCl_3$): δ(ppm) 7.52 (d, J = 8.2 Hz, 2H), 7.46 (d, J = 8.1 Hz, 2H), 7.40 (bs, 1H), 7.30 (d, J = 8.4 Hz, 2H), 7.22 (d, J = 8.0 Hz, 2H), 2.42 (s, 3H), 2.20 (s, 3H).

^{13}C NMR (151 MHz, $CDCl_3$): δ(ppm) 168.5, 144.8, 141.0, 140.3, 137.6, 129.5, 127.6, 122.3, 119.8, 24.8, 21.7.

HRMS (EI) Calculated for $C_{14}H_{12}NaO_4S_2$: 321.0493; found: *m/z* 321.0475.

S-(benzo[d][1,3]dioxol-5-yl) 4-methylbenzenesulfonothioate 3.3-43t

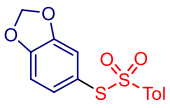

The reaction was conducted according to the general procedure **3-5** using 5-Iodo-1,3-benzodioxole (6.5 µL, 12.4 mg, 0.05 mmol), tetrabutylammonium thiotosylate (21.5 mg, 0.05 mmol), $AgSbF_6$ (20.6 mg, 0.06 mmol), gold complex **3.3-31$_{Cl}$** (0.26 mg, 0.5 µmol) and DCE (0.5 mL). Yield calculated by comparing the relative integration of the internal standard peaks with those of product (80%).

Purification by column chromatography (Hexane:EtOAc = 10:1).

3.3-43t was obtained as a white solid: 12.0 mg, 77% yield.

^{1}H NMR (300 MHz, $CDCl_3$): δ(ppm) 7.51 (d, J = 8.3 Hz, 2H), 7.24 (d, J = 8.2 Hz, 2H), 6.88 – 6.67 (m, 3H), 6.03 (s, 2H), 2.43 (s, 3H).

^{13}C NMR (151 MHz, $CDCl_3$): δ(ppm) 150.8, 148.4, 144.7, 140.4, 132.0, 129.6, 127.8, 120.1, 116.3, 109.1, 102.1, 21.8.

HRMS (ESI) Calculated $C_{14}H_{12}NaO_4S_2^+$ $[M+Na]^+$: 331.0069; found: *m/z* 331.0075.

S-(2-chlorophenyl) 4-methylbenzenesulfonothioate 3.3-43u

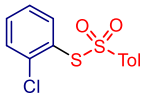

The reaction was conducted according to the general procedure **3-5** using 1-chloro-2-iodobenzene (6.1 µL, 11.9 mg, 0.05 mmol), tetrabutylammonium thiotosylate (21.5 mg, 0.05 mmol), $AgSbF_6$ (20.6 mg, 0.06 mmol), gold complex **3.3-31$_{Cl}$** (0.26 mg, 0.5 µmol) and DCE (0.5 mL). Yield calculated by comparing the relative integration of the internal standard peaks with those of product (89%). NMR data match those reported in the literature.[108]

S-(2-bromophenyl) 4-methylbenzenesulfonothioate 3.3-43v

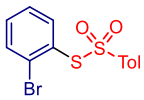

The reaction was conducted according to the general procedure **3-5** using 1-bromo-2-iodobenzene (14.1 mg, 0.05 mmol), tetrabutylammonium thiotosylate (21.5 mg, 0.05 mmol), $AgSbF_6$ (20.6 mg, 0.06 mmol), gold complex **3.3-31$_{Cl}$** (0.26 mg, 0.5 µmol) and DCE (0.5 mL). Yield calculated by comparing the relative integration of the internal standard peaks with those of product (88%). NMR data match those reported in the literature.[108]

S-(4-chlorophenyl) 4-methylbenzenesulfonothioate 3.3-43w

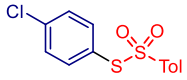

The reaction was conducted according to the general procedure **3-5** using 1-chloro-4-iodobenzene (11.9 mg, 0.05 mmol), tetrabutylammonium thiotosylate (21.5 mg, 0.05 mmol), $AgSbF_6$ (20.6 mg, 0.06 mmol), gold complex **3.3-31$_{Cl}$** (0.26 mg, 0.5 µmol) and DCE (0.5 mL). Yield

calculated by comparing the relative integration of the internal standard peaks with those of product (91%). NMR data match those reported in the literature.[108]

S-(4-bromophenyl) 4-methylbenzenesulfonothioate 3.3-43x

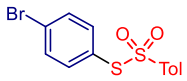

The reaction was conducted according to the general procedure **3-5** using 1-bromo-4-iodobenzene (14.1 mg, 0.05 mmol), tetrabutylammonium thiotosylate (21.5 mg, 0.05 mmol), $AgSbF_6$ (20.6 mg, 0.06 mmol), gold complex **3.3-31$_{Cl}$** (0.26 mg, 0.5 µmol) and DCE (0.5 mL). Yield calculated by comparing the relative integration of the internal standard peaks with those of product (91%). NMR data match those reported in the literature.[108]

S-(2,6-difluorophenyl) 4-methylbenzenesulfonothioate 3.3-43y

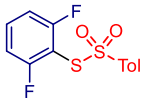

The reaction was conducted according to the general procedure **3-5** using 1,3-difluoro-2-iodobenzene (12.0 mg, 0.05 mmol), tetrabutylammonium thiotosylate (21.5 mg, 0.05 mmol), $AgSbF_6$ (20.6 mg, 0.06 mmol), gold complex **3.3-31$_{Cl}$** (0.52 mg, 1.0 µmol) and DCE (0.5 mL). Yield calculated by comparing the relative integration of the internal standard peaks with those of product (75%).

Purification by flash column chromatography (Hexane:EtOAc = 3:1).

3.3-43y was obtained as a white solid: 11.0 mg, 73% yield.

^{1}H NMR (300 MHz, $CDCl_3$): δ(ppm) 7.63 (d, J = 8.4 Hz, 2H), 7.53 (tt, J = 8.4, 6.2 Hz, 1H), 7.30 (d, J = 7.9 Hz, 2H), 7.06 – 6.96 (m, 2H), 2.48 (s, 3H).

^{13}C NMR (151 MHz, $CDCl_3$): δ(ppm) 164.5 (d, J = 3.0 Hz), 162.8 (d, J = 3.0 Hz), 145.4, 141.3, 134.8 (t, J = 10.4 Hz), 129.8, 127.6, 112.3 (d, J = 3.9 Hz), 112.2 (d, J = 3.8 Hz), 105.3 (t, J = 21.9 Hz), 21.9.

^{19}F NMR (283 MHz, $CDCl_3$): δ(ppm) -101.7.

HRMS (ESI) Calculated $C_{13}H_{10}F_2NaO_2S_2^+$ $[M+Na]^+$: 322.9982; found: *m/z* 322.9988.

S-(3-bromo-5-chlorophenyl) 4-methylbenzenesulfonothioate 3.3-43aa

The reaction was conducted according to the general procedure **3-5** using 1-bromo-3-chloro-5-iodobenzene (15.8 mg, 0.05 mmol), tetrabutylammonium thiotosylate (21.5 mg, 0.05 mmol), $AgSbF_6$ (20.6 mg, 0.06 mmol), gold complex **3.3-31$_{Cl}$** (0.52 mg, 1.0 µmol) and DCE (0.5 mL). Yield calculated by comparing the relative integration of the internal standard peaks with those of product (91%).

Purification by flash column chromatography (Hexane:EtOAc = 10:1).

3.3-43aa was obtained as a white solid: 15.6 mg, 83% yield.

^{1}H NMR (300 MHz, $CDCl_3$): δ(ppm) 7.64 (t, J = 1.8 Hz, 1H), 7.54 (d, J = 8.4 Hz, 2H), 7.40 – 7.27 (m, 4H), 2.49 (s, 3H).

^{13}C NMR (151 MHz, $CDCl_3$): δ(ppm) 145.7, 139.7, 137.2, 135.7, 134.9, 134.2, 131.2, 129.8, 127.9, 122.9, 21.8.

HRMS (ESI) Calculated $C_{13}H_{10}BrClNaO_2S_2^+$ $[M+Na]^+$: 398.8886; found: *m/z* 398.8892.

S-(4-bromo-3-chloro-2-fluorophenyl) 4-methylbenzenesulfonothioate 3.3-43ab

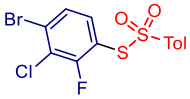

The reaction was conducted according to the general procedure **3-5** using 1-bromo-2-chloro-3-fluoro-4-iodobenzene (16.7 mg, 0.05 mmol), tetrabutylammonium thiotosylate (21.5 mg, 0.05 mmol), $AgSbF_6$ (20.6 mg, 0.06 mmol), gold complex **3.3-31$_{Cl}$** (1.3 mg, 2.5 µmol) and DCE (0.5 mL). Yield calculated by comparing the relative integration of the internal standard peaks with those of product (88%).

Purification by column chromatography (Hexane:EtOAc = 10:1).

3.3-43ab was obtained as a white solid: 16.0 mg, 81% yield.

^{1}H NMR (300 MHz, $CDCl_3$): δ(ppm) 7.57 (d, J = 8.4 Hz, 2H), 7.52 (dd, J = 8.5, 1.7 Hz, 1H), 7.38 – 7.28 (m, 3H), 2.49 (s, 3H).

^{13}C NMR (151 MHz, $CDCl_3$): δ(ppm) 159.1 (d, J = 257.3 Hz), 145.8, 140.5, 136.7, 129.9, 129.4 (d, J = 4.6 Hz), 128.7, 127.7, 124.1 (d, J = 20.7 Hz), 116.4 (d, J = 19.0 Hz), 21.9.

^{19}F NMR (283 MHz, $CDCl_3$): δ(ppm) -98.0.

HRMS (EI) Calculated for $C_{13}H_9BrClFO_2S_2$: 393.8900; found: *m* 393.8819.

S-(3,4-dichlorophenyl) 4-methylbenzenesulfonothioate 3.3-43ac

The reaction was conducted according to the general procedure **3-5** using 1,2-dichloro-4-iodobenzene (13.6 mg, 0.05 mmol), tetrabutylammonium thiotosylate (21.5 mg, 0.05 mmol), $AgSbF_6$ (20.6 mg, 0.06 mmol), gold complex **3.3-31$_{Cl}$** (0.52 mg, 1.0 µmol) and DCE (0.5 mL). Yield calculated by comparing the relative integration of the internal standard peaks with those of product (99%).

Purification by flash column chromatography (Hexane:EtOAc = 10:1).

3.3-43ac was obtained as a white solid: 15.5 mg, 93% yield.

^{1}H NMR (300 MHz, $CDCl_3$): δ(ppm) 7.53 (d, J = 8.4 Hz, 2H), 7.47 (d, J = 8.3 Hz, 1H), 7.41 (d, J = 2.1 Hz, 1H), 7.34 – 7.24 (m, 3H), 2.48 (s, 3H).

^{13}C NMR (151 MHz, $CDCl_3$): δ(ppm) 145.5, 140.0, 137.8, 136.5, 135.6, 133.5, 131.3, 129.8, 128.0, 127.8, 21.8.

HRMS (ESI) Calculated $C_{13}H_{10}Cl_2NaO_2S_2^+$ $[M+Na]^+$: 354.9391; found: *m/z* 354.9397.

S-(4-formylphenyl) 4-methylbenzenesulfonothioate 3.3-43ad

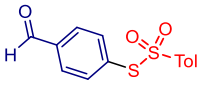

The reaction was conducted according to the general procedure **3-5** using 4-iodobenzaldehyde (11.6 mg, 0.05 mmol), tetrabutylammonium thiotosylate (21.5 mg, 0.05 mmol), $AgSbF_6$ (20.6 mg, 0.06 mmol), gold complex **3.3-31$_{Cl}$** (0.52 mg, 1.0 µmol) and DCE (0.5 mL). Yield calculated by comparing the relative integration of the internal standard peaks with those of product (73%).

Purification by flash column chromatography (Hexane:EtOAc = 3:1).

3.3-43ad was obtained as a white solid: 10.0 mg, 69% yield.

^{1}H NMR (300 MHz, $CDCl_3$): δ(ppm) 10.06 (s, 1H), 7.84 (d, J = 8.6 Hz, 2H), 7.57 (d, J = 8.0 Hz, 2H), 7.47 (d, J = 8.4 Hz, 2H), 7.22 (d, J = 8.0 Hz, 2H), 2.43 (s, 3H).

^{13}C NMR (151 MHz, $CDCl_3$): δ(ppm) 191.4, 145.4, 140.4, 137.8, 137.0, 135.0, 130.2, 129.7, 127.7, 21.8.

HRMS (EI) Calculated for $C_{14}H_{12}O_3S_2$: 292.0228; found: *m* 292.0254.

S-(2-formyl-4-methoxyphenyl) 4-methylbenzenesulfonothioate 3.3-43ae

The reaction was conducted according to the general procedure **3-5** using 2-iodo-5-methoxybenzaldehyde (13.1 mg, 0.05 mmol), tetrabutylammonium thiotosylate (21.5 mg, 0.05 mmol), $AgSbF_6$ (20.6 mg, 0.06 mmol), gold complex **3.3-31$_{Cl}$** (0.52 mg, 1.0 µmol) and DCE (0.5 mL). Yield calculated by comparing the relative integration of the internal standard peaks with those of product (43%). Purification by preparative TLC (Hexane:EtOAc = 3:1).

3.3-43ae was obtained as a white solid: 6.6 mg, 41% yield.

^{1}H NMR (300 MHz, $CDCl_3$): δ(ppm) 10.02 (s, 1H), 7.46 (d, J = 3.0 Hz, 1H), 7.44 – 7.37 (m, 3H), 7.25 – 7.20 (m, 2H), 7.11 (dd, J = 8.6, 3.0 Hz, 1H), 3.91 (s, 3H), 2.43 (s, 3H).

^{13}C NMR (151 MHz, $CDCl_3$): δ(ppm) 190.2, 162.8, 145.6, 140.8, 139.6, 139.4, 129.9, 127.6, 122.4, 121.5, 112.4, 56.0, 21.9.

HRMS (ESI) Calculated $C_{15}H_{14}NaO_4S_2^+$ $[M+Na]^+$: 345.0226; found: *m/z* 345.0231.

S-(4-acetylphenyl) 4-methylbenzenesulfonothioate 3.3-43af

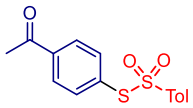

The reaction was conducted according to the general procedure **3-5** using 1-(4-iodophenyl)ethan-1-one (13.1 mg, 0.05 mmol), tetrabutylammonium thiotosylate (21.5 mg, 0.05 mmol), $AgSbF_6$ (20.6 mg, 0.06 mmol), gold complex **3.3-31$_{Cl}$** (0.52 mg, 1.0 µmol) and DCE (0.5 mL). Yield calculated by comparing the relative integration of the internal standard peaks with those of product (74%). Purification by preparative TLC (Hexane:EtOAc = 3:1).

3.3-43af was obtained as a white solid: 11.0 mg, 72% yield.

^{1}H NMR (600 MHz, $CDCl_3$): δ(ppm) 7.90 (d, J = 8.4 Hz, 2H), 7.48 (dd, J = 14.0, 8.3 Hz, 4H), 7.22 (d, J = 7.8 Hz, 2H), 2.62 (s, 3H), 2.43 (s, 3H).

^{13}C NMR (151 MHz, $CDCl_3$): δ(ppm) 197.2, 145.2, 140.4, 138.7, 136.5, 133.3, 129.6, 128.9, 127.6, 26.8, 21.7.

HRMS (EI) Calculated for $C_{15}H_{14}O_3S_2$: 306.0384; found: *m* 306.0356.

methyl 2-(tosylthio)benzoate 3.3-43ag

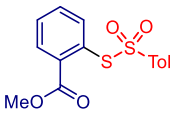

The reaction was conducted according to the general procedure **3-5** using methyl 2-iodobenzoate (7.3 µL, 13.1 mg, 0.05 mmol), tetrabutylammonium thiotosylate (21.5 mg, 0.05 mmol), $AgSbF_6$ (20.6 mg, 0.06 mmol), gold complex **3.3-31$_{Cl}$** (0.52 mg, 1.0 µmol) and DCE (0.5 mL). Yield calculated by comparing the relative integration of the internal standard peaks with those of product (56%). NMR data match those reported in the literature.[109]

methyl 4-(tosylthio)benzoate 3.3-43ah

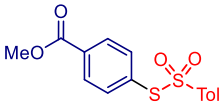

The reaction was conducted according to the general procedure **3-5** using methyl 4-iodobenzoate (13.1 mg, 0.05 mmol), tetrabutylammonium thiotosylate (21.5 mg, 0.05 mmol), $AgSbF_6$ (20.6 mg, 0.06 mmol), gold complex **3.3-31$_{Cl}$** (0.26 mg, 0.5 µmol) and DCE (0.5 mL). Yield calculated by comparing the relative integration of the internal standard peaks with those of product (99%). NMR data match those reported in the literature.[105]

S-(2-cyanophenyl) 4-methylbenzenesulfonothioate 3.3-43ai

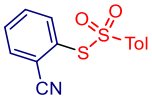

The reaction was conducted according to the general procedure **3-5** using 2-iodobenzonitrile (11.4 mg, 0.05 mmol), tetrabutylammonium thiotosylate (21.5 mg, 0.05 mmol), $AgSbF_6$ (20.6 mg, 0.06 mmol), gold complex **3.3-31$_{Cl}$** (1.30 mg, 2.5 µmol) and DCE (0.5 mL). Yield calculated by comparing the relative integration of the internal standard peaks with those of product (53%).

Purification by flash chromatography (Hexane:EtOAc = 10:1).

3.3-43ai was obtained as a white solid: 7.0 mg, 48% yield.

^{1}H NMR (300 MHz, $CDCl_3$): δ(ppm) 7.87 – 7.78 (m, 1H), 7.78 – 7.56 (m, 3H), 7.49 (d, J = 8.4 Hz, 2H), 7.30 – 7.22 (m, 2H), 2.44 (s, 3H).

^{13}C NMR (151 MHz, $CDCl_3$): δ(ppm) 145.9, 140.0, 139.0, 134.0, 133.5, 131.8, 131.3, 130.0, 127.8, 120.1, 115.8, 21.9.

HRMS (EI) Calculated for $C_{14}H_{11}NO_2S_2$: 289.0231; found: *m* 289.0212.

S-(4-cyanophenyl) 4-methylbenzenesulfonothioate 3.3-43aj

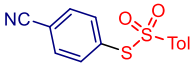

The reaction was conducted according to the general procedure **3-5** using 4-iodobenzonitrile (11.4 mg, 0.05 mmol), tetrabutylammonium thiotosylate (21.5 mg, 0.05 mmol), $AgSbF_6$ (20.6 mg, 0.06 mmol), gold complex **3.3-31$_{Cl}$** (0.52 mg, 1.0 µmol) and DCE (0.5 mL). Yield calculated by comparing the relative integration of the internal standard peaks with those of product (57%).

Purification by flash chromatography (Hexane:EtOAc = 10:1).

3.3-43aj was obtained as a white solid: 8.0 mg, 55% yield.

^{1}H NMR (300 MHz, $CDCl_3$): δ(ppm) 7.63 (d, J = 8.1 Hz, 2H), 7.52 (d, J = 8.2 Hz, 2H), 7.47 (d, J = 8.2 Hz, 2H), 7.25 (d, J = 8.2 Hz, 2H), 2.44 (s, 3H).

^{13}C NMR (151 MHz, $CDCl_3$): δ(ppm) 145.6, 140.3, 136.9, 134.0, 132.9, 129.8, 127.7, 117.8, 115.1, 21.9.
HRMS (ESI) Calculated for $C_{14}H_{11}NNaO_2S_2$ $[M+]^+$: 312.0123; found: *m/z* 312.0054.

S-(3-nitrophenyl) 4-methylbenzenesulfonothioate 3.3-43ak

The reaction was conducted according to the general procedure **3-5** using 1-iodo-3-nitrobenzene (12.4 mg, 0.05 mmol), tetrabutylammonium thiotosylate (21.5 mg, 0.05 mmol), $AgSbF_6$ (20.6 mg, 0.06 mmol), gold complex **3.3-31$_{Cl}$** (0.52 mg, 1.0 µmol) and DCE (0.5 mL). Yield calculated by comparing the relative integration of the internal standard peaks with those of product (74%). NMR data match those reported in the literature.[110]

S-(3-(trifluoromethyl)phenyl) 4-methylbenzenesulfonothioate 3.3-43al

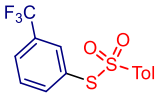

The reaction was conducted according to the general procedure **3-5** using 1-iodo-3-(trifluoromethyl)benzene (7.2 µL, 13.6 mg, 0.05 mmol), tetrabutylammonium thiotosylate (21.5 mg, 0.05 mmol), $AgSbF_6$ (20.6 mg, 0.06 mmol), gold complex **3.3-31$_{Cl}$** (0.52 mg, 1.0 µmol) and DCE (0.5 mL). Yield calculated by comparing the relative integration of the internal standard peaks with those of product (72%).

Purification by flash chromatography (Hexane:EtOAc = 10:1).

3.3-43al was obtained as a white solid: 11.2 mg, 67% yield.

^{1}H NMR (300 MHz, $CDCl_3$): δ(ppm) 7.71 (t, J = 7.3 Hz, 2H), 7.59 – 7.47 (m, 1H), 7.48 – 7.35 (m, 3H), 7.27 – 7.18 (m, 2H), 2.42 (s, 3H).

^{13}C NMR (151 MHz, $CDCl_3$): δ(ppm) 145.5, 140.2, 139.8, 133.3 (q, J = 3.8 Hz), 131.9 (q, J = 33.2 Hz), 130.1, 129.7, 129.6, 128.1 (q, J = 3.6 Hz), 127.8, 123.3 (q, J = 272.7 Hz), 21.8.

^{19}F NMR (283 MHz, $CDCl_3$) δ(ppm) -63.0.

HRMS (EI) Calculated for $C_{14}H_{11}F_3O_2S_2$: 332.0153; found: *m* 332.0151.

S-(4-(trifluoromethyl)phenyl) 4-methylbenzenesulfonothioate 3.3-43am

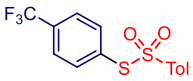

The reaction was conducted according to the general procedure **3-5** using 1-iodo-4-(trifluoromethyl)benzene (7.3 µL, 13.6 mg, 0.05 mmol), tetrabutylammonium thiotosylate (21.5 mg, 0.05 mmol), $AgSbF_6$ (20.6 mg, 0.06 mmol), gold complex **3.3-31$_{Cl}$** (0.26 mg, 0.5 µmol) and DCE (0.5 mL). Yield calculated by comparing the relative integration of the internal standard peaks with those of product (95%). NMR data match those reported in the literature.[111]

S-(3,5-bis(trifluoromethyl)phenyl) 4-methylbenzenesulfonothioate 3.3-43an

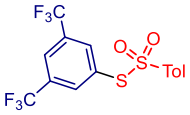

The reaction was conducted according to the general procedure **3-5** using 1-iodo-3,5-bis(trifluoromethyl)benzene (8.8 µL, 17.0 mg, 0.05 mmol), tetrabutylammonium thiotosylate (21.5 mg, 0.05 mmol), $AgSbF_6$ (20.6 mg, 0.06 mmol), gold complex **3.3-31$_{Cl}$** (0.52 mg, 1.0 µmol) and DCE (0.5 mL). Yield calculated by comparing the relative integration of the internal standard peaks with those of product (37%).

Purification by preparative TLC (Hexane:EtOAc = 3:1).

3.3-43an was obtained as a white solid: 7.0 mg, 35% yield.

^{1}H NMR (300 MHz, $CDCl_3$): δ(ppm) 7.95 (s, 1H), 7.74 (s, 2H), 7.45 (d, J = 8.4 Hz, 2H), 7.26 (d, J = 8.0 Hz, 2H), 2.44 (s, 3H).

^{13}C NMR (151 MHz, $CDCl_3$): δ(ppm) 146.0, 139.2, 136.6 – 136.4 (m), 132.7 (q, J = 34.1 Hz), 131.4, 129.8, 127.8, 125.0 – 124.5 (m), 125.2 – 119.6 (m), 21.6.

^{19}F NMR (283 MHz, $CDCl_3$) δ(ppm) -63.0.

HRMS (ESI) Calculated for $C_{15}H_{10}F_6NaO_2S_2$ $[M+Na]^+$: 422,9919; found: *m/z* 400.9842.

dimethyl 5-(tosylthio)isophthalate 3.3-43ao

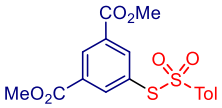

The reaction was conducted according to the general procedure **3-5** using dimethyl 5-iodoisophthalate (16.0 mg, 0.05 mmol), tetrabutylammonium thiotosylate (21.5 mg, 0.05 mmol), $AgSbF_6$ (20.6 mg, 0.06 mmol), gold complex **3.3-31$_{Cl}$** (0.52 mg, 1.0 µmol) and DCE (0.5 mL). Yield calculated by comparing the relative integration of the internal standard peaks with those of product (72%).

Purification by preparative TLC (Hexane:EtOAc = 3:1).

3.3-43ao was obtained as a white solid: 11.4 mg, 60% yield.

^{1}H NMR (300 MHz, $CDCl_3$): δ(ppm) 8.76 (t, J = 1.6 Hz, 1H), 8.16 (d, J = 1.6 Hz, 2H), 7.46 (d, J = 8.4 Hz, 2H), 7.23 (d, J = 8.1 Hz, 2H), 3.94 (s, 6H), 2.42 (s, 3H).

^{13}C NMR (151 MHz, $CDCl_3$): δ(ppm) 165.0, 145.5, 141.4, 140.0, 133.2, 132.0, 129.8, 127.8, 52.9, 43.6, 21.8.

HRMS (ESI) Calculated for $C_{17}H_{16}NaO_6S_2^+$ $[M+Na]^+$: 403.0281; found: *m/z* 403.0286.

S-(thiophen-2-yl) 4-methylbenzenesulfonothioate 3.3-43ap

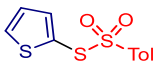

The reaction was conducted according to the general procedure **3-5** using 2-iodothiophene (5.5 µL, 10.5 mg, 0.05 mmol), tetrabutylammonium thiotosylate (21.5 mg, 0.05 mmol), $AgSbF_6$ (20.6 mg, 0.06 mmol), gold complex **3.3-31$_{Cl}$** (0.26 mg, 0.5 µmol) and DCE (0.5 mL). Yield calculated by comparing the relative integration of the internal standard peaks with those of product (84%). NMR data match those reported in the literature.[110]

(S,S'-(thiophene-2,5-diyl) bis(4-methylbenzenesulfonothioate 3.3-43aq

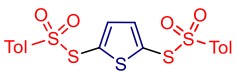

The reaction was conducted according to the general procedure **3-5** using 2,5-diiodothiophene (16.8 mg, 0.05 mmol), tetrabutylammonium thiotosylate (43.0 mg, 0.10 mmol), $AgSbF_6$ (37.8 mg, 0.11 mmol), gold complex **3.3-31$_{Cl}$** (0.52 mg, 1.0 µmol) and DCE (0.5 mL). Yield calculated by comparing the relative integration of the internal standard peaks with those of product (74%).

Purification by column chromatography (Hexane:EtOAc = 10:1). The compound could not be isolated under pure and was obtained in mixture with an impurity. The purity of the isolated material was assessed to be > 80%.

3.3-43aq was obtained as a white solid: 15.0 mg, 66% yield (purity > 80%). Data provided below are for this isolate material.

^{1}H NMR (600 MHz, $CDCl_3$): δ(ppm) 7.58 (d, J = 8.3 Hz, 4H), 7.32 (d, J = 8.6 Hz, 4H), 7.09 (s, 2H), 2.46 (s, 6H).

^{13}C NMR (151 MHz, $CDCl_3$): δ(ppm) 145.7, 139.5, 139.4, 134.5, 129.9, 127.9, 21.8.

HRMS (EI) Calculated for $C_{18}H_{16}O_4S_5$: 455.9653; found: *m* 455.9658.

(*E*)-*S*-styryl 4-methylbenzenesulfonothioate 3.3-43at

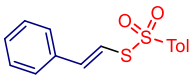

The reaction was conducted according to the general procedure **3-5** using (*E*)-(2-iodovinyl)benzene (11.5 mg, 0.05 mmol), tetrabutylammonium thiotosylate (21.5 mg, 0.05 mmol), $AgSbF_6$ (20.6 mg, 0.06 mmol), gold complex **3.3-31$_{Cl}$** (0.26 mg, 0.5 µmol) and DCE (0.5 mL). Yield calculated by comparing the relative integration of the internal standard peaks with those of product (85%).

Purification by column chromatography (Hexane:EtOAc = 10:1).

3.3-43at was obtained as a white solid: 12.0 mg, 83% yield.

^{1}H NMR (300 MHz, $CDCl_3$): δ(ppm) 7.75 (d, J = 8.4 Hz, 2H), 7.36 (s, 5H), 7.33 – 7.28 (m, 2H), 7.01 – 6.72 (m, 2H), 2.44 (s, 3H).

^{13}C NMR (151 MHz, $CDCl_3$): δ(ppm) 145.3, 145.0, 141.3, 135.1, 129.8, 129.8, 129.0, 127.5, 127.4, 115.0, 21.8.

HRMS (EI) Calculated for $C_{15}H_{14}O_2S_2$: 290.0435; found: *m* 290.0422.

2-(tosylthio)phenyl 4-methylbenzenesulfonate 3.3-43au

The reaction was conducted according to the general procedure **3-5** using 2-iodophenyl 4-methylbenzenesulfonate (18.7 mg, 0.05 mmol), tetrabutylammonium thiotosylate (21.5 mg, 0.05 mmol), $AgSbF_6$ (20.6 mg, 0.06 mmol), gold complex **3.3-31$_{Cl}$** (0.26 mg, 0.5 µmol) and DCE (0.5 mL). Yield calculated by comparing the relative integration of the internal standard peaks with those of product (63%).

Purification by preparative TLC (Hexane:EtOAc = 4:1).

3.3-43au was obtained as a white solid: 9.0 mg, 41% yield.

^{1}H NMR (300 MHz, $CDCl_3$): δ(ppm) 7.73 – 7.58 (m, 3H), 7.53 – 7.45 (m, 1H), 7.39 – 7.29 (m, 5H), 7.28 – 7.22 (m, 1H), 7.12 (d, J = 8.7 Hz, 2H), 2.47 (s, 3H), 2.40 (s, 3H).

^{13}C NMR (151 MHz, $CDCl_3$): δ(ppm) 150.4, 146.0, 145.1, 140.7, 139.4, 133.4, 132.2, 129.9, 129.6, 128.7, 128.0, 127.5, 123.9, 122.6, 21.9, 21.8.

HRMS (EI) Calculated for$C_{20}H_{18}O_5S_3$: 434.0316; found: *m* 434.0308.

(*E*)-S-(oct-1-en-1-yl) 4-methylbenzenesulfonothioate 3.3-43av

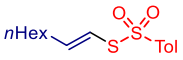

The reaction was conducted according to the general procedure **3-5** using (*E*)-1-iodooct-1-ene (11.9 mg, 0.05 mmol), tetrabutylammonium thiotosylate (21.5 mg, 0.05 mmol), $AgSbF_6$ (20.6 mg, 0.06 mmol), gold complex **3.3-31$_{Cl}$** (0.26 mg, 0.5 µmol) and DCE (0.5 mL). Yield calculated by comparing the relative integration of the internal standard peaks with those of product (93%).

Purification by flash column chromatography (Hexane:EtOAc = 10:1).

3.3-43av was obtained as a colourless oil: 13.0 mg, 87% yield.

^{1}H NMR (300 MHz, $CDCl_3$): δ(ppm) 7.74 (d, J = 8.4 Hz, 2H), 7.31 (d, J = 7.9 Hz, 2H), 6.23 – 5.98 (m, 2H), 2.44 (s, 3H), 2.24 – 2.10 (m, 2H), 1.41 – 1.16 (m, 8H), 0.97 – 0.79 (m, 3H).

^{13}C NMR (75 MHz, $CDCl_3$): δ(ppm) 151.1, 144.6, 141.0, 129.5, 127.4, 115.1, 33.3, 31.5, 28.6, 28.2, 22.5, 21.6, 14.0.

HRMS (EI) Calculated for $C_{15}H_{22}O_2S_2$: 298.1061; found: *m* 298.1032.

3.5.6. Structural diversifications of thiotosylate 3.3-43a

3.5.6.1. Synthesis of 1-(4-fluorophenyl)-2-phenyldisulfane 3.3-44a

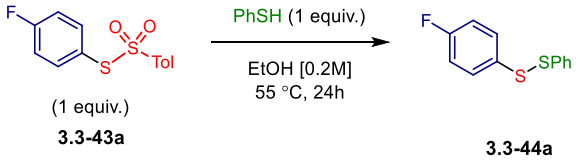

Following a procedure previously reported.[112] In a screw-cap vial containing a magnetic stir bar was added compound **3.3-43a** (10.0 mg, 0.03 mmol), PhSH (3.6 µL, 3.9 mg) and EtOH (0.15 mL). The vial was then screwed and isolated with parafilm before the reaction mixture was stirred and heated at 55 °C for 24h. Upon completion of the reaction, the mixture was filtered through a plug of Celite. $CDCl_3$ was used to rinse the pad and dilute the filtrate. Trifluorotoluene (1.0 mg), used as an internal standard, was added to the filtrate and the resulting solution was then analyzed by ^{19}F NMR spectroscopy. The yield (72%) was calculated by comparing the relative integration of the internal standard peaks with those of the product (see **Appendix Figure 6.2-12**). NMR data were compared to those reported in the literature.[113]

3.5.6.2. Synthesis of 4-((4-fluorophenyl)thio)morpholine 3.3-44b

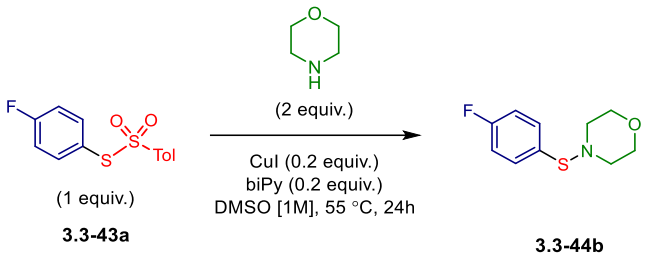

Following a procedure previously reported.[112] In a screw-cap vial containing a magnetic stir bar was added compound **3.3-43a** (20.0 mg, 0.06 mmol), CuI (2.6 mg, 14.2 µmol), biPy (2.2 mg, 14.2 µmol), morpholine (12.2 µL, 12.4 mg, 0.12 mmol), and DMSO (0.06 mL). The vial was then screwed and isolated with parafilm before the reaction mixture was stirred and heated at 55 °C for 24h. Upon completion of the reaction, the mixture was filtered through a plug of Celite. $CDCl_3$ was used to rinse the pad and dilute the filtrate. Trifluorotoluene (1.0 mg), used as an internal standard, was added to the filtrate and the resulting solution was then analyzed by ^{19}F NMR spectroscopy. The yield (62%) was calculated by comparing the relative integration of the internal standard peaks with those of the product (see **Appendix Figure 6.2-13**). NMR data were compared to those reported in the literature.[114]

3.5.6.3. Synthesis of S-(4-fluorophenyl) diphenylphosphinothioate 3.3-44c

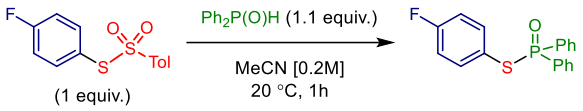

(1 equiv.)

3.3-43a **3.3-44c**

Following a procedure previously reported.[105] In a screw-cap vial containing a magnetic stir bar was added compound **3.3-43a** (20.0 mg, 0.06 mmol), $Ph_2P(O)H$ (13.3 mg, 0.07 mmol), and MeCN (0.3 mL). The vial was then screwed and isolated with parafilm before the reaction mixture was stirred at 20 °C for 1h. Upon completion of the reaction, the mixture was filtered through a plug of Celite. $CDCl_3$ was used to rinse the pad and dilute the filtrate. 1,3,5-trimethylbenzene (1.8 mg), used as an internal standard, was added to the filtrate and the resulting solution was then analyzed by ^1H NMR spectroscopy. The yield (95%) was calculated by comparing the relative integration of the internal standard peaks with those of the product (see **Appendix Figure 6.2-14**). NMR data were compared to those reported in the literature.[105]

3.5.6.4. Synthesis of chlorotetrafluoro(4-fluorophenyl)-λ⁶-sulfane 3.3-44d

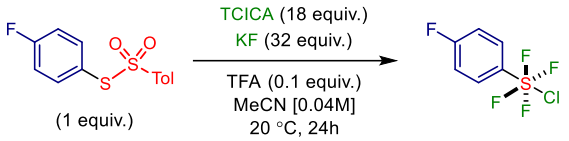

(1 equiv.)

3.3-43a **3.3-44d**

The following procedure was adapted from a procedure by Cornella and coworkers.[115] Inside a nitrogen-filled glovebox, a magnetic stir bar was placed inside a screw-cap 1 dram vial, followed by compound **3.3-43a** (10.0 mg, 0.03 mmol), TCICA (125.3 mg, 0.54 mmol), KF (55.7 mg, 0.96 mmol), MeCN (0.8 mL) and TFA (0.2 µL, 0.3 mg, 3 µmol). The vial was then sealed, transferred outside a glovebox and the reaction mixture was stirred at 20 °C for 24h. Upon completion of the reaction, the mixture was filtered through a Celite plug. $CDCl_3$ was used to rinse the pad and dilute the filtrate. Trifluorotoluene (1.0 mg), used as an internal standard, was added to the filtrate and the resulting solution was then analyzed by ^{19}F NMR spectroscopy. The yield (80%) was calculated by comparing the relative integration of the internal standard peaks with those of the product (see **Appendix Figure 6.2-15**). NMR data were compared to those reported in the literature.[116]

3.5.6.5. Synthesis of (4-fluorophenyl)(trifluoromethyl)sulfane 3.3-44e

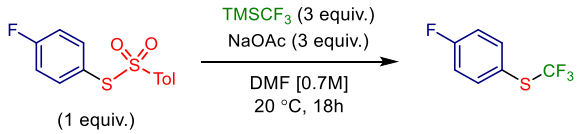

(1 equiv.)

3.3-43a **3.3-44e**

Following a procedure previously reported.[117] Inside a nitrogen-filled glovebox, a magnetic stir bar was placed inside a screw-cap 1 dram vial, followed by compound **3.3-43a** (20.0 mg, 0.06

mmol), $TMSCF_3$ (8.9 µL, 8.5 mg, 0.18 mmol), NaOAc (14.8 mg, 0.18 mmol) and DMF (0.8 mL). The vial was then sealed and the reaction mixture was stirred at 20 °C for 18 hours. Upon completion of the reaction, the mixture was filtered through a Celite plug. $CDCl_3$ was used to rinse the pad and dilute the filtrate. Trifluorotoluene (1.0 mg), used as an internal standard, was added to the filtrate and the resulting solution was then analyzed by ^{19}F NMR spectroscopy. The yield (77%) was calculated by comparing the relative integration of the internal standard peaks with those of the product (see **Appendix Figure 6.2-16**). NMR data were compared to those reported in the literature.[118]

3.5.6.6. Synthesis of 4-((4-fluorophenyl)thio)phenol 3.3-44f

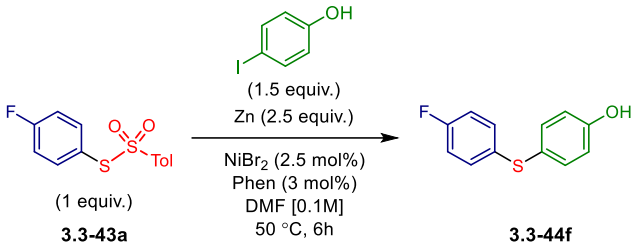

Following a procedure previously reported.[93] In a screw-cap vial containing a magnetic stir bar was added compound **3.3-43a** (10.0 mg, 0.03 mmol), 4-iodophenol (9.9 mg, 0.04 mmol), Zn (4.9 mg, 0.75 mmol), $NiBr_2$ (0.2 mg, 0.75 µmol), Phen (0.2 mg, 0.9 µmol) and DMF (0.3 mL). The vial was then sealed and the reaction mixture was stirred at 50 °C for 6 hours. Upon completion of the reaction, the mixture was filtered through a Celite plug, using $CDCl_3$ as the eluent. $CDCl_3$ was used to rinse the pad and dilute the filtrate. Trifluorotoluene (1.5 mg), used as an internal standard, was added to the filtrate and the resulting solution was then analyzed by ^{19}F NMR spectroscopy. The yield (95%) was calculated by comparing the relative integration of the internal standard peaks with those of the product (see **Appendix Figure 6.2-17**). NMR data were compared to those reported in the literature.[119]

3.5.6.7. Synthesis of (4-fluorophenyl)(phenylethynyl)sulfane 3.3-44g

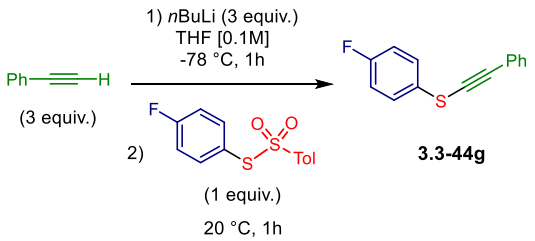

A 5 mL flask, equipped with a magnetic stir bar, was flame-dried and subsequently filled with an atmosphere of nitrogen. To this flask was added a solution of ethynylbenzene (19.7 µL, 18.4 mg, 0.18 mmol) in THF (1.6 mL) and the system was cooled to -78 °C. A solution of *n*BuLi in hexane

(0.07 mL, 2.5M, 0.18 mmol) was then added dropwise to the solution, and the resulting reaction mixture was stirred at this temperature for 1 hour. Compound **3.3-43a** (20.0 mg, 0.06 mmol), in solution in THF (0.2 mL) was then added and the reaction mixture was slowly warmed up to 20 °C. After stirring for an additional 1 hour at this temperature, the mixture was quenched with water and extracted with DCM. The organic phases were dried of $MgSO_4$ and concentrated under vacuum. The residue was dissolved in $CDCl_3$. Trifluorotoluene (1 mg), used as an internal standard, was added to the filtrate and the resulting solution was then analyzed by ^{19}F NMR spectroscopy. The yield (73%) was calculated by comparing the relative integration of the internal standard peaks with those of the product (see **Appendix Figure 6.2-18**). NMR data were compared to those reported in the literature.[120]

3.5.7. Synthesis of cross-coupling product 3.3-45

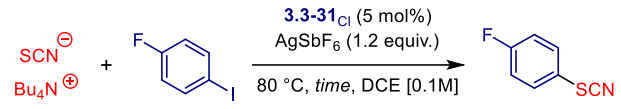

(1 equiv.) **3.3-42a** (1 equiv.) **3.3-45**

Inside a nitrogen-filled glovebox, $AgSbF_6$ (20.6 mg, 0.06 mmol) was added to a 1 dram vial containing a stir bar. The vial was taken outside the glovebox. In separate vial, a solution of *p*-fluoroiodobenzene (6.4 µL, 10.9 mg, 0.05 mmol), tetrabutylammonium cyanate (15.0 mg, 0.05 mmol) and gold complex **3.3-31$_{Cl}$** (1.3 mg, 2.5 µmol) in DCE (0.5 mL) was prepared. This solution was added to the vial containing $AgSbF_6$. The vial was capped, vigorously shaken, isolated with parafilm and placed in a 80 °C preheated oil-bath. After stirring the mixture at 80 °C for the required time (3 – 24h, see **equation 3**), the reaction mixture was passed through a plug of celite. A small amount of $CDCl_3$ was used to rinse the pad and dilute the filtrate. A few µL of 1,3,5-trimethylbenzene, used as an internal standard, were added to this solution. The resulting solution was then analyzed by ^1H NMR spectroscopy. The yield was calculated by comparing the relative integration of the internal standard peaks with those of the product **3.3-45**[121] (see **Appendix Figure 6.2-19** for representative example).

3.5.8. Other data and experiments

3.5.8.1. Role of Ag^+ in Au(I)Au/(III) RedOx catalysis (alkene/ArI exchange)

A stoichiometric experiment was run to demonstrate that in the presence of Ag^+ the rate of the alkene to ArI exchange at the Au(I) center was increased, what overall leads to a more oxidative addition process. When Ag^+ is omitted, Bourissou and coworkers previously showed that the alkene to ArI exchange and subsequent oxidative addition could take place but way more slowly (days).[42]

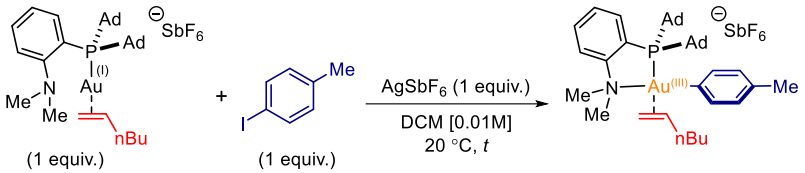

A NMR tube was charged with a solution of complex **3.3-35**$_{Alk\text{-}Md}$ (5 mg, 5.3 µmol) in DCM (0.05 mL) was added 1-iodo-4-methylbenzene (1.2 mg, 5.3 µmol) and $AgSbF_6$ (1.8 mg, 5.3 µmol) and the reaction mixture was monitored by ^{31}P NMR (see **Appendix Figure 6.2-20**).

3.5.8.2. Mechanistic experiments on the thiotosylation of ArI

• Synthesis of thiotosylate Au(I) complex **3.3-35**$_{STs\text{-}Cl}$:

A suspension of AgSTs (13.6 mg, 0.05 mmol) in DCM was cooled to -78 °C, and a solution of complex **3.3-31**$_{Cl}$ (20 mg, 0.04 mmol) in dry DCM (4 ml) was slowly added. The reaction mixture was then allowed to warm to room temperature and stirred for 2 additional hours. The mixture was then filtered through Celite using DCM as the eluent. The filtrate was concentrated under reduced pressure to afford 16.8 mg of the desired product as a yellowish solid (65%).

^{1}H NMR (300 MHz, CD_2Cl_2) δ(ppm) 8.27 (d, J = 1.4 Hz, 1H), 8.19 (s, 1H), 7.85 (d, J = 8.3 Hz, 2H), 7.24 (d, J = 8.6 Hz, 2H), 3.49 (d, J = 6.5 Hz, 3H), 2.40 (s, 3H), 1.45 (d, J = 16.8 Hz, 18H).

^{13}C NMR (151 MHz, CD_2Cl_2) δ(ppm) 154.3, 148.4, 142.6, 141.7, 140.5, 133.1, 129.2, 125.5, 41.2 (d, J = 21.1 Hz), 30.0 (d, J = 8.1 Hz), 21.2. Due to the significant broadening, signals for C_{quat}. are not visible.

^{31}P NMR (122 MHz, CD_2Cl_2) δ(ppm) 117.1 (bs)

HRMS (ESI) Calculated for $C_{20}H_{31}AuClN_3O_2PS_2^+$ $[M+H]^+$: 672.0944; found: *m/z* 672.0953.

• Thiotosylate Au(I) complex **3.3-35**$_{STs\text{-}Cl}$ as the resting state in the cross-coupling reaction:

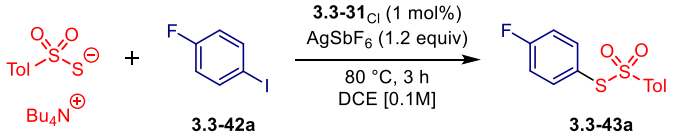

Inside a nitrogen-filled glovebox, $AgSbF_6$ (20.6 mg, 0.06 mmol) was added to a 1 dram vial containing a stir bar. The vial was taken outside the glovebox. In separate vial, a solution of p-fluoroiodobenzene (6.4 µL, 10.9 mg, 0.05 mmol), tetrabutylammonium thiotosylate (21.5 mg, 0.05 mmol) and gold complex **3.3-31**$_{Cl}$ (0.26 mg, 0.5 µmol) in DCE (0.5 mL) was prepared. This solution was added to the vial containing $AgSbF_6$. The vial was capped, vigorously shaken, isolated

with parafilm and placed in a 80 °C preheated oil-bath. After 3 hours, an aliquot was analyzed by HRMS. The Au(I) thiotosylate complex **3.3-35$_{STs-Cl}$** was detected (see **Appendix Figure 6.2-21**).

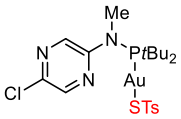

HRMS (ESI) Calculated for $C_{20}H_{31}AuClN_3O_2PS_2^+$ $[M+H]^+$: 672.0944; found: *m/z* 672.0953.

3.5.8.3. Importance of Ag^+ salt on the course of the cross-coupling reaction

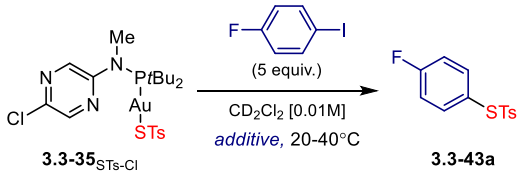

3.3-35$_{STs-Cl}$ **3.3-43a**

A screw cap NMR tube was charged with a solution of complex **3.3-35$_{STs-Cl}$** (3.5 mg, 5.2 µmol) in CD_2Cl_2 (0.5 mL). Subsequently, 1-fluoro-4-iodobenzene (3.0 µL, 5.8 mg, 26.0 µmol), trifluorotoluene (0.5 µl) and the corresponding additive ($AgSbF_6$ (1.8 mg, 5.2 µmol) *or* $TBAPF_6$ (2.0 mg, 5.2 µmol)) were added. The reaction mixture was kept at the designated temperature and monitored by ^{19}F spectroscopy to observe the formation of **3.3-43a** (see **Appendix Figures 6.2-22**).

While the use of $AgSbF_6$ as the additive led to the quantitative formation of the cross coupling product **3.3-43a**, no product was observed in the absence of $AgSbF_6$ or when it was replaced by the $TBAPF_6$- ammonium salt. This experiment in addition to the following one demonstrate that the Ag^+ salts are crucial to induce the oxidative addition step by promoting the STs to ArI exchange at the Au(I) center in Au(I) complex **3.3-35$_{STs-Cl}$**.

• Ag^+ is not required to induce the cross coupling reaction from Au(III) oxidative complex **3.3-45**:

This reaction was run using MeDalPhos as the ligand since the corresponding Au(III) oxidative complex with ClKarPhos was found too instable to be isolated.

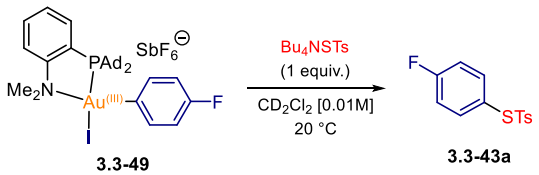

3.3-49 **3.3-43a**

A screw cap NMR tube was charged with a solution of complex **3.3-49** (5 mg, 4.6 µmol) in CD_2Cl_2 (0.5 mL). Subsequently, tetrabutylammonium thiotosylate (2.0 mg, 4.6 µmol) and

trifluorotoluene (0.5 µL) were added. The reaction mixture was kept at 20 ◦C and monitored by ^{19}F and ^{31}P spectroscopy to observe the formation of **3.3-43a** (see **Appendix Figures 6.2-23**).

The ^{31}P NMR monitoring of the reaction showed that the initial signal of the Au(III) complex **3.3-49** (δ= 75.97 ppm) disappeared upon addition of TsSNEt4 to provide a new broadened signal with a slightly lower chemical shift ($\delta\approx$ 75.5 ppm). This signal tends to get more defined during the course of the reaction. It is believed that an equilibrium exists between 62 and the corresponding LAu(III)STs complex resulting from the substitution of the iodide by the STs motif. The broad signal at ($\delta\approx$ 75.5 ppm) might be the result of this equilibrium. The new peak at $\delta\approx$ 58.12 ppm is proposed to be the LAu(I)STs complex resulting from the reductive elimination process with subsequent coordination with TsS^- .

3.5.8.4. Robustness of Au(I) complex 3.3-11_H

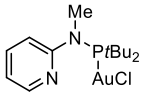

Complex **3.3-11_H** (2 mg, 0.08 mmol) was placed in a screw-cap NMR tube, and a methanol-d4 was added (0.5 mL), followed by the addition of a few µL of 1,3,5-trimethylbenzene, used as an internal standard. A ^1H NMR spectrum of the mixture was recorded at t=0 to determine the relative concentration of the complex with respect to the standard. The solution was then kept at 20°C for 14 days, after which time another ^1H NMR analysis revealed no detectable degradation. The solution was then heated in an oil bath at 60°C and, after 7 days, a ^1H NMR analysis showed a 10% degradation of the complex. The concentration of complex **3.3-11_H** was calculated by comparing the relative integration of the internal standard peaks with those of the product (**Appendix Figures 6.2-24**).

3.6. List of references

(1) Biffis, A.; Centomo, P.; Del Zotto, A.; Zecca, M. Pd Metal Catalysts for Cross-Couplings and Related Reactions in the 21st Century: A Critical Review. *Chem. Rev.* **2018**, *118* (4), 2249–2295. https://doi.org/10.1021/acs.chemrev.7b00443.

(2) Ruiz-Castillo, P.; Buchwald, S. L. Applications of Palladium-Catalyzed C–N Cross-Coupling Reactions. *Chem. Rev.* **2016**, *116* (19), 12564–12649. https://doi.org/10.1021/acs.chemrev.6b00512.

(3) Chen, X.; Engle, K. M.; Wang, D.-H.; Yu, J.-Q. Palladium(II)-Catalyzed C-H Activation/C-C Cross-Coupling Reactions: Versatility and Practicality. *Angew. Chemie Int. Ed.* **2009**, *48* (28), 5094–5115. https://doi.org/10.1002/anie.200806273.

(4) Campeau, L.-C.; Hazari, N. Cross-Coupling and Related Reactions: Connecting Past Success to the Development of New Reactions for the Future. *Organometallics* **2019**, *38* (1), 3–35. https://doi.org/10.1021/acs.organomet.8b00720.

(5) Bratsch, S. G. Standard Electrode Potentials and Temperature Coefficients in Water at 298.15 K. *J. Phys. Chem. Ref. Data* **1989**, *18* (1), 1–21. https://doi.org/10.1063/1.555839.

(6) Nevado, C. Gold Catalysis: Recent Developments and Future Trends. *Chimia (Aarau).* **2010**, *64* (4 SE-Scientific Articles), 247. https://doi.org/10.2533/chimia.2010.247.

(7) Garcia, P.; Malacria, M.; Aubert, C.; Gandon, V.; Fensterbank, L. Gold-Catalyzed Cross-Couplings: New Opportunities for C-C Bond Formation. *ChemCatChem* **2010**, *2* (5), 493–497. https://doi.org/10.1002/cctc.200900319.

(8) Hopkinson, M. N.; Gee, A. D.; Gouverneur, V. Au^{I}/Au^{III} Catalysis: An Alternative Approach for C-C Oxidative Coupling. *Chem. – A Eur. J.* **2011**, *17* (30), 8248–8262. https://doi.org/10.1002/chem.201100736.

(9) Wegner, H. A.; Auzias, M. Gold for C-C Coupling Reactions: A Swiss-Army-Knife Catalyst? *Angew. Chemie Int. Ed.* **2011**, *50* (36), 8236–8247. https://doi.org/10.1002/anie.201101603.

(10) Kar, A.; Mangu, N.; Kaiser, H. M.; Beller, M.; Tse, M. K. A General Gold-Catalyzed Direct Oxidative Coupling of Non-Activated Arenes. *Chem. Commun.* **2008**, No. 3, 386–388. https://doi.org/10.1039/B714928J.

(11) Cui, L.; Zhang, G.; Zhang, L. Homogeneous Gold-Catalyzed Efficient Oxidative Dimerization of Propargylic Acetates. *Bioorg. Med. Chem. Lett.* **2009**, *19* (14), 3884–3887. https://doi.org/10.1016/j.bmcl.2009.03.127.

(12) Zhang, G.; Peng, Y.; Cui, L.; Zhang, L. Gold-Catalyzed Homogeneous Oxidative Cross-Coupling Reactions. *Angew. Chemie Int. Ed.* **2009**, *48* (17), 3112–3115. https://doi.org/10.1002/anie.200900585.

(13) Ball, L. T.; Green, M.; Lloyd-Jones, G. C.; Russell, C. A. Arylsilanes: Application to Gold-Catalyzed Oxyarylation of Alkenes. *Org. Lett.* **2010**, *12* (21), 4724–4727.

https://doi.org/10.1021/ol1019162.

(14) Brenzovich, W. E. J.; Brazeau, J.-F.; Toste, F. D. Gold-Catalyzed Oxidative Coupling Reactions with Aryltrimethylsilanes. *Org. Lett.* **2010**, *12* (21), 4728–4731. https://doi.org/10.1021/ol102194c.

(15) Winston, M. S.; Wolf, W. J.; Toste, F. D. Photoinitiated Oxidative Addition of CF_3I to Gold(I) and Facile Aryl-CF_3 Reductive Elimination. *J. Am. Chem. Soc.* **2014**, *136* (21), 7777–7782. https://doi.org/10.1021/ja503974x.

(16) Liu, S.; Kang, K.; Liu, S.; Wang, D.; Wei, P.; Lan, Y.; Shen, Q. The Difluoromethylated Organogold(III) Complex Cis-[Au(PCy_3)(4-F-C_6H_4)(CF_2H)(Cl)]: Preparation, Characterization, and Its C(sp2)–CF_2H Reductive Elimination. *Organometallics* **2018**, *37* (21), 3901–3908. https://doi.org/10.1021/acs.organomet.8b00579.

(17) Sahoo, B.; Hopkinson, M. N.; Glorius, F. Combining Gold and Photoredox Catalysis: Visible Light-Mediated Oxy- and Aminoarylation of Alkenes. *J. Am. Chem. Soc.* **2013**, *135* (15), 5505–5508. https://doi.org/10.1021/ja400311h.

(18) Shu, X.; Zhang, M.; He, Y.; Frei, H.; Toste, F. D. Dual Visible Light Photoredox and Gold-Catalyzed Arylative Ring Expansion. *J. Am. Chem. Soc.* **2014**, *136* (16), 5844–5847. https://doi.org/10.1021/ja500716j.

(19) Hopkinson, M. N.; Tlahuext-Aca, A.; Glorius, F. Merging Visible Light Photoredox and Gold Catalysis. *Acc. Chem. Res.* **2016**, *49* (10), 2261–2272. https://doi.org/10.1021/acs.accounts.6b00351.

(20) Huang, L.; Rudolph, M.; Rominger, F.; Hashmi, A. S. K. Photosensitizer-Free Visible-Light-Mediated Gold-Catalyzed 1,2-Difunctionalization of Alkynes. *Angew. Chemie Int. Ed.* **2016**, *55* (15), 4808–4813. https://doi.org/10.1002/anie.201511487.

(21) Deng, J.-R.; Chan, W.-C.; Chun-Him Lai, N.; Yang, B.; Tsang, C.-S.; Chi-Bun Ko, B.; Lai-Fung Chan, S.; Wong, M.-K. Photosensitizer-Free Visible Light-Mediated Gold-Catalysed Cis-Difunctionalization of Silyl-Substituted Alkynes. *Chem. Sci.* **2017**, *8* (11), 7537–7544. https://doi.org/10.1039/C7SC02294H.

(22) Xie, J.; Sekine, K.; Witzel, S.; Krämer, P.; Rudolph, M.; Rominger, F.; Hashmi, A. S. K. Light-Induced Gold-Catalyzed Hiyama Arylation: A Coupling Access to Biarylboronates. *Angew. Chemie Int. Ed.* **2018**, *57* (51), 16648–16653. https://doi.org/10.1002/anie.201806427.

(23) Taschinski, S.; Döpp, R.; Ackermann, M.; Rominger, F.; de Vries, F.; Menger, M. F. S. J.; Rudolph, M.; Hashmi, A. S. K.; Klein, J. E. M. N. Light-Induced Mechanistic Divergence in Gold(I) Catalysis: Revisiting the Reactivity of Diazonium Salts. *Angew. Chemie Int. Ed.* **2019**, *58* (47), 16988–16993. https://doi.org/10.1002/anie.201908268.

(24) Dong, B.; Peng, H.; Motika, S. E.; Shi, X. Gold Redox Catalysis through Base-Initiated Diazonium Decomposition toward Alkene, Alkyne, and Allene Activation. *Chem. – A Eur. J.* **2017**, *23* (46), 11093–11099. https://doi.org/10.1002/chem.201701970.

(25) Witzel, S.; Xie, J.; Rudolph, M.; Hashmi, A. S. K. Photosensitizer-Free, Gold-Catalyzed C–C Cross-Coupling of Boronic Acids and Diazonium Salts Enabled by Visible Light. *Adv. Synth. Catal.* **2017**, *359* (9), 1522–1528. https://doi.org/10.1002/adsc.201700121.

(26) Guenther, J.; Mallet-Ladeira, S.; Estevez, L.; Miqueu, K.; Amgoune, A.; Bourissou, D. Activation of Aryl Halides at Gold(I): Practical Synthesis of (P,C) Cyclometalated Gold(III) Complexes. *J. Am. Chem. Soc.* **2014**, *136* (5), 1778–1781. https://doi.org/10.1021/ja412432k.

(27) Marelli, E.; Monot, J.; Martin-Vaca, B.; Mallet-Ladeira, S.; García-Rodeja, Y.; Miqueu, K.; Bourissou, D. Base-Triggered Oxidative Addition to Gold. *Chem. – A Eur. J.* **2023**, *29* (37), e202301091. https://doi.org/10.1002/chem.202301091.

(28) Beucher, H.; Schörgenhumer, J.; Merino, E.; Nevado, C. Chelation-Assisted C–C Bond Activation of Biphenylene by Gold(I) Halides. *Chem. Sci.* **2021**, *12* (45), 15084–15089. https://doi.org/10.1039/D1SC03814A.

(29) Joost, M.; Zeineddine, A.; Estévez, L.; Mallet−Ladeira, S.; Miqueu, K.; Amgoune, A.; Bourissou, D. Facile Oxidative Addition of Aryl Iodides to Gold(I) by Ligand Design: Bending Turns on Reactivity. *J. Am. Chem. Soc.* **2014**, *136* (42), 14654–14657. https://doi.org/10.1021/ja506978c.

(30) Fürstner, A.; Davies, P. W.; Fürstner, A.; Davies, P. W. Catalytic Carbophilic Activation: Catalysis by Platinum and Gold π-Acids. *Angew. Chemie Int. Ed.* **2007**, *46* (19), 3410–3449. https://doi.org/10.1002/ANIE.200604335.

(31) Carvajal, M. A.; Novoa, J. J.; Alvarez, S. Choice of Coordination Number in D10 Complexes of Group 11 Metals. *J. Am. Chem. Soc.* **2004**, *126* (5), 1465–1477. https://doi.org/10.1021/ja038416a.

(32) Crespo, O.; Gimeno, M. C.; Laguna, A.; Jones, P. G. Two-, Three- and Four-Co-Ordinate Gold(I) Complexes of 1,2-Bis(Diphenylphosphino)-1,2-Dicarba-Closo-Dodecaborane. *J. Chem. Soc. Dalt. Trans.* **1992**, No. 10, 1601–1605. https://doi.org/10.1039/DT9920001601.

(33) Joost, M.; Estévez, L.; Miqueu, K.; Amgoune, A.; Bourissou, D. Oxidative Addition of Carbon–Carbon Bonds to Gold. *Angew. Chemie Int. Ed.* **2015**, *54* (17), 5236–5240. https://doi.org/10.1002/anie.201500458.

(34) Harper, M. J.; Arthur, C. J.; Crosby, J.; Emmett, E. J.; Falconer, R. L.; Fensham-Smith, A. J.; Gates, P. J.; Leman, T.; McGrady, J. E.; Bower, J. F.; Russel, C. A. Oxidative Addition, Transmetalation, and Reductive Elimination at a 2,2′-Bipyridyl-Ligated Gold Center. *J. Am. Chem. Soc.* **2018**, *140* (12), 4440–4445. https://doi.org/10.1021/jacs.8b01411.

(35) Cadge, J. A.; Bower, J. F.; Russell, C. A. A Systematic Study of the Effects of Complex Structure on Aryl Iodide Oxidative Addition at Bipyridyl-Ligated Gold(I) Centers. *Angew. Chemie Int. Ed.* **2021**, *60* (47), 24976–24983. https://doi.org/10.1002/anie.202108744.

(36) Cadge, J. A.; Sparkes, H. A.; Bower, J. F.; Russell, C. A. Oxidative Addition of Alkenyl and

Alkynyl Iodides to a Au^{I} Complex. *Angew. Chemie Int. Ed.* **2020**, *59* (16), 6617–6621. https://doi.org/10.1002/anie.202000473.

(37) Serra, J.; Whiteoak, C. J.; Acuña-Parés, F.; Font, M.; Luis, J. M.; Lloret-Fillol, J.; Ribas, X. Oxidant-Free Au(I)-Catalyzed Halide Exchange and Csp^2–O Bond Forming Reactions. *J. Am. Chem. Soc.* **2015**, *137* (41), 13389–13397. https://doi.org/10.1021/jacs.5b08756.

(38) Serra, J.; Parella, T.; Ribas, X. Au(III)-Aryl Intermediates in Oxidant-Free C–N and C–O Cross-Coupling Catalysis. *Chem. Sci.* **2017**, *8* (2), 946–952. https://doi.org/10.1039/C6SC03699F.

(39) Zeineddine, A.; Estévez, L.; Mallet-Ladeira, S.; Miqueu, K.; Amgoune, A.; Bourissou, D. Rational Development of Catalytic Au(I)/Au(III) Arylation Involving Mild Oxidative Addition of Aryl Halides. *Nat. Commun.* **2017**, *8* (1), 565. https://doi.org/10.1038/s41467-017-00672-8.

(40) Lundgren, R. J.; Sappong-Kumankumah, A.; Stradiotto, M. A Highly Versatile Catalyst System for the Cross-Coupling of Aryl Chlorides and Amines. *Chem. – A Eur. J.* **2010**, *16* (6), 1983–1991. https://doi.org/10.1002/chem.200902316.

(41) Rodriguez, J.; Zeineddine, A.; Sosa Carrizo, E. D.; Miqueu, K.; Saffon-Merceron, N.; Amgoune, A.; Bourissou, D. Catalytic Au(I)/Au(III) Arylation with the Hemilabile MeDalphos Ligand: Unusual Selectivity for Electron-Rich Iodoarenes and Efficient Application to Indoles. *Chem. Sci.* **2019**, *10* (30), 7183–7192. https://doi.org/10.1039/C9SC01954E.

(42) Rigoulet, M.; Thillaye du Boullay, O.; Amgoune, A.; Bourissou, D. Gold(I)/Gold(III) Catalysis That Merges Oxidative Addition and π-Alkene Activation. *Angew. Chemie Int. Ed.* **2020**, *59* (38), 16625–16630. https://doi.org/10.1002/anie.202006074.

(43) Tathe, A. G.; Chintawar, C. C.; Bhoyare, V. W.; Patil, N. T. Ligand-Enabled Gold-Catalyzed 1,2-Heteroarylation of Alkenes. *Chem. Commun.* **2020**, *56* (65), 9304–9307. https://doi.org/10.1039/D0CC03707A.

(44) Zhang, S.; Wang, C.; Ye, X.; Shi, X. Intermolecular Alkene Difunctionalization via Gold-Catalyzed Oxyarylation. *Angew. Chemie Int. Ed.* **2020**, *59* (46), 20470–20474. https://doi.org/10.1002/anie.202009636.

(45) Chintawar, C. C.; Yadav, A. K.; Patil, N. T. Gold-Catalyzed 1,2-Diarylation of Alkenes. *Angew. Chemie Int. Ed.* **2020**, *59* (29), 11808–11813. https://doi.org/10.1002/anie.202002141.

(46) Rodriguez, J.; Vesseur, D.; Tabey, A.; Mallet-Ladeira, S.; Miqueu, K.; Bourissou, D. Au(I)/Au(III) Catalytic Allylation Involving π-Allyl Au(III) Complexes. *ACS Catal.* **2022**, *12* (2), 993–1003. https://doi.org/10.1021/acscatal.1c04580.

(47) Holmsen, M. S. M.; Nova, A.; Øien-Ødegaard, S.; Heyn, R. H.; Tilset, M. A Highly Asymmetric Gold(III) η^3-Allyl Complex. *Angew. Chemie Int. Ed.* **2020**, *59* (4), 1516–1520. https://doi.org/10.1002/anie.201912315.

(48) Rodriguez, J.; Szalóki, G.; Sosa Carrizo, E. D.; Saffon-Merceron, N.; Miqueu, K.; Bourissou, D. Gold(III) π-Allyl Complexes. *Angew. Chemie Int. Ed.* **2020**, *59* (4), 1511–1515. https://doi.org/10.1002/anie.201912314.

(49) Bhoyare, V. W.; Sosa Carrizo, E. D.; Chintawar, C. C.; Gandon, V.; Patil, N. T. Gold-Catalyzed Heck Reaction. *J. Am. Chem. Soc.* **2023**, *145* (16), 8810–8816. https://doi.org/10.1021/jacs.3c02544.

(50) Bhoyare V. W.; Tathe A. G; Gandon V.; Patil, N. T.; Unlocking the Chain-Walking Process in Gold Catalysis. *ChemRxiv* **2023**.

(51) Akram, M. O.; Das, A.; Chakrabarty, I.; Patil, N. T. Ligand-Enabled Gold-Catalyzed C(sp2)–N Cross-Coupling Reactions of Aryl Iodides with Amines. *Org. Lett.* **2019**, *21* (19), 8101–8105. https://doi.org/10.1021/acs.orglett.9b03082.

(52) Rodriguez, J.; Adet, N.; Saffon-Merceron, N.; Bourissou, D. Au(I)/Au(III)-Catalyzed C–N Coupling. *Chem. Commun.* **2020**, *56* (1), 94–97. https://doi.org/10.1039/C9CC07666B.

(53) Tathe, A. G.; Urvashi; Yadav, A. K.; Chintawar, C. C.; Patil, N. T. Gold-Catalyzed 1,2-Aminoarylation of Alkenes with External Amines. *ACS Catal.* **2021**, *11* (8), 4576–4582. https://doi.org/10.1021/acscatal.1c00789.

(54) Chen, G.; Xu, B. Hydrogen Bond Donor and Unbalanced Ion Pair Promoter-Assisted Gold-Catalyzed Carbon-Oxygen Cross-Coupling of (Hetero)Aryl Iodides with Alcohols. *ACS Catal.* **2023**, *13* (3), 1823–1829. https://doi.org/10.1021/acscatal.2c05890

(55) Das, A.; Patil, N. T. Ligand-Enabled Gold-Catalyzed C(sp2)–O Cross-Coupling Reactions. *ACS Catal.* **2023**, *13* (6), 3847–3853. https://doi.org/10.1021/acscatal.3c00338.

(56) Li, W.; Lu, Z.; Hammond, G. B.; Xu, B. Unbalanced-Ion-Pair-Catalyzed Nucleophilic Fluorination Using Potassium Fluoride. *Org. Lett.* **2021**, *23* (24), 9640–9644. https://doi.org/10.1021/acs.orglett.1c03887.

(57) McDaniel, J. W.; Stauber, J. M.; Doud, E. A.; Spokoyny, A. M.; Murphy, J. M. An Organometallic Gold(III) Reagent for ^{18}F Labeling of Unprotected Peptides and Sugars in Aqueous Media. *Org. Lett.* **2022**, *24* (28), 5132–5136. https://doi.org/10.1021/acs.orglett.2c01965.

(58) Stauber, J. M.; Rheingold, A. L.; Spokoyny, A. M. Gold(III) Aryl Complexes as Reagents for Constructing Hybrid Peptide-Based Assemblies via Cysteine S-Arylation. *Inorg. Chem.* **2021**, *60* (7), 5054–5062. https://doi.org/10.1021/acs.inorgchem.1c00087.

(59) Messina, M. S.; Stauber, J. M.; Waddington, M. A.; Rheingold, A. L.; Maynard, H. D.; Spokoyny, A. M. Organometallic Gold(III) Reagents for Cysteine Arylation. *J. Am. Chem. Soc* **2018**, *140*, 7. https://doi.org/10.1021/jacs.8b04115.

(60) Doud, E.; Tilden, J.; Treacy, J.; Chao, E.; Montgomery, H.; Kunkel, G.; Adhami, N.; Kerr, T.; Rheingold, A.; Frost, C.; Houk, K.; Maynard, H.; Spokoyny, A. Breaking Kinetic Record for Cysteine Bioconjugation with Organometallic Reagents. *ChemRxiv* **2023**.

(61) Mudshinge, S. R.; Yang, Y.; Xu, B.; Hammond, G. B.; Lu, Z. Gold (I/III)-Catalyzed Trifluoromethylthiolation and Trifluoromethylselenolation of Organohalides. *Angew. Chemie Int. Ed.* **2022**, *61* (12), e202115687. https://doi.org/10.1002/anie.202115687.

(62) Tathe, A. G.; Patil, N. T. Ligand-Enabled Gold-Catalyzed C(sp2)–S Cross-Coupling Reactions. *Org. Lett.* **2022**, *24* (24), 4459–4463. https://doi.org/10.1021/acs.orglett.2c01692.

(63) Patil, N. T.; Sancheti, S.P.; Singh, Y.; Mane, M. V. Gold-Catalyzed 1,2-Dicarbofunctionalization of Alkynes. *ChemRxiv* **2023**.

(64) Ye, X.; Wang, C.; Zhang, S.; Tang, Q.; Wojtas, L.; Li, M.; Shi, X. Chiral Hemilabile P,N-Ligand-Assisted Gold Redox Catalysis for Enantioselective Alkene Aminoarylation. *Chem. – A Eur. J.* **2022**, *28* (34), e202201018. https://doi.org/10.1002/chem.202201018.

(65) Chintawar, C. C.; Bhoyare, V. W.; Mane, M. V; Patil, N. T. Enantioselective Au(I)/Au(III) Redox Catalysis Enabled by Chiral (P,N)-Ligands. *J. Am. Chem. Soc.* **2022**, *144* (16), 7089–7095. https://doi.org/10.1021/jacs.2c02799.

(66) Font, P.; Valdés, H.; Guisado-Barrios, G.; Ribas, X. Hemilabile MIC^N Ligands Allow Oxidant-Free Au(I)/Au(III) Arylation-Lactonization of γ-Alkenoic Acids. *Chem. Sci.* **2022**, *13* (32), 9351–9360. https://doi.org/10.1039/D2SC01966C.

(67) Gao, P.; Xu, J.; Zhou, T.; Liu, Y.; Bisz, E.; Dziuk, B.; Lalancette, R.; Szostak, R.; Zhang, D.; Szostak, M. L-Shaped Heterobidentate Imidazo[1,5-a]Pyridin-3-Ylidene (N,C)-Ligands for Oxidant-Free Au^{I}/Au^{III} Catalysis. *Angew. Chemie Int. Ed.* **2023**, *62* (12), e202218427. https://doi.org/10.1002/anie.202218427.

(68) Scott, S. C.; Cadge, J. A.; Boden, G. K.; Bower, J. F.; Russell, C. A. A Hemilabile NHC-Gold Complex and Its Application to the Redox Neutral 1,2-Oxyarylation of Feedstock Alkenes. *Angew. Chemie Int. Ed.* **2023**, *62* (23), e202301526. https://doi.org/10.1002/anie.202301526.

(69) Chu, J.; Munz, D.; Jazzar, R.; Melaimi, M.; Bertrand, G. Synthesis of Hemilabile Cyclic (Alkyl)(Amino)Carbenes (CAACs) and Applications in Organometallic Chemistry. *J. Am. Chem. Soc.* **2016**, *138* (25), 7884–7887. https://doi.org/10.1021/jacs.6b05221.

(70) Reiersølmoen, A. C.; Battaglia, S.; Orthaber, A.; Lindh, R.; Erdélyi, M.; Fiksdahl, A. P,N-Chelated Gold(III) Complexes: Structure and Reactivity. *Inorg. Chem.* **2021**, *60* (5), 2847–2855. https://doi.org/10.1021/acs.inorgchem.0c02720.

(71) Navarro, M.; Tabey, A.; Szalóki, G.; Mallet-Ladeira, S.; Bourissou, D. Stable Au(III) Complexes Bearing Hemilabile P^N and C^N Ligands: Coordination of the Pendant Nitrogen upon Oxidation of Gold. *Organometallics* **2021**, *40* (11), 1571–1576. https://doi.org/10.1021/acs.organomet.1c00258.

(72) Szalóki, G.; Babinot, J.; Martin-Diaconescu, V.; Mallet-Ladeira, S.; García-Rodeja, Y.; Miqueu, K.; Bourissou, D. Ligand-Enabled Oxidation of Gold(I) Complexes with o-Quinones. *Chem. Sci.* **2022**, *13* (35), 10499–10505. https://doi.org/10.1039/D2SC03724F.

(73) Genoux, A.; Biedrzycki, M.; Merino, E.; Rivera-Chao, E.; Linden, A.; Nevado, C. Synthesis and Characterization of Bidentate (P^N)Gold(III) Fluoride Complexes: Reactivity Platforms for Reductive Elimination Studies. *Angew. Chemie Int. Ed.* **2021**, *60* (8), 4164–4168. https://doi.org/10.1002/anie.202009359.

(74) Cadge, J. A.; Gates, P. J.; Bower, J. F.; Russell, C. A. Migratory Insertion of CO into a Au–C Bond. *J. Am. Chem. Soc.* **2022**, *144* (43), 19719–19725. https://doi.org/10.1021/jacs.2c10432.

(75) Rodriguez, J.; Tabey, A.; Mallet-Ladeira, S.; Bourissou, D. Oxidative Additions of Alkynyl/Vinyl Iodides to Gold and Gold-Catalyzed Vinylation Reactions Triggered by the MeDalphos Ligand. *Chem. Sci.* **2021**, *12* (22), 7706–7712. https://doi.org/10.1039/D1SC01483H.

(76) Gopalakrishnan, J. Aminophosphines: Their Chemistry and Role as Ligands and Synthons. *Appl. Organomet. Chem.* **2009**, *23* (8), 291–318. https://doi.org/https://doi.org/10.1002/aoc.1515.

(77) Dorta, R.; Stevens, E. D.; Scott, N. M.; Costabile, C.; Cavallo, L.; Hoff, C. D.; Nolan, S. P. Steric and Electronic Properties of N-Heterocyclic Carbenes (NHC): A Detailed Study on Their Interaction with $Ni(CO)_4$. *J. Am. Chem. Soc.* **2005**, *127* (8), 2485–2495. https://doi.org/10.1021/ja0438821.

(78) Rigoulet, M.; Miqueu, K.; Bourissou, D. Mechanistic Insights about the Ligand-Enabled Oxy-Arylation/Vinylation of Alkenes via Au(I)/Au(III) Catalysis. *Chem. – A Eur. J.* **2022**, *28* (60), e202202110. https://doi.org/10.1002/chem.202202110.

(79) Navarro, M.; Toledo, A.; Joost, M.; Amgoune, A.; Mallet-Ladeira, S.; Bourissou, D. π Complexes of P^P and P^N Chelated Gold(I). *Chem. Commun.* **2019**, *55* (55), 7974–7977. https://doi.org/10.1039/C9CC04266K.

(80) Navarro, M.; Toledo, A.; Mallet-Ladeira, S.; Sosa Carrizo, E. D.; Miqueu, K.; Bourissou, D. Versatility and Adaptative Behaviour of the P^N Chelating Ligand MeDalphos within Gold(i) π Complexes. *Chem. Sci.* **2020**, *11* (10), 2750–2758. https://doi.org/10.1039/C9SC06398F.

(81) Neese, F. The ORCA Program System. *WIREs Comput. Mol. Sci.* **2012**, *2* (1), 73–78. https://doi.org/10.1002/wcms.81.

(82) Neese, F. Software Update: The ORCA Program System, Version 4.0. *WIREs Comput. Mol. Sci.* **2018**, *8* (1), e1327. https://doi.org/10.1002/wcms.1327.

(83) Bursch, M.; Mewes, J.-M.; Hansen, A.; Grimme, S. Best-Practice DFT Protocols for Basic Molecular Computational Chemistry. *Angew. Chemie Int. Ed.* **2022**, *61* (42), e202205735. https://doi.org/10.1002/anie.202205735.

(84) Grimme, S.; Hansen, A.; Ehlert, S.; Mewes, J.-M. R2SCAN-3c: A “Swiss Army Knife” Composite Electronic-Structure Method. *J. Chem. Phys.* **2021**, *154* (6), 64103. https://doi.org/10.1063/5.0040021.

(85) Dohm, S.; Hansen, A.; Steinmetz, M.; Grimme, S.; Checinski, M. P. Comprehensive Thermochemical Benchmark Set of Realistic Closed-Shell Metal Organic Reactions. *J. Chem. Theory Comput.* **2018**, *14* (5), 2596–2608. https://doi.org/10.1021/acs.jctc.7b01183.

(86) Kung, K. K.-Y.; Ko, H.-M.; Cui, J.-F.; Chong, H.-C.; Leung, Y.-C.; Wong, M.-K. Cyclometalated Gold(III) Complexes for Chemoselective Cysteine Modification via Ligand Controlled C–S Bond-Forming Reductive Elimination. *Chem. Commun.* **2014**, *50* (80), 11899–11902. https://doi.org/10.1039/C4CC04467C.

(87) Currie, L.; Rocchigiani, L.; Hughes, D. L.; Bochmann, M. Carbon–Sulfur Bond Formation by Reductive Elimination of Gold(III) Thiolates. *Dalt. Trans.* **2018**, *47* (18), 6333–6343. https://doi.org/10.1039/C8DT00906F.

(88) Peng, H.; Cai, R.; Xu, C.; Chen, H.; Shi, X. Nucleophile Promoted Gold Redox Catalysis with Diazonium Salts: C–Br, C–S and C–P Bond Formation through Catalytic Sandmeyer Coupling. *Chem. Sci.* **2016**, *7* (9), 6190–6196. https://doi.org/10.1039/C6SC01742H.

(89) Caballero-Muñoz, A.; Rosas-Ortega, M.; Díaz-Salazar, H.; Porcel, S. C–S Cross-Coupling of Aryldiazonium Salts with Thiols Mediated by Gold. *European J. Org. Chem.* **2023**, *26* (30), e202300203. https://doi.org/10.1002/ejoc.202300203.

(90) Kepp, K. P. A Quantitative Scale of Oxophilicity and Thiophilicity. *Inorg. Chem.* **2016**, *55* (18), 9461–9470. https://doi.org/10.1021/acs.inorgchem.6b01702.

(91) Beletskaya, I. P.; Ananikov, V. P. Transition-Metal-Catalyzed C–S, C–Se, and C–Te Bond Formations via Cross-Coupling and Atom-Economic Addition Reactions. Achievements and Challenges. *Chem. Rev.* **2022**, *122* (21), 16110–16293. https://doi.org/10.1021/acs.chemrev.1c00836.

(92) Kanemoto, K.; Furuhashi, K.; Morita, Y.; Komatsu, T.; Fukuzawa, S. Acid-Mediated Sulfonylthiolation of Arenes via Selective Activation of SS-Morpholino Dithiosulfonate. *Org. Lett.* **2021**, *23* (5), 1582–1587. https://doi.org/10.1021/acs.orglett.0c04289.

(93) Jiang, Y.-F.; Zhu, W.-C.; Liu, X.-Y.; Tian, S.-Y.; Han, J.-H.; Rao, W.; Shen, S.-S.; Sheng, D.; Wang, S.-Y. Synthesis of 1,3-Dibenzenesulfonylpolysulfane (DBSPS) and Its Application in the Preparation of Aryl Thiosulfonates from Boronic Acids. *Org. Lett.* **2023**, *25* (10), 1776–1781. https://doi.org/10.1021/acs.orglett.3c00526.

(94) Reeves, J. T.; Camara, K.; Han, Z. S.; Xu, Y.; Lee, H.; Busacca, C. A.; Senanayake, C. H. The Reaction of Grignard Reagents with Bunte Salts: A Thiol-Free Synthesis of Sulfides. *Org. Lett.* **2014**, *16* (4), 1196–1199. https://doi.org/10.1021/ol500067f.

(95) Chen, X.-Y.; Pu, M.; Cheng, H.-G.; Sperger, T.; Schoenebeck, F. Arylation of Axially Chiral Phosphorothioate Salts by Dinuclear PdI Catalysis. *Angew. Chemie Int. Ed.* **2019**, *58* (33), 11395–11399. https://doi.org/10.1002/anie.201906063.

(96) Römbke, P.; Schier, A.; Wiesbrock, F.; Schmidbaur, H. Gold(I) Thiosulfonate Complexes. *Inorganica Chim. Acta* **2003**, *347*, 123–128. https://doi.org/10.1016/S0020-

1693(02)01445-7.

(97) Zheng, H.; Fan, Y.; Song, Y.; Chen, J. S.; You, E.; Labalme, S.; Lin, W. Site Isolation in Metal–Organic Layers Enhances Photoredox Gold Catalysis. *J. Am. Chem. Soc.* **2022**, *144* (24), 10694–10699. https://doi.org/10.1021/jacs.2c03062.

(98) Peterson, L. J.; Wolfe, J. P. Palladium-Catalyzed Alkene Carboamination Reactions of Electron-Poor Nitrogen Nucleophiles. *Adv. Synth. Catal.* **2015**, *357* (10), 2339–2344. https://doi.org/10.1002/adsc.201500334.

(99) Qi, X.; Zhou, R.; Peng, J.-B.; Ying, J.; Wu, X.-F. Selenium-Catalyzed Carbonylative Synthesis of 2-Benzimidazolones from 2-Nitroanilines with TFBen as the CO Source. *European J. Org. Chem.* **2019**, *2019* (31–32), 5161–5164. https://doi.org/10.1002/ejoc.201801739.

(100) Zhang, Z.; Niwa, T.; Watanabe, K.; Hosoya, T. 11C-Cyanation of Aryl Fluorides via Nickel and Lithium Chloride-Mediated C−F Bond Activation. *Angew. Chemie Int. Ed.* **2023**, *62* (22), e202302956. https://doi.org/10.1002/anie.202302956.

(101) Finck, L.; Oestreich, M. Transition-Metal-Free Coupling of Polyfluorinated Arenes and Functionalized, Masked Aryl Nucleophiles. *Chem. – A Eur. J.* **2021**, *27* (43), 11061–11064. https://doi.org/10.1002/chem.202101731.

(102) Kim, S.; Goldfogel, M. J.; Gilbert, M. M.; Weix, D. J. Nickel-Catalyzed Cross-Electrophile Coupling of Aryl Chlorides with Primary Alkyl Chlorides. *J. Am. Chem. Soc.* **2020**, *142* (22), 9902–9907. https://doi.org/10.1021/jacs.0c02673.

(103) Yeh, M.-C. P.; Yeh, W.-J.; Tu, L.-H.; Wu, J.-R. $CeCl_3 \cdot 7H_2O$–NaI Catalyzed Intramolecular Addition Reactions of 7-Hydroxy-1,3-Dienes: A Facile Approach to Hexahydrobenzofurans and Tetrahydrofurans. *Tetrahedron* **2006**, *62* (31), 7466–7470. /https://doi.org/10.1016/j.tet.2006.05.026.

(104) Qiu, S.; Wei, Y.; Liu, G. Palladium-Catalyzed Intramolecular Hydroamination of Allenes Coupled to Aerobic Alcohol Oxidation. *Chem. – A Eur. J.* **2009**, *15* (12), 2751–2754. https://doi.org/10.1002/chem.200802381.

(105) Yang, B.; Zhang, X.-Y.; Yue, H.-Q.; Li, W.-Z.; Li, M.; Lu, L.; Wu, Z.-Q.; Li, J.; Sun, K.; Yang, S.-D. A Promoter-Free Protocol for the Synthesis of Selenophosphates and Thiophosphates via a Spontaneous Process at Room Temperature. *Adv. Synth. Catal.* **2022**, *364* (20), 3528–3538. https://doi.org/10.1002/adsc.202200625.

(106) Raghuvanshi, D. S.; Verma, N. An Iodine-Mediated New Avenue to Sulfonylation Employing N-Hydroxy Aryl Sulfonamide as a Sulfonylating Agent. *Org. Biomol. Chem.* **2021**, *19* (21), 4760–4767. https://doi.org/10.1039/D1OB00036E.

(107) Cai, W.; Gu, Z. Selective Ortho Thiolation Enabled by Tuning the Ancillary Ligand in Palladium/Norbornene Catalysis. *Org. Lett.* **2019**, *21* (9), 3204–3209. https://doi.org/10.1021/acs.orglett.9b00923.

(108) Zhang, X.; Cui, T.; Zhang, Y.; Gu, W.; Liu, P.; Sun, P. Electrochemical Oxidative Cross-

Coupling Reaction to Access Unsymmetrical Thiosulfonates and Selenosulfonates. *Adv. Synth. Catal.* **2019**, *361* (9), 2014–2019. https://doi.org/10.1002/ADSC.201900047.

(109) Kanemoto, K.; Yoshida, S.; Hosoya, T. Synthesis of Alkynyl Sulfides by Copper-Catalyzed Thiolation of Terminal Alkynes Using Thiosulfonates. *Org. Lett.* **2019**, *21* (9), 3172–3177. https://doi.org/10.1021/acs.orglett.9b00875.

(110) Wang, D.; He, Q.; Shi, K.; Xiong, M.; Zhou, Y.; Pan, Y. Transition-Metal-Free Synthesis of Unsymmetrical Disulfides via Three-Component Reaction of Thiosulfonates, Thiourea and Alkyl Halides. *Adv. Synth. Catal.* **2021**, *363* (11), 2767–2772. https://doi.org/10.1002/ADSC.202100165.

(111) Huang, C. M.; Li, J.; Wang, S. Y.; Ji, S. J. TFA Promoted Multi-Component Reaction of Aryldiazonium with Sodium Metabisulphite and Thiols: Construction of Thiosulfonate under Transition-Metal Free Conditions. *Chinese Chem. Lett.* **2020**, *31* (7), 1923–1926. https://doi.org/10.1016/J.CCLET.2019.12.032.

(112) Taniguchi, N. Unsymmetrical Disulfide and Sulfenamide Synthesis via Reactions of Thiosulfonates with Thiols or Amines. *Tetrahedron* **2017**, *73* (15), 2030–2035. https://doi.org/10.1016/j.tet.2017.02.047.

(113) Suga, S.; Matsumoto, K.; Ueoka, K.; Yoshida, J. Indirect Cation Pool Method. Rapid Generation of Alkoxycarbenium Ion Pools from Thioacetals. *J. Am. Chem. Soc.* **2006**, *128* (24), 7710–7711. https://doi.org/10.1021/ja0625778.

(114) Liu, S.; Qi, Z.; Zhang, Z.; Qian, B. Iodine/Manganese Dual Catalysis for Oxidative Dehydrogenation Coupling of Amines with Thiols. *Org. Lett.* **2019**, *21* (19), 7722–7725. https://doi.org/10.1021/acs.orglett.9b02545.

(115) Wang, L.; Cornella, J. A Unified Strategy for Arylsulfur(VI) Fluorides from Aryl Halides: Access to Ar-SOF_3 Compounds. *Angew. Chemie Int. Ed.* **2020**, *59* (52), 23510–23515. https://doi.org/10.1002/anie.202009699.

(116) Kordnezhadian, R.; Zogu, A.; Borgarelli, C.; Van Lommel, R.; Demaerel, J.; De Borggraeve, W. M.; Ismalaj, E. De-Risking S-F Bond Formation: A Gas Cylinder-Free Strategy to Access S(IV) and S(VI) Fluorinated Compounds. *Chem. – A Eur. J.* **2023**, *29* (39), e202300361. /https://doi.org/10.1002/chem.202300361.

(117) Luo, Z.; Yang, X.; Tsui, G. C. Perfluoroalkylation of Thiosulfonates: Synthesis of Perfluoroalkyl Sulfides. *Org. Lett.* **2020**, *22* (15), 6155–6159. https://doi.org/10.1021/acs.orglett.0c02235.

(118) Shen, F.; Zheng, H.; Xue, X.-S.; Lu, L.; Shen, Q. Transition-Metal-Free Ipso-Trifluoromethylthiolation of Lithium Aryl Boronates. *Org. Lett.* **2019**, *21* (16), 6347–6351. https://doi.org/10.1021/acs.orglett.9b02236.

(119) Xiao, F.; Tang, M.; Huang, H.; Deng, G.-J. Site-Selective Synthesis of Aryl Sulfides via Oxidative Aromatization of Cyclohexanones with Thiophenols. *J. Org. Chem.* **2022**, *87* (1), 512–523. https://doi.org/10.1021/acs.joc.1c02530.

(120) Feng, Q.; Huang, H.; Sun, J. Ru-Catalyzed [3 + 2] Cycloaddition of Nitrile Oxides and Electron-Rich Alkynes with Reversed Regioselectivity. *Org. Lett.* **2021**, *23* (7), 2431–2436. https://doi.org/10.1021/acs.orglett.1c00273.

(121) Gao, Y.; Sparascio, S.; Terlizzi, L. Di; Serra, M.; Yue, G.; Lu, Y.; Fagnoni, M.; Zhao, X.; Protti, S. Synthesis of Aryl Thiocyanates and Aryl Selenocyanates via Visible-Light Activation of Arylazo Sulfones. *Adv. Synth. Catal.* **2023**, *365* (7), 1082–1087. https://doi.org/10.1002/adsc.202300008.

4. Chapter 4. Conclusion and outlook

The research described in this thesis opens up an avenue for possible future explorations and developments in the field of gold chemistry. In **Chapter 2**, we successfully demonstrated the use of tri-(*ortho*-biaryl)phosphine ligands in Au(I) chemistry, providing an innovative alternative to previous methods that relied primarily relied on supramolecular ligands. Our findings indicate that a more straightforward ligand design can yield selectivity on par with, or even exceeding, that of more intricate supramolecular structures.

The importance of this discovery is underscored by the common observation[1] that Au^+ typically serves as an electronic intermediary between the ligand and reacting enynes, a phenomenon that leads to a diverse product range dictated by substrate substituents rather than the catalyst or ligand. What underscores the significance of this discovery is the general understanding that Au^+ functions as an electronic buffer between the ligand and reacting enynes. This phenomenon orchestrates a broad array of products guided by the substrate's substituents, rather than the catalyst or ligand itself. Our investigation contributes to a contemporary shift in the field, where catalyst confinement has become a central research theme. The confinement achieved through our simpler ligand design is therefore a noteworthy and promising advance, potentially simplifying procedures and broadening the application of gold catalysis.

However, these ligands present certain limitations, mostly related to their specific cone-shaped geometry. While well-suited for linear Au(I) complexes, where they effectively translate the necessary steric information along the ligand-metal (L-Au) axis, they may not be compatible with other metals exhibiting geometries such as tetrahedral or octahedral.

Despite these constraints, the ligands offer ample unexplored opportunities for use and modification. For example, we have demonstrated the potential for various substitutions on the aromatic rings of the phosphines. The studied substitutions have not been directly involved in chemical reactions, leaving open the possibility for using specific functional groups instead of mere placeholders (**Scheme 4-1, A**), thereby creating bifunctional ligands capable of facilitating unique reactions.

An illustrative example of this innovative strategy was recently demonstrated by Zhang and Qian, who employed a chiral bifunctional phosphine ligand to selectively form products with good yields and exceptional enantioselectivity (**Scheme 4-1, B**).[2] In this research, the scientists employed a chiral bifunctional phosphine ligand **4-1** to selectively achieve the formation of products **4-2** with good yields and excellent enantioselectivity. The pivotal element in this breakthrough, as proposed by the researchers, was the cooperative interaction between the metal and the tertiary amine group within the ligand. This collaboration facilitated the asymmetric catalytic deprotonation of the propargylic C–H bond.

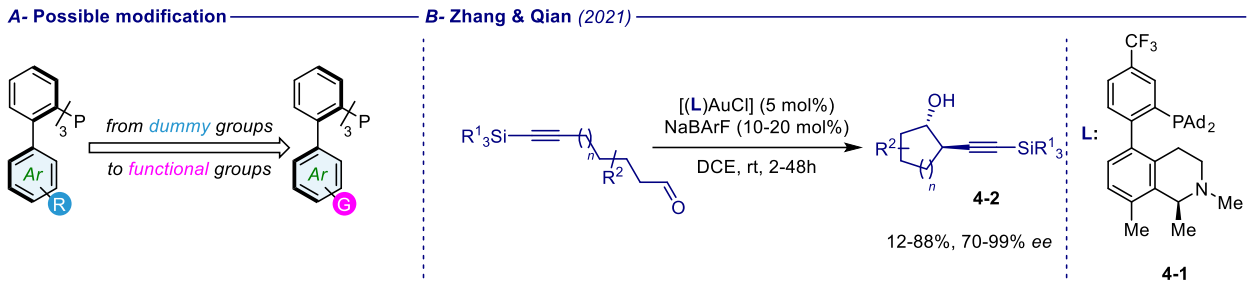

Scheme 4-1. Possible modifications, inspired by the work of Zhang & Qian.

Beyond these preliminary explorations, the potential to modify one, two, or all three aryl rings of the developed tri-(*ortho*-biaryl)phosphine ligands adds yet another layer of complexity and opportunity. These alterations might significantly impact the reactivity of corresponding gold complexes, broadening their applicability. The introduction of chiral functional groups could open doors to enantioselective reactions, further enhancing the utility of these ligands.

Another intriguing aspect of these ligands is their potential application in stabilizing otherwise unstable or highly reactive intermediates. This concept was highlighted during the preparation of our manuscript when interesting research by Campos and Navarro was published.[3] In their study, they utilized a similar tri-(ortho-biaryl)phosphine ligand to stabilize a gold(I)−ethylene π-complex **4-3** (**Scheme 4-2, A**). They found that the use of a bulky ligand was crucial for stabilization, as attempts to prepare the related $[(Ph_3P)Au\text{-}(C_2H_4)]^+$ complex resulted in immediate decomposition, forming $[(PPh_3)_2Au]^+$ and Au(0). They attributed this phenomenon to the inability of the relatively small PPh_3 ligand to stabilize the corresponding Au(I)−ethylene adduct towards bimolecular decomposition.

Furthermore, the researchers illustrated how this bulky tri-(*ortho*-biaryl)phosphine ligand could be deployed in the Au(I)-catalyzed hydroamination of ethylene by imidazolidine-2-one to form product **4-4** in excellent yield (**Scheme 4-2, B**). This example underscores the broad applicability and potential of the ligands, not only in stabilizing complex structures but also in catalyzing specific reactions.

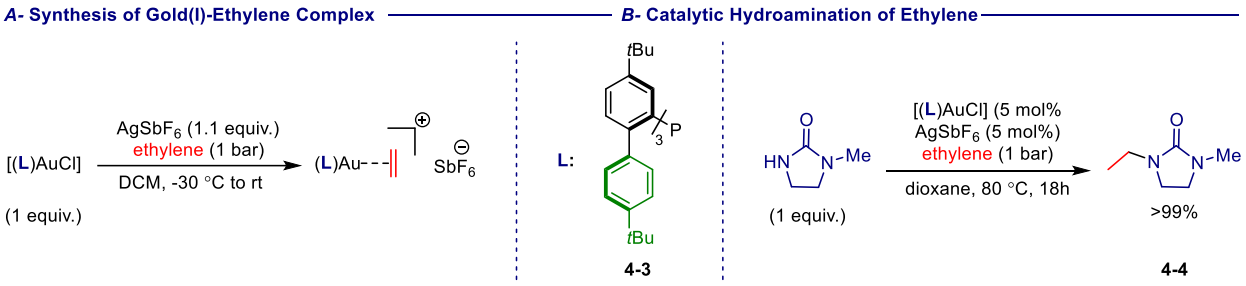

Scheme 4-2. Example of stabilization of reactive species.

The possibility of substituting the ortho-aryl moiety of the phosphine ligand with a more flexible structure, such as cyclohexane, represents yet another compelling avenue for exploration (**Scheme 4-3**). By introducing this structural alteration, the system could gain greater flexibility,

allowing it to change its conformation to a certain extent, while preserving its overall geometry. This adjustment could enhance compatibility with specific substrates and reactions.

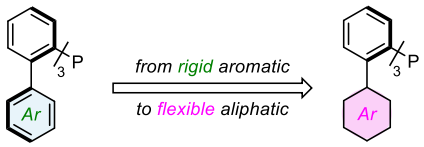

Scheme 4-3. Flexible structure.

By manipulating the number of substitutions, such as changing one or more ortho-aryl rings within the ligand's framework, it is feasible to fine-tune the ligand's flexibility. Furthermore, incorporating an aliphatic ring in place of the ortho-aryl group could facilitate the introduction of chiral substituents. This modification could lead to the execution of enantioselective reactions, broadening the application scope of these ligands and potentially offering new opportunities for innovation within the field of catalysis.

In summary, the research presented in **Chapter 2** opens up the possibilities for further innovation and discovery in this field. In conclusion, the tri-(*ortho*-biaryl)phosphine ligands offer a rich landscape for exploration and adaptation. Whether through subtle modifications to increase reactivity, introducing chiral functionality for enantioselective reactions, or employing the ligands to stabilize reactive intermediates, the possibilities for advancing the field of gold catalysis are manifold and promising.

In **Chapter 3**, we explored a new family of hemilabile bidentate (P^N) ligands, distinct from MeDalPhos, with the ability to facilitate C(sp^2)-I oxidative addition to the Au(I) center . This was achieved by replacing the Me_2NAr portion of MeDalPhos with a 2-NMe pyridine moiety, thereby increasing the ligand's hemilability and allowing for greater structural and electronic flexibility. These innovative ligands performed as well as or better than MeDalPhos in a range of model reactions and alkene arylation reactions. Furthermore, their utility was highlighted in performing the thiotosylation of aryl iodides, an unprecedented metal-catalyzed C-S cross-coupling reaction, in which they enabled high yields even at a catalyst loading of as little as 0.3 mol % of the relevant Au(I)-complex.

The potential future work on these ligands extends far, allowing for detailed investigations in both the modification of the core ligand and applications with gold as well as other metals. The application of (P^N) ligands in chiral catalysis is a well-established practice,[4] thereby providing numerous architectural possibilities to delve into with respect to Au(I)/Au(III) catalysis. What is surprising is the lack of research exploring this phosphaneyl architecture, a gap likely stemming from the prevailing belief that these ligands would be unstable due to the presence of the N-P bond. Our research challenges this notion, demonstrating remarkable stability of these ligands even in methanol at 60 ◦C. This key finding may inspire additional development and application of this unique architectural approach.

Additionally, we described a new C-S coupling reaction that distinguishes itself from conventional methods. Specifically, this reaction cannot be accomplished using traditional palladium catalysis, often the first option considered for developing a cross-coupling reaction. This result highlights the orthogonality between gold and palladium catalysis, potentially motivating other researchers to seek out distinctive Au-catalyzed cross-coupling reactions.

Moreover, we have uncovered a broad and rich reactivity of the thiotosylation products, a field that has surprisingly been given little attention in terms of synthesis procedures and exploration of reactivity. We have demonstrated that these products can act as valuable building blocks for accessing a wide variety of sulfur-containing molecules, including those of significant medicinal interest. The novelty of these findings may indeed ignite further development and study of these intriguing molecules. Future work in this field could include new approaches to establish these molecules as routinely used in modern synthesis, since they might serve as viable alternatives to thiols, which are notoriously for their unpleasant odor.

Furthermore, our research has also underlined a critical factor known as the "silver effect" within the context of Au(I)/Au(III) catalysis. We discovered that the role of silver is not merely to abstract a halide from the gold complex. Rather, silver serves a dual function by also freeing the Au(I) species from the nucleophile, enabling it to undergo oxidative addition with aryl iodide. This finding enhances our comprehension of crucial steps in Au(I)/Au(III) catalysis and may lead to a deeper understanding of the underlying mechanisms.

This also brings attention to one of the major limitations in Au(I)/Au(III) chemistry, which is the dependence on stoichiometric quantities of silver salts. The utilization of silver not only contributes to the overall cost but can also pose challenges in terms of environmental sustainability. Future avenues of research should, therefore, focus on identifying economical and environmentally friendly alternatives to silver salts. However, our study emphasizes that any such alternatives must meet specific criteria. They must be able not only to abstract the halide from the gold complex but also to liberate the Au(I) species from the nucleophile. This dual functionality is essential and may guide the design and synthesis of new reagents that can emulate the unique role played by silver in these reactions, paving the way for innovative advances in this field of chemistry.

Our investigations have further demonstrated that the newly developed ligands, possessing a more electron-withdrawing character compared to the conventional MeDalPhos, facilitate the reductive elimination process. This feature might prove essential for certain applications. Specifically, we draw attention to recent findings in Patil's work (**Scheme 4-4**),[5] where the researchers encountered an unexpected necessity for an electronically poor iodoarene to facilitate the reductive elimination step from electron-rich organogold(III) alkoxide complexes **4-5**. This observation contrasts sharply with the common preference for electron-rich iodoarenes in cross-coupling reactions mediated by Au(I)/Au(III) catalysis. It might be possible that employing more electron-withdrawing ligands would facilitate this reaction and promote the subsequent development of this field.

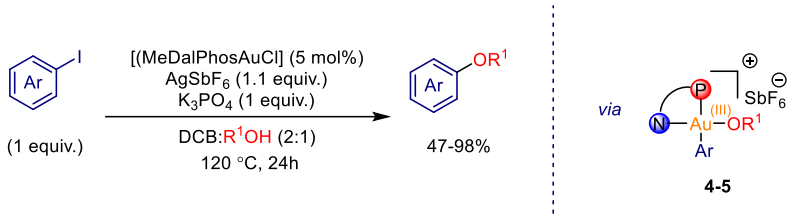

Scheme 4-4. Gold-catalyzed C(sp2)-O cross-coupling.

Our research on the properties and functionality of a new family of hemilabile bidentate (P^N) ligands demonstrates their exceptional stability, versatility, and ability to catalyze previously unattainable reactions. These findings, detailed in an evolving field of Au(I)/Au(III) catalysis, open new avenues of exploration, shed light on the underlying mechanisms, and pave the way for innovative applications in various chemical fields. A notable aspect is the diverse role of silver and the potential of thiotosylation products, which make a contribution to this field by proposing alternatives to traditional compounds and revealing hidden aspects of catalysis.

4.1. Claims to Original Research

- Development of tri-(*ortho*-biaryl)phosphine ligands and corresponding gold complexes to create confined reaction spaces.
- Successful achievement of a variety of ligand-induced effects, including increased or reversed selectivity, substrate selection, control of *E/Z* selectivity, regioselective reactions and protection of reaction sites.

- Development of a new family of ligands for Au(I)/Au(III) catalysis
- Extensive mechanistic studies on Au(I)/Au(III) catalysis that provide new insights.
- Discovery and development of a novel gold-catalyzed thiotosylation cross-coupling reaction.
- Investigative studies on the previously unexplored silver effect in Au(I)/Au(III) catalysis.
- Achievement of the highest reported turnover number (TON) in the Au(I)/Au(III) catalysis that reaches up to 310.

4.2. List of references

(1) Mato, M.; Franchino, A.; García-Morales, C.; Echavarren, A. M. Gold-Catalyzed Synthesis of Small Rings. *Chem. Rev.* **2021**, *121* (14), 8613–8684. https://doi.org/10.1021/acs.chemrev.0c00697.

(2) Li, T.; Cheng, X.; Qian, P.; Zhang, L. Gold-Catalysed Asymmetric Net Addition of Unactivated Propargylic C–H Bonds to Tethered Aldehydes. *Nat. Catal.* **2021**, *4* (2), 164–171. https://doi.org/10.1038/s41929-020-00569-8.

(3) Navarro, M.; Alférez, M. G.; de Sousa, M.; Miranda-Pizarro, J.; Campos, J. Dicoordinate Au(I)–Ethylene Complexes as Hydroamination Catalysts. *ACS Catal.* **2022**, *12* (7), 4227–4241. https://doi.org/10.1021/acscatal.1c05823.

(4) Biswas, A.; Pan, S.; Samanta, R. Cu(II)-Catalyzed Construction of Heterobiaryls Using 1-Diazonaphthoquinones: A General Strategy for the Synthesis of QUINOX and Related P,N Ligands. *Org. Lett.* **2022**, *24* (8), 1631–1636. https://doi.org/10.1021/acs.orglett.2c00127.

(5) Das, A.; Patil, N. T. Ligand-Enabled Gold-Catalyzed C(sp^2)–O Cross-Coupling Reactions. *ACS Catal.* **2023**, *13* (6), 3847–3853. https://doi.org/10.1021/acscatal.3c00338.

5. Publications and presentations

5.1. Publications of work in this thesis

Muratov, K.; Zaripov, E.; Berezovski, M. V.; Gagosz, F. "DFT-guided Development of New Hemilabile (P^N) Ligands for Gold-(I/III) RedOx Catalysis : Application to the Thiotosylation of Aryl Iodides."*J. Am. Chem. Soc.* **2024***, 146* (6), 3660–3674

Muratov, K.; F. Gagosz, F. Confinement-Induced Selectivities in Gold(I) Catalysis—The Benefit of Using Bulky Tri-(ortho-biaryl)phosphine Ligands. *Angew. Chem. Int. Ed*. **2022**, *61*, e202203452. https://doi.org/10.1002/anie.202203452. [***Selected as Hot Paper***]

5.2. Publications not presented in this thesis

(*Co-first authors, contributed equally)

Campeau, D.*; León Rayo, D. F.*; Mansour, A.*; **Muratov, K**.*; Gagosz, F. Gold-Catalyzed Reactions of Specially Activated Alkynes, Allenes, and Alkenes. Chem. Rev. **2020**, *121* (14), 8756–8867. https://doi.org/10.1021/acs.chemrev.0c00788

5.3. Presentations of work in this thesis

Muratov, K.; Gagosz, F. Structure-activity relationships in Au(III) catalysis, *Canadian Chemistry Conference and Exhibition 2023*, Vancouver, BC, oral presentation

Muratov, K.; Gagosz, F. Sterically hindered phosphines as confined ligands for selective gold(I) catalysis, *Canadian Chemistry Conference and Exhibition 2022*, Calgary, AB, oral presentation

Muratov, K.; Gagosz, F. Sterically hindered phosphines as ligands for selective gold catalysis, *QOMSBOC 2021*, virtual poster

Muratov, K.; Gagosz, F. Sterically hindered phosphines as ligands for selective gold catalysis, Ottawa-Carleton Chemistry Institute Day, **2021**, virtual presentation

Muratov, K.; Gagosz, F. Sterically hindered phosphines as ligands for selective gold catalysis, *Chemistry and Biochemistry Graduate Research Conference 2020*, Virtual presentation

6. Appendix

6.1. Appendix for Chapter 2

6.1.1. Cycloisomerization of enyne 2.3-17 (Chapter 2, Scheme 2.3-5)

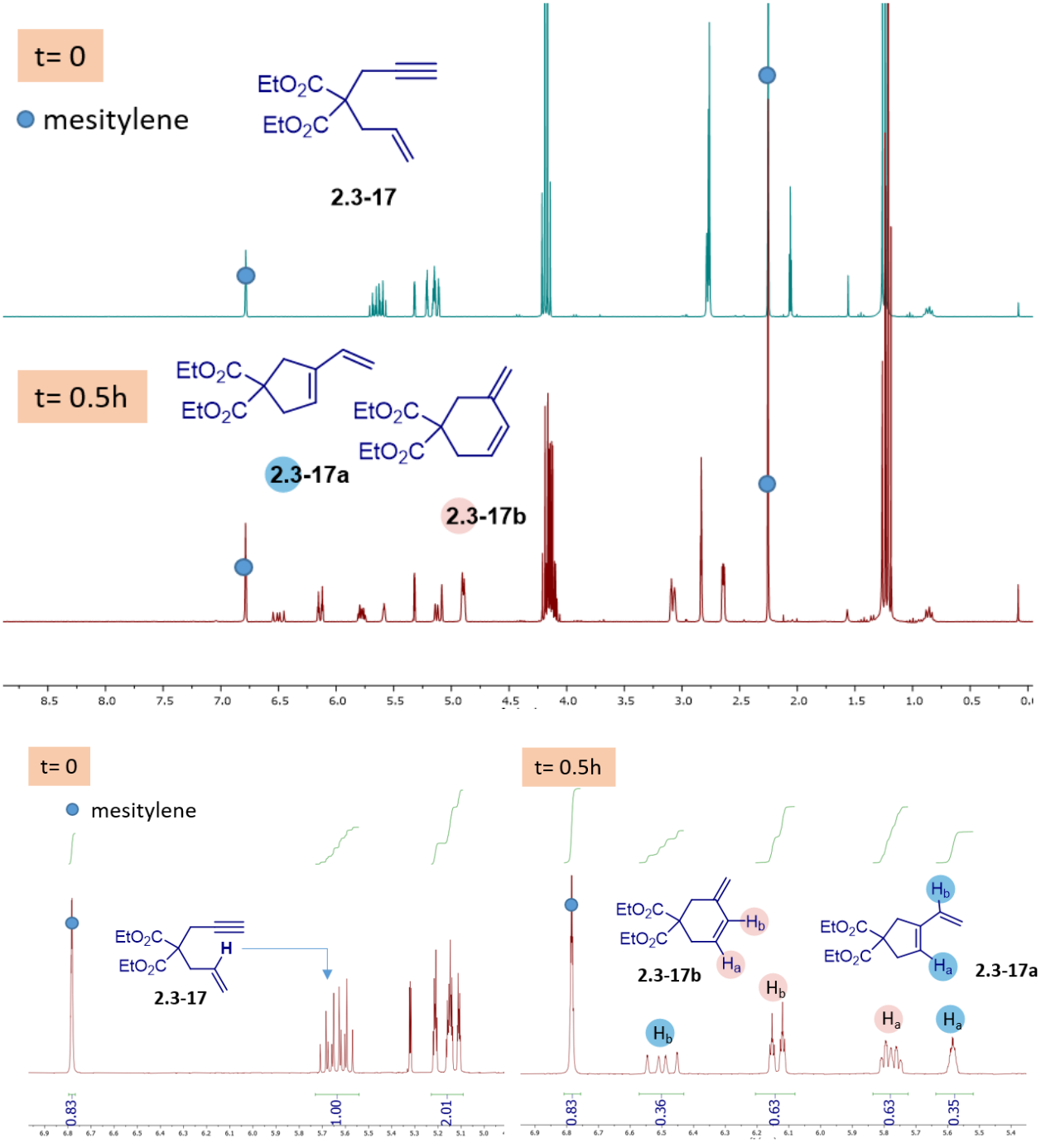

Figure 6.1-1. ^{1}H NMR spectra @t= 0 and t= 0.5h for [Au] = **2.3-22.**

6.1.2. Cycloisomerization of enyne 2.3-24 (Chapter 2, Scheme 2.3-6, A)

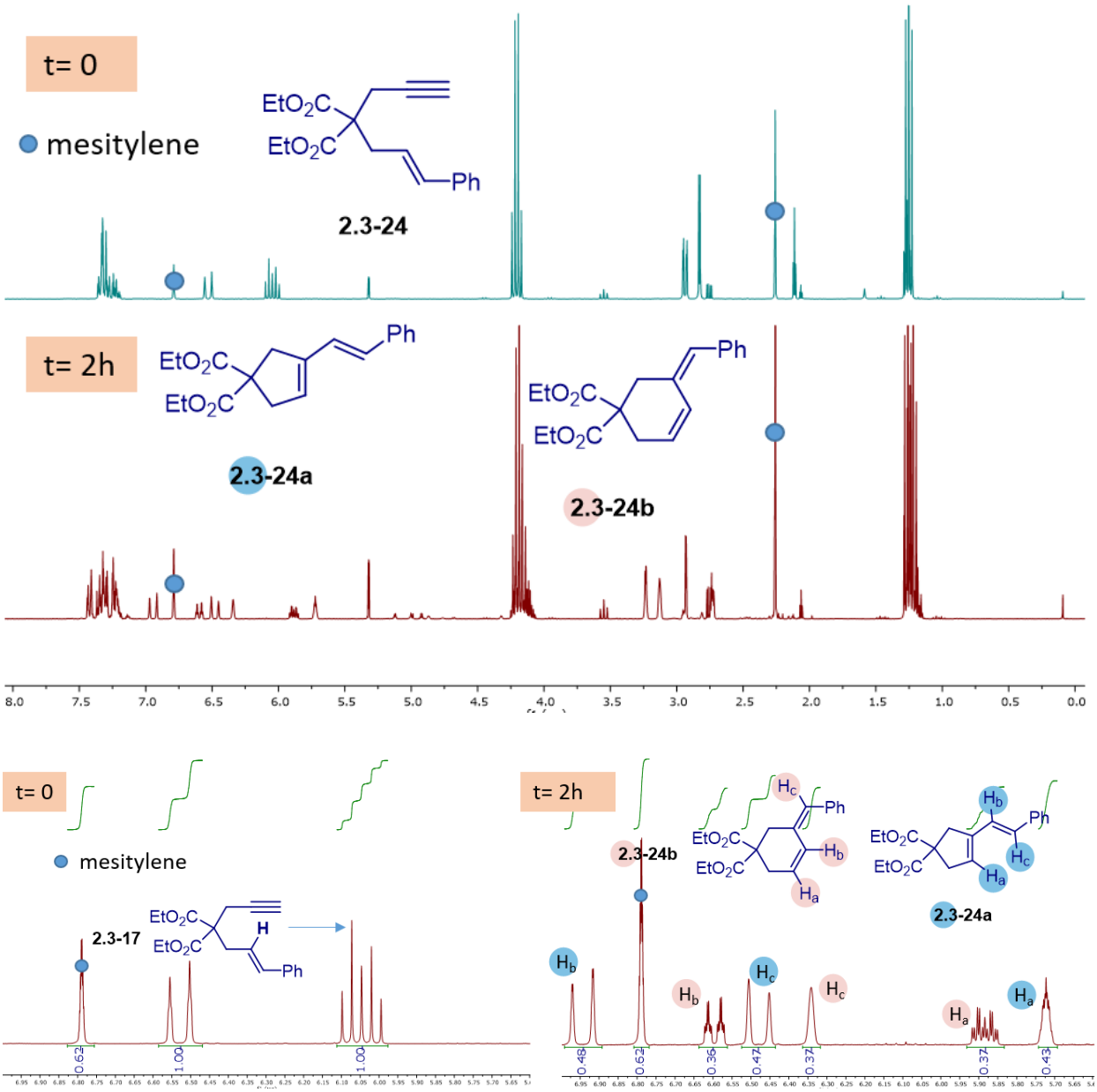

Figure 6.1-2. ^{1}H NMR spectra @t= 0 and t= 2h for [Au] = **2.3-20.**

6.1.3. Cycloisomerization of enyne 2.3-25 (Chapter 2, Scheme 2.3-6, B)

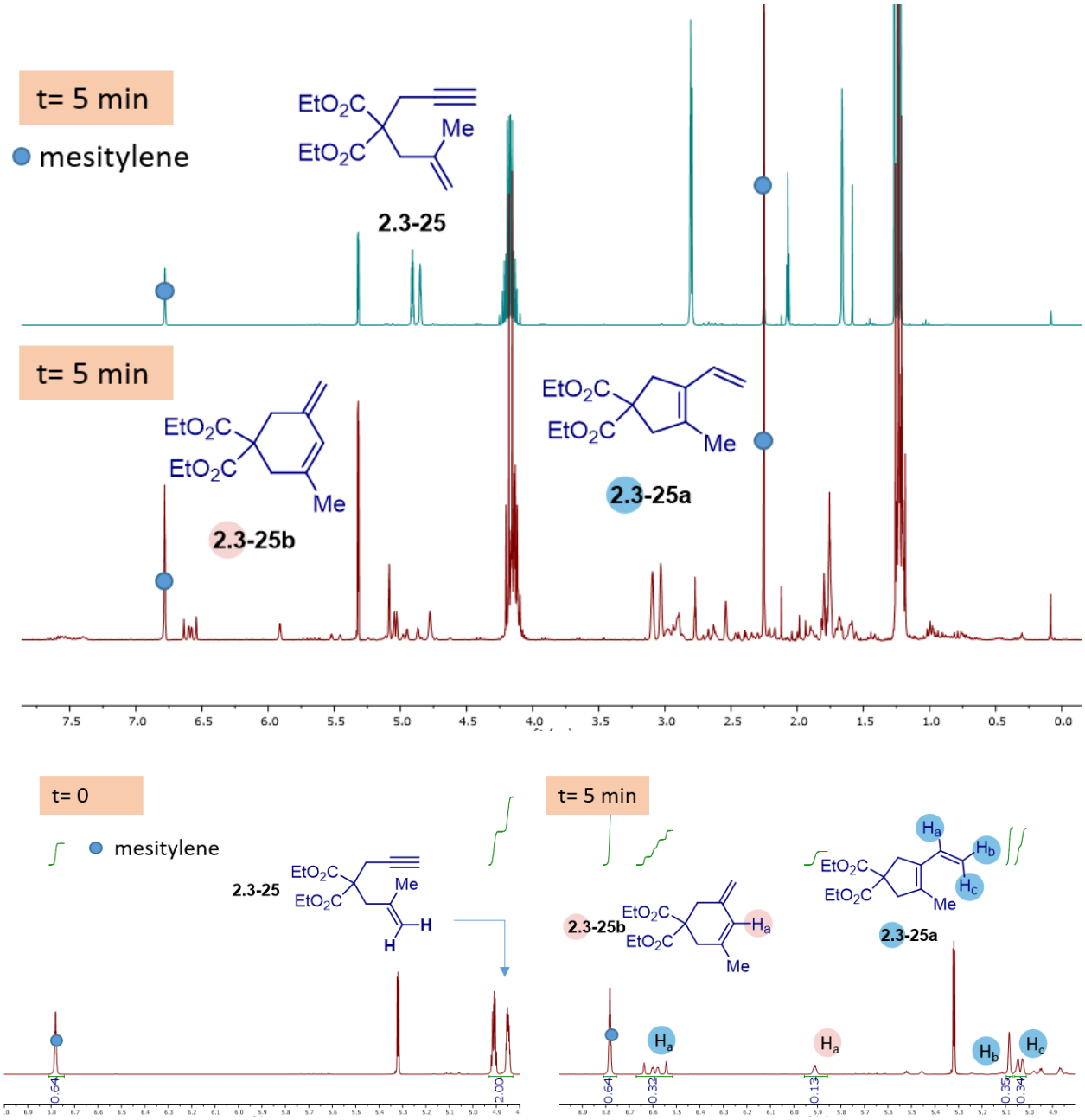

Figure 6.1-3. ^{1}H NMR spectra @t= 0 and t= 5min for [Au] = **2.3-20.**

6.1.4. Cycloisomerization of enyne 2.3-26 (Chapter 2, Scheme 2.3-6, C)

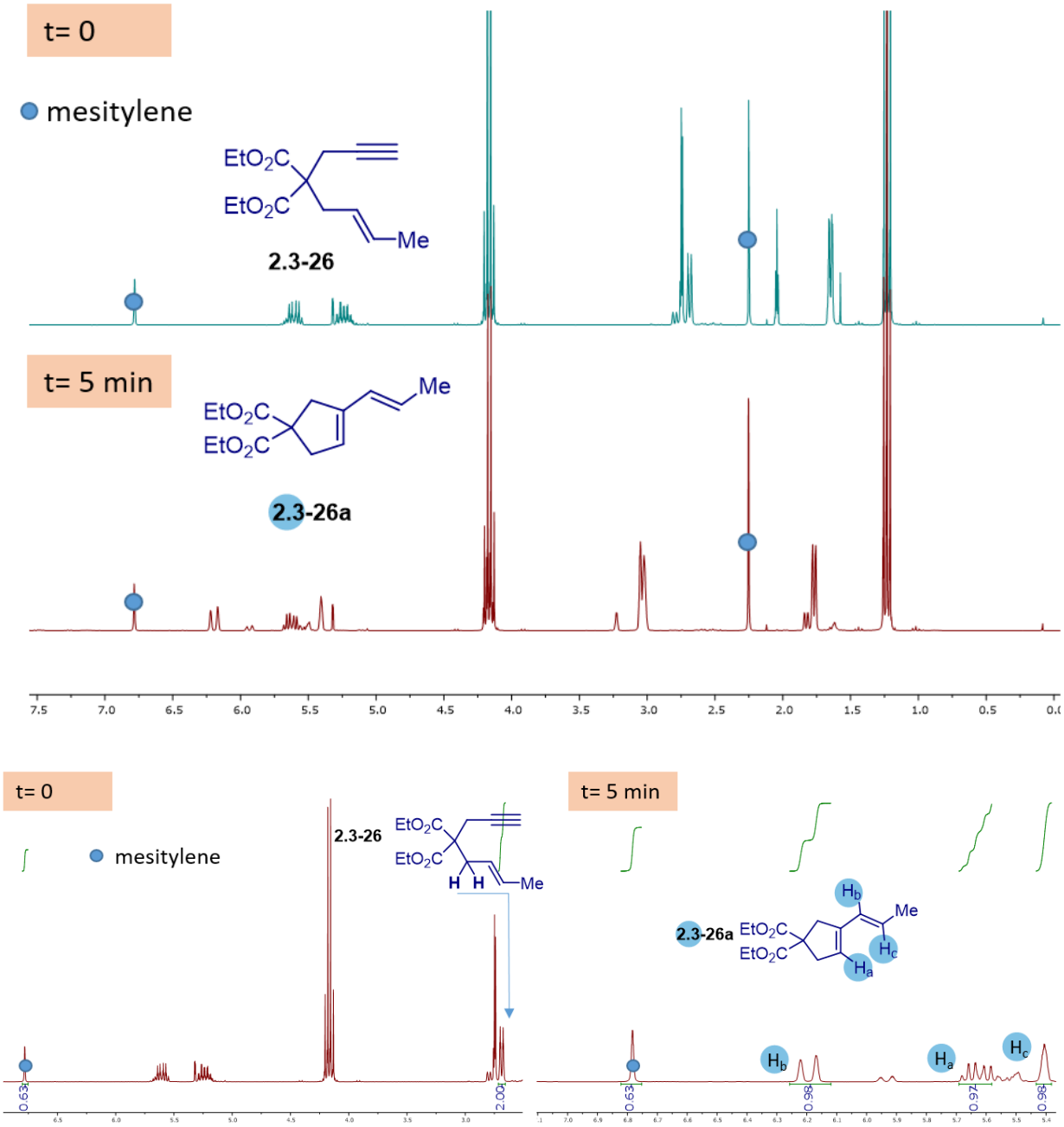

Figure 6.1-4. ^{1}H NMR spectra @t= 0 and t= 5min for [Au] = **2.3-6$_{H}$.**

6.1.5. Cycloisomerization of enyne 2.3-27 (Chapter 2, Scheme 2.3-6, D)

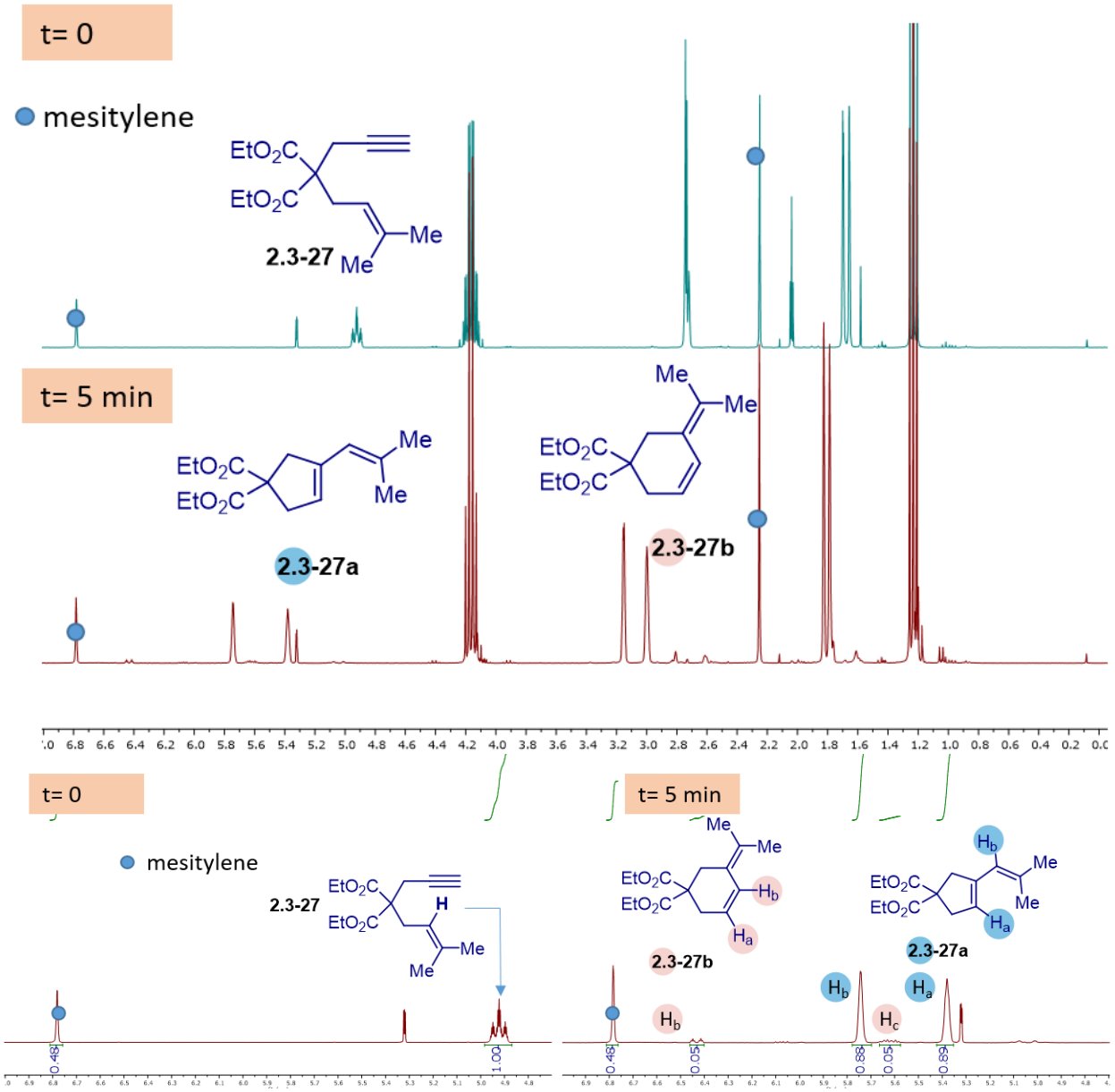

Figure 6.1-5. ^{1}H NMR spectra @t= 0 and t= 5min for [Au] = **2.3-6$_H$.**

6.1.6. Cycloisomerization of enyne 2.3-28 (Chapter 2, Scheme 2.3-7, A)

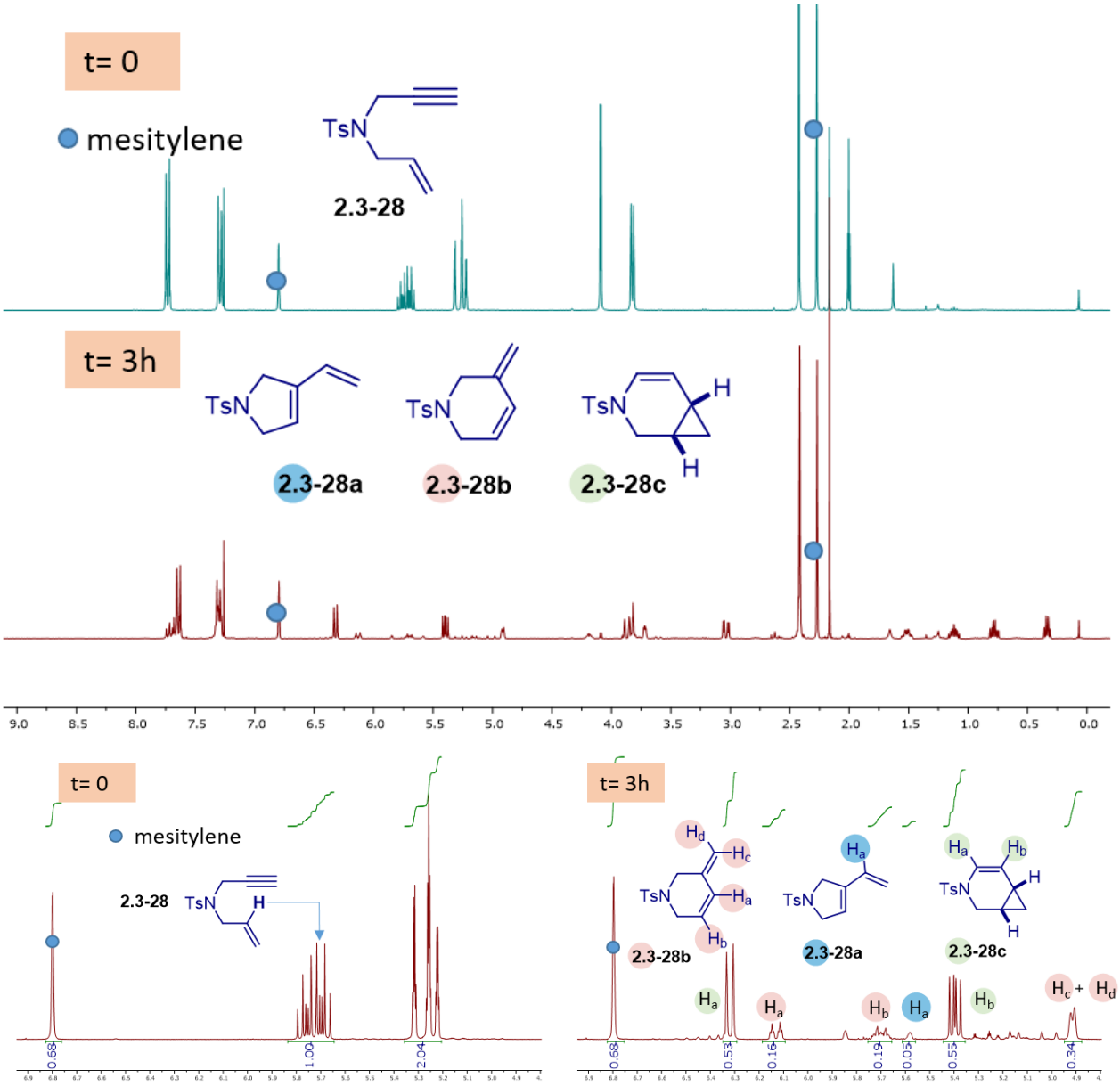

Figure 6.1-6. ^{1}H NMR spectra @t= 0 and t= 3h for [Au] = **2.3-22.**

6.1.7. Cycloisomerization of enyne 2.3-29 (Chapter 2, Scheme 2.3-7, B)

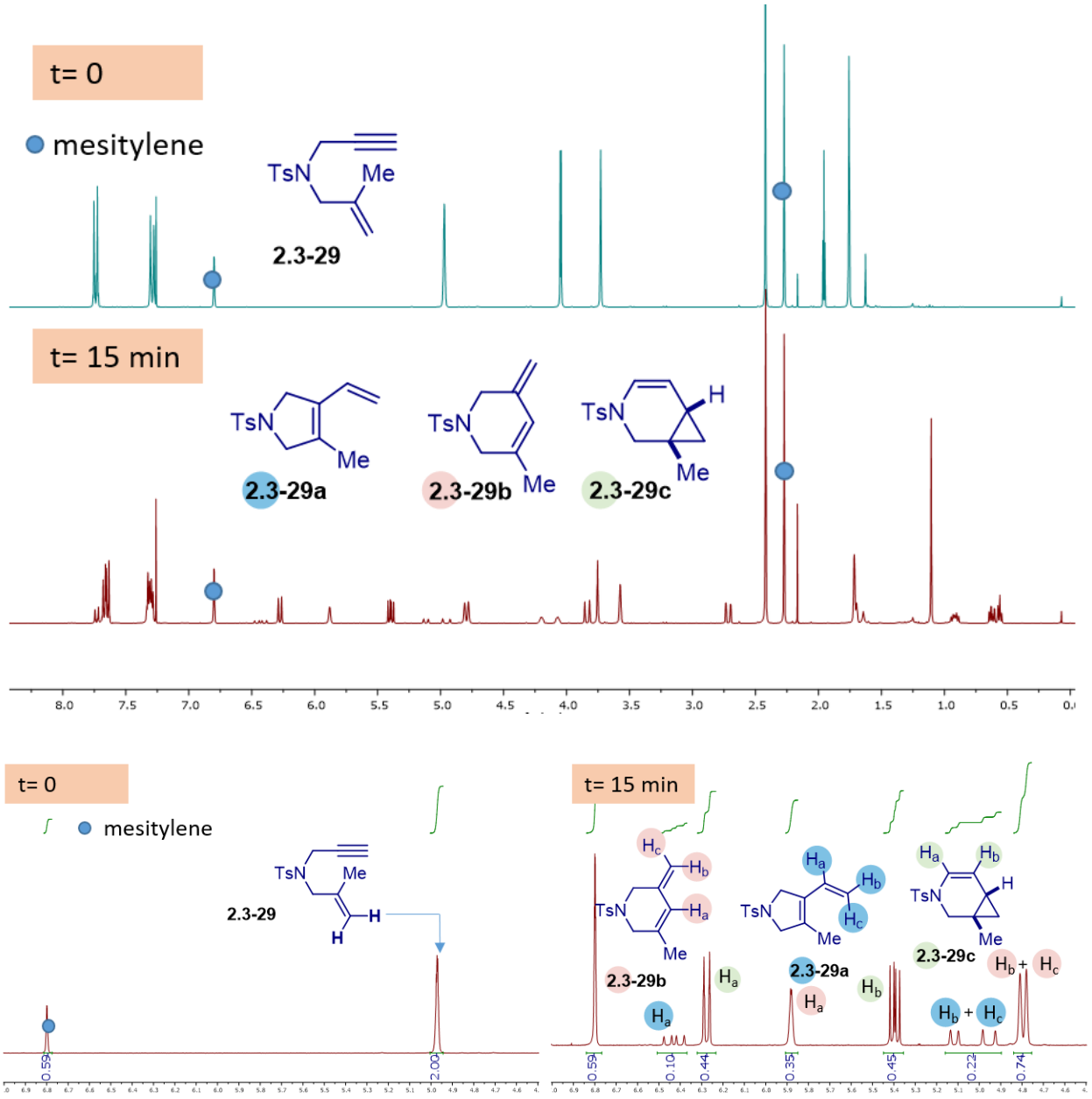

Figure 6.1-7. ^{1}H NMR spectra @t= 0 and t= 15min for [Au] = **2.3-22.**

6.1.8. Cycloisomerization of enyne 2.3-30 (Chapter 2, Scheme 2.3-8, A)

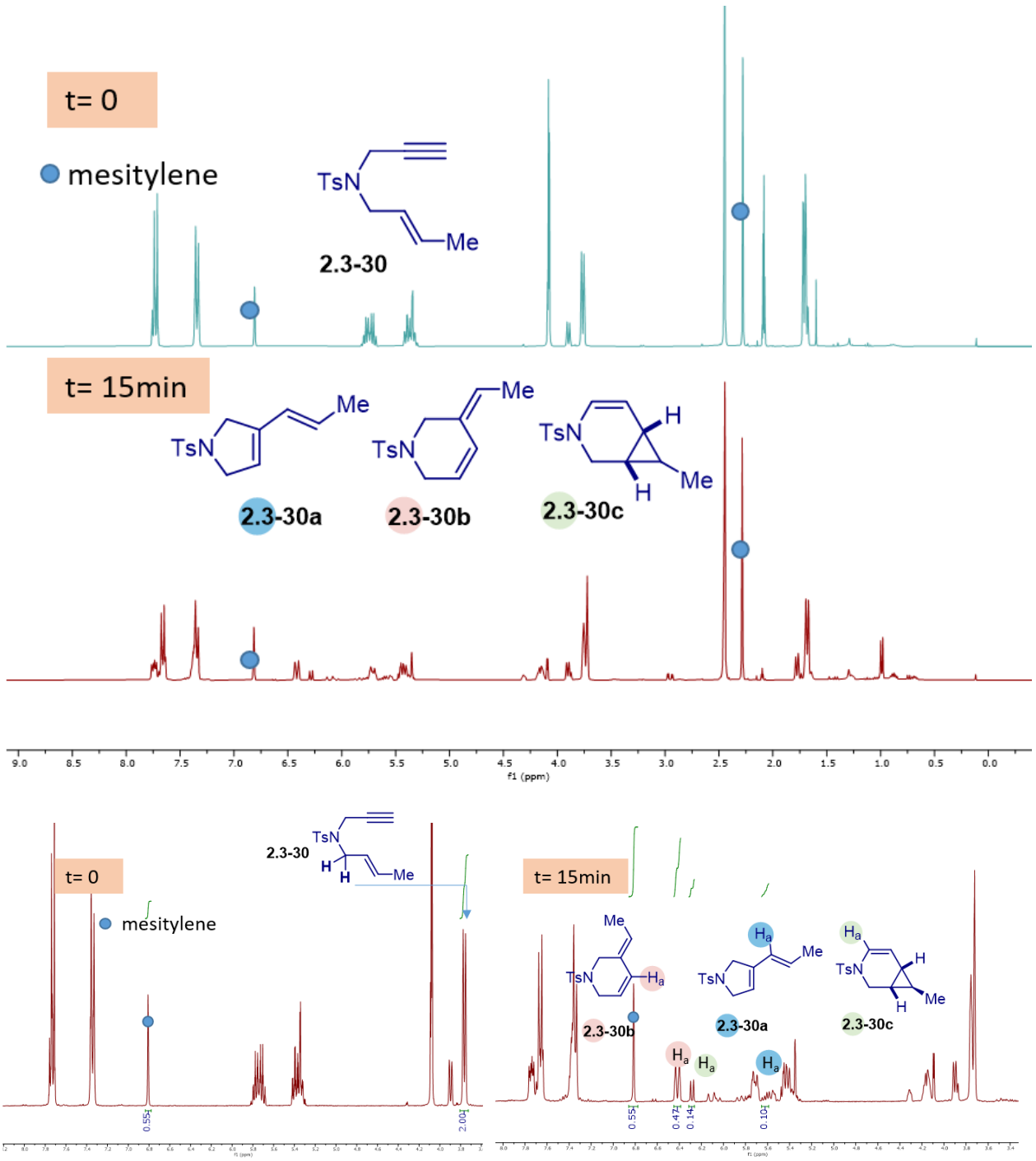

Figure 6.1-8. ^{1}H NMR spectra @t= 0 and t= 15min for [Au] = **2.3-21.**

6.1.9. Cycloisomerization of enyne 2.3-31 (Chapter 2, Scheme 2.3-8, B)

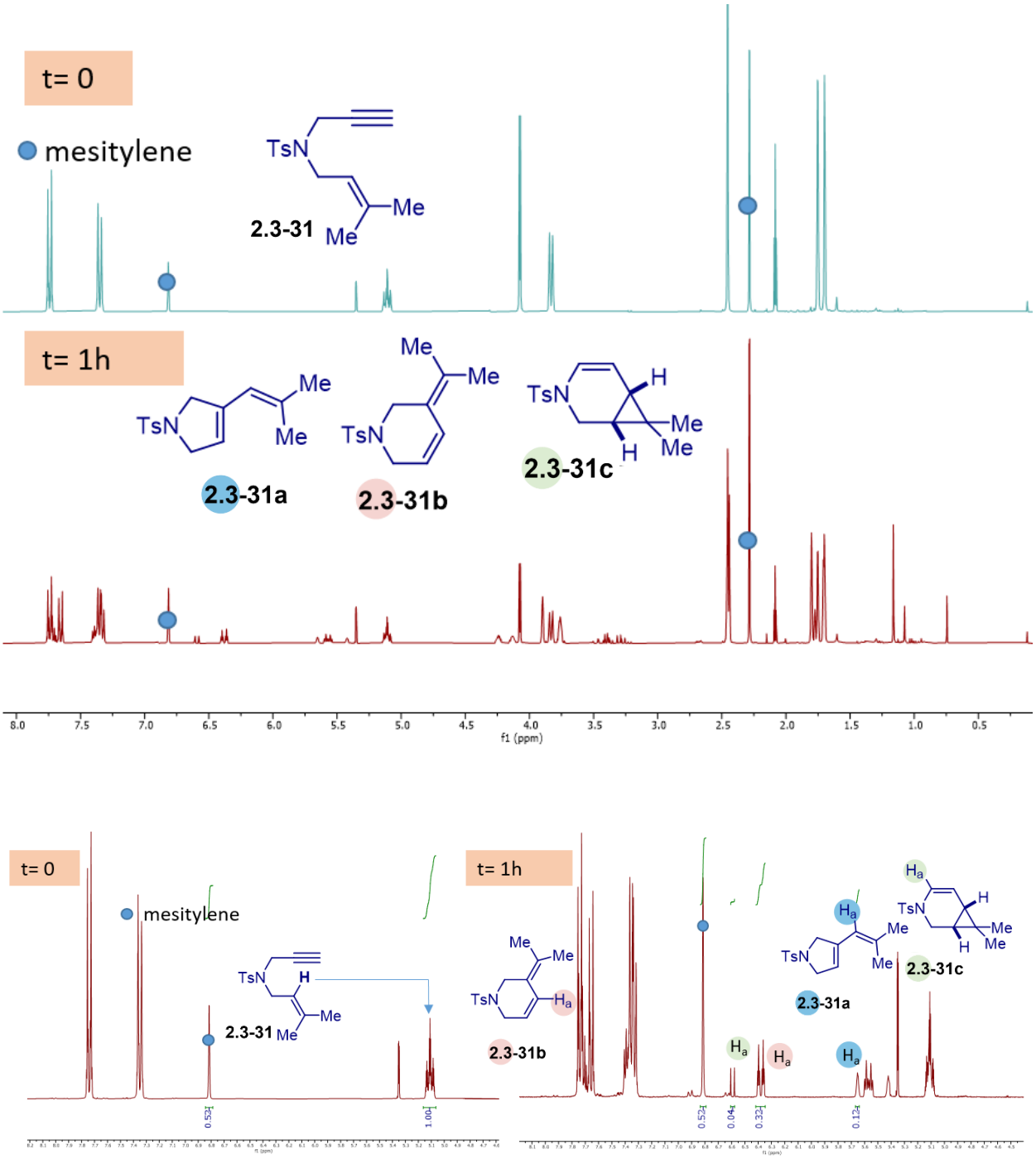

Figure 6.1-9. ^{1}H NMR spectra @t= 0 and t= 15min for [Au] = **2.3-6$_{pnPe}$.**

6.1.10. Interrupted cycloisomerization of enyne 2.3-24 with styrene (Chapter 2, Scheme 2.3-9)

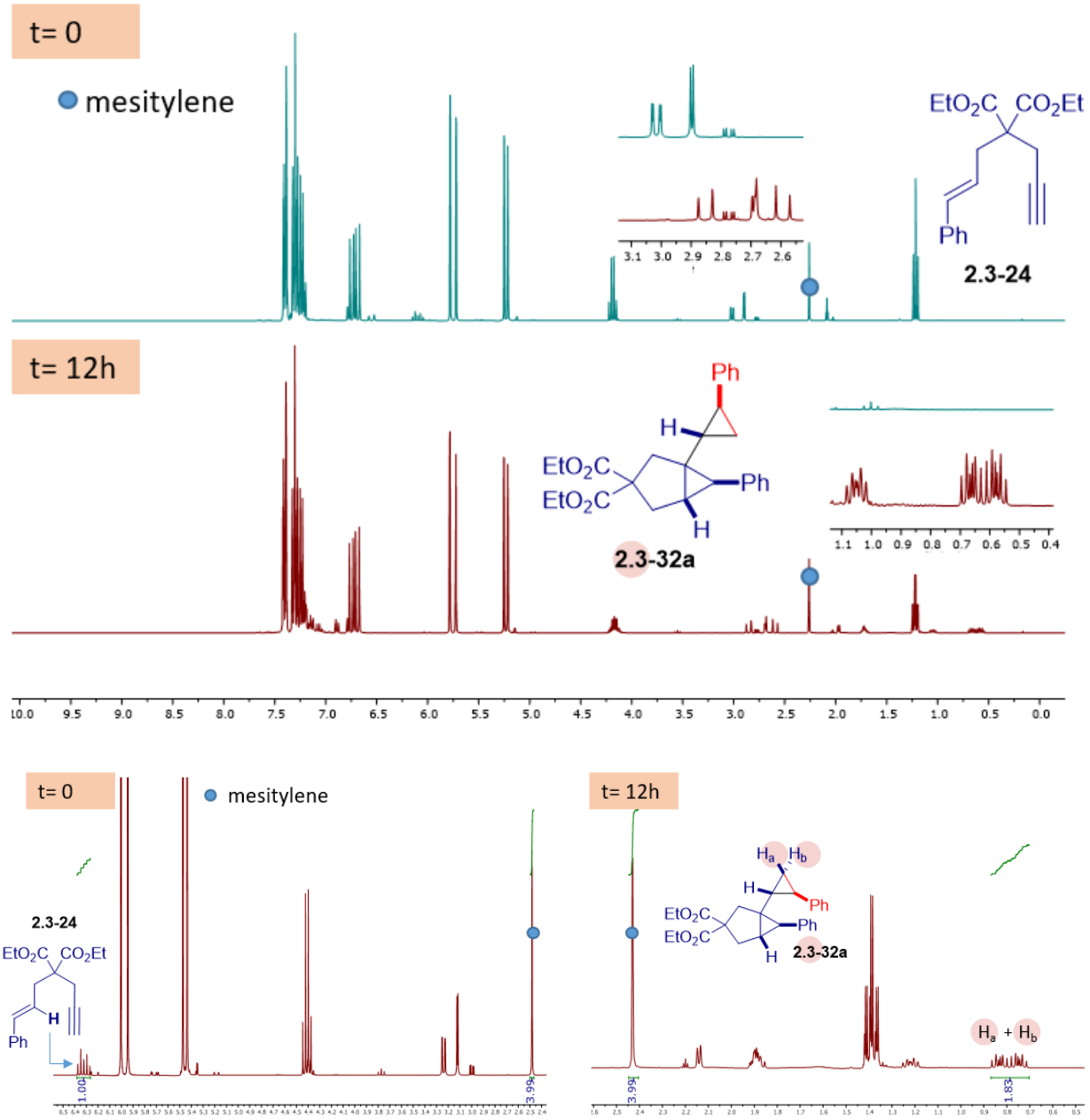

Figure 6.1-10. ^{1}H NMR spectra @t= 0 and t= 12h for [Au] = **2.3-21.**

6.1.11. Interrupted cycloisomerization of enyne 2.3-24 with 1,3-dimethoxybenzene (Chapter 2, Scheme 2.3-9)

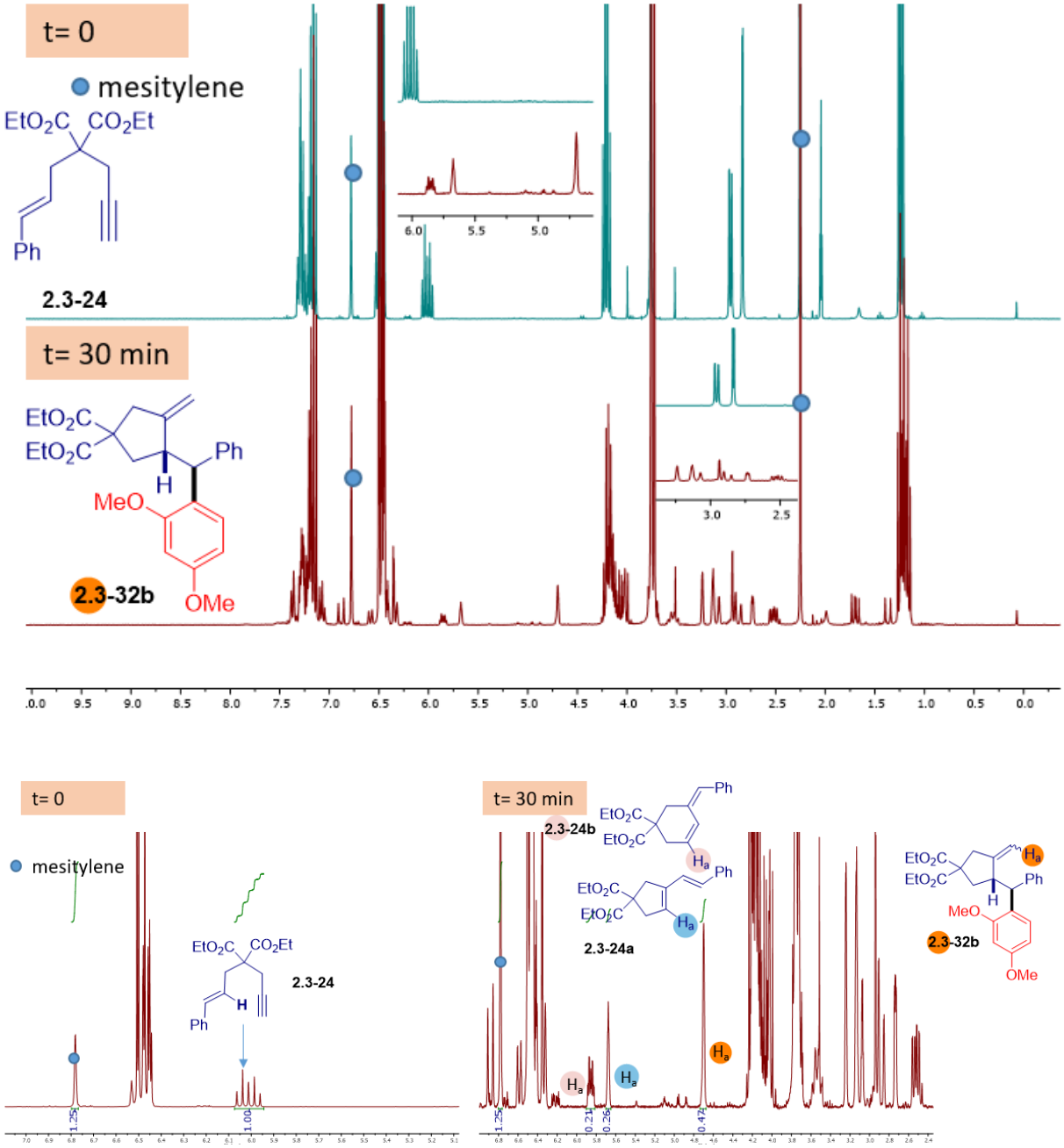

Figure 6.1-11. ^{1}H NMR spectra @t= 0 and t= 30min for [Au] = **2.3-21.**

6.1.12. Interrupted cycloisomerization of N-cinnamyl-4-methyl-N-(prop-2-yn-1-yl)benzenesulfonamide 2.3-33 with indole (Chapter 2, Scheme 2.3-10, A)

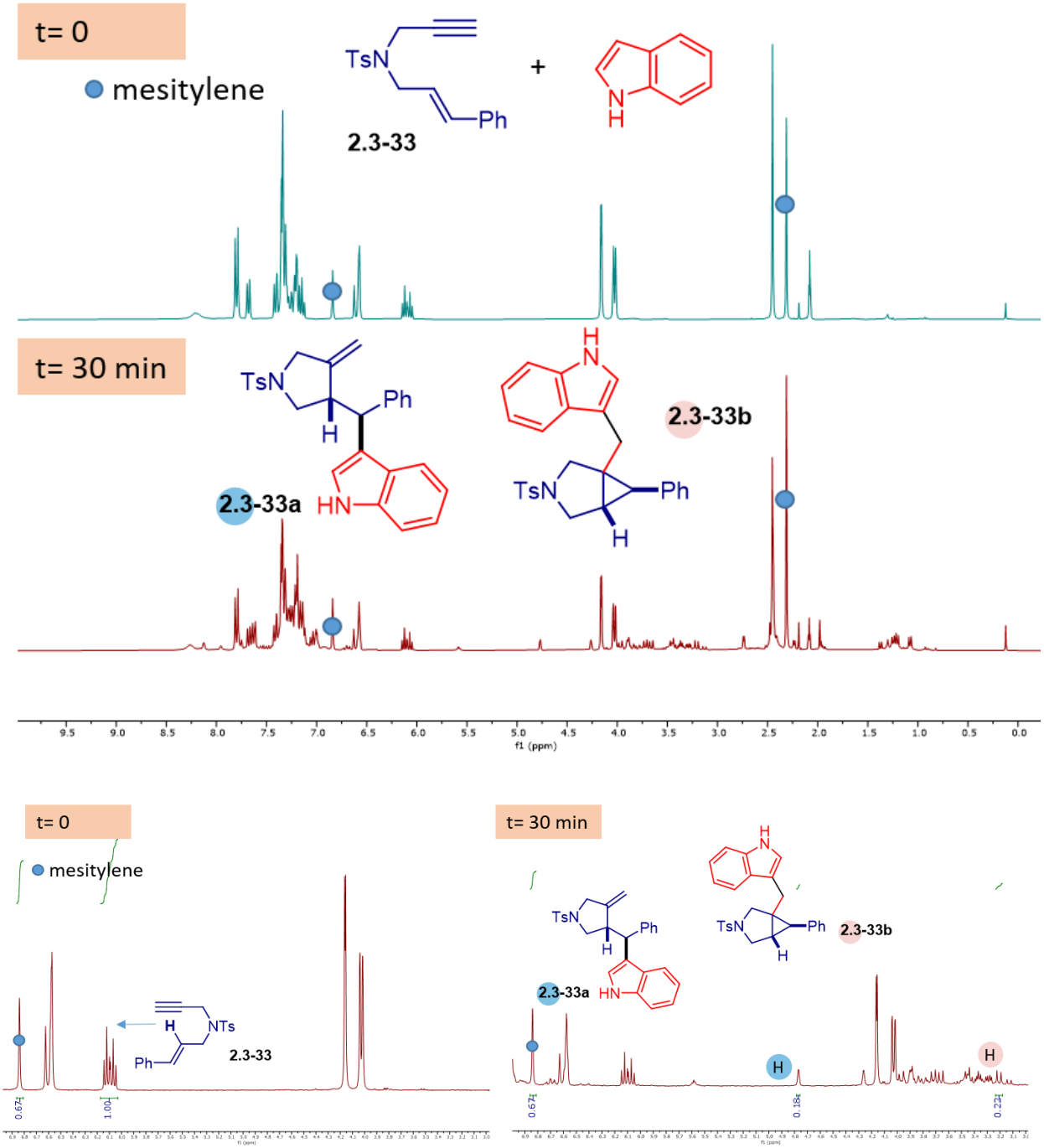

Figure 6.1-12. ^{1}H NMR spectra @t= 0 and t= 30min for [Au] = **2.3-23.**

6.1.13. Interrupted cycloisomerization of ethyl 2-diazo-2-phenylacetate 2.3-34 with styrene (Chapter 2, Scheme 2.3-10, B)

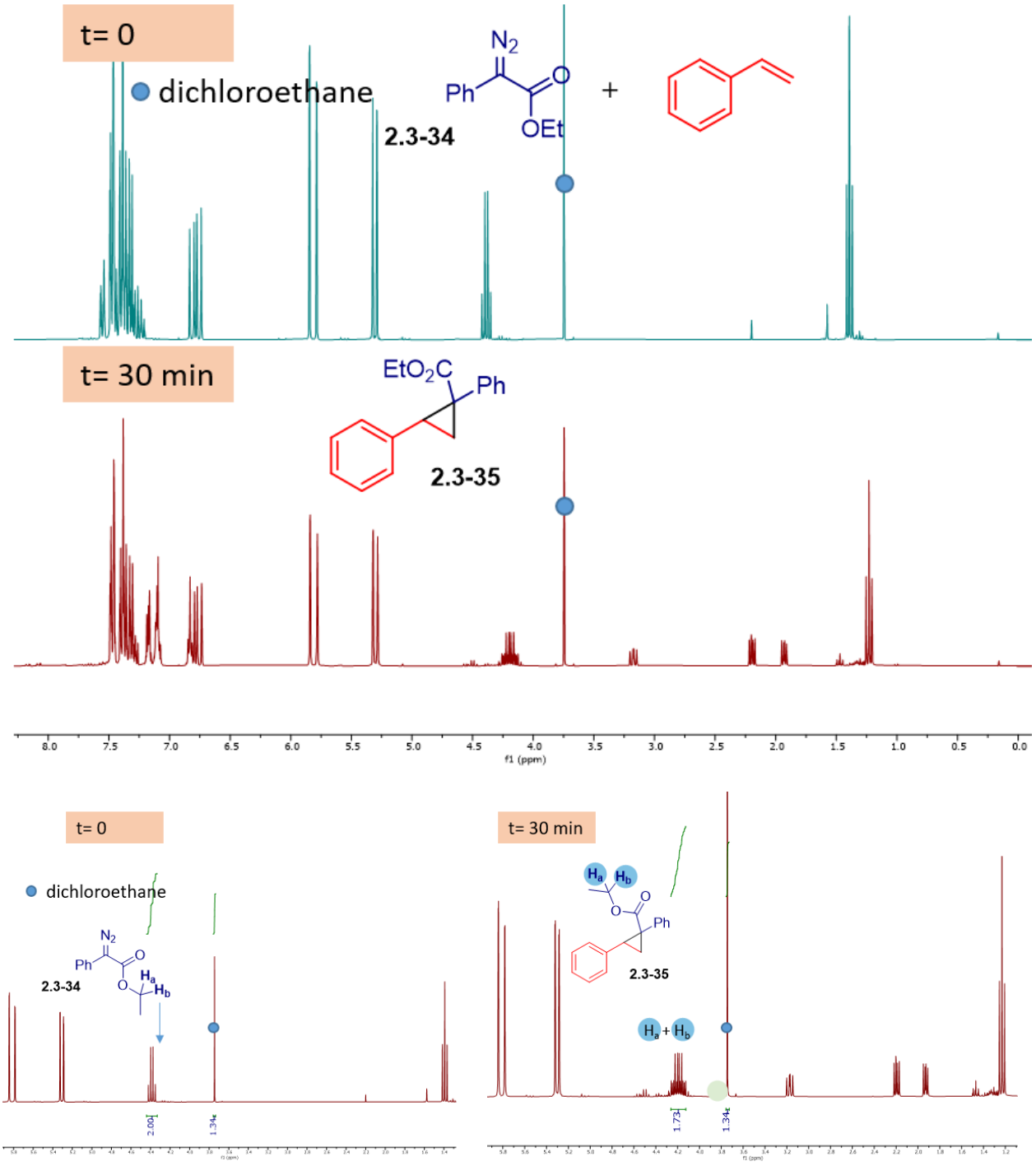

Figure 6.1-13. ^{1}H NMR spectra @t= 0 and t= 30min for [Au] = **2.3-21.**

6.1.14. Cycloisomerization of enyne 2.3-35 (Chapter 2, Scheme 2.3-11, A)

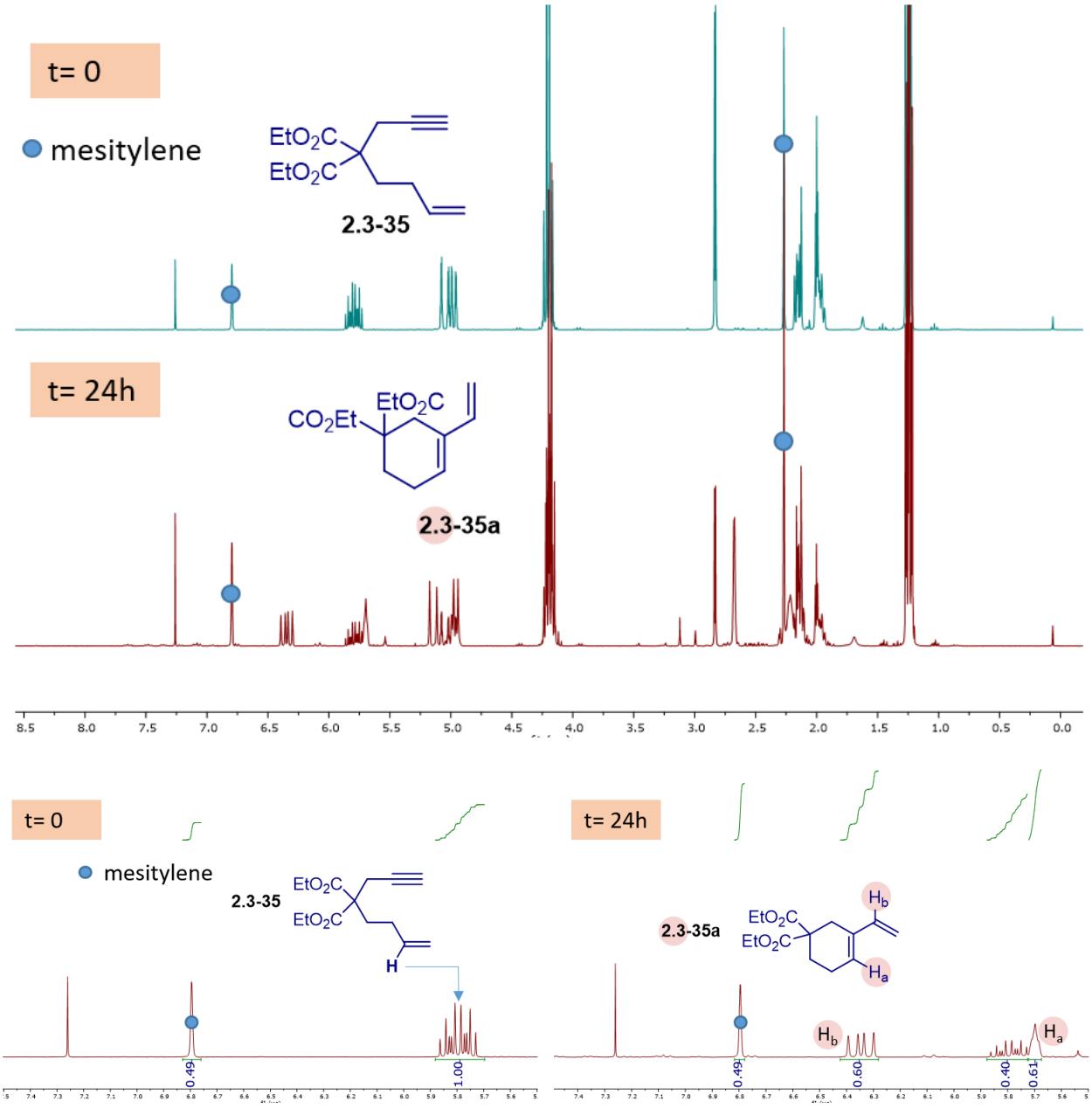

Figure 6.1-14. ^{1}H NMR spectra @t= 0 and t= 24h for [Au] = **2.3-19.**

6.1.15. Cycloisomerization of enyne 2.3-36 (Chapter 2, Scheme 2.3-11, A)

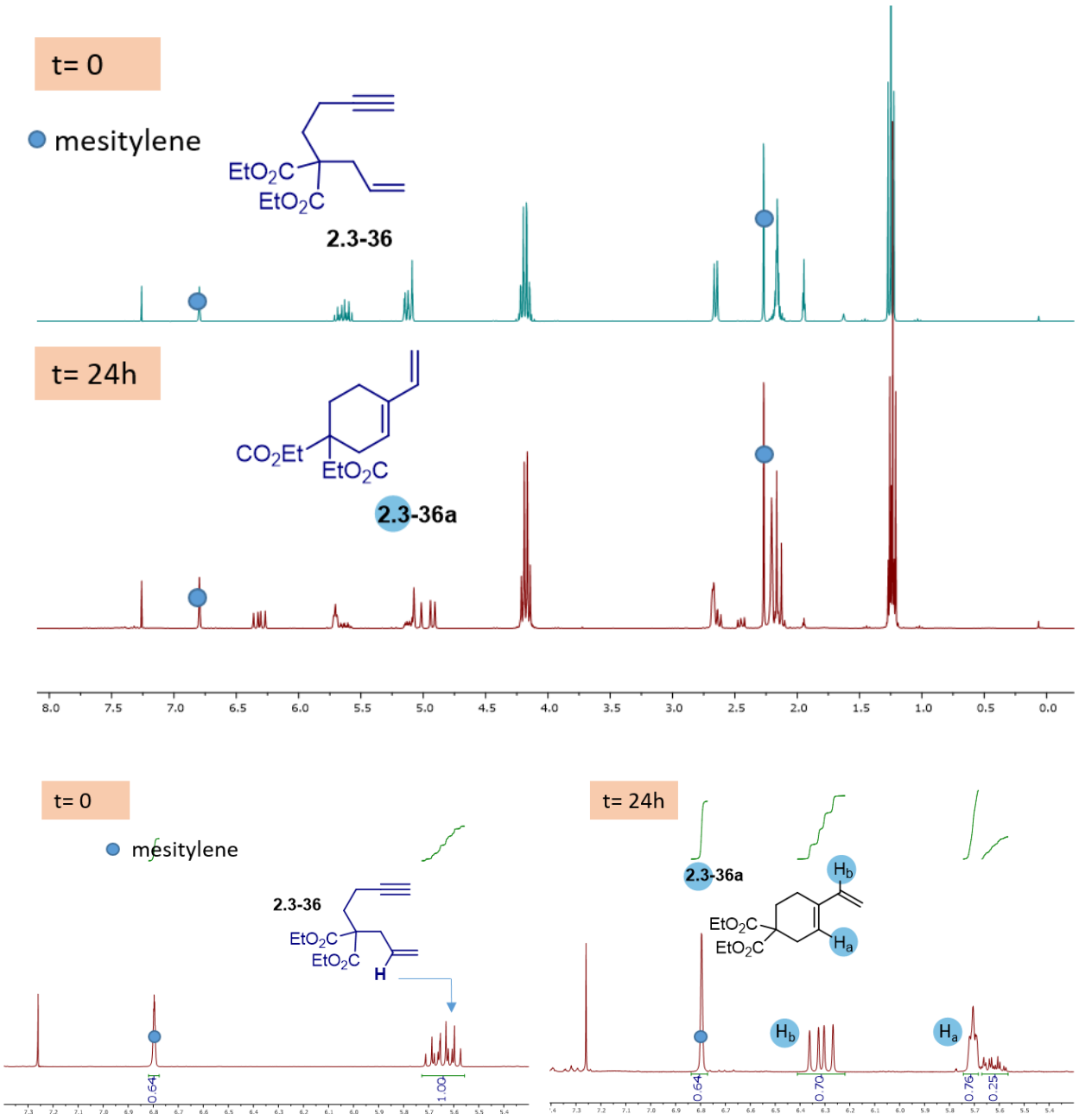

Figure 6.1-15. ^{1}H NMR spectra @t= 0 and t= 24h for [Au] = **2.3-6$_{H}$.**

6.1.16. Competetive cycloisomerization of enynes 2.3-35 and 2.3-36 (Chapter 2, Scheme 2.3-11, B)

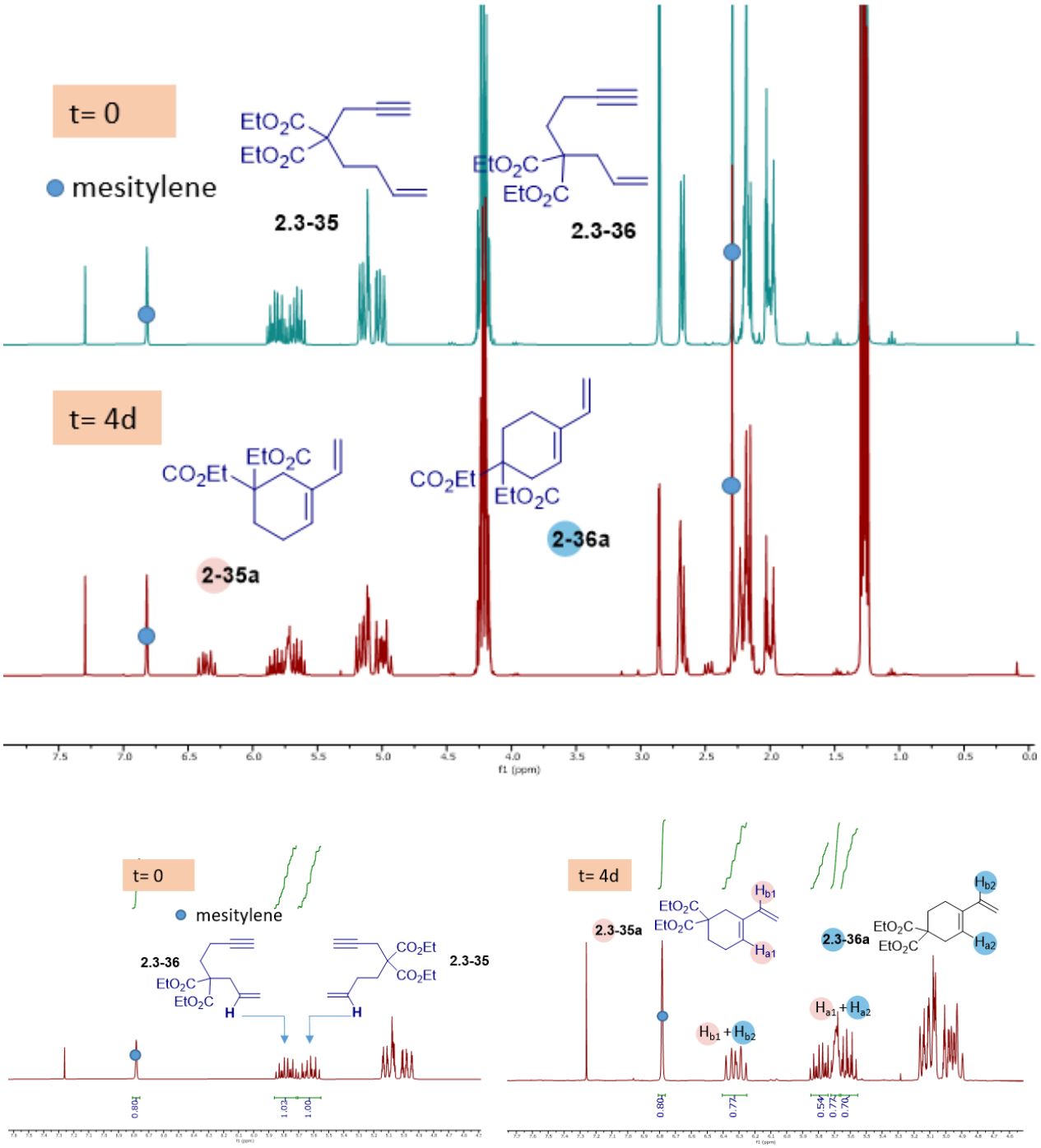

Figure 6.1-16. ^{1}H NMR spectra @t= 0 and t= 24h for [Au] = **2.3-6$_{H}$.**

6.1.17. Cycloisomerization of enyne 2.3-37 (Chapter 2, Scheme 2.3-12)

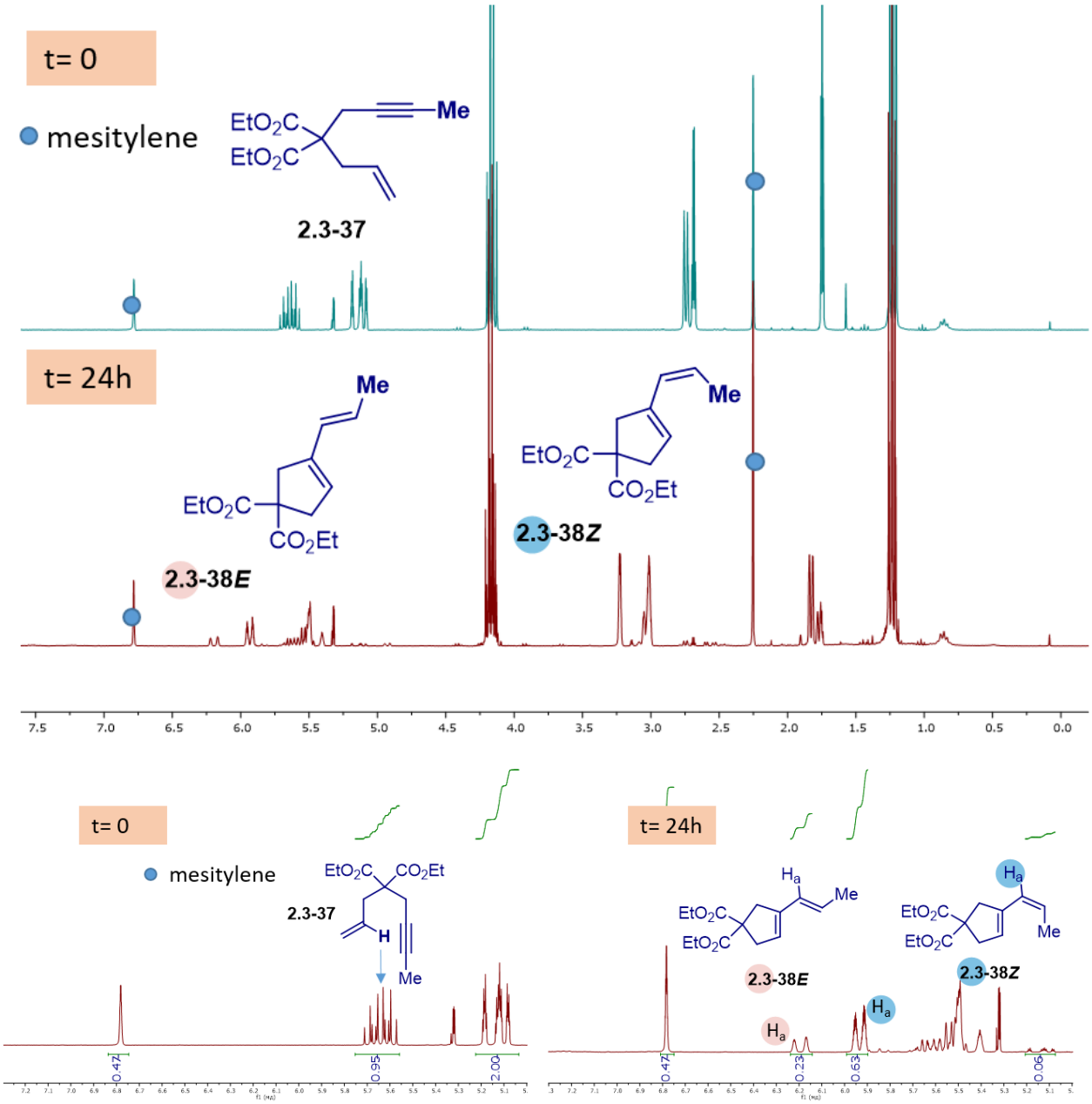

Figure 6.1-17. ^{1}H NMR spectra @t= 0 and t= 24h for [Au] = **2.3-7.**

6.1.18. Hydration of alkyne 2.3-38 (Chapter 2, Scheme 2.3-13, A)

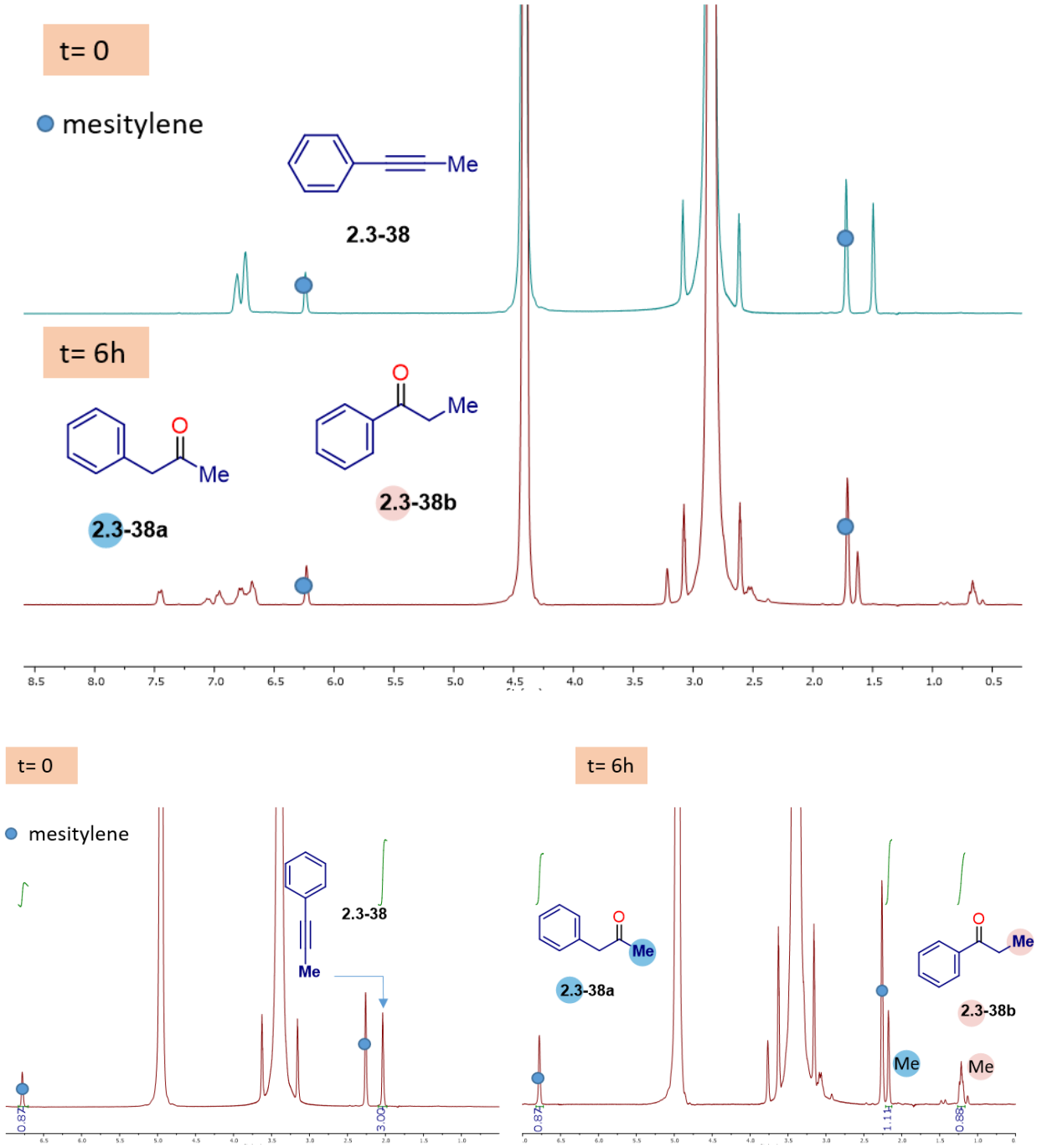

Figure 6.1-18. ^{1}H NMR spectra @t= 0 and t= 6h for L = JohnPhos.

6.1.19. Hydration of alkyne 2.3-39 (Chapter 2, Scheme 2.3-13, B)

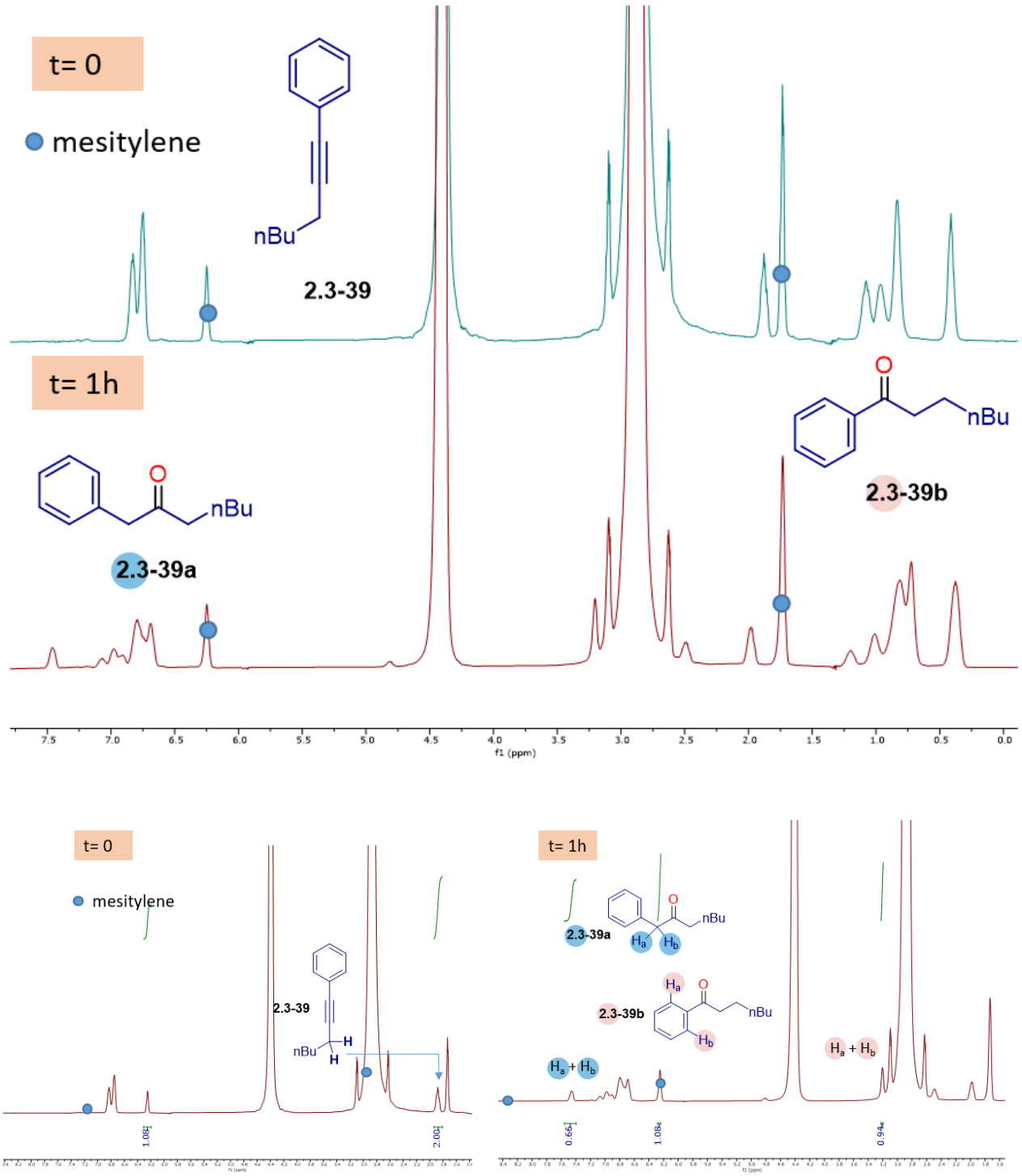

Figure 6.1-19. ^{1}H NMR spectra @t= 0 and t= 1h for L = IPr.

6.1.20. Competetive hydration of alkynes 2.3-38 and 2.3-39 (Chapter 2, Scheme 2.3-14, A)

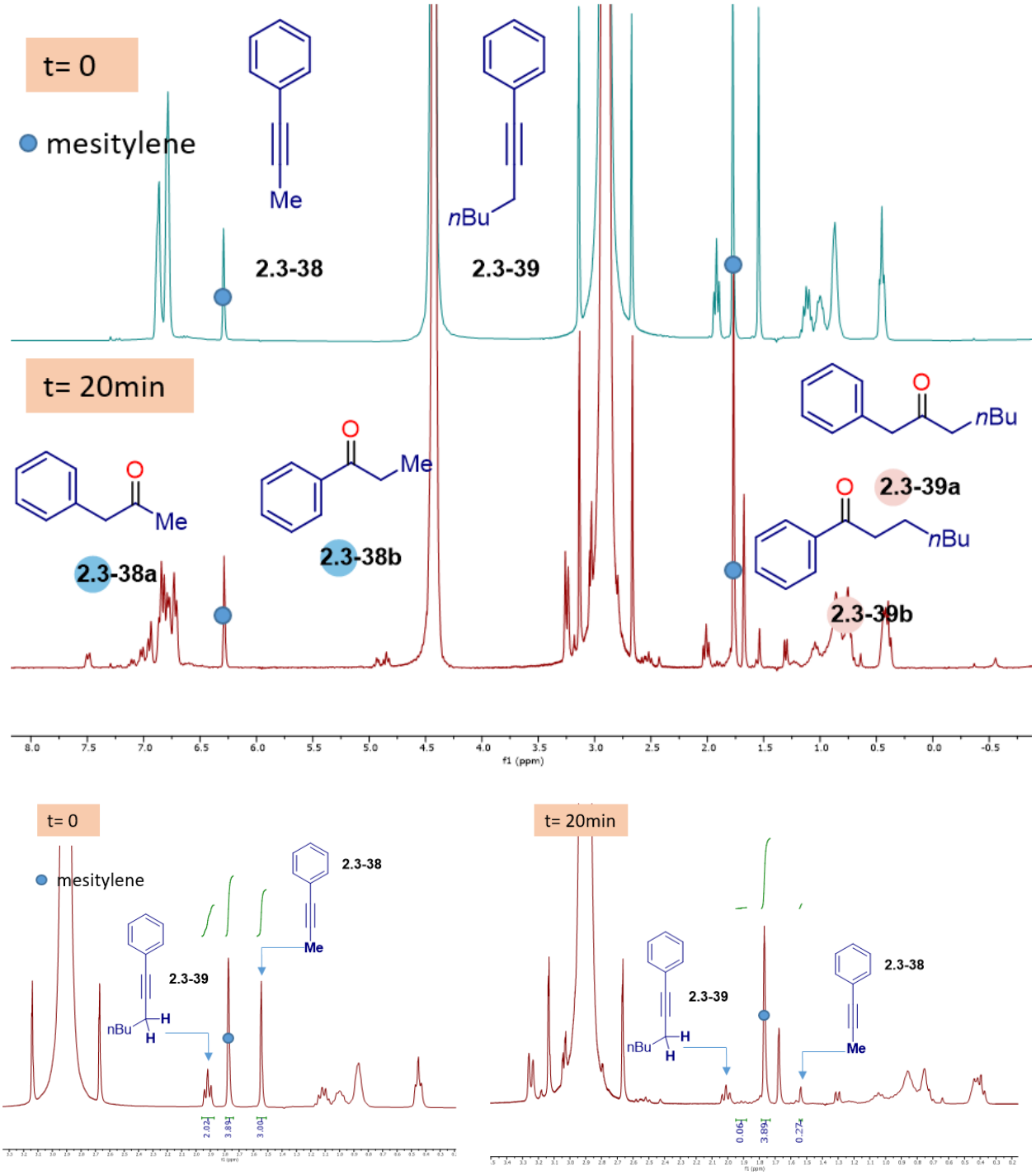

Figure 6.1-20. ^{1}H NMR spectra @t= 0 and t= 20min for L = IPr.

6.1.21. Competetive hydration of alkynes 2.3-40 and 2.3-41 (Chapter 2, Scheme 2.3-14, B)

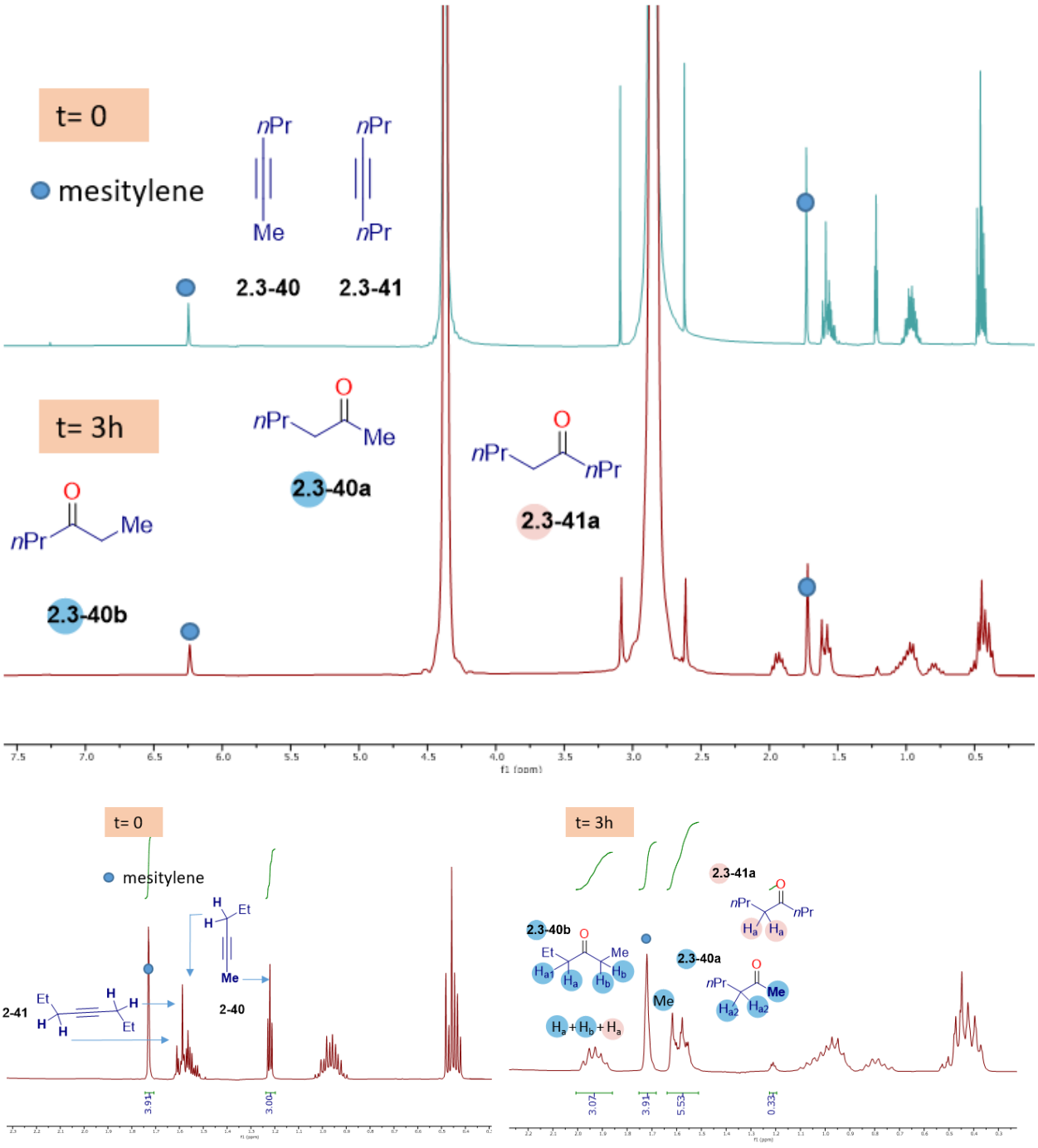

Figure 6.1-21. ^{1}H NMR spectra @t= 0 and t= 3h for L = **2.3-4$_{H}$.**

6.1.22. SCXRD analysis and data

Crystallographic data were collected from single crystals mounted on MiTeGen dual thickness MicroMounts using Parabar oil. Data were collected on a Bruker ApexII single crystal diffractometer equipped with a graphite monochromator. The instrument was equipped with a

sealed tube Mo Kα source ($\lambda = 0.71073$ Å), an ApexII CCD detector and a dry compressed air-cooling system. All samples were cooled to 203(2) K during data collection. Raw data collection and processing were performed with the Apex3 software package from Bruker. Initial unit cell parameters were determined from 36 data frames from select ω scans. Semi-empirical absorption corrections based on equivalent reflections were applied.[1] Systematic absences in the diffraction dataset and unit-cell parameters were consistent with the assigned space group. The initial structural solutions were determined using ShelxT direct methods,[2] and refined with full-matrix least-squares procedures based on F^2 using ShelXL or ShelXle.[3] Hydrogen atoms were placed geometrically and refined using a riding model.

X-ray of 2.3-5$_H$, CCDC deposition number: 2138316

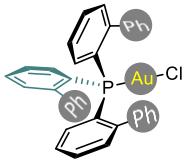

2-5$_H$

White crystals of **2.3-5$_H$** suitable for X-Ray crystallography analysis were obtained *via* slow diffusion of a layer of pentane over a solution of **2.3-5$_H$** in DCM.

ORTEP drawing of **2.3-5$_H$**:

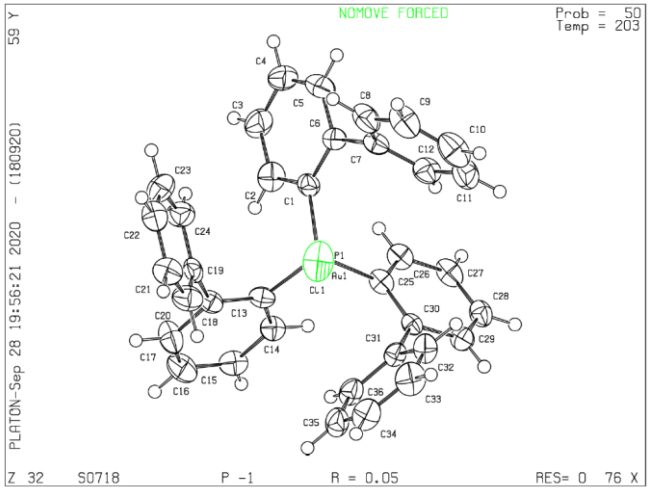

Datablock: S0718

```
Bond precision:  C-C = 0.0096 A          Wavelength=0.71073

Cell:          a=10.1476(8)      b=10.8176(8)      c=14.9610(12)
               alpha=84.074(2)   beta=78.059(2)    gamma=64.348(2)
Temperature:   203 K

                Calculated                Reported
Volume          1448.2(2)                 1448.2(2)
Space group     P -1                      P -1
Hall group      -P 1                      -P 1
Moiety formula  C36 H27 Au Cl P           C36 H27 Au Cl P
Sum formula     C36 H27 Au Cl P           C36 H27 Au Cl P
Mr              722.97                    722.96
Dx,g cm-3       1.658                     1.658
Z               2                         2
Mu (mm-1)       5.250                     5.250
F000            708.0                     708.0
F000'           704.80
h,k,lmax        14,15,21                  14,15,21
Nref            8888                      8871
Tmin,Tmax       0.471,0.753               0.623,0.746
Tmin'           0.325

Correction method= # Reported T Limits: Tmin=0.623 Tmax=0.746
AbsCorr = MULTI-SCAN

Data completeness= 0.998          Theta(max)= 30.558

R(reflections)= 0.0531( 5331)     wR2(reflections)= 0.0885( 8871)

S = 0.950                 Npar= 352
```

X-ray of 2.3-5$_{mtBu}$, CCDC deposition number: 2138315

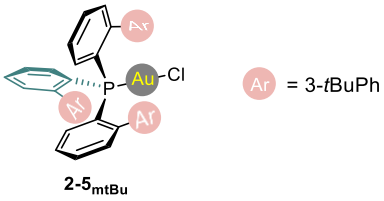

2-5$_{mtBu}$

White crystals of **2.3-5$_{mtBu}$**·CH_2Cl_2 suitable for X-Ray crystallography analysis were obtained *via* slow diffusion of a layer of pentane over a solution of **2.3-5$_{mtBu}$** in DCM.

ORTEP drawing of **2.3-5$_{mtBu}$**:

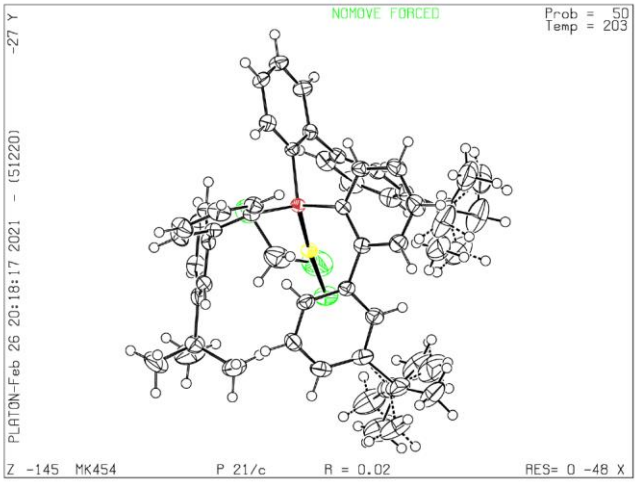

Datablock: MK454

Bond precision: C-C = 0.0038 A Wavelength=0.71073

Cell: a=17.5156(9) b=11.7499(6) c=22.0155(11)
alpha=90 beta=101.468(1) gamma=90
Temperature: 203 K

	Calculated	Reported
Volume	4440.5(4)	4440.5(4)
Space group	P 21/c	P 21/c
Hall group	-P 2ybc	-P 2ybc
Moiety formula	C48 H51 Au Cl P, C H2 Cl2	C49 H53 Au Cl3 P
Sum formula	C49 H53 Au Cl3 P	C49 H53 Au Cl3 P
Mr	976.20	976.20
Dx,g cm-3	1.460	1.460
Z	4	4
Mu (mm-1)	3.562	3.562
F000	1968.0	1968.0
F000'	1962.81	
h,k,lmax	22,15,28	22,15,28
Nref	10360	10298
Tmin,Tmax	0.733,0.768	0.602,0.746
Tmin'	0.395	

Correction method= # Reported T Limits: Tmin=0.602 Tmax=0.746
AbsCorr = MULTI-SCAN

Data completeness= 0.994 Theta(max)= 27.651

R(reflections)= 0.0236(8641) wR2(reflections)= 0.0517(10298)

S = 1.019 Npar= 567

X-ray of 2.3-5$_{pnPe}$, CCDC deposition number: 2138317

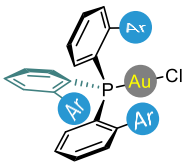

2-5$_{nPe}$

Ar = 4-*n*PentPh

White crystals of **2.3-5$_{pnPe}$** suitable for X-Ray crystallography analysis were obtained *via* slow diffusion of a layer of pentane over a solution of **2.3-5$_{pnPe}$** in DCM.

ORTEP drawing of **2.3-5$_{pnPe}$**:

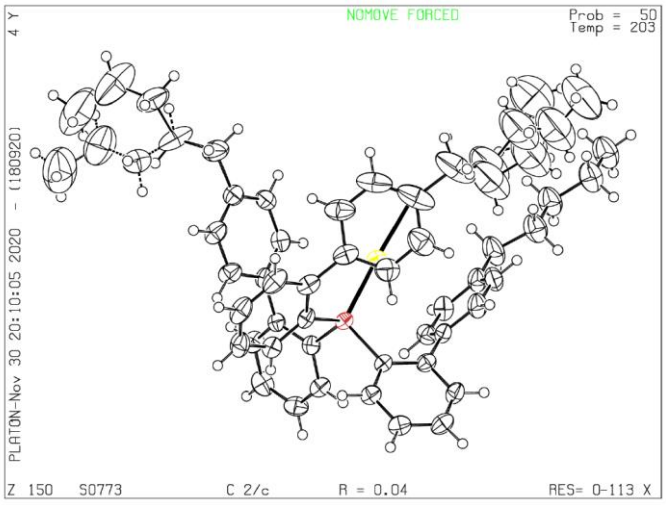

Datablock: S0773

```
Bond precision:   C-C = 0.0076 A          Wavelength=0.71073

Cell:             a=31.620(5)     b=14.515(3)          c=20.726(4)
                  alpha=90        beta=111.050(5)      gamma=90
Temperature:      203 K

                 Calculated                Reported
Volume           8878(3)                   8877(3)
Space group      C 2/c                     C 2/c
Hall group       -C 2yc                    -C 2yc
Moiety formula   C51 H57 Au Cl P           C51 H57 Au Cl P
Sum formula      C51 H57 Au Cl P           C51 H57 Au Cl P
Mr               933.36                    933.35
Dx,g cm-3        1.397                     1.397
Z                8                         8
Mu (mm-1)        3.443                     3.443
F000             3792.0                    3792.0
F000'            3779.26
h,k,lmax         43,20,28                  43,20,28
Nref             12454                     12423
Tmin,Tmax        0.524,0.794               0.648,0.746
Tmin'            0.471

Correction method= # Reported T Limits: Tmin=0.648 Tmax=0.746
AbsCorr = MULTI-SCAN

Data completeness= 0.998          Theta(max)= 29.574

R(reflections)= 0.0439( 7289)     wR2(reflections)= 0.0932( 12423)

S = 0.998                 Npar= 553
```

6.1.23. Calculation of percent buried volumes (V_{Bur}%) and generation of topographic steric maps (TSM)

The percent buried volumes (V_{Bur}%) and topographic steric maps (TSM) were calculated and generated using the SambVca 2.1[4,5] software available online.[3]

The following parameters were employed: r= 3.5 Å (radius of the sphere around the metal center), d= 2.23 Å (X-ray average P–Au bond distances) for phosphine-AuCl complexes **2.3-9 – 2-13**, **2.3-5**, and **2.3-13** or d= 1.99 Å for IPr-AuCl **2.3-14**; bondi radii scaled by 1.17; Au, counteranion and solvent molecule removed for calculation; H omitted for calculation; mesh spacing for numerical integration (0.05 instead of 0.1 for a better resolution of the topographic steric map).

• Au-Cl complex **2.3-8** V_{Bur}%= 30.8%

[3] https://www.molnac.unisa.it/OMtools/sambvca2.1/index.html

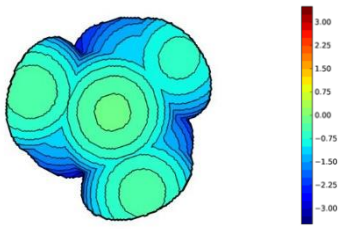

Calculations performed using SCXRD data from the literature.[6]

- Au-Cl complex (**2.3-9**) V_{Bur}%= 42.4%

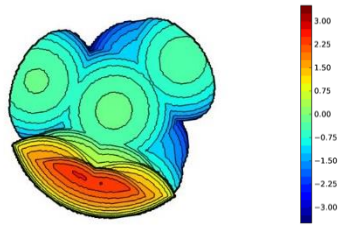

Calculations performed using SCXRD data from the literature.[7]

- Au-Cl complex (**2.3-10**) V_{Bur}%= 53.6%

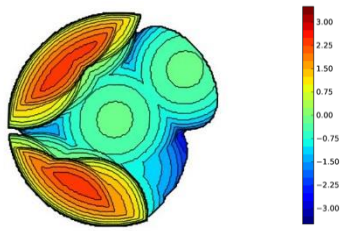

Calculations performed using SCXRD data from the literature.[8]

- Au-Cl complex (**2.3-11**) V_{Bur}%= 50.7%

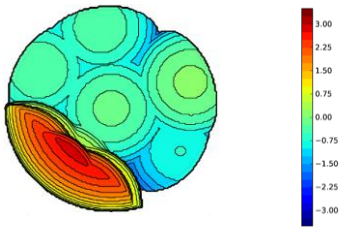

Calculations performed using SCXRD data from the literature.[9]

- Au-Cl complex (**2.3-12**) V_{Bur}%= 53.4%

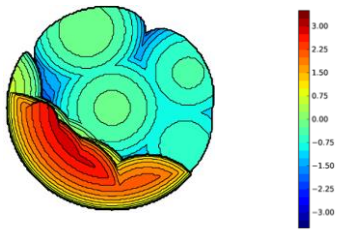

Calculations performed using SCXRD data from the literature.[10]

- Au-Cl complex (**2.3-13**) V_{Bur}%= 46.3%

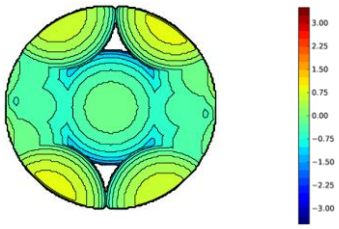

Calculations performed using SCXRD data from the literature.[11]

- Simulated Au complex (**2.3-14**) V_{Bur}%= 32.1%

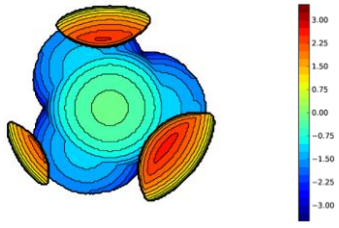

Calculations performed using SCXRD data of the *tris*-alkynylsilyl ligand **1b** from the literature.[12]

- Au-Cl complex (**2.3-15**) V_{Bur}%= 37.6%

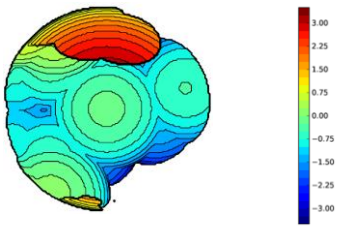

Calculations performed using SCXRD data of complex **A** from the literature.[13]

- Au-Cl complex (**2.3-5$_H$**) $V_{Bur\%}$= 64.5%

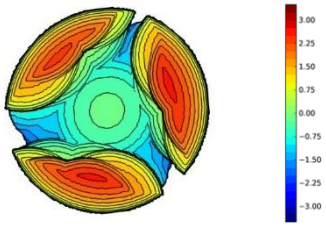

Calculations performed using SCXRD data from the present work. See section SCXRD analyses

• Au-Cl complex (**2.3-5$_{mtBu}$**) $V_{Bur\%}$= 67.5%

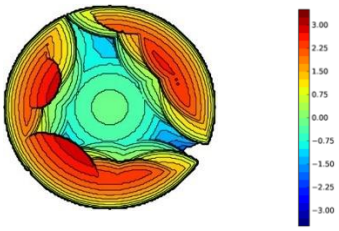

Calculations performed using SCXRD data from the present work. See section SCXRD analyses

• Au-Cl complex (**2.3-5$_{nPe}$**) $V_{Bur\%}$= 63.5%

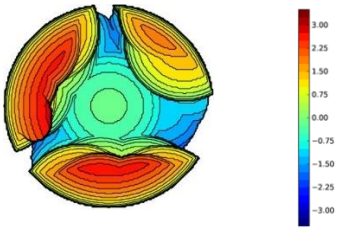

Calculations performed using SCXRD data from the present work. See section SCXRD analyses

6.1.23. Calculation of G_{Au} parameters, equivalent cone angles (ECA) and generation of solid angle spherical projections (SASP)

The percent G_{Au} parameters, the equivalent cone angles (ECA) and the solid angle spherical projections were calculated using the Solid-G software and its extension SolidAngleGL[14] which can be downloaded online.[4]

The default software parameters were used for the calculations of G_{Au}(L) (P atom or carbene center to Au distances employed are those from the corresponding SCXRD data). The steric projections coloured in red were generated using a bound sphere with a radius of 8 Å and a granulometry of 900.

[4] https://xray.chem.wisc.edu/solid-g/

• Au-Cl complex (**2.3-8**) G_{Au}= 28.5% ECA= 128.5°

Calculations performed using SCXRD data from the literature.[6]

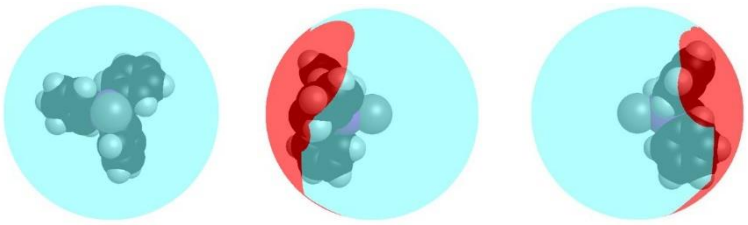

• Au-Cl complex (**2.3-9**) G_{Au}= 39.8% ECA= 156.6°

Calculations performed using SCXRD data from the literatue.[7]

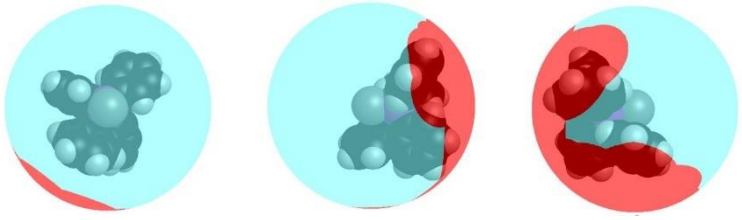

• Au-Cl complex (**2.3-10**) G_{Au}= 50.9% ECA= 182.0°

Calculations performed using SCXRD data from the literature.[8]

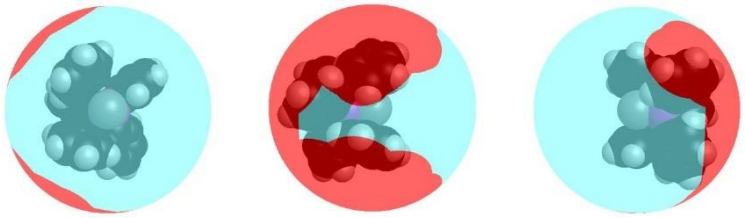

• Au-Cl complex (**2.3-11**) G_{Au}= 47.3% ECA= 173.7°

Calculations performed using SCXRD data from the literature.[9]

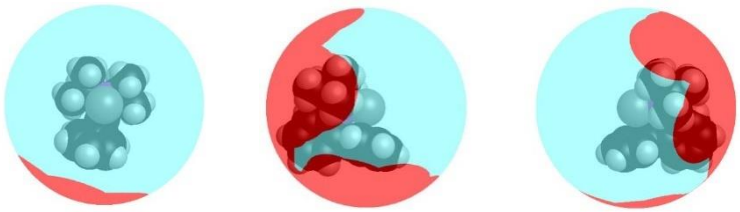

- Au-Cl complex (**2.3-12**) G_{Au}= 56.1% ECA= 194.1°

Calculations performed using SCXRD data from the literature.[10]

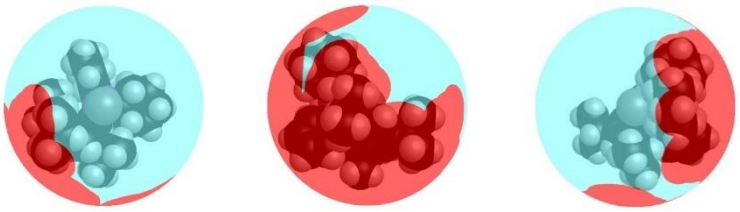

- Au-Cl complex (**2.3-13**) G_{Au}= 47.6% ECA= 174.5°

Calculations performed using SCXRD data from the literature.[11]

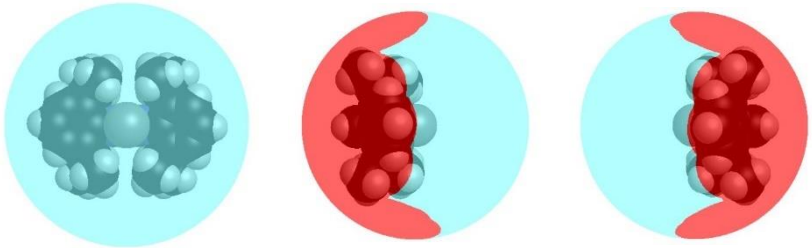

- Simulated Au complex (**2.3-14**) G_{Au}= 55.1% ECA= 181.6°

Calculations performed using SCXRD data of the *tris*-alkynylsilyl ligand **1b** from the literature.[12]

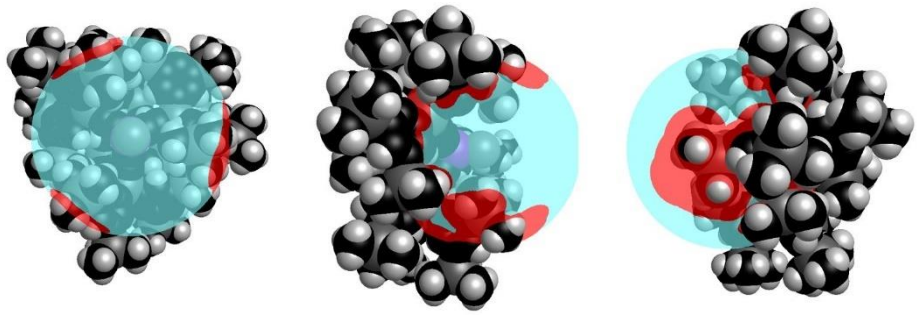

• Au-Cl complex (**2.3-15**) G_{Au}= 65.4% ECA= 216.0°

Calculations performed using SCXRD data of complex **A** from the literature.[13]

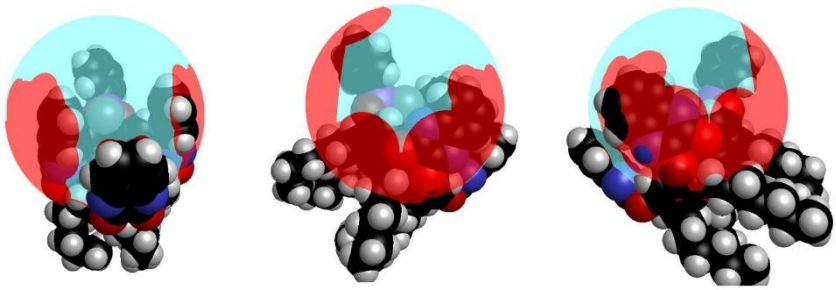

• Au-Cl complex (**2.3-5$_H$**) G_{Au}= 61.8% ECA= 207.3°

Calculations performed using SCXRD data from the present work. See section SCXRD analyses

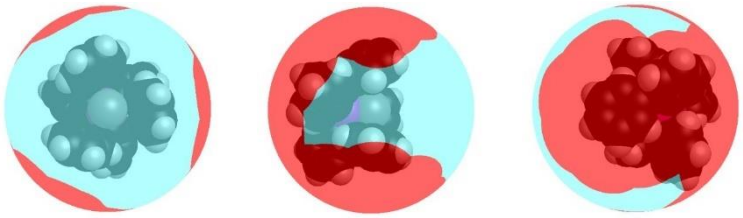

• Au-Cl complex (**2.3-5$_{mtBu}$**) G_{Au}= 74.0% ECA= 237.4°

Calculations performed using SCXRD data from the present work. See section SCXRD analyses

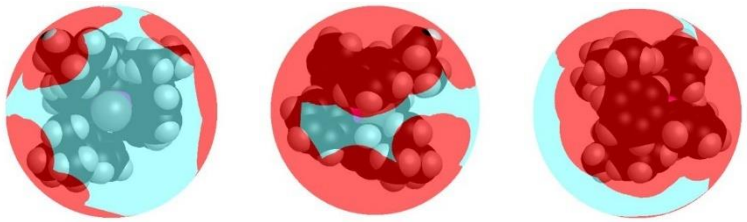

• Au-Cl complex (**2.3-5$_{nPe}$**) G_{Au}= 67.5% ECA= 216.5°

Calculations performed using SCXRD data from the present work. See section SCXRD analyses

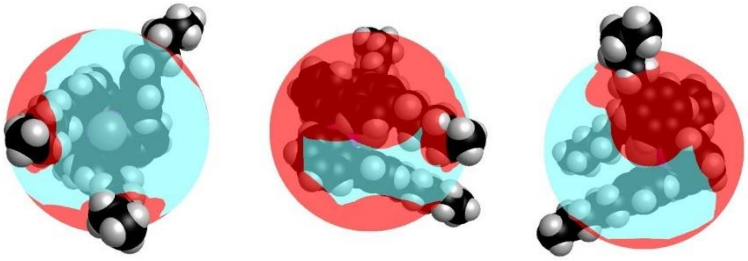

6.1.24. List of references

(1) Blessing, R. H. An Empirical Correction for Absorption Anisotropy. *Acta Crystallogr. Sect. A* **1995**, *51* (1), 33–38. https://doi.org/10.1107/S0108767394005726.

(2) Sheldrick, G. M. A Short History of SHELX. *Acta Crystallogr. Sect. A* **2008**, *64* (1), 112–122. https://doi.org/10.1107/S0108767307043930.

(3) Hübschle, C. B.; Sheldrick, G. M.; Dittrich, B. ShelXle: A Qt Graphical User Interface for SHELXL. *J. Appl. Crystallogr.* **2011**, *44* (6), 1281–1284. https://doi.org/10.1107/S0021889811043202.

(4) Falivene, L.; Credendino, R.; Poater, A.; Petta, A.; Serra, L.; Oliva, R.; Scarano, V.; Cavallo, L. SambVca 2. A Web Tool for Analyzing Catalytic Pockets with Topographic Steric Maps. *Organometallics* **2016**, *35* (13), 2286–2293. https://doi.org/10.1021/acs.organomet.6b00371.

(5) Falivene, L.; Cao, Z.; Petta, A.; Serra, L.; Poater, A.; Oliva, R.; Scarano, V.; Cavallo, L. Towards the Online Computer-Aided Design of Catalytic Pockets. *Nat. Chem.* **2019**, *11* (10), 872–879. https://doi.org/10.1038/s41557-019-0319-5.

(6) Dunstan, S. P. C.; Healy, P. C.; Sobolev, A. N.; Tiekink, E. R. T.; White, A. H.; Williams, M. L.

Isomorphism in the Structural Chemistry of Two-Coordinate Adducts of Diphenyl(2-Formylphenyl)Phosphine and Triphenylphosphine with Gold(I) Halides. *J. Mol. Struct.* **2014**, *1072*, 253–259. https://doi.org/10.1016/j.molstruc.2014.05.020.

(7) Barnes, N. A.; Flower, K. R.; Fyyaz, S. A.; Godfrey, S. M.; McGown, A. T.; Miles, P. J.; Pritchard, R. G.; Warren, J. E. Can the Solid State Structures of the Dihalogen Adducts R_3EX_2 (E = P, As; R = Alkyl, Aryl; X = Br, I) with the Molecular Spoke Geometry Be Considered Good Mimics of the Gold(I) Systems [$(R_3E)AuX$] (E = As, P; R = Alkyl, Aryl; X = Cl, Br, I)? *CrystEngComm* **2010**, *12* (3), 784–794. https://doi.org/10.1039/B917245A.

(8) Griebel, C.; Hodges, D. D.; Yager, B. R.; Liu, F. L.; Zhou, W.; Makaravage, K. J.; Zhu, Y.; Norman, S. G.; Lan, R.; Day, C. S.; Jones, A. C. Bisbiphenyl Phosphines: Structure and Synthesis of Gold(I) Alkene π-Complexes with Variable Phosphine Donicity and Enhanced Stability. *Organometallics* **2020**, *39* (14), 2665–2671. https://doi.org/10.1021/acs.organomet.0c00278.

(9) Grirrane, A.; Álvarez, E.; García, H.; Corma, A. Deactivation of Cationic Cu^{I} and Au^{I} Catalysts for A^3 Coupling by CH_2Cl_2: Mechanistic Implications of the Formation of Neutral Cu^{I} and Au^{I} Chlorides. *Angew. Chemie Int. Ed.* **2014**, *53* (28), 7253–7258. https://doi.org/10.1002/anie.201403973.

(10) Touil, M.; Bechem, B.; Hashmi, A. S. K.; Engels, B.; Omary, M. A.; Rabaâ, H. Theoretical Study of Weak CC Double Bond Coordination in a Gold (I) Catalyst Precursor. *J. Mol. Struct. THEOCHEM* **2010**, *957* (1), 21–25. https://doi.org/10.1016/j.theochem.2010.06.030.

(11) de Frémont, P.; Scott, N. M.; Stevens, E. D.; Nolan, S. P. Synthesis and Structural Characterization of N-Heterocyclic Carbene Gold(I) Complexes. *Organometallics* **2005**, *24* (10), 2411–2418. https://doi.org/10.1021/om050111c.

(12) Ochida, A.; Sawamura, M. Phosphorus Ligands with a Large Cavity: Synthesis of Triethynylphosphines with Bulky End Caps and Application to the Rhodium-Catalyzed Hydrosilylation of Ketones. *Chem. – An Asian J.* **2007**, *2* (5), 609–618. https://doi.org/10.1002/asia.200700006.

(13) Martín-Torres, I.; Ogalla, G.; Yang, J.-M.; Rinaldi, A.; Echavarren, A. M. Enantioselective Alkoxycyclization of 1,6-Enynes with Gold(I)-Cavitands: Total Synthesis of Mafaicheenamine C. *Angew. Chemie Int. Ed.* **2021**, *60* (17), 9339–9344. https://doi.org/10.1002/anie.202017035.

(14) Guzei, I. A.; Wendt, M. An Improved Method for the Computation of Ligand Steric Effects Based on Solid Angles. *Dalt. Trans.* **2006**, No. 33, 3991–3999. https://doi.org/10.1039/B605102B.

6.2. Appendix for Chapter 3

6.2.1. First set of pyridine-based ligands tested

The following ligand were initially tested using exp1 & 2 described in **Scheme 3.3-2** of the thesis. When a negative result was obtained with Exp1, the ligand was not tested in Exp2.

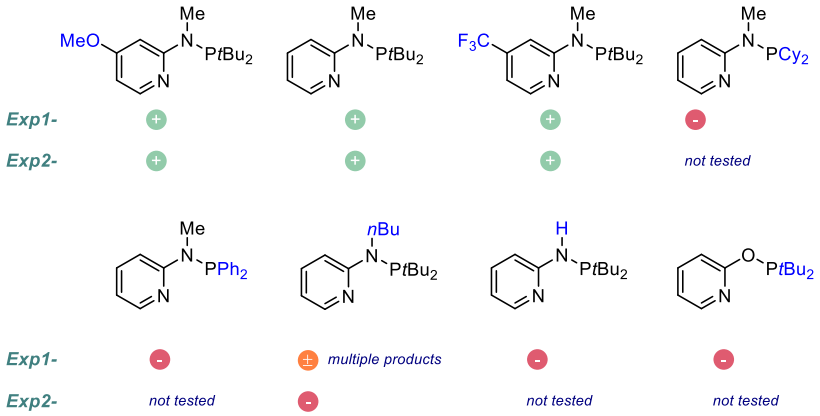

Figure 6.2-1. First set of pyridine-based ligands tested.

6.2.2. Alkoxyarylation with pent-4-en-1-ol 3.3-16a (Chapter 3, Scheme 3.3-4, A)

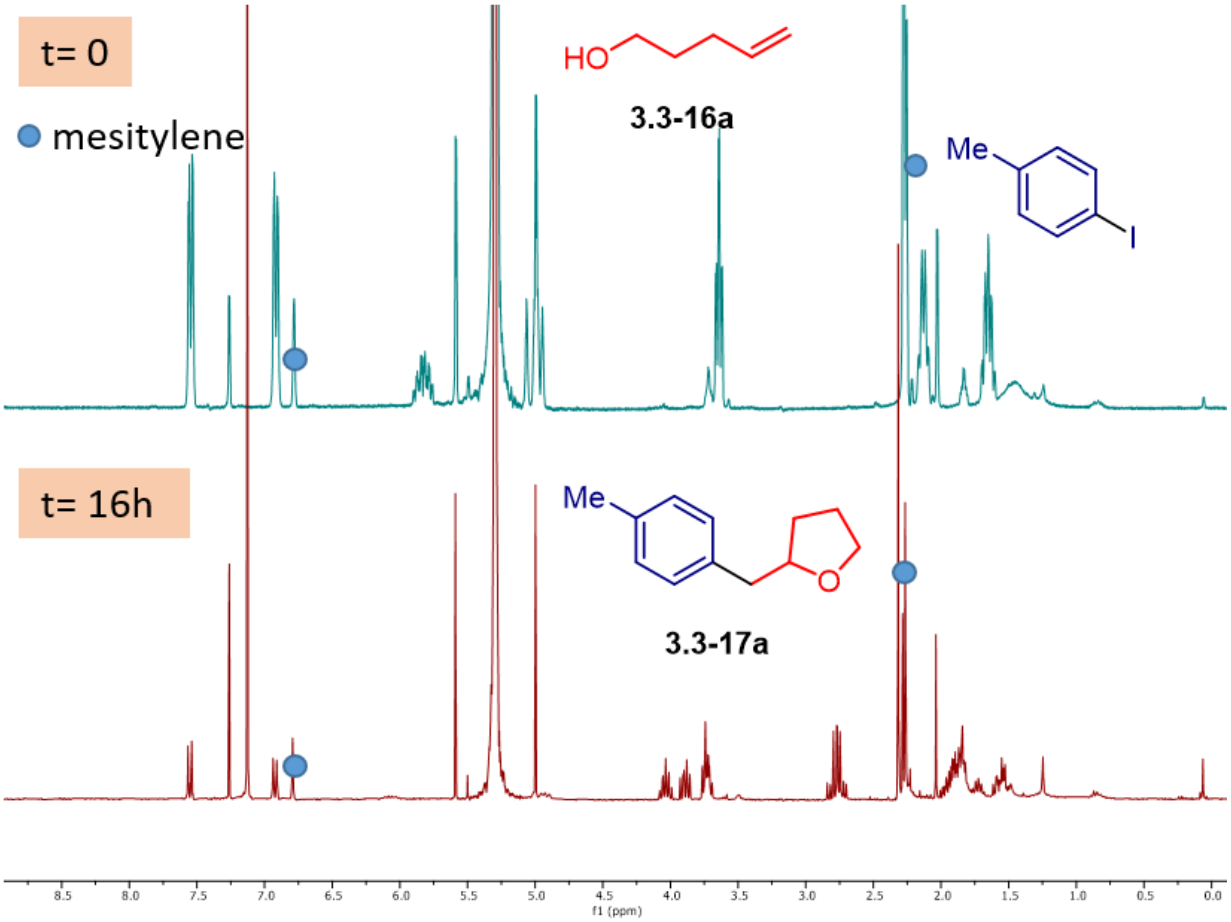

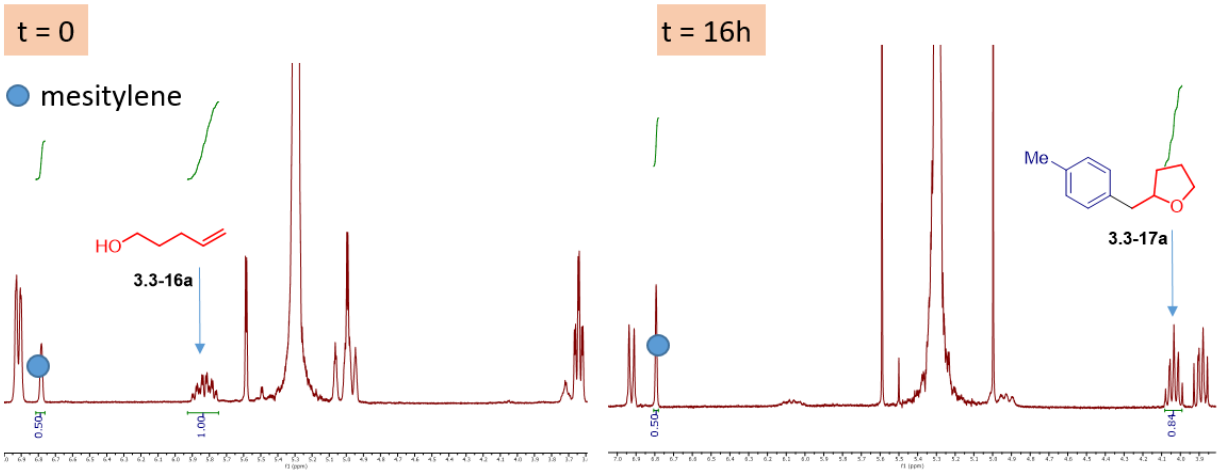

Figure 6.2-2. A representative ^{1}H NMR spectra @t= 0 and t= 16h with complex **3.3-31$_{Cl}$.**

6.2.3. Amidoarylation with *N*-tosyl aminopentene 3.3-16b (Chapter 3, Scheme 3.3-4, A)

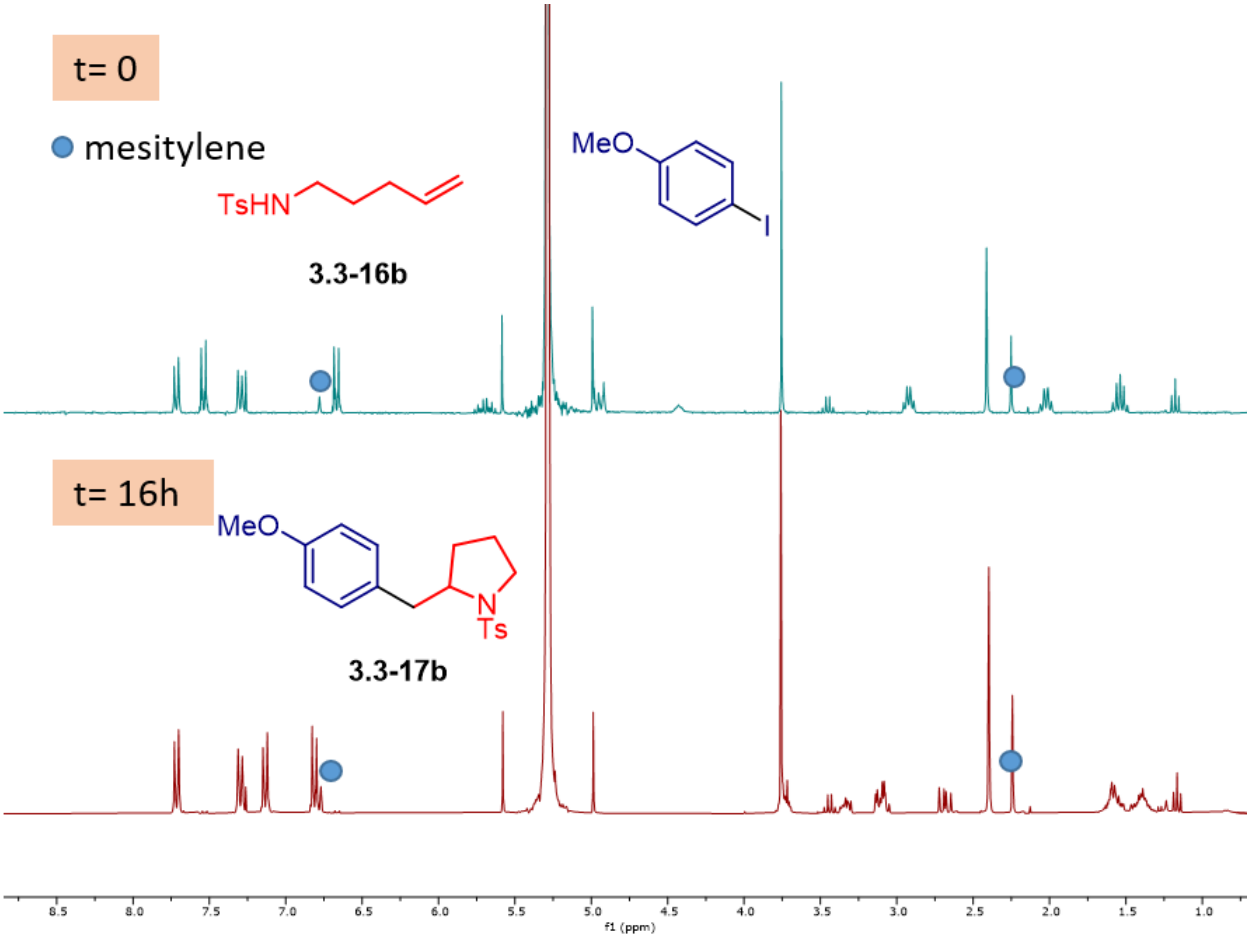

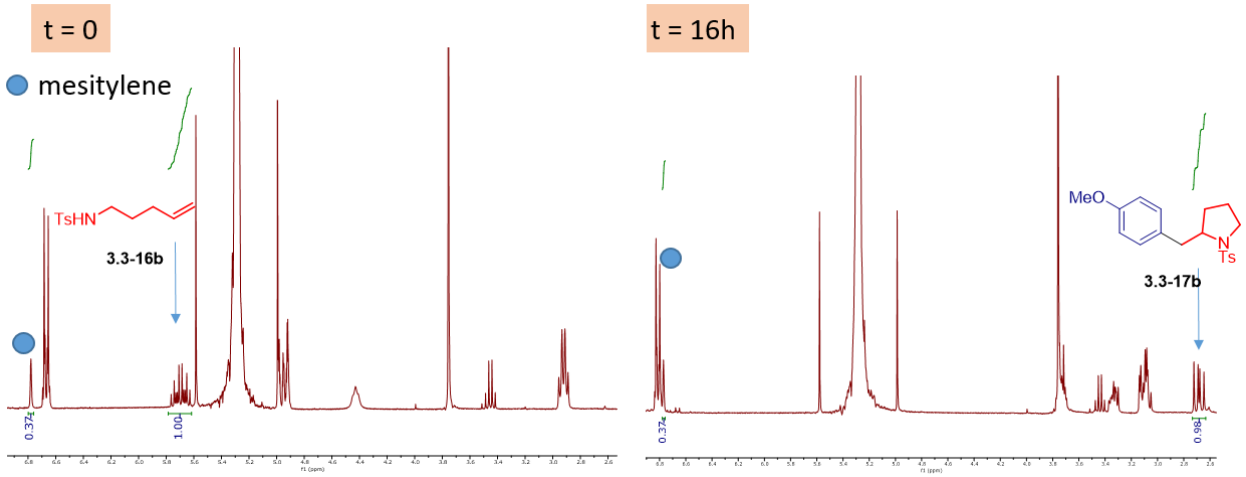

Figure 6.2-3. A representative ^{1}H NMR spectra @t= 0 and t= 16h with complex **3.3-31$_{Cl}$.**

6.2.4. Amination with 2-nitroaniline 3.3-24 (Chapter 3, Scheme 3.3-5)

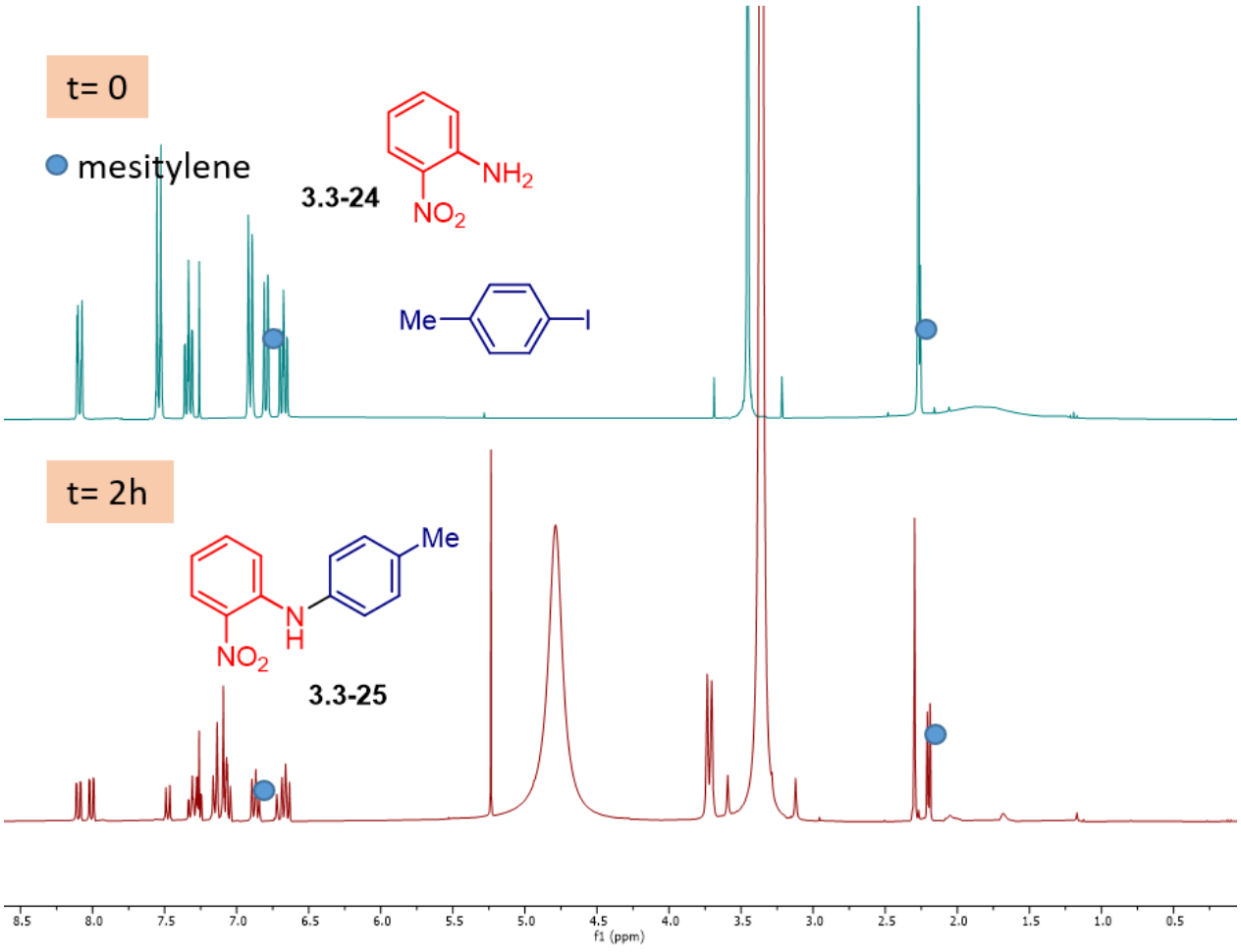

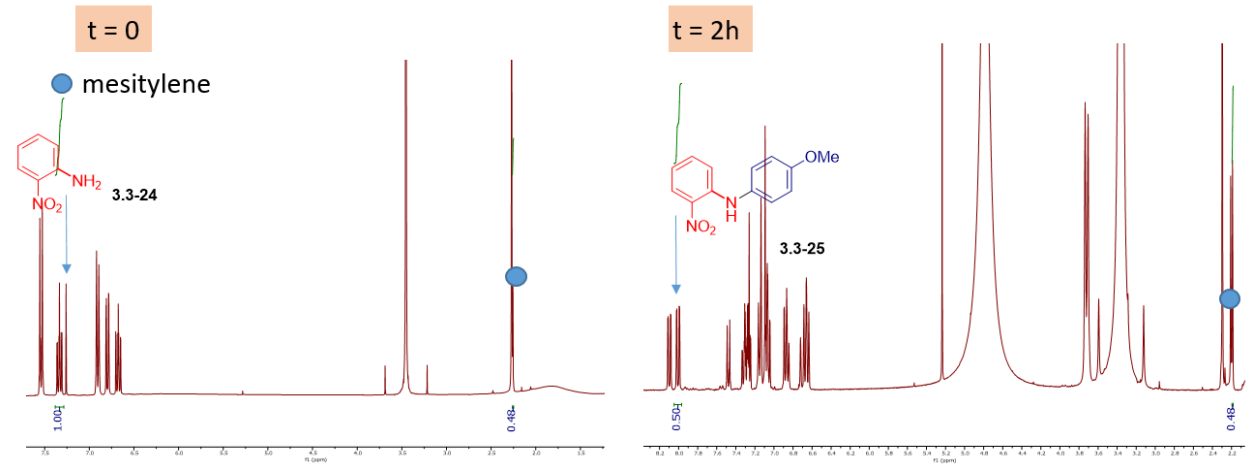

Figure 6.2-4. A representative ^{1}H NMR spectra @t= 0 and t= 2h with ligand **3.3-18** (MeDalPhos).

6.2.5. Heck reaction with hex-1-ene (Chapter 3, Scheme 3.3-5)

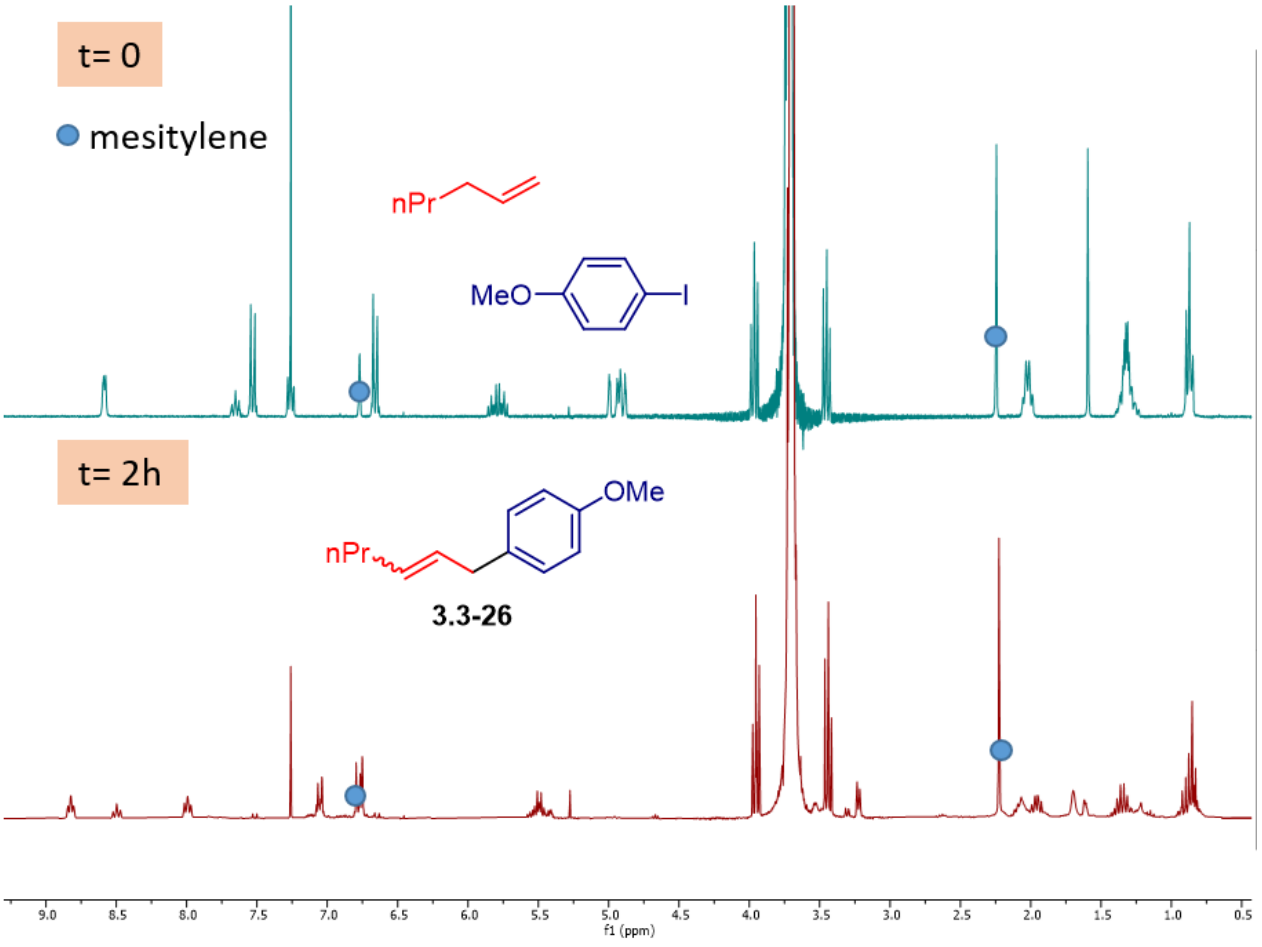

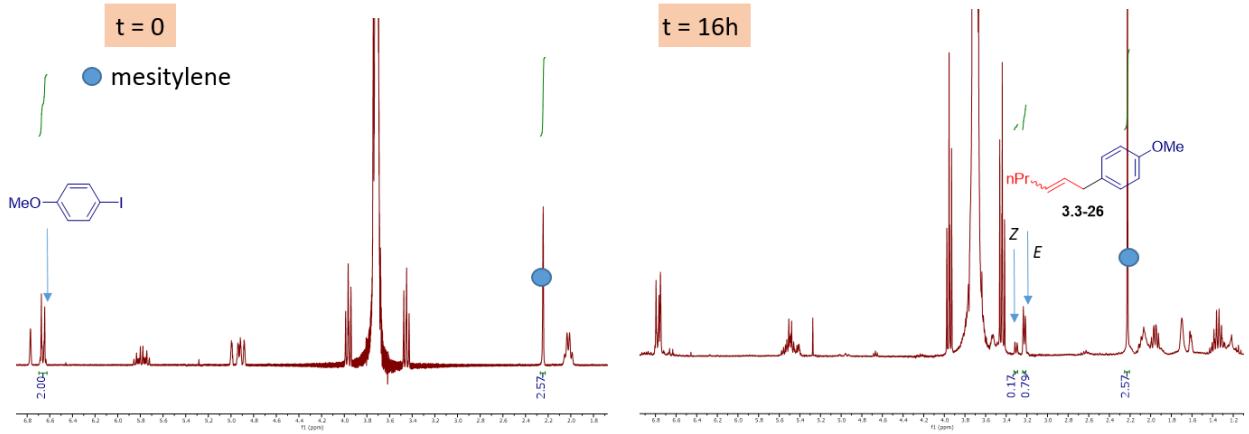

Figure 6.2-5. A representative ^{1}H NMR spectra @t= 0 and t= 2h with ligand **3.3-18** (MeDalPhos) and *base* = **pyridine**.

6.2.6. Transmetallation with tributyl(thiophen-2-yl)stannane 3.3-27a (Chapter 3, Scheme 3.3-6, A)

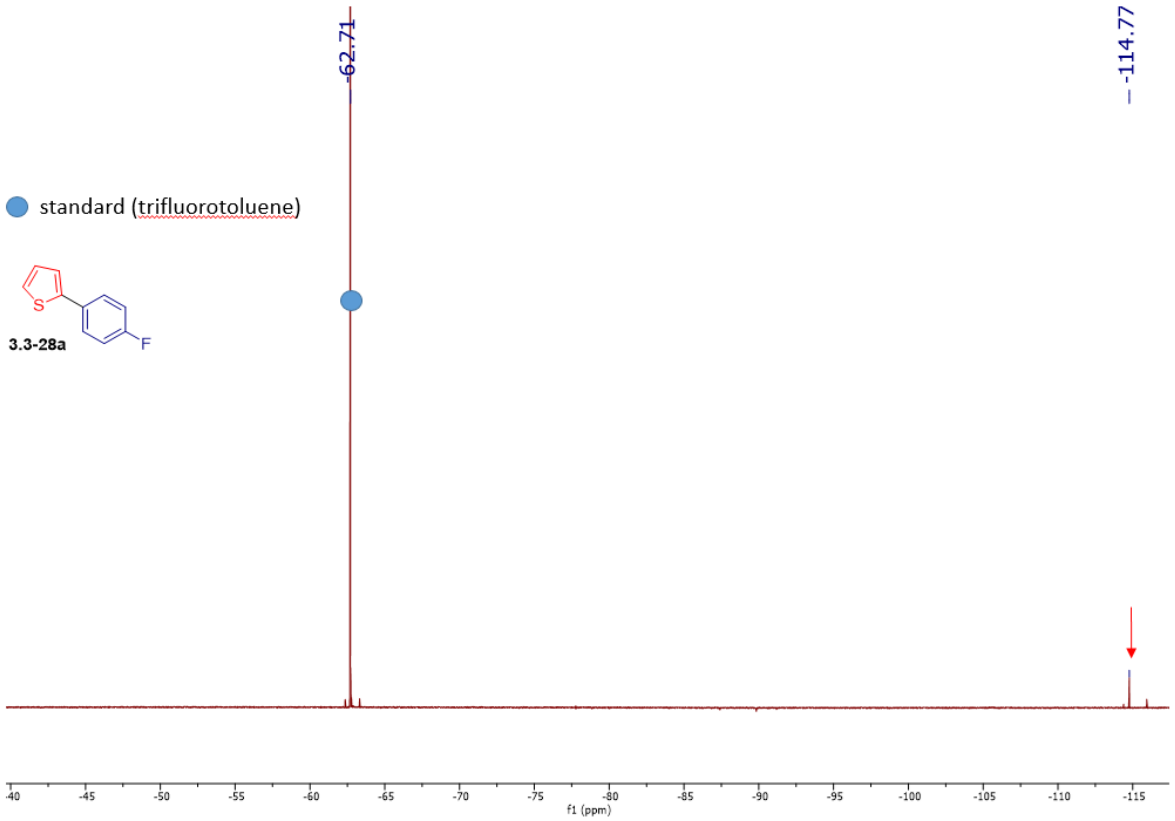

Figure 6.2-6. A representative ^{1}H NMR spectra @t= 0 and t= 12h with ligand **3.3-18** (MeDalPhos).

6.2.7. Transmetallation with silver reagent 3.3-27b (Chapter 3, Scheme 3.3-6, A)

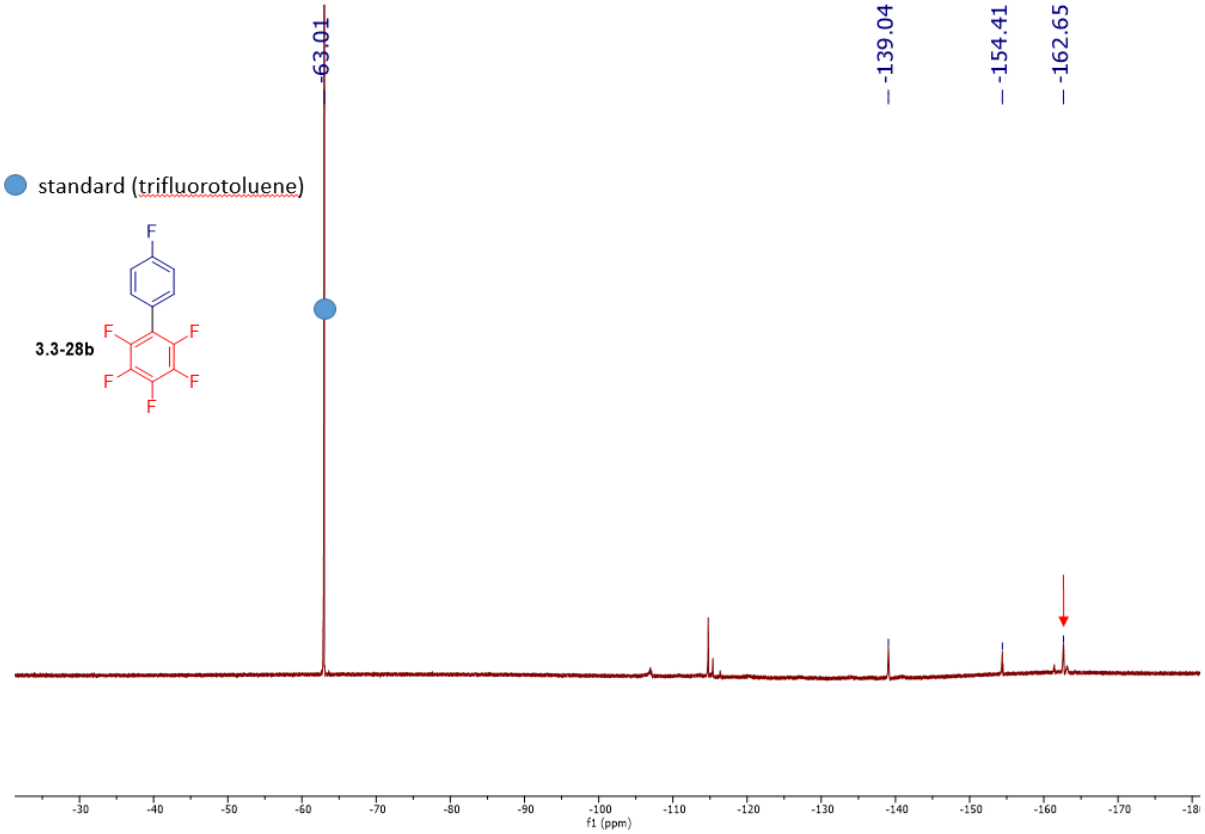

Figure 6.2-7. A representative ^{1}H NMR spectra @t= 0 and t= 6h with ligand **3.3-15**$_{H}$.

6.2.8. Alkoxyarylation with hex-5-en-1-ol 3.3-16c (Chapter 3, Scheme 3.3-8)

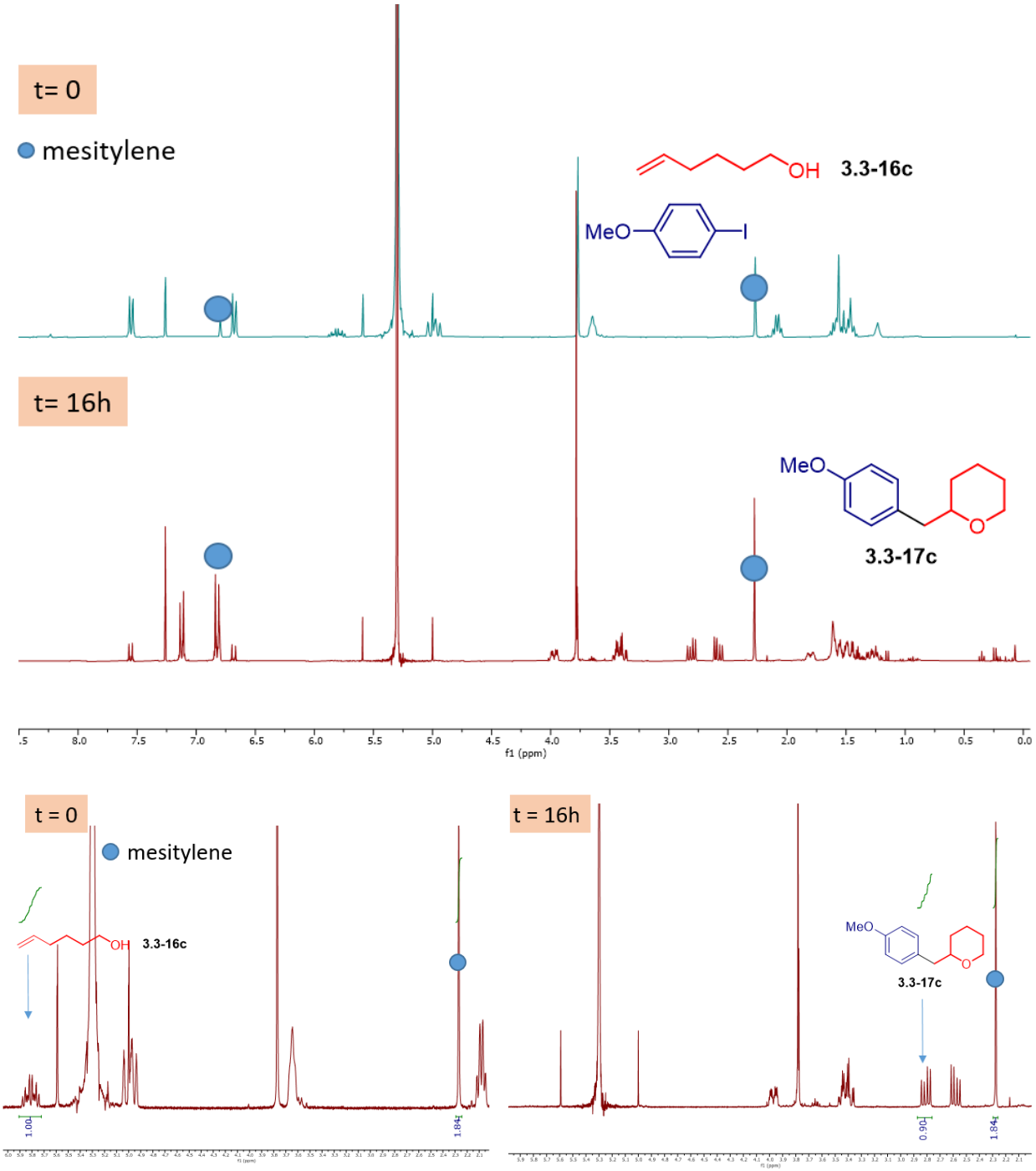

Figure 6.2-8. A representative ^{1}H NMR spectra @t= 0 and t= 16h with complex **3.3-31$_{Cl}$.**

6.2.9. Alkoxyarylation with (*E*)-(2-iodovinyl)benzene and pent-4-en-1-ol 3.3-16a (Chapter 3, Scheme 3.3-8)

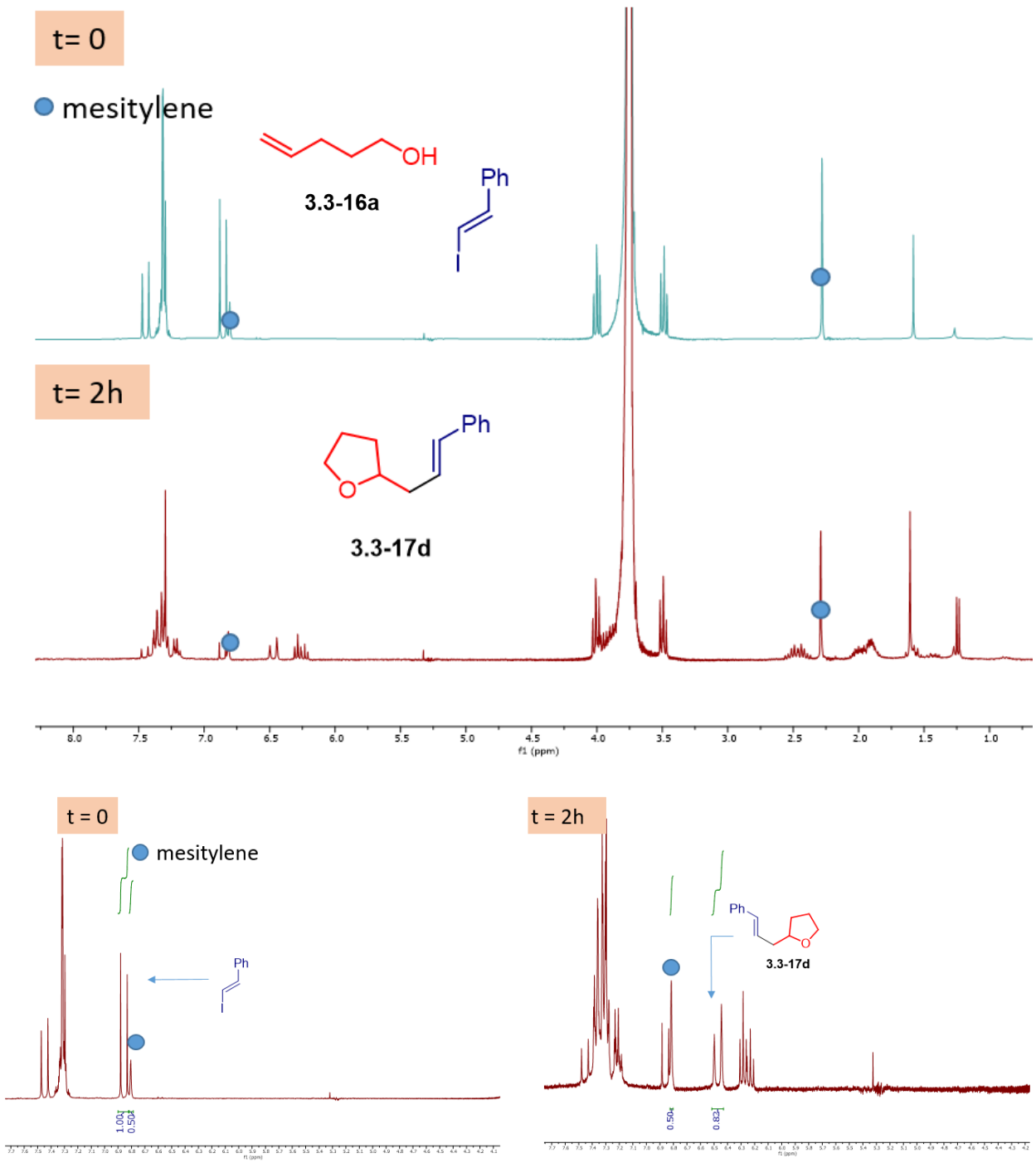

Figure 6.2-9. A representative ^{1}H NMR spectra @t= 0 and t= 2h with complex **3.3-31$_{Cl}$.**

6.2.10. Amidoarylation with (*E*)-(2-iodovinyl)benzene and *N*-tosyl aminopentene 3.3-16b (Chapter 3, Scheme 3.3-8)

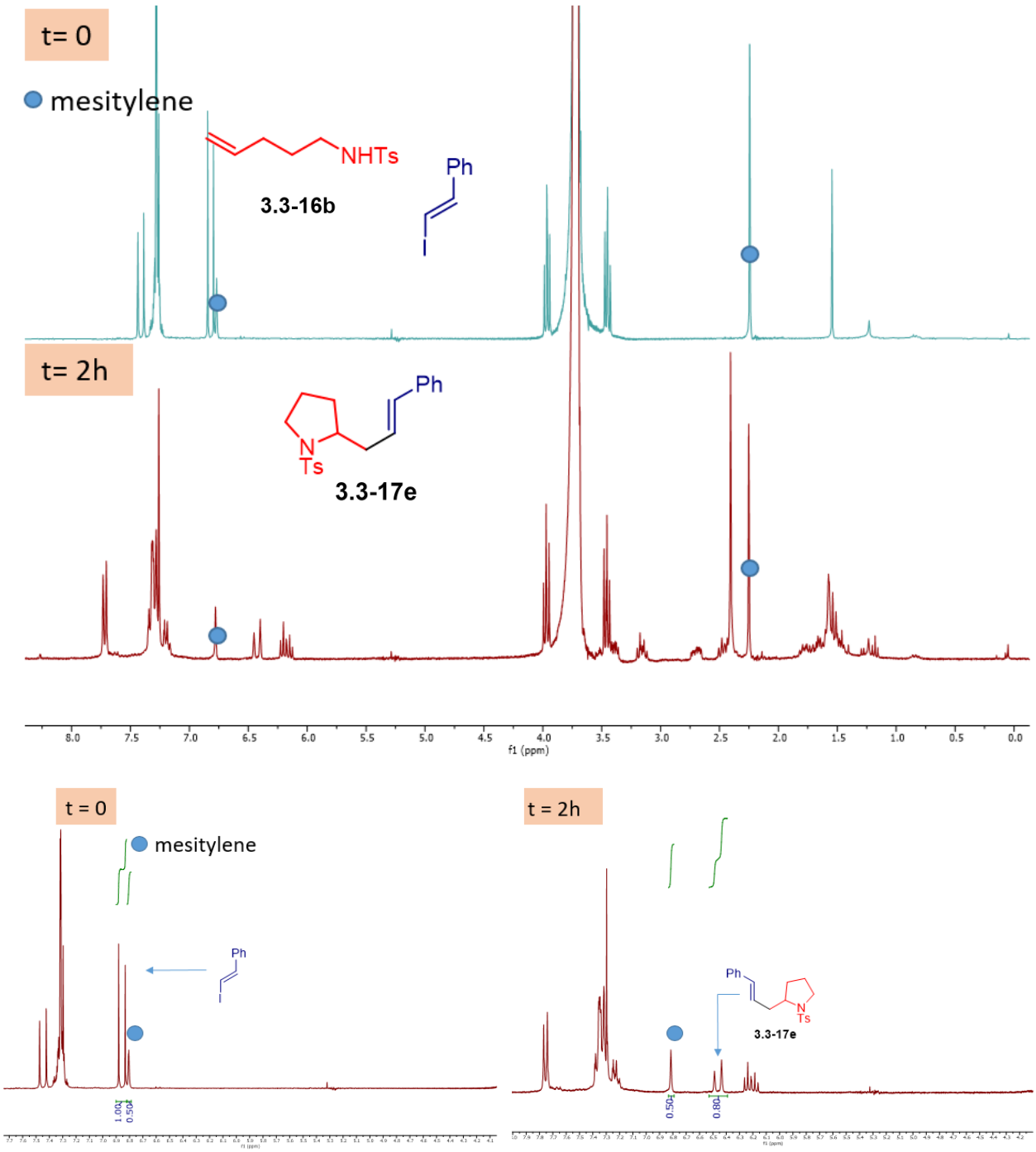

Figure 6.2-10. A representative ^{1}H NMR spectra @t= 0 and t= 2h with complex **3.3-31$_{Cl}$.**

6.2.11. General procedure for the calculation of yield of cross-coupling products 3.3-43 (Chapter 3, Scheme 3.3-11)

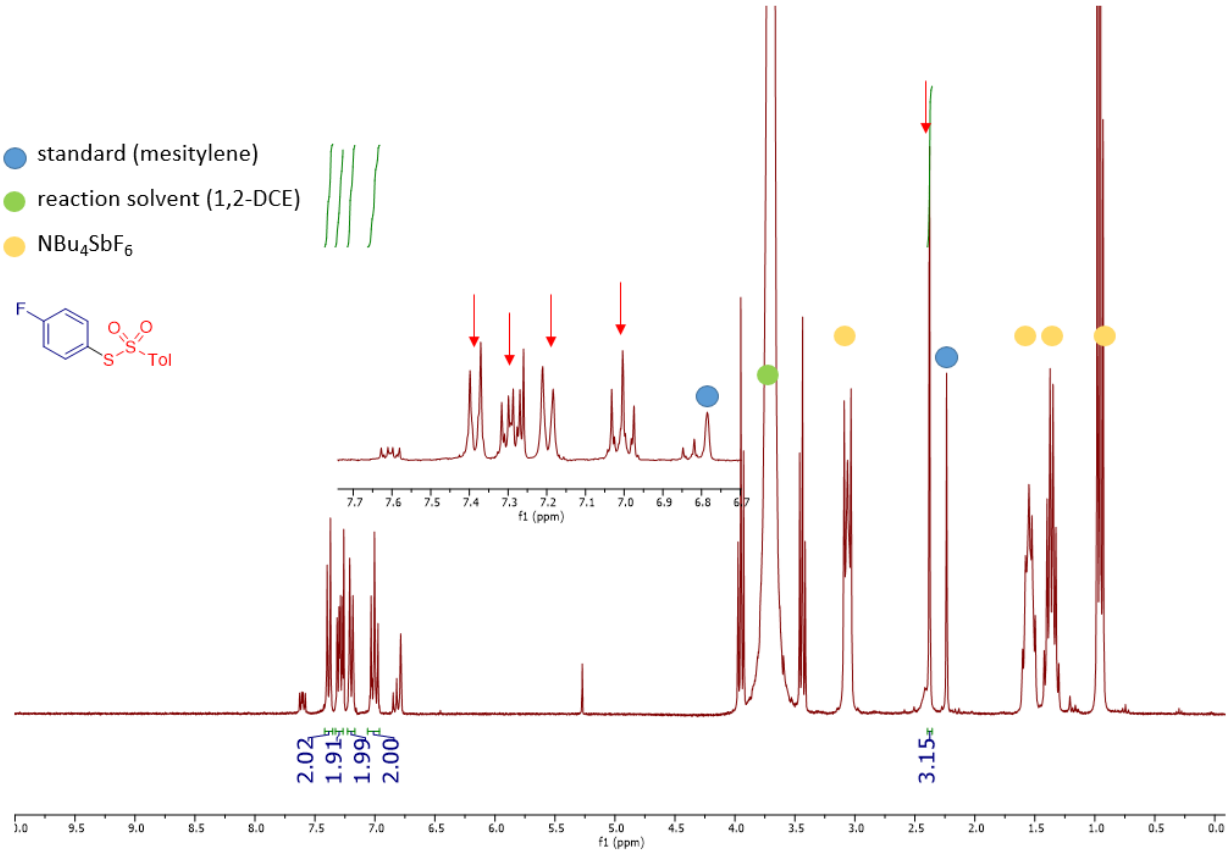

Figure 6.2-11. ^{1}H NMR analysis of the crude reaction mixture with *S*-(4-fluorophenyl) 4-methylbenzenesulfonothioate **3.3-43a.**

6.2.12. Calculation of yield of diversification product 3.3-44a (Chapter 3, Scheme 3.3-12)

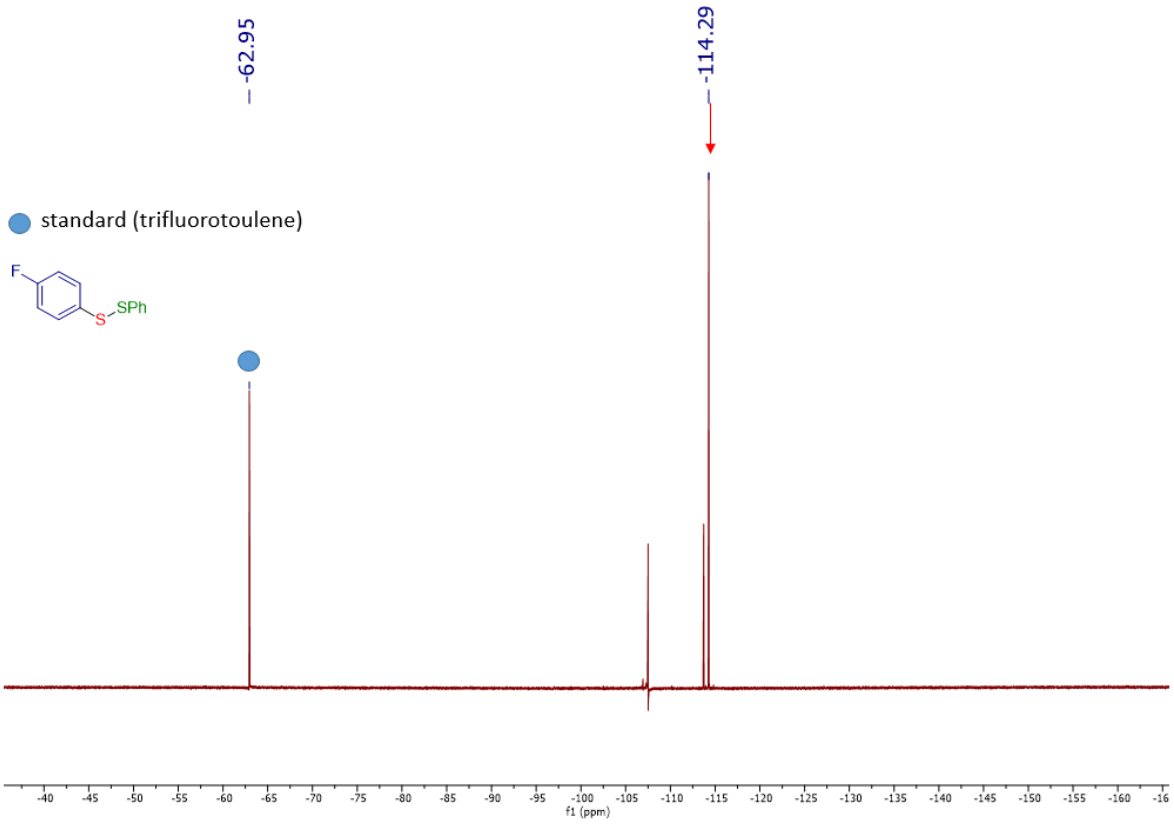

Figure 6.2-12. ^{19}F NMR analysis of the crude reaction mixture with 1-(4-fluorophenyl)-2-phenyldisulfane **3.3-44a**.

6.2.13. Calculation of yield of diversification product 3.3-44b (Chapter 3, Scheme 3.3-12)

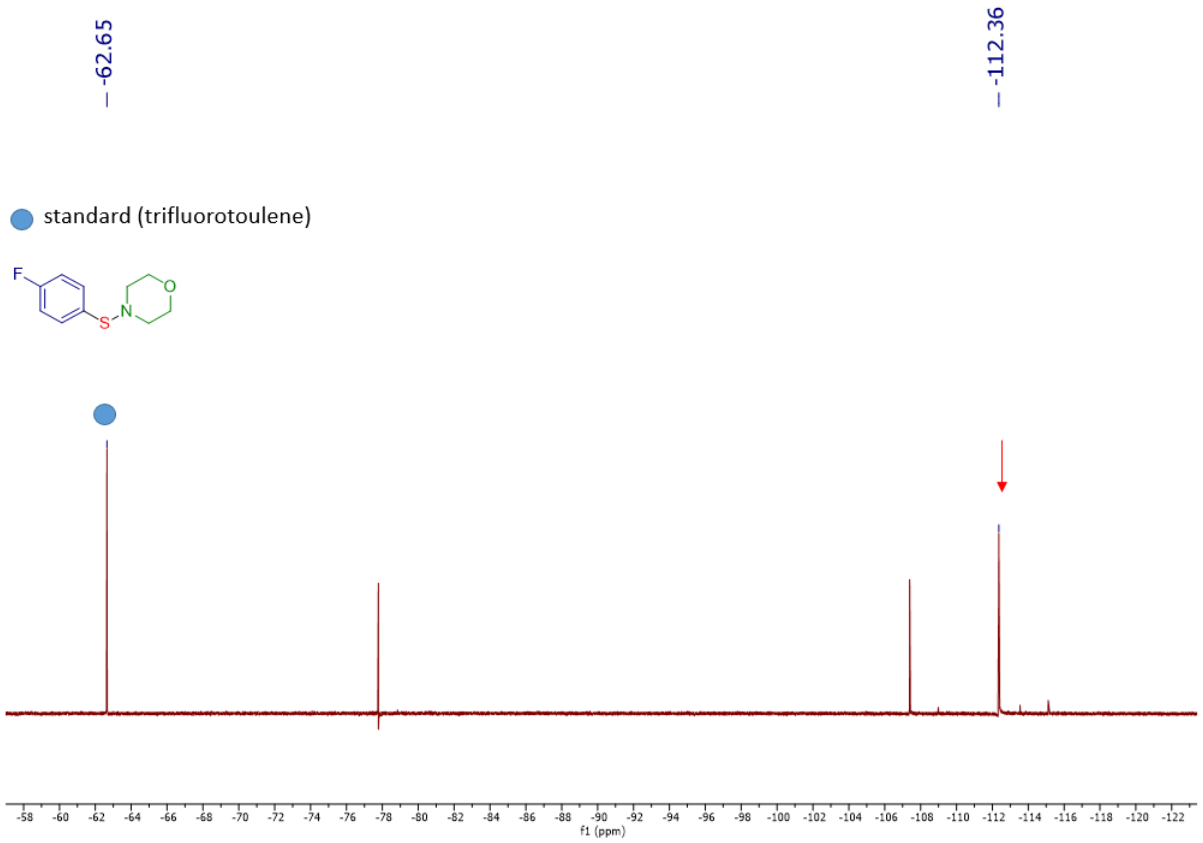

Figure 6.2-13. ^{19}F NMR analysis of the crude reaction mixture with 4-((4-fluorophenyl)thio)morpholine **3.3-44b.**

6.2.14. Calculation of yield of diversification product 3.3-44c (Chapter 3, Scheme 3.3-12)

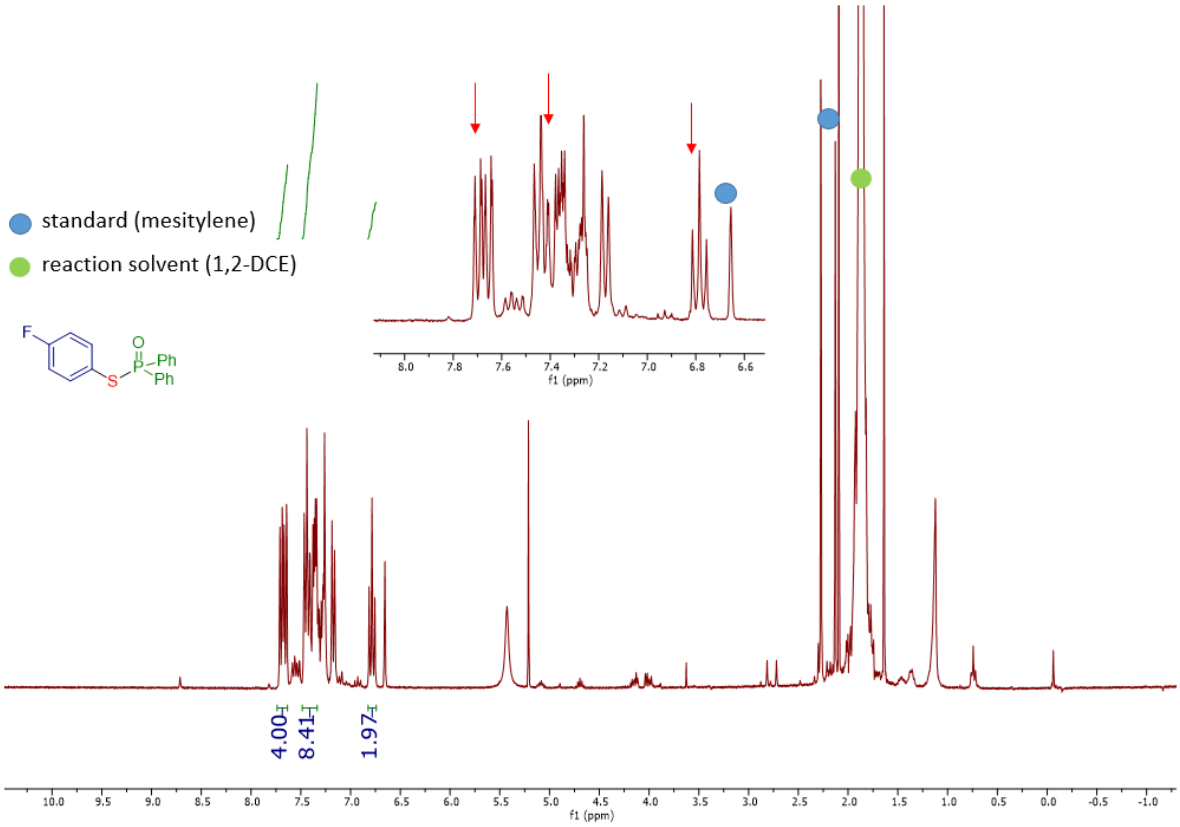

Figure 6.2-14. ^{1}H NMR analysis of the crude reaction mixture with S-(4-fluorophenyl) diphenylphosphinothioate **3.3-44c**.

6.2.15. Calculation of yield of diversification product 3.3-44d (Chapter 3, Scheme 3.3-12)

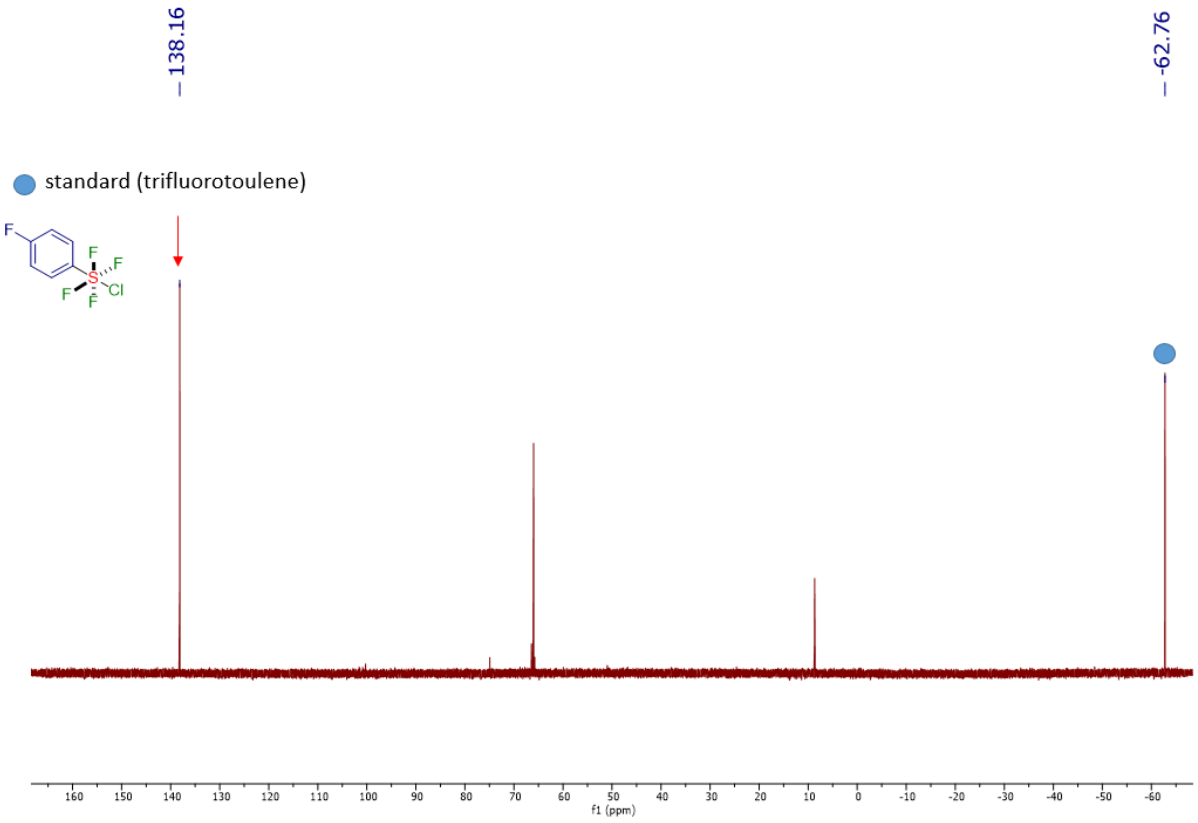

Figure 6.2-15. ^{19}F NMR analysis of the crude reaction mixture with chlorotetrafluoro(4-fluorophenyl)-λ^6-sulfane **3.3-44d**.

6.2.16. Calculation of yield of diversification product 3.3-44e (Chapter 3, Scheme 3.3-12)

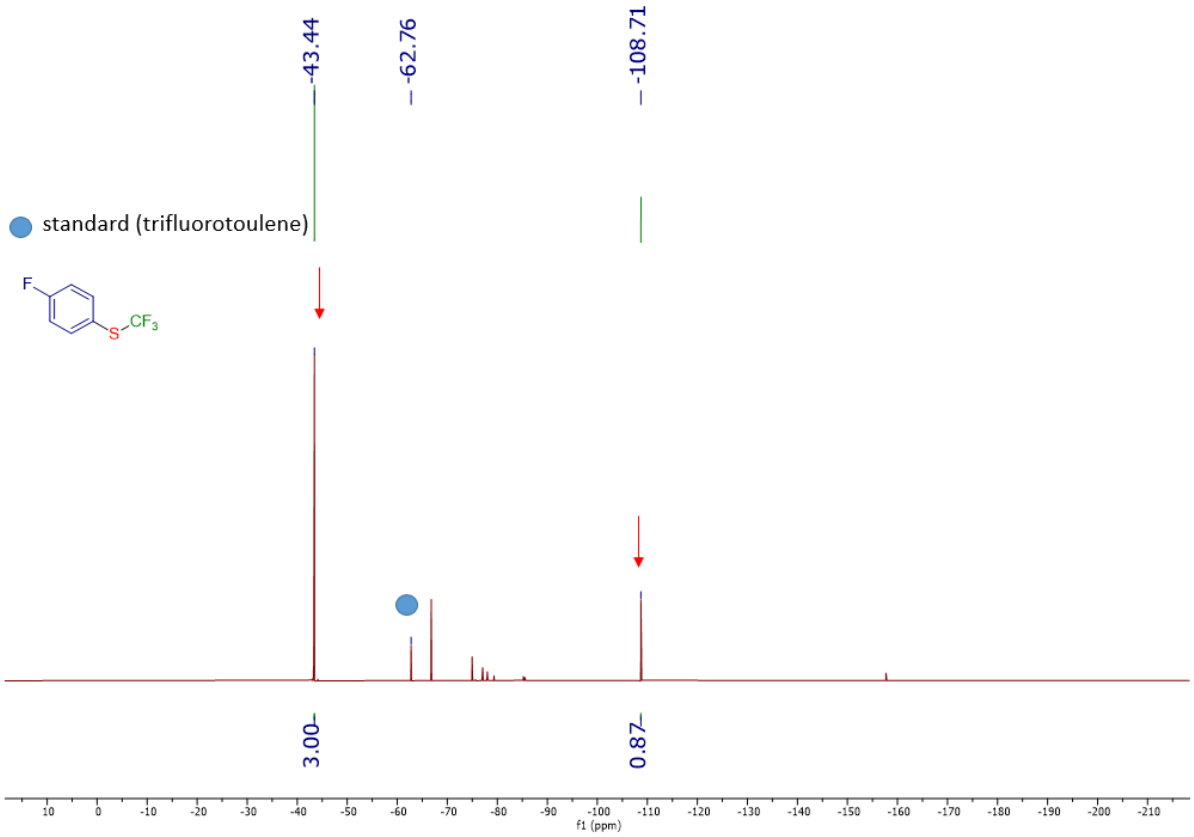

Figure 6.2-16. ^{19}F NMR analysis of the crude reaction mixture with (4-fluorophenyl)(trifluoromethyl)sulfane **3.3-44e**.

6.2.17. Calculation of yield of diversification product 3.3-44f (Chapter 3, Scheme 3.3-12)

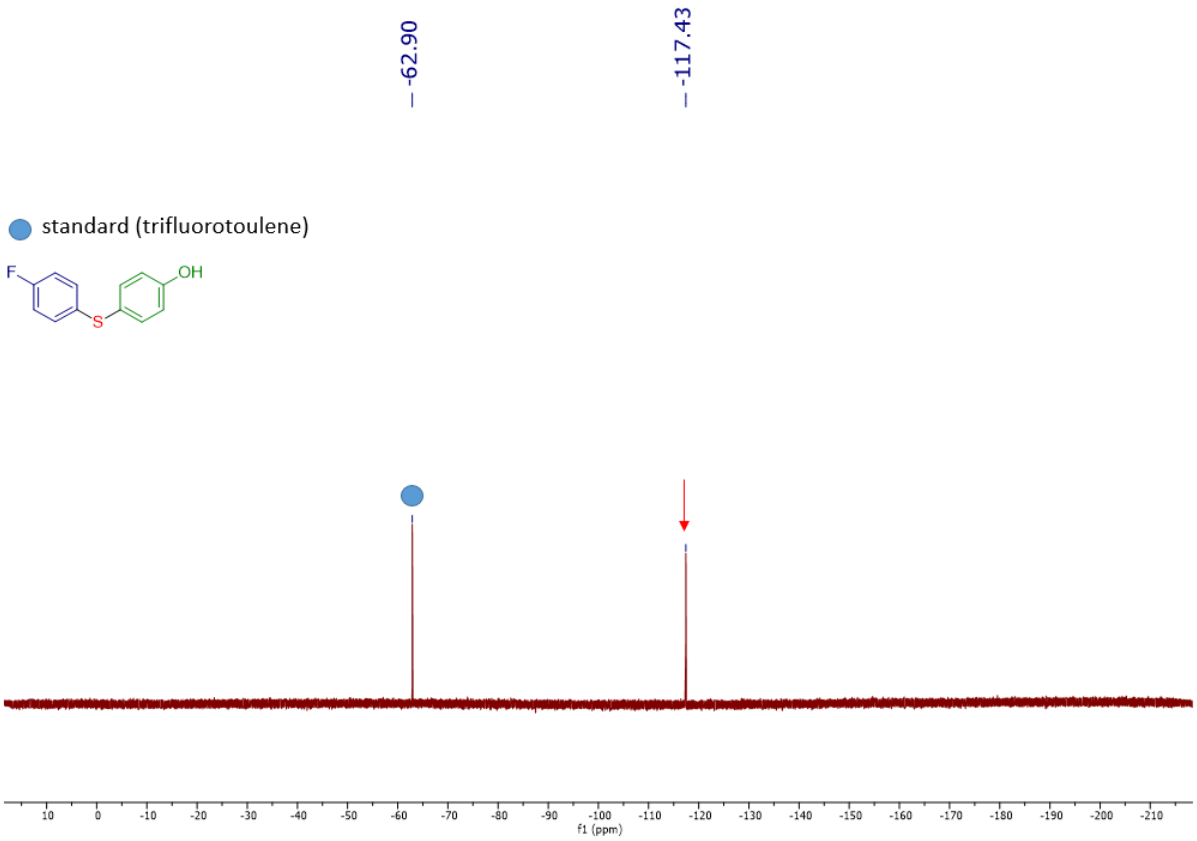

Figure 6.2-17. ^{19}F NMR analysis of the crude reaction mixture with 4-((4-fluorophenyl)thio)phenol **3.3-44f**.

6.2.18. Calculation of yield of diversification product 3.3-44g (Chapter 3, Scheme 3.3-12)

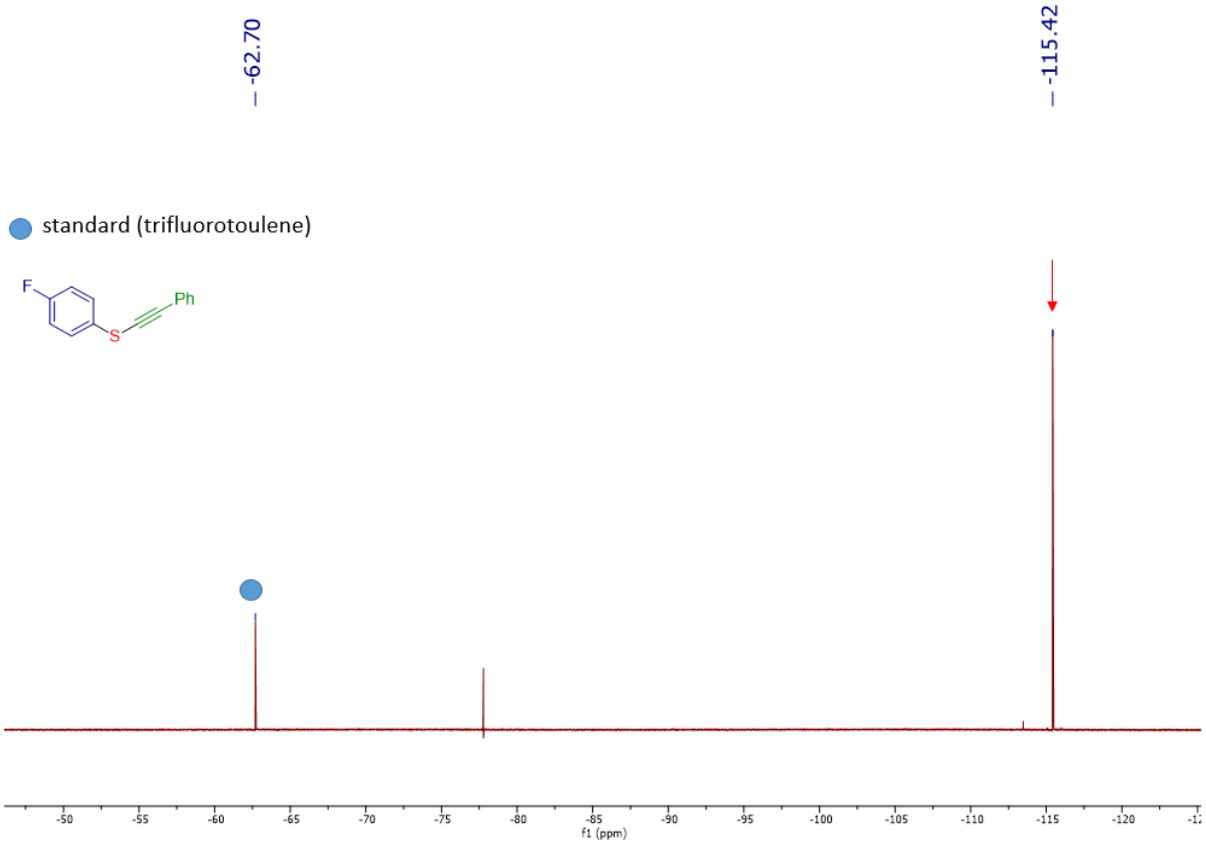

Figure 6.2-18. ^{19}F NMR analysis of the crude reaction mixture with (4-fluorophenyl)(phenylethynyl)sulfane **3.3-44g**.

6.2.19. Synthesis of cross-coupling product 3.3-45 (Chapter 3, Equation 3)

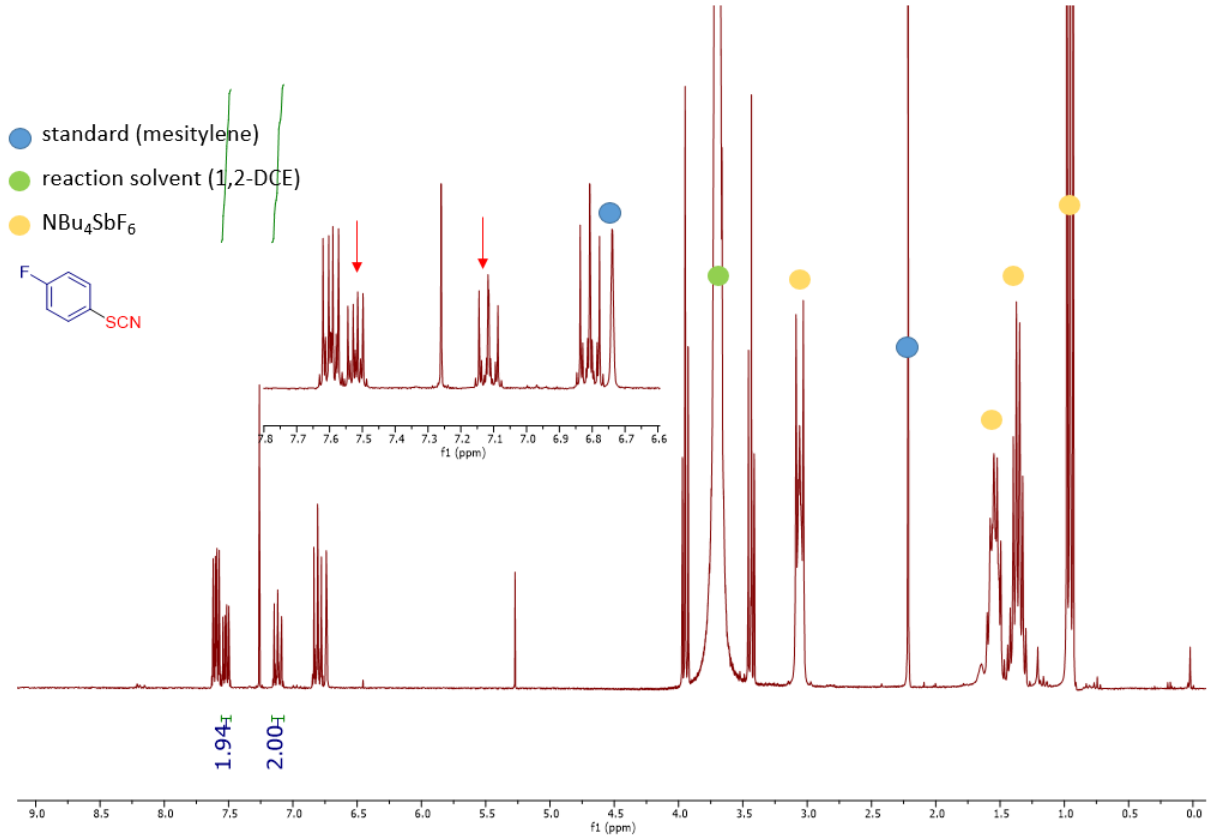

Figure 6.2-19. ^{1}H NMR analysis of the crude reaction mixture with 1-fluoro-4-thiocyanatobenzene **3.3-45.**

6.2.20. Role of Ag^{+} in Au(I)/Au(III) redox catalysis (alkene/ArI exchange) (Chapter 3, Scheme 3.3-13, A)

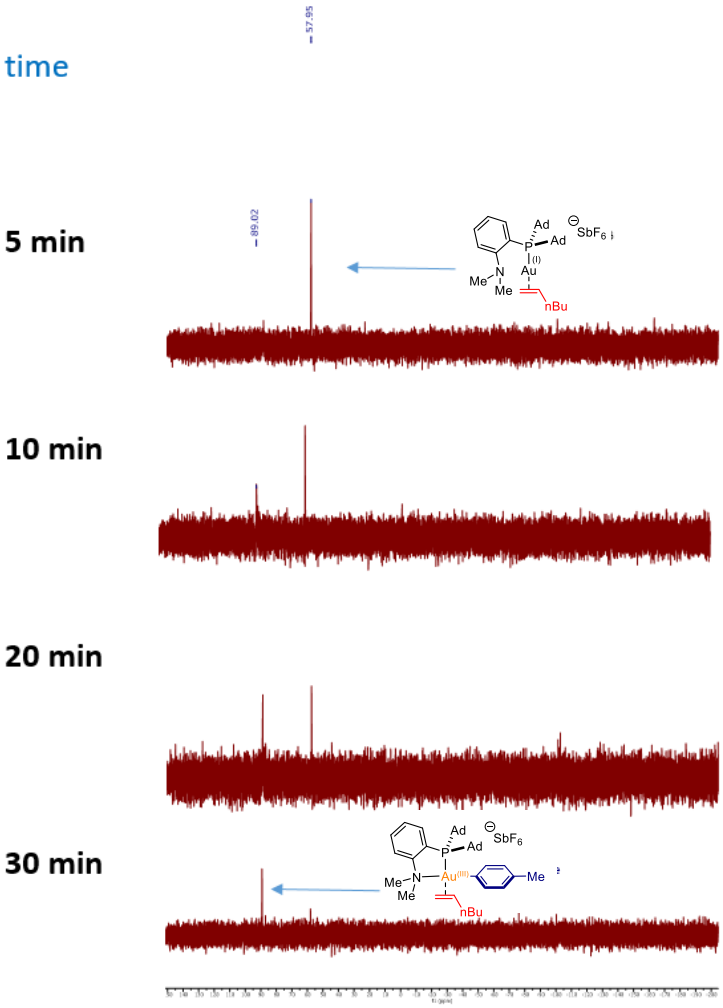

Figure 6.2-20. ^{31}P NMR spectra @t= 5, 10, 20 and 30 min.

6.2.21. Thiotosylate Au(I) complex 3.3-35$_{STs-Cl}$ as the resting state in the cross-coupling reaction (Chapter 3, Scheme 3.3-12, A)

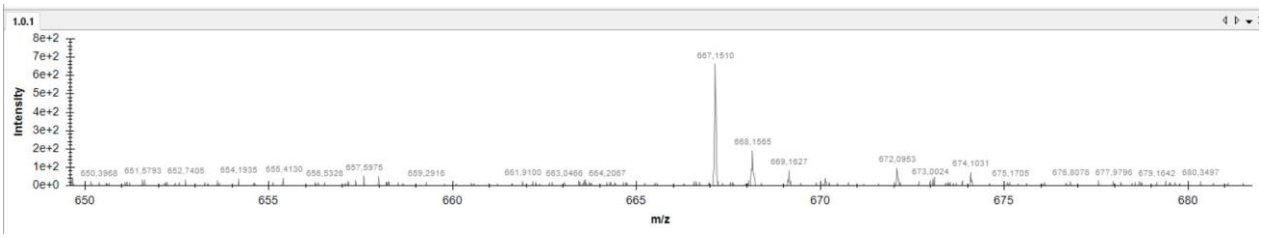

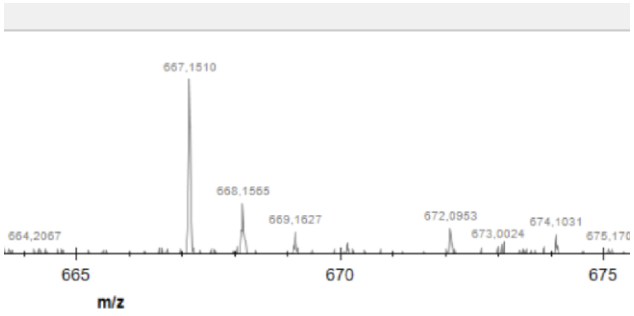

Figure 6.2-21. HRMS of the reaction mixture.

6.2.22. Importance of Ag^+ salt on the course of the cross-coupling reaction (Chapter 3, Scheme 3.3-12, B)

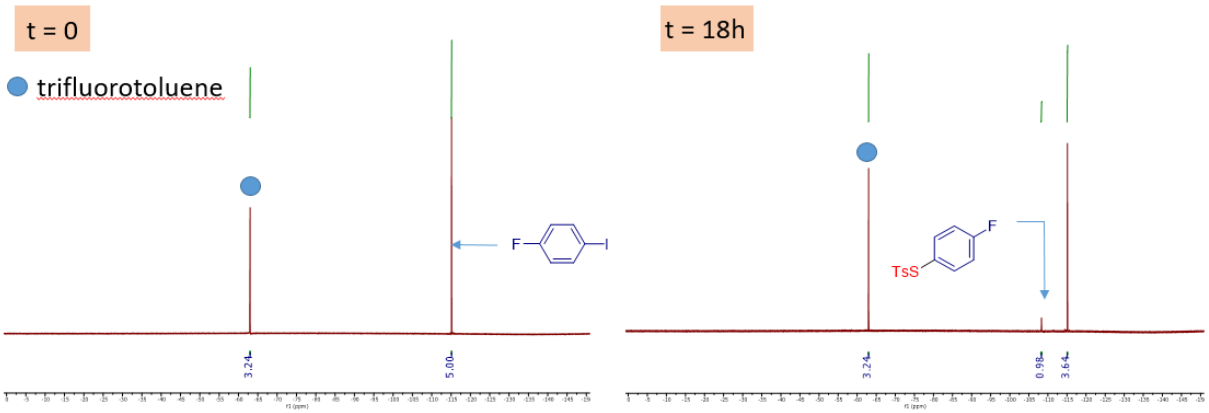

Figure 6.2-22-1. H NMR spectra @t= 0 and t= 18h for additive = $AgSbF_6$.

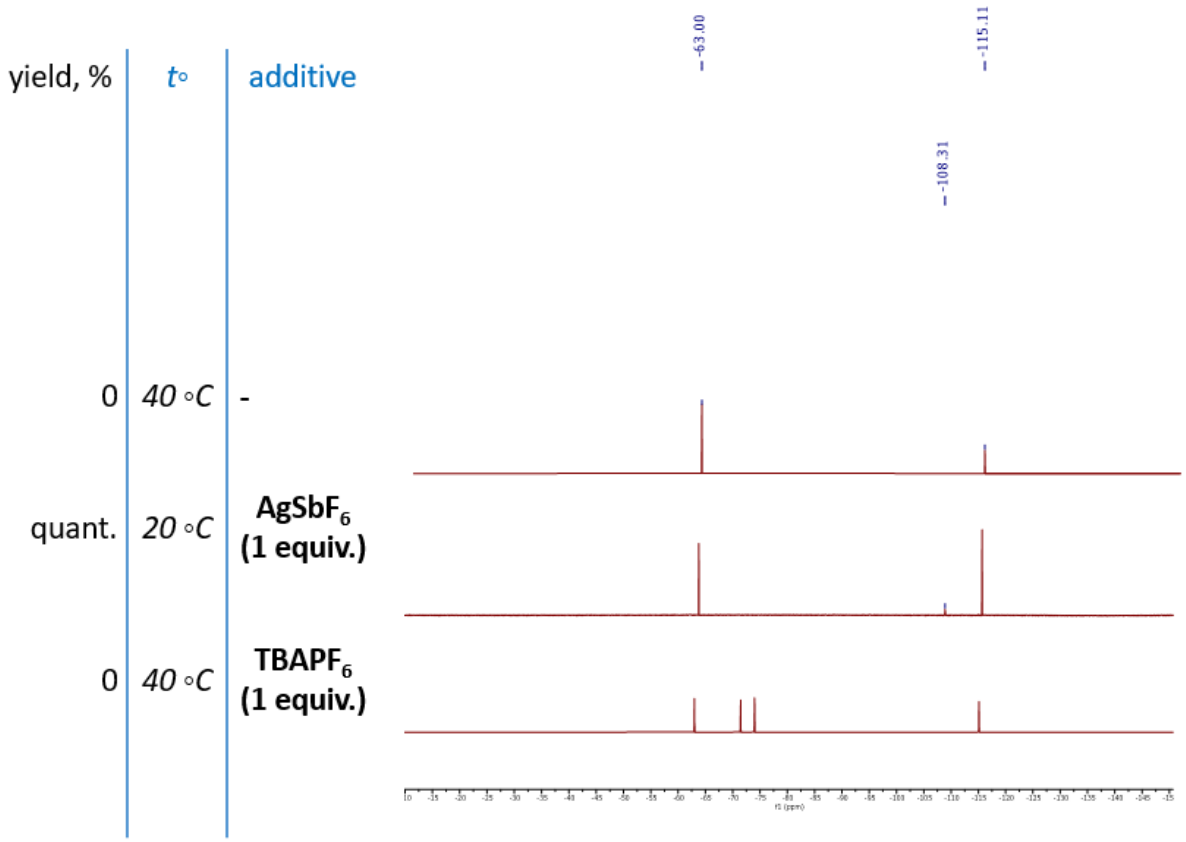

Figure 6.2-22-2. ^{19}F NMR spectra @t= 18h.

6.2.23. Ag^+ is not required to induce the cross coupling reaction from Au(III) oxidative complex 3.3-49 (Chapter 3, Scheme 3.3-13, B)

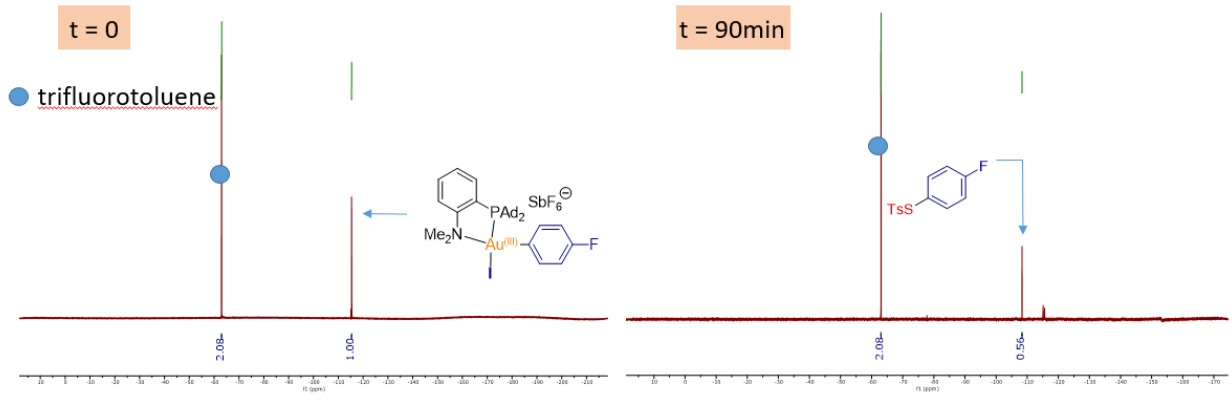

Figure 6.2-23-1. ^{1}H NMR spectra @t= 0 and t= 90min.

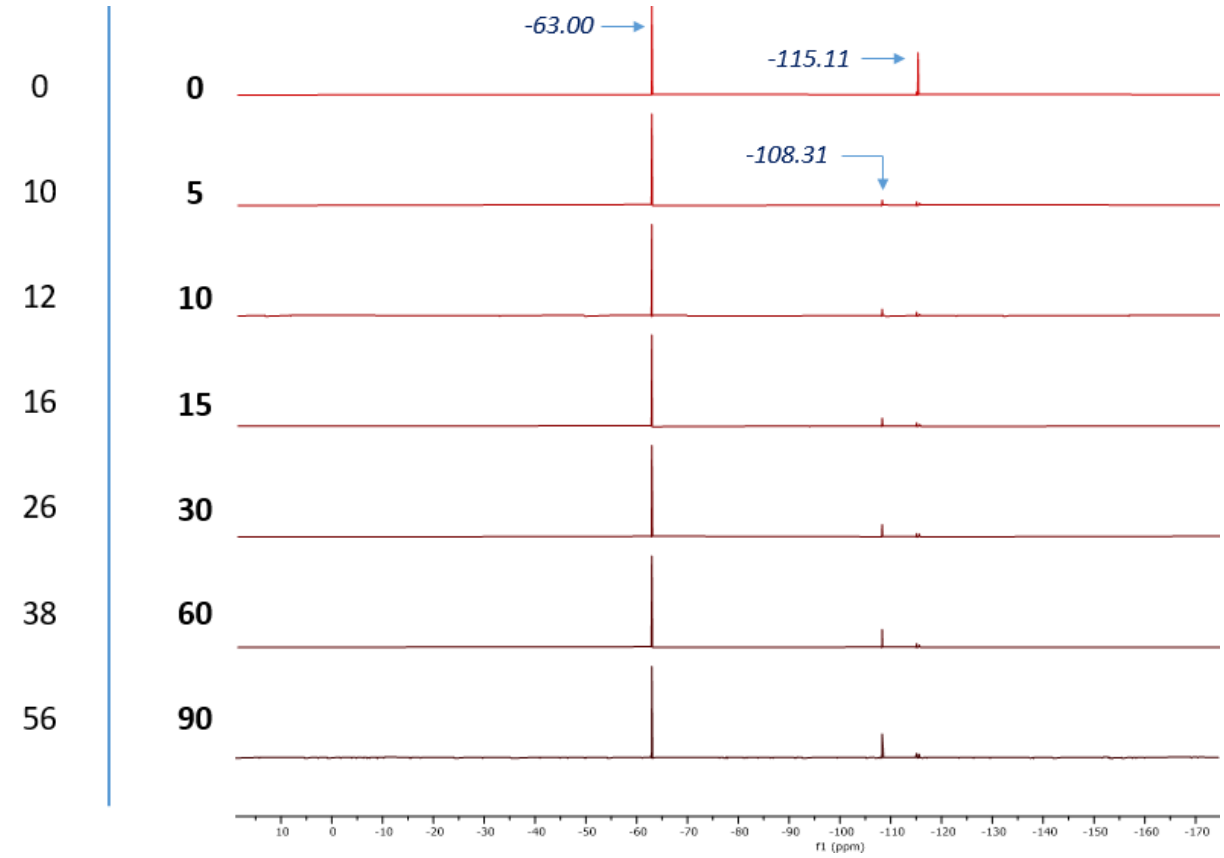

Figure 6.2-23-2. Stacked ^{19}F NMR spectra @t= 0-90min.

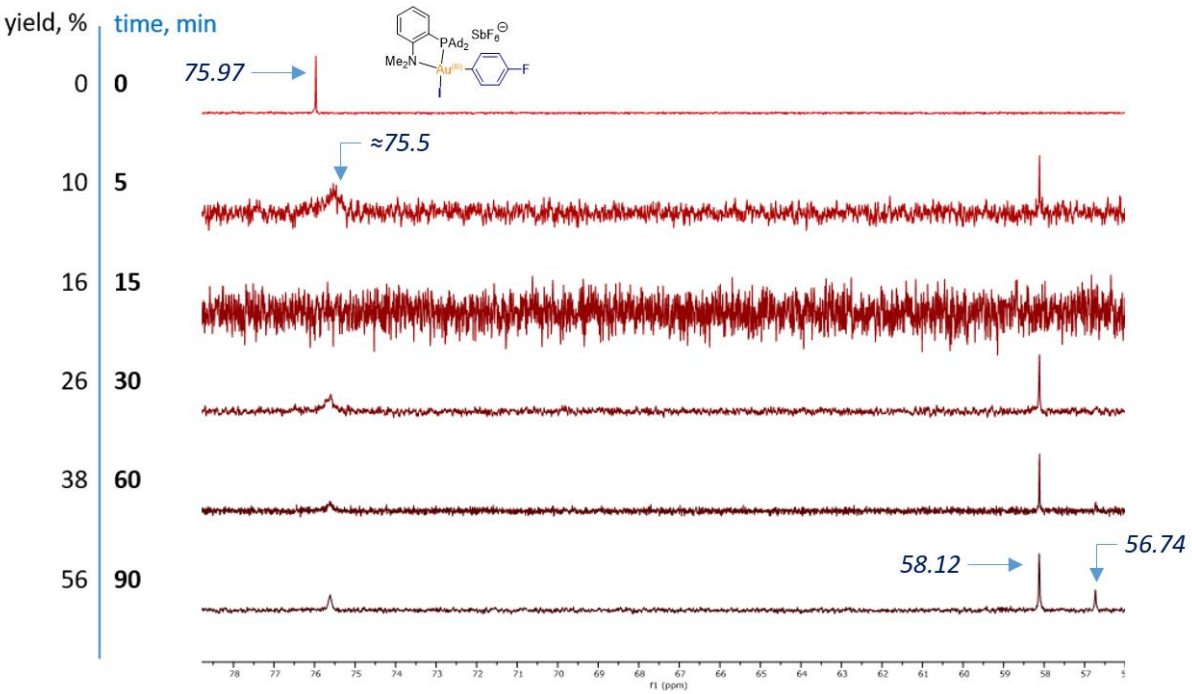

Figure 6.2-23-3. Stacked ^{31}P NMR spectra @t= 0-90min.

time (min)	yield (%)
5	10
10	12
15	16
30	26
60	38
90	56

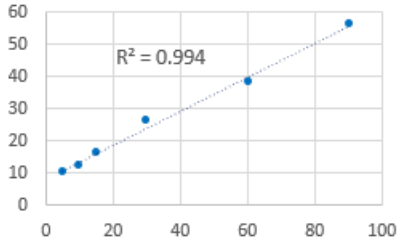

Figure 6.2-23-4. Yields of product **3.3-43a**.

6.2.24. Robustness of Au(I) complex 3.3-11$_H$ (Chapter 3)

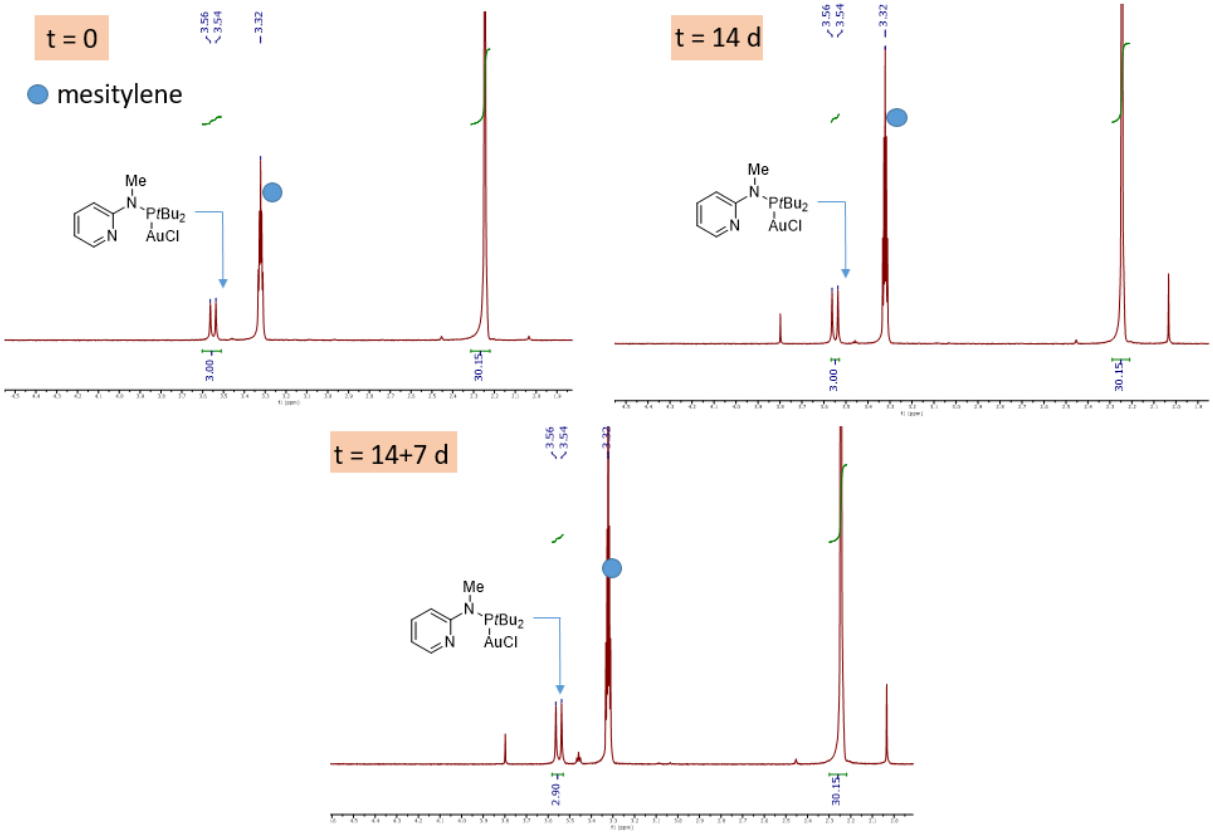

Figure 6.2-24. ^{1}H NMR spectra @t= 0, 14 d and 14+7 d.

6.2.25. SCXRD analysis and data

Crystallographic data were collected from single crystals mounted on MiTeGen dual thickness MicroMounts using Parabar oil. Data were collected on a Bruker ApexII single crystal diffractometer equipped with a graphite monochromator. The instrument was equipped with a

sealed tube Mo Kα source ($\lambda = 0.71073$ Å), an ApexII CCD detector and a dry compressed air-cooling system. All samples were cooled to 203(2) K during data collection. Raw data collection and processing were performed with the Apex3 software package from Bruker.[5] Initial unit cell parameters were determined from 36 data frames from select ω scans. Semi-empirical absorption corrections based on equivalent reflections were applied.[1] Systematic absences in the diffraction dataset and unit-cell parameters were consistent with the assigned space group. The initial structural solutions were determined using ShelxT direct methods,[2] and refined with full-matrix least-squares procedures based on F^2 using ShelXL or ShelXle.[3] Hydrogen atoms were placed geometrically and refined using a riding model.

X-ray of 3.3-12$_H$, CCDC deposition number: 2287345

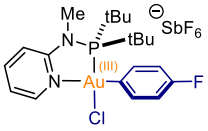

White crystals of **3.3-12**$_H$ suitable for X-Ray crystallography analysis were obtained *via* slow diffusion of a layer of pentane over a solution of **3.3-12**$_H$ in DCM.

ORTEP drawing of **3.3-12**$_H$:

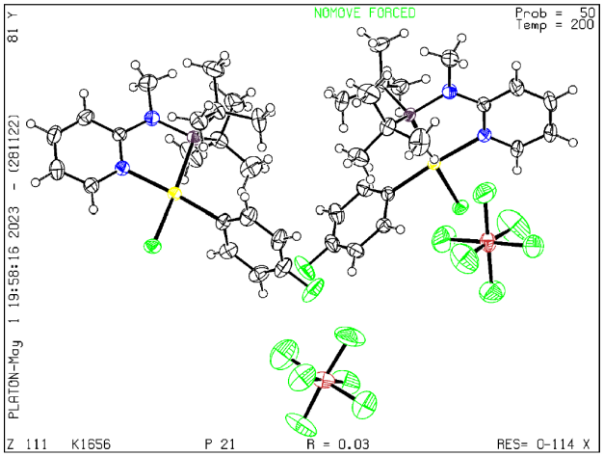

[5] APEX Softward Suite v 2010 Bruker AXS Inc. Madison Wisconsin USA, **2010**.

Datablock: K1656

```
Bond precision:   C-C = 0.0093 A          Wavelength=0.71073

Cell:             a=12.3545(7)     b=15.1818(9)         c=14.8190(9)
                  alpha=90         beta=108.834(1)      gamma=90
Temperature:      200 K

                  Calculated                  Reported
Volume            2630.7(3)                   2630.7(3)
Space group       P 21                        P 21
Hall group        P 2yb                       P 2yb
Moiety formula    C20 H29 Au Cl F N2 P, F6 Sb C20 H29 Au Cl F N2 P, F6 Sb
Sum formula       C20 H29 Au Cl F7 N2 P Sb    C20 H29 Au Cl F7 N2 P Sb
Mr                815.60                      815.59
Dx,g cm-3         2.059                       2.059
Z                 4                           4
Mu (mm-1)         6.820                       6.820
F000              1552.0                      1552.0
F000'             1543.68
h,k,lmax          19,23,22                    19,23,22
Nref              20368[ 10509]               20058
Tmin,Tmax         0.305,0.472                 0.538,0.747
Tmin'             0.133

Correction method= # Reported T Limits: Tmin=0.538 Tmax=0.747
AbsCorr = MULTI-SCAN

Data completeness= 1.91/0.98        Theta(max)= 33.344

R(reflections)= 0.0295( 17008)                wR2(reflections)=
                                              0.0568( 20058)
S = 0.906                  Npar= 609
```

X-ray of 3.3-13$_H$, CCDC deposition number: 2287348

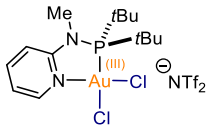

White crystals of **3.3-13$_H$** suitable for X-Ray crystallography analysis were obtained *via* slow diffusion of a layer of pentane over a solution of **3.3-13$_H$** in DCM.

ORTEP drawing of **3.3-13$_H$**:

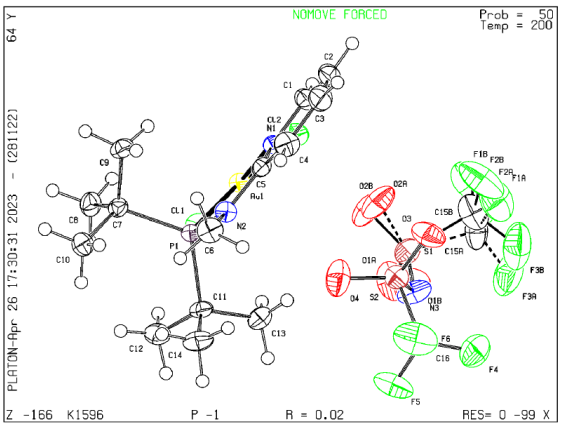

Datablock: K1596

Bond precision: C-C = 0.0042 A Wavelength=0.71073

Cell: a=8.4670(3) b=12.2133(5) c=14.4357(6)
alpha=114.387(2) beta=90.013(2) gamma=100.116(2)
Temperature: 200 K

	Calculated	Reported
Volume	1334.06(9)	1334.05(9)
Space group	P -1	P -1
Hall group	-P 1	-P 1
Moiety formula	C2 F6 N O4 S2, C14 H25 Au Cl2 N2 P	C14 H25 Au Cl2 N2 P, C2 F6 N O4 S2
Sum formula	C16 H25 Au Cl2 F6 N3 O4 P S2	C16 H25 Au Cl2 F6 N3 O4 P S2
Mr	800.35	800.34
Dx,g cm-3	1.992	1.992
Z	2	2
Mu (mm-1)	6.001	6.001
F000	776.0	776.0
F000'	773.78	
h,k,lmax	11,16,19	11,16,19
Nref	6671	6650
Tmin,Tmax	0.213,0.542	0.576,0.746
Tmin'	0.105	

Correction method= # Reported T Limits: Tmin=0.576 Tmax=0.746
AbsCorr = MULTI-SCAN

Data completeness= 0.997 Theta(max)= 28.364

6.2.26. DFT calculations[6]

[6] Conducted by Prof. Fabien Gagosz.

6.2.26.1. General information

DFT calculations were performed with ORCA 5.0.2.[4,5] Structures were calculated and optimized using the R^{2}SCAN-3c[6] composite method (def2-mTZVPP basis set,[6] def2-mTZVPP/J auxiliary basis set[6]). Effective core potential (ECP) were employed for gold (replacing 60 core electrons) and iodine (replacing 28 core electrons) as described by the standard def2-ECP basis sets.[7–13] Resolution of Identity (RI) approximation to speed up calculations.[14–16] Vibrational frequency calculations were performed at the same level (R^{2}SCAN-3c) that had been applied for geometry optimization at the gas phase, 1 atm, and 298.15 K. Normal modes of vibration were analyzed to assure that either 0 (intermediate) or 1 (transition state) imaginary frequencies were obtained. Intrinsic reaction coordinate (IRC)[17] calculations were performed on transition state structure to assign connectivity with preceding and following minima.

To have a better accuracy, the Gibbs free energies were computed *via* single-point calculations at the PWPB95/def2-TZVPP level of theory[18,19] using R^{2}SCAN-3c-optimized structures and the corresponding def2-TZVPP/J[20] auxiliary basis set. Dispersion effects were considered with the implementation of Grimme D4 correction.[21] The solvent effects on the relative energies were evaluated with the Solvation Model based on solute electron Density (SMD)[22] via single-point calculations at the PWPB95-D4/def2-TZVPP level. This level of theory was denoted PWPB95-D4/def2-TZVPP + SMD(1,2-dichloroethane or dichloromethane)//R^{2}SCAN-3c.

6.2.26.2. Calculations presented in Scheme 3.3-6

Calculations with MeDalPhos **3.3-18**, as the ligand

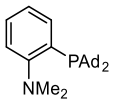

3.3-18

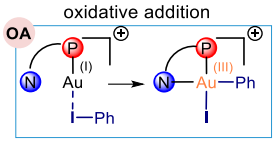

OA_{MDP}-SM → [OA_{MDP}-TS]‡ → OA_{MDP}-Pdt

Species	Negative frequencies (vib. Freq.)	Electronic Energy R2SCAN-3c (Hartree)	Free Energy correction (Hartrees)	Solvation Energy (Hartrees)	Electronic Energy PWPB95/def2-TZVPP + Solvation Energy (Hartree)	ΔG (kcal/mol)
OA_{MDP}-SM	0	-2151.893972	0.658343	-0.084985	-2151.428239	0
OA_{MDP}-TS	1 (-163)	-2151.880282	0.659774	-0.083962	-2151.408705	13.1
OA_{MDP}-Pdt	0	-2151.247093	0.663453	-0.096835	-2151.443726	-6.5

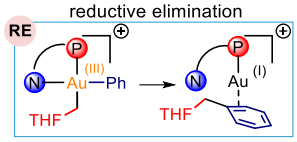

$RE_{MDP}\text{-SM} \rightarrow [RE_{MDP}\text{-SM}]^{\ddagger} \rightarrow RE_{MDP}\text{-Pdt}$

Species	Negative frequencies (vib. Freq.)	Electronic Energy R2SCAN-3c (Hartree)	Free Energy correction (Hartrees)	Solvation Energy (Hartrees)	Electronic Energy PWPB95/def2-TZVPP + Solvation Energy (Hartree)	ΔG (kcal/mol)
RE_{MDP}-SM	0	-1637.538846	0.793225	-0.099100	-2124.900398	0
RE_{MDP}-TS	1 (-348)	-2125.198937	0.790080	-0.094586	-2124.869520	17.4
RE_{MDP}-Pdt	0	-2125.268871	0.790757	-0.088113	-2124.938475	-25.4

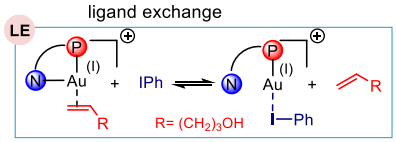

MDP-Alk + IPh $\xrightarrow{\Delta G}$ OA_{MDP}-SM + Alk

Species	Electronic Energy R2SCAN-3c (Hartree)	Free Energy correction (Hartrees)	Solvation Energy (Hartrees)	Electronic Energy PWPB95/def2-TZVPP + Solvation Energy (Hartree)	ΔG (kcal/mol)
MDP-Alk	-1894.261374	0.713506	-0.091289	-1893.962349	8.9
IPh	-529.321841	0.057904	-0.010565	-529.140605	
OA_{MDP}-SM	-2151.893972	0.658343	-0.084985	-2151.428239	
Alk	-271.675754	0.111211	-0.010746	-271.6586172	

Calculations with **3.3-15$_{OMe}$**, as the ligand

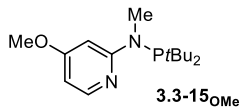

Electronic Energy R2SCAN-3c (Hartree)	Hirshfeld charge on N_{pyr} (e)
-1113.704814	-0.182

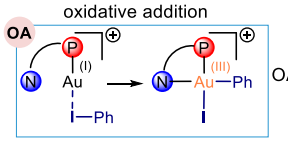

$OA_{3.3\text{-}15OMe}\text{-SM} \rightarrow [OA_{3.3\text{-}15OMe}\text{-TS}]^{\ddagger} \rightarrow OA_{3.3\text{-}15OMe}\text{-Pdt}$

Species	Negative frequencies (vib. Freq.)	Electronic Energy R2SCAN-3c (Hartree)	Free Energy correction (Hartrees)	Solvation Energy (Hartrees)	Electronic Energy PWPB95/def2-TZVPP + Solvation Energy (Hartree)	ΔG (kcal/mol)
$OA_{3.3\text{-}15OMe}$-SM	0	-1778.711279	0.432211	-0.080857	-1778.307000	0
$OA_{3.3\text{-}15OMe}$-TS	1 (-153)	-1778.6983581	0.433788	-0.078390	-1778.287651	13.1
$OA_{3.3\text{-}15OMe}$-Pdt	0	-1778.7336797	0.436971	-0.090808	-1778.326855	-9.5

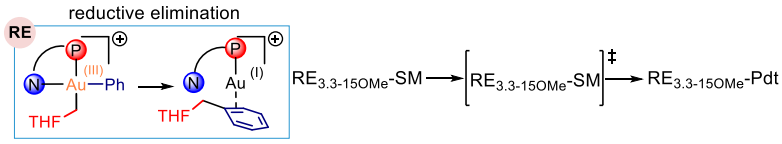

Species	Negative frequencies (vib. Freq.)	Electronic Energy R2SCAN-3c (Hartree)	Free Energy correction (Hartrees)	Solvation Energy (Hartrees)	Electronic Energy PWPB95/def2-TZVPP + Solvation Energy (Hartree)	ΔG (kcal/mol)
$RE_{3.3\text{-}15OMe}$-SM	0	-1752.053688	0.565819	-0.091549	-1751.783779	0
$RE_{3.3\text{-}15OMe}$-TS	1 (-382)	-1752.020397	0.564215	-0.088112	-1751.749439	20.5
$RE_{3.3\text{-}15OMe}$-Pdt	0	-1752.090421	0.565984	-0.080483	-1751.818961	-22.0

Species	Electronic Energy R2SCAN-3c (Hartree)	Free Energy correction (Hartrees)	Solvation Energy (Hartrees)	Electronic Energy PWPB95/def2-TZVPP + Solvation Energy (Hartree)	ΔG (kcal/mol)
$3.3\text{-}15_{OMe}$-Alk	-1521.085333	0.487807	-0.084465	-1520.845344	11.3
IPh	-529.321841	0.057904	-0.010565	-529.140605	
$OA3._{3.3\text{-}15OMe}$-SM	-1778.711279	0.432211	-0.080857	-1778.307000	
Alk	-271.675754	0.111211	-0.010746	-271.6586172	

Calculations with **$3.3\text{-}15_{H}$**, as the ligand

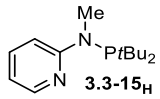 **3.3-15$_H$**	Electronic Energy R2SCAN-3c (Hartree)	Hirshfeld charge on N_{pyr} (e)
	-999.195839	-0.170

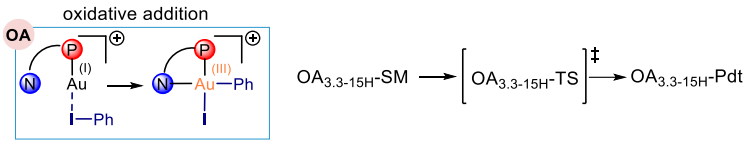

Species	Negative frequencies (vib. Freq.)	Electronic Energy R2SCAN-3c (Hartree)	Free Energy correction (Hartrees)	Solvation Energy (Hartrees)	Electronic Energy PWPB95/def2-TZVPP + Solvation Energy (Hartree)	ΔG (kcal/mol)
$OA_{3.3\text{-}15H}$-SM	0	-1664.198891	0.402687	-0.081627	-1663.802280	0
$OA_{3.3\text{-}15H}$-TS	1 (-156)	-1664.185391	0.404161	-0.079197	-1663.782211	13.5
$OA_{3.3\text{-}15H}$-Pdt	0	-1664.218168	0.407345	-0.093204	-1663.819877	-8.1

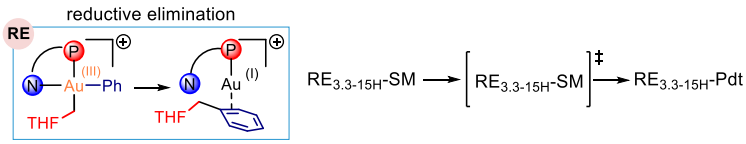

Species	Negative frequencies (vib. Freq.)	Electronic Energy R2SCAN-3c (Hartree)	Free Energy correction (Hartrees)	Solvation Energy (Hartrees)	Electronic Energy PWPB95/def2-TZVPP + Solvation Energy (Hartree)	ΔG (kcal/mol)
$RE_{3.3\text{-}15H}$SM	0	-1637.538846	0.537396	-0.093246	-1637.276665	0
$RE_{3.3\text{-}15H}$-TS	1 (-377)	-1637.507136	0.534430	-0.088971	-1637.243913	18.7
$RE_{3.3\text{-}15H}$-Pdt	0	-1637.578361	0.536279	-0.080951	-1637.314580	-24.5

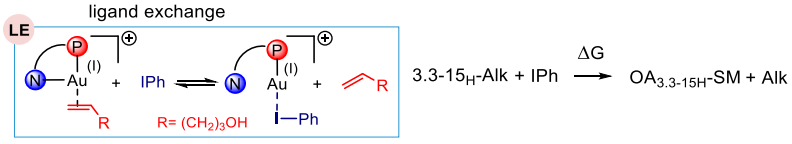

Species	Electronic Energy R2SCAN-3c (Hartree)	Free Energy correction (Hartrees)	Solvation Energy (Hartrees)	Electronic Energy PWPB95/def2-TZVPP + Solvation Energy (Hartree)	ΔG (kcal/mol)

3.3-15$_H$-Alk	-1406.571480	0.458079	-0.085568	-1406.339489	10.7
IPh	-529.321841	0.057904	-0.010565	-529.140605	
OA$_{3.3\text{-}15H}$-SM	-1664.198891	0.402687	-0.081627	-1663.802280	
Alk	-271.675754	0.111211	-0.010746	-271.6586172	

Calculations with **3.3-15$_{CF3}$**, as the ligand

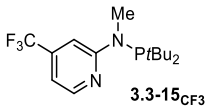 3.3-15$_{CF3}$	Electronic Energy R2SCAN-3c (Hartree)	Hirshfeld charge on N_{pyr} (e)
	-1336.252641	-0.161

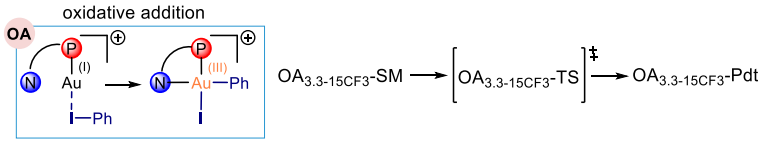

Species	Negative frequencies (vib. Freq.)	Electronic Energy R2SCAN-3c (Hartree)	Free Energy correction (Hartrees)	Solvation Energy (Hartrees)	Electronic Energy PWPB95/def2-TZVPP + Solvation Energy (Hartree)	ΔG (kcal/mol)
OA$_{3.3\text{-}15CF3}$-SM	0	-2001.249066	0.402403	-0.085900	-2000.843235	0
OA$_{3.3\text{-}15CF3}$-TS	1 (-155)	-2001.234784	0.404027	-0.083687	-2000.822390	14.1
OA$_{3.3\text{-}15CF3}$-Pdt	0	-2001.265923	0.407015	-0.097508	-2000.857960	-6.3

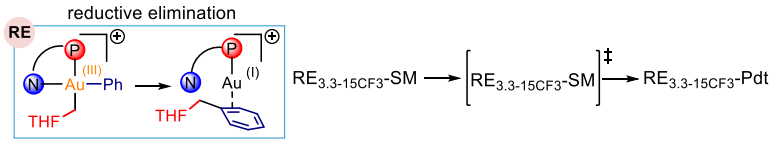

Species	Negative frequencies (vib. Freq.)	Electronic Energy R2SCAN-3c (Hartree)	Free Energy correction (Hartrees)	Solvation Energy (Hartrees)	Electronic Energy PWPB95/def2-TZVPP + Solvation Energy (Hartree)	ΔG (kcal/mol)
RE$_{3.3\text{-}15CF3}$SM	0	-1974.586960	0.537143	-0.097536	-1974.315050	0
RE$_{3.3\text{-}15CF3}$-TS	1 (-371)	-1974.556163	0.534689	-0.093811	-1974.283784	18.1

$RE_{3.3\text{-}15CF3}$-Pdt	0	-1974.629501	0.536169	-0.084593	-1974.356130	-26.4

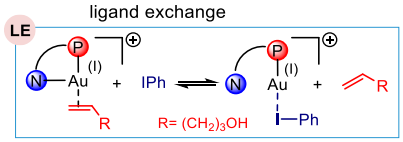

$3.3\text{-}15_{CF3}$-Alk + IPh $\xrightarrow{\Delta G}$ $OA_{3.3\text{-}15CF3}$-SM + Alk

Species	Electronic Energy R2SCAN-3c (Hartree)	Free Energy correction (Hartrees)	Solvation Energy (Hartrees)	Electronic Energy PWPB95/def2-TZVPP + Solvation Energy (Hartree)	ΔG (kcal/mol)
$3.3\text{-}15_{CF3}$-Alk	-1743.620069	0.457771	-0.090519	-1743.379044	9.9
IPh	-529.321841	0.057904	-0.010565	-529.140605	
$OA_{3.3\text{-}15CF3}$-SM	-2001.249066	0.402403	-0.085900	-2000.843235	
Alk	-271.675754	0.111211	-0.010746	-271.6586172	

Calculations with **$3.3\text{-}30_H$**, as the ligand

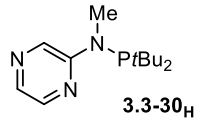

$3.3\text{-}30_H$

Electronic Energy R2SCAN-3c (Hartree)	Hirshfeld charge on N_{pyr} (e)
-1015.228937	-0.156

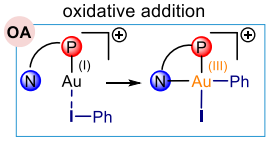

$OA_{3.3\text{-}30H}$-SM $\rightarrow$ [$OA_{3.3\text{-}30H}$-TS]‡ $\rightarrow$ $OA_{3.3\text{-}30H}$-Pdt

Species	Negative frequencies (vib. Freq.)	Electronic Energy R2SCAN-3c (Hartree)	Free Energy correction (Hartrees)	Solvation Energy (Hartrees)	Electronic Energy PWPB95/def2-TZVPP + Solvation Energy (Hartree)	ΔG (kcal/mol)
$OA_{3.3\text{-}30H}$-SM	0	-1680.225551	0.390280	-0.086520	-1679.835470	0
$OA_{3.3\text{-}30H}$-TS	1 (-159)	-1680.210871	0.391839	-0.084217	-1679.813934	14.5
$OA_{3.3\text{-}30H}$-Pdt	0	-1680.241529	0.394869	-0.097503	-1679.849046	-5.6

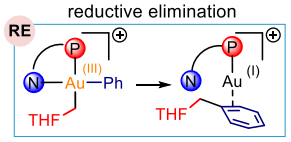

$RE_{3.3\text{-}30H}\text{-SM} \rightarrow [RE_{3.3\text{-}30H}\text{-SM}]^{\ddagger} \rightarrow RE_{3.3\text{-}30H}\text{-Pdt}$

Species	Negative frequencies (vib. Freq.)	Electronic Energy R2SCAN-3c (Hartree)	Free Energy correction (Hartrees)	Solvation Energy (Hartrees)	Electronic Energy PWPB95/def2-TZVPP + Solvation Energy (Hartree)	ΔG (kcal/mol)
$RE_{3.3\text{-}30H}SM$	0	-1653.562957	0.525085	-0.098584	-1653.306953	0
$RE_{3.3\text{-}30H}$-TS	1 (-367)	-1653.532277	0.521788	-0.094669	-1653.275517	17.7
$RE_{3.3\text{-}30H}$-Pdt	0	-1653.605978	0.524163	-0.085125	-1653.348426	-26.6

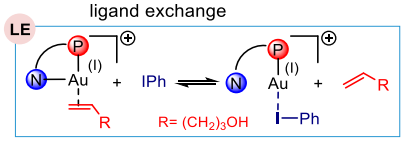

$3.3\text{-}30_H\text{-Alk} + \text{IPh} \xrightarrow{\Delta G} OA_{3.3\text{-}30H}\text{-SM} + \text{Alk}$

Species	Electronic Energy R2SCAN-3c (Hartree)	Free Energy correction (Hartrees)	Solvation Energy (Hartrees)	Electronic Energy PWPB95/def2-TZVPP + Solvation Energy (Hartree)	ΔG (kcal/mol)
$3.3\text{-}30_H$-Alk	-1422.595775	0.445675	-0.090955	-1422.370386	9.3
IPh	-529.321841	0.057904	-0.010565	-529.140605	
$OA_{3.3\text{-}30H}$-SM	-1680.225551	0.390280	-0.086520	-1679.835470	
Alk	-271.675754	0.111211	-0.010746	-271.6586172	

Calculations with **3.3-30$_{Cl}$**, as the ligand

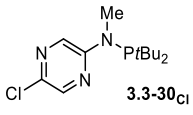

Electronic Energy R2SCAN-3c (Hartree)	Hirshfeld charge on N_{pyr} (e)
-1474.813798	-0.147

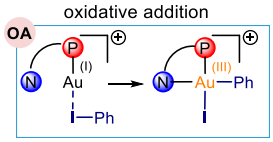

$OA_{3.3\text{-}30Cl}\text{-SM} \rightarrow [OA_{3.3\text{-}30Cl}\text{-TS}]^{\ddagger} \rightarrow OA_{3.3\text{-}30Cl}\text{-Pdt}$

Species	Negative frequencies (vib. Freq.)	Electronic Energy R2SCAN-3c (Hartree)	Free Energy correction (Hartrees)	Solvation Energy (Hartrees)	Electronic Energy PWPB95/def2-TZVPP + Solvation Energy (Hartree)	ΔG (kcal/mol)
$OA_{3.3\text{-}30Cl}$-SM	0	-2139.806717	0.379024	-0.090200	-2139.406292	0
$OA_{3.3\text{-}30Cl}$-TS	1 (-158)	-2139.791055	0.380551	-0.088469	-2139.383972	14.9
$OA_{3.3\text{-}30Cl}$-Pdt	0	-2139.819864	0.383315	-0.101719	-2139.417050	-4.1

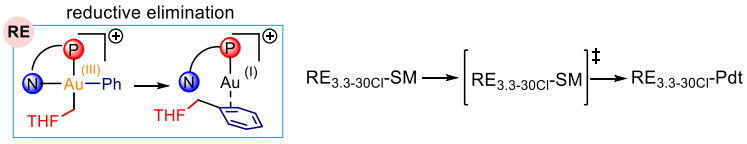

Species	Negative frequencies (vib. Freq.)	Electronic Energy R2SCAN-3c (Hartree)	Free Energy correction (Hartrees)	Solvation Energy (Hartrees)	Electronic Energy PWPB95/def2-TZVPP + Solvation Energy (Hartree)	ΔG (kcal/mol)
$RE_{3.3\text{-}30Cl}$SM	0	-2113.141831	0.513633	-0.101855	-2112.875326	0
$RE_{3.3\text{-}30Cl}$-TS	1 (-357)	-2113.112631	0.511038	-0.098372	-2112.845577	17.0
$RE_{3.3\text{-}30Cl}$-Pdt	0	-2113.188749	0.513171	-0.088525	-2112.920447	-28.6

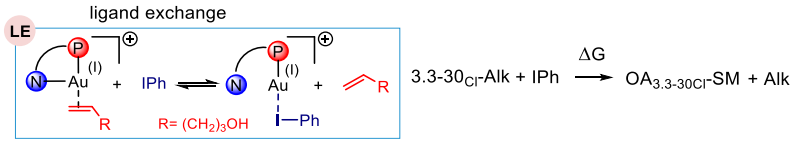

Species	Electronic Energy R2SCAN-3c (Hartree)	Free Energy correction (Hartrees)	Solvation Energy (Hartrees)	Electronic Energy PWPB95/def2-TZVPP + Solvation Energy (Hartree)	ΔG (kcal/mol)
$3.3\text{-}30_{Cl}$-Alk	-1882.175123	0.434124	-0.095321	-1881.939761	8.6
IPh	-529.321841	0.057904	-0.010565	-529.140605	
$OA_{3.3\text{-}30Cl}$-SM	-2139.806717	0.379024	-0.090200	-2139.406292	
Alk	-271.675754	0.111211	-0.010746	-271.6586172	

Correlations q(N)/ΔG

Predictive models:

RE step

• 3-point data set

ΔG≠ (RE) = -121.72qN - 1.6903 R^2 = 0.9651 ΔG (RE) = -214.07qN - 60.856 R^2 = 0.9998

• 4-point data set

ΔG≠ (RE) = -112.29qN - 0.0334 R^2 = 0.9672 ΔG (RE) = -190.87qN - 56.777 R^2 = 0.9803

• 5-point data set

ΔG≠ (RE) = -99.486qN + 2.1675 R^2 = 0.9595 ΔG (RE) = -188.6qN - 56.388 R^2 = 0.9889

OA step

• 3-point data set

ΔG≠ (OA) = 46.129qN + 21.463 R^2 = 0.9566 ΔG (OA) = -149.28x + 17.523 R^2 = 0.9706

• 4-point data set

ΔG≠ (OA) = 53.137qN + 22.695 R^2 = 0.9586 ΔG (OA) = -154.25qN + 18.397 R^2 = 0.9826

• 5-point data set

ΔG≠ (OA) = 55.122qN + 23.036 R^2 = 0.9775 ΔG (OA) = -159.7qN + 19.332 R^2 = 0.9899

LE step

• 3-point data set

ΔG (LE) = -68.906qN - 1.1261 R^2 = 0.9584

• 4-point data set

ΔG (LE) = -79.044qN - 2.9078 R^2 = 0.9604

• 5-point data set

ΔG (LE) = -82.387qN - 3.4823 R^2 = 0.9783

6.2.26.3. Calculations presented in Scheme 3.3-9, B

The relative stabilities of the complexes were calculated considering the following ligand exchange. MeDalPhos was used as the ligand.

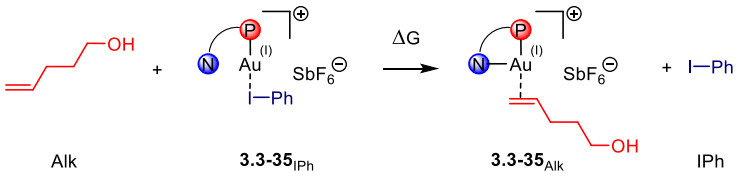

Alk **3.3-35**$_{IPh}$ **3.3-35**$_{Alk}$ IPh

Species	Electronic Energy R2SCAN-3c (Hartree)	Free Energy correction (Hartrees)	Solvation Energy (Hartrees)	Electronic Energy PWPB95/def2-TZVPP + Solvation Energy (Hartree)	ΔG (kcal/mol)
3.3-35$_{Alk}$	-2734.045760	0.717107	-0.068353	-2733.466862	-9.9
IPh	-529.321841	0.057904	-0.010565	-529.140605	
3.3-35$_{IPh}$	-2991.676680	0.663129	-0.065183	-2990.932420	
Alk	-271.675754	0.111211	-0.010746	-271.6586172	

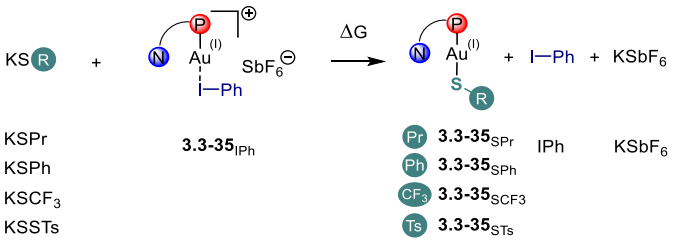

Species	Electronic Energy R2SCAN-3c (Hartree)	Free Energy correction (Hartrees)	Solvation Energy (Hartrees)	Electronic Energy PWPB95/def2-TZVPP + Solvation Energy (Hartree)	ΔG (kcal/mol)
3.3-35$_{SPr}$	-2139.448249	0.664337	-0.043955	-2139.098191	
IPh	-529.321841	0.057904	-0.010565	-529.140605	
$KSbF_6$	-1439.548607	-0.022377	-0.024815	-1439.306281	-44.2
3.3-35$_{IPh}$	-2991.676680	0.663129	-0.065183	-2990.932420	
KSPr	-1116.576885	0.061551	-0.035571	-1116.567037	
3.3-35$_{SPh}$	-2252.547904	0.659996	-0.049888	-2252.186212	
IPh	-529.321841	0.057904	-0.010565	-529.140605	
$KSbF_6$	-1439.548607	-0.022377	-0.024815	-1439.306281	-39.3
3.3-35$_{IPh}$	-2991.676680	0.663129	-0.065183	-2990.932420	
KSPh	-1229.6924739	0.057359	-0.035969	-1229.663076	
3.3-35$_{SCF3}$	-2358.604662	0.584877	-0.041209	-2358.256351	
IPh	-529.321841	0.057904	-0.010565	-529.140605	
$KSbF_6$	-1439.548607	-0.022377	-0.024815	-1439.306281	-33.2
3.3-35$_{IPh}$	-2991.676680	0.663129	-0.065183	-2990.932420	
KSCF3	-1335.759560	-0.017719	-0.025460	-1335.742961	
3.3-35$_{STs}$	-2801.131810	0.668198	-0.056740	-2800.780965	
IPh	-529.321841	0.057904	-0.010565	-529.140605	
$KSbF_6$	-1439.548607	-0.022377	-0.024815	-1439.306281	-27.6
3.3-35$_{IPh}$	-2991.676680	0.663129	-0.065183	-2990.932420	
KSTs	-1778.297921	0.064071	-0.032352	-1778.274872	

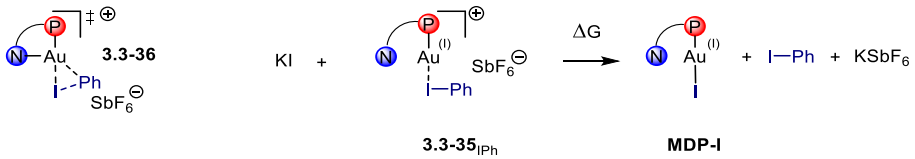

Species	Negative frequencies (vib. Freq.)	Electronic Energy R2SCAN-3c (Hartree)	Free Energy correction (Hartrees)	Solvation Energy (Hartrees)	Electronic Energy PWPB95/def2-TZVPP + Solvation Energy (Hartree)	ΔG (kcal/mol)
3.3-36	1 (-163)	-2991.662987	0.663695	-0.063669	-2990.911783	
MDP-I	0	-1920.549555	0.573707	-0.040246	-1920.067588	
IPh	0	-529.321841	0.057904	-0.010565	-529.140605	
$KSbF_6$	0	-1439.548607	-0.022377	-0.024815	-1439.306281	-28.9
3.3-35$_{IPh}$	0	-2991.676680	0.663129	-0.065183	-2990.932420	
KI	0	-897.7044887	-0.025120	-0.035537	-897.5647426	

6.2.26.4. Calculations presented in Scheme 3.3-13, A

Calculations were performed with ClKarPhos (**3.3-30**$_{Cl}$) as the ligand.

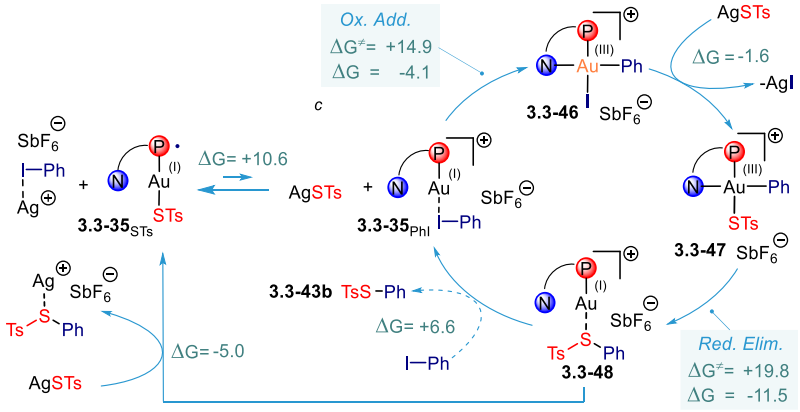

Species	Negative frequencies (vib. Freq.)	Electronic Energy R2SCAN-3c (Hartree)	Free Energy correction (Hartrees)	Solvation Energy (Hartrees)	Electronic Energy PWPB95/def2-TZVPP + Solvation Energy (Hartree)	ΔG (kcal/mol)

3.3-35$_{PhI}$	0	-2139.806717	0.379024	-0.090200	-2139.406292	0
TS(3.3-35$_{PhI}$**→3.3-46)**	1 (-158)	-2139.791055	0.380551	-0.088469	-2139.383972	14.9
3.3-46	0	-2139.819864	0.383315	-0.101719	-2139.417050	-4.1
3.3-47	0	-3020.409983 6	0.477906	-0.106116	-3020.128751	0
TS(3.3-47→3.3-48)	1 (-234)	-3020.384516	0.474161	-0.094549	-3020.093435	+19.8
3.3-48	0	-3020.430440	0.4753361	-0.092566	-3020.144472	-11.5
3.3-35$_{PhI}SbF_6$	0	-2979.598646	0.384143	-0.062890	-2978.912429	
TS(3.3-35$_{PhI}$**→3.3-46)**SbF_6	1 (-150)	-2979.580275	0.384718	-0.062540	-2978.887790	
3.3-46SbF_6	0	-2979.614627	0.388672	-0.068942	-2978.924955	
3.3-48SbF_6	0	-3860.217639	0.479583	-0.071202	-3859.652613	
3.3-35$_{STs}$	0	-2789.052575	0.390093	-0.056525	-2788.759583	
AgSTs	0	-1325.394454	0.063115	-0.033028	-1325.237750	
Et_4NSTs	0	-1549.830936	0.329537	-0.067364	-1549.807331	

Et_4NSbF_6	0	-1211.0880127	0.242778	-0.053200	-1210.844865	
AgI	0	-444.821260	-0.025717	-0.021073	-444.5343867	
$Ag(TsS\text{-}Ph)SbF_6$	0	-2396.5788446	0.152308	-0.042449	-2396.1383878	
$Ag(IPh)SbF_6$	0	-1515.9681740	0.056376	-0.032188	-1515.406659	
PhI	0	-529.321841	0.057904	-0.010565	-529.140605	
TsS-Ph	0	-1409.919403	0.150920	-0.028131	-1409.867768	

6.2.27. List of references

(1) Blessing, R. H. An Empirical Correction for Absorption Anisotropy. *Acta Crystallogr. Sect. A* **1995**, *51* (1), 33–38. https://doi.org/10.1107/S0108767394005726.

(2) Sheldrick, G. M. A Short History of *SHELX*. *Acta Crystallogr. Sect. A* **2008**, *64* (1), 112–122. https://doi.org/10.1107/S0108767307043930.

(3) Hübschle, C. B.; Sheldrick, G. M.; Dittrich, B. *ShelXle*: A Qt Graphical User Interface for *SHELXL*. *J. Appl. Crystallogr.* **2011**, *44* (6), 1281–1284. https://doi.org/10.1107/S0021889811043202.

(4) Neese, F. The ORCA Program System. *WIREs Comput. Mol. Sci.* **2012**, *2* (1), 73–78. https://doi.org/10.1002/wcms.81.

(5) Neese, F. Software Update: The ORCA Program System, Version 4.0. *WIREs Comput. Mol. Sci.* **2018**, *8* (1), e1327. https://doi.org/https://doi.org/10.1002/wcms.1327.

(6) Grimme, S.; Hansen, A.; Ehlert, S.; Mewes, J.-M. R2SCAN-3c: A “Swiss Army Knife” Composite Electronic-Structure Method. *J. Chem. Phys.* **2021**, *154* (6), 64103. https://doi.org/10.1063/5.0040021.

(7) Dolg, M.; Stoll, H.; Preuss, H. Energy-adjusted Ab Initio Pseudopotentials for the Rare Earth Elements. *J. Chem. Phys.* **1989**, *90* (3), 1730–1734. https://doi.org/10.1063/1.456066.

(8) Andrae, D.; Häußermann, U.; Dolg, M.; Stoll, H.; Preuß, H. Energy-Adjustedab Initio Pseudopotentials for the Second and Third Row Transition Elements. *Theor. Chim. Acta* **1990**, *77* (2), 123–141. https://doi.org/10.1007/BF01114537.

(9) Metz, B.; Stoll, H.; Dolg, M. Small-Core Multiconfiguration-Dirac–Hartree–Fock-Adjusted Pseudopotentials for Post-d Main Group Elements: Application to PbH and PbO. *J. Chem. Phys.* **2000**, *113* (7), 2563–2569. https://doi.org/10.1063/1.1305880.

(10) Peterson, K. A.; Figgen, D.; Goll, E.; Stoll, H.; Dolg, M. Systematically Convergent Basis Sets with Relativistic Pseudopotentials. II. Small-Core Pseudopotentials and Correlation Consistent Basis Sets for the Post-d Group 16–18 Elements. *J. Chem. Phys.* **2003**, *119* (21), 11113–11123. https://doi.org/10.1063/1.1622924.

(11) Leininger, T.; Nicklass, A.; Küchle, W.; Stoll, H.; Dolg, M.; Bergner, A. The Accuracy of the Pseudopotential Approximation: Non-Frozen-Core Effects for Spectroscopic Constants of Alkali Fluorides XF (X = K, Rb, Cs). *Chem. Phys. Lett.* **1996**, *255* (4), 274–280. https://doi.org/10.1016/0009-2614(96)00382-X.

(12) Kaupp, M.; Schleyer, P. v. R.; Stoll, H.; Preuss, H. Pseudopotential Approaches to Ca, Sr, and Ba Hydrides. Why Are Some Alkaline Earth MX_2 Compounds Bent? *J. Chem. Phys.* **1991**, *94* (2), 1360–1366. https://doi.org/10.1063/1.459993.

(13) Cao, X.; Dolg, M. Valence Basis Sets for Relativistic Energy-Consistent Small-Core Lanthanide Pseudopotentials. *J. Chem. Phys.* **2001**, *115* (16), 7348–7355. https://doi.org/10.1063/1.1406535.

(14) Eichkorn, K.; Treutler, O.; Öhm, H.; Häser, M.; Ahlrichs, R. Auxiliary Basis Sets to Approximate Coulomb Potentials. *Chem. Phys. Lett.* **1995**, *242* (6), 652–660. https://doi.org/10.1016/0009-2614(95)00838-U.

(15) Eichkorn, K.; Weigend, F.; Treutler, O.; Ahlrichs, R. Auxiliary Basis Sets for Main Row Atoms and Transition Metals and Their Use to Approximate Coulomb Potentials. *Theor. Chem. Acc.* **1997**, *97* (1), 119–124. https://doi.org/10.1007/s002140050244.

(16) Weigend, F. A Fully Direct RI-HF Algorithm: Implementation, Optimised Auxiliary Basis Sets, Demonstration of Accuracy and Efficiency. *Phys. Chem. Chem. Phys.* **2002**, *4* (18), 4285–4291. https://doi.org/10.1039/B204199P.

(17) Fukui, K. The Path of Chemical Reactions - the IRC Approach. *Acc. Chem. Res.* **1981**, *14* (12), 363–368. https://doi.org/10.1021/ar00072a001.

(18) Goerigk, L.; Grimme, S. Efficient and Accurate Double-Hybrid-Meta-GGA Density Functionals—Evaluation with the Extended GMTKN30 Database for General Main Group Thermochemistry, Kinetics, and Noncovalent Interactions. *J. Chem. Theory Comput.* **2011**, *7* (2), 291–309. https://doi.org/10.1021/ct100466k.

(19) Weigend, F.; Ahlrichs, R. Balanced Basis Sets of Split Valence, Triple Zeta Valence and Quadruple Zeta Valence Quality for H to Rn: Design and Assessment of Accuracy. *Phys. Chem. Chem. Phys.* **2005**, *7* (18), 3297–3305. https://doi.org/10.1039/B508541A.

(20) Weigend, F. Accurate Coulomb-Fitting Basis Sets for H to Rn. *Phys. Chem. Chem. Phys.* **2006**, *8* (9), 1057–1065. https://doi.org/10.1039/B515623H.

(21) Caldeweyher, E.; Ehlert, S.; Hansen, A.; Neugebauer, H.; Spicher, S.; Bannwarth, C.; Grimme, S. A Generally Applicable Atomic-Charge Dependent London Dispersion Correction. *J. Chem. Phys.* **2019**, *150* (15), 154122. https://doi.org/10.1063/1.5090222.

(22) Marenich, A. V; Cramer, C. J.; Truhlar, D. G. Universal Solvation Model Based on Solute Electron Density and on a Continuum Model of the Solvent Defined by the Bulk Dielectric Constant and Atomic Surface Tensions. *J. Phys. Chem. B* **2009**, *113* (18), 6378–6396. https://doi.org/10.1021/jp810292n.

7. Collective NMR data

7.1. NMR data for Chapter 2.

tris([1,1'-biphenyl]-2-yl)phosphane 2.3-4$_H$)

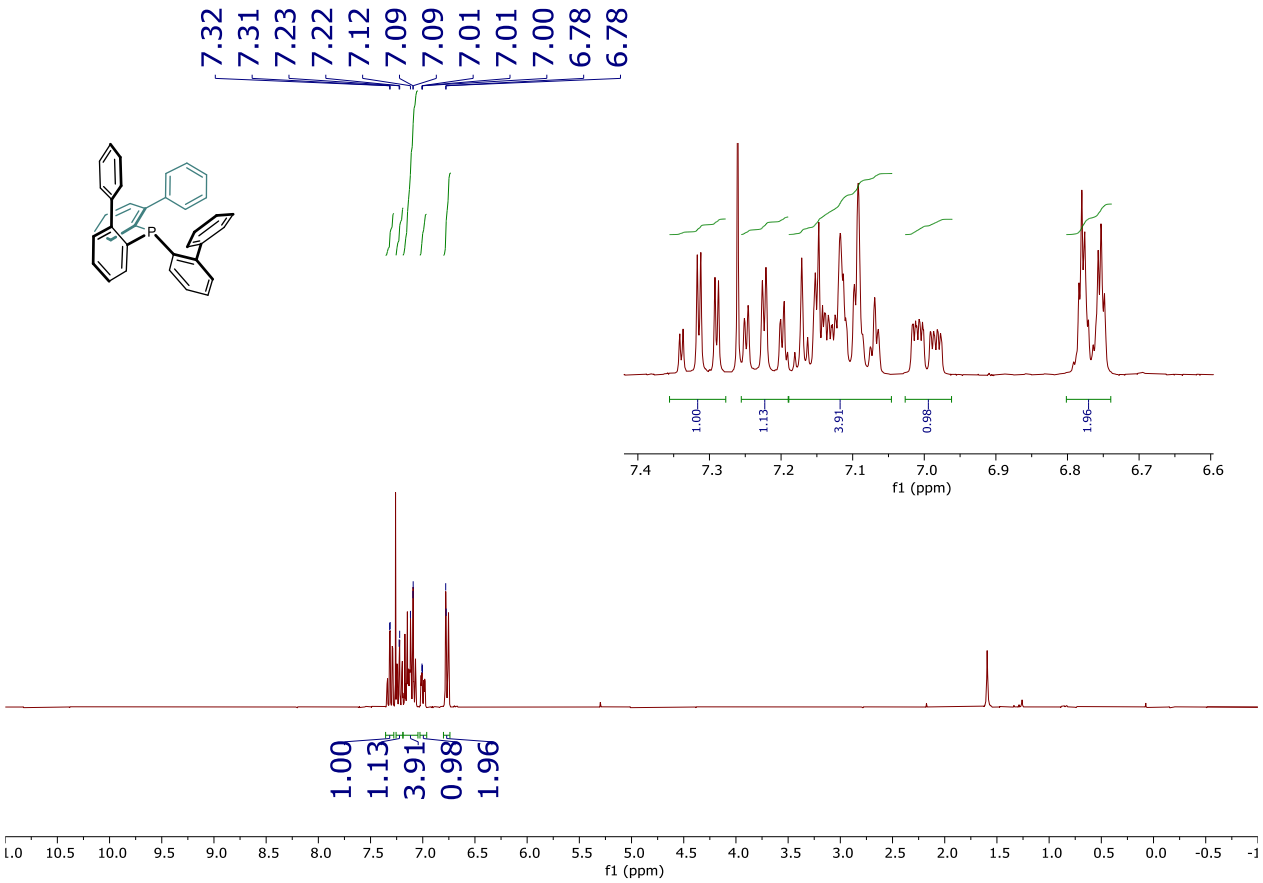

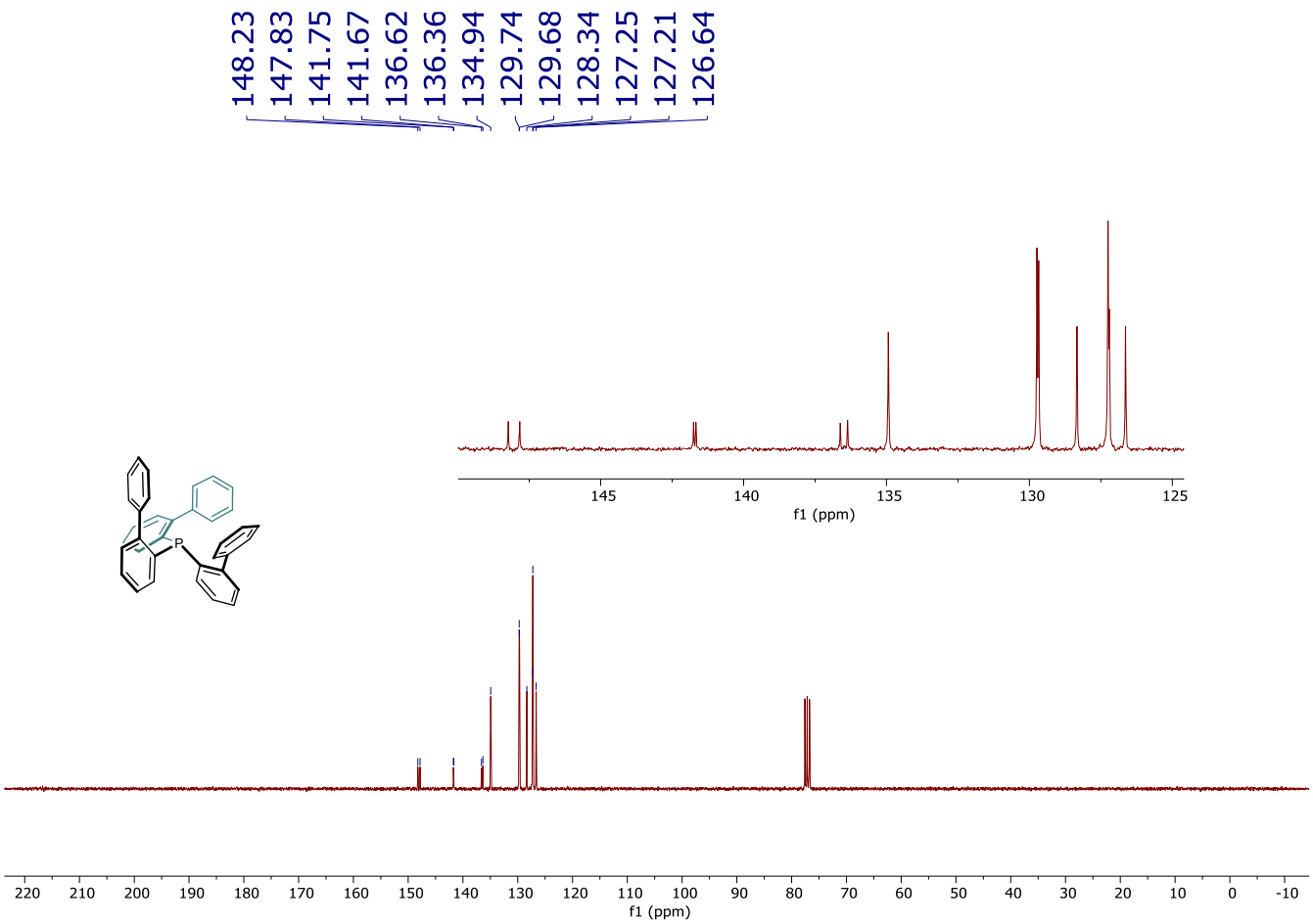
148.23
147.83
141.75
141.67
136.62
136.36
134.94
129.74
129.68
128.34
127.25
127.21
126.64
P
145
140
135
130
125
f1 (ppm)
220
210
200
190
180
170
160
150
140
130
120
110
100
90
80
70
60
50
40
30
20
10
0
-10
f1 (ppm)

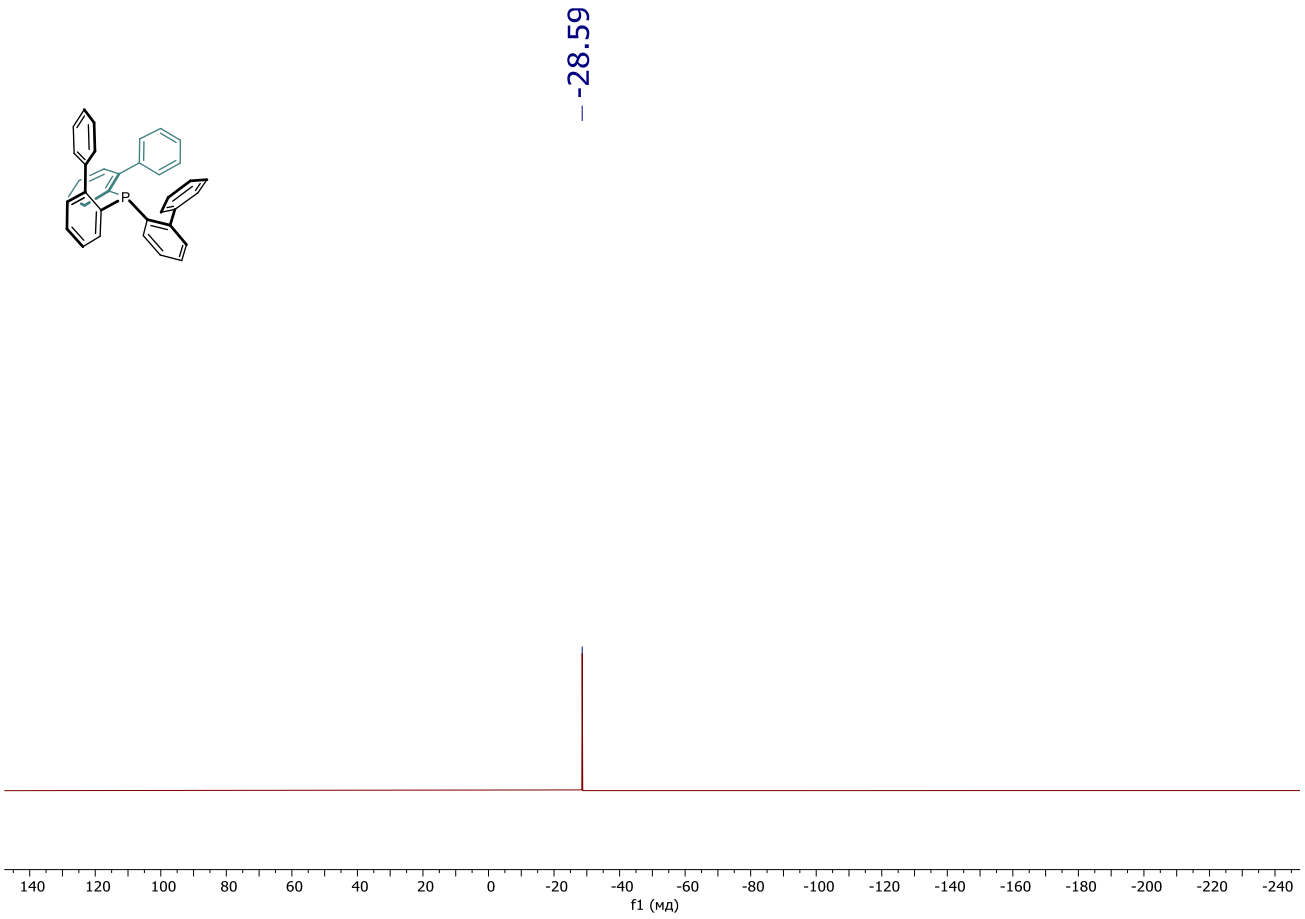
-28.59
P
140
120
100
80
60
40
20
0
-20
-40
-60
-80
-100
-120
-140
-160
-180
-200
-220
-240
f1 (мд)

tris(3'-(tert-butyl)-[1,1'-biphenyl]-2-yl)phosphane 2.3-4$_{mtBu}$

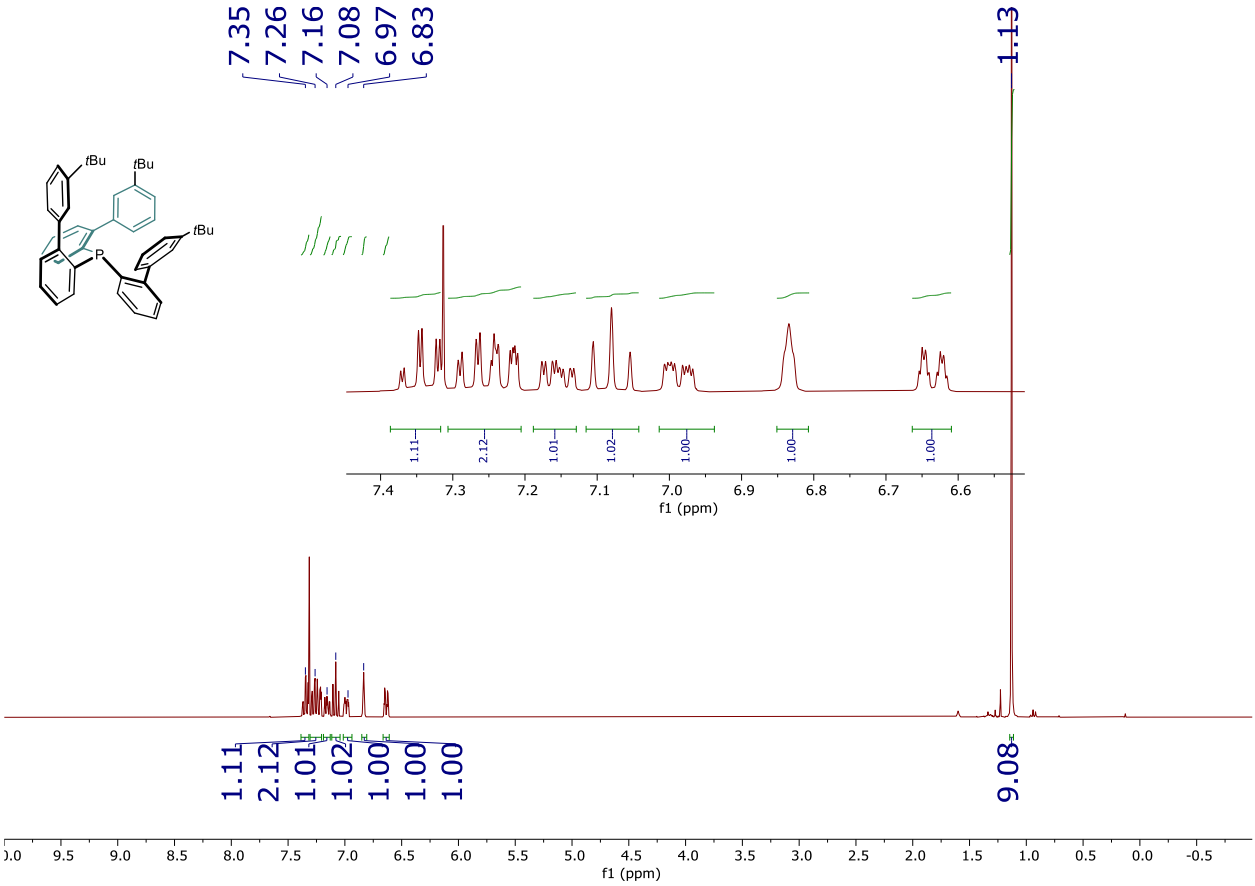

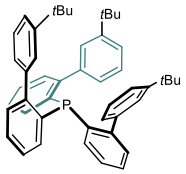

149.78
148.74
148.35
141.33
141.25
136.95
136.69
134.83
129.66
129.61
128.17
127.10
127.04
126.98
126.79
126.73
123.60

34.51
31.34

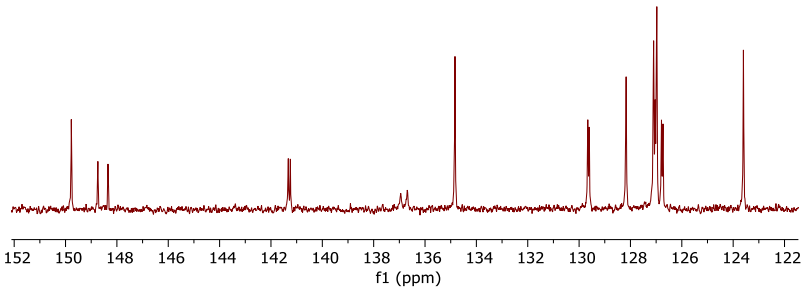

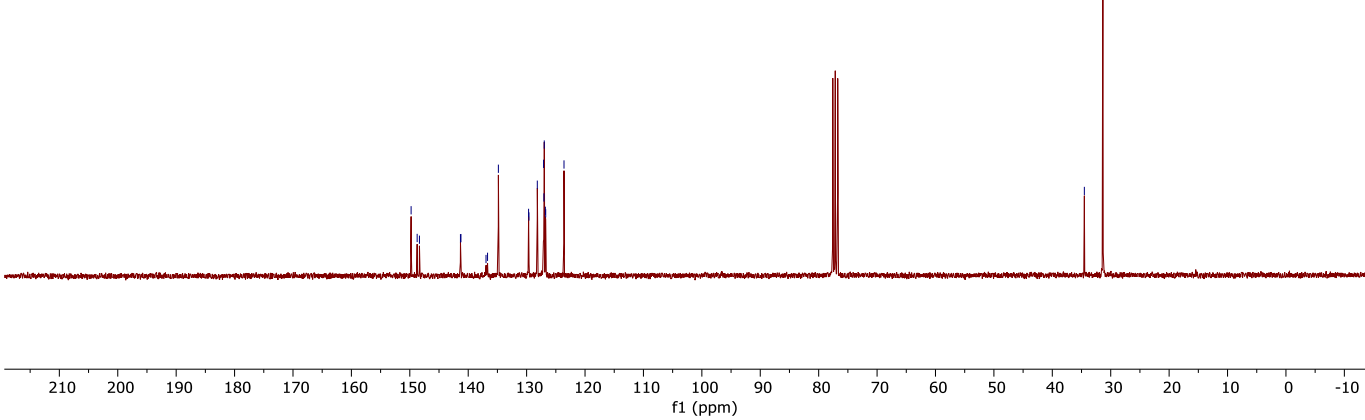

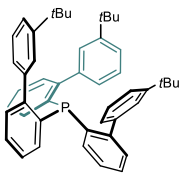

-26.34

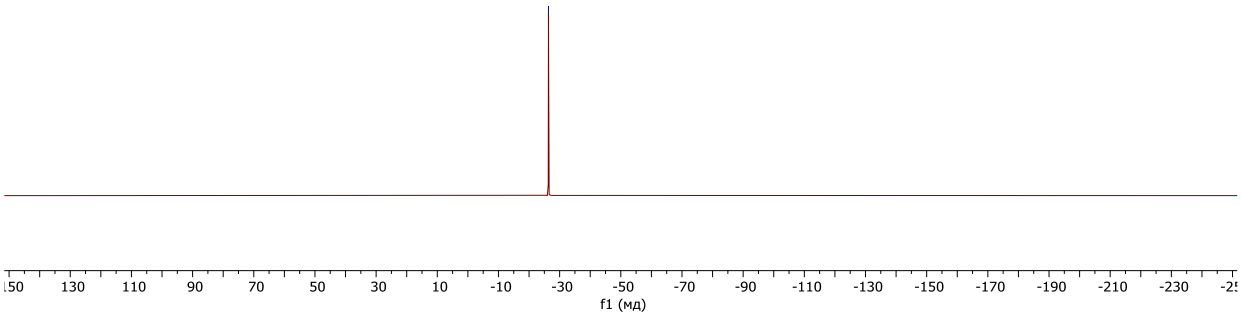

tris(3'-butyl-[1,1'-biphenyl]-2-yl)phosphane 2.3-4$_{mnBu}$

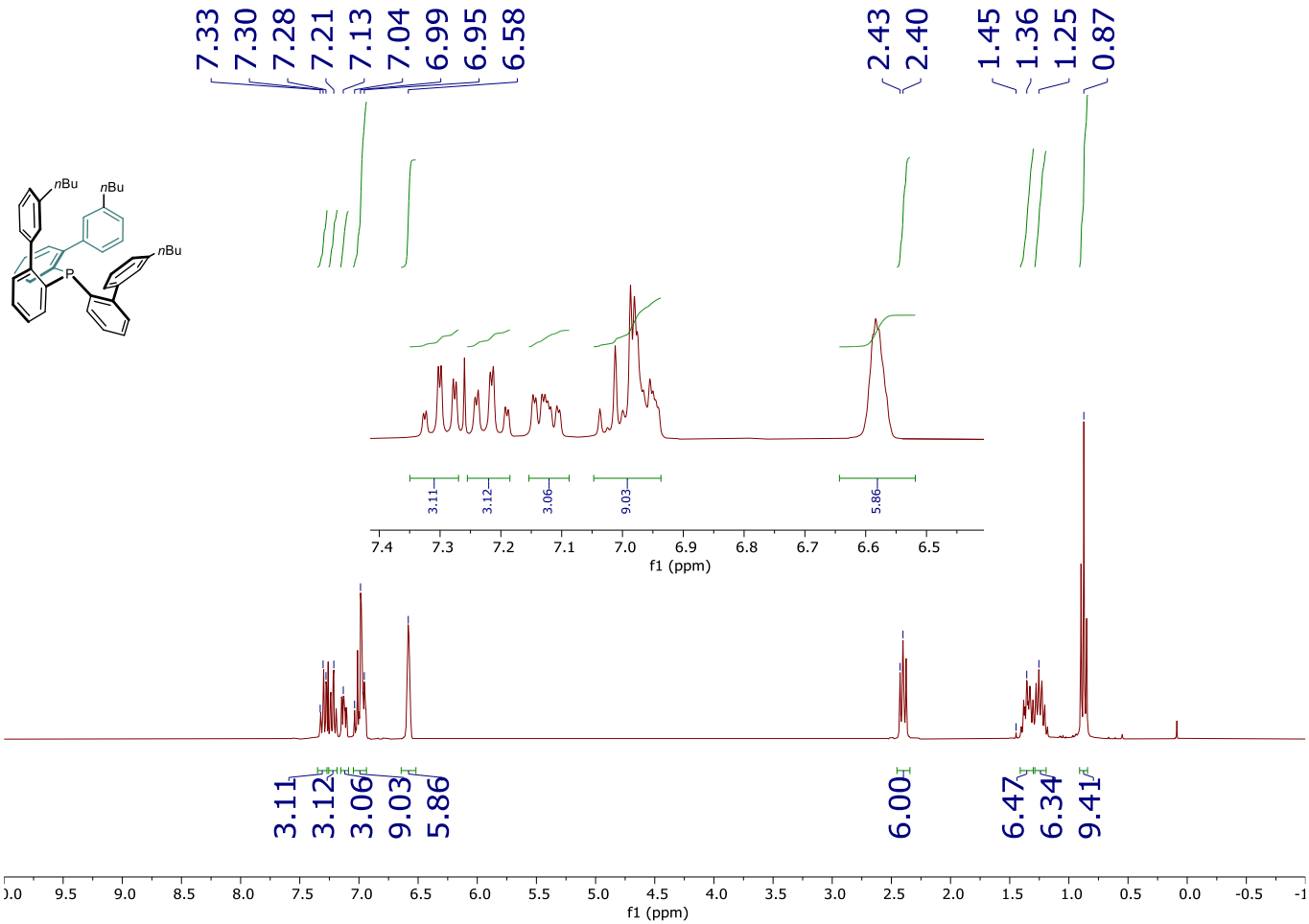

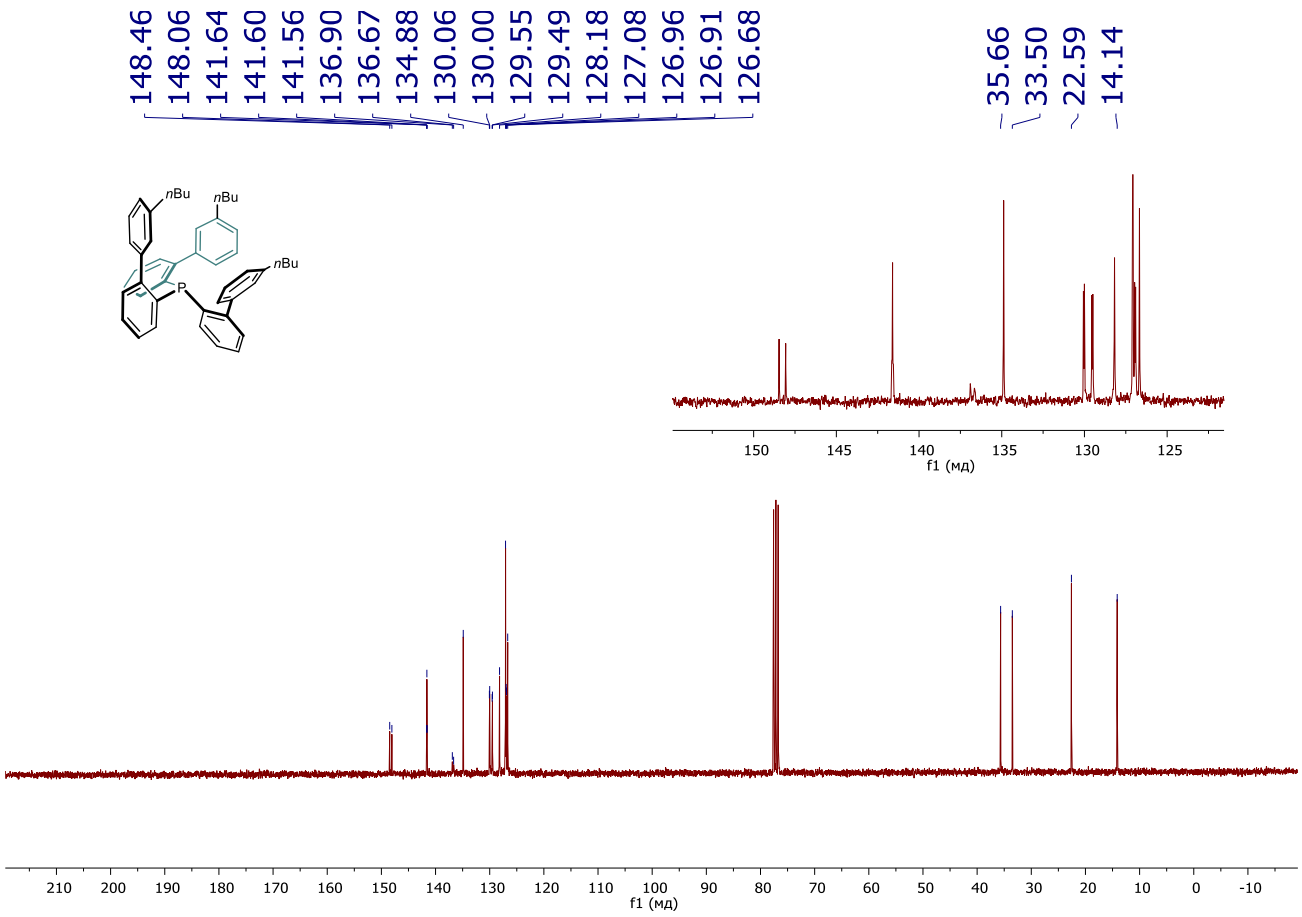
148.46
148.06
141.64
141.60
141.56
136.90
136.67
134.88
130.06
130.00
129.55
129.49
128.18
127.08
126.96
126.91
126.68
35.66
33.50
22.59
14.14
nBu
nBu
nBu
P
150
145
140
135
130
125
f1 (мд)
210
200
190
180
170
160
150
140
130
120
110
100
90
80
70
60
50
40
30
20
10
0
-10
f1 (мд)

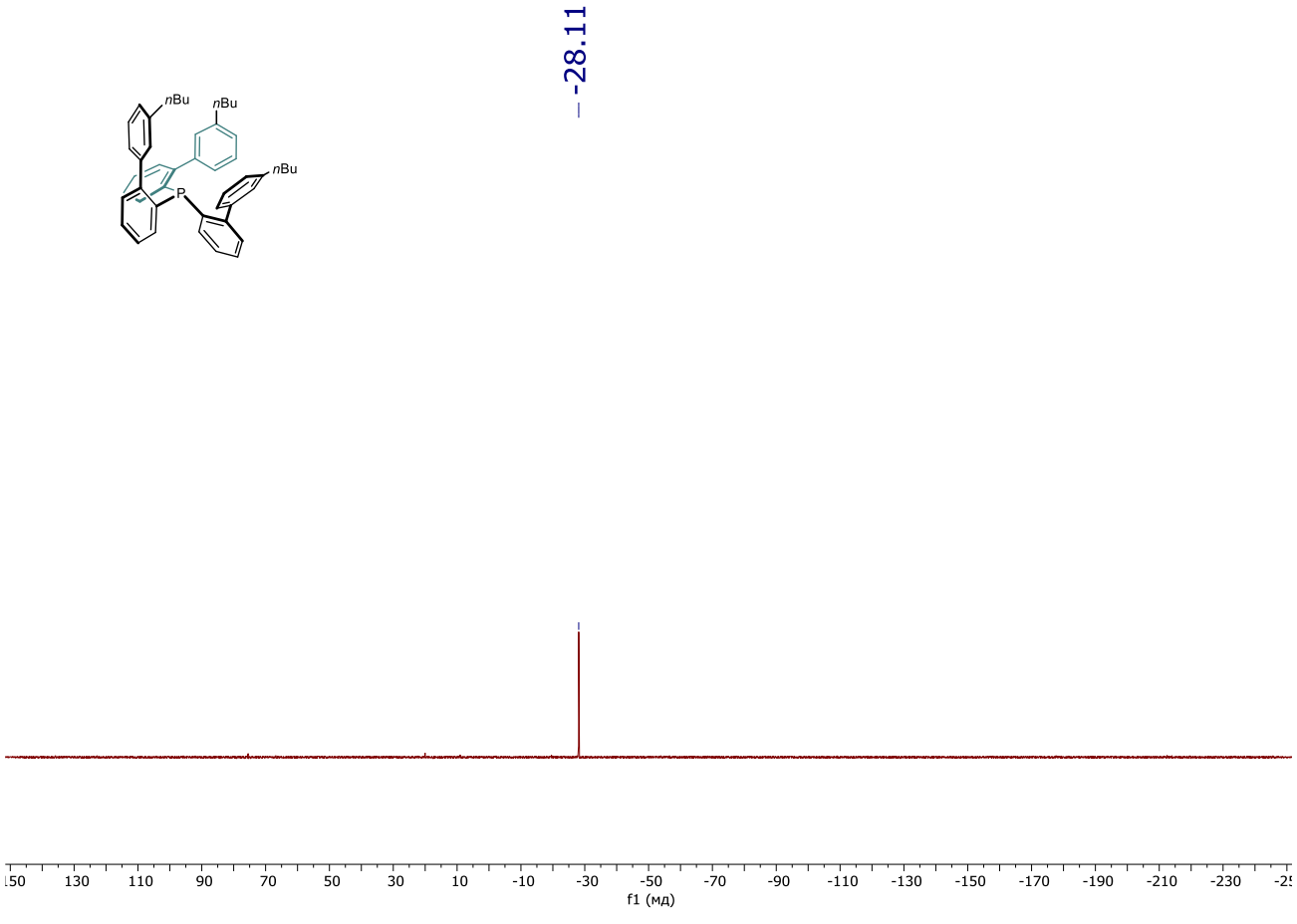
-28.11
nBu
nBu
nBu
P
50
130
110
90
70
50
30
10
-10
-30
-50
-70
-90
-110
-130
-150
-170
-190
-210
-230
f1 (мд)

tris(4'-(*tert*-butyl)-[1,1'-biphenyl]-2-yl)phosphane 2.3-4$_{ptBu}$

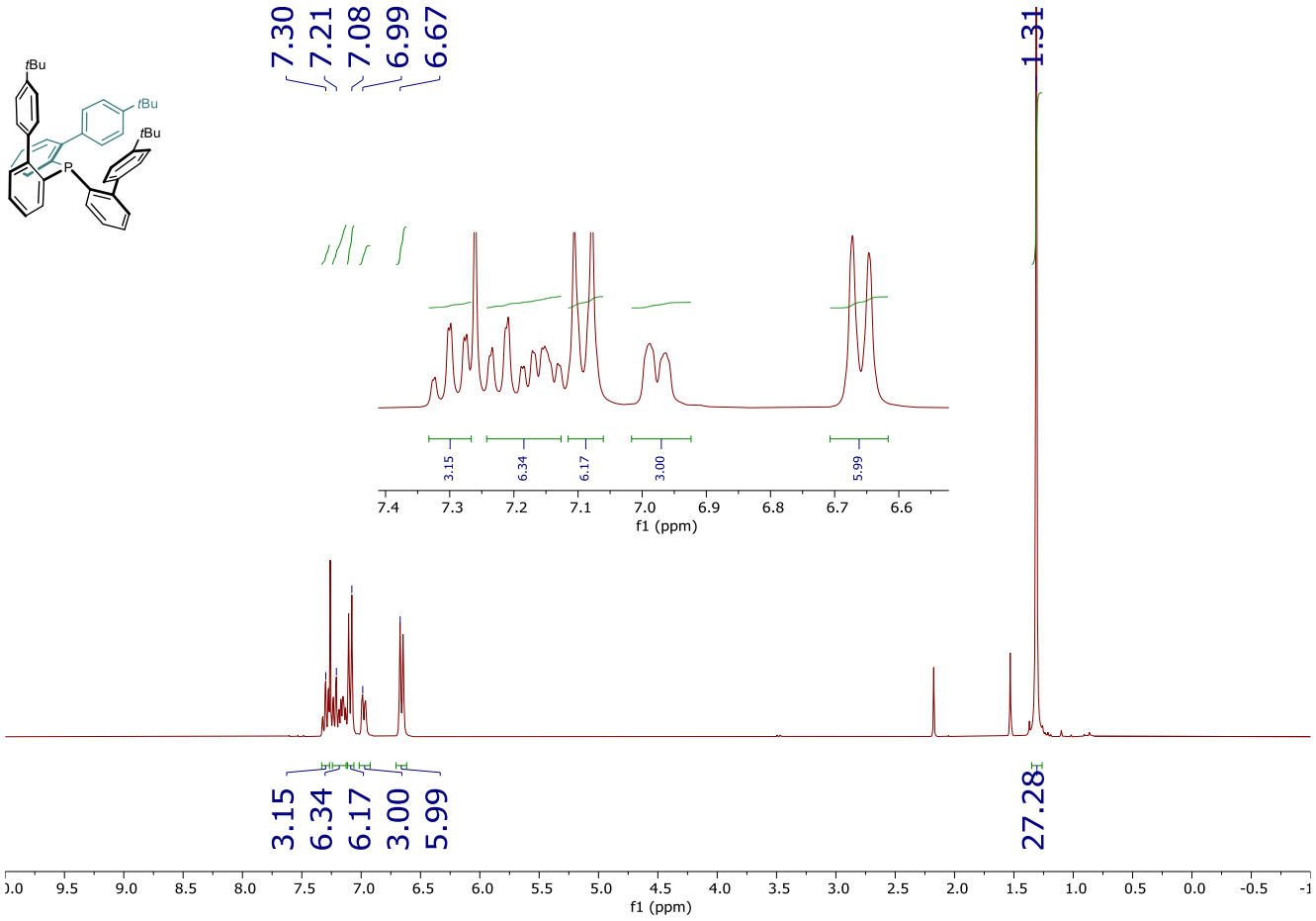

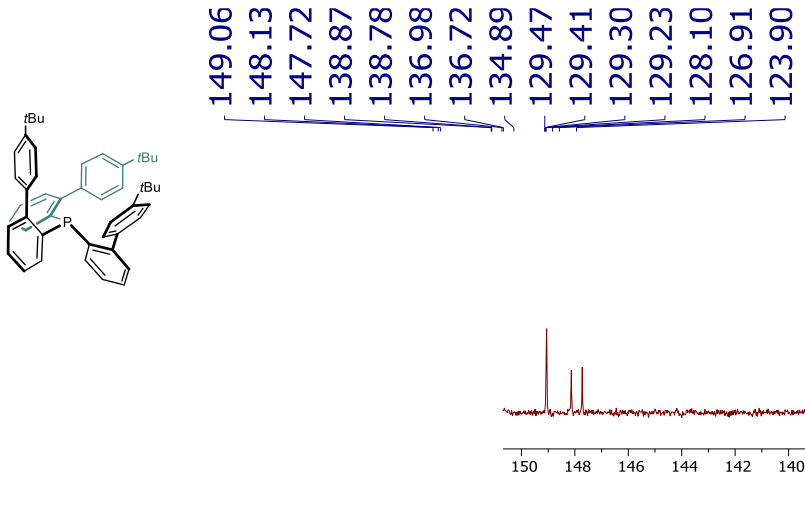
149.06
148.13
147.72
138.87
138.78
136.98
136.72
134.89
129.47
129.41
129.30
129.23
128.10
126.91
123.90
34.43
31.44
tBu
tBu
tBu
P
150 148 146 144 142 140 138 136 134 132 130 128 126 124
f1 (мд)

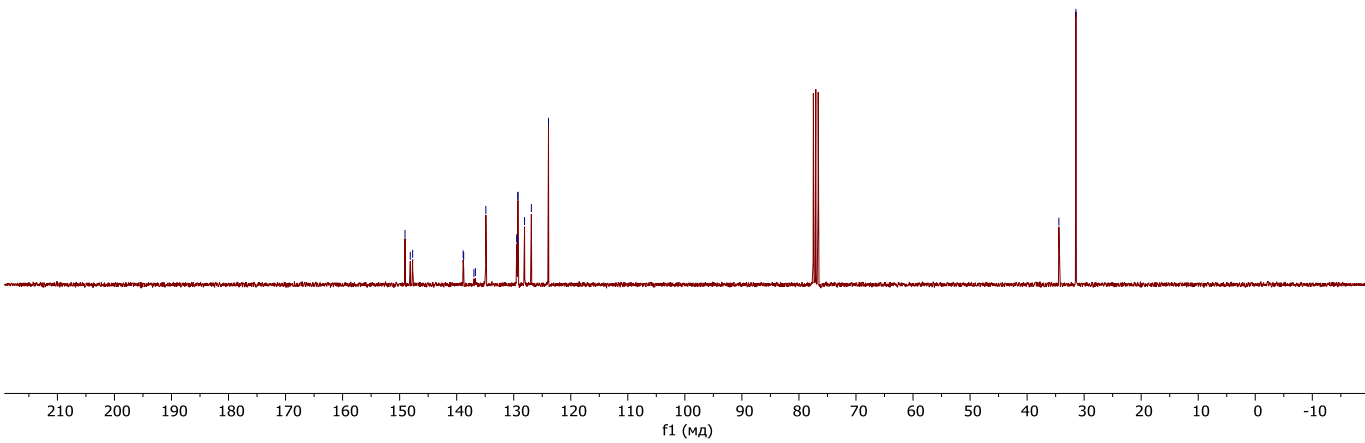
210 200 190 180 170 160 150 140 130 120 110 100 90 80 70 60 50 40 30 20 10 0 -10
f1 (мд)

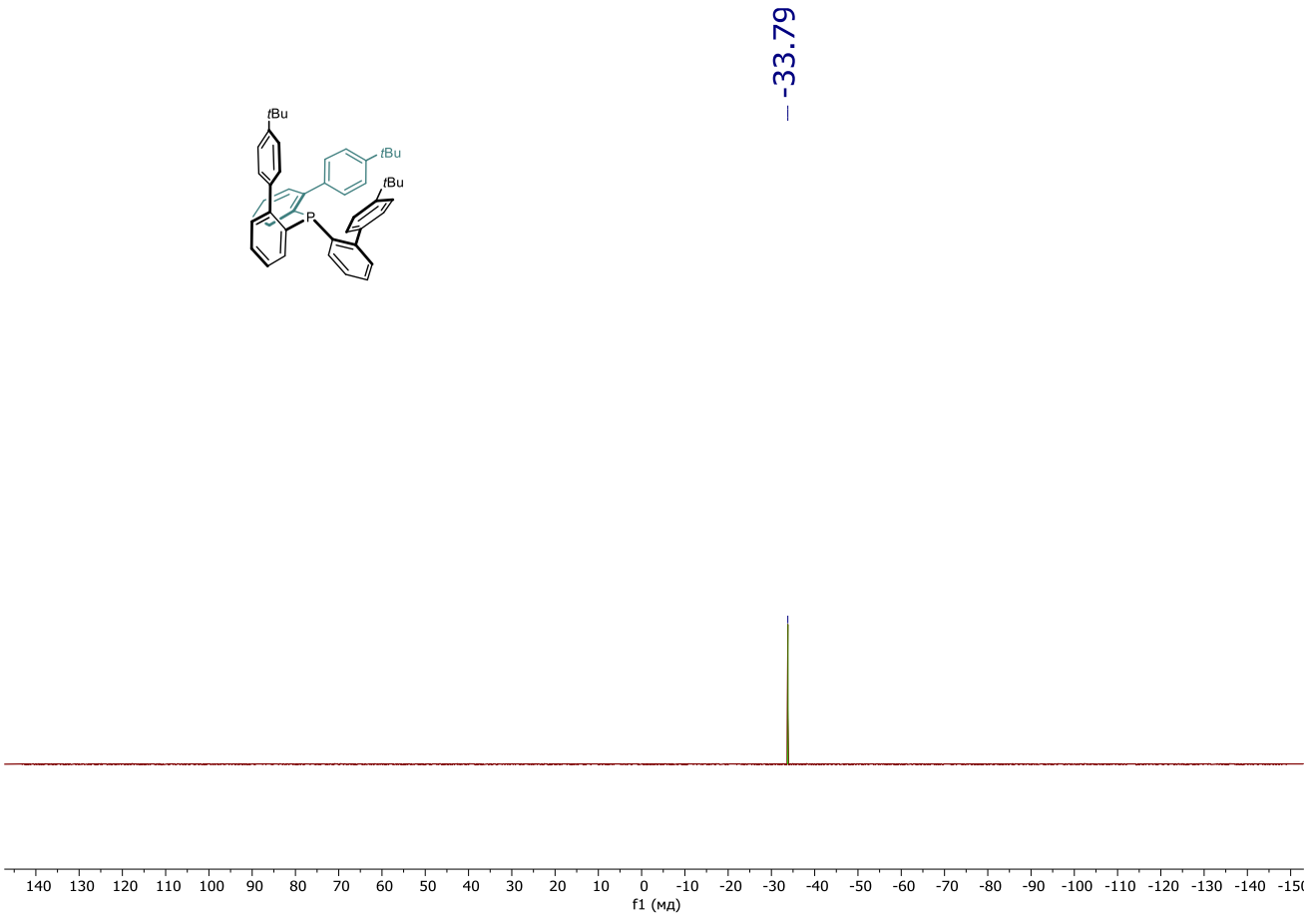
-33.79
tBu
tBu
tBu
P
140 130 120 110 100 90 80 70 60 50 40 30 20 10 0 -10 -20 -30 -40 -50 -60 -70 -80 -90 -100 -110 -120 -130 -140 -150
f1 (мд)

tris(4'-pentyl-[1,1'-biphenyl]-2-yl)phosphane 2.3-4$_{pnPe}$

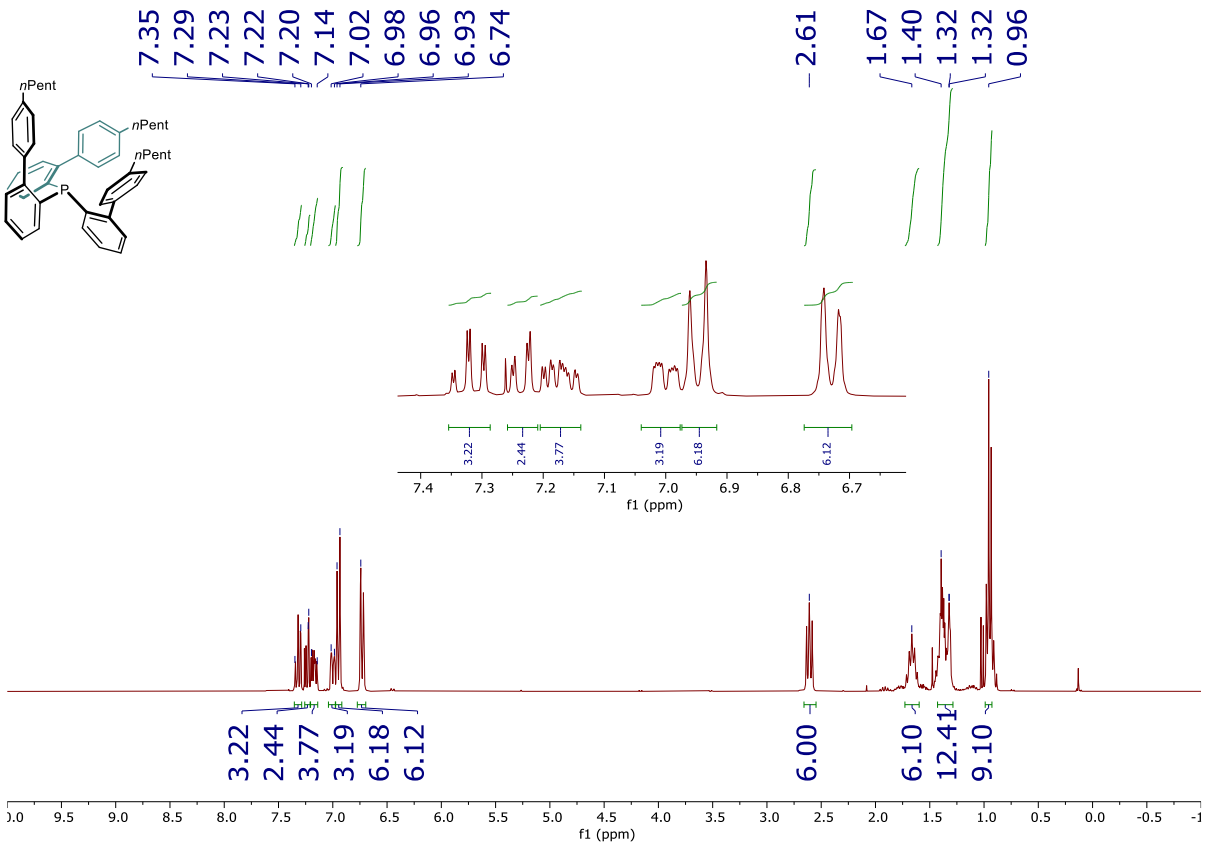

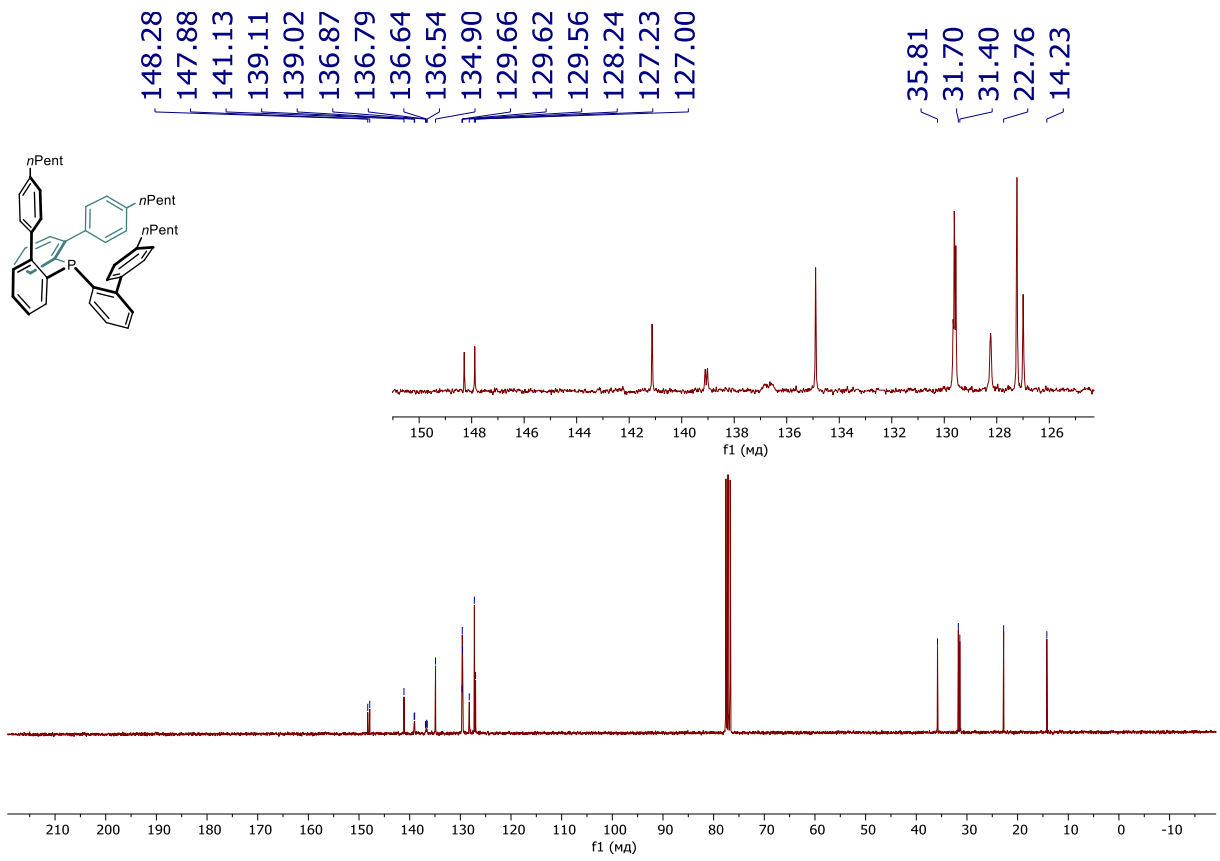

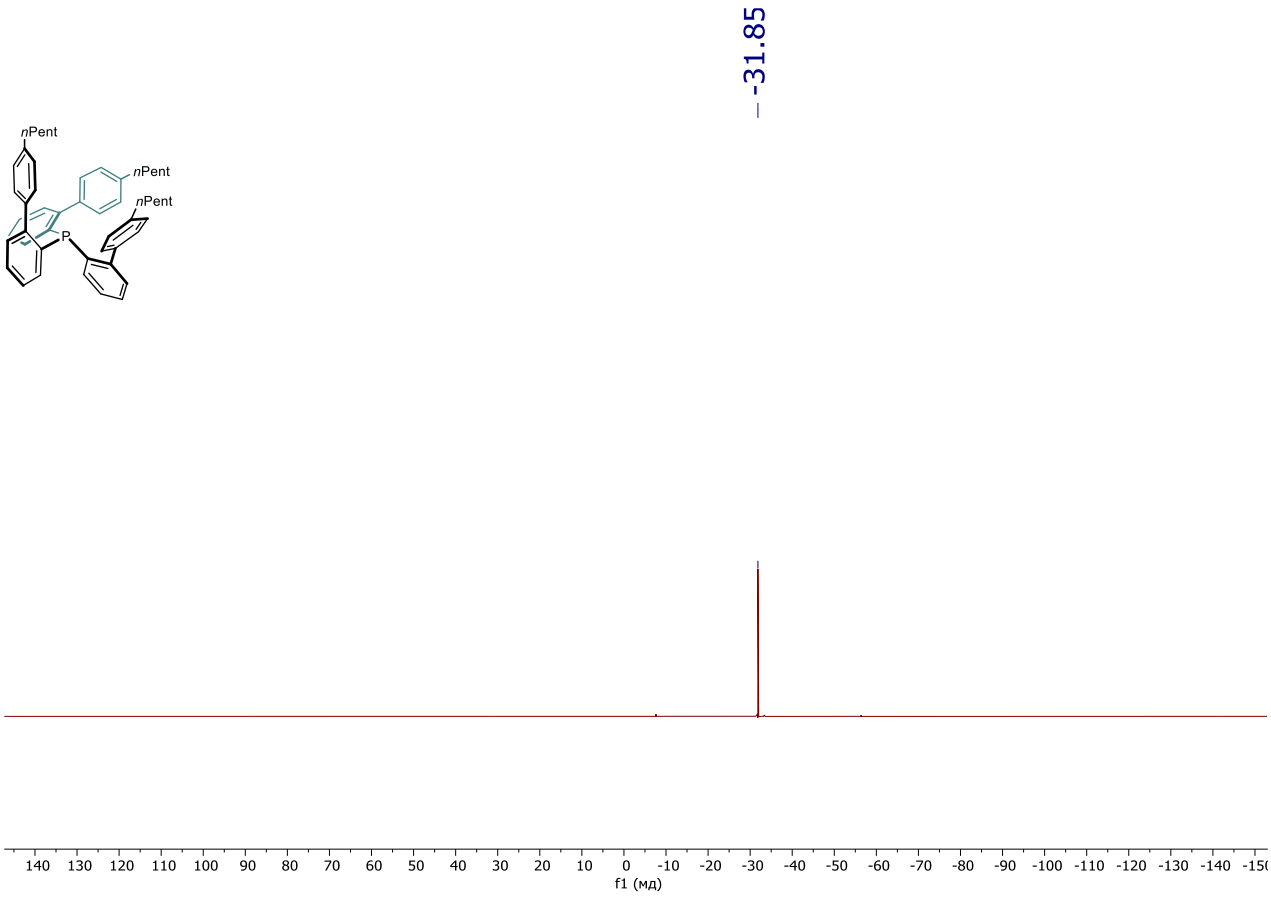

tris(2-(naphthalen-2-yl)phenyl)phosphane 2.3-4$_{2Nap}$

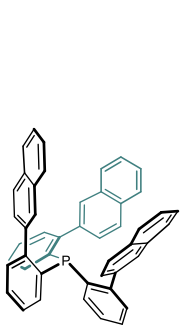

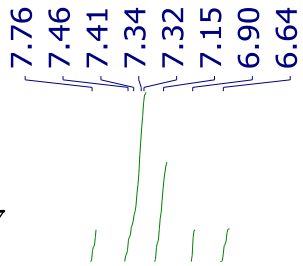

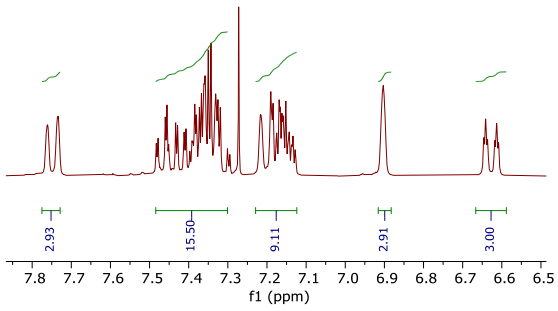

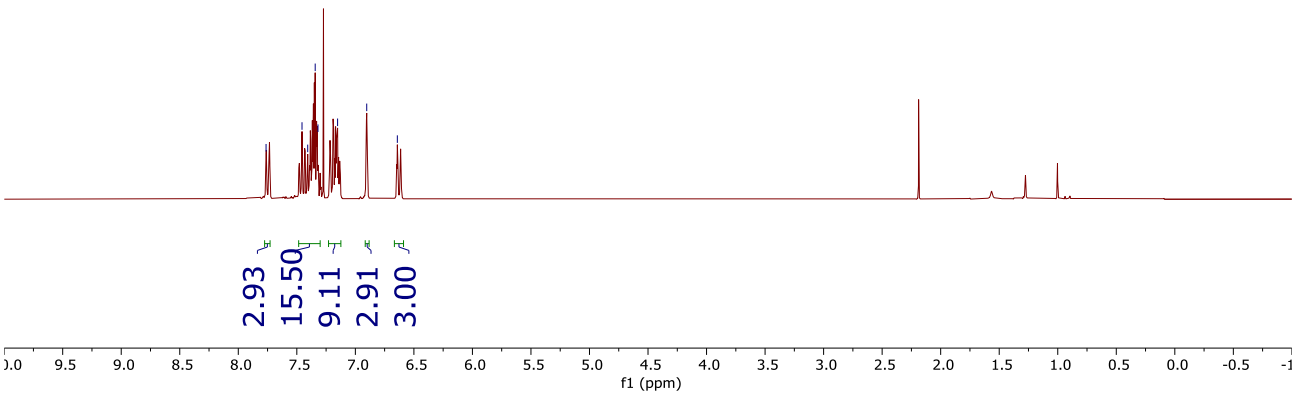

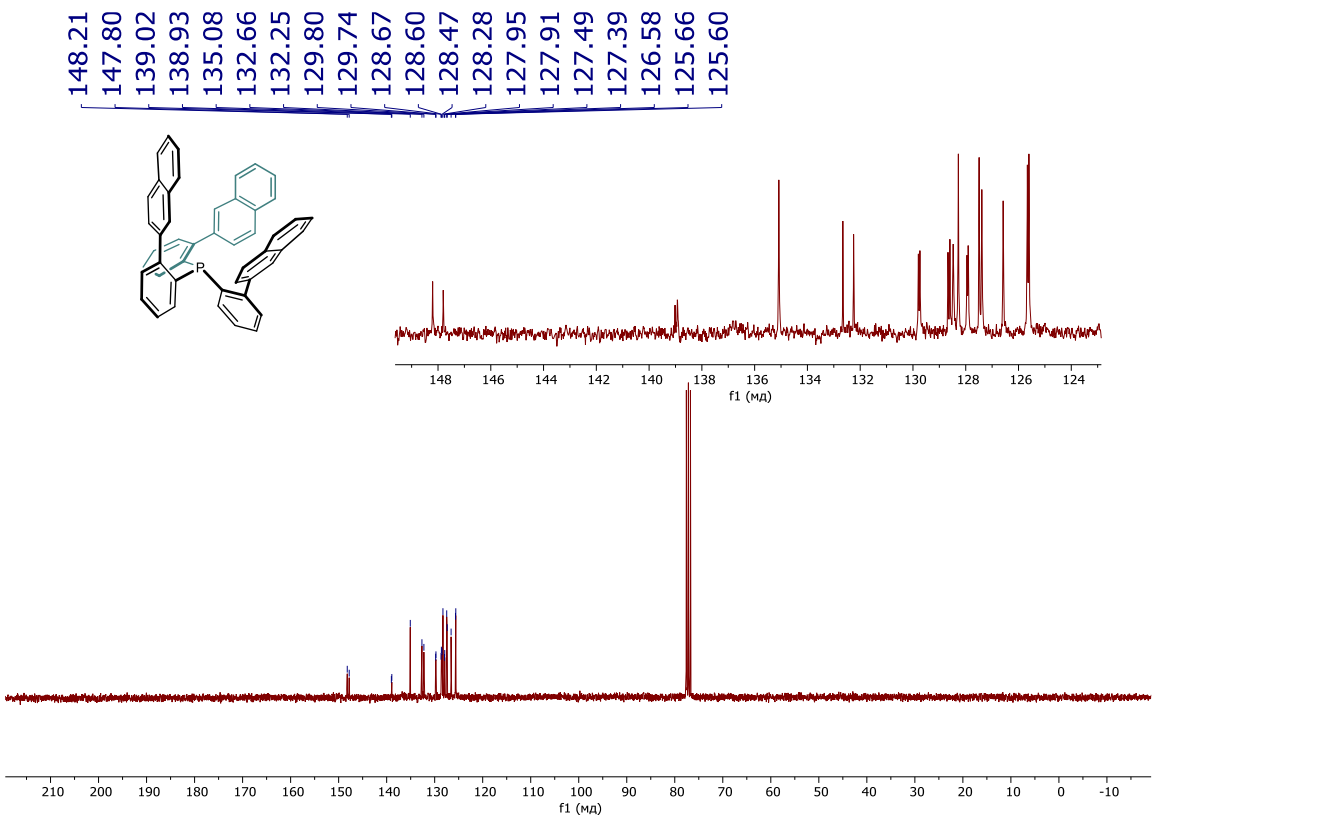

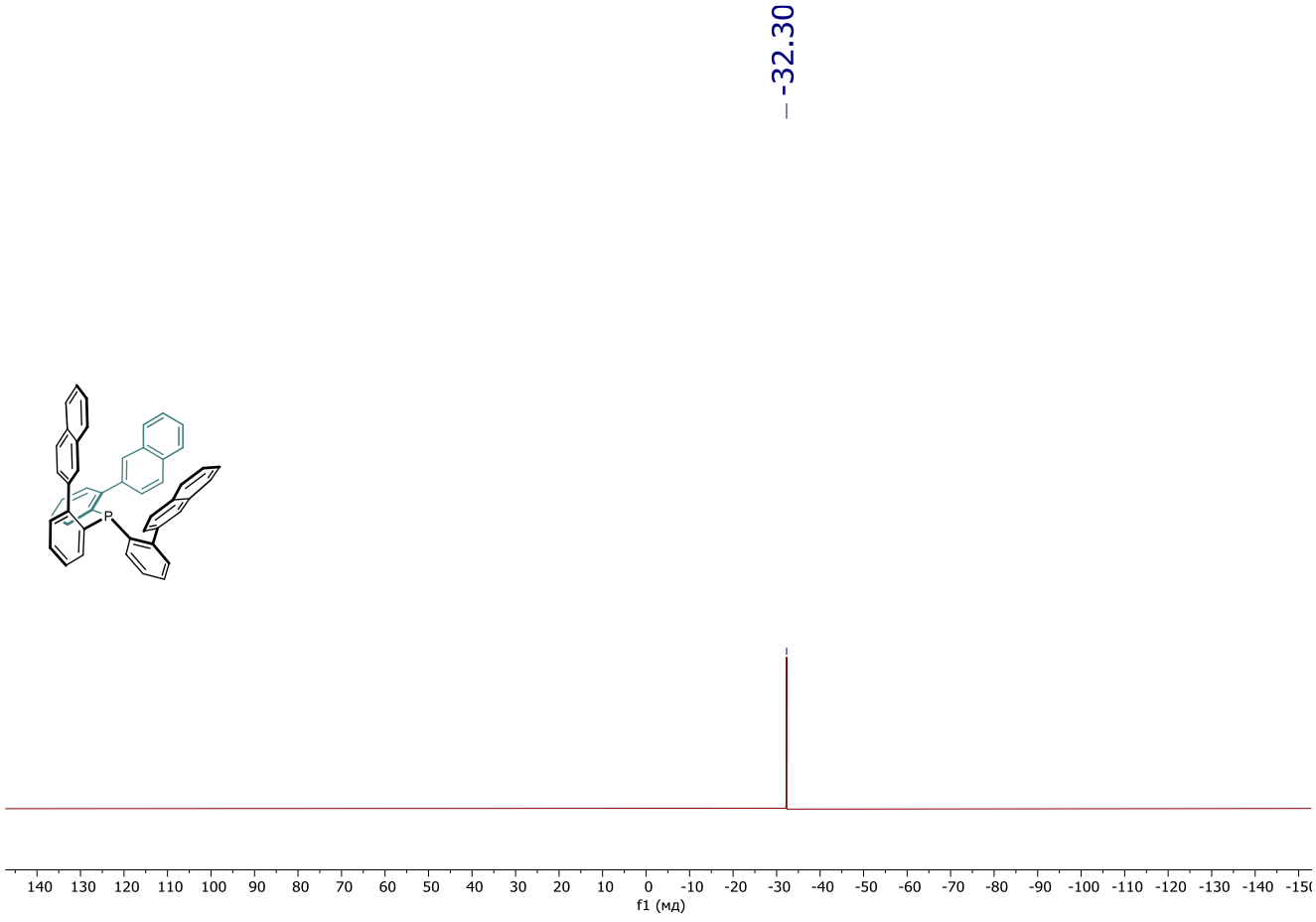

tris(5-(trifluoromethyl)-[1,1'-biphenyl]-2-yl)phosphane 2.3-4$_{CF3}$

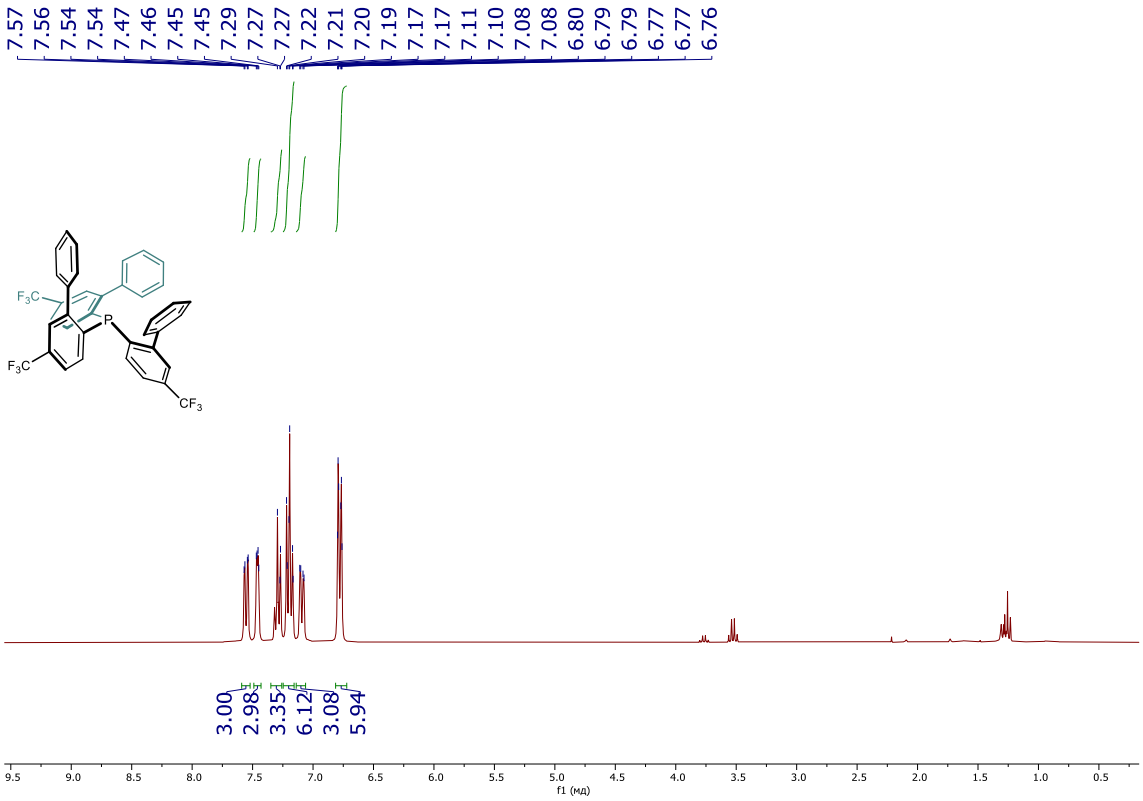
7.57
7.56
7.54
7.54
7.47
7.46
7.45
7.45
7.29
7.27
7.27
7.22
7.21
7.20
7.19
7.17
7.17
7.11
7.10
7.08
7.08
6.80
6.79
6.79
6.77
6.77
6.76
F3C
P
F3C
CF3
3.00
2.98
3.35
6.12
3.08
5.94
f1 (мд)

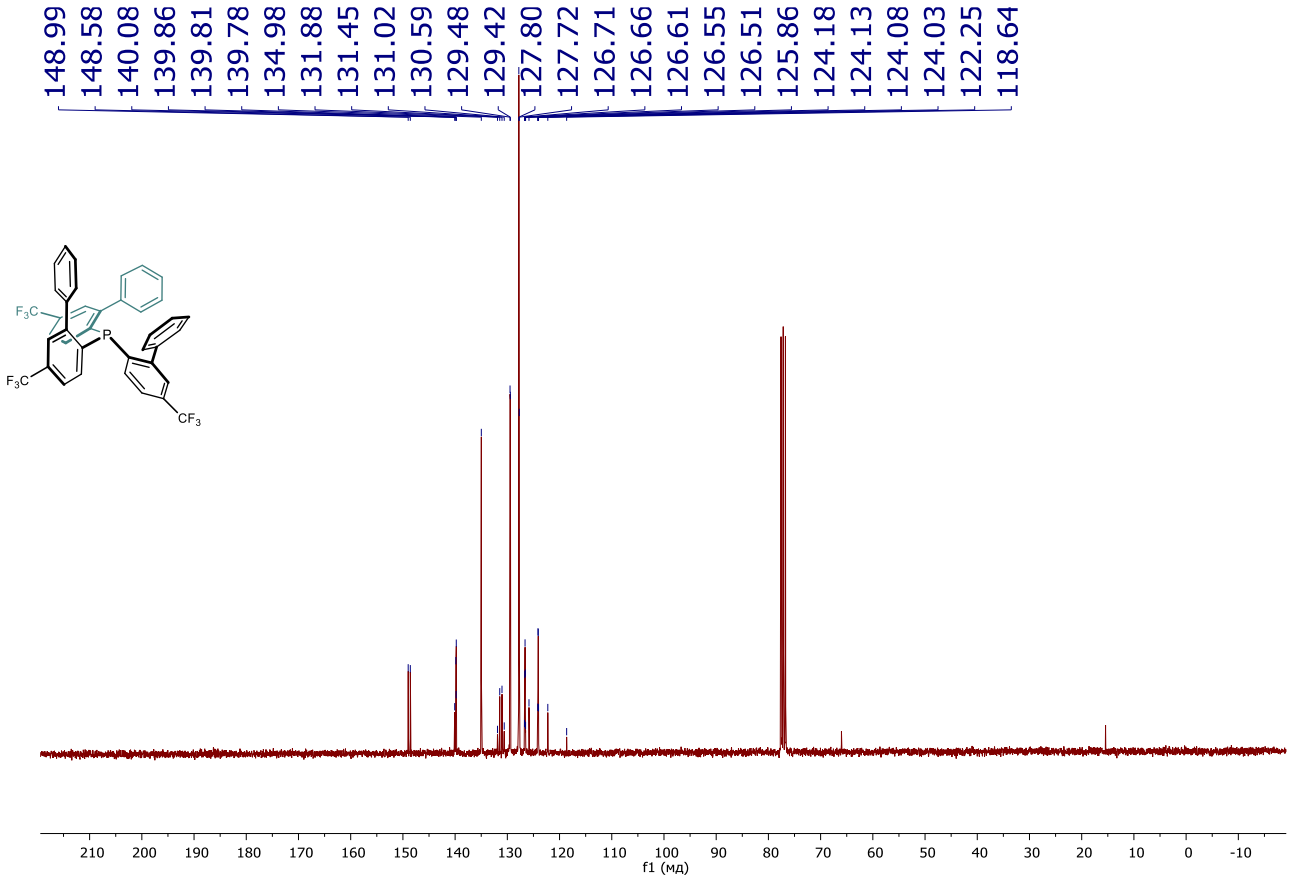
148.99
148.58
140.08
139.86
139.81
139.78
134.98
131.88
131.45
131.02
130.59
129.48
129.42
127.80
127.72
126.71
126.66
126.61
126.55
126.51
125.86
124.18
124.13
124.08
124.03
122.25
118.64
F3C
P
F3C
CF3
f1 (мд)

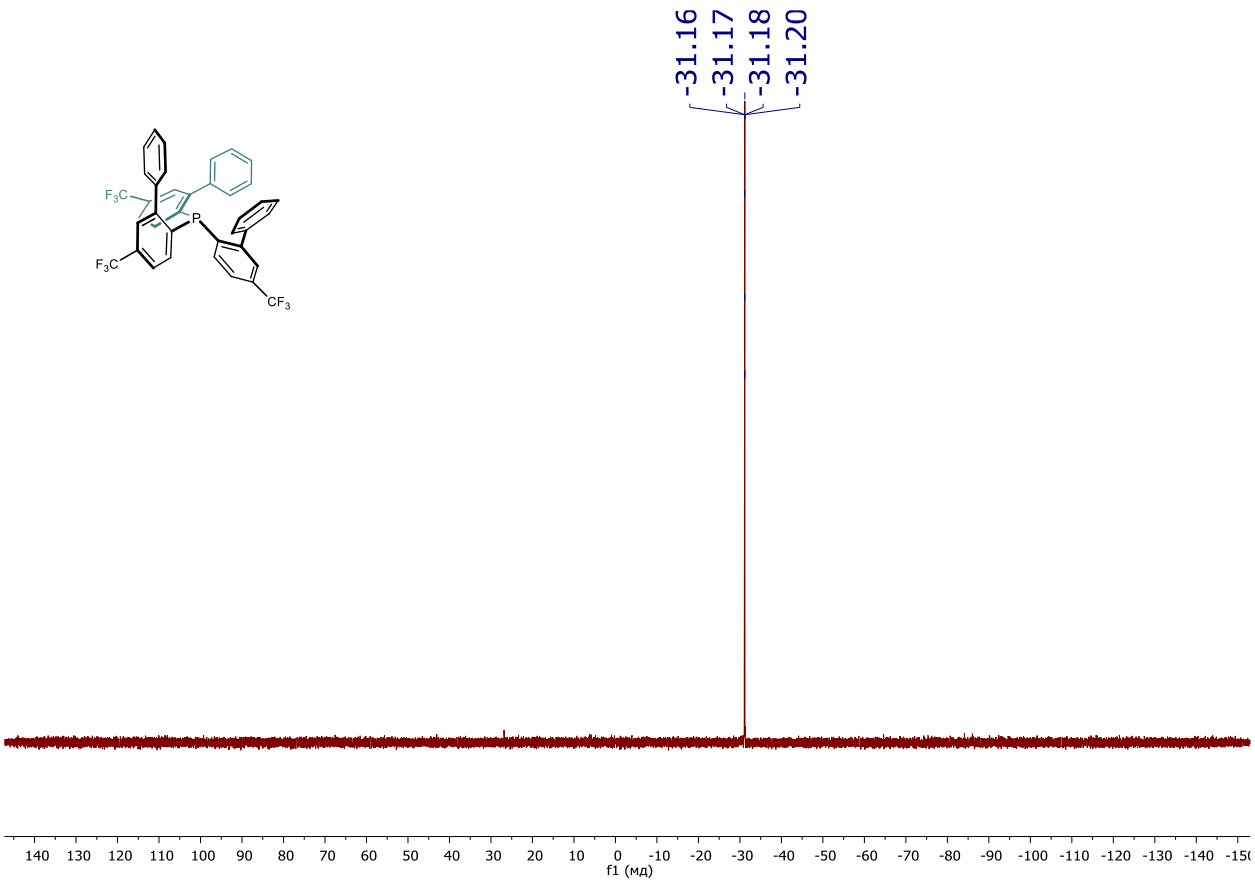

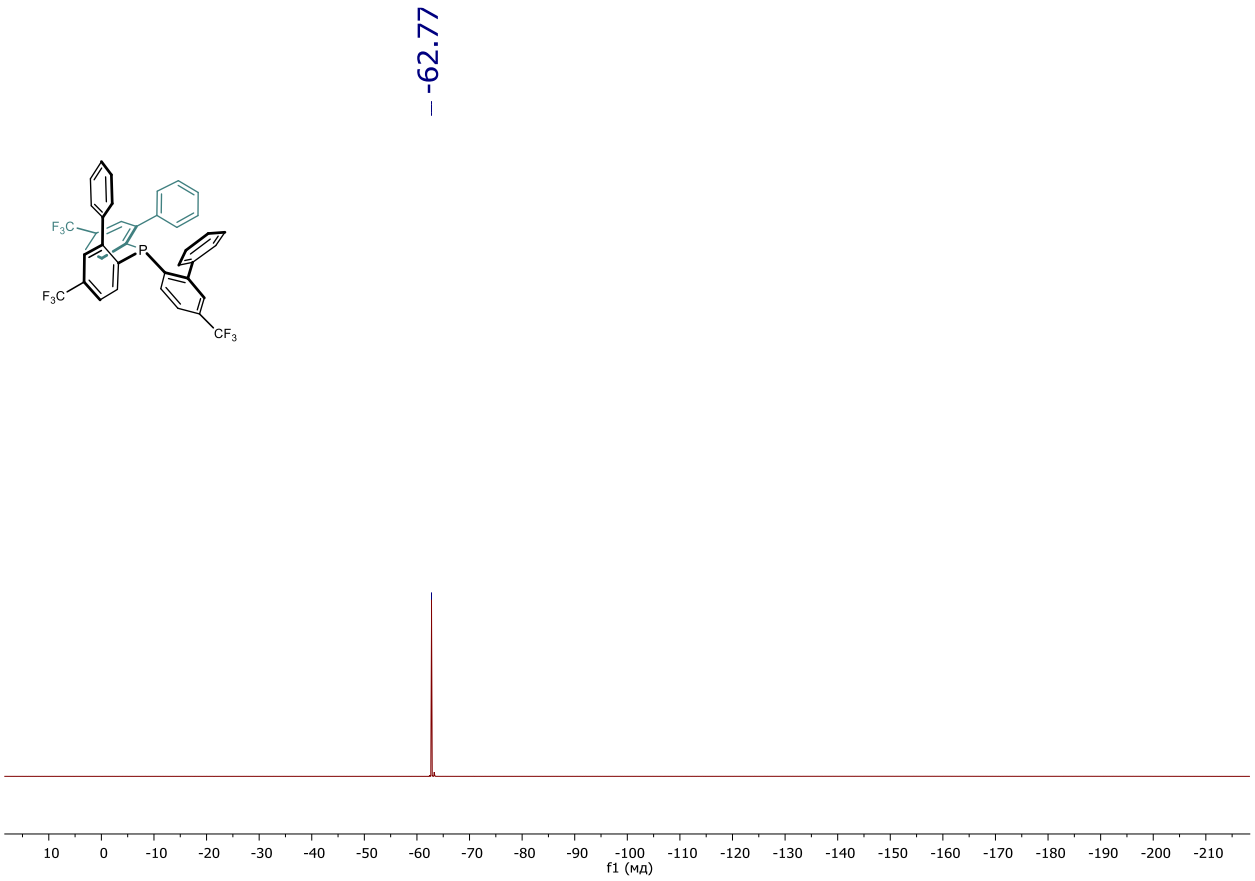

Gold (I) chloride complex 2.3-5$_H$

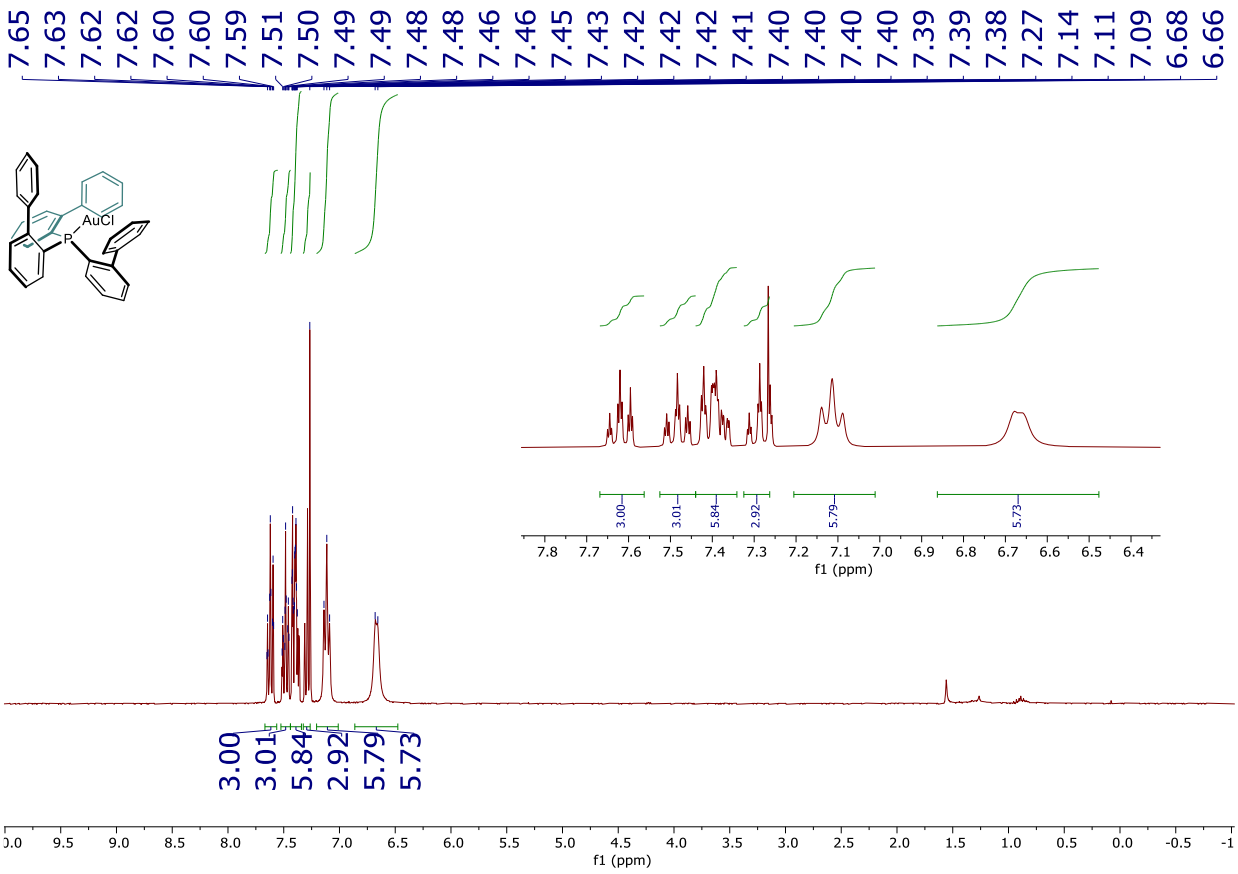
7.65 7.63 7.62 7.62 7.60 7.60 7.59 7.51 7.50 7.49 7.49 7.48 7.48 7.46 7.46 7.45 7.43 7.42 7.42 7.42 7.41 7.40 7.40 7.40 7.40 7.39 7.39 7.38 7.27 7.14 7.11 7.09 6.68 6.66
AuCl
P
3.00 3.01 5.84 2.92 5.79 5.73
f1 (ppm)

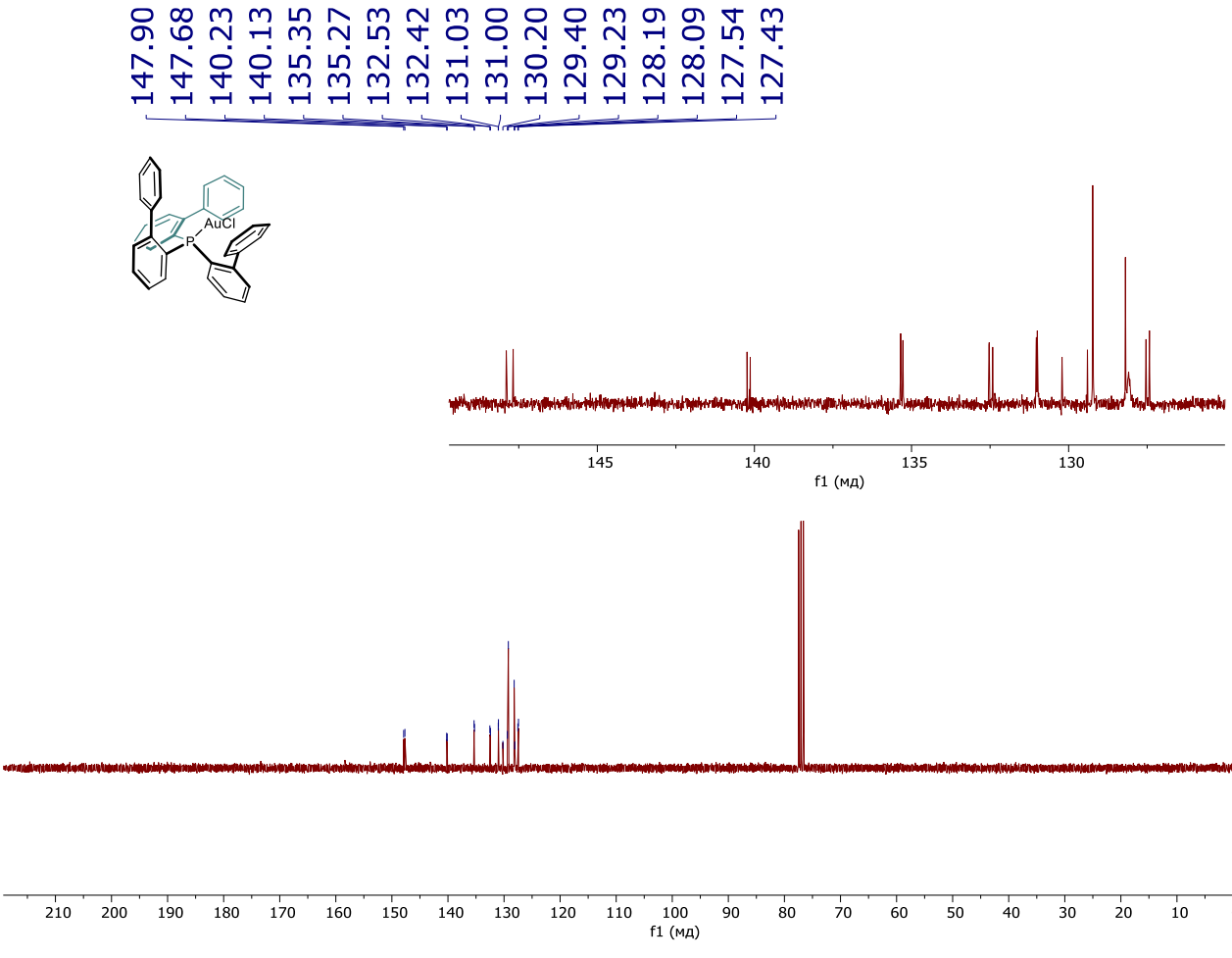
147.90 147.68 140.23 140.13 135.35 135.27 132.53 132.42 131.03 131.00 130.20 129.40 129.23 128.19 128.09 127.54 127.43
AuCl
P
f1 (мд)
f1 (мд)

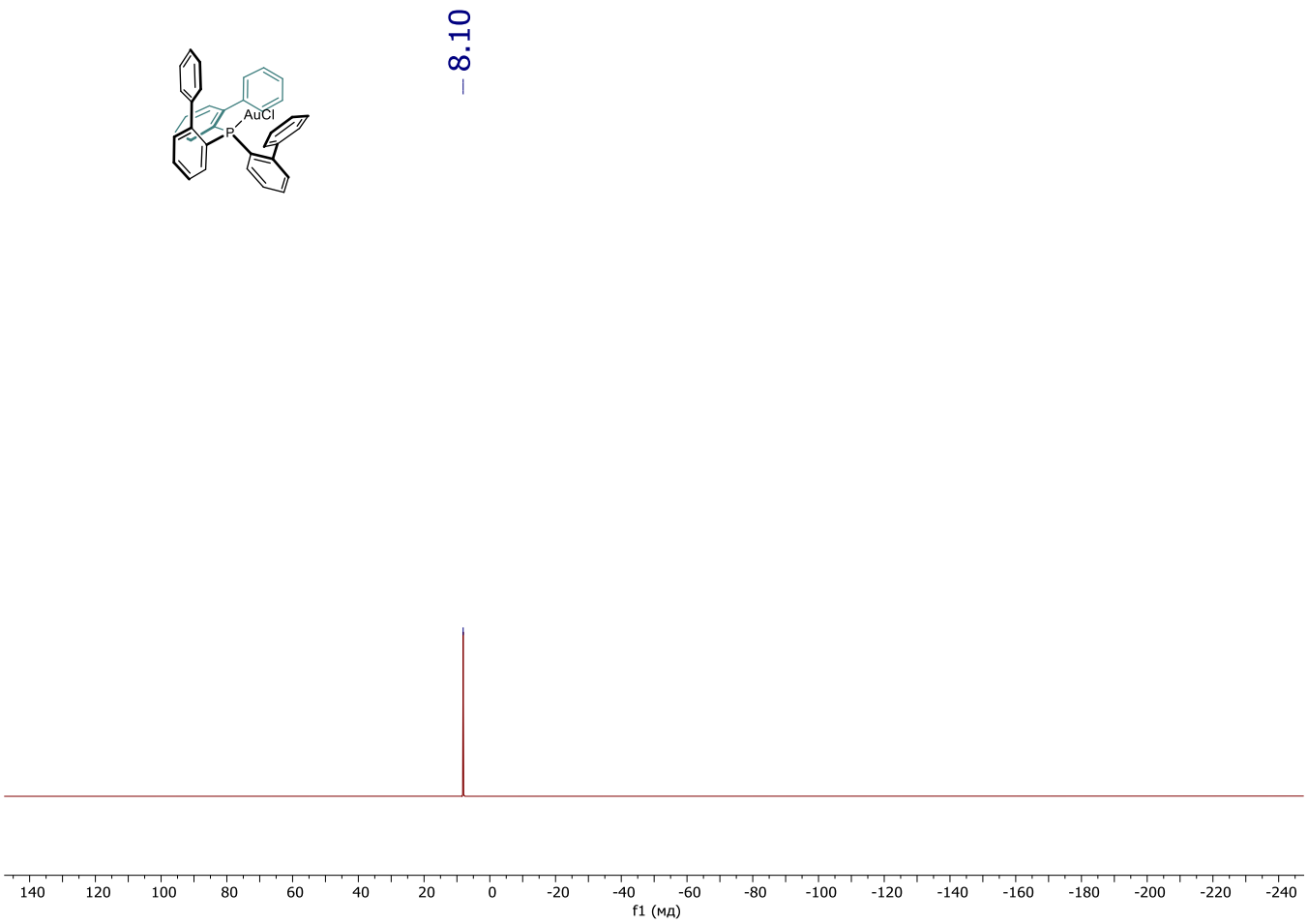

Gold (I) chloride complex 2.3-5$_{mtBu}$

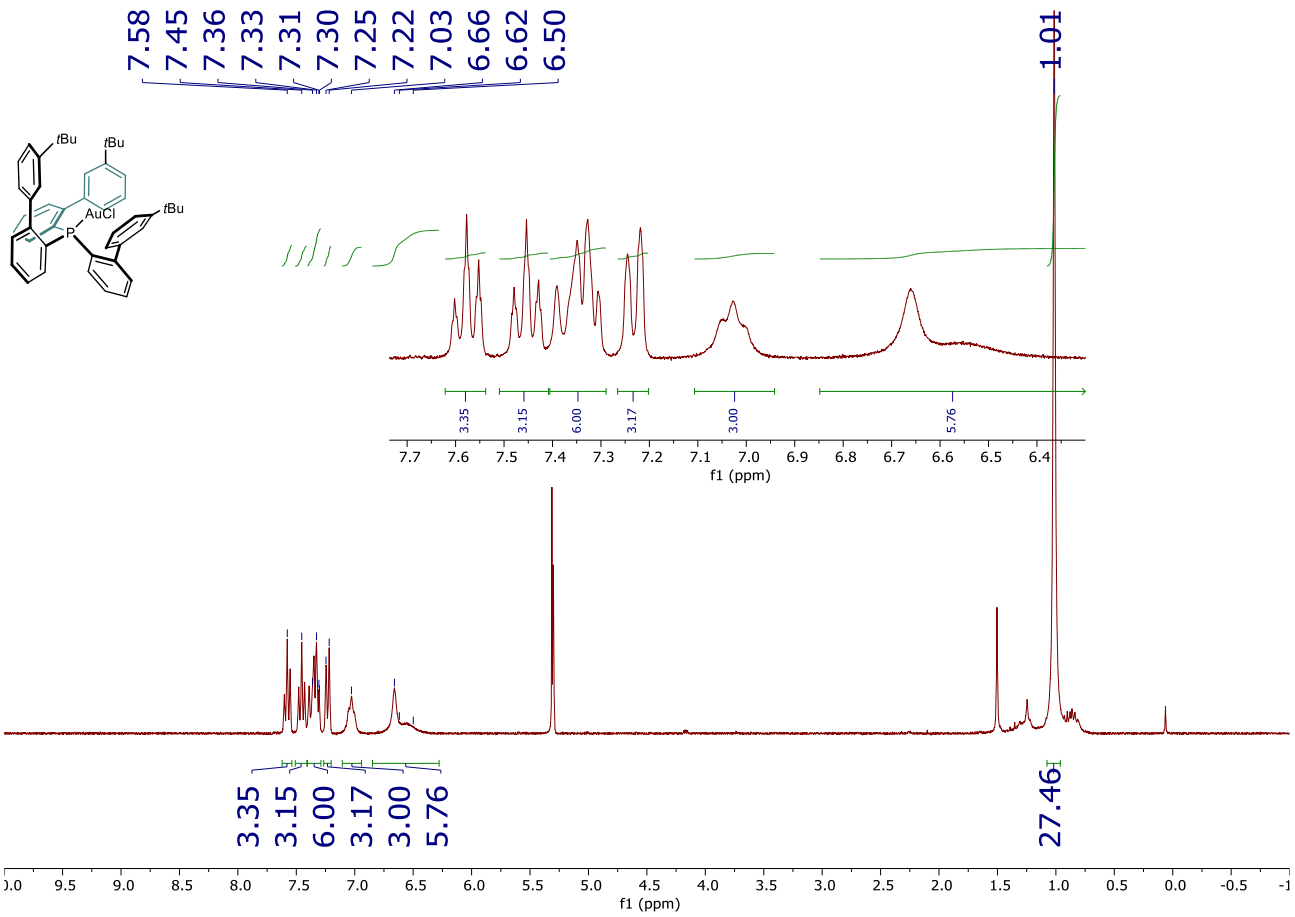
7.58
7.45
7.36
7.33
7.31
7.30
7.25
7.22
7.03
6.66
6.62
6.50
1.01
tBu
tBu
AuCl
tBu
P
3.35
3.15
6.00
3.17
3.00
5.76
f1 (ppm)
3.35
3.15
6.00
3.17
3.00
5.76
27.46
f1 (ppm)

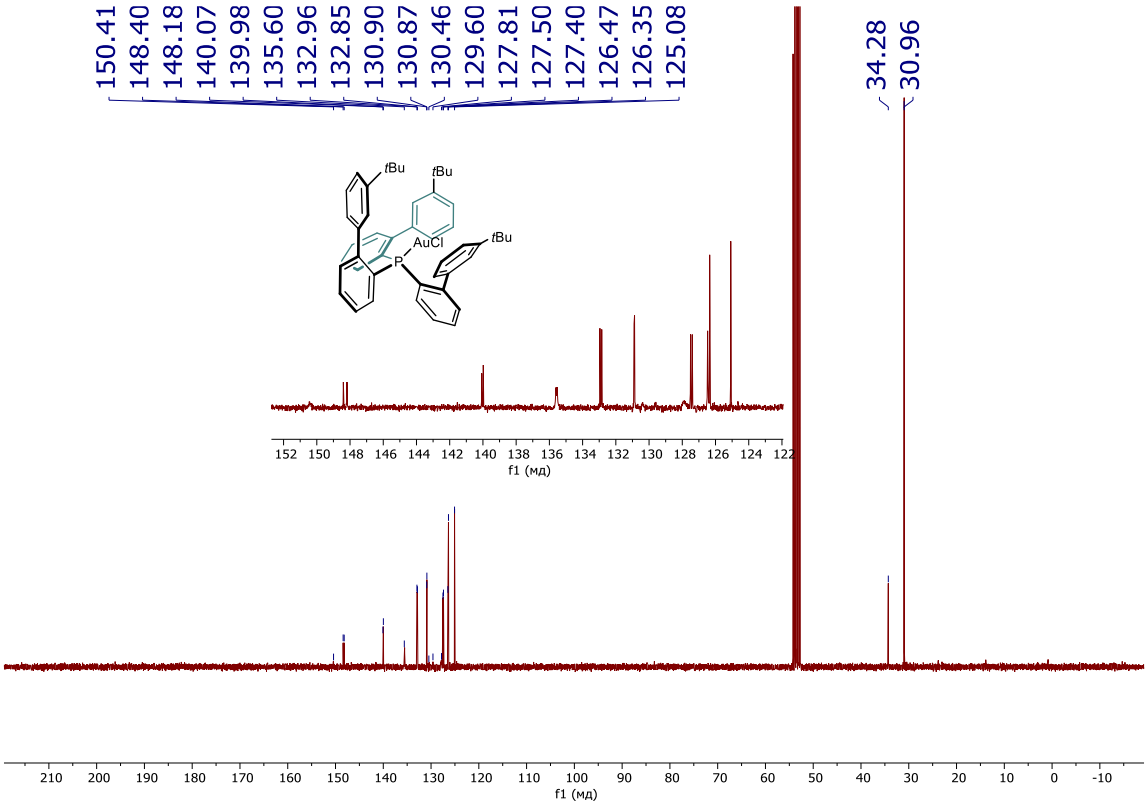

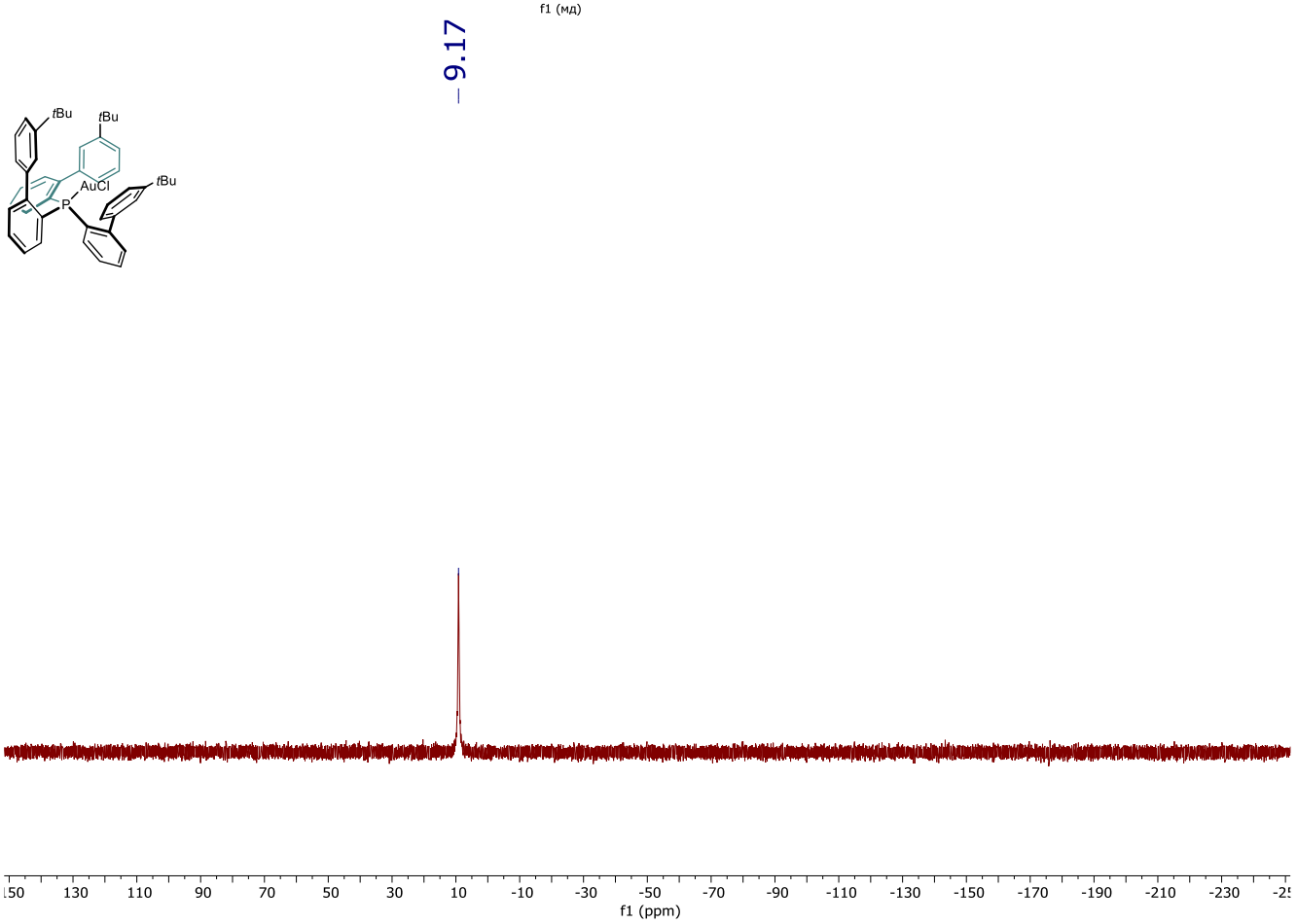

Gold (I) chloride complex 2.3-5$_{mnBu}$

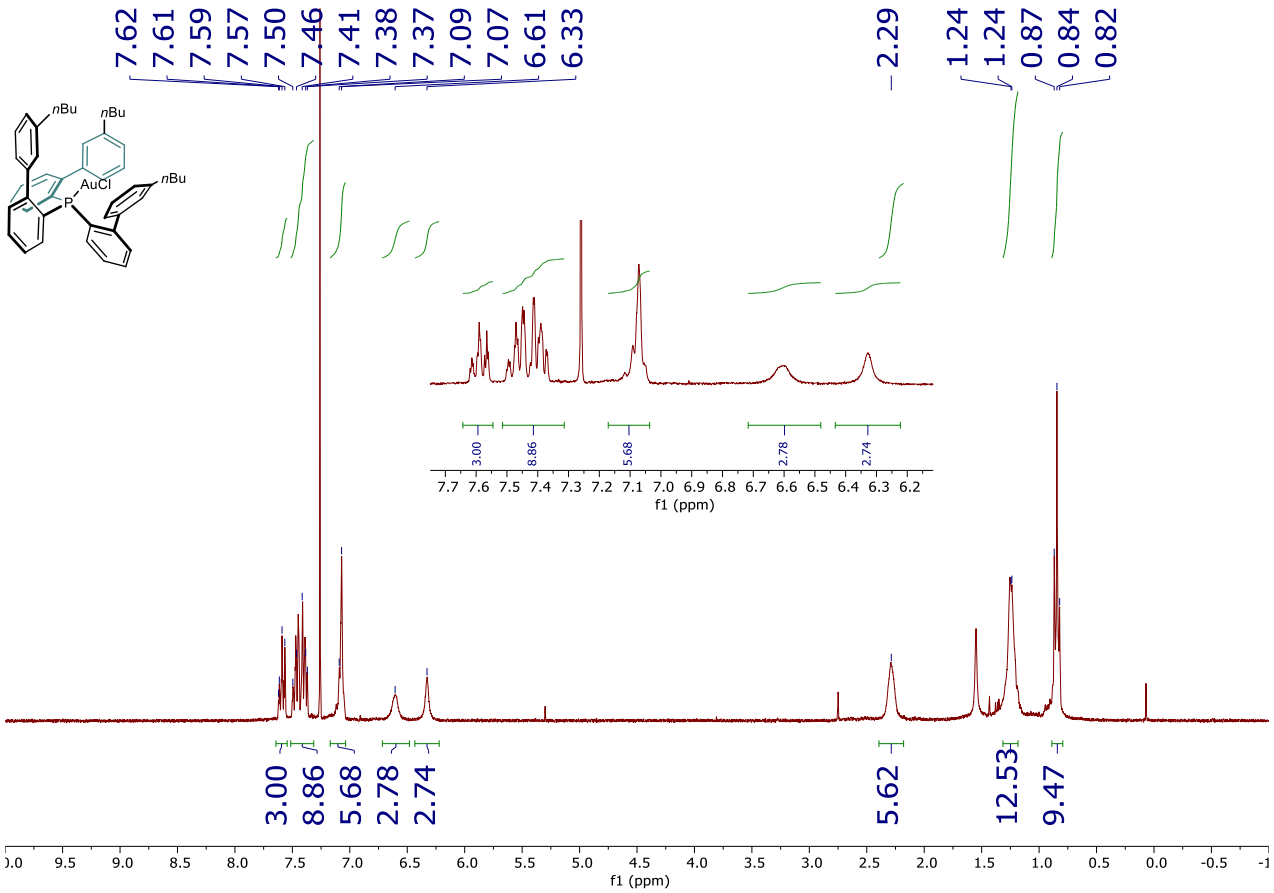
7.62
7.61
7.59
7.57
7.50
7.46
7.41
7.38
7.37
7.09
7.07
6.61
6.33
2.29
1.24
1.24
0.87
0.84
0.82
nBu
nBu
AuCl
nBu
P
3.00
8.86
5.68
2.78
2.74
5.62
12.53
9.47
f1 (ppm)

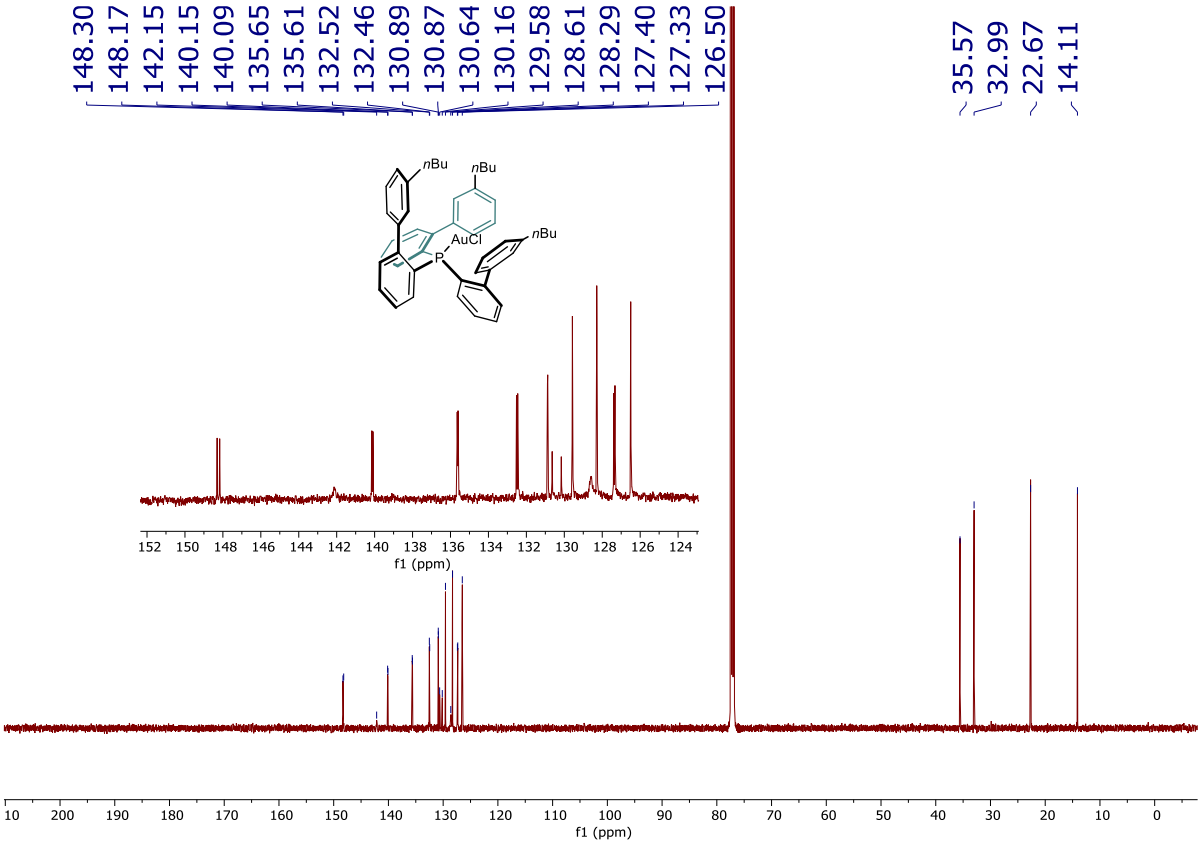
148.30
148.17
142.15
140.15
140.09
135.65
135.61
132.52
132.46
130.89
130.87
130.64
130.16
129.58
128.61
128.29
127.40
127.33
126.50
35.57
32.99
22.67
14.11
nBu
nBu
AuCl
nBu
P
f1 (ppm)

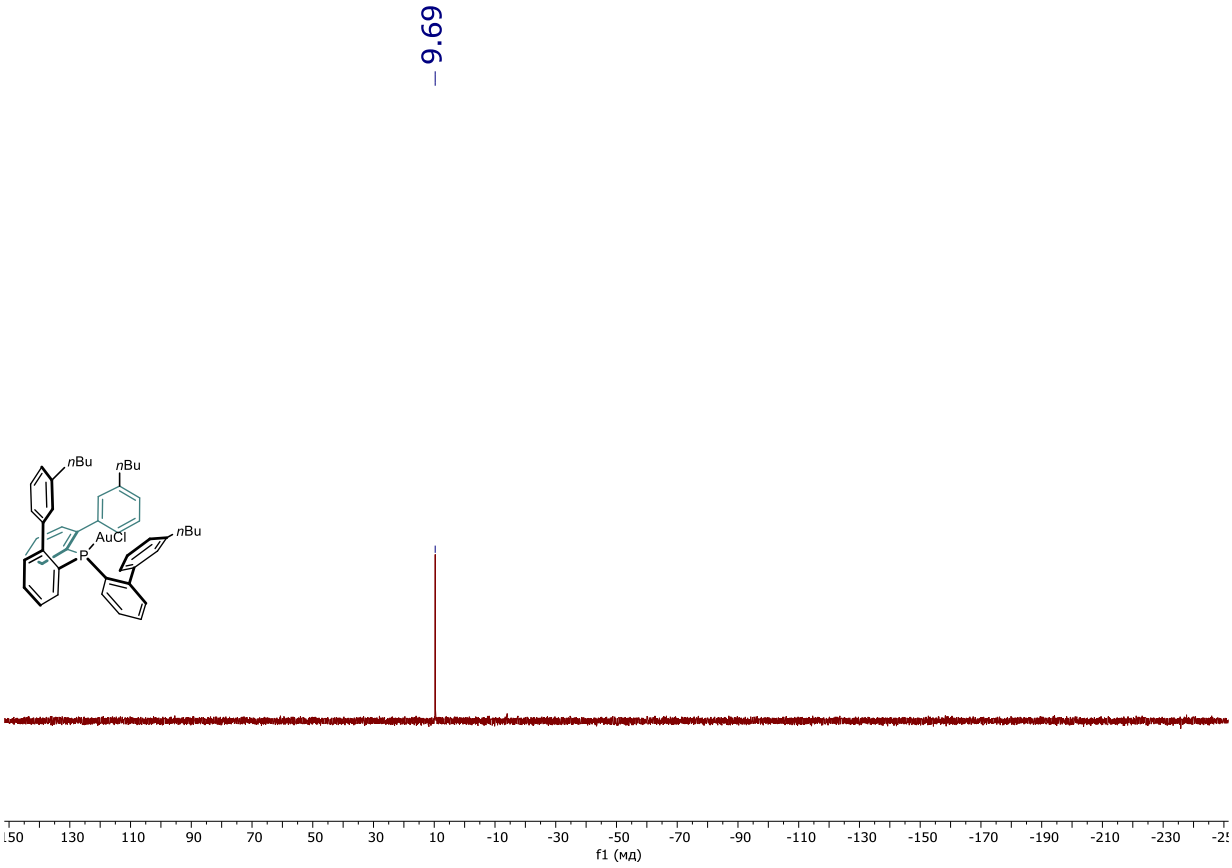

Gold (I) chloride complex 2.3-5$_{ptBu}$

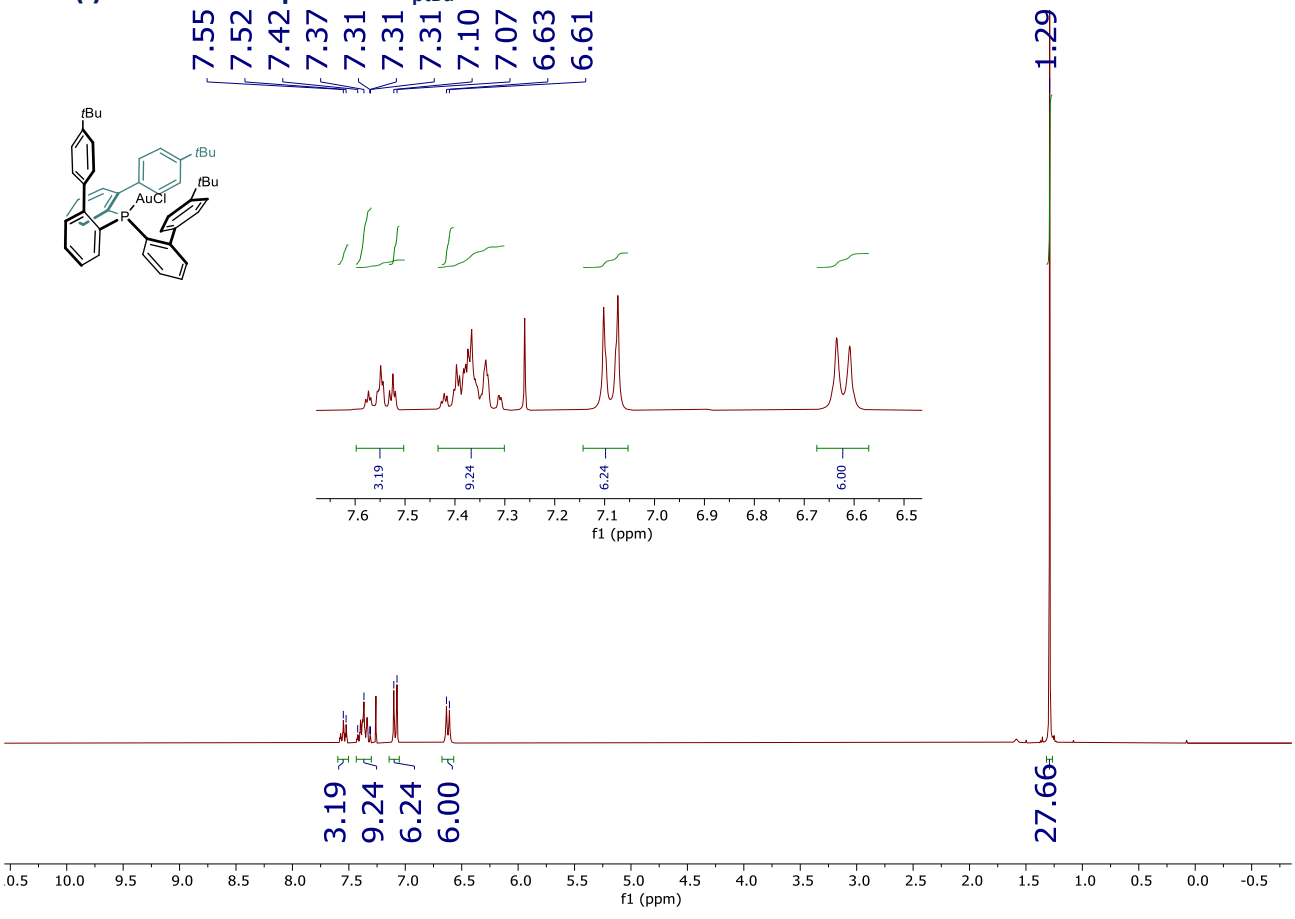

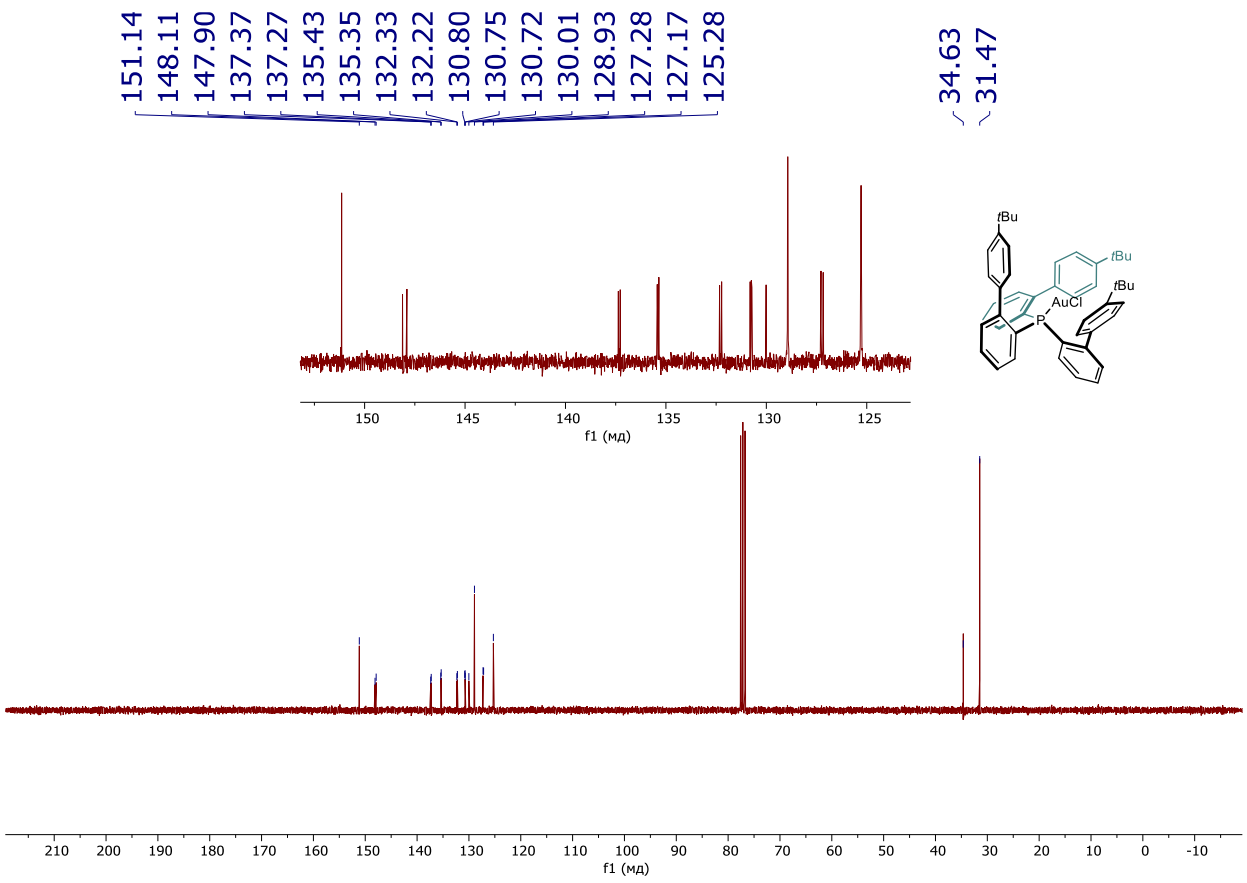
151.14
148.11
147.90
137.37
137.27
135.43
135.35
132.33
132.22
130.80
130.75
130.72
130.01
128.93
127.28
127.17
125.28
34.63
31.47
tBu
tBu
tBu
AuCl
P
150
145
140
135
130
125
f1 (мд)
210
200
190
180
170
160
150
140
130
120
110
100
90
80
70
60
50
40
30
20
10
0
-10
f1 (мд)

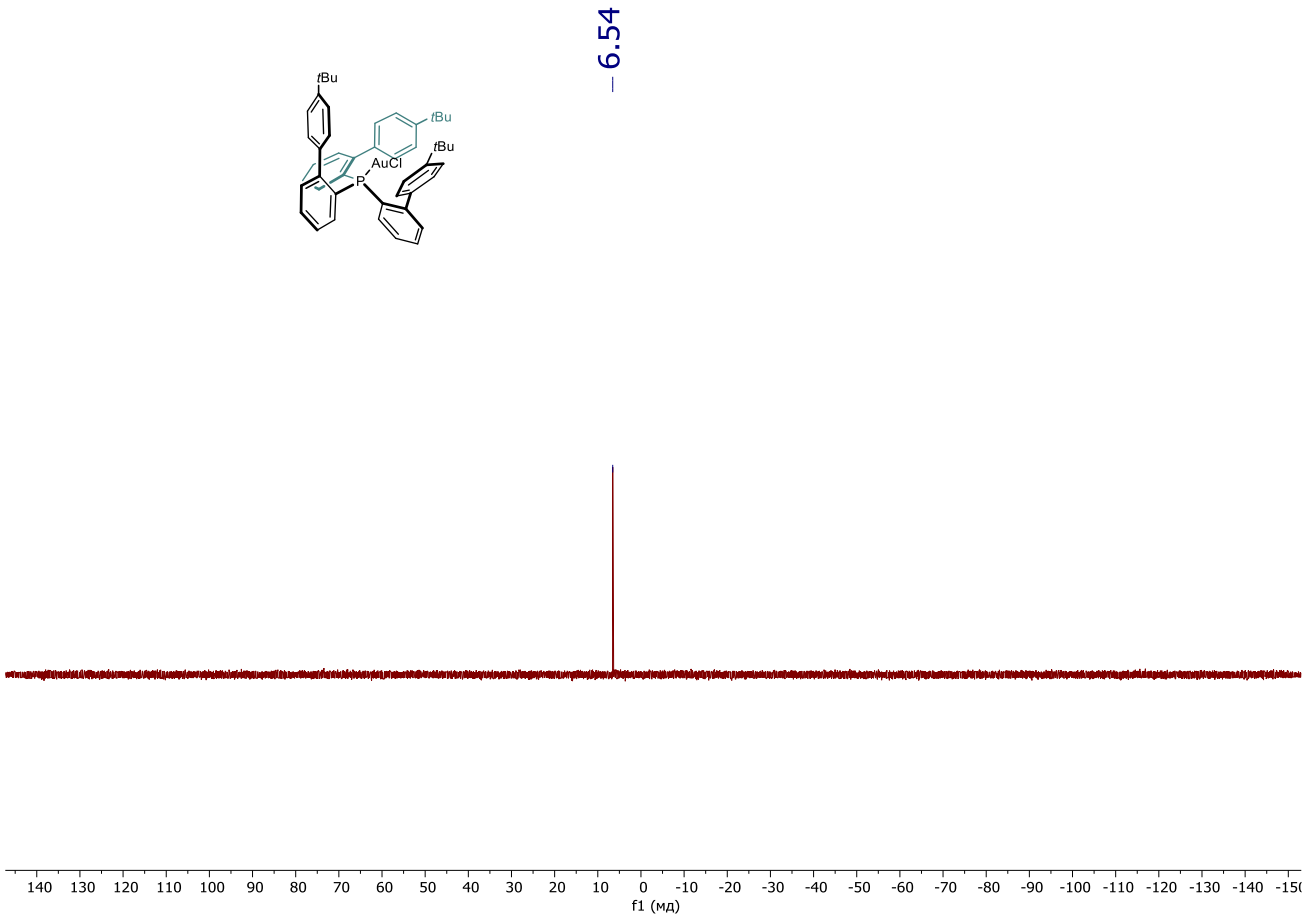
6.54
tBu
tBu
tBu
AuCl
P
140
130
120
110
100
90
80
70
60
50
40
30
20
10
0
-10
-20
-30
-40
-50
-60
-70
-80
-90
-100
-110
-120
-130
-140
f1 (мд)

Gold (I) chloride complex 2.3-5$_{pnPe}$

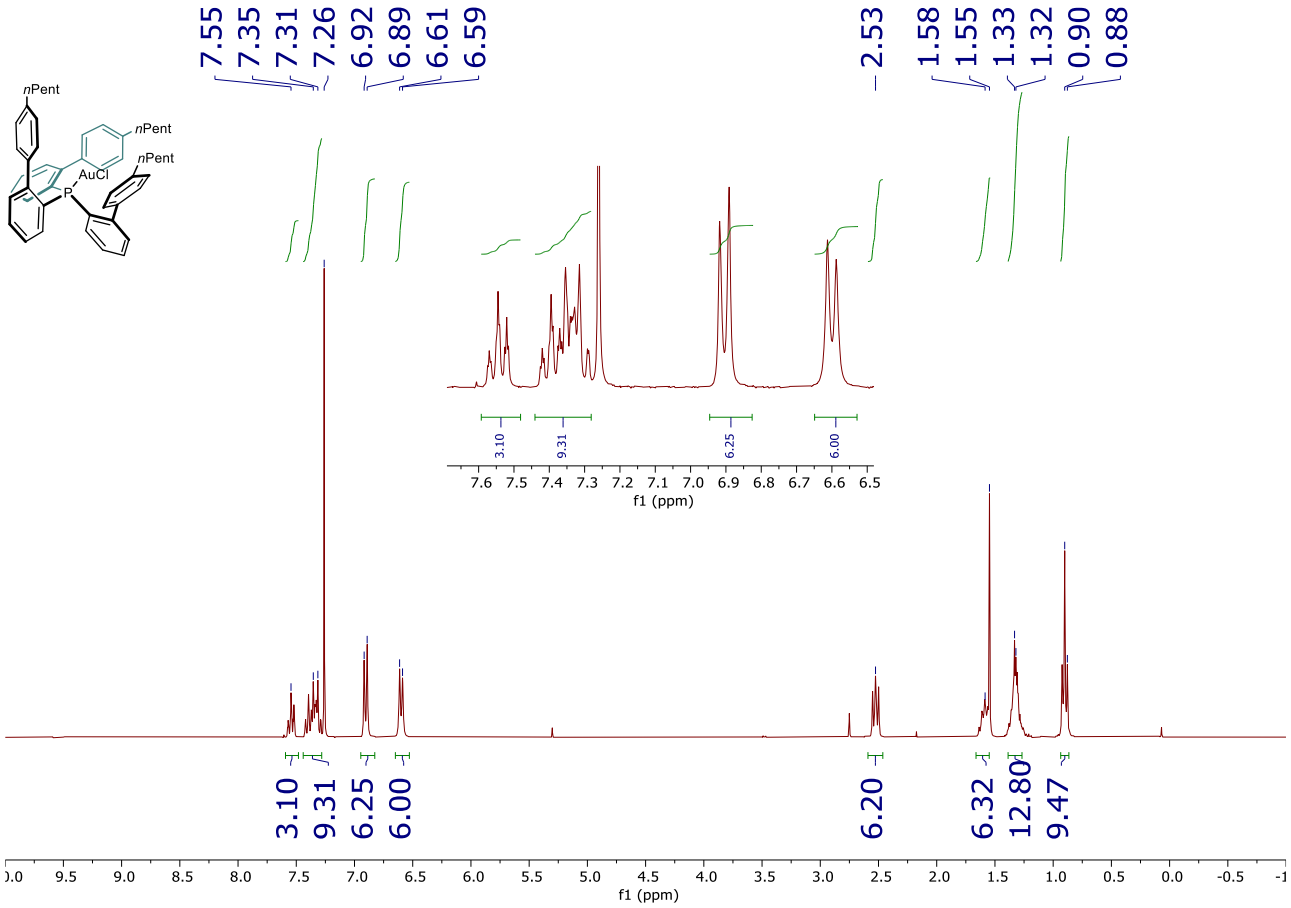

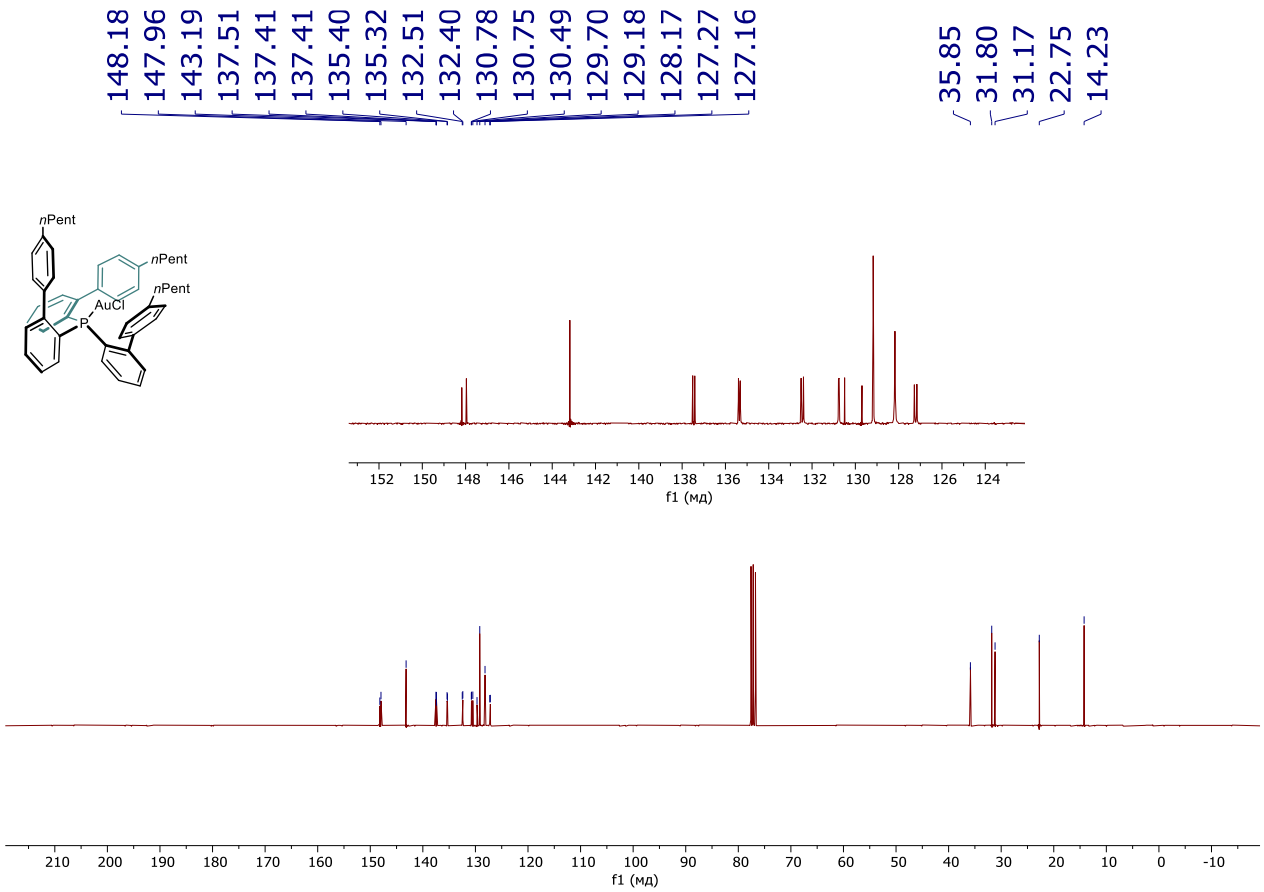

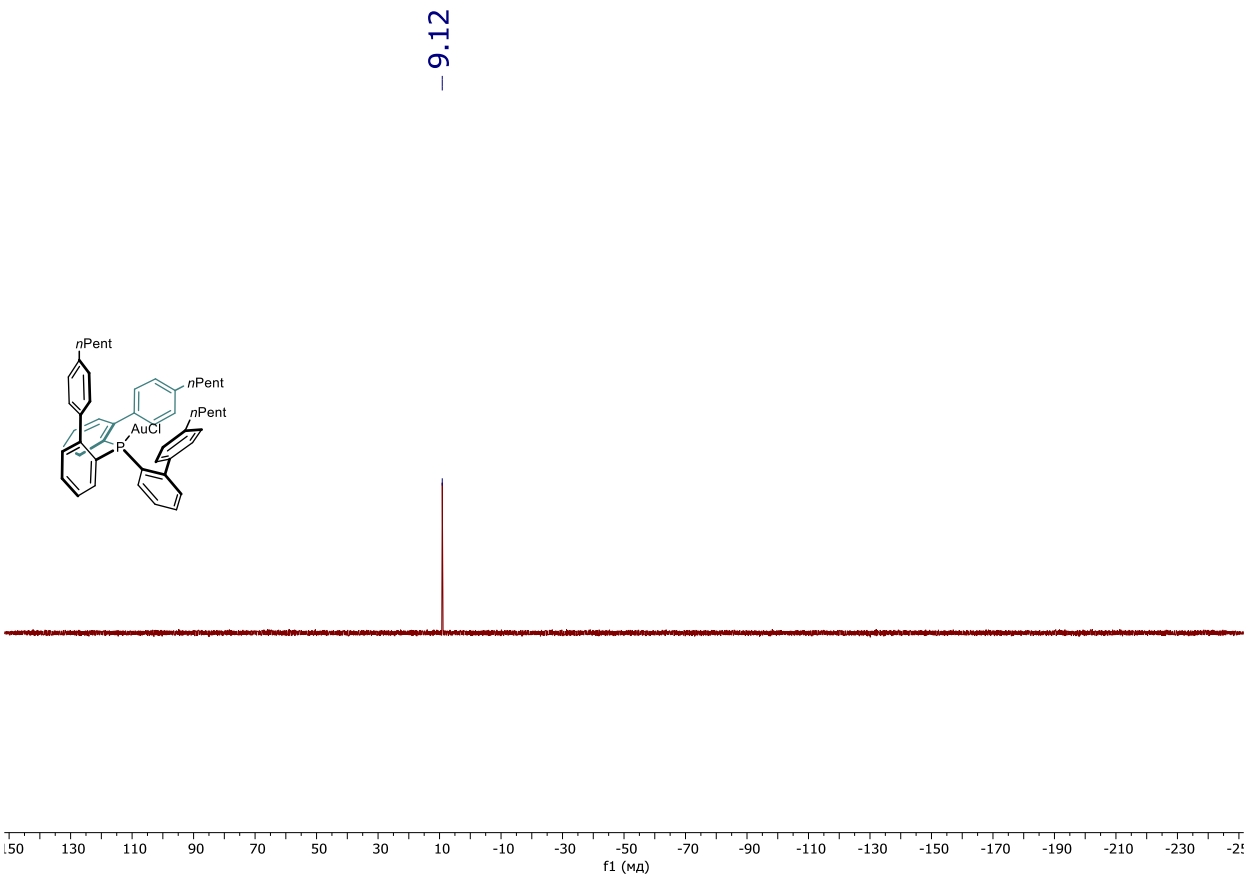

Gold (I) chloride complex 2.3-5$_{2Nap}$

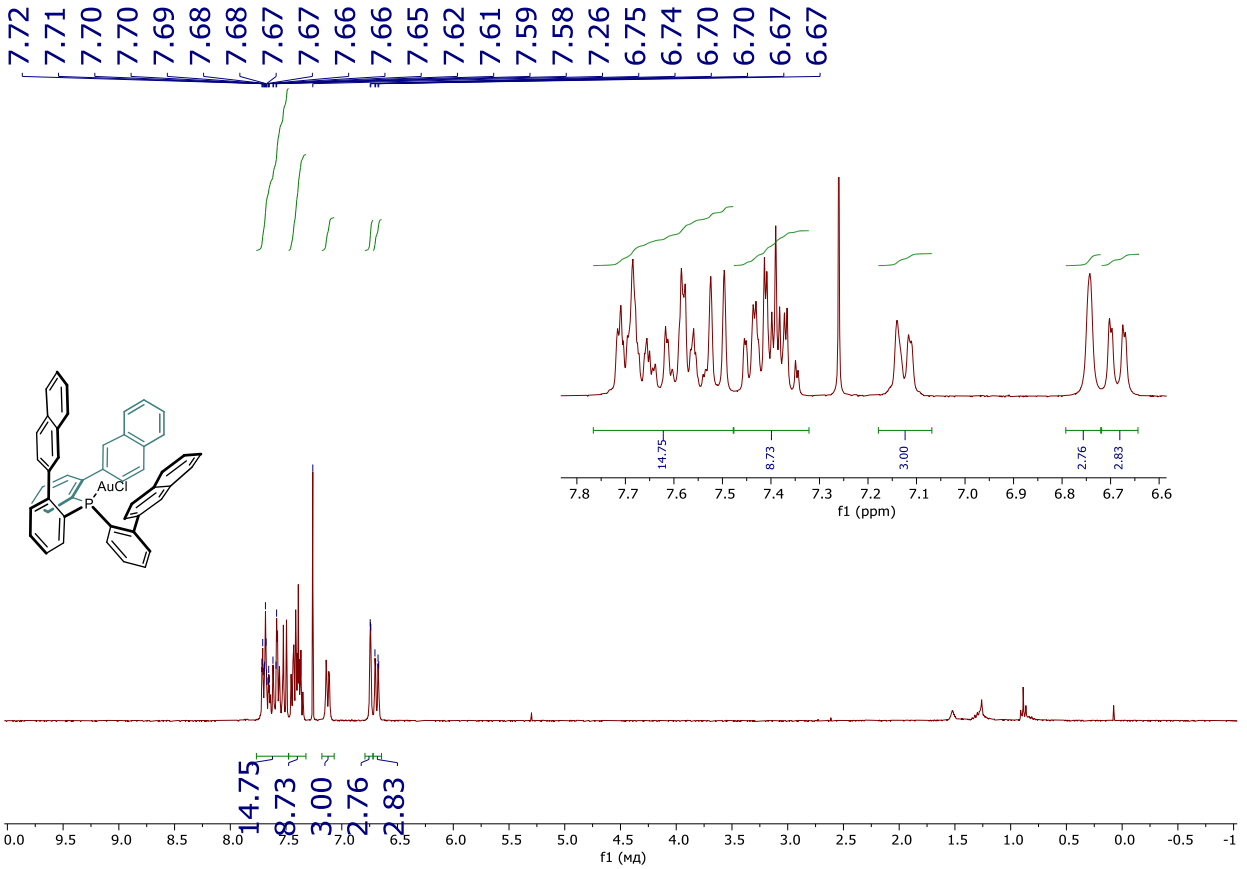

147.99
147.77
137.34
137.24
135.67
135.60
132.77
132.47
132.36
132.04
130.84
130.81
130.79
129.98
128.81
128.56
127.91
127.73
127.52
127.51
127.41
126.75
126.12
126.01

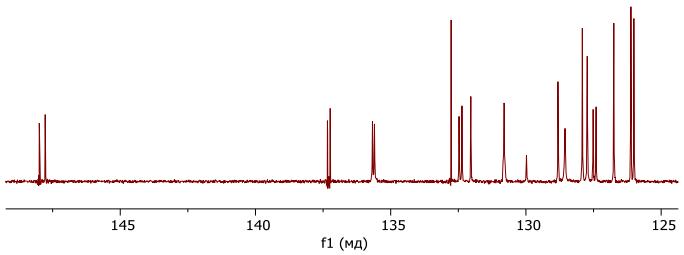

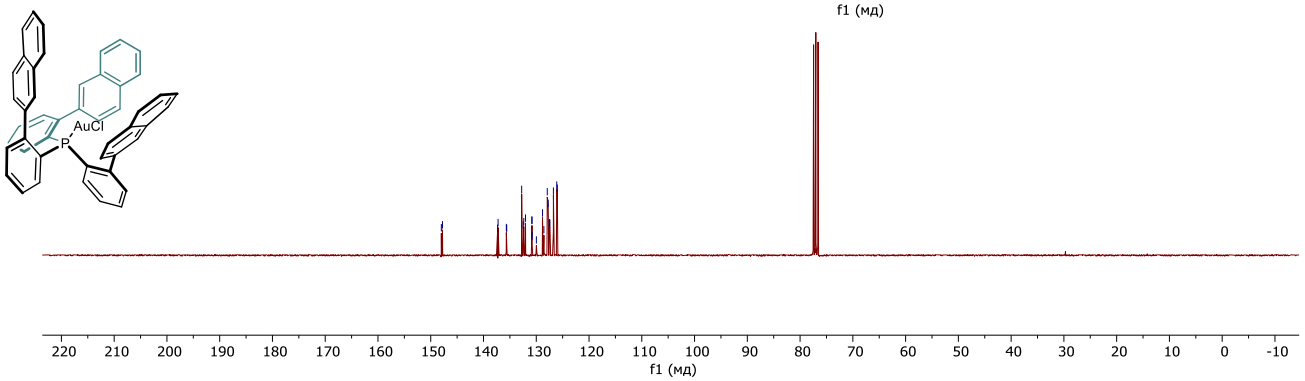

7.72

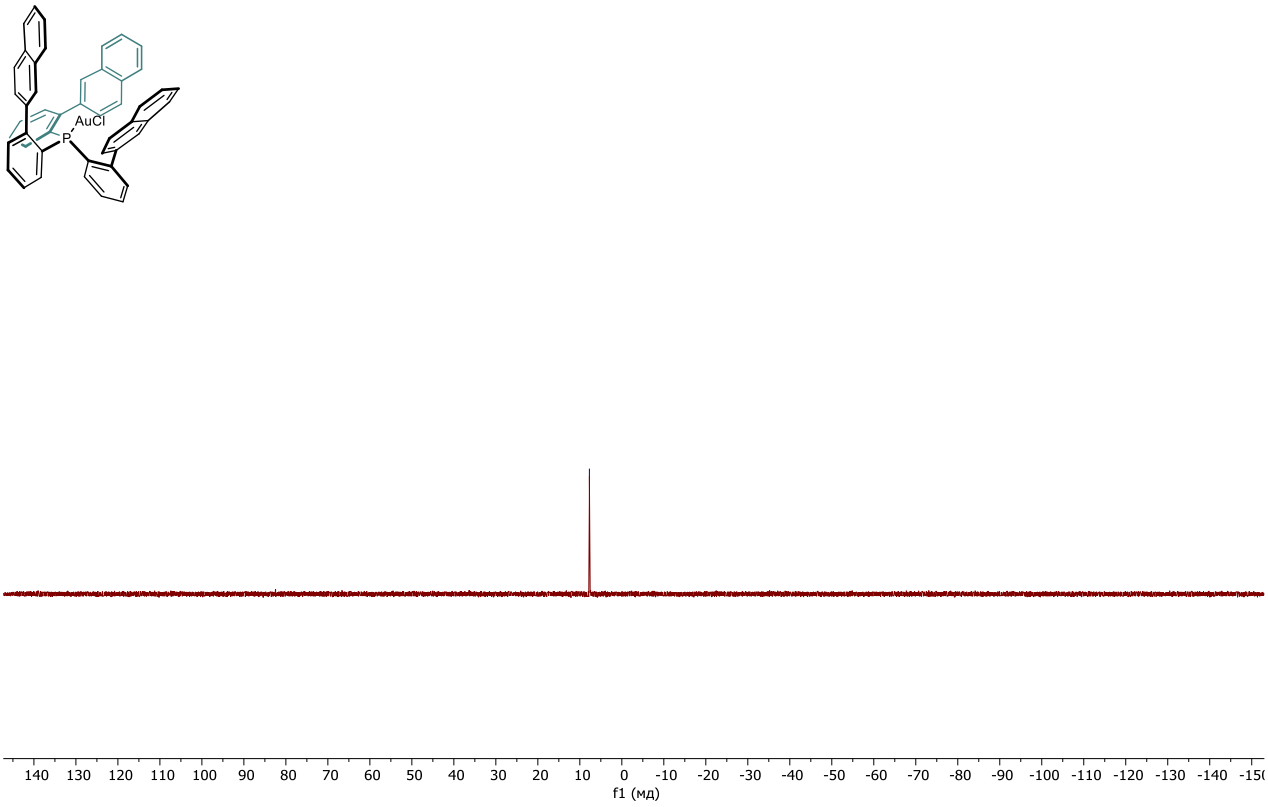

Gold (I) chloride complex 2.3-5$_{CF3}$

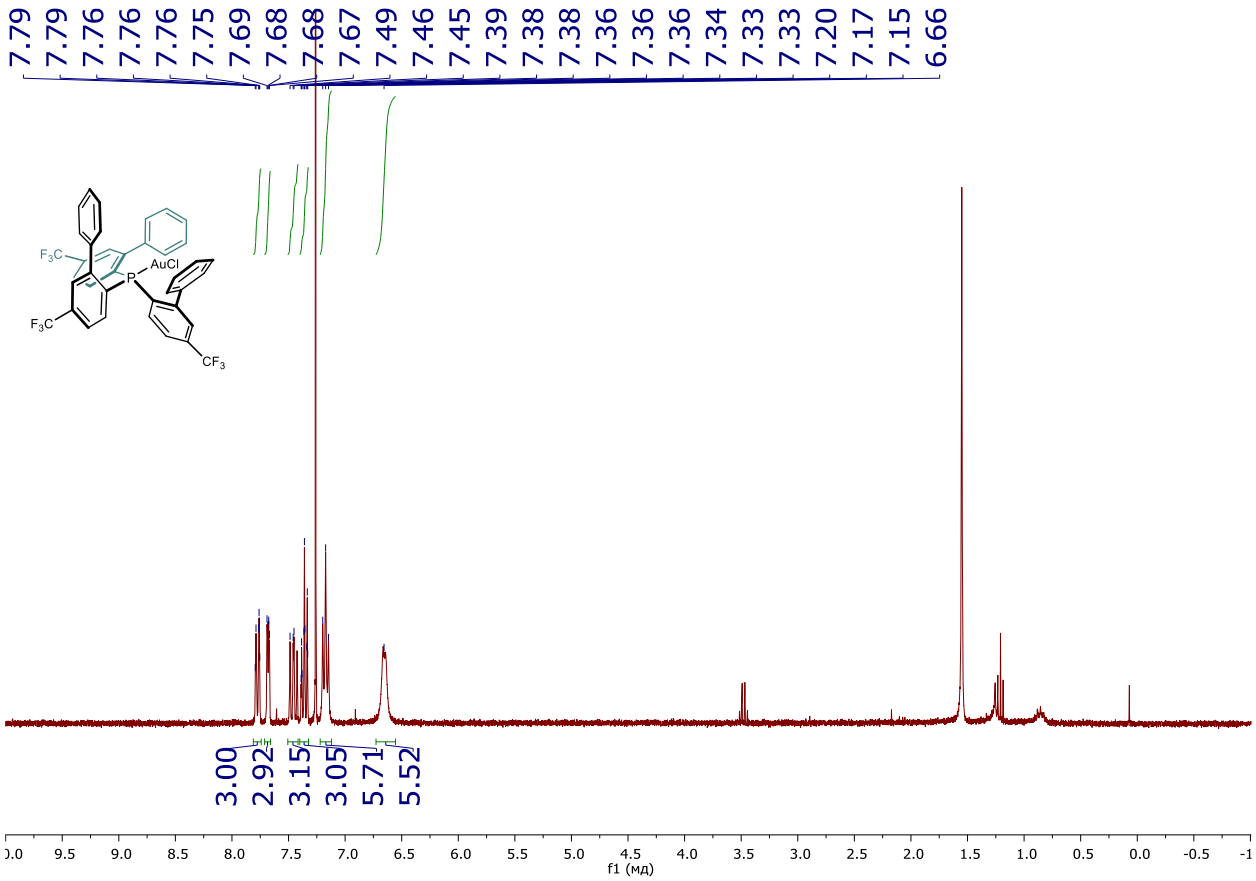

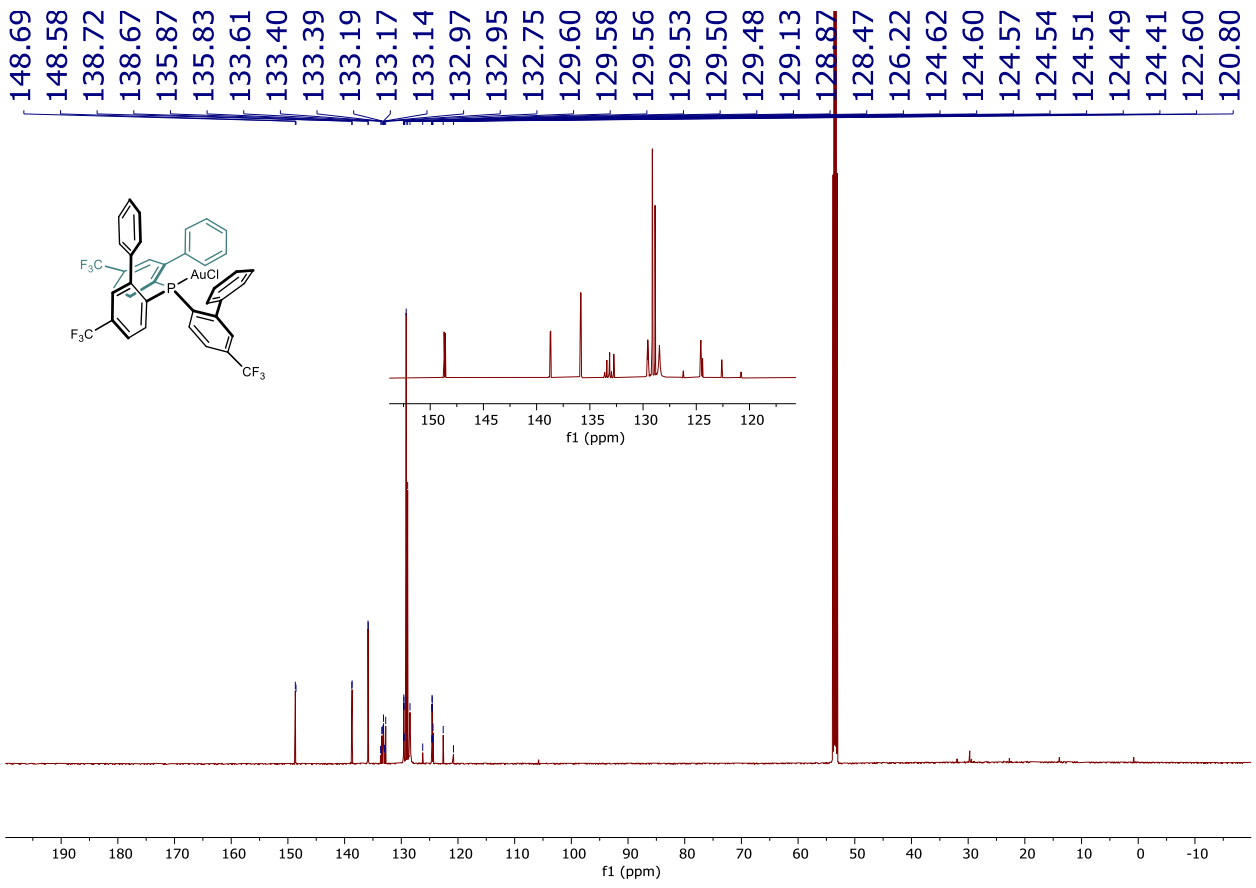

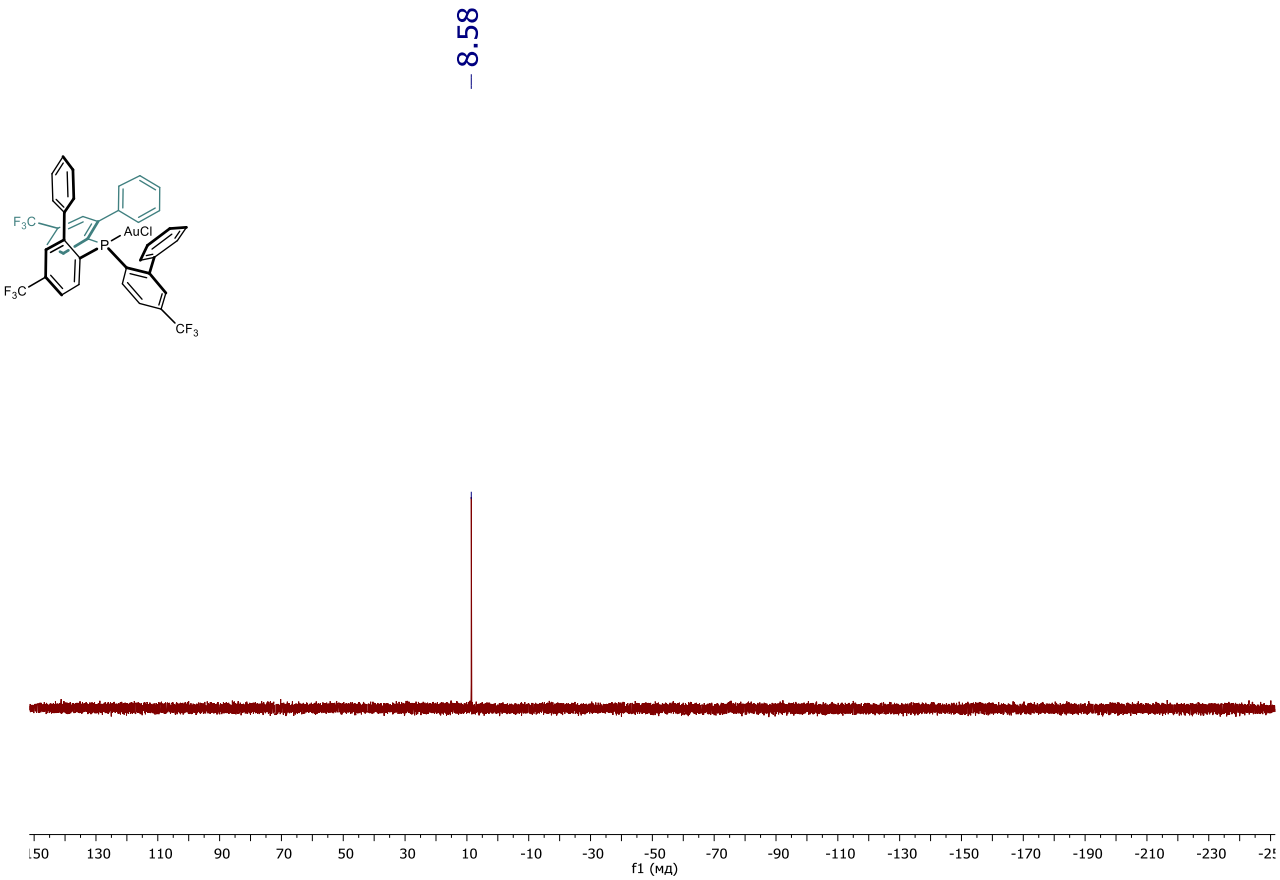
8.58
F3C
AuCl
P
F3C
CF3
f1 (мд)

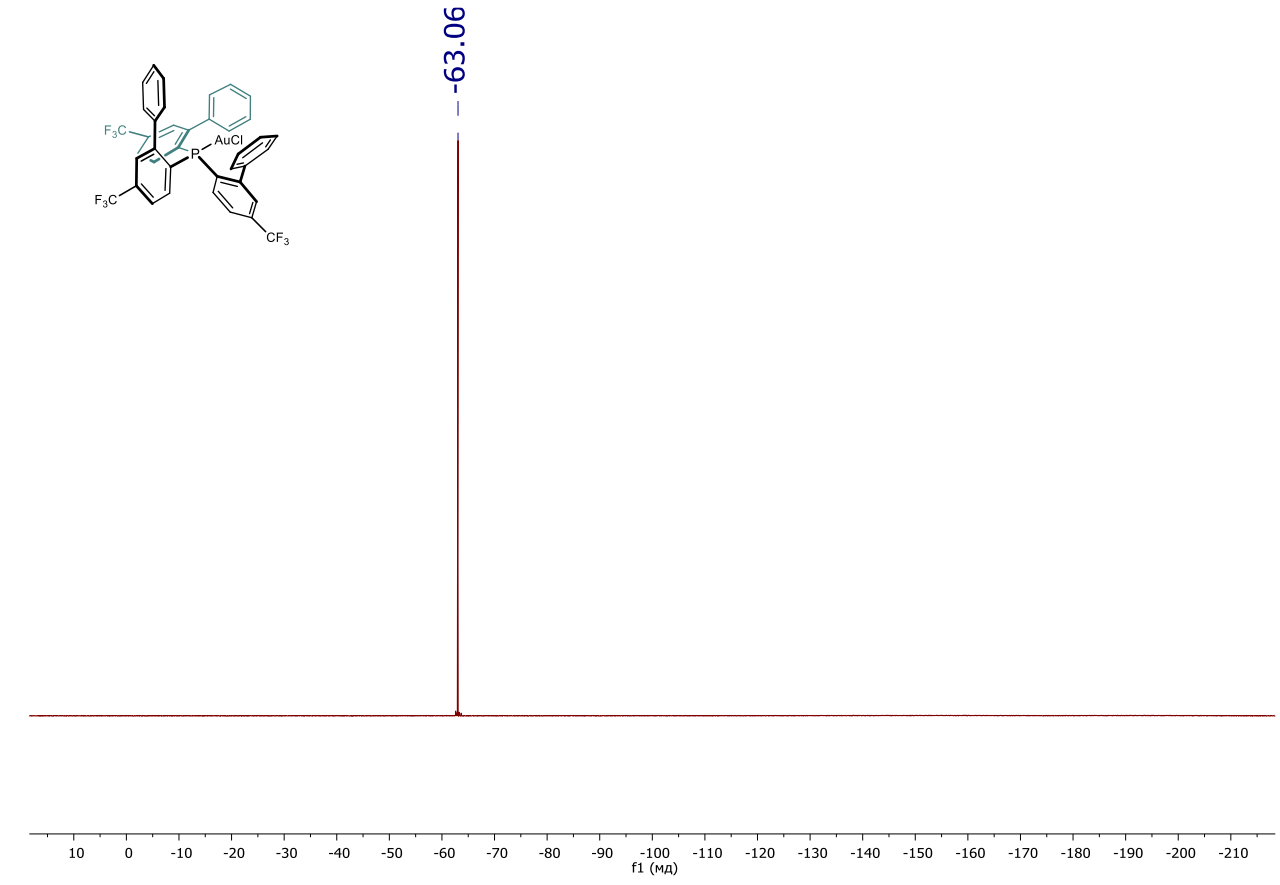
-63.06
F3C
AuCl
P
F3C
CF3
f1 (мд)

Gold (I) complex 2.3-19

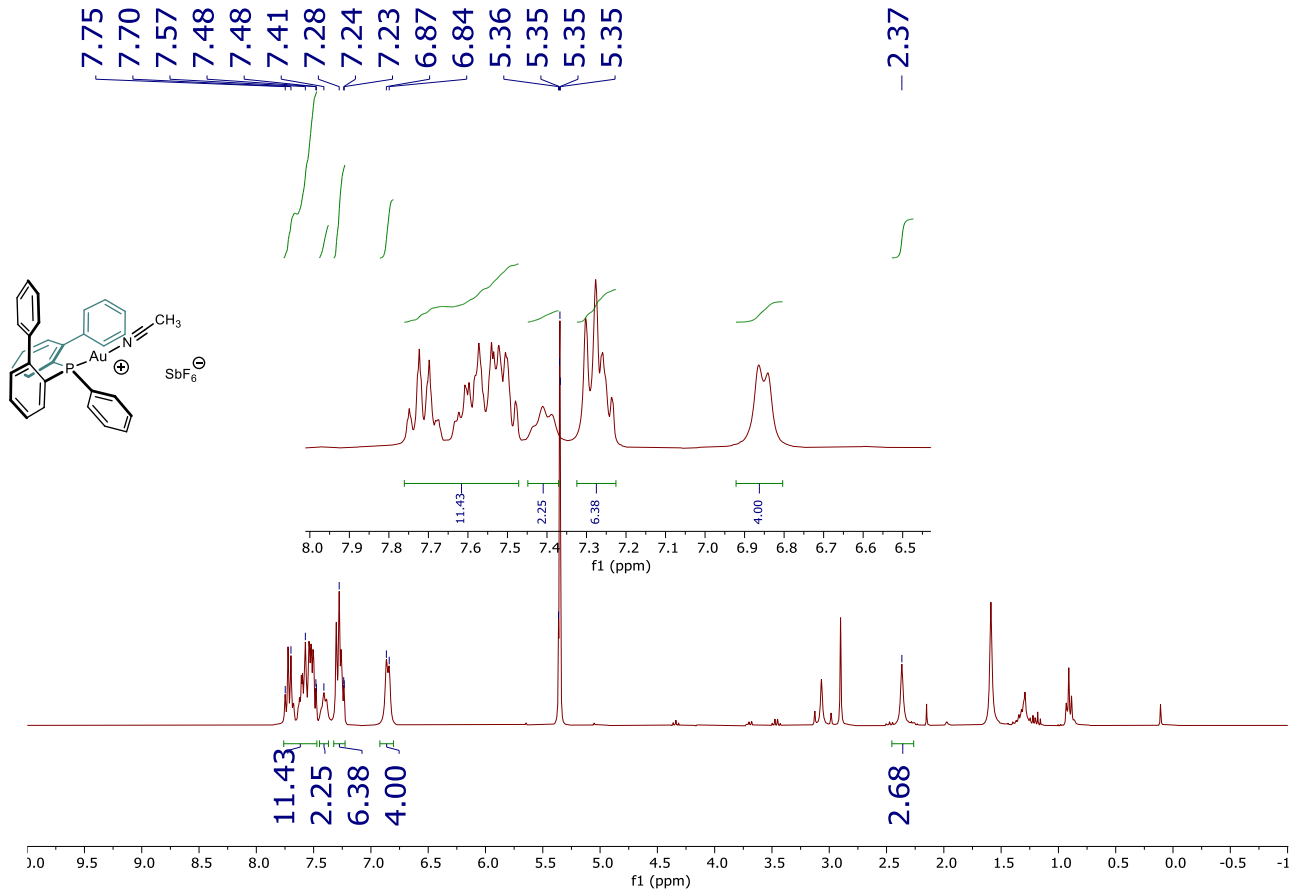

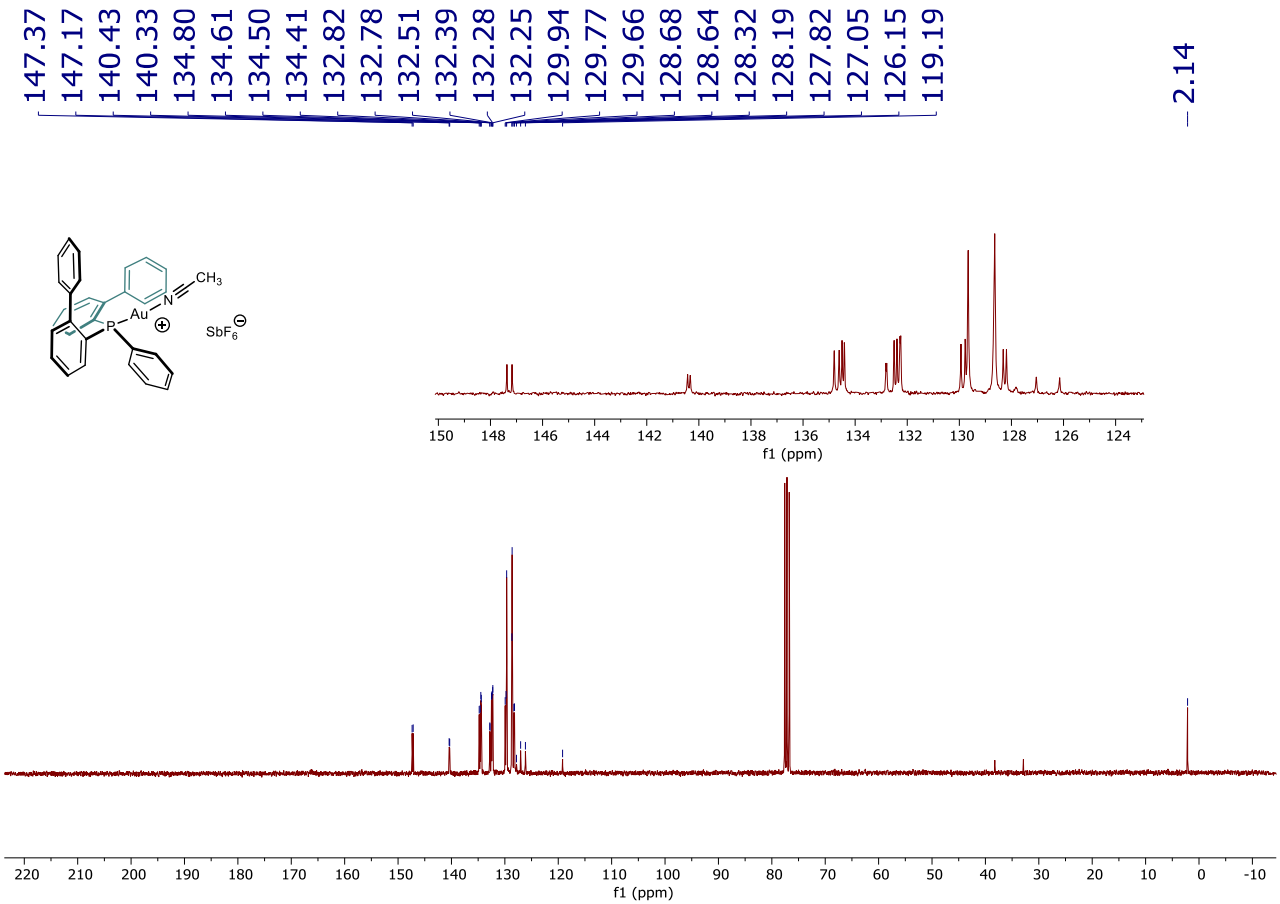

8.21

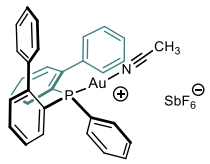

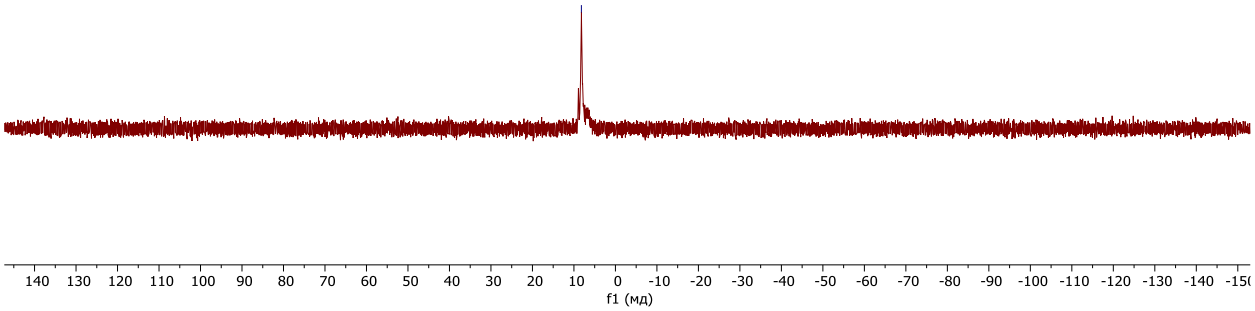

Gold (I) complex 2.3-6_H

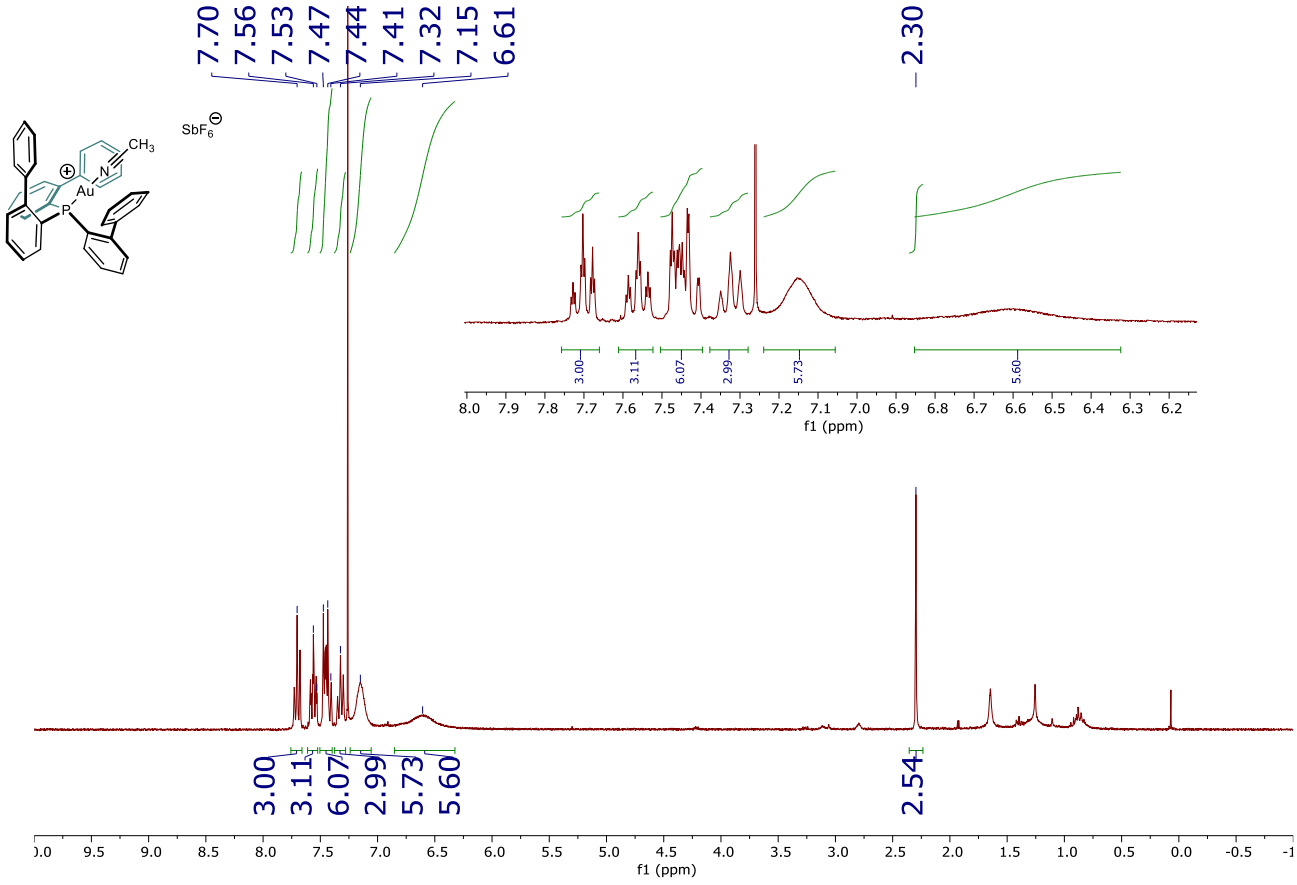
7.70
7.56
7.53
7.47
7.44
7.41
7.32
7.15
6.61
2.30
SbF6
CH3
N
Au
P
3.00
3.11
6.07
2.99
5.73
5.60
2.54
f1 (ppm)

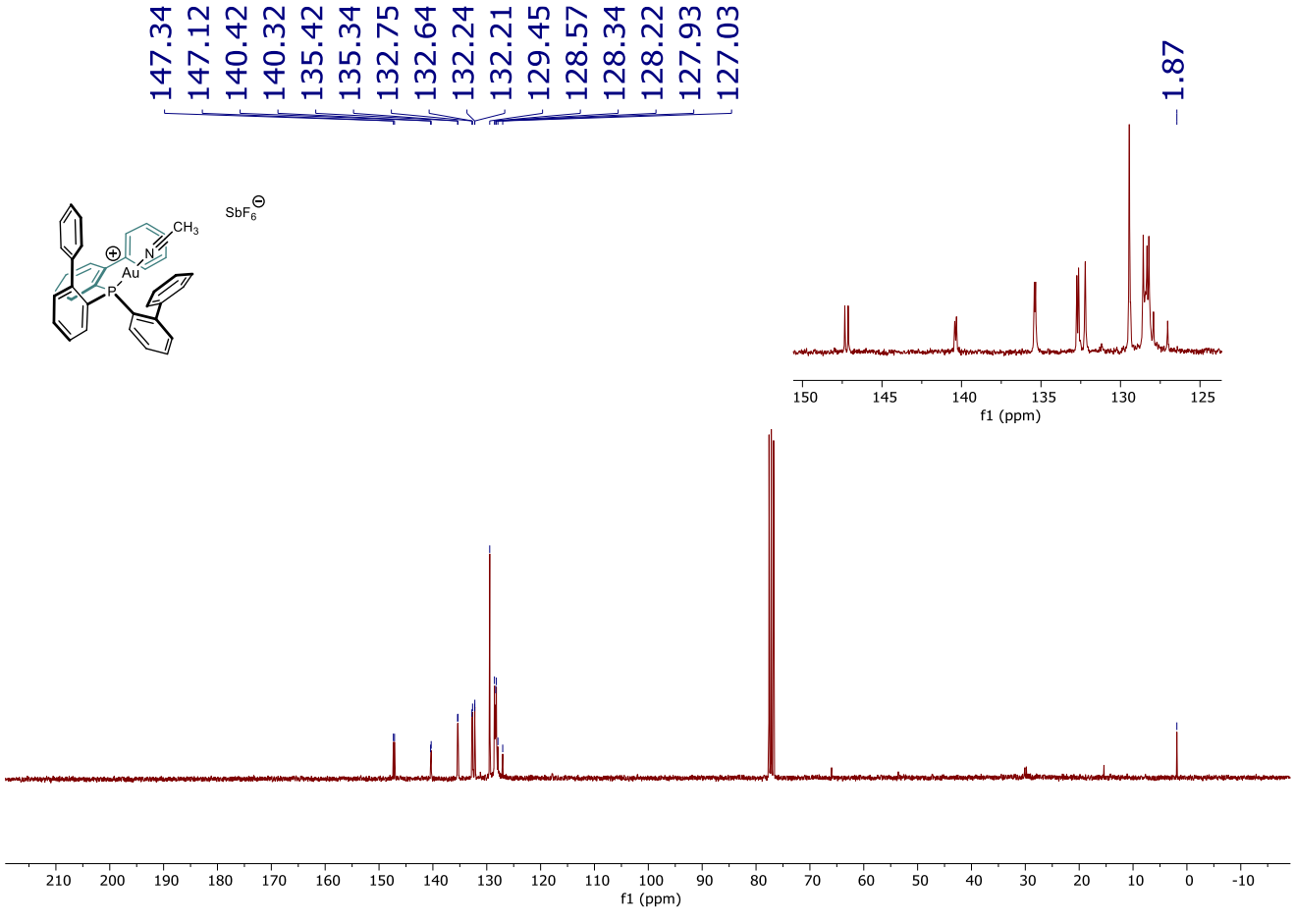
147.34
147.12
140.42
140.32
135.42
135.34
132.75
132.64
132.24
132.21
129.45
128.57
128.34
128.22
127.93
127.03
1.87
SbF6
CH3
N
Au
P
f1 (ppm)

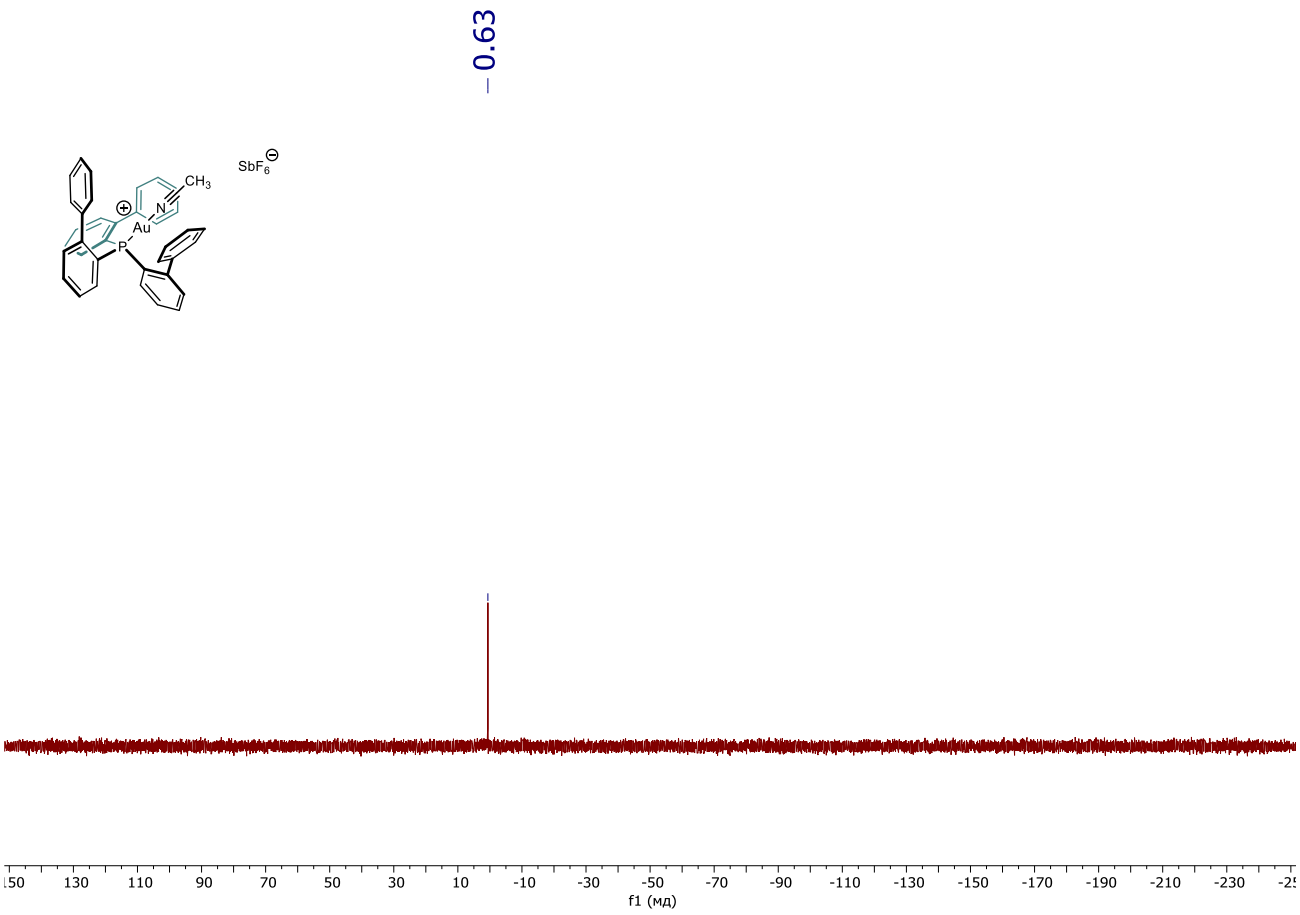

Gold (I) complex 2.3-6$_{mtBu}$

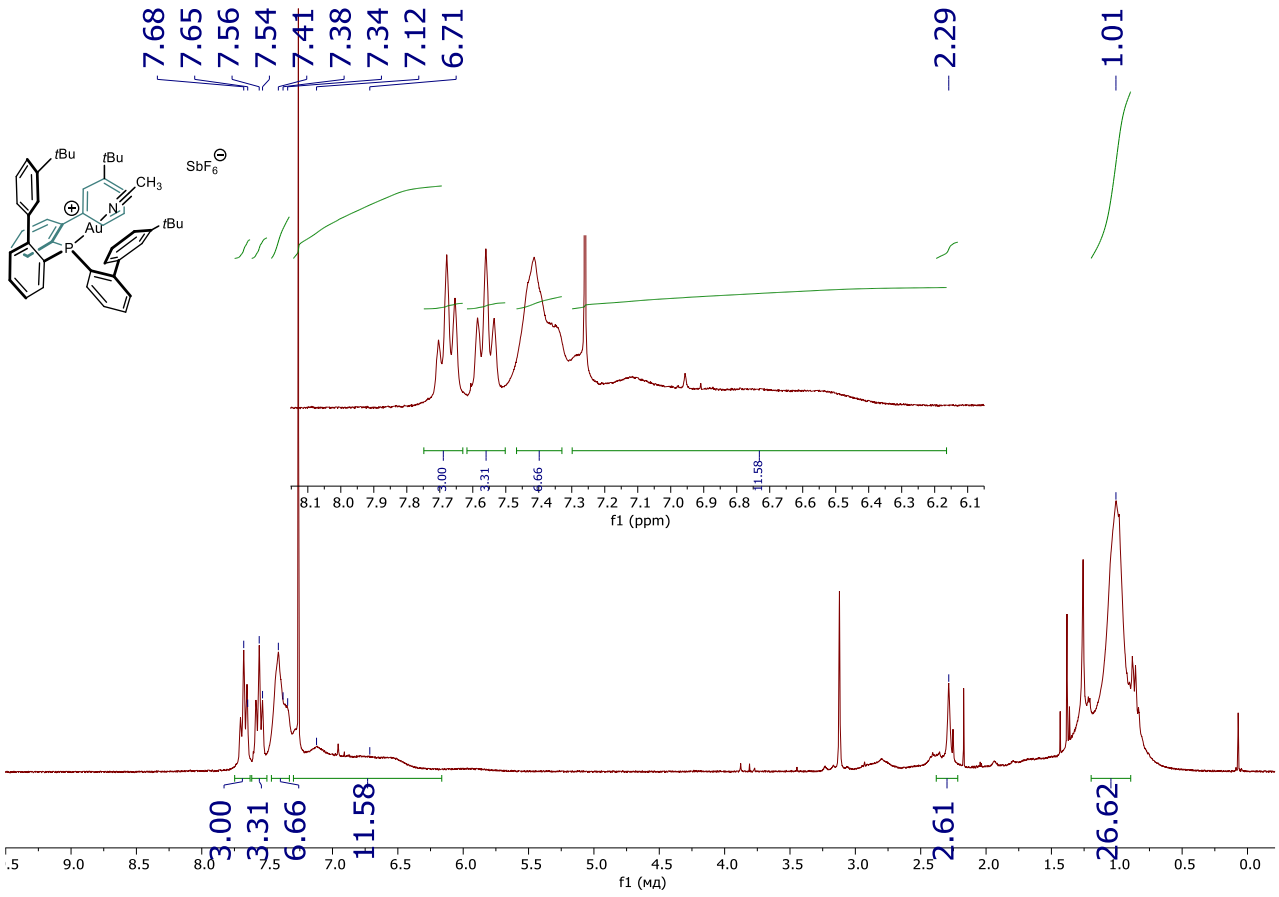
7.68
7.65
7.56
7.54
7.41
7.38
7.34
7.12
6.71
2.29
1.01
tBu
tBu
CH3
N
Au
P
tBu
SbF6
3.00
3.31
6.66
11.58
2.61
26.62
f1 (мд)
f1 (ppm)

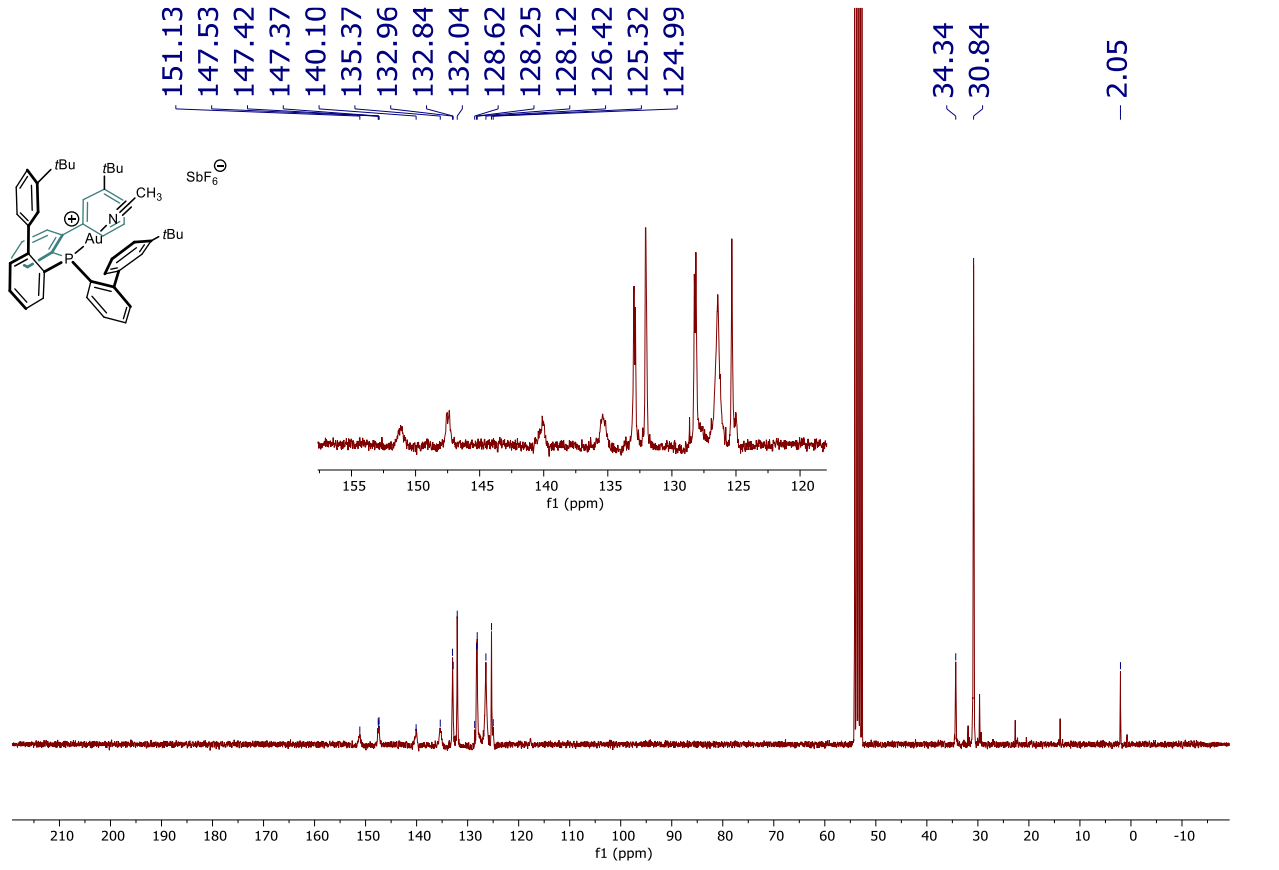
151.13
147.53
147.42
147.37
140.10
135.37
132.96
132.84
132.04
128.62
128.25
128.12
126.42
125.32
124.99
34.34
30.84
2.05
tBu
tBu
CH3
N
Au
P
tBu
SbF6
f1 (ppm)
f1 (ppm)

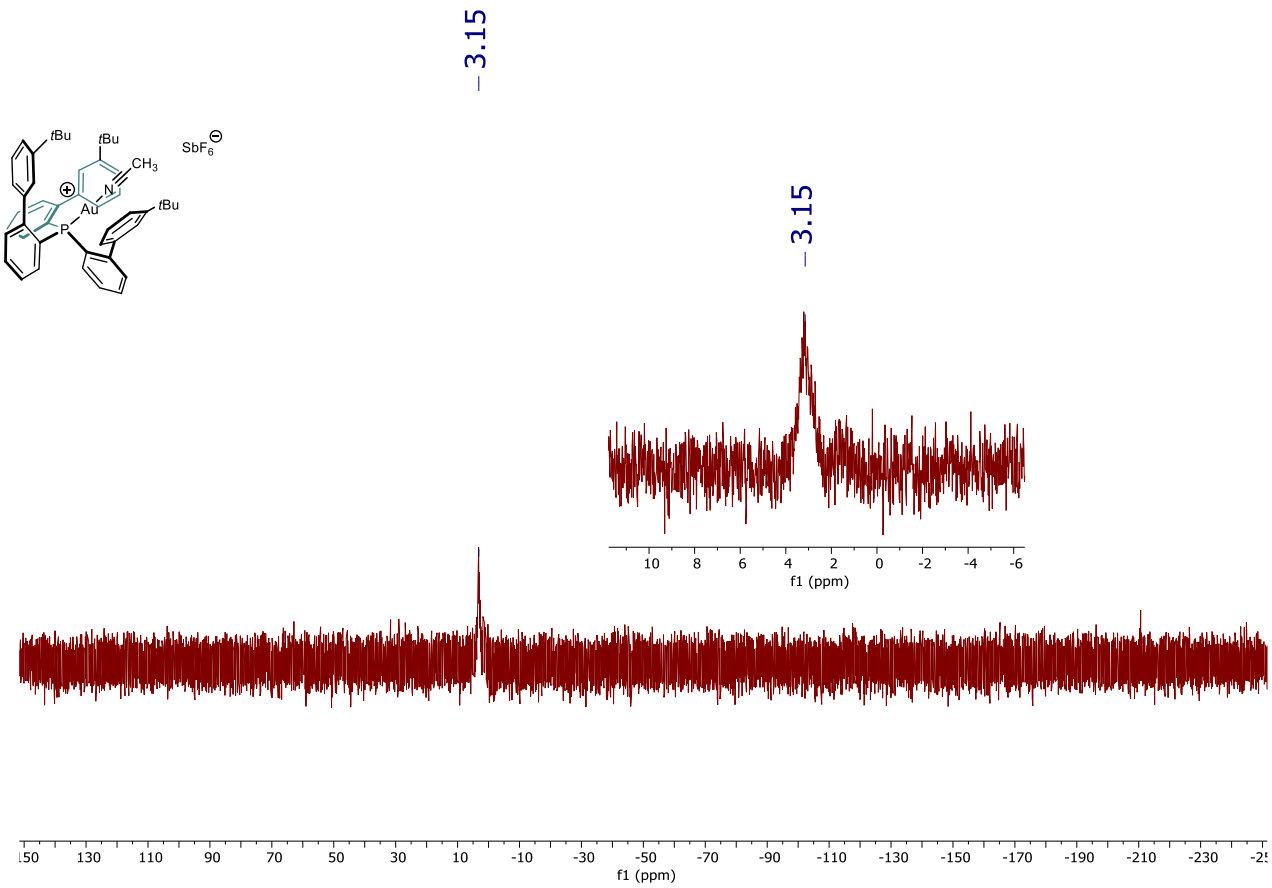

Gold (I) complex 2.3-6$_{mnBu}$

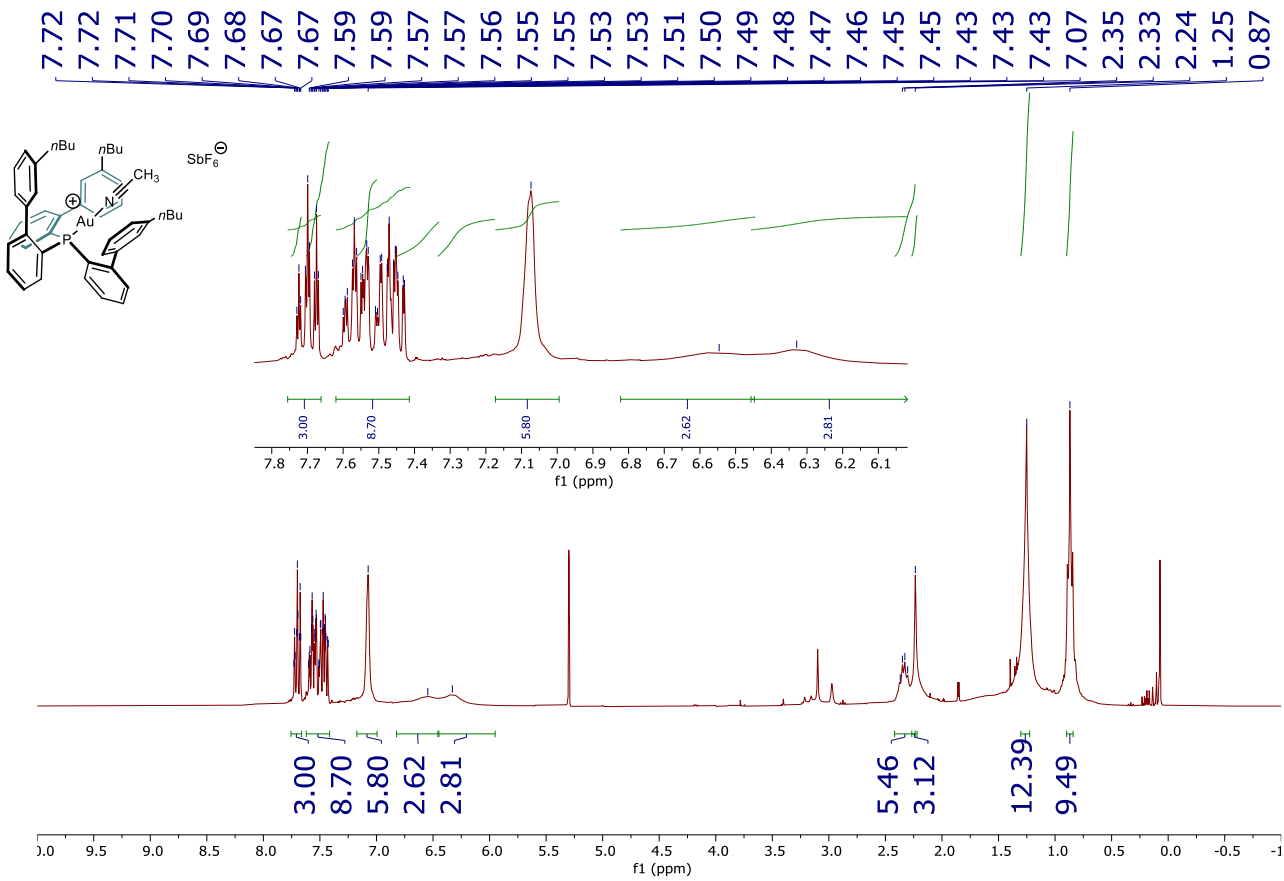
7.72 7.72 7.71 7.70 7.69 7.68 7.67 7.67 7.59 7.59 7.57 7.57 7.56 7.55 7.55 7.53 7.53 7.51 7.50 7.49 7.48 7.47 7.46 7.45 7.45 7.43 7.43 7.43 7.07 2.35 2.33 2.24 1.25 0.87
nBu
nBu
CH3
N
Au
P
nBu
SbF6
3.00 8.70 5.80 2.62 2.81
f1 (ppm)
3.00 8.70 5.80 2.62 2.81 5.46 3.12 12.39 9.49
f1 (ppm)

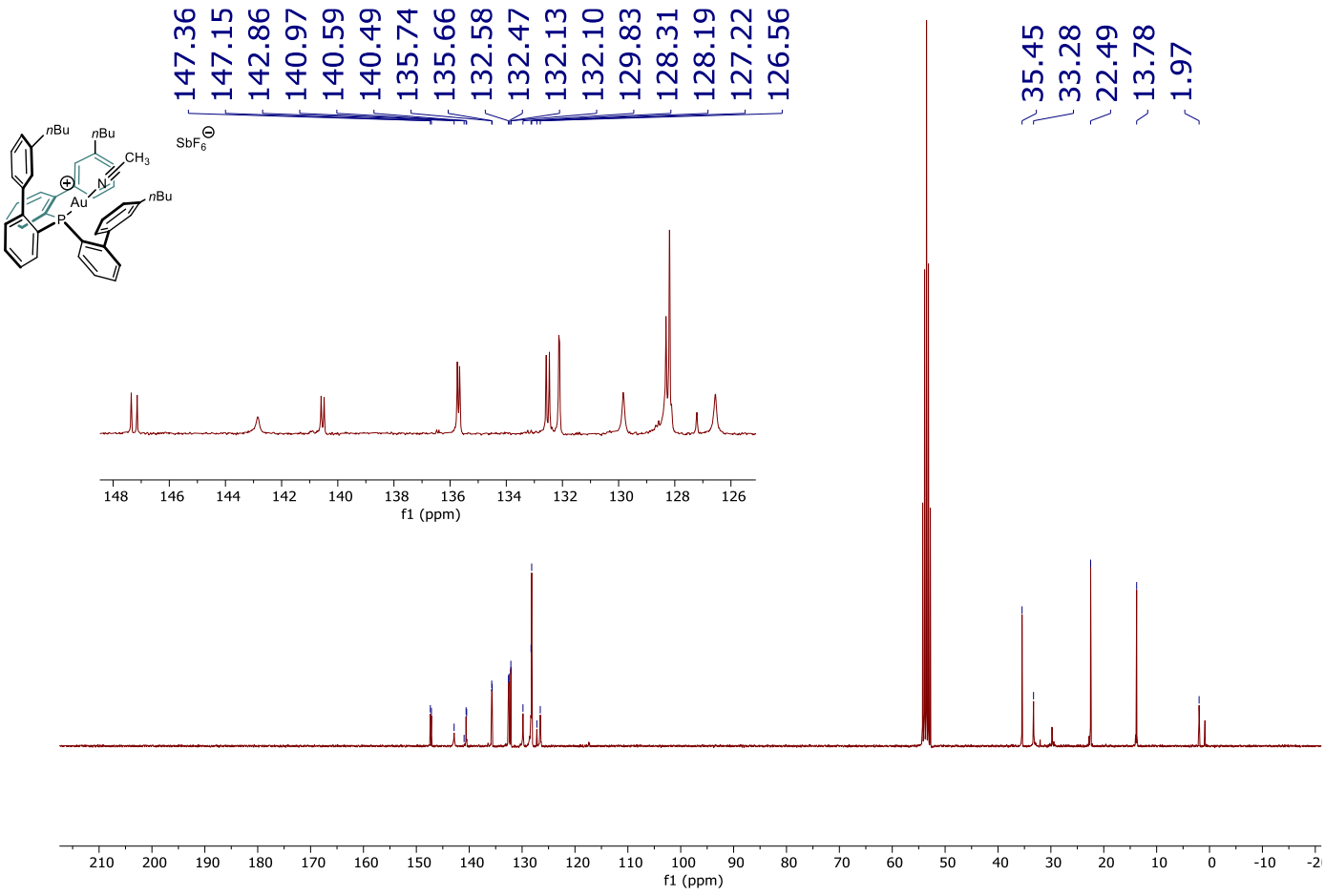
147.36 147.15 142.86 140.97 140.59 140.49 135.74 135.66 132.58 132.47 132.13 132.10 129.83 128.31 128.19 127.22 126.56
35.45 33.28 22.49 13.78 1.97
nBu
nBu
CH3
N
Au
P
nBu
SbF6
f1 (ppm)
f1 (ppm)

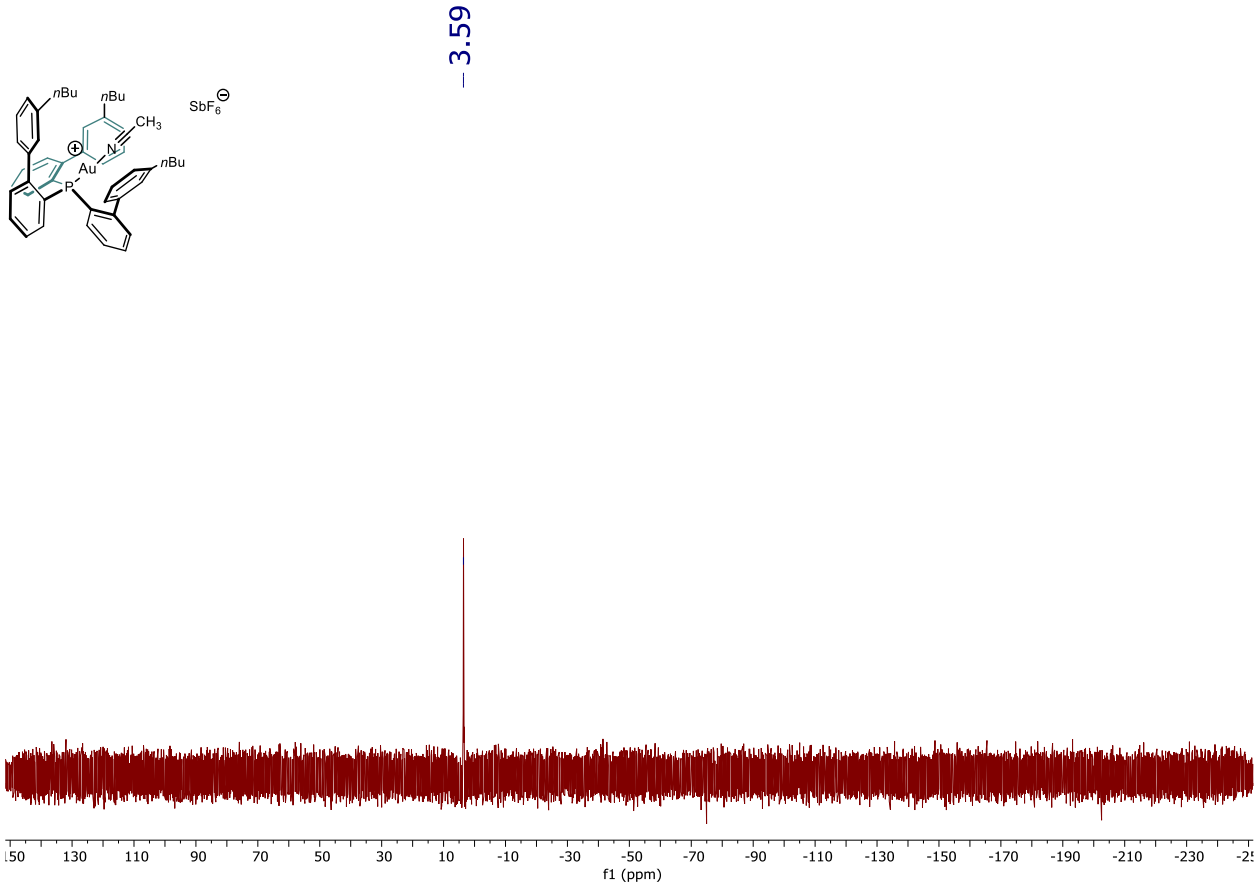

Gold (I) complex 2.3-6$_{ptBu}$

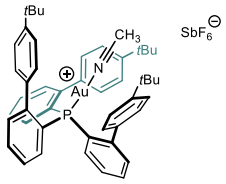

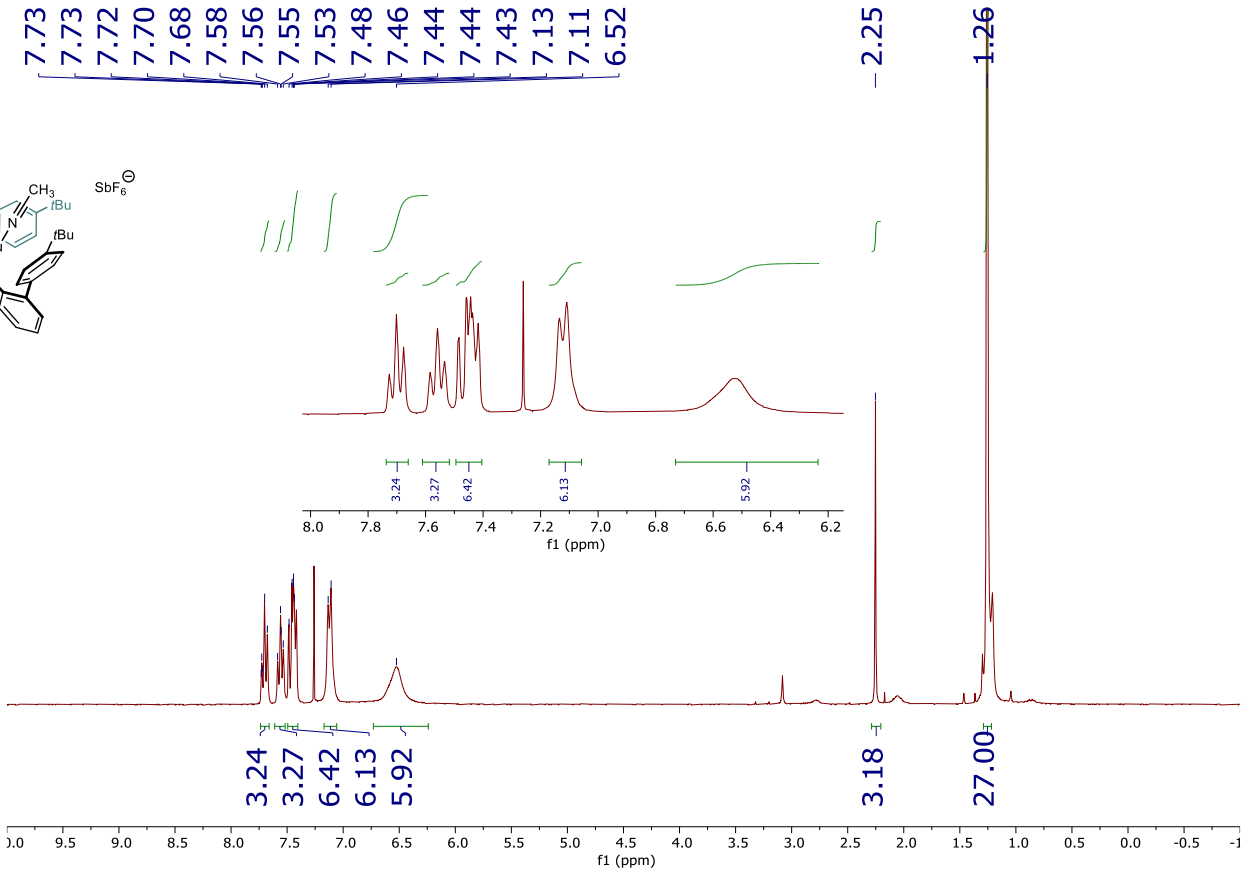

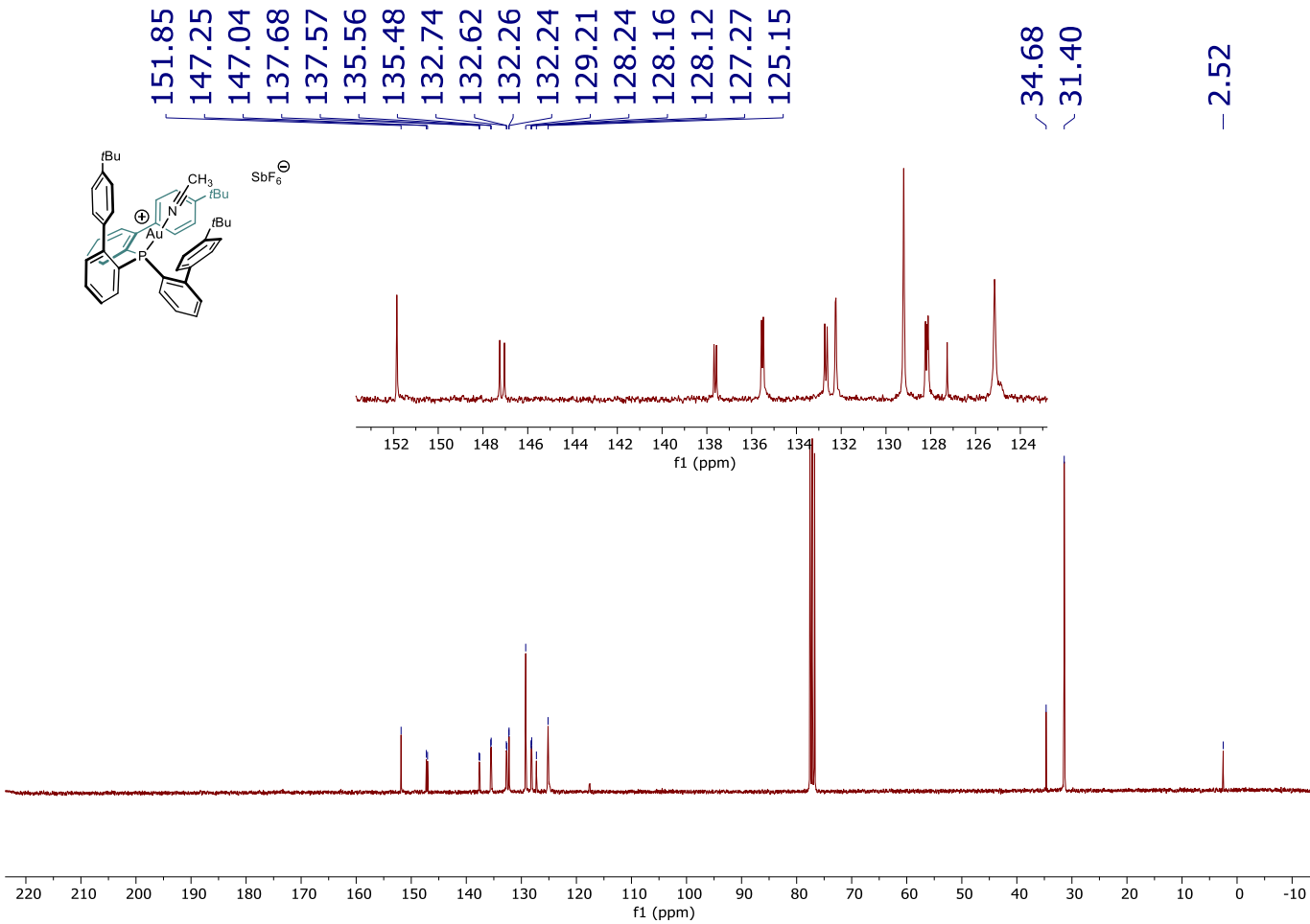
151.85
147.25
147.04
137.68
137.57
135.56
135.48
132.74
132.62
132.26
132.24
129.21
128.24
128.16
128.12
127.27
125.15
34.68
31.40
2.52
tBu
CH3
tBu
N
Au
tBu
P
SbF6
f1 (ppm)

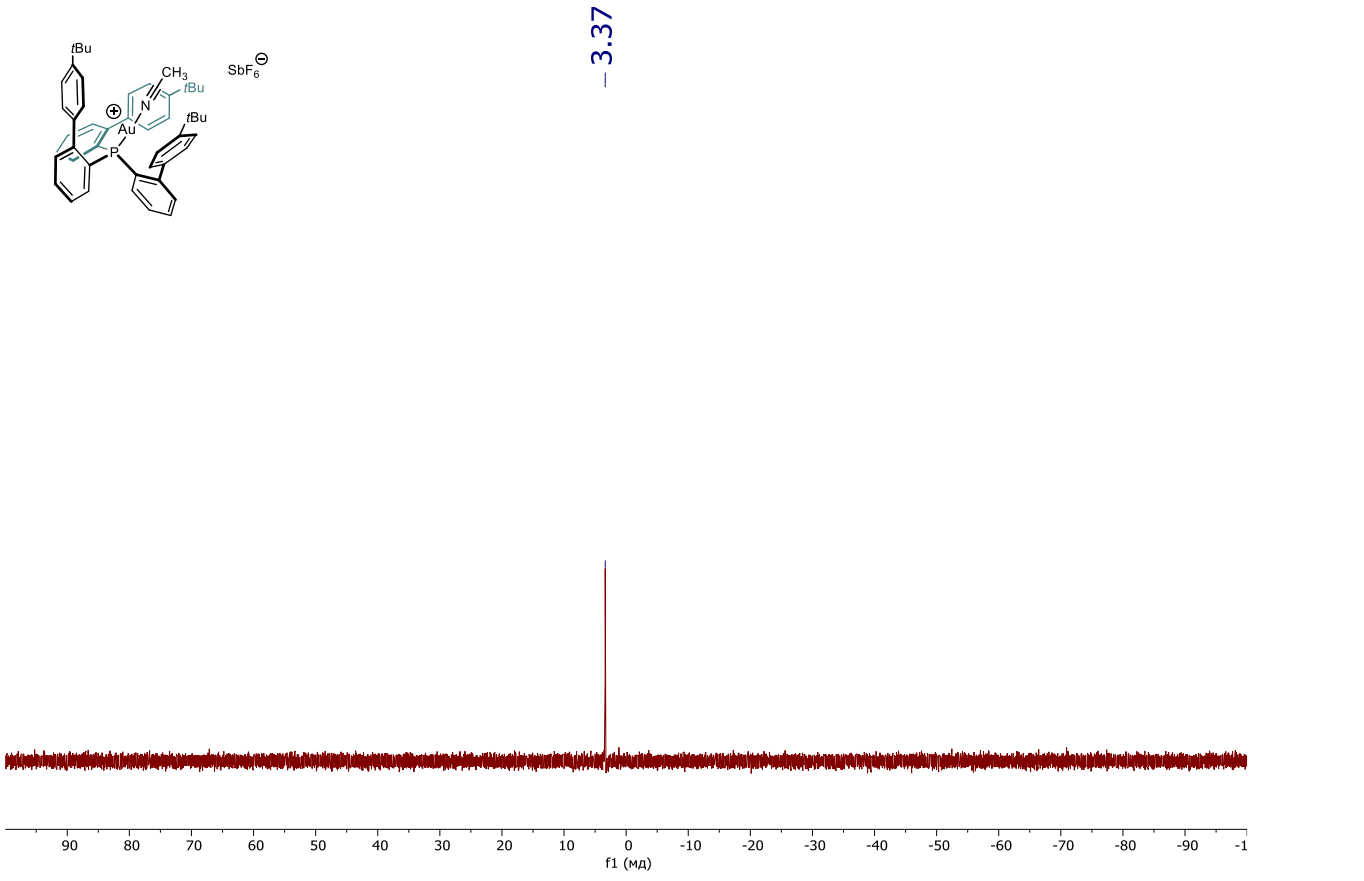
3.37
tBu
CH3
tBu
N
Au
tBu
P
SbF6
f1 (мд)

Gold (I) complex 2.3-6$_{pnPe}$

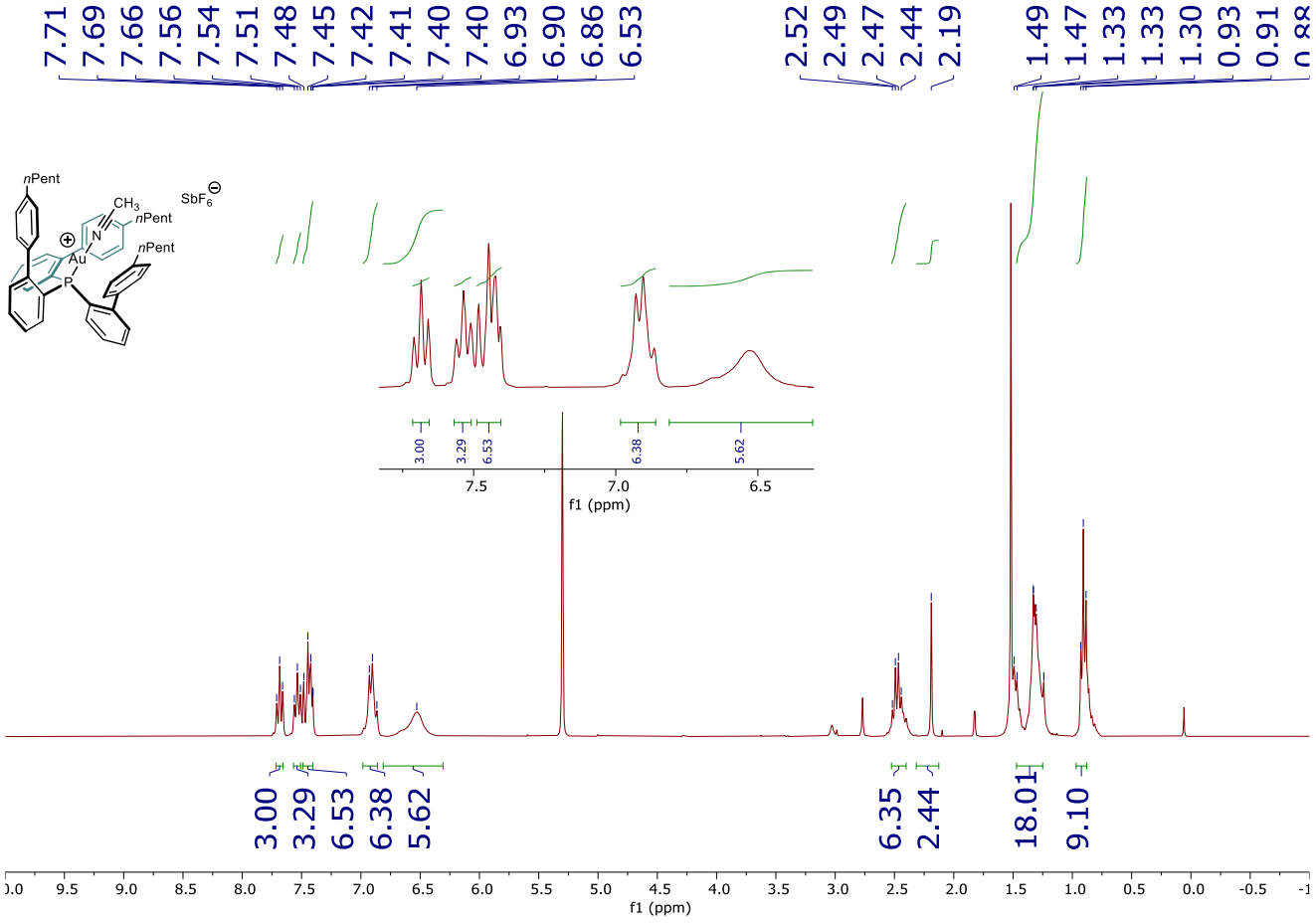

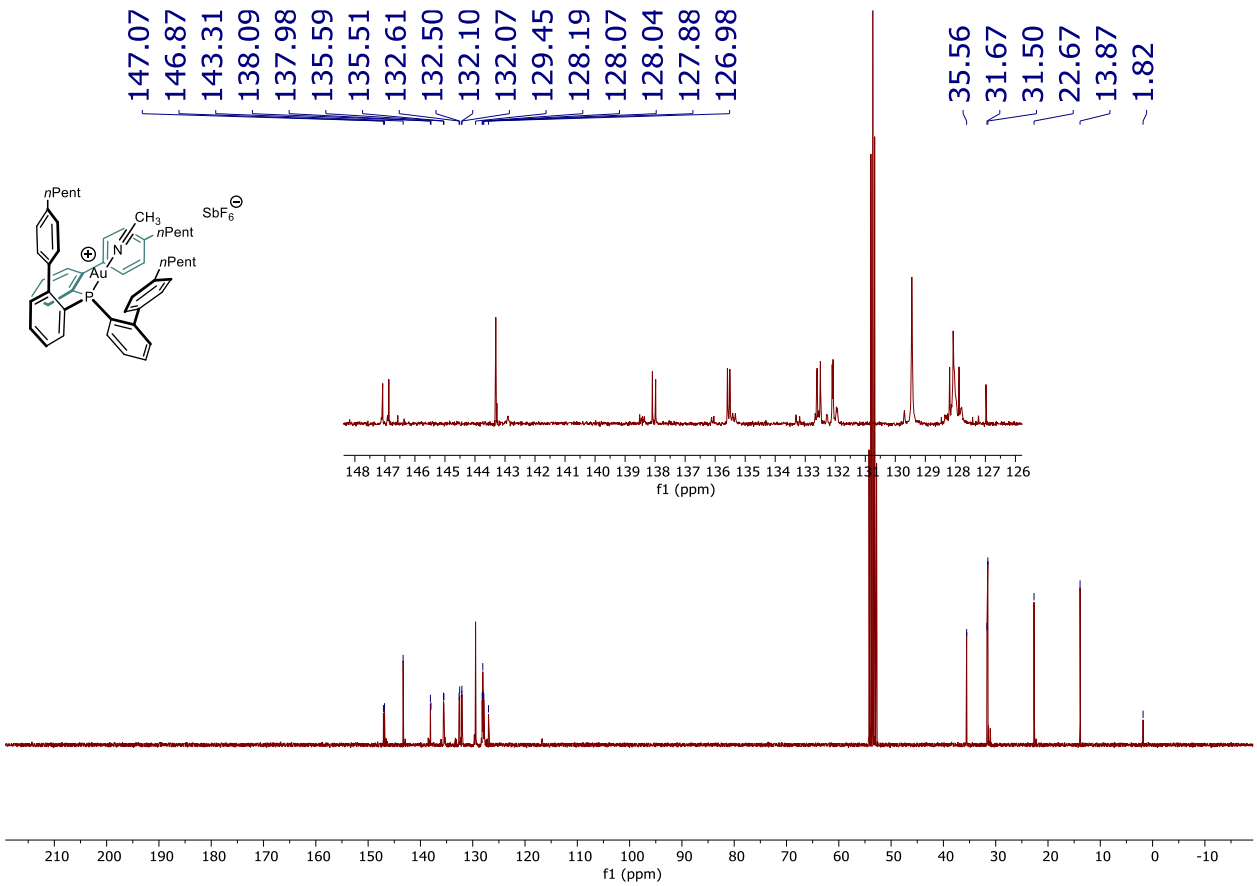

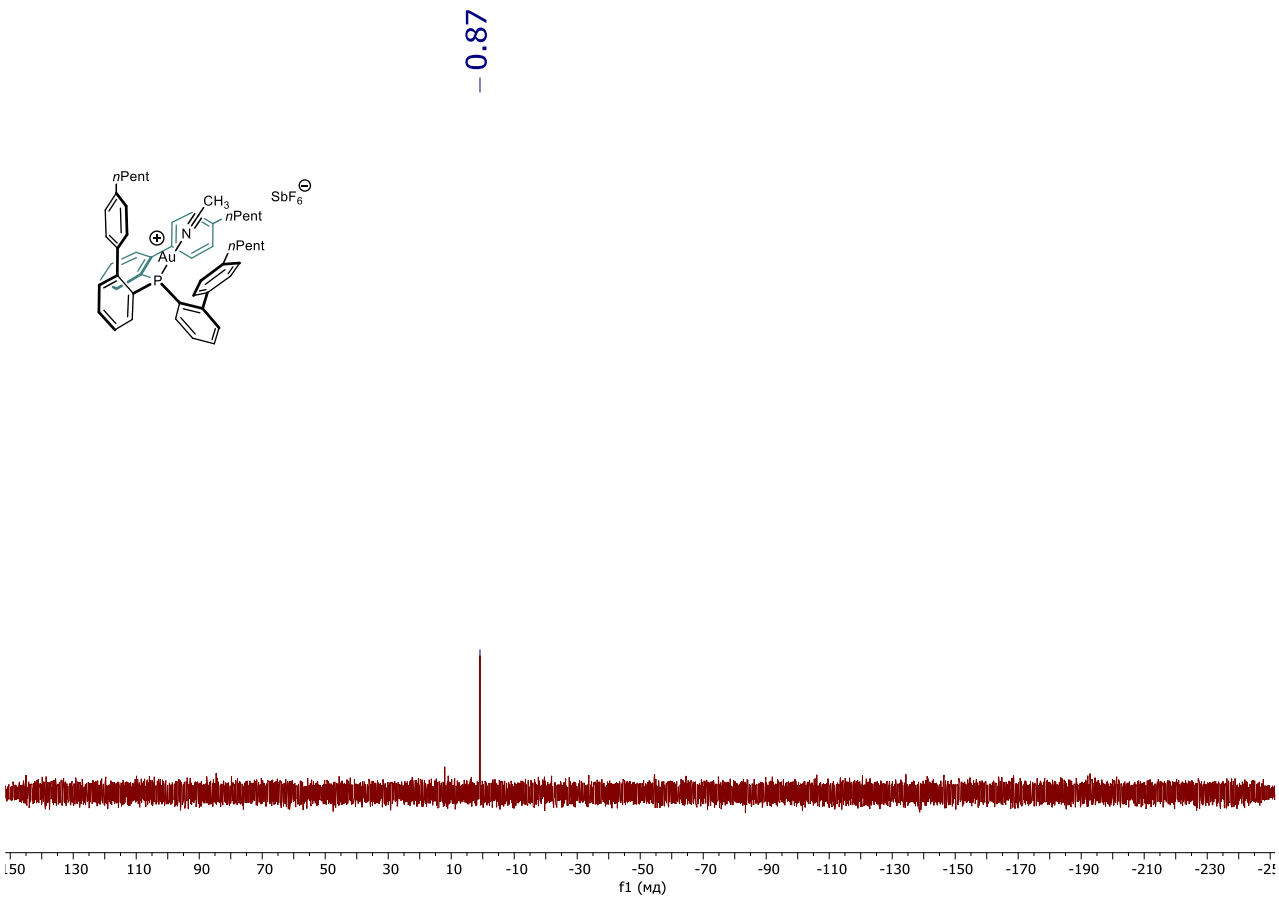

Gold (I) complex 2.3-6_{2Nap}

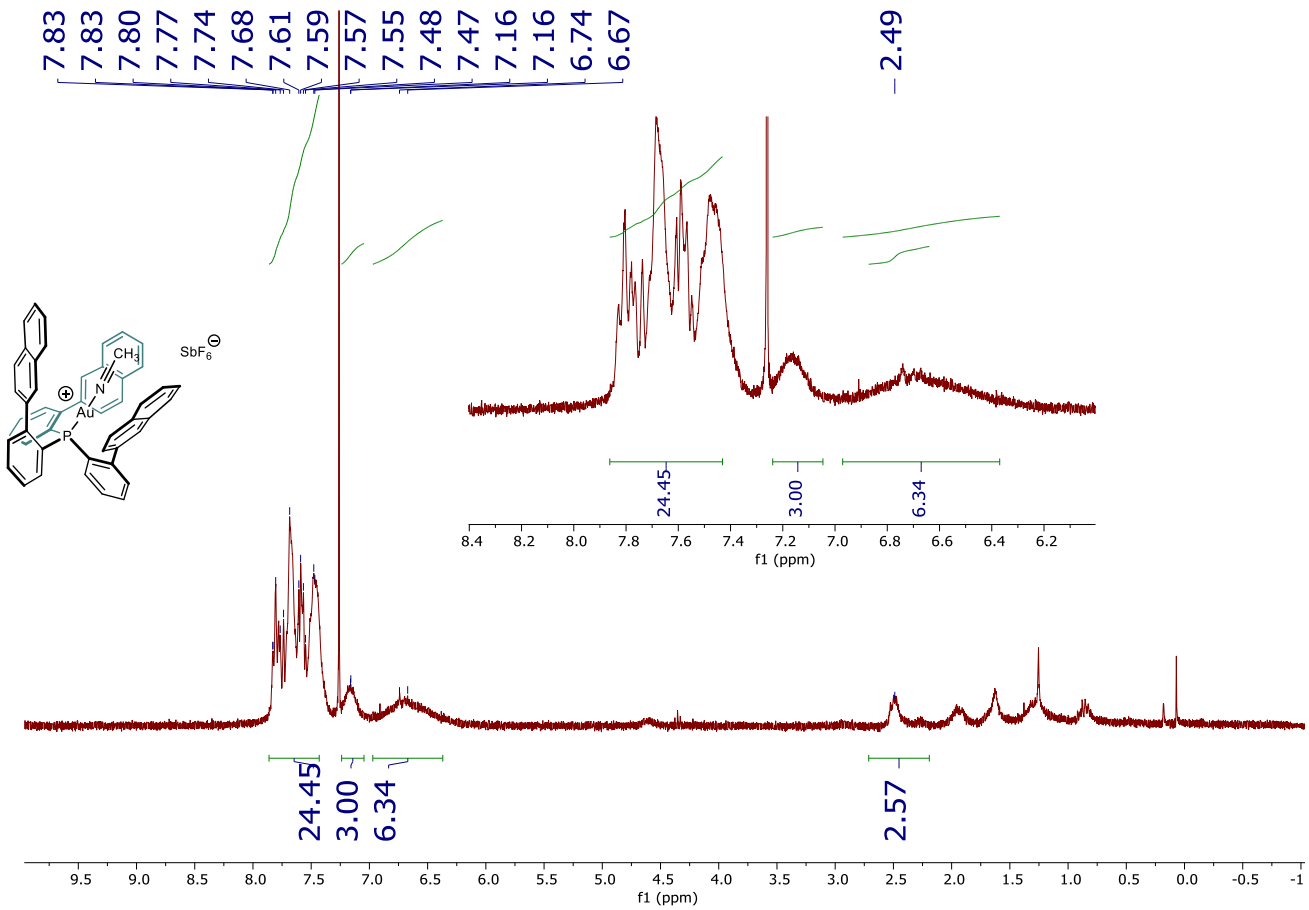
7.83
7.83
7.80
7.77
7.74
7.68
7.61
7.59
7.57
7.55
7.48
7.47
7.16
7.16
6.74
6.67
2.49
24.45
3.00
6.34
2.57
f1 (ppm)

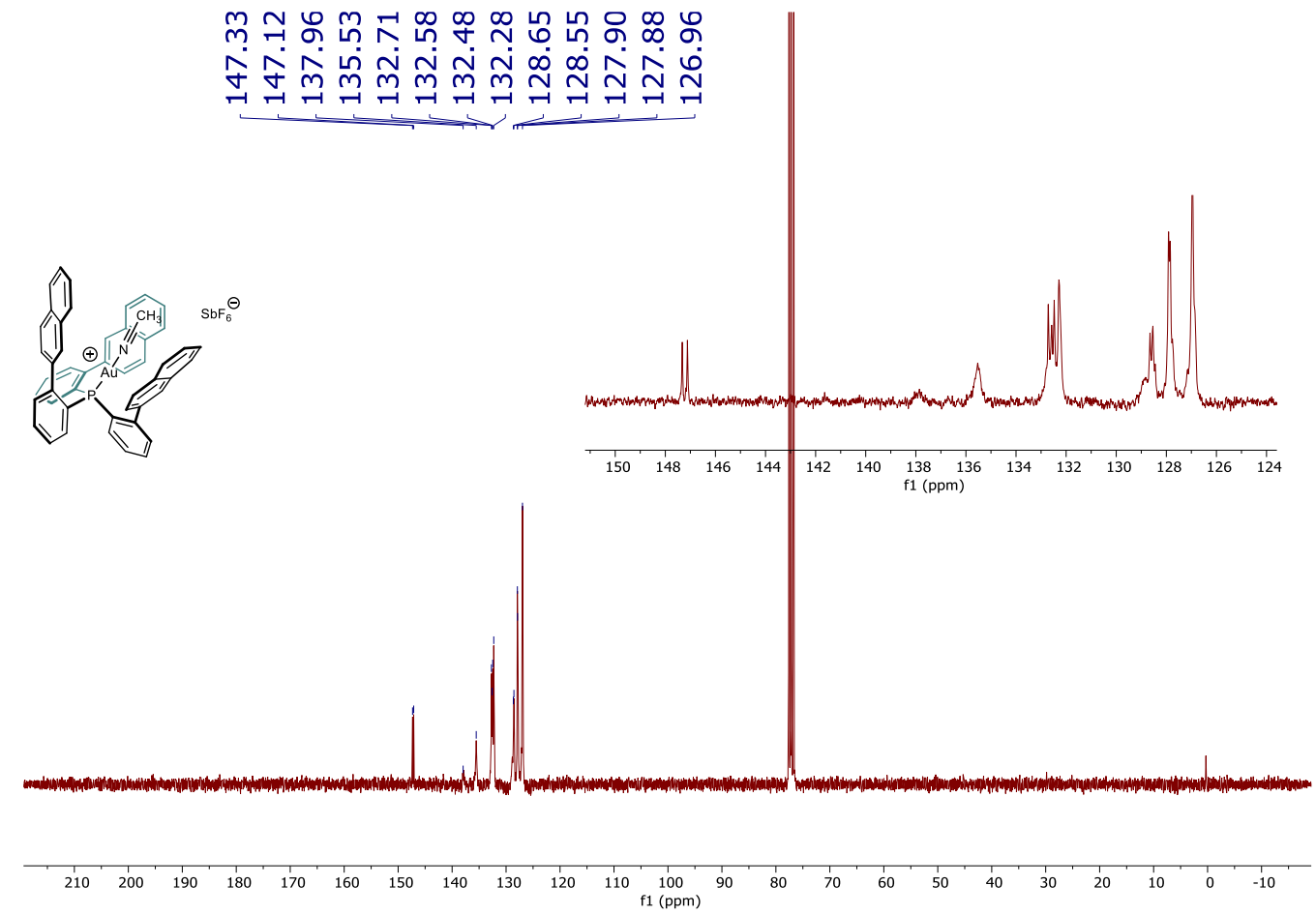
147.33
147.12
137.96
135.53
132.71
132.58
132.48
132.28
128.65
128.55
127.90
127.88
126.96
f1 (ppm)

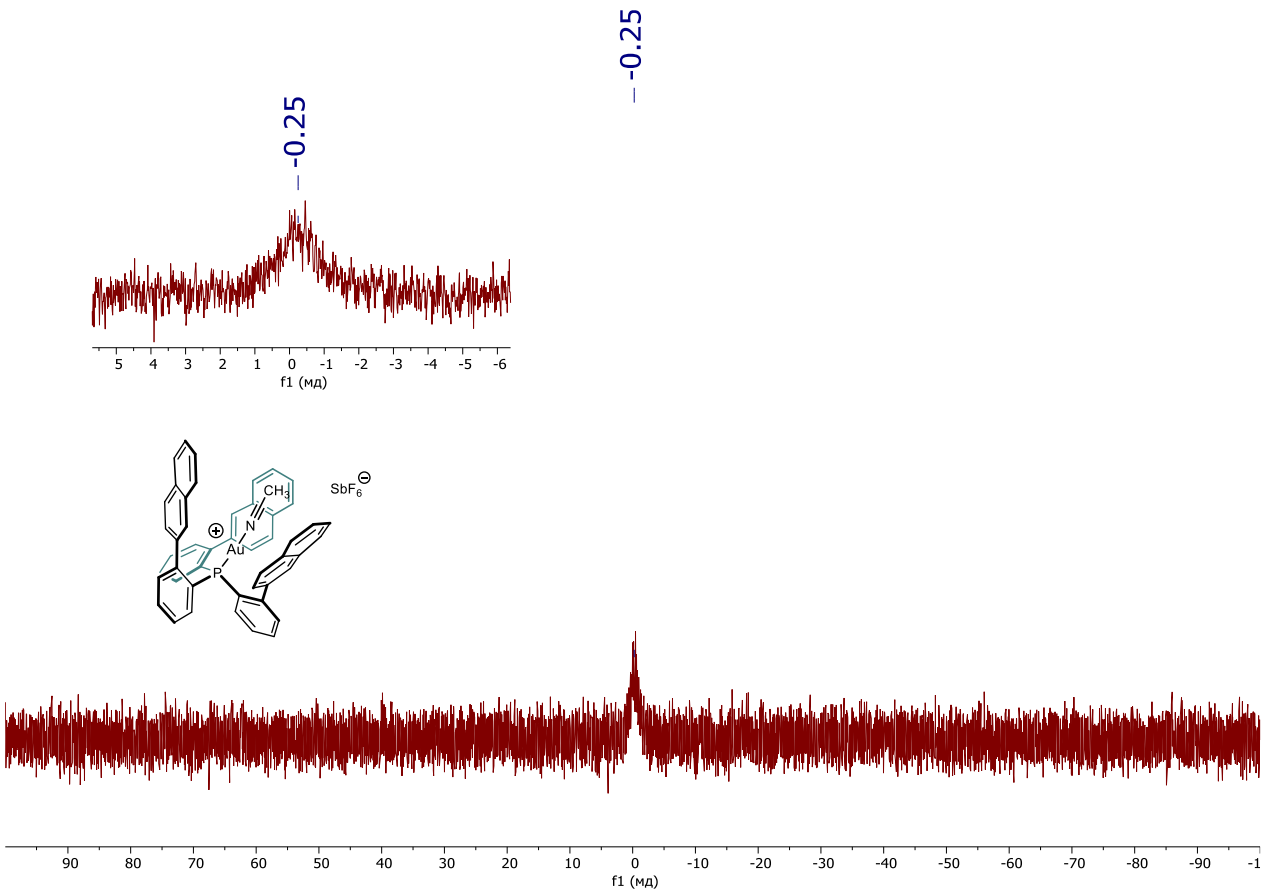

Gold (I) complex 2.3-6$_{CF3}$

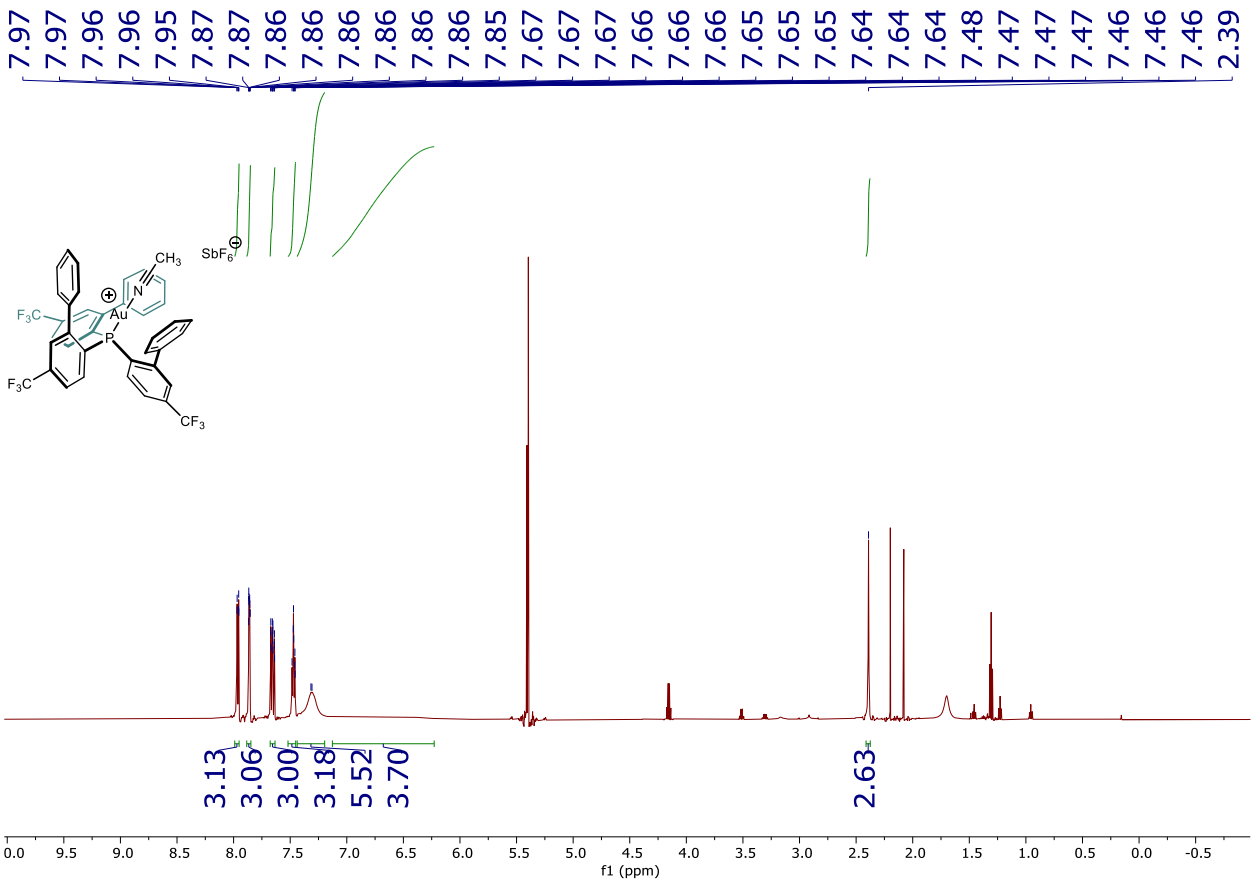
7.97 7.97 7.96 7.96 7.95 7.87 7.87 7.86 7.86 7.86 7.86 7.86 7.85 7.67 7.67 7.67 7.66 7.66 7.66 7.65 7.65 7.65 7.64 7.64 7.64 7.48 7.47 7.47 7.47 7.46 7.46 7.46 2.39
SbF6
CH3
N
Au
P
F3C
F3C
CF3
3.13 3.06 3.00 3.18 5.52 3.70
2.63
f1 (ppm)

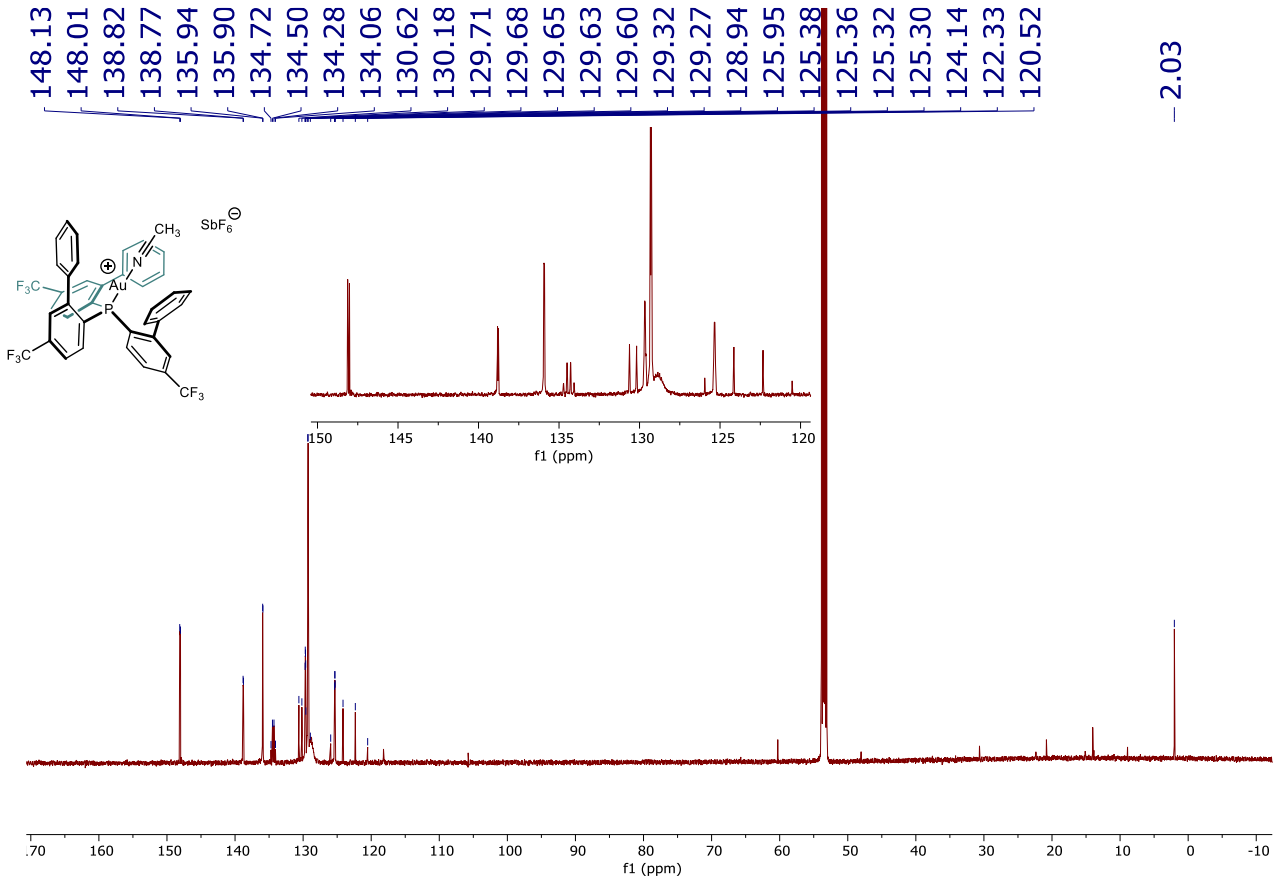
148.13 148.01 138.82 138.77 135.94 135.90 134.72 134.50 134.28 134.06 130.62 130.18 129.71 129.68 129.65 129.63 129.60 129.32 129.27 128.94 125.95 125.38 125.36 125.32 125.30 124.14 122.33 120.52
2.03
SbF6
CH3
N
Au
P
F3C
F3C
CF3
f1 (ppm)
f1 (ppm)

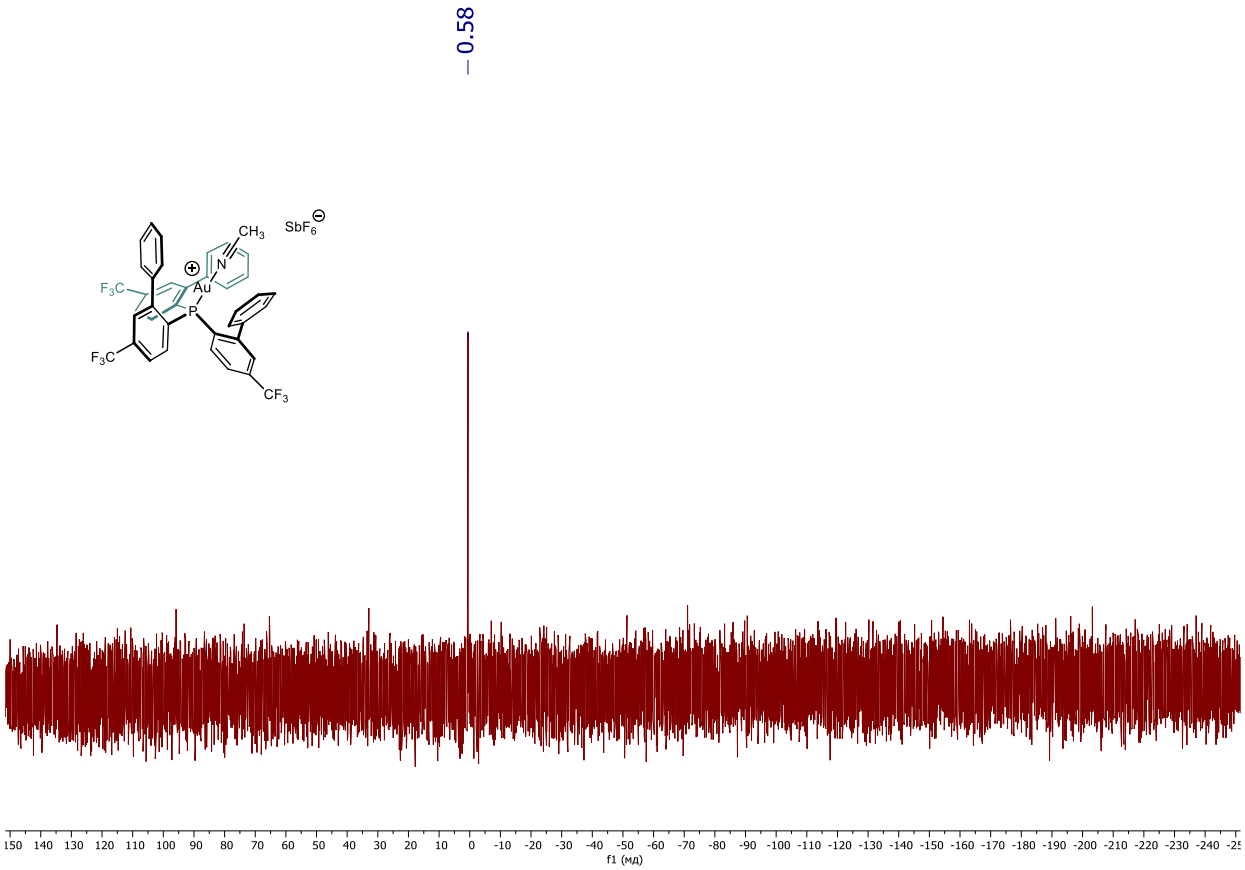
0.58
CH3
SbF6
N
Au
P
F3C
F3C
CF3
f1 (мд)

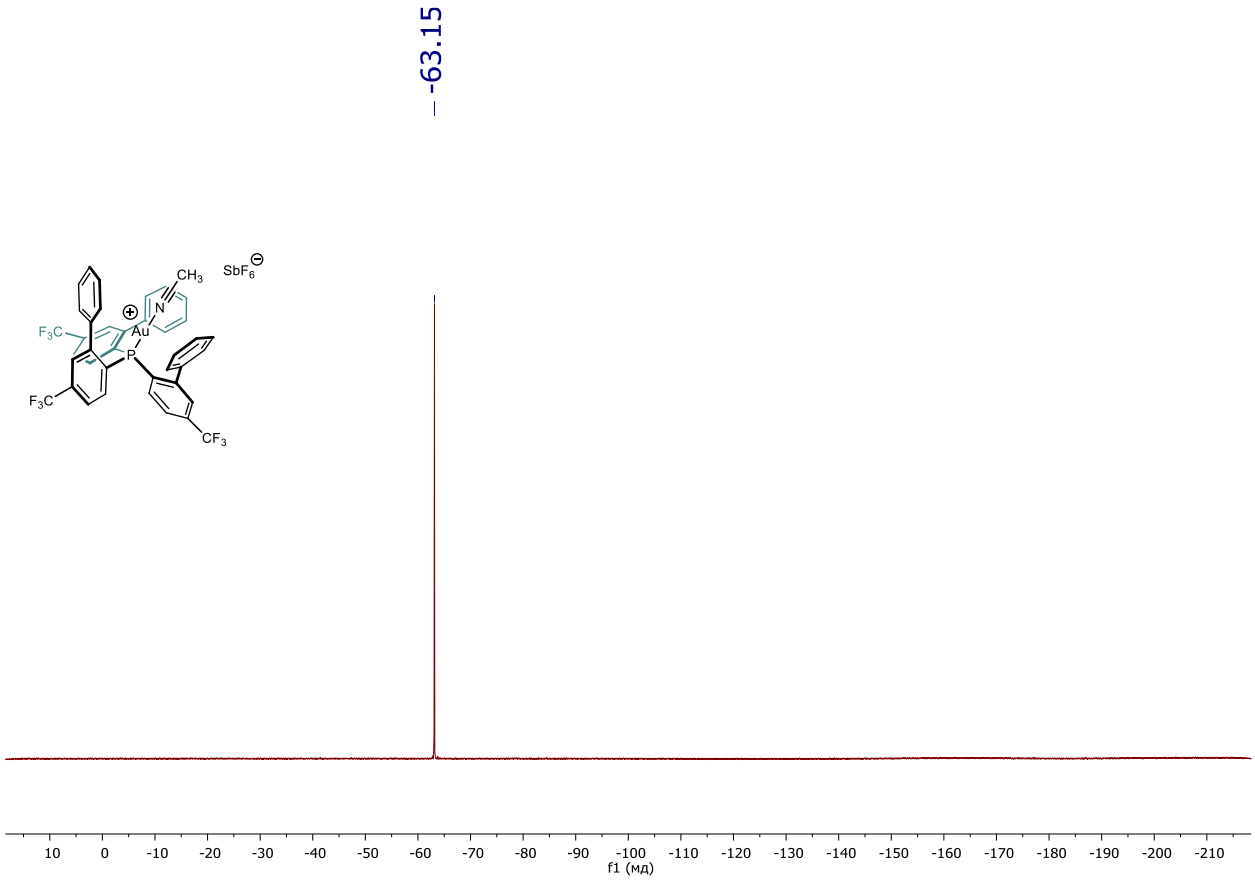
-63.15
CH3
SbF6
N
Au
P
F3C
F3C
CF3
f1 (мд)

Gold (I) complex 2.3-42

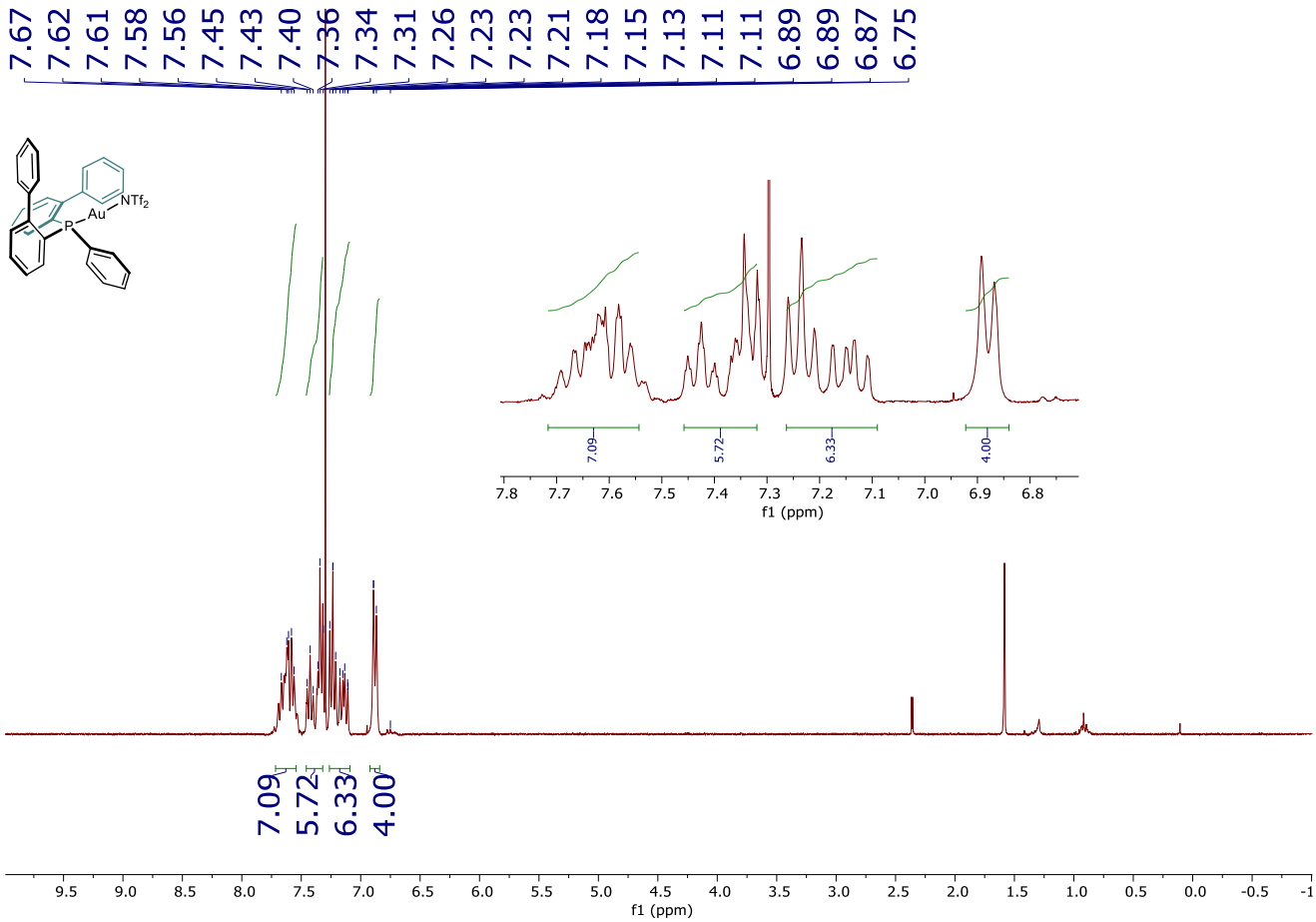

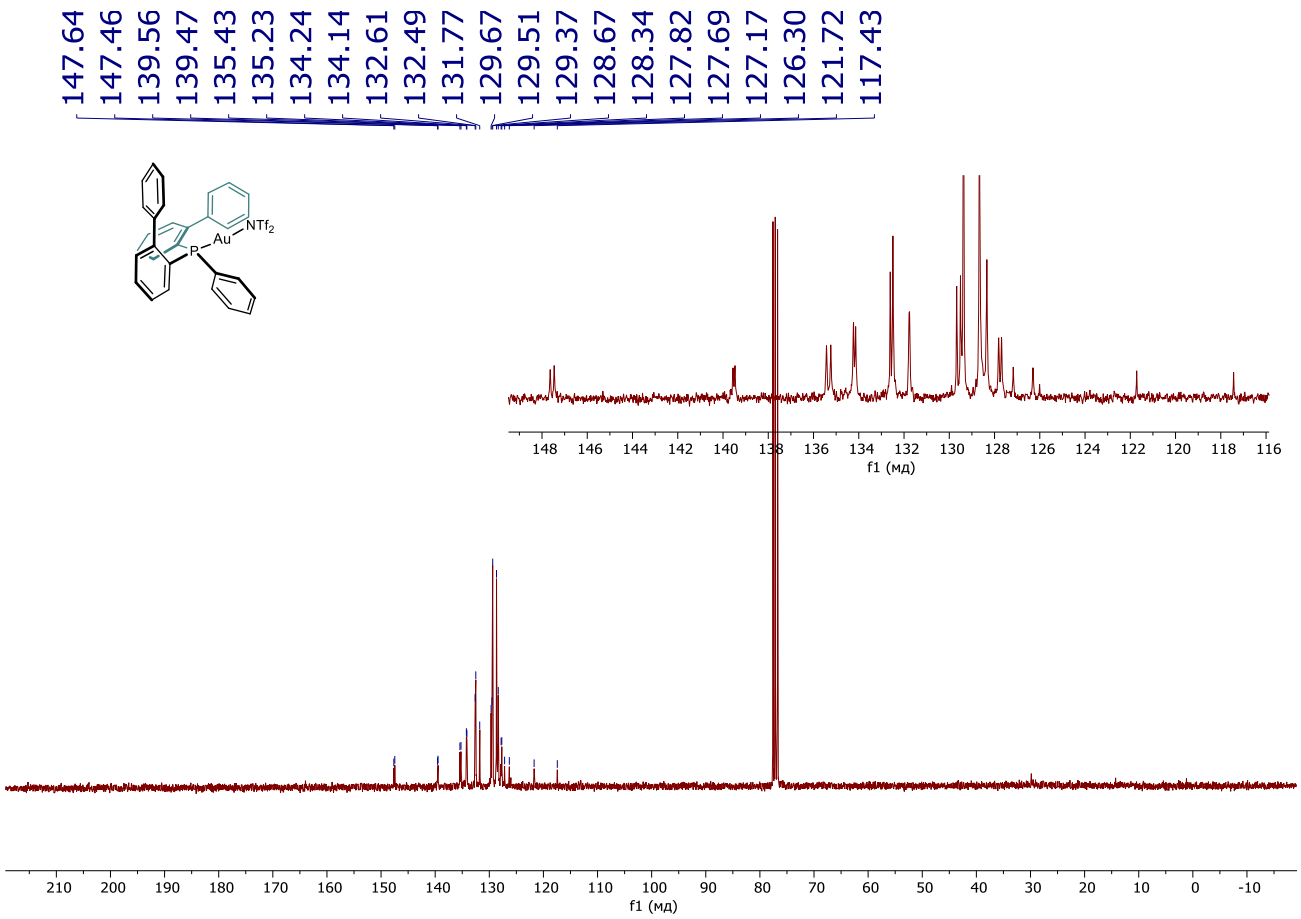
147.64
147.46
139.56
139.47
135.43
135.23
134.24
134.14
132.61
132.49
131.77
129.67
129.51
129.37
128.67
128.34
127.82
127.69
127.17
126.30
121.72
117.43
NTf2
Au
P
f1 (мд)
f1 (мд)

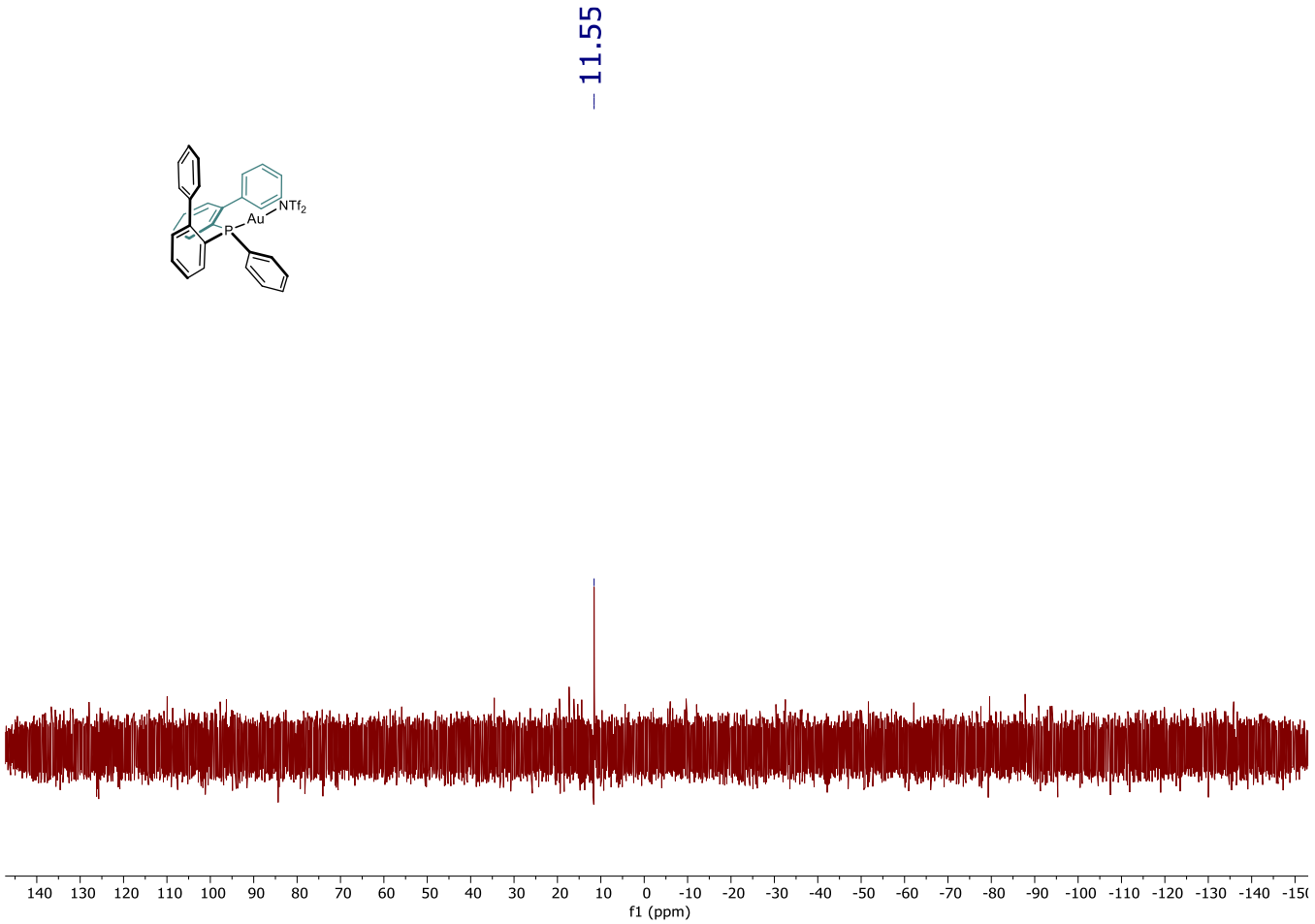
11.55
NTf2
Au
P
f1 (ppm)

Gold (I) complex 2.3-7

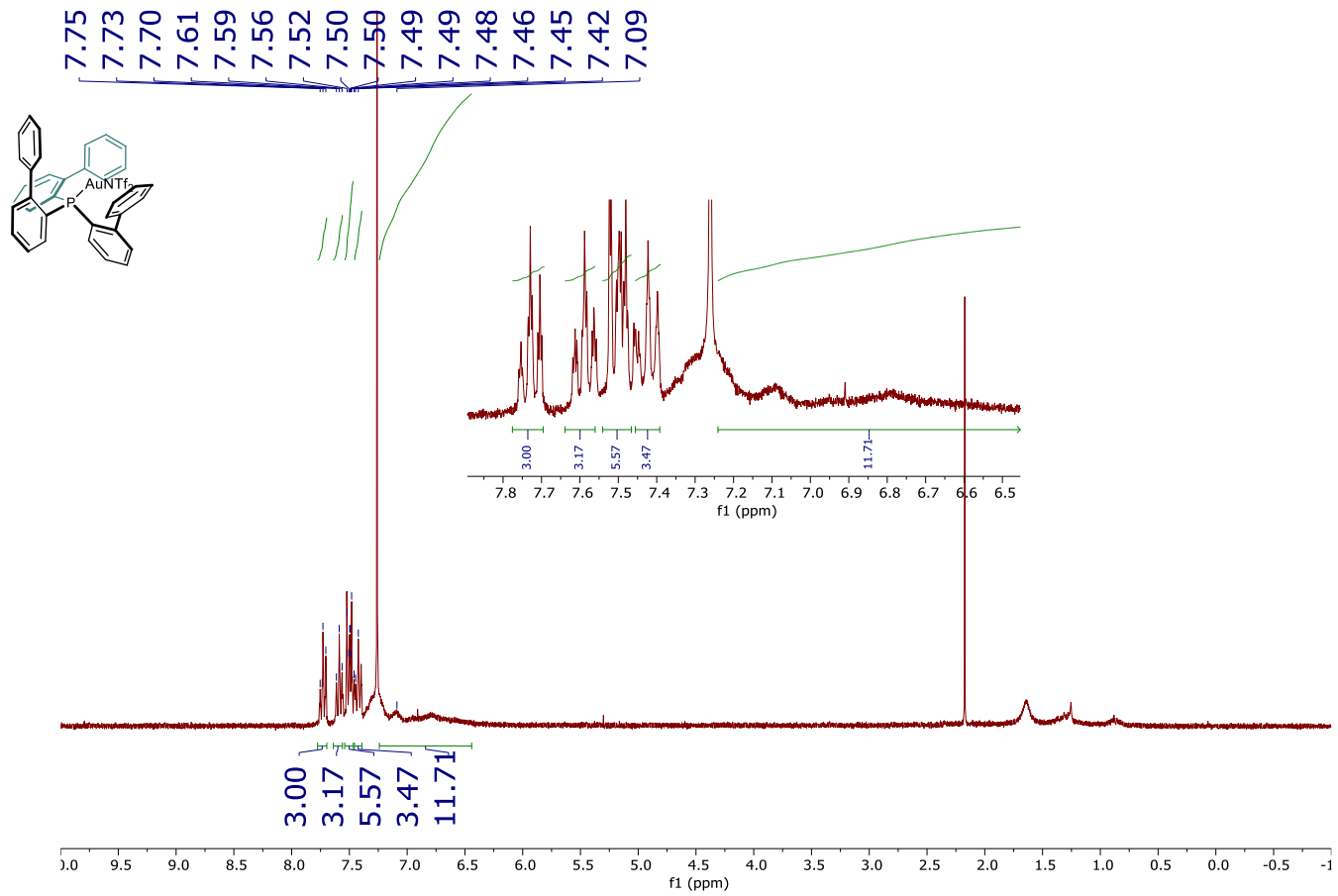

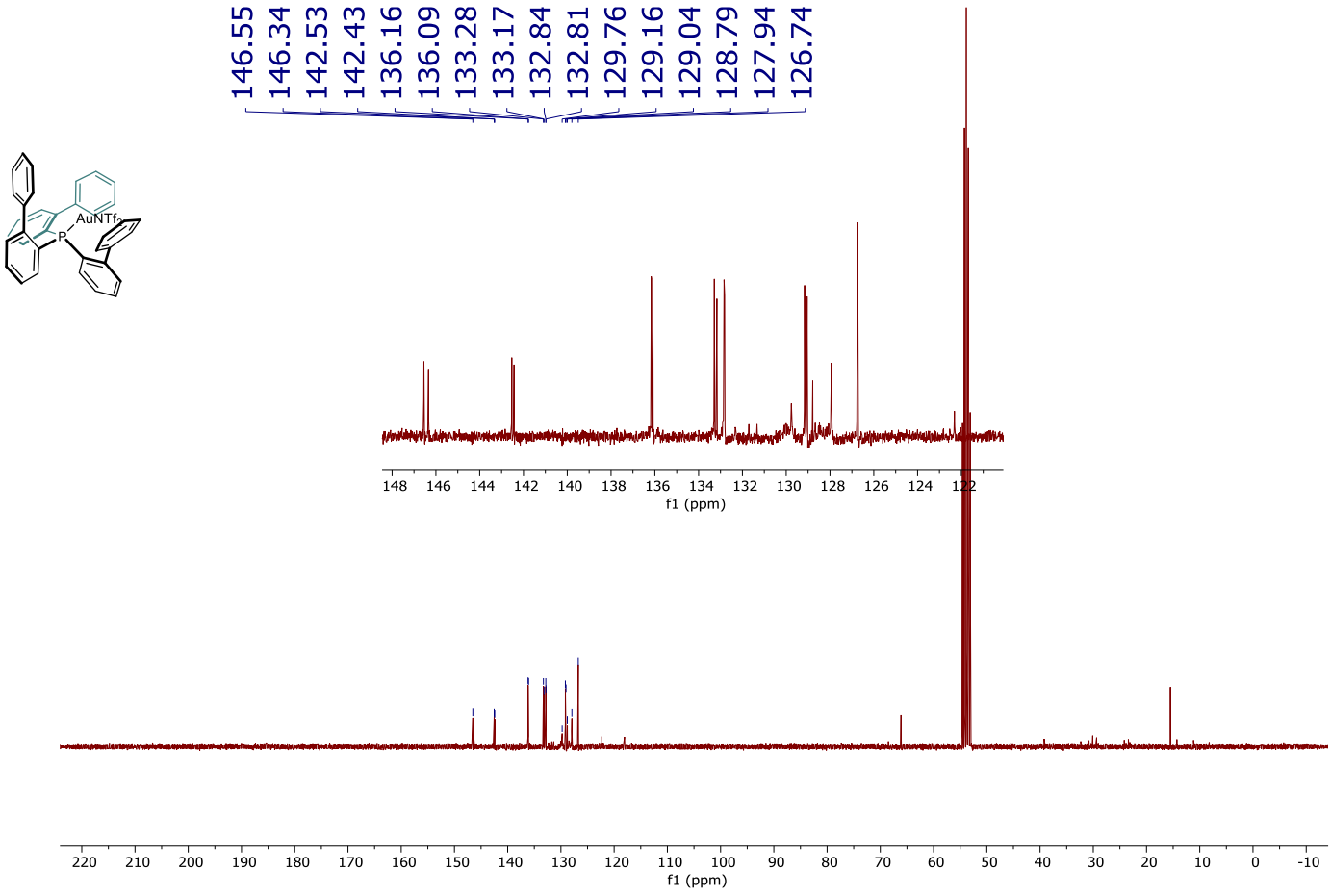

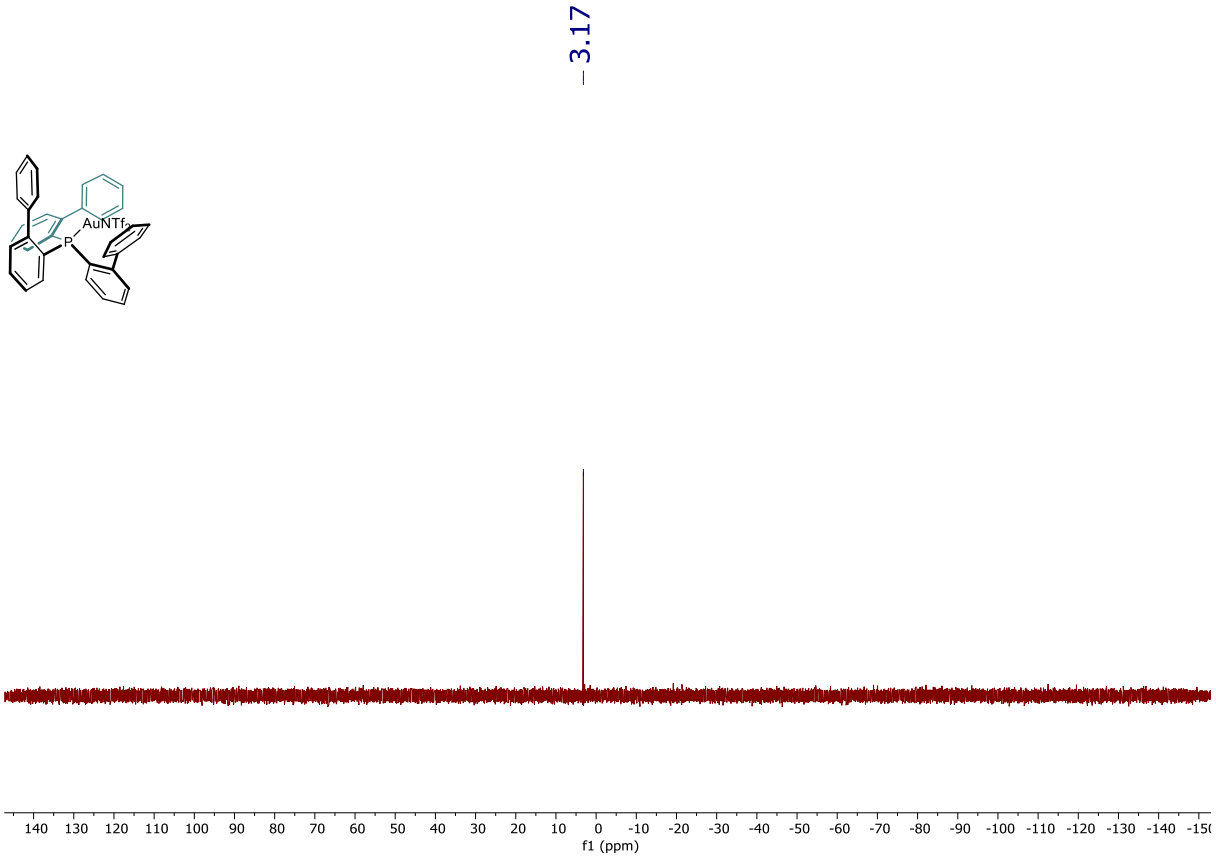

Diethyl 6-phenyl-1-(2-phenylcyclopropyl)bicyclo[3.1.0]hexane-3,3-dicarboxylate 2.3-32a

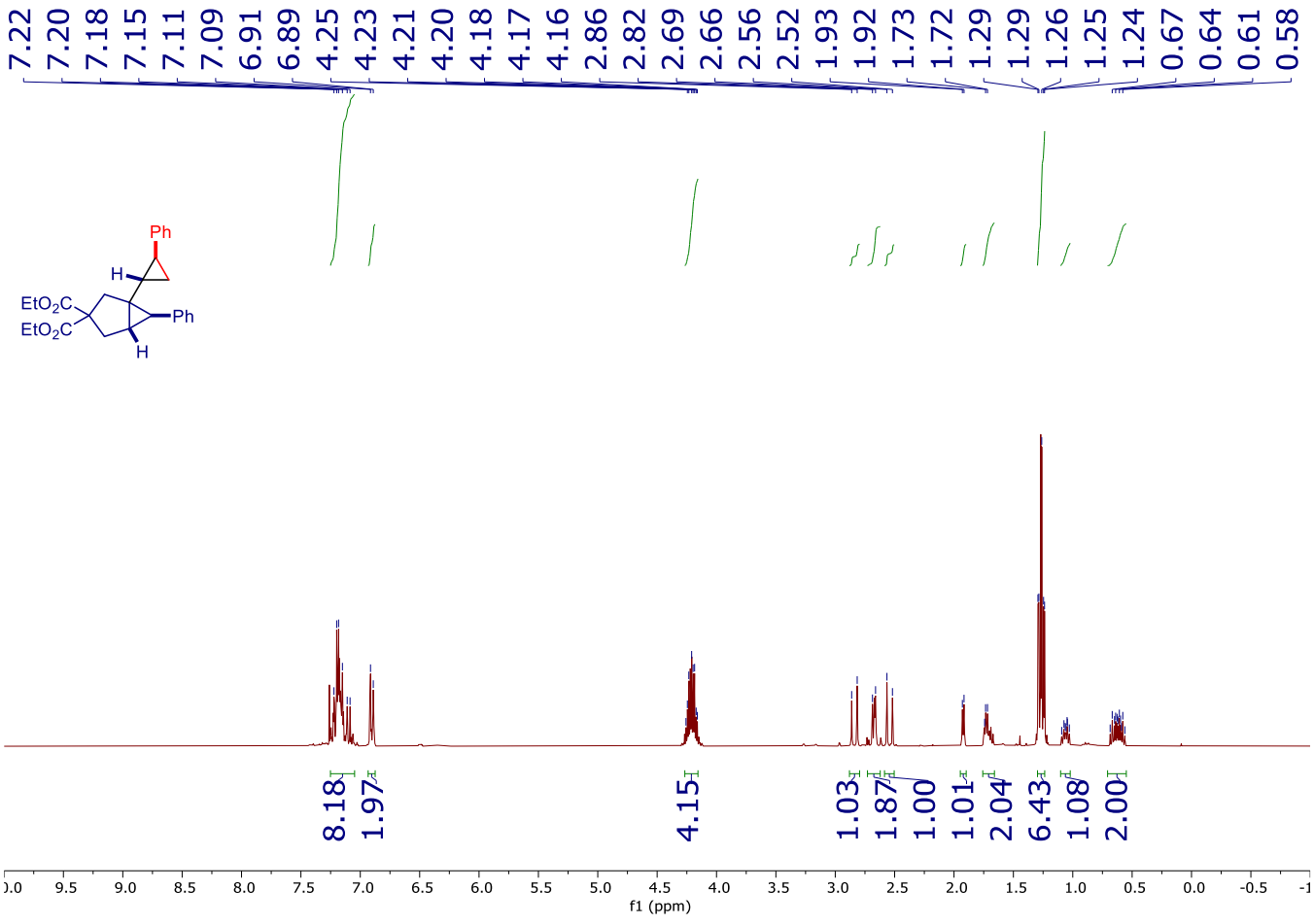

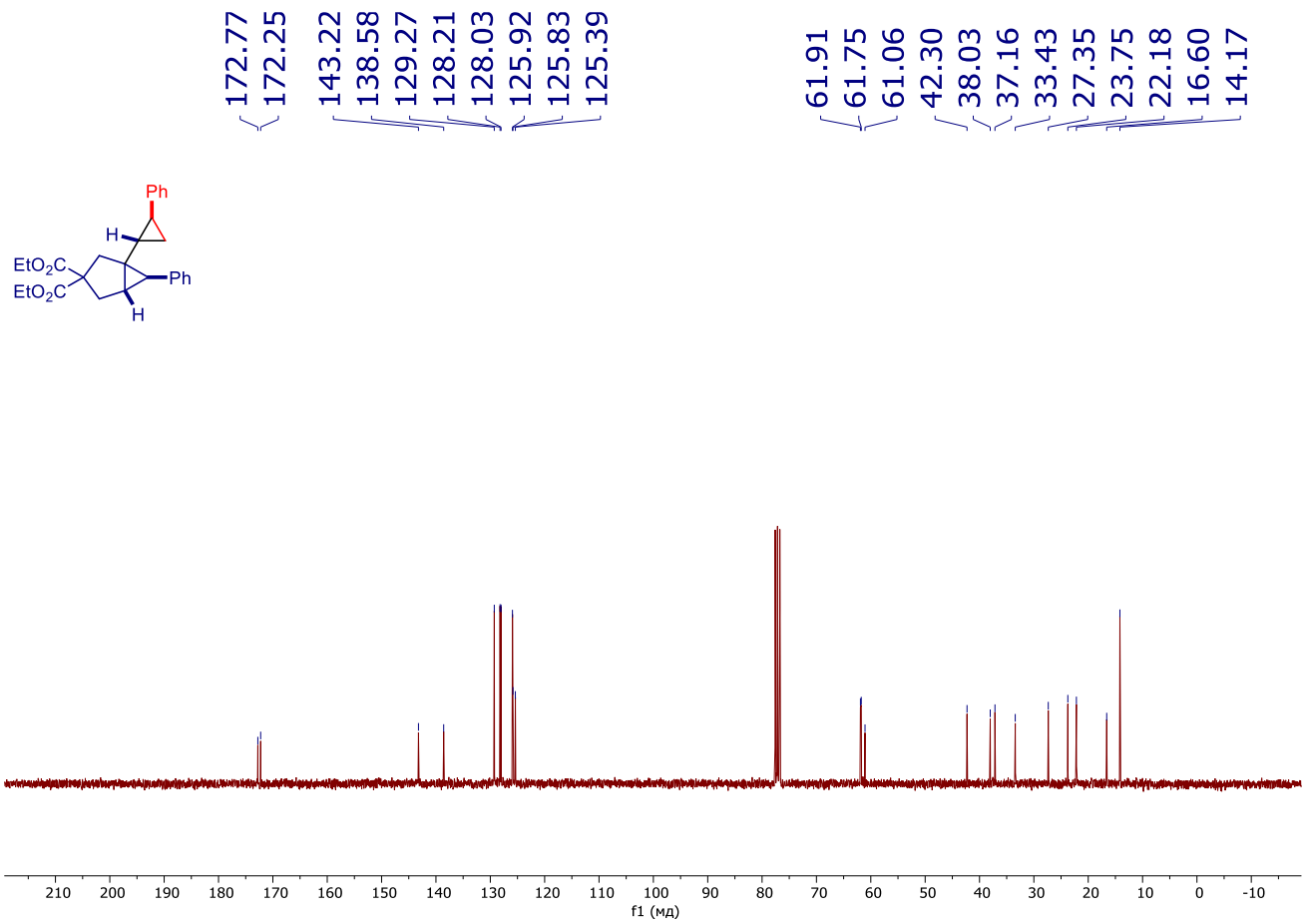

Diethyl 3-((2,4-dimethoxyphenyl)(phenyl)methyl)-4-methylenecyclopentane-1,1-dicarboxylate 2.3-32b

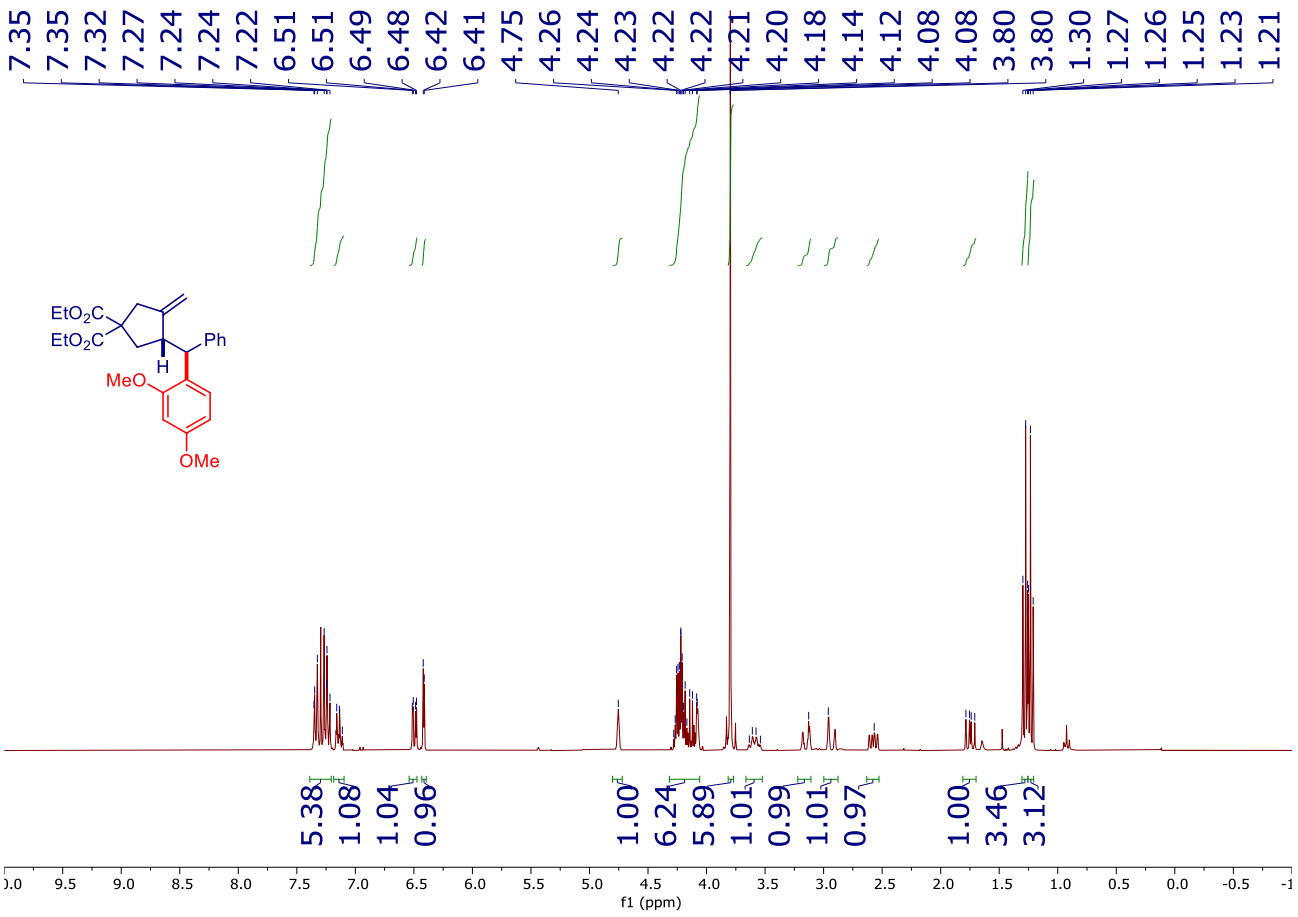
7.35 7.35 7.32 7.27 7.24 7.24 7.22 6.51 6.51 6.49 6.48 6.42 6.41 4.75 4.26 4.24 4.23 4.22 4.22 4.21 4.20 4.18 4.14 4.12 4.08 4.08 3.80 3.80 1.30 1.27 1.26 1.25 1.23 1.21
EtO2C
EtO2C
Ph
H
MeO
OMe
5.38 1.08 1.04 0.96 1.00 6.24 5.89 1.01 0.99 1.01 0.97 1.00 3.46 3.12
f1 (ppm)

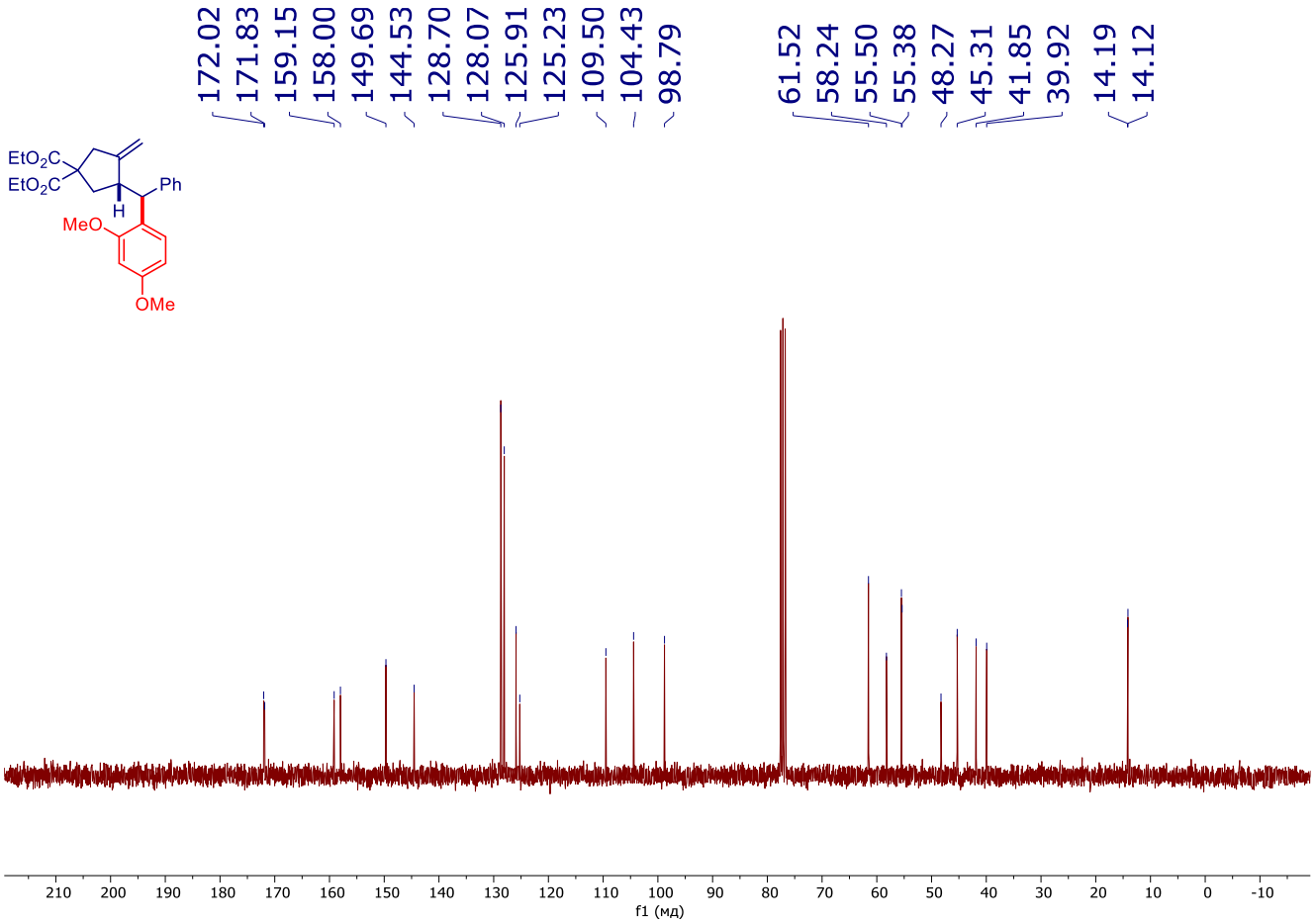
172.02 171.83 159.15 158.00 149.69 144.53 128.70 128.07 125.91 125.23 109.50 104.43 98.79 61.52 58.24 55.50 55.38 48.27 45.31 41.85 39.92 14.19 14.12
EtO2C
EtO2C
Ph
H
MeO
OMe
f1 (мд)

Diethyl 4-vinylcyclohex-3-ene-1,1-dicarboxylate 2.3-36a

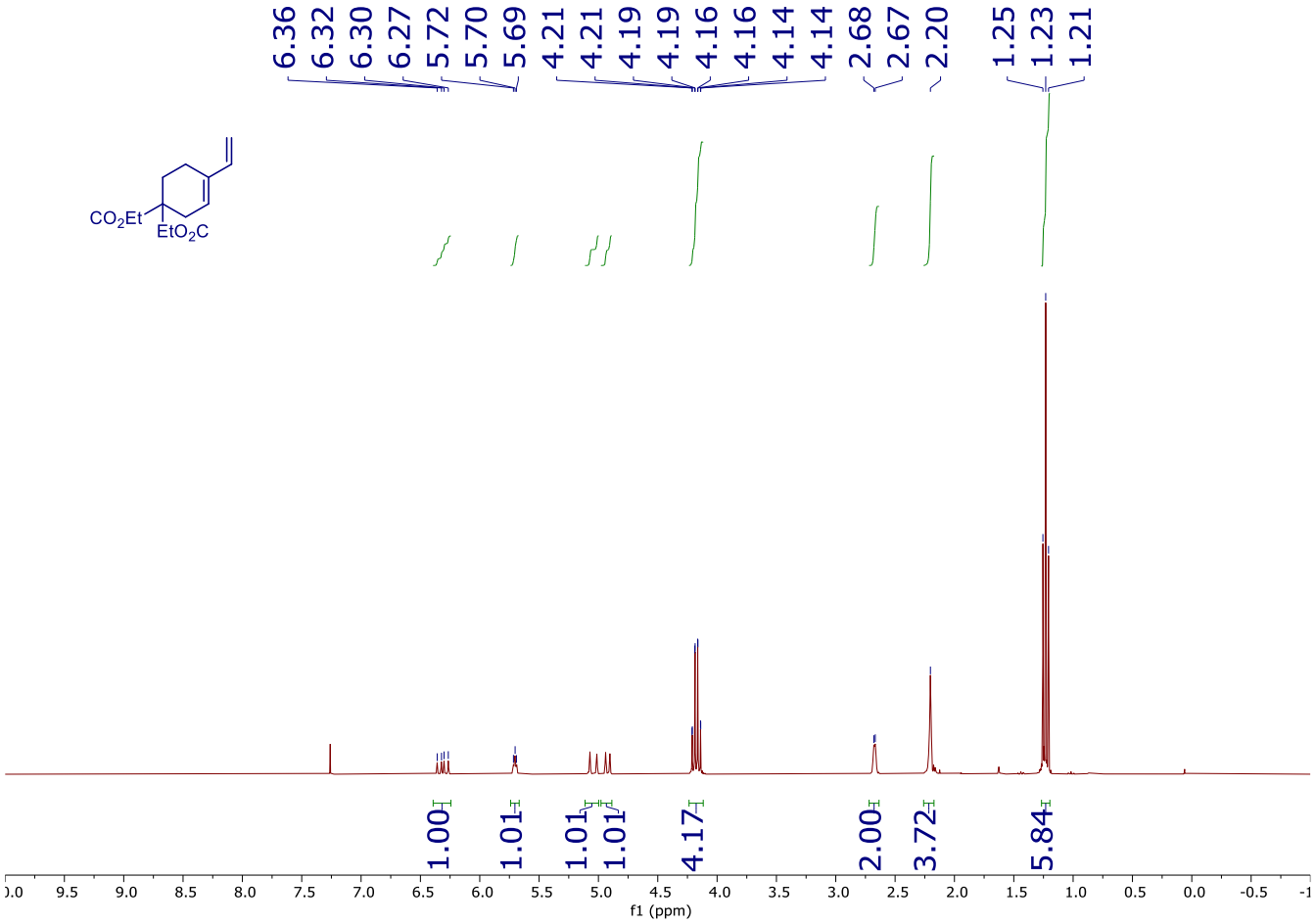

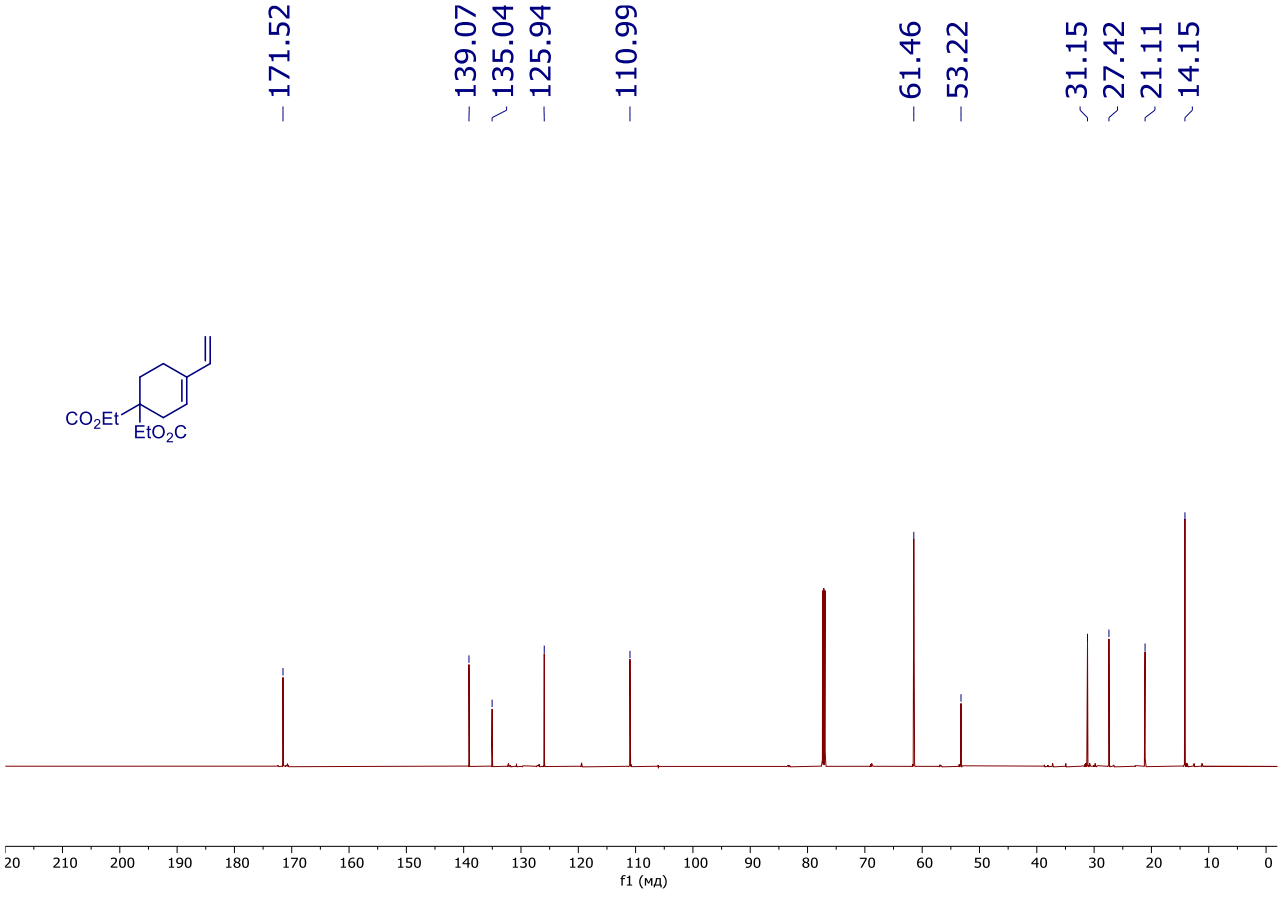

7.2. NMR data for Chapter 3.

N-(di-tert-butylphosphaneyl)-N-methylpyridin-2-amine 3.3-15$_H$

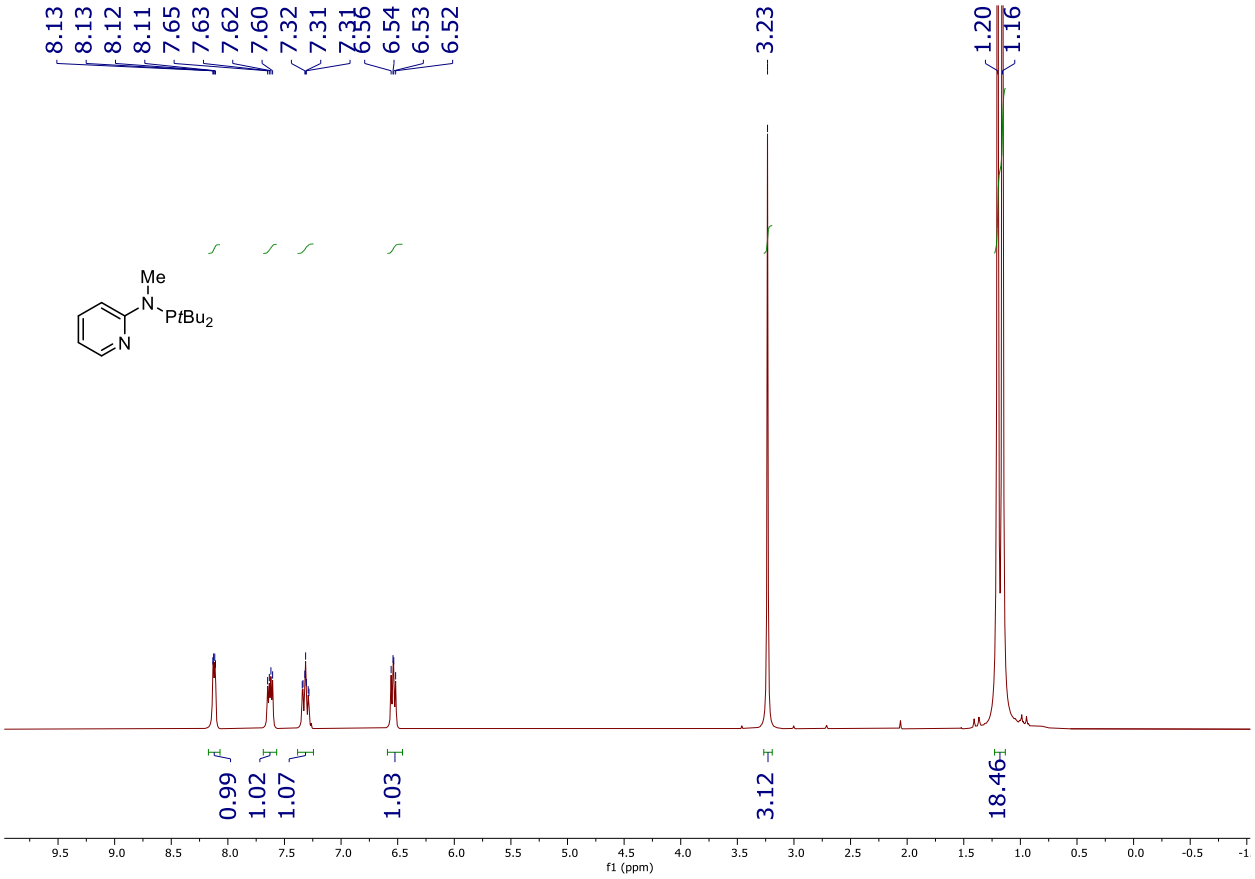

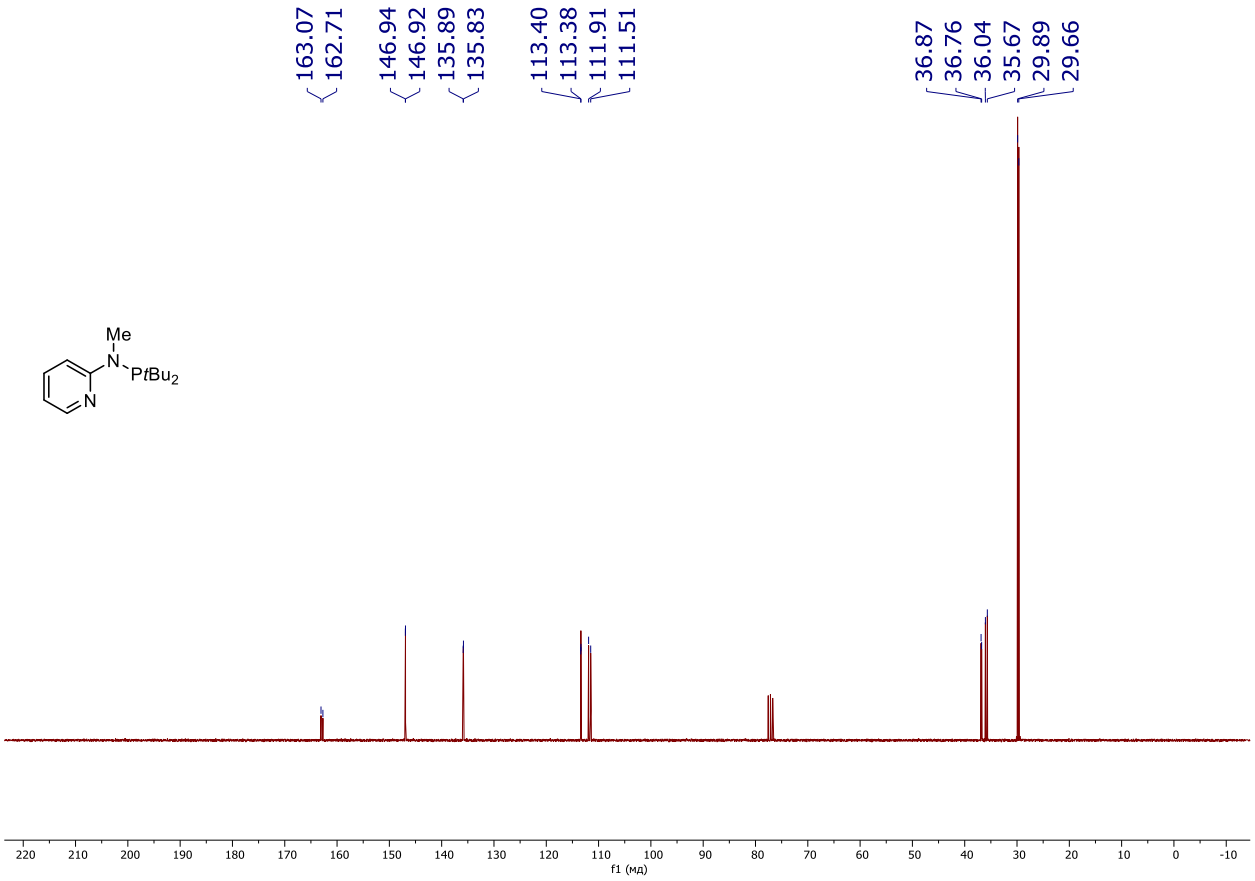

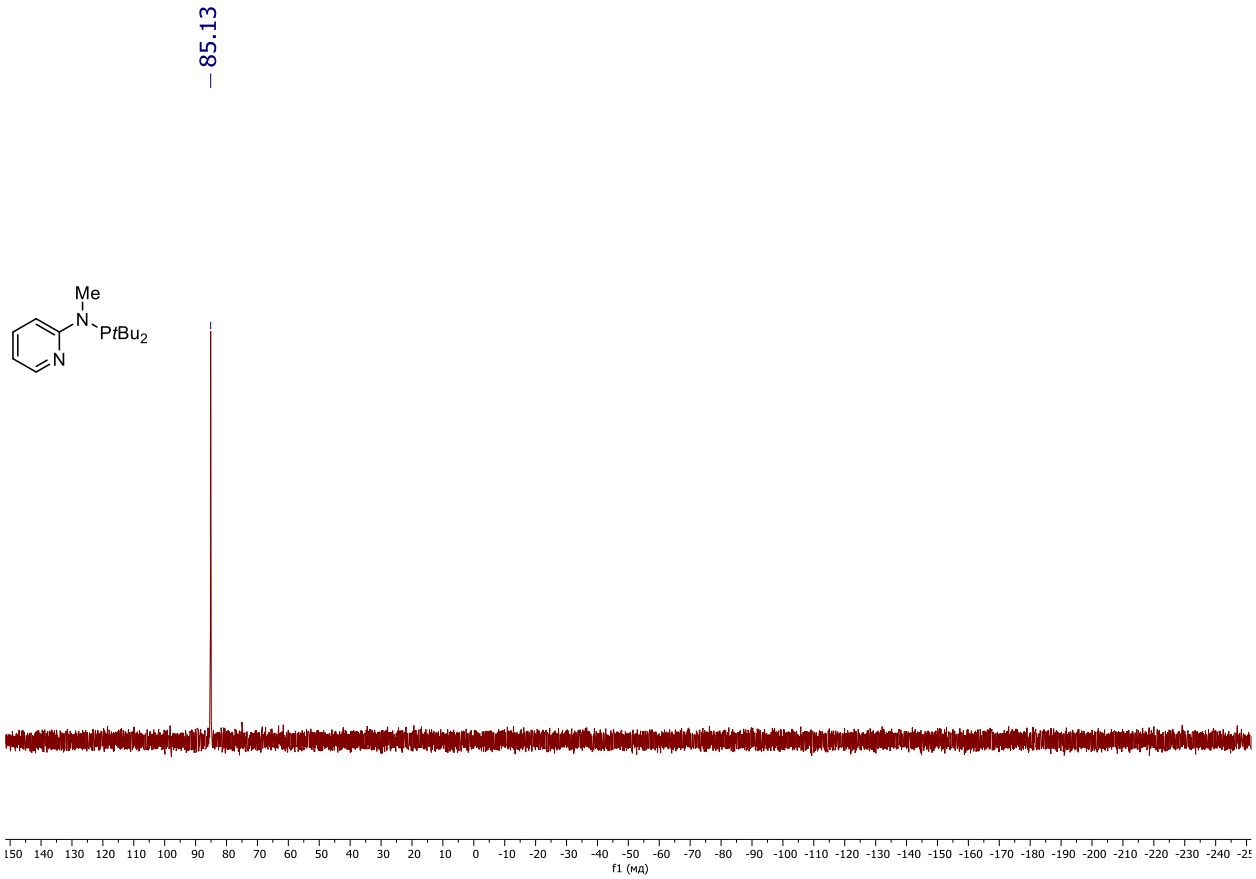

N-(di-tert-butylphosphaneyl)-4-methoxy-N-methylpyridin-2-amine 3.3-15$_{OMe}$

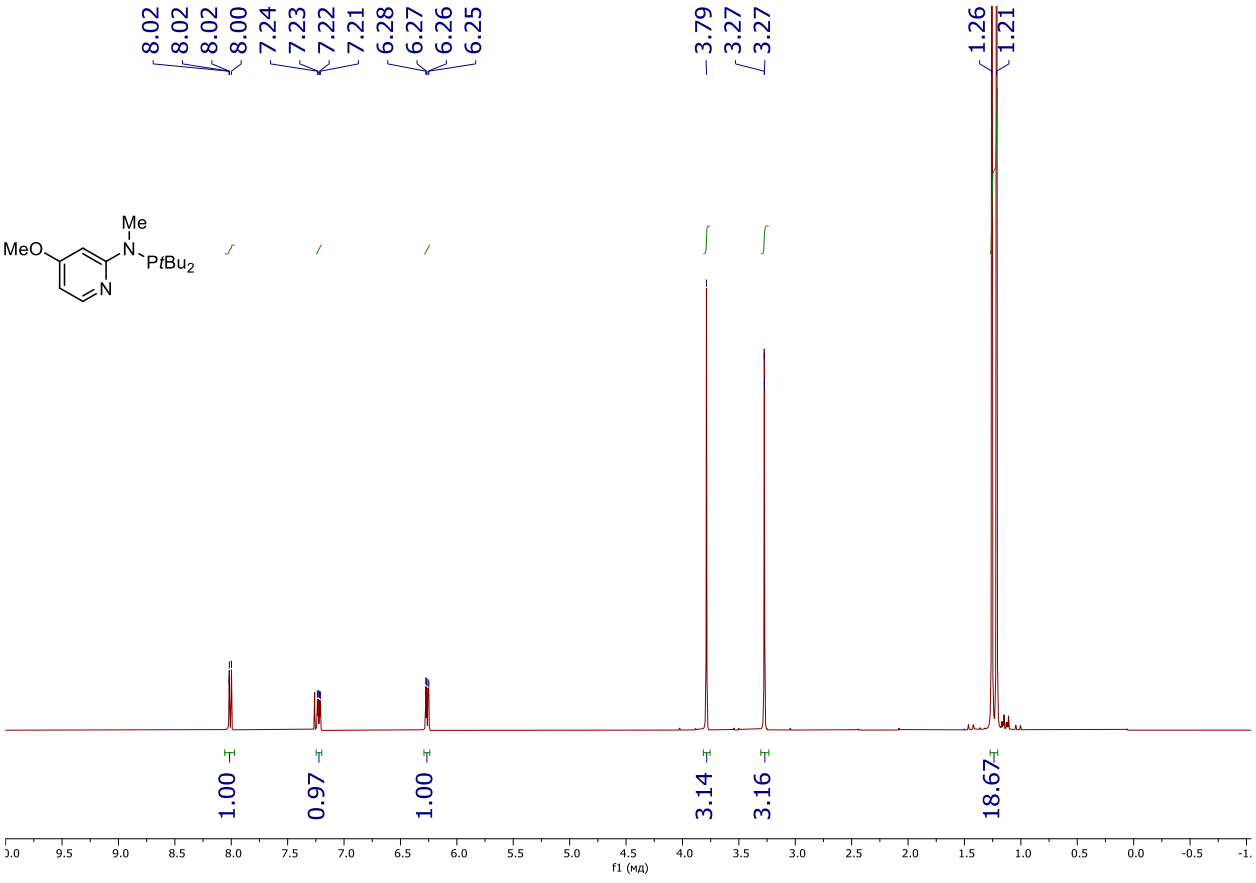

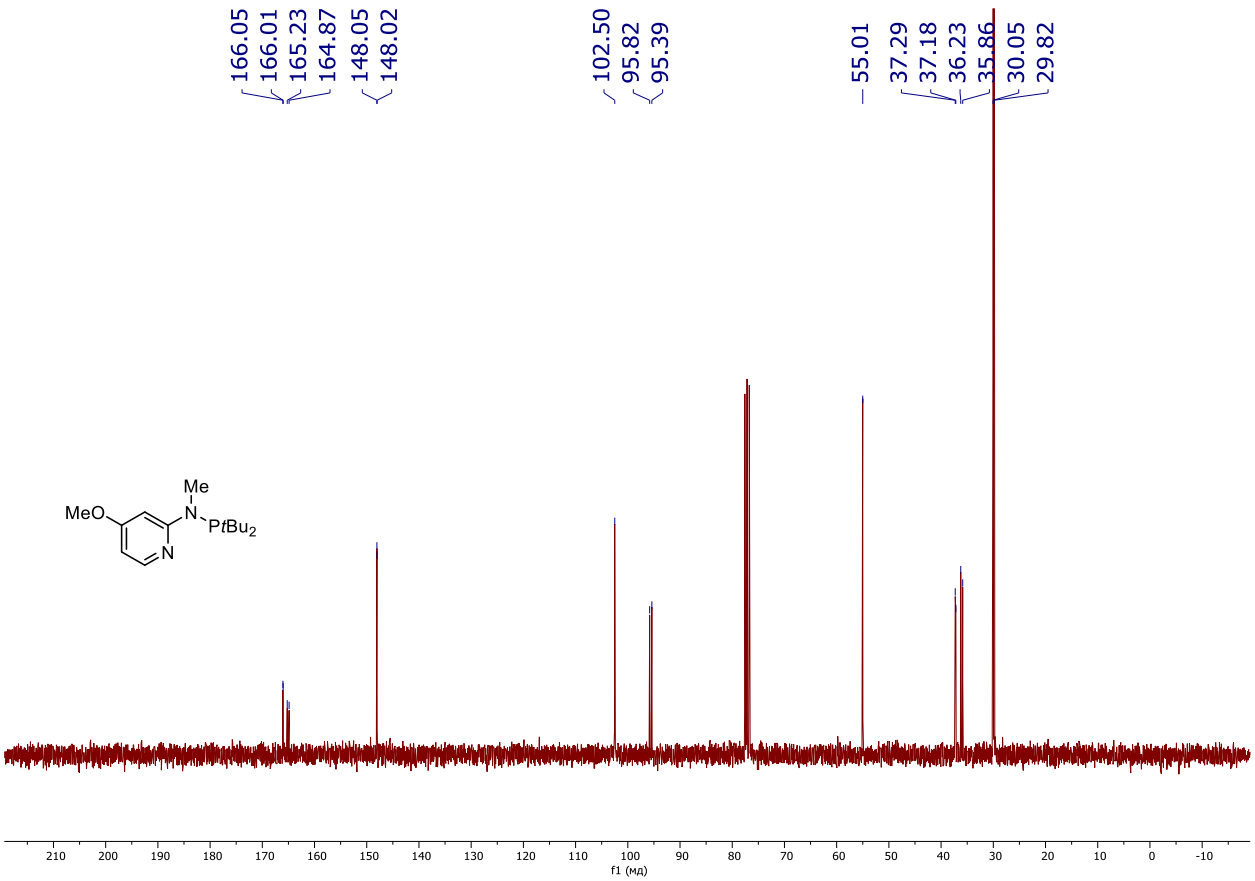

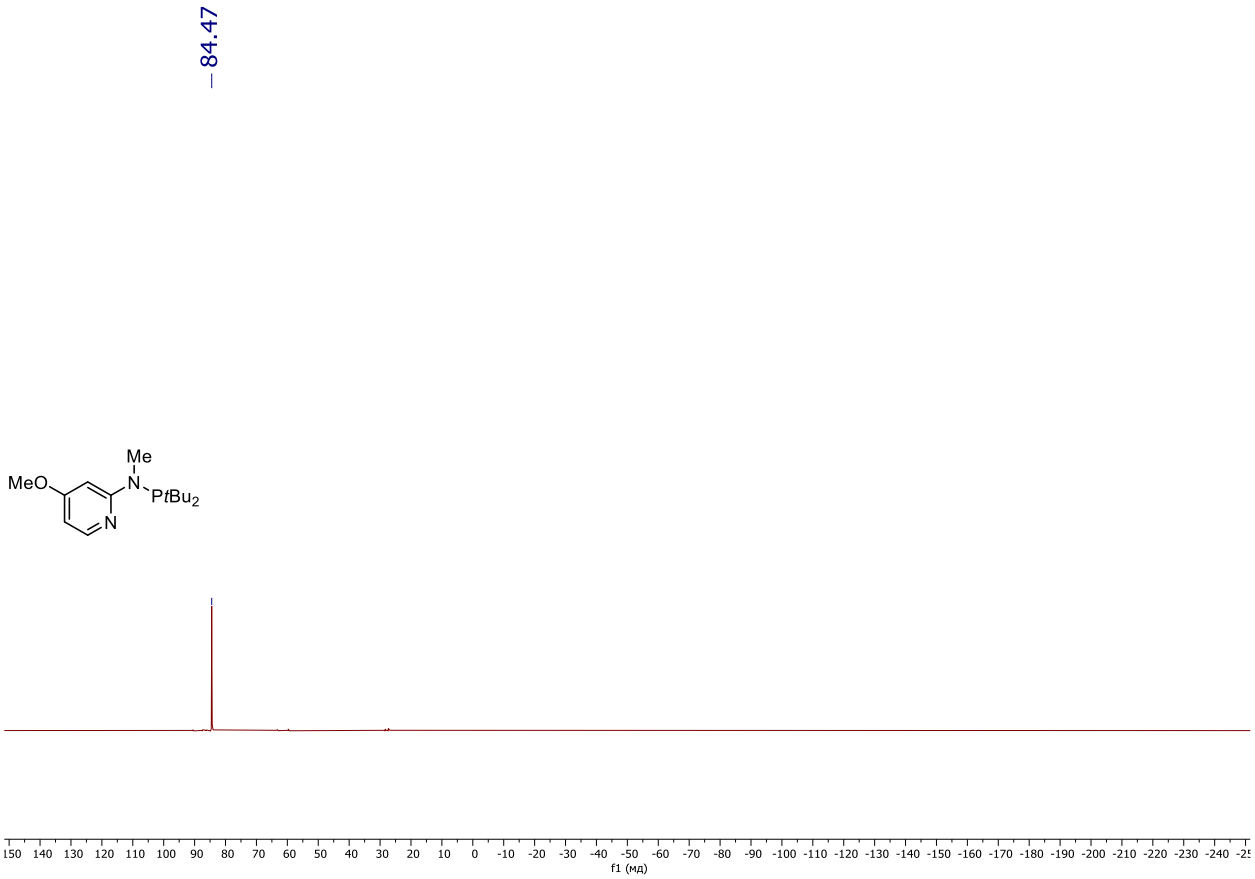

N-(di-tert-butylphosphaneyl)-N-methyl-4-(trifluoromethyl)pyridin-2-amine 3.3-15$_{CF3}$

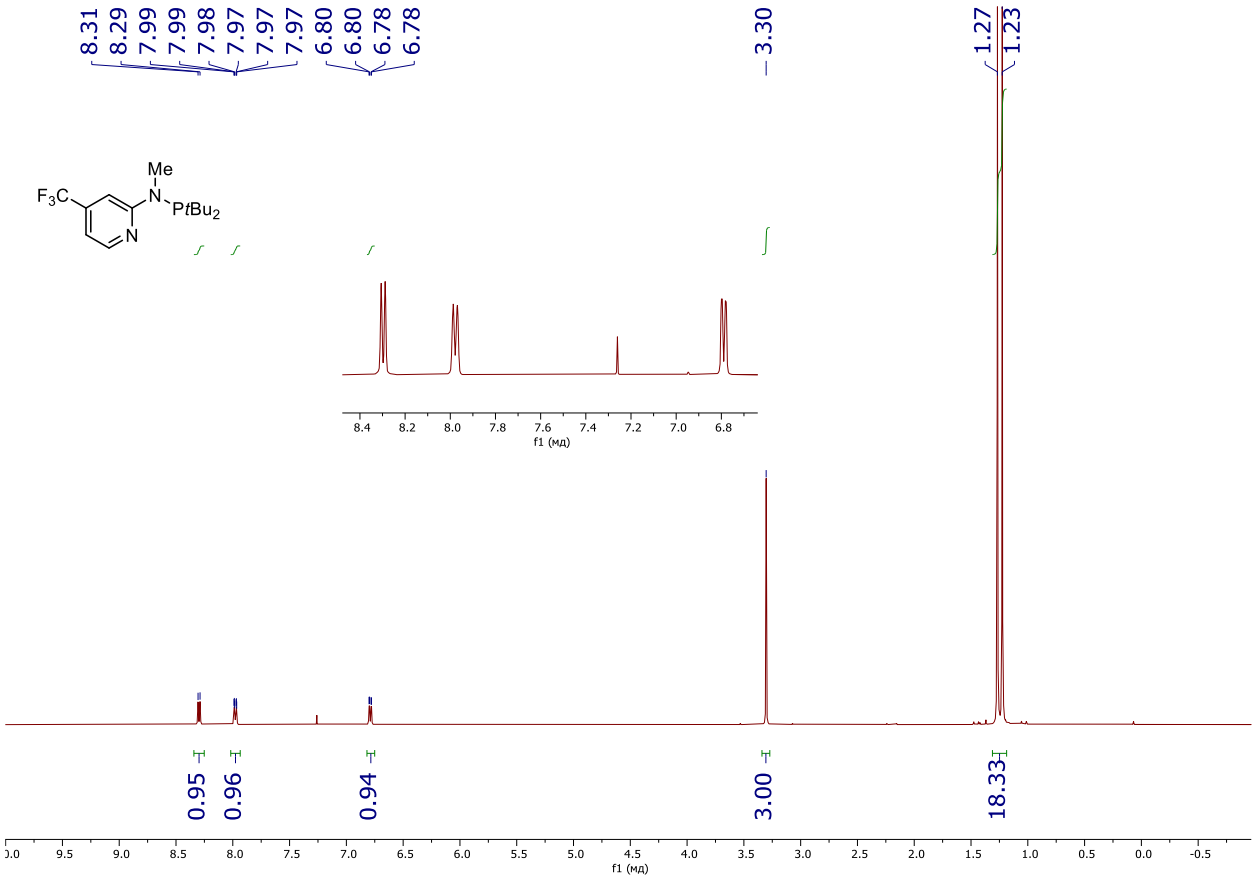
8.31
8.29
7.99
7.99
7.98
7.97
7.97
7.97
6.80
6.80
6.78
6.78
3.30
1.27
1.23
Me
N
PtBu2
F3C
N
0.95
0.96
0.94
3.00
18.33
f1 (мд)

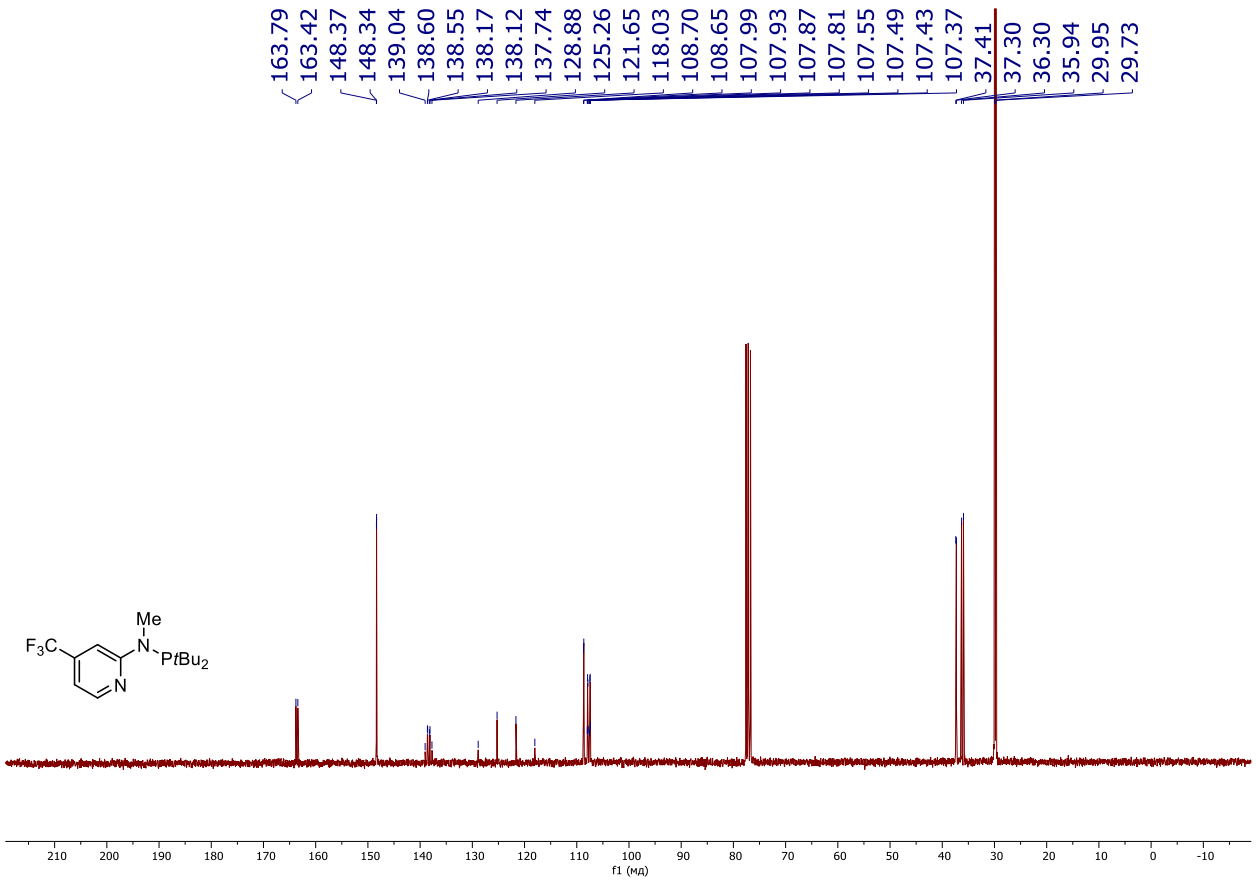
163.79
163.42
148.37
148.34
139.04
138.60
138.55
138.17
138.12
137.74
128.88
125.26
121.65
118.03
108.70
108.65
107.99
107.93
107.87
107.81
107.55
107.49
107.43
107.37
37.41
37.30
36.30
35.94
29.95
29.73
Me
N
PtBu2
F3C
N
f1 (мд)

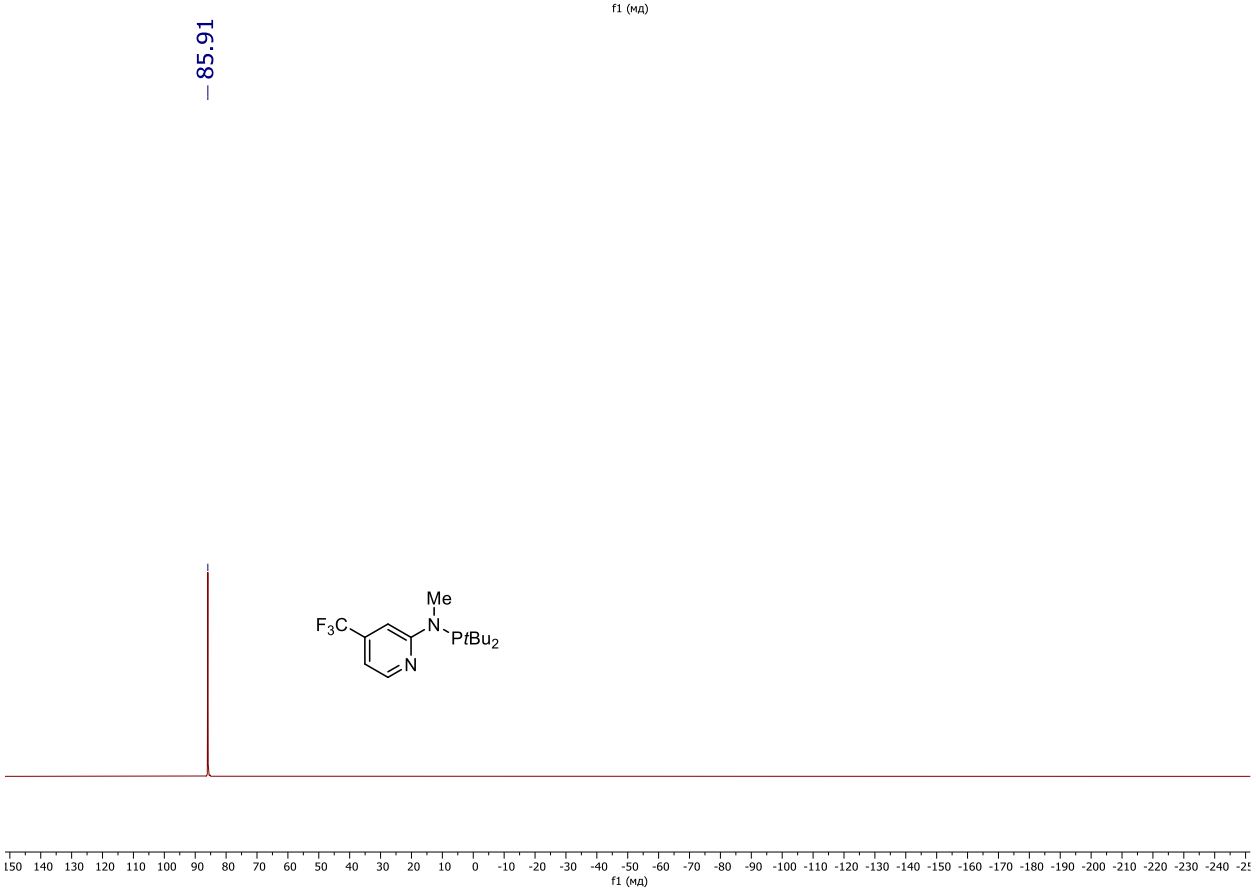
85.91
Me
N
PtBu2
F3C
N
f1 (мд)

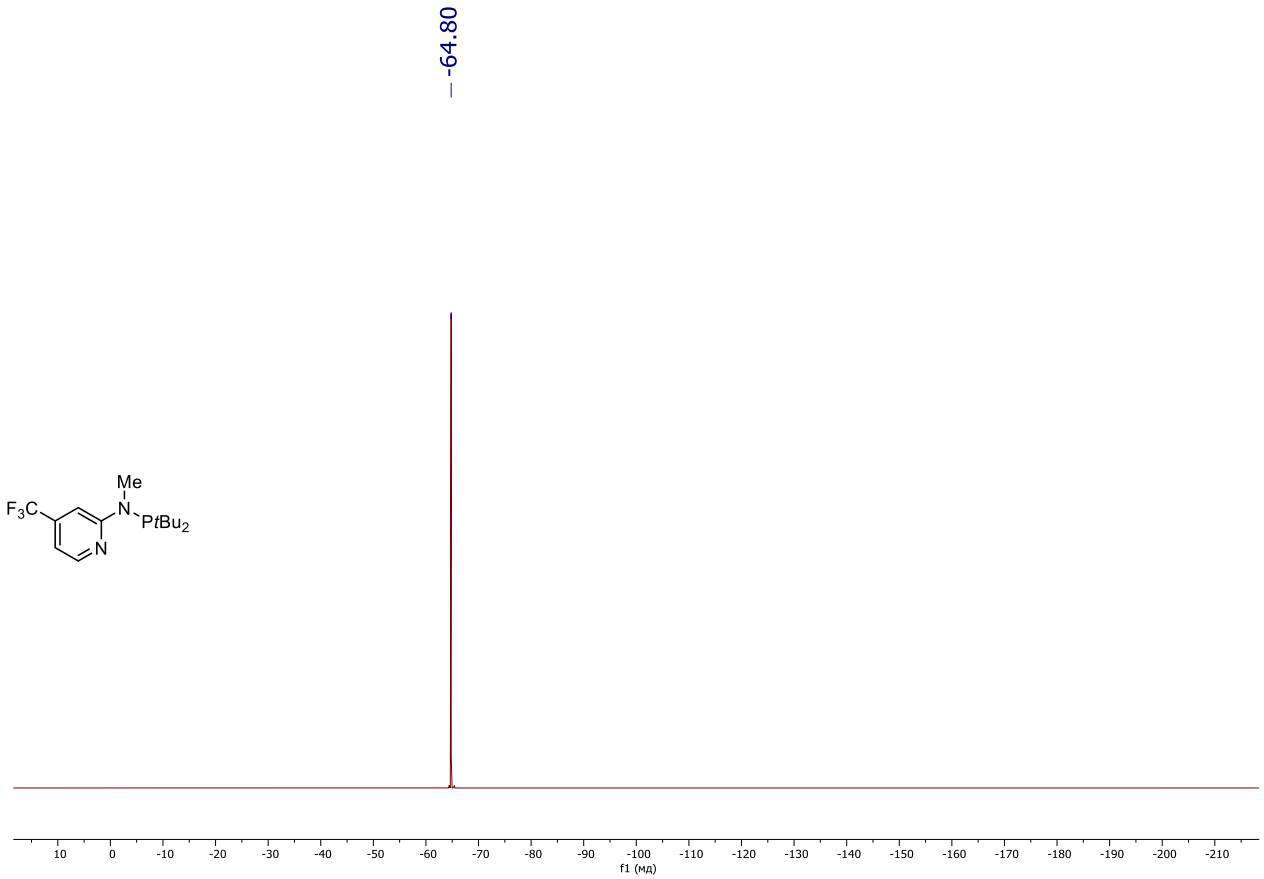

N-(di-tert-butylphosphaneyl)-N-methylpyrazin-2-amine 3.3-26$_H$

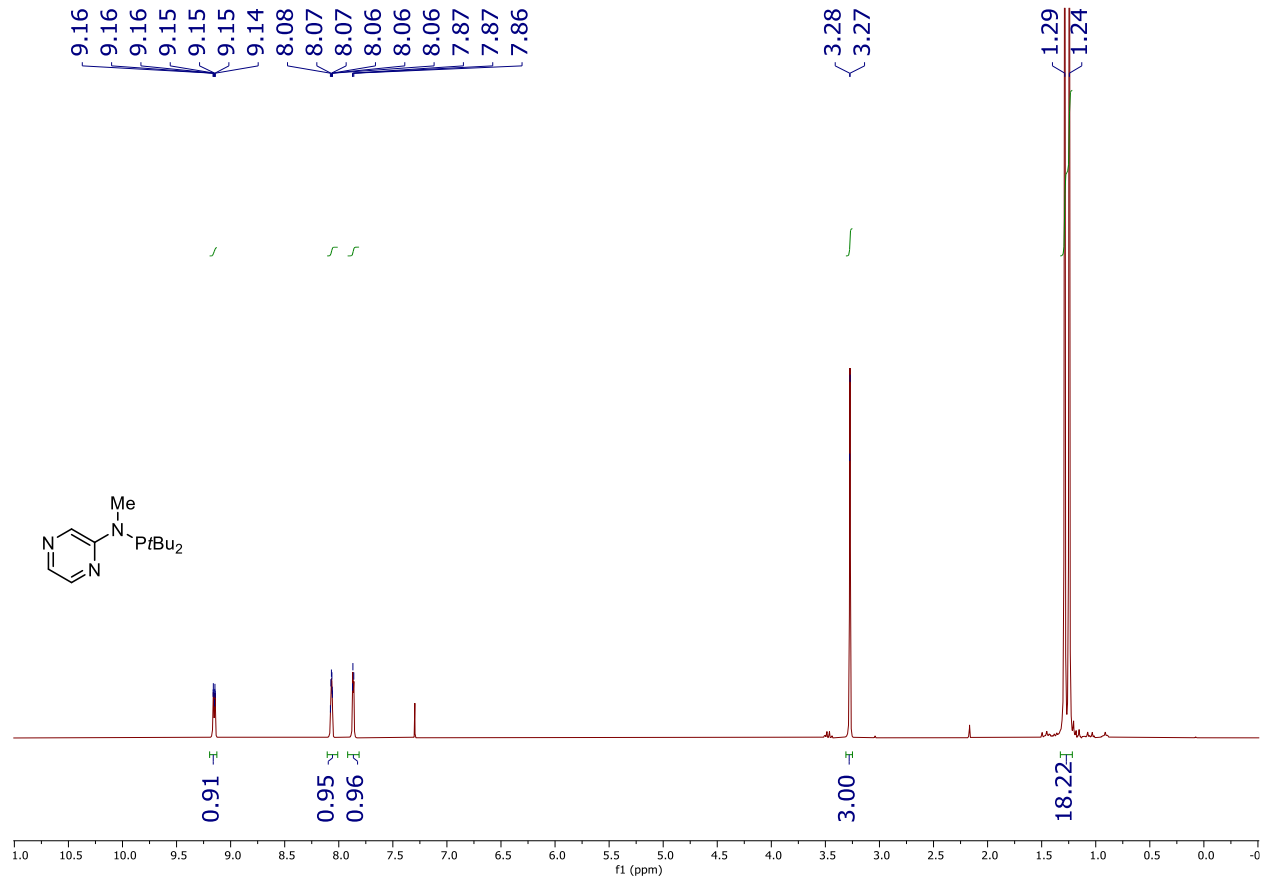

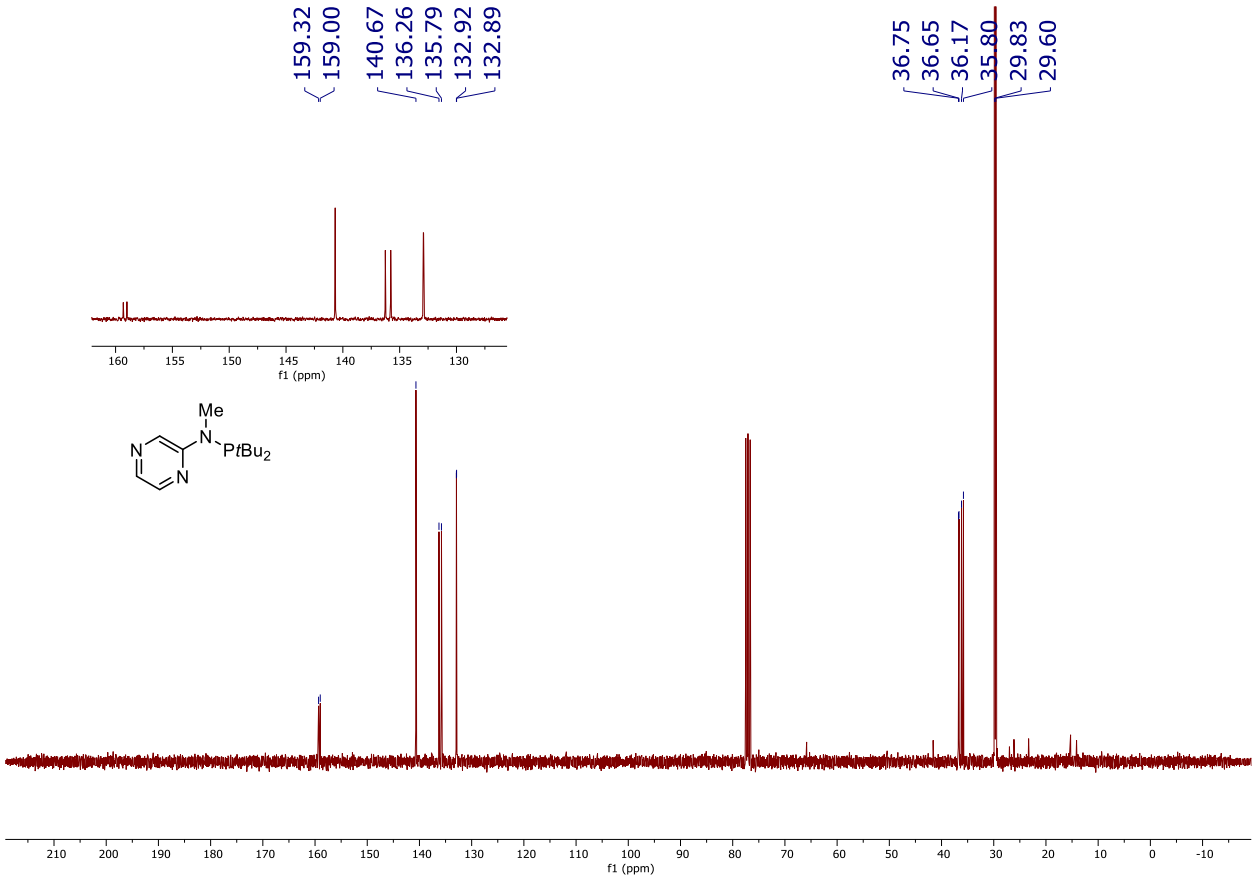

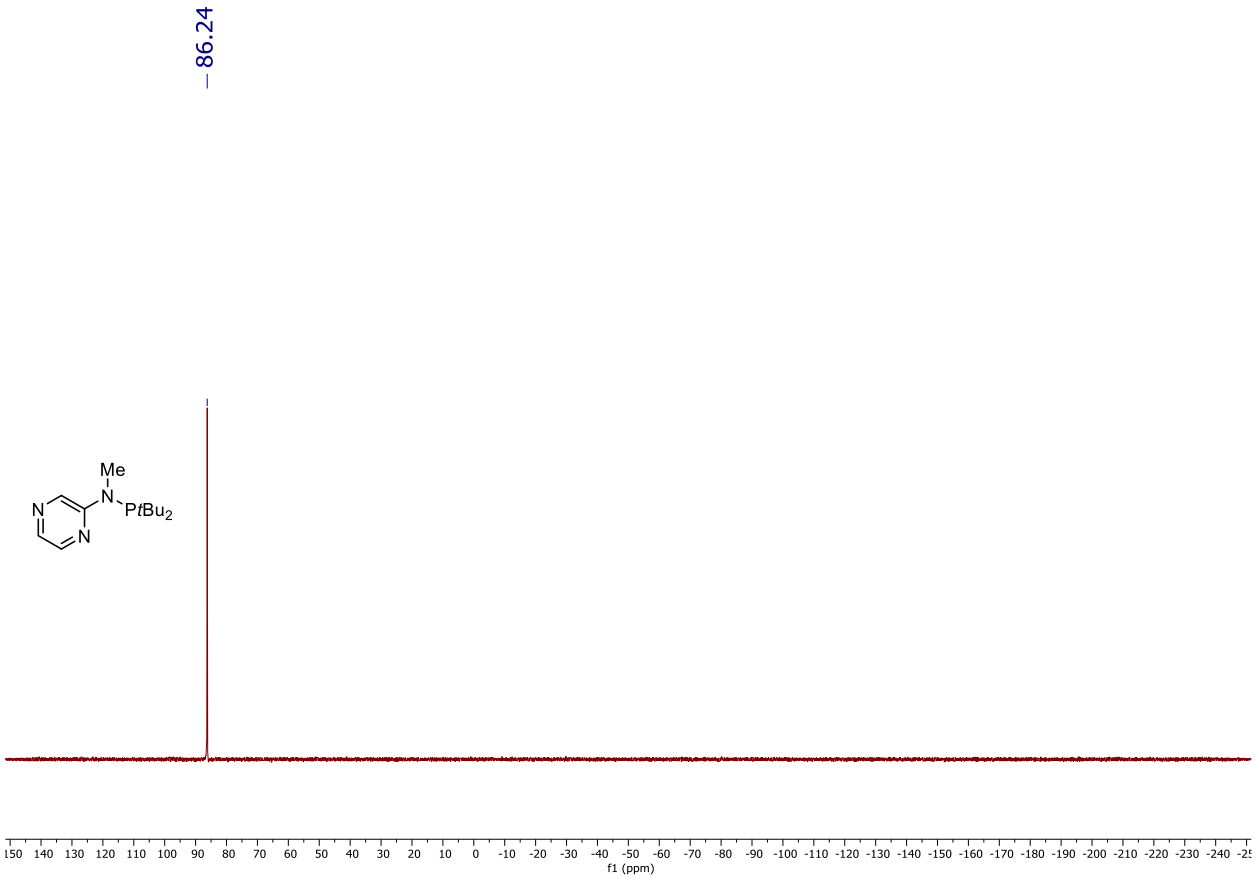

N-(di-tert-butylphosphaneyl)-N-methylpyrazin-2-amine 3.3-26$_{Cl}$

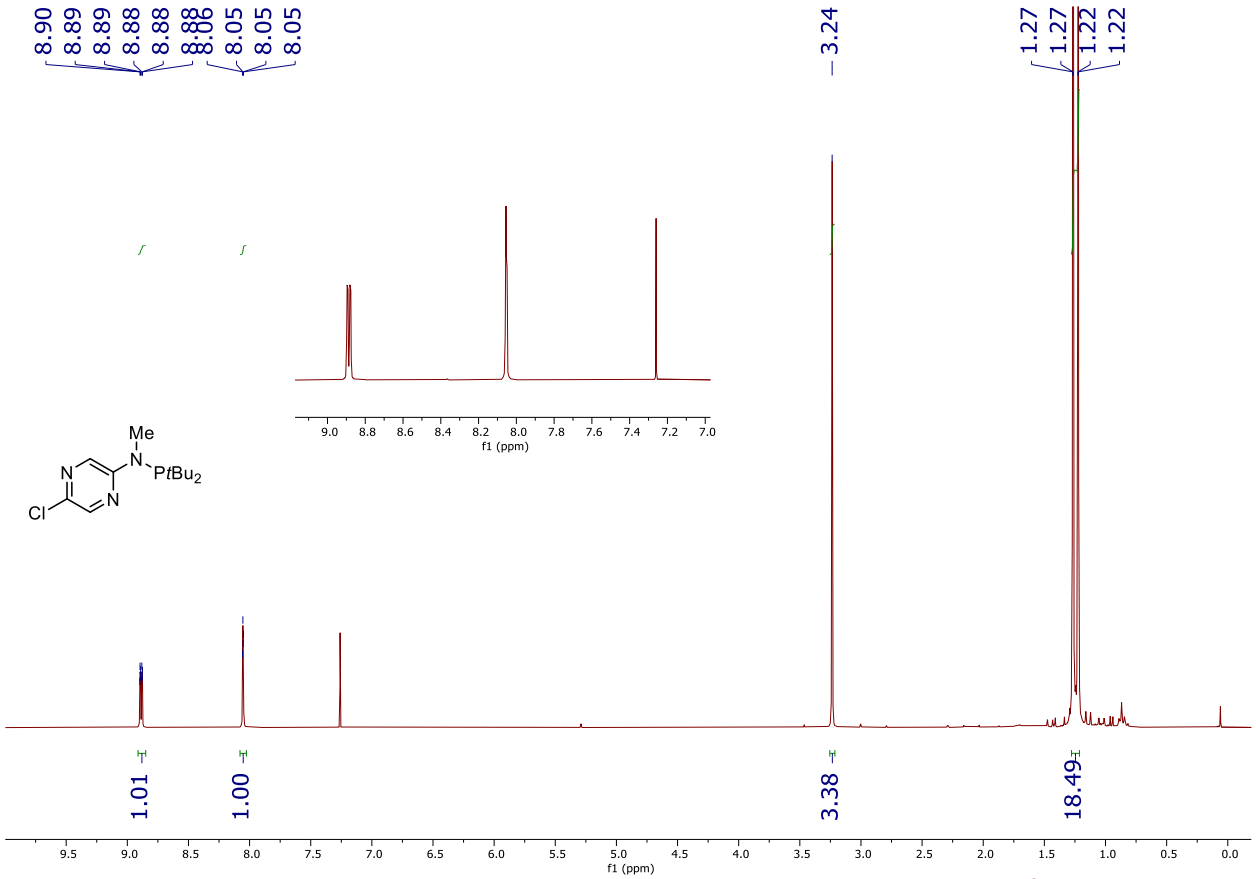
8.90
8.89
8.89
8.88
8.88
8.06
8.05
8.05
8.05
3.24
1.27
1.27
1.22
1.22
Me
N
PtBu2
Cl
N
N
1.01
1.00
3.38
18.49
f1 (ppm)

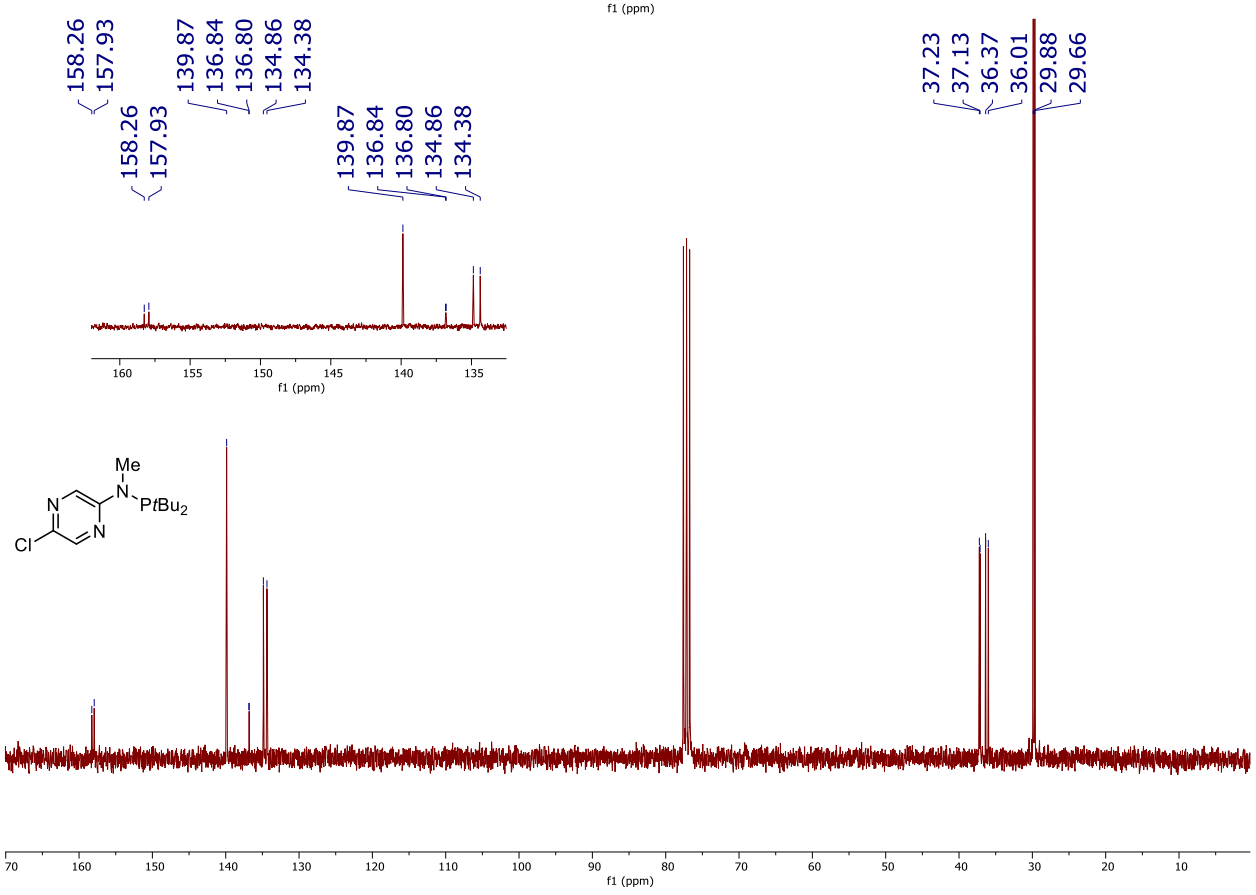
158.26
157.93
139.87
136.84
136.80
134.86
134.38
37.23
37.13
36.37
36.01
29.88
29.66
Me
N
PtBu2
Cl
N
N
f1 (ppm)

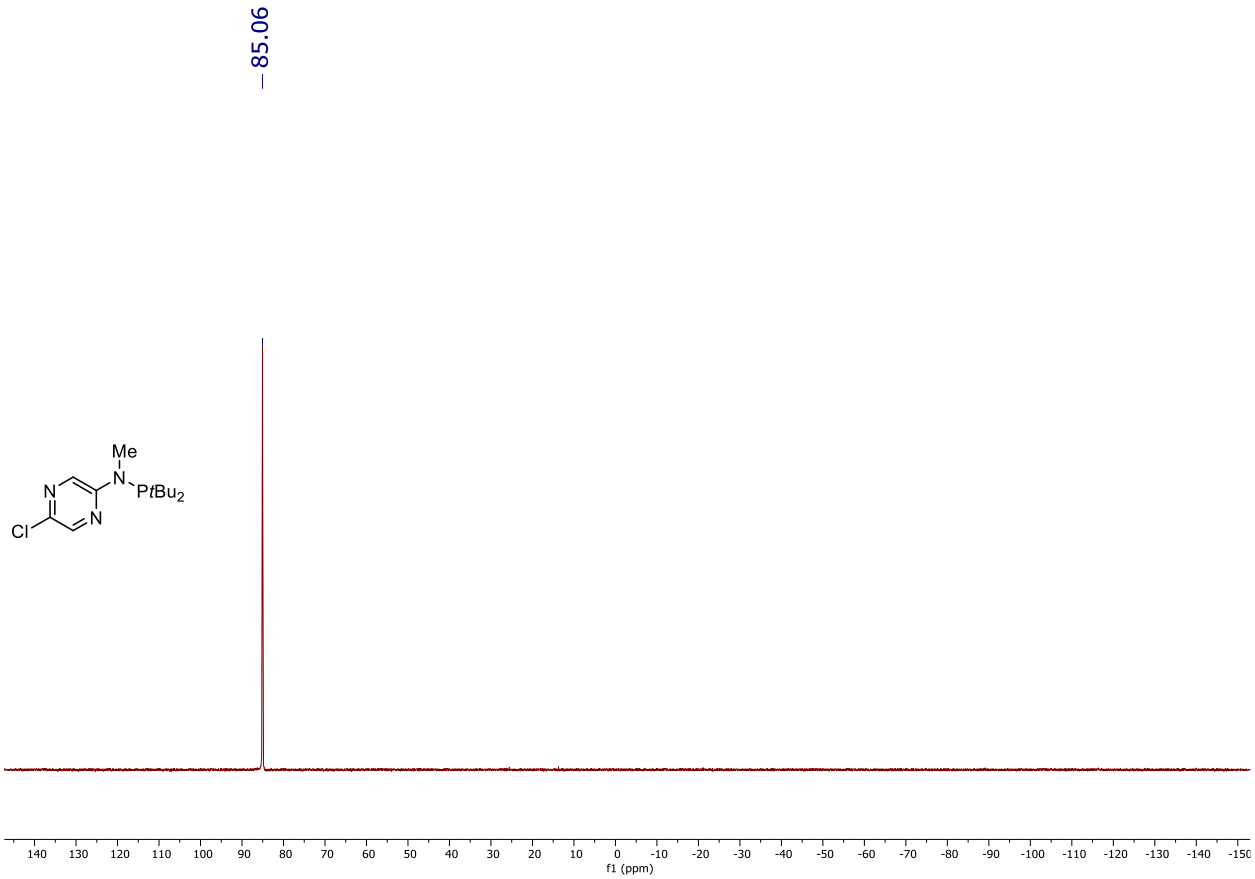

Gold (I) complex 3.3-11$_H$

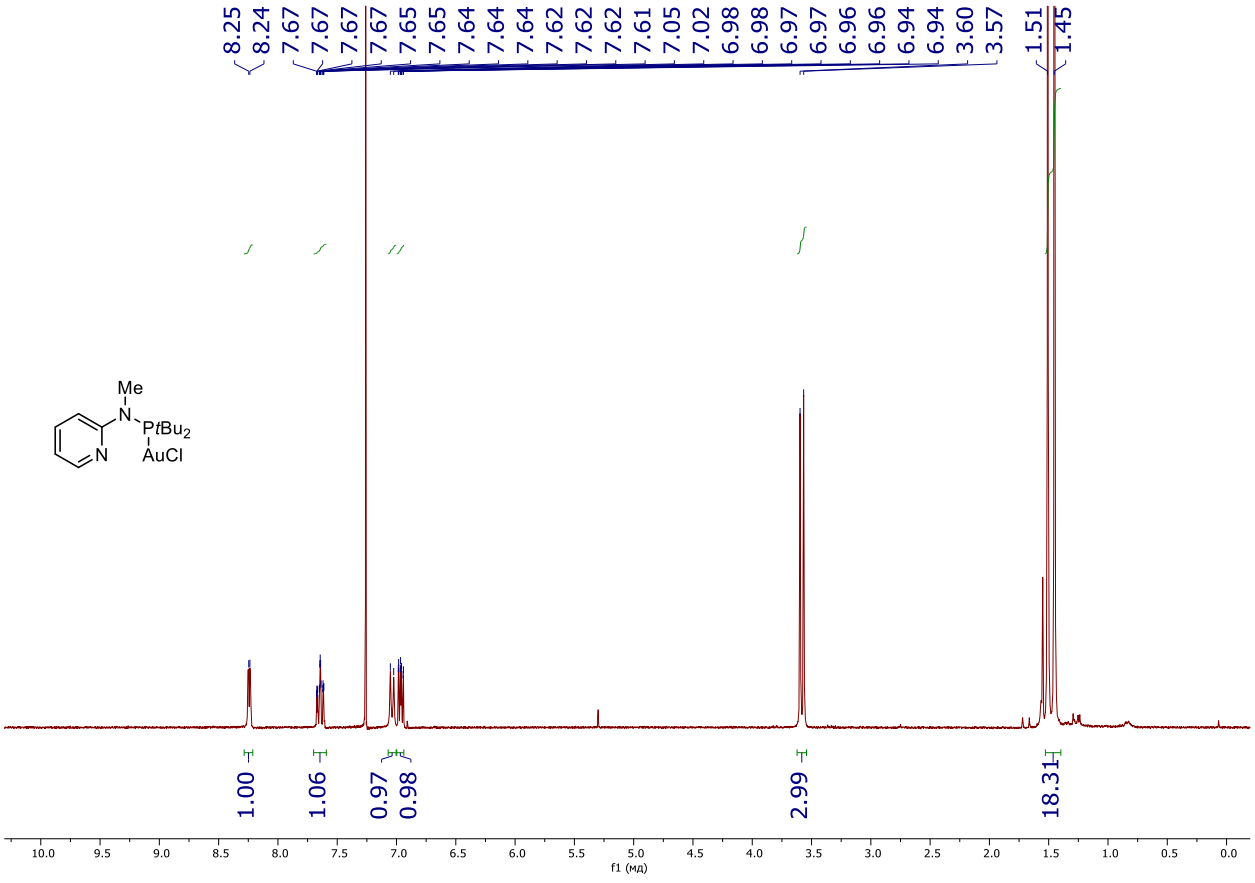

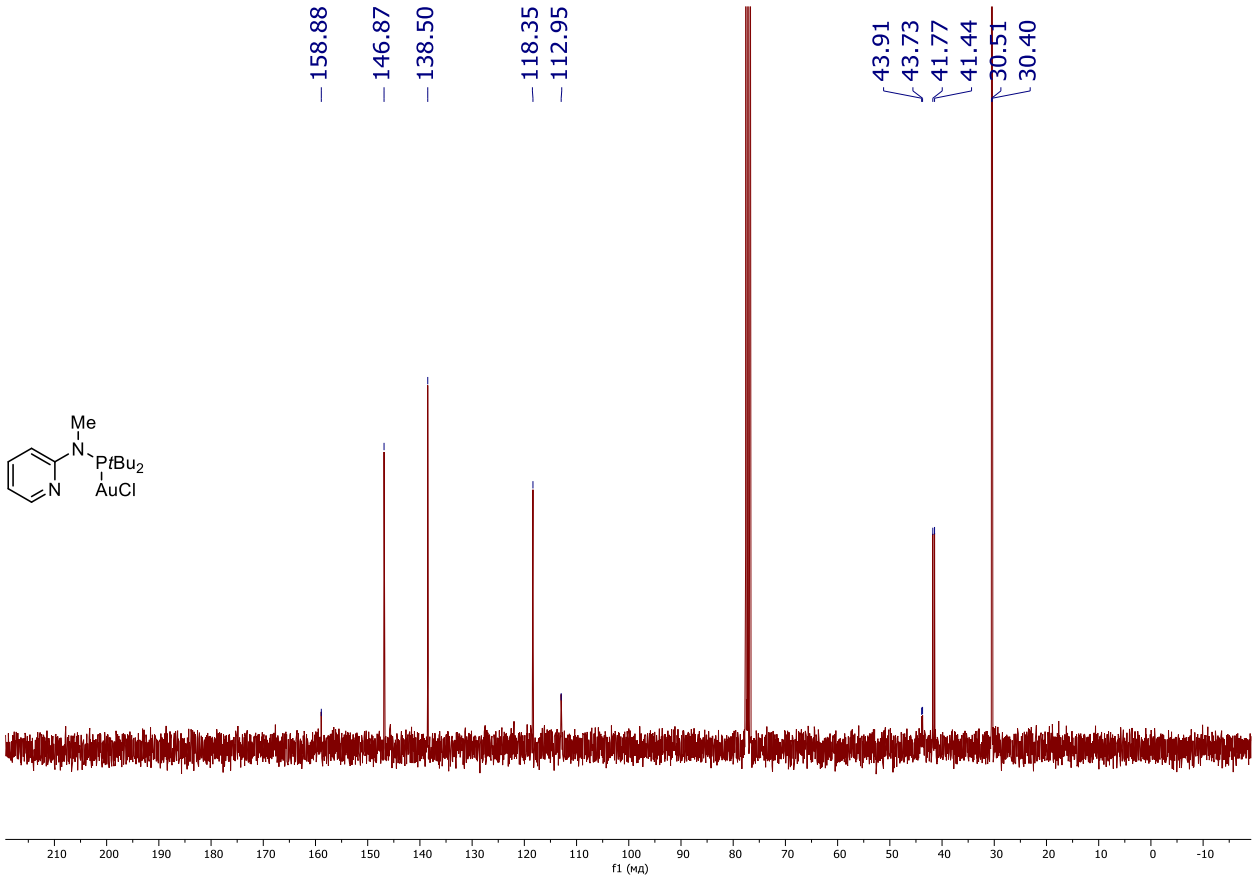

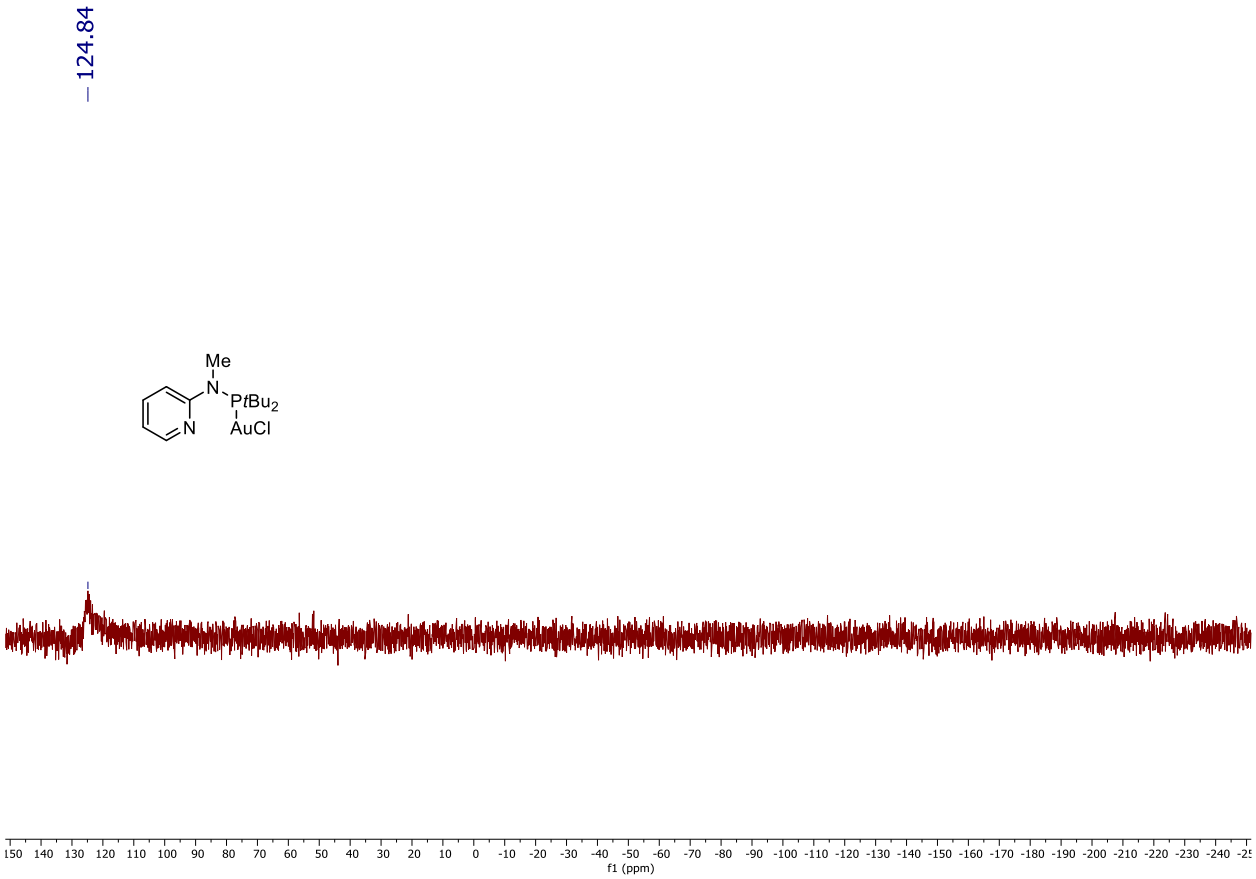

Gold (I) complex 3.3-11$_{OMe}$

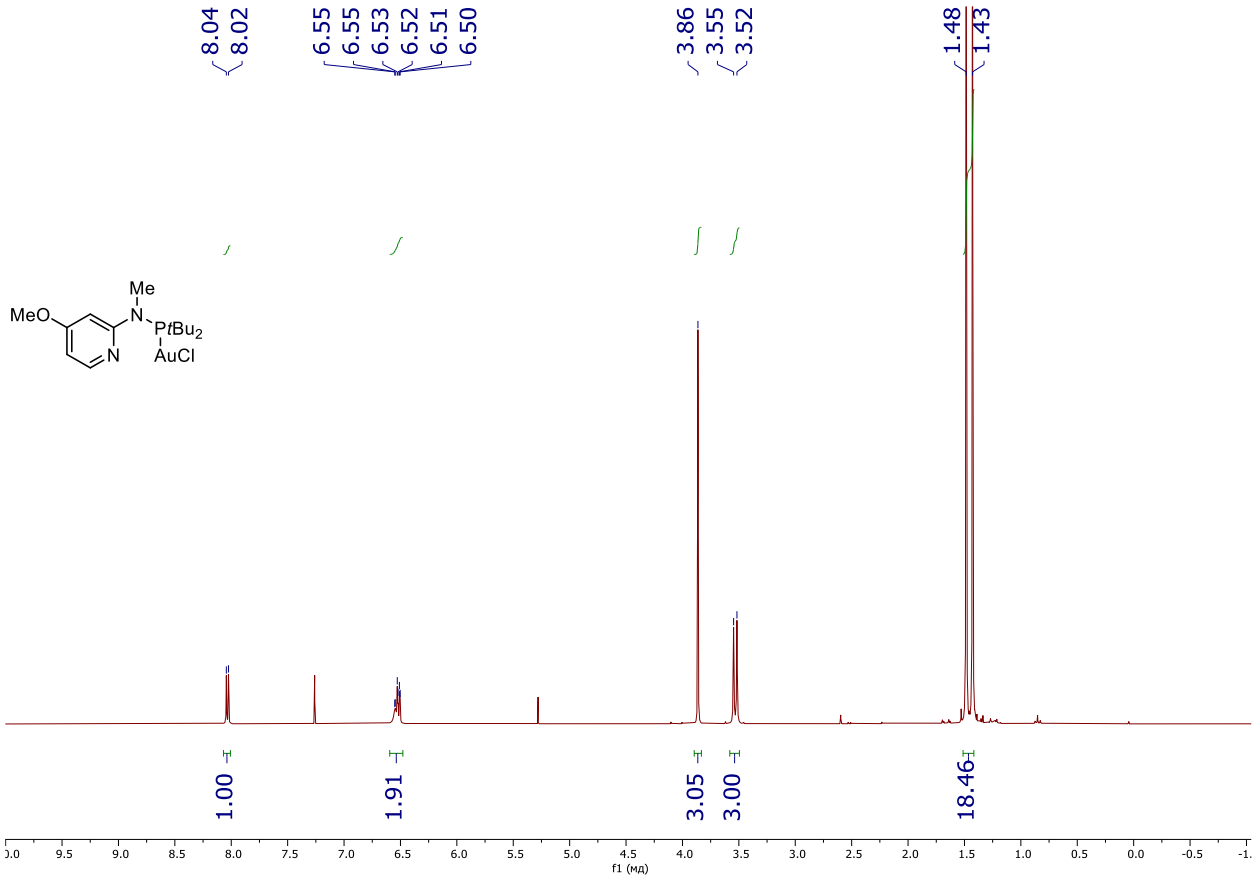
8.04
8.02
6.55
6.55
6.53
6.52
6.51
6.50
3.86
3.55
3.52
1.48
1.43
Me
MeO
N
PtBu2
AuCl
N
1.00
1.91
3.05
3.00
18.46
f1 (мд)

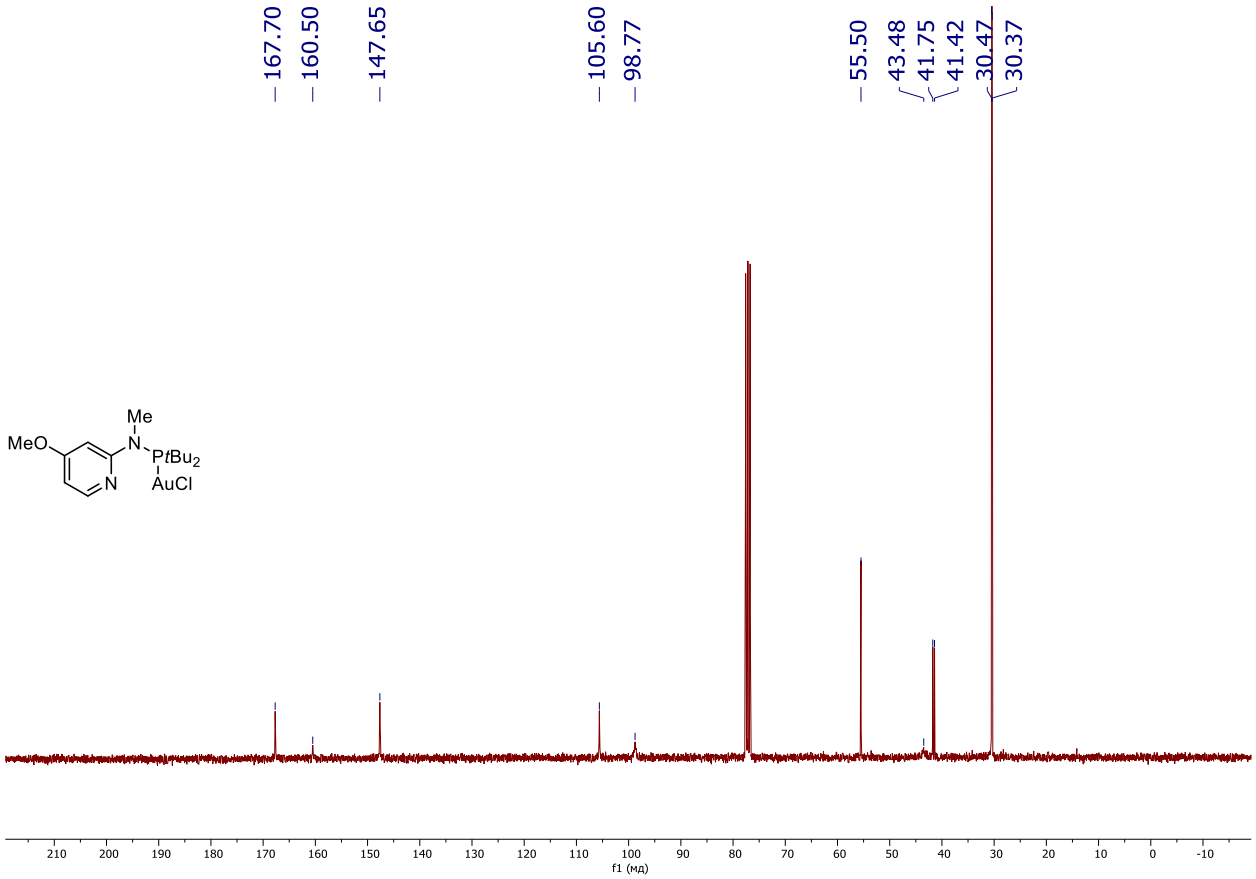
167.70
160.50
147.65
105.60
98.77
55.50
43.48
41.75
41.42
30.47
30.37
Me
MeO
N
PtBu2
AuCl
N
f1 (мд)

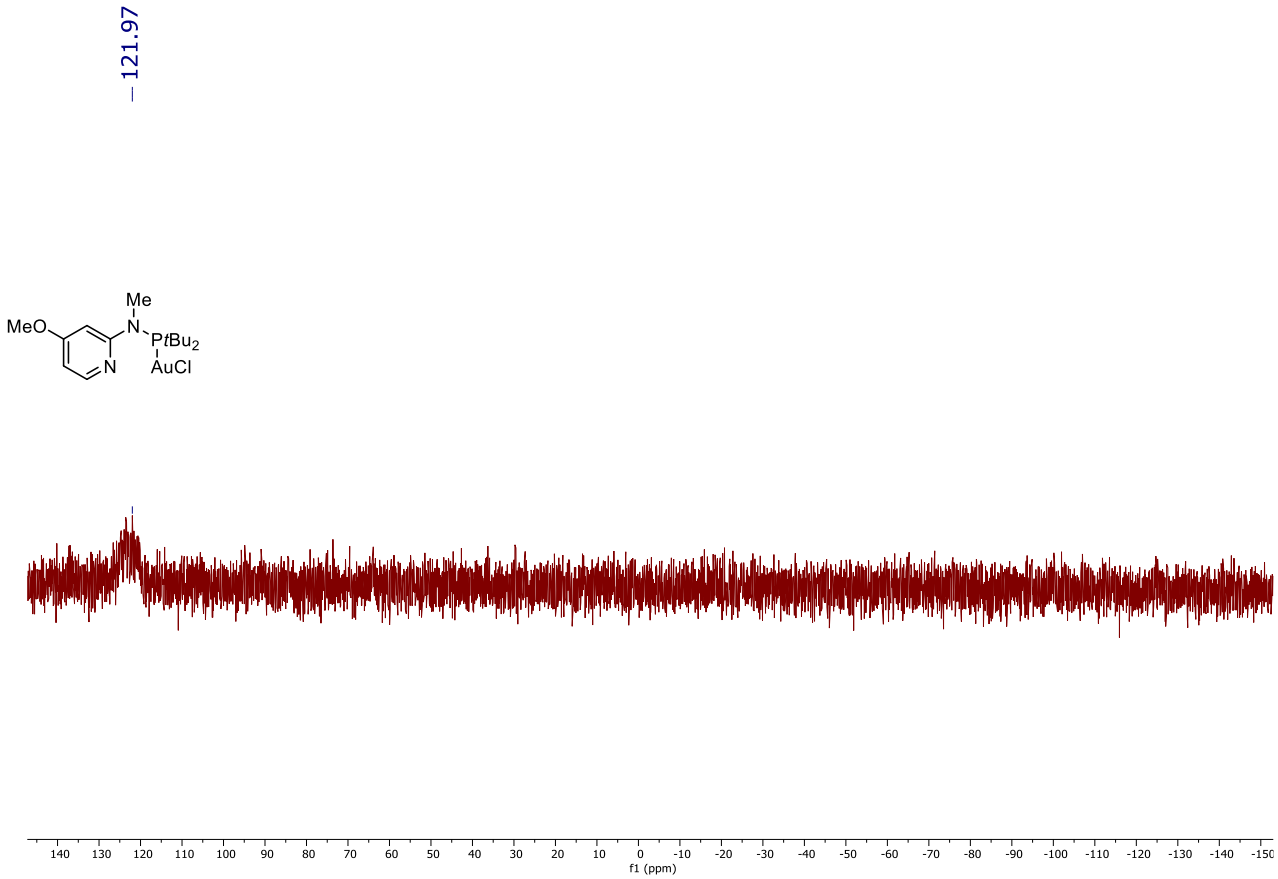

Gold (I) complex 3.3-11$_{CF3}$

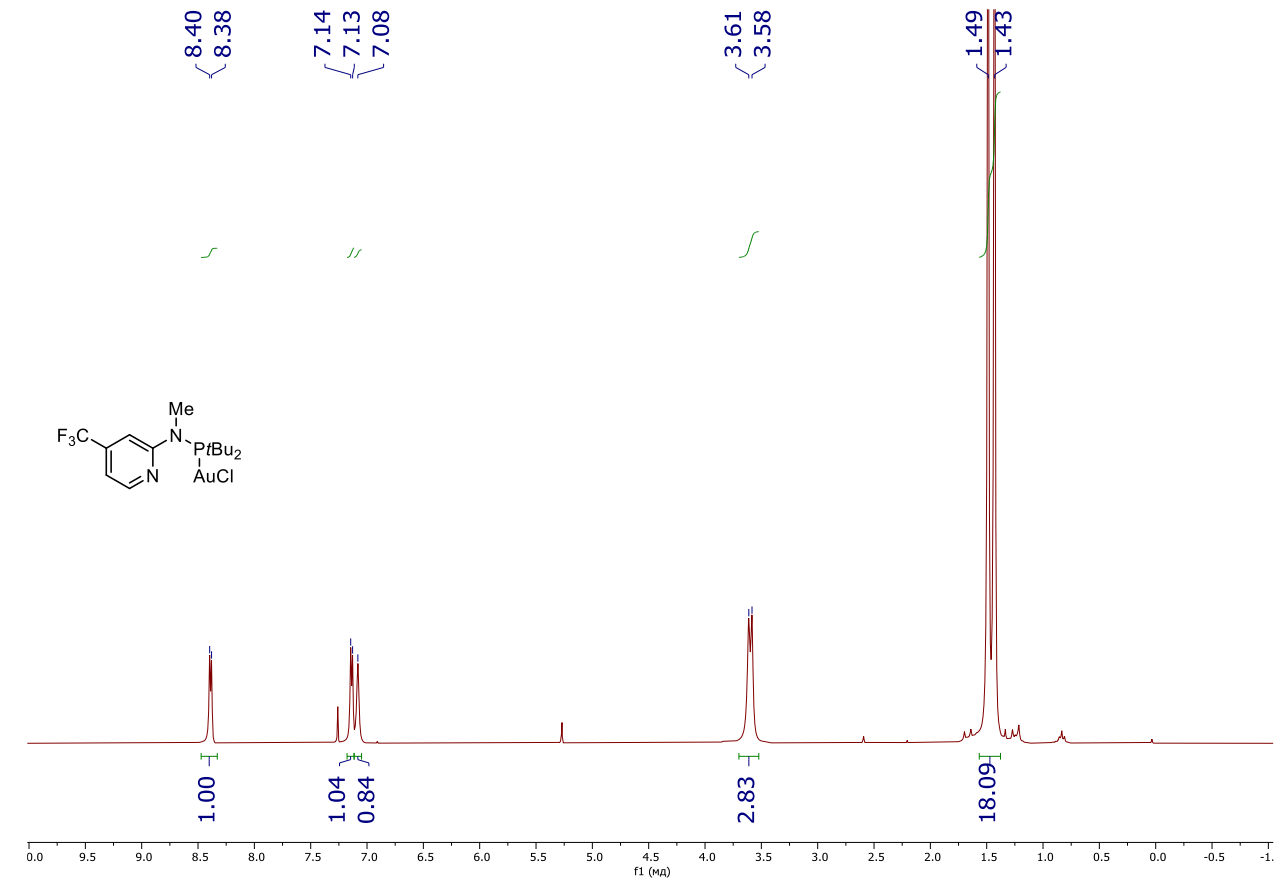

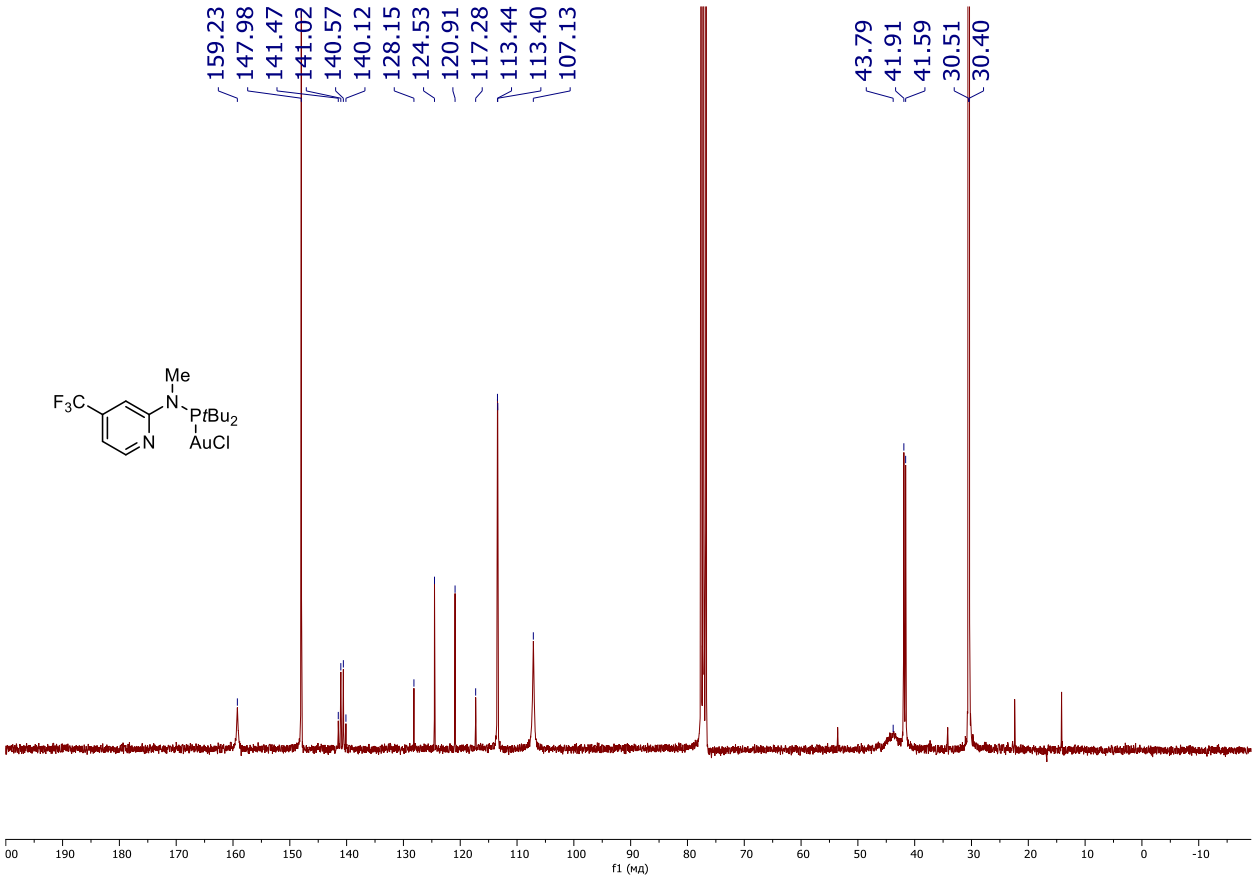
159.23
147.98
141.47
141.02
140.57
140.12
128.15
124.53
120.91
117.28
113.44
113.40
107.13
43.79
41.91
41.59
30.51
30.40
Me
N
F3C
PtBu2
AuCl
f1 (мд)

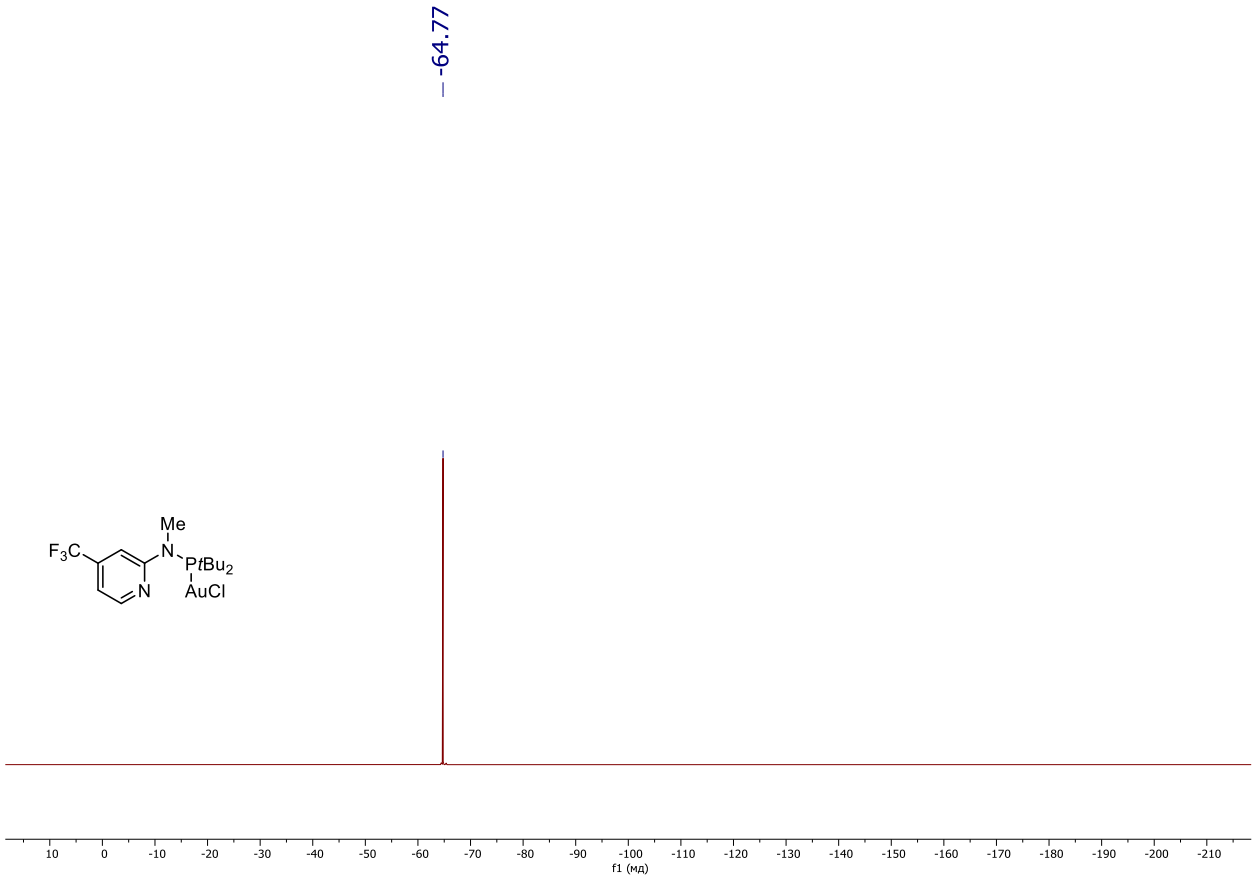
-64.77
Me
N
F3C
PtBu2
AuCl
f1 (мд)

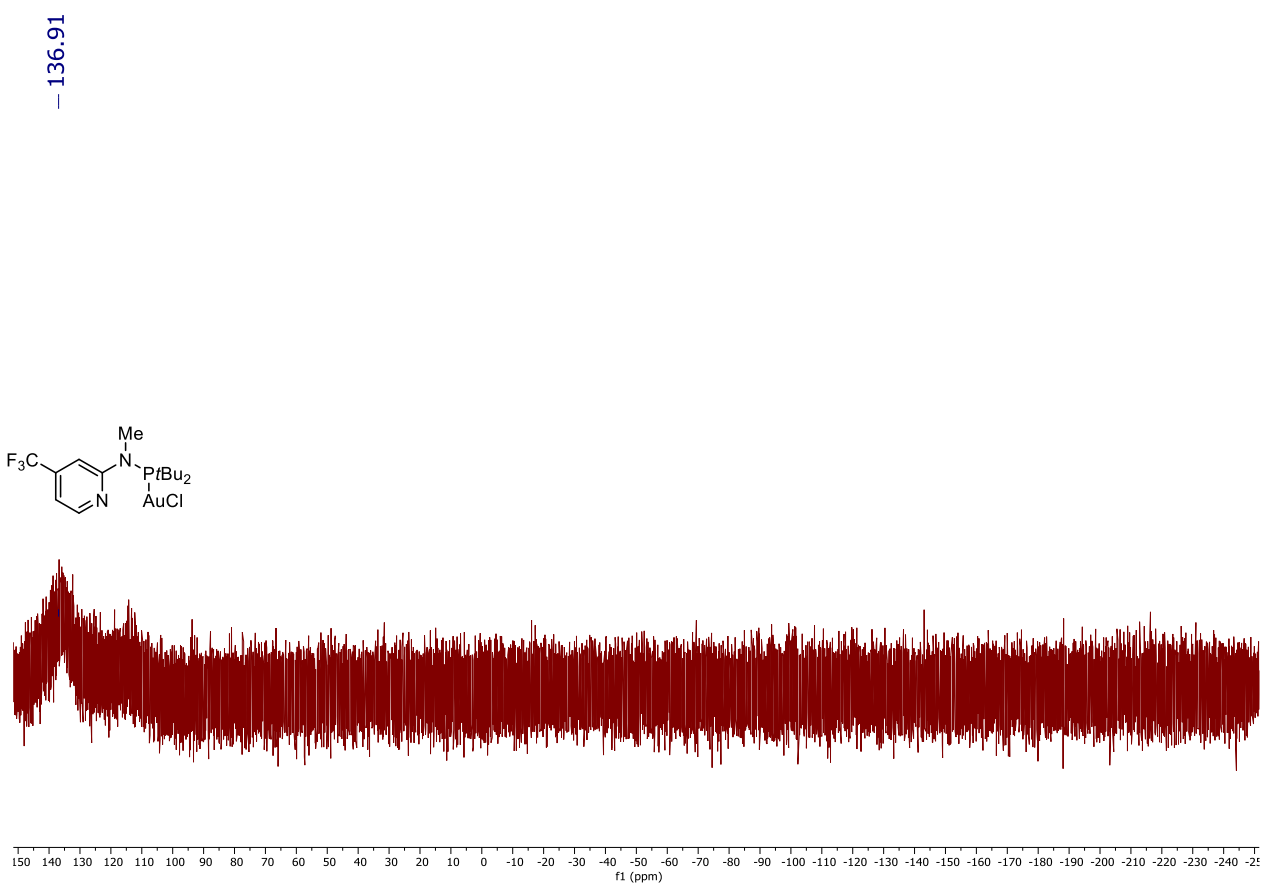

Gold (I) complex 3.3-27$_H$

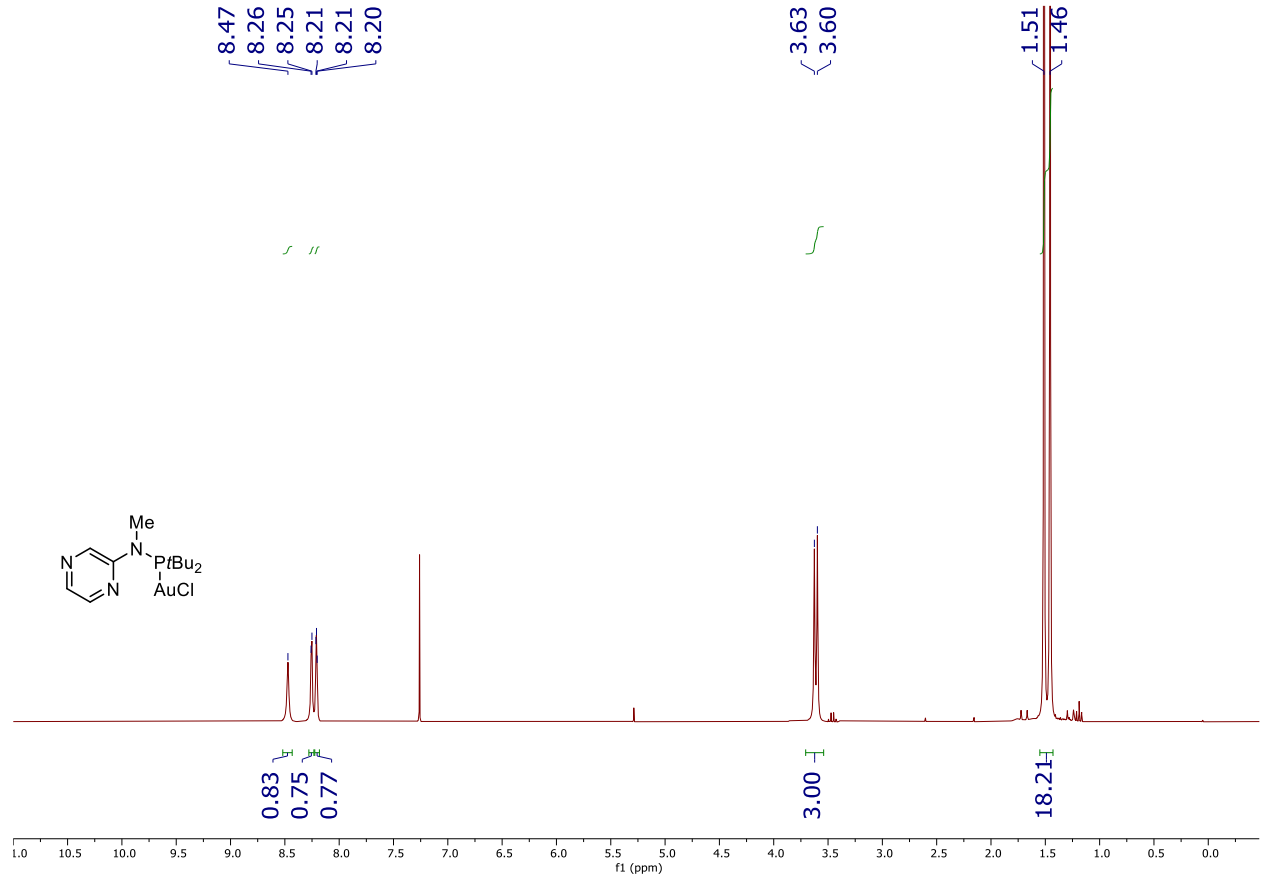

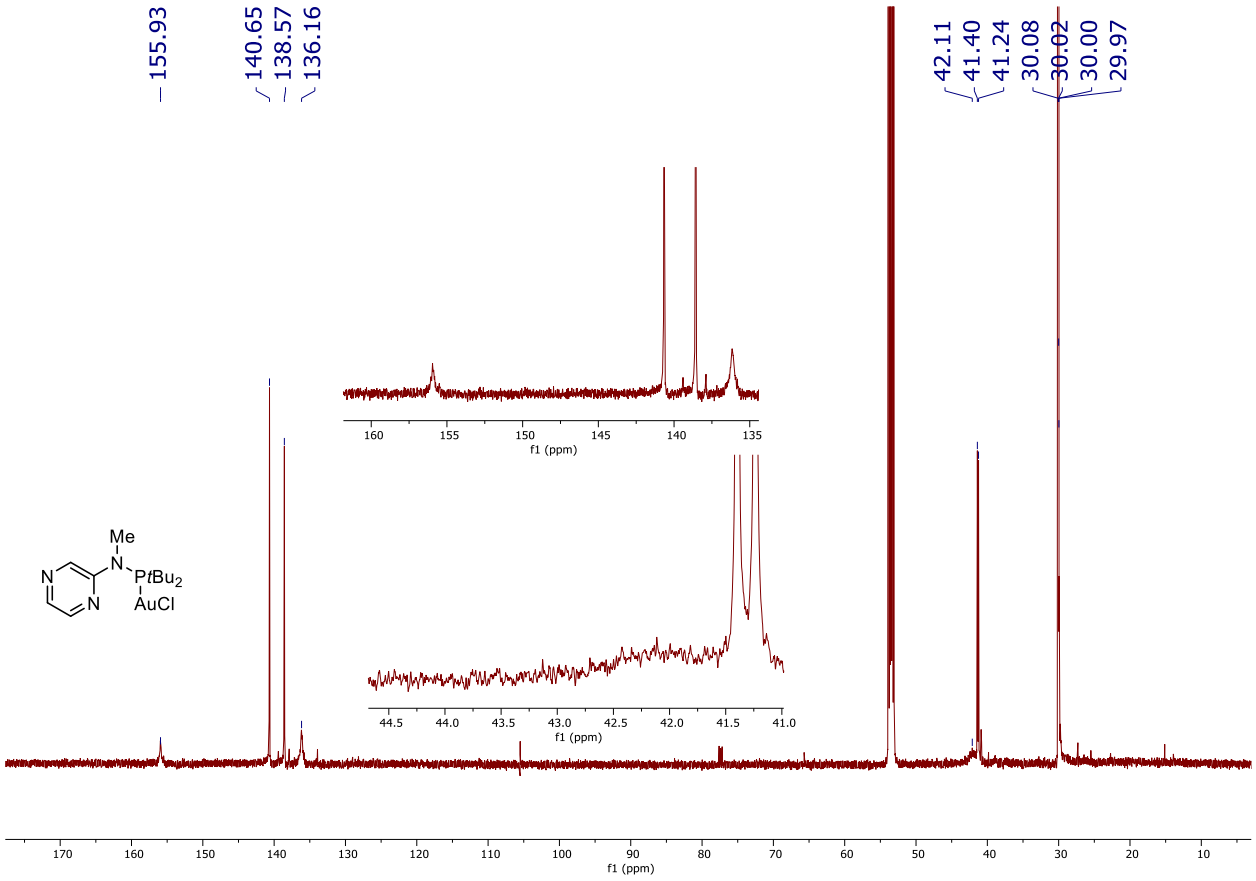

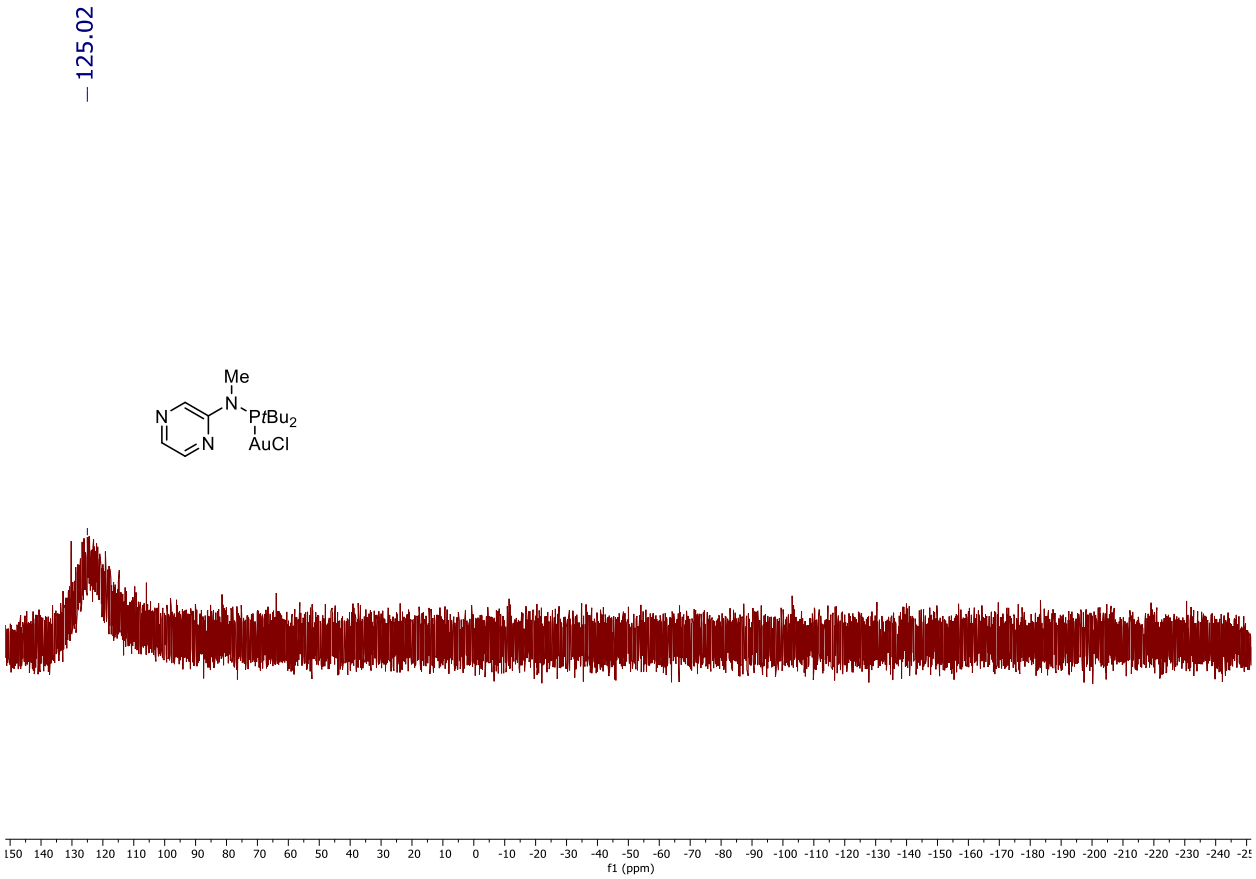

Gold (I) complex 3.3-27$_{Cl}$

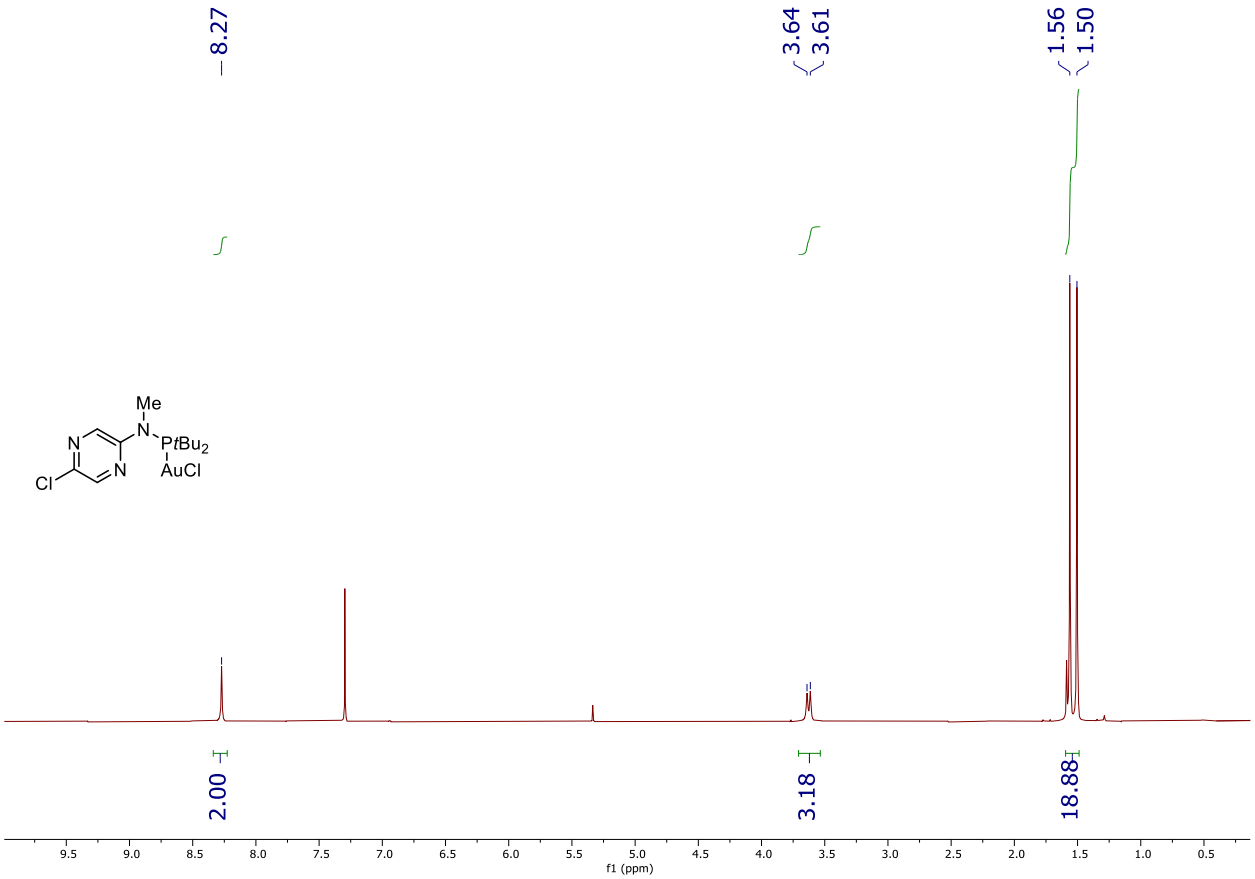
8.27
3.64
3.61
1.56
1.50
Me
N
N
PtBu2
AuCl
Cl
N
2.00
3.18
18.88
f1 (ppm)

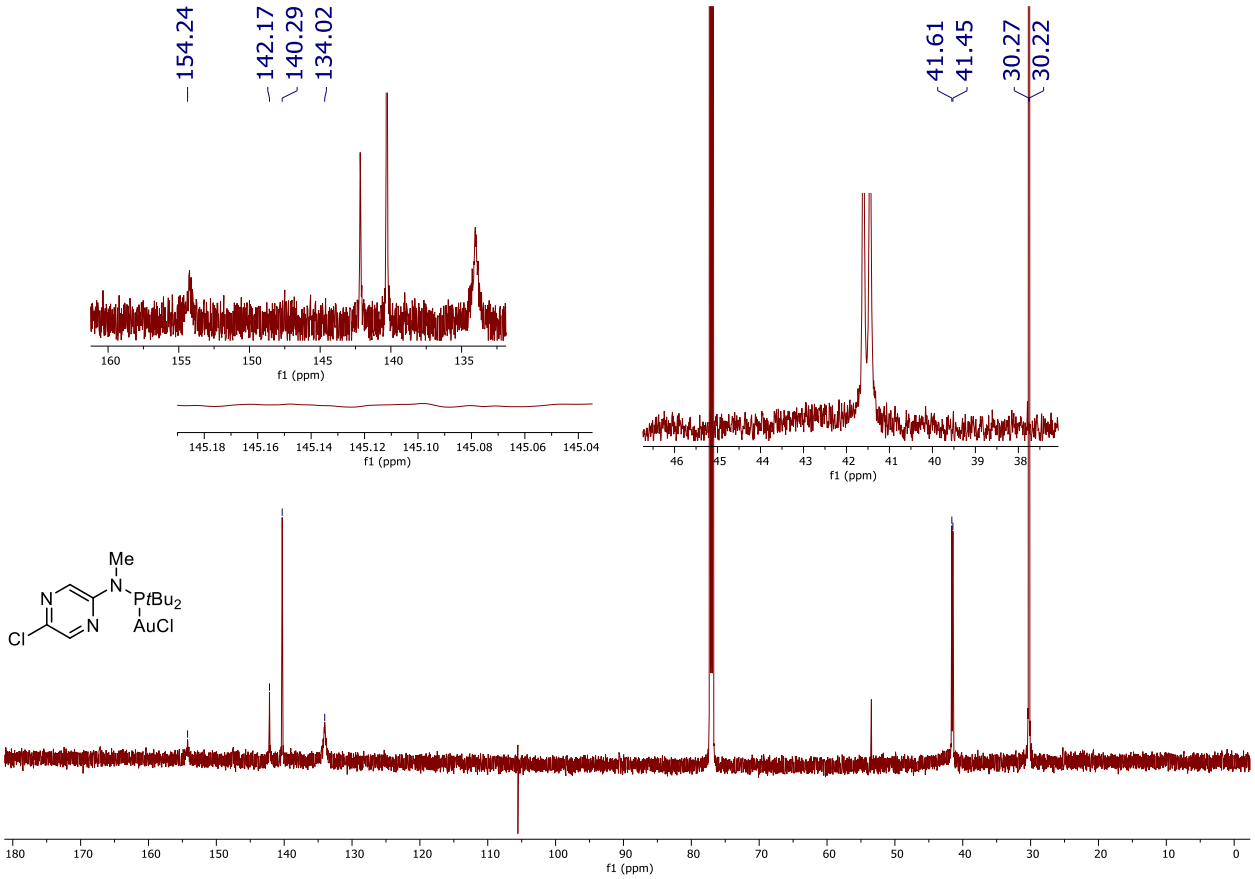
154.24
142.17
140.29
134.02
41.61
41.45
30.27
30.22
f1 (ppm)
Me
N
N
PtBu2
AuCl
Cl
N

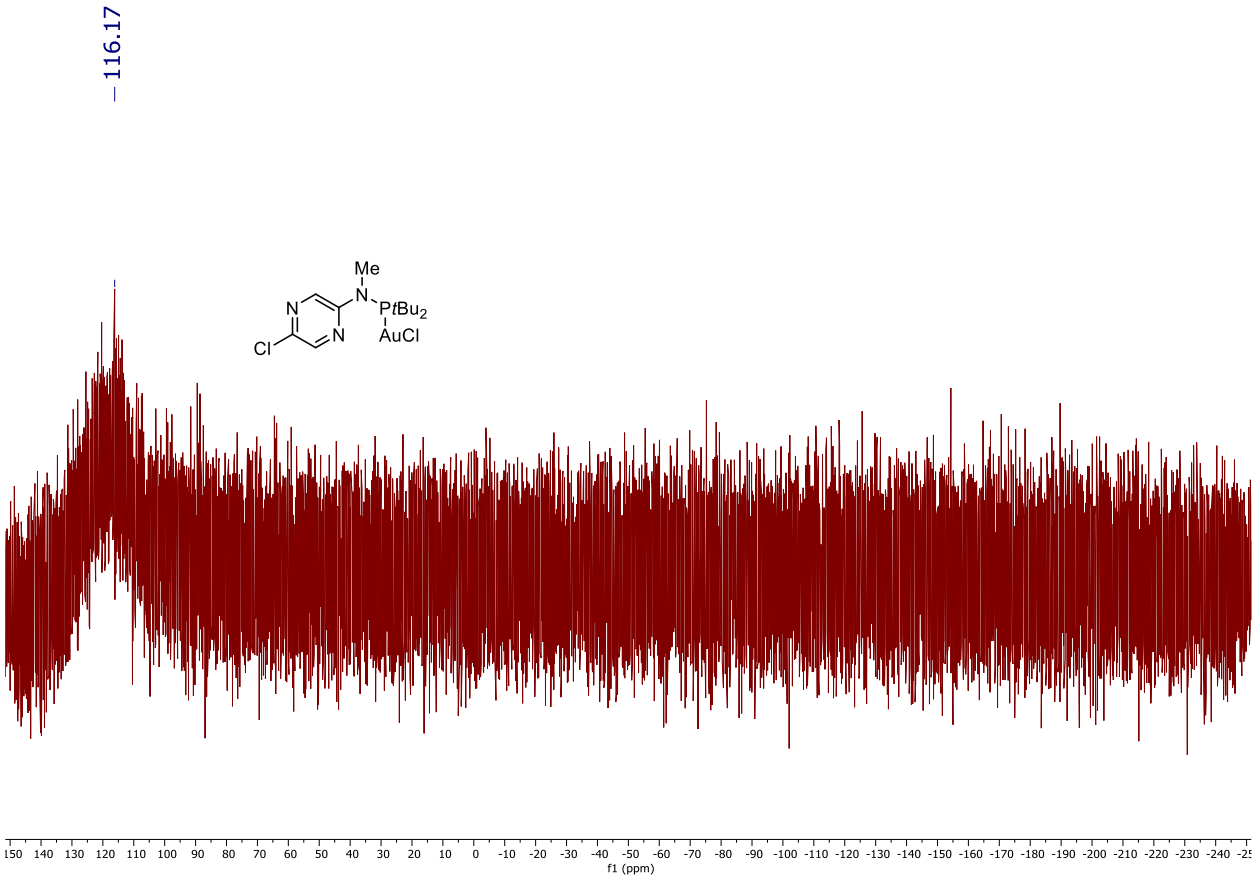

Gold (III) complex 3.3-12$_H$

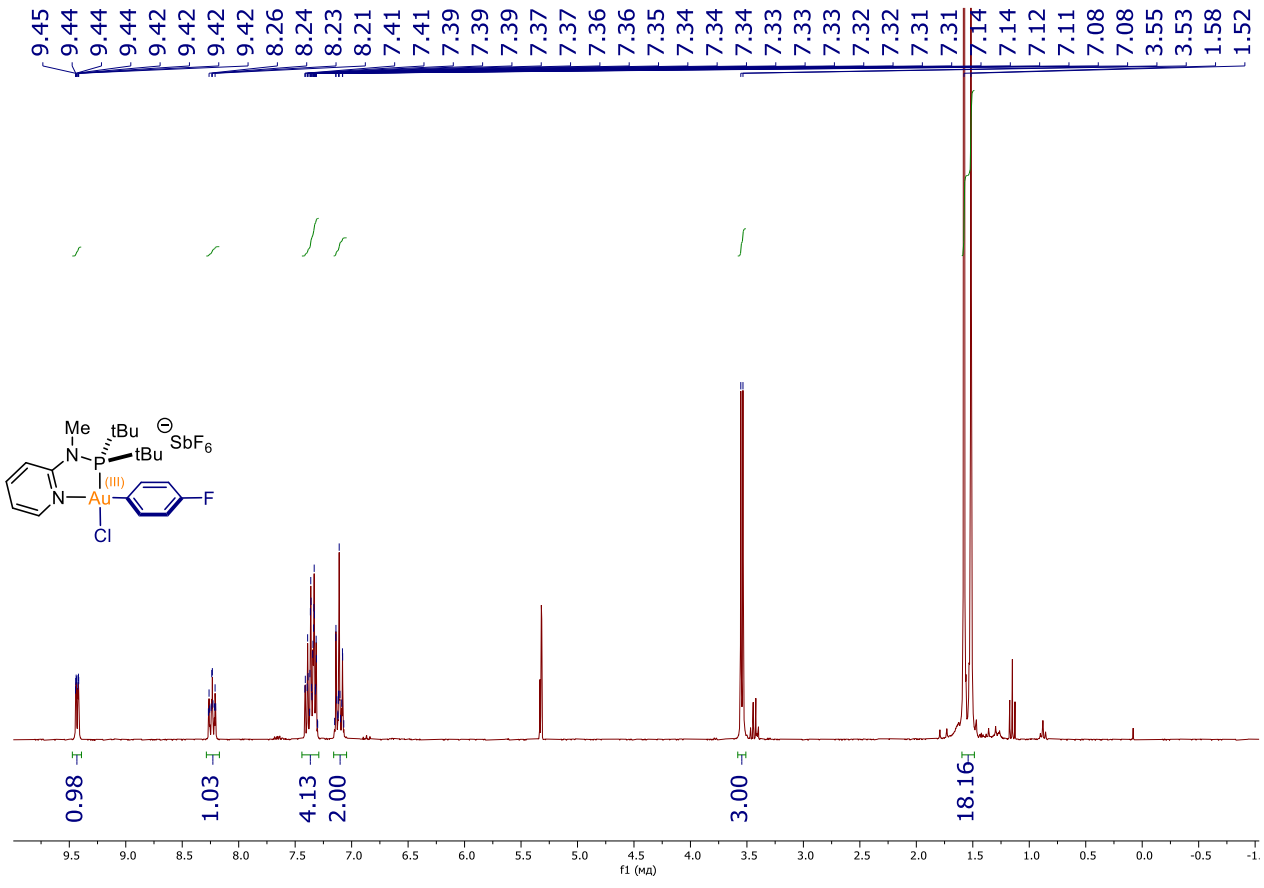

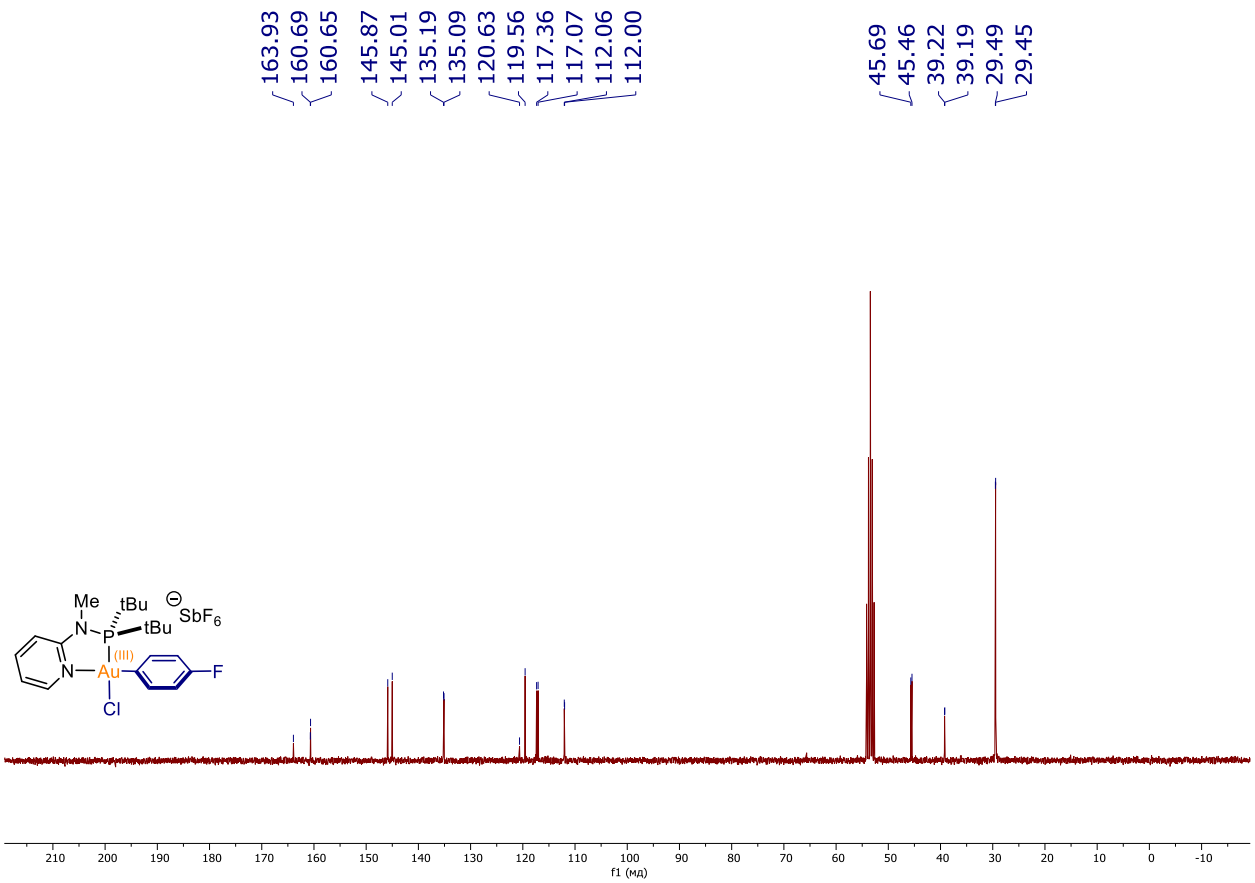
163.93
160.69
160.65
145.87
145.01
135.19
135.09
120.63
119.56
117.36
117.07
112.06
112.00
45.69
45.46
39.22
39.19
29.49
29.45
Me
tBu
tBu
SbF6
P
N
N
Au
(III)
Cl
F
f1 (мд)

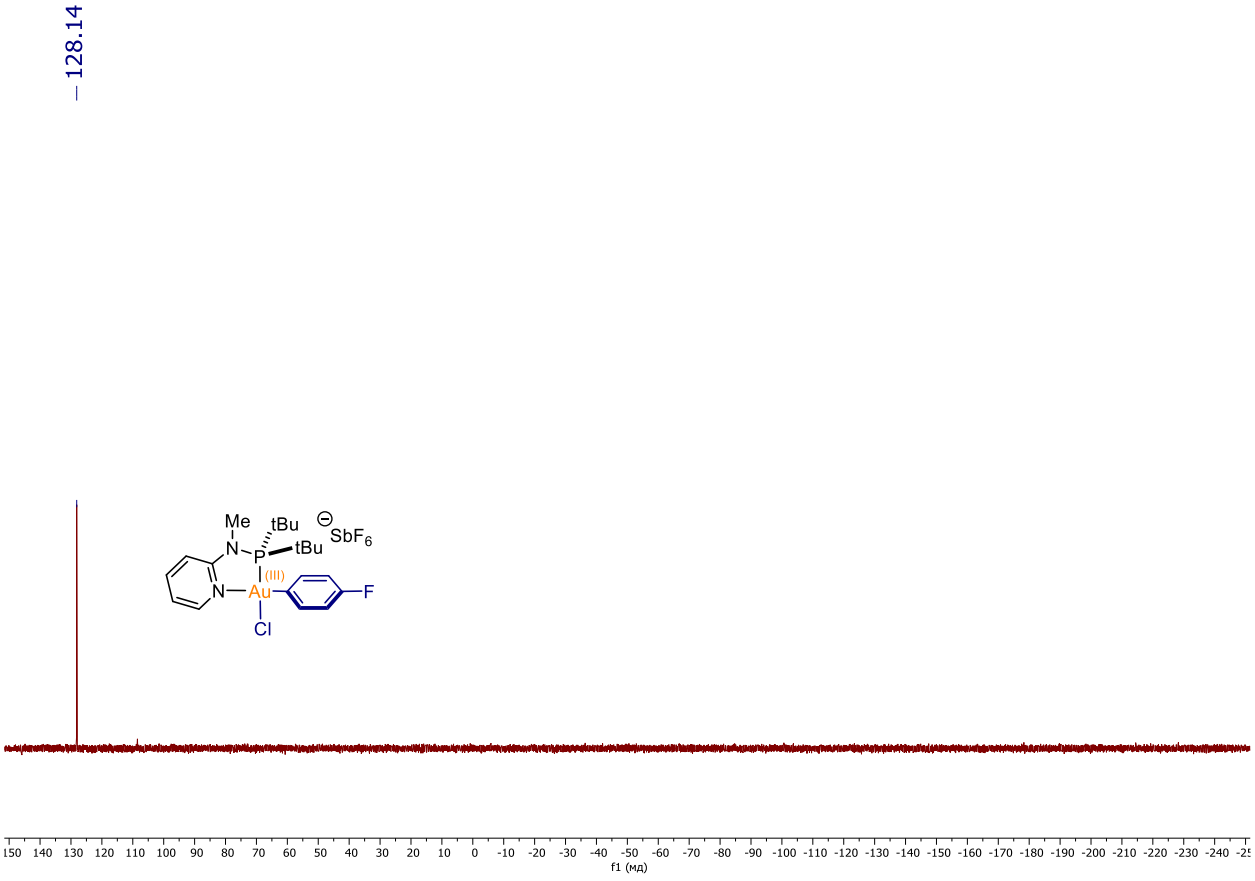
128.14
Me
tBu
tBu
SbF6
P
N
N
Au
(III)
Cl
F
f1 (мд)

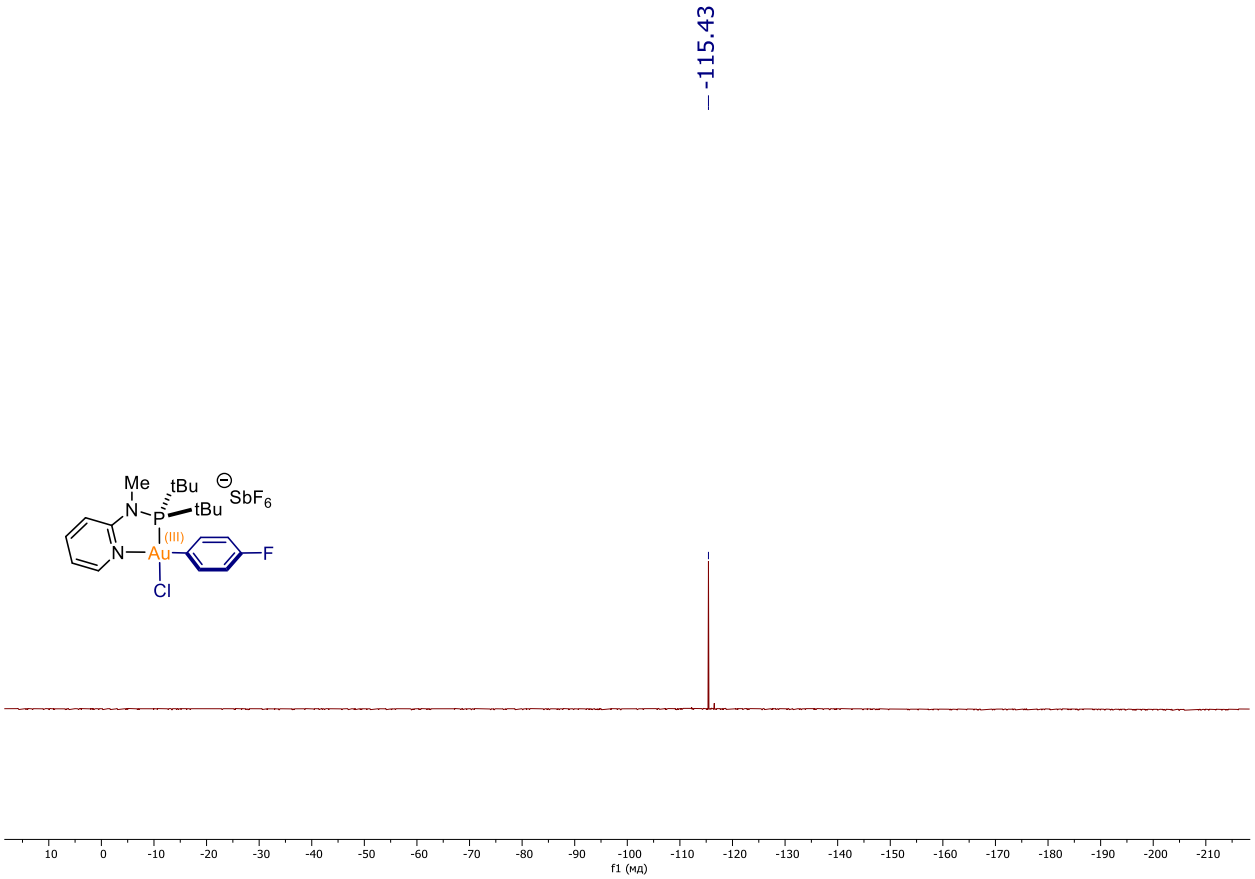

Gold (III) complex 3.3-12$_{OMe}$

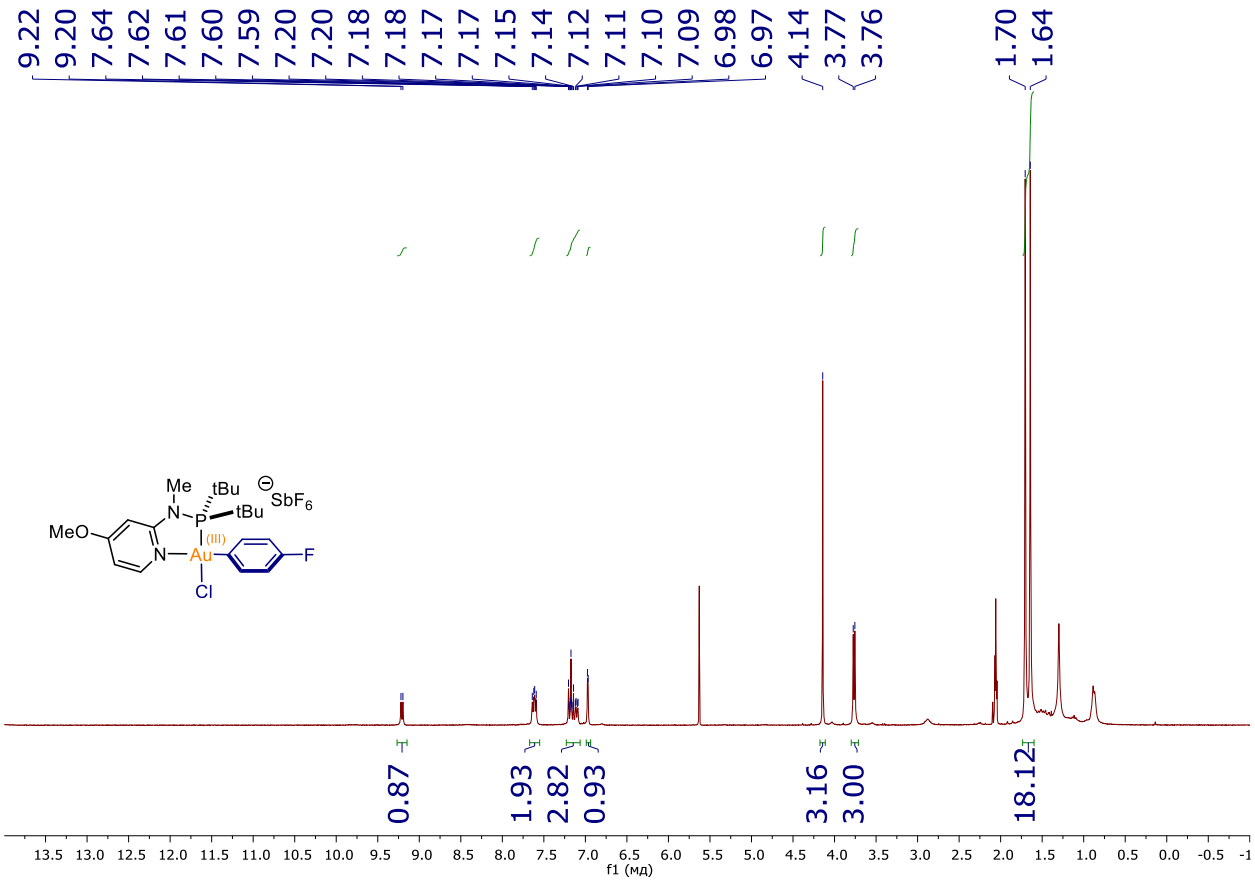

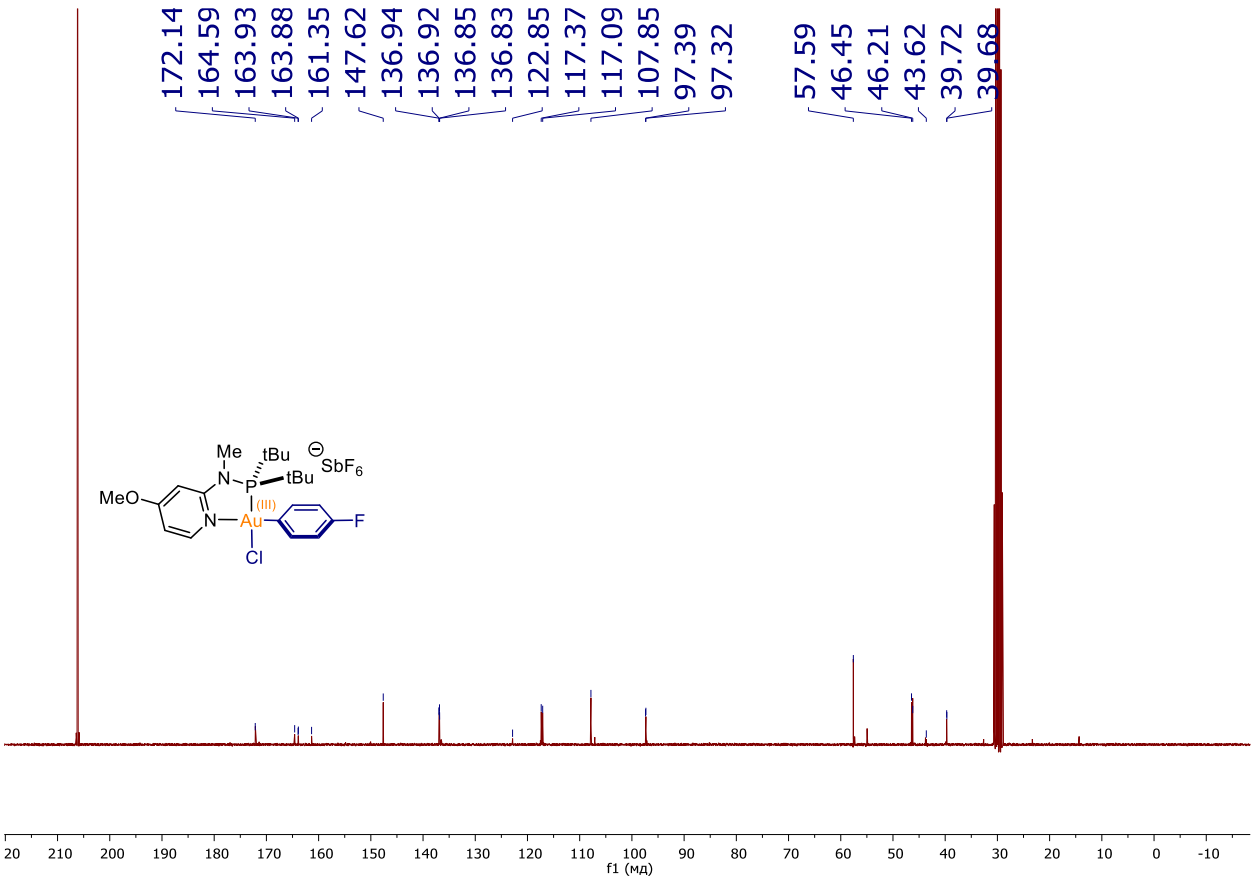
172.14
164.59
163.93
163.88
161.35
147.62
136.94
136.92
136.85
136.83
122.85
117.37
117.09
107.85
97.39
97.32
57.59
46.45
46.21
43.62
39.72
39.68
Me
tBu
tBu
SbF6
MeO
N
P
Au
(III)
F
Cl
20 210 200 190 180 170 160 150 140 130 120 110 100 90 80 70 60 50 40 30 20 10 0 -10
f1 (мд)

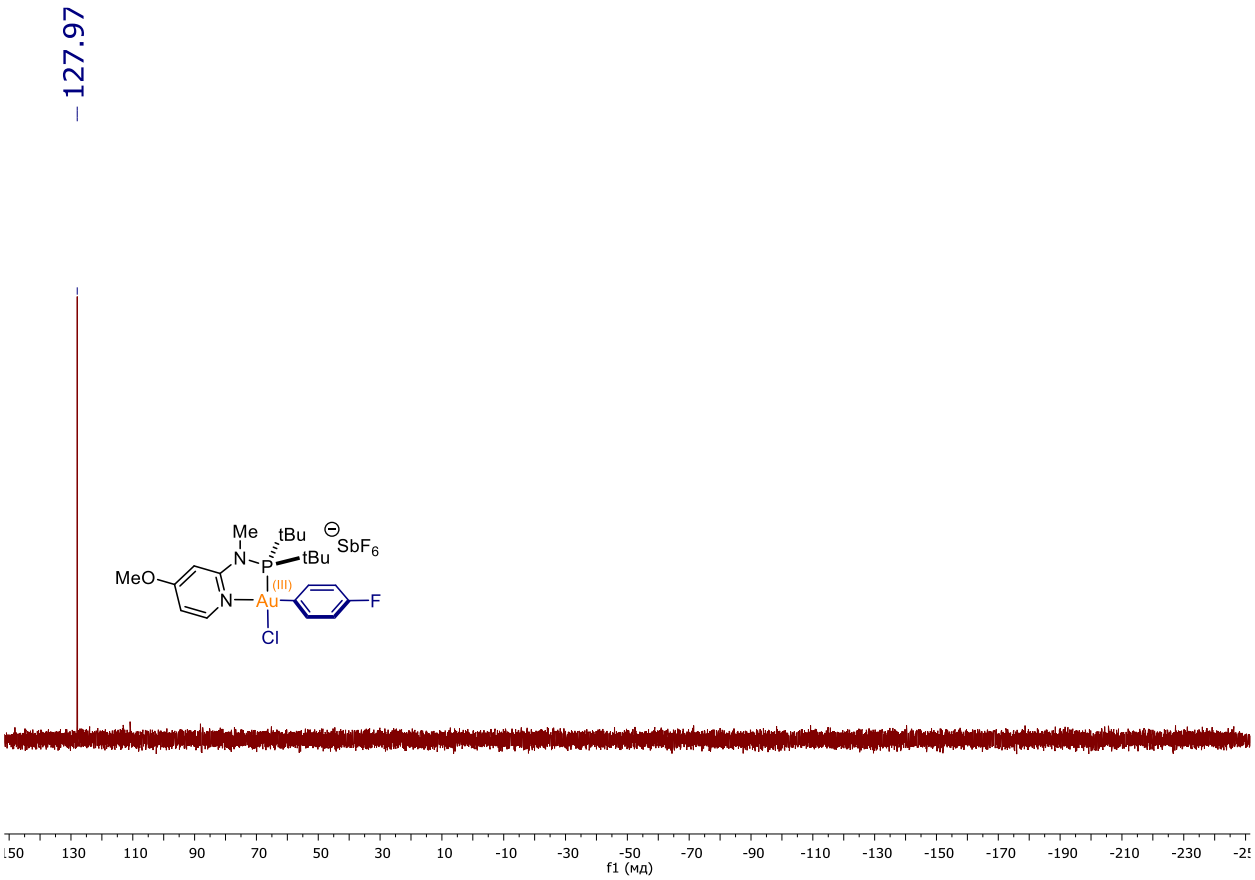
127.97
Me
tBu
tBu
SbF6
MeO
N
P
Au
(III)
F
Cl
150 130 110 90 70 50 30 10 -10 -30 -50 -70 -90 -110 -130 -150 -170 -190 -210 -230
f1 (мд)

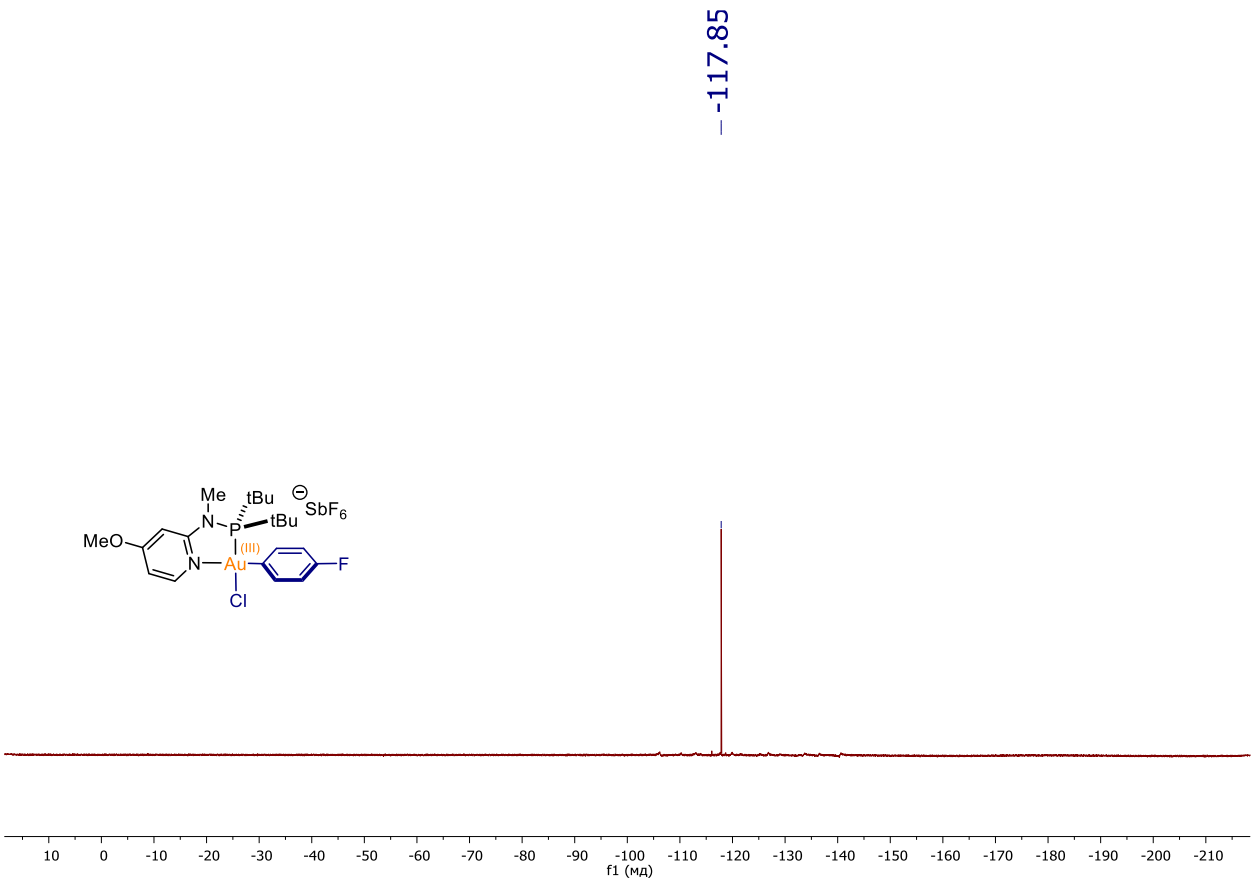

Gold (III) complex 3.3-12$_{CF3}$

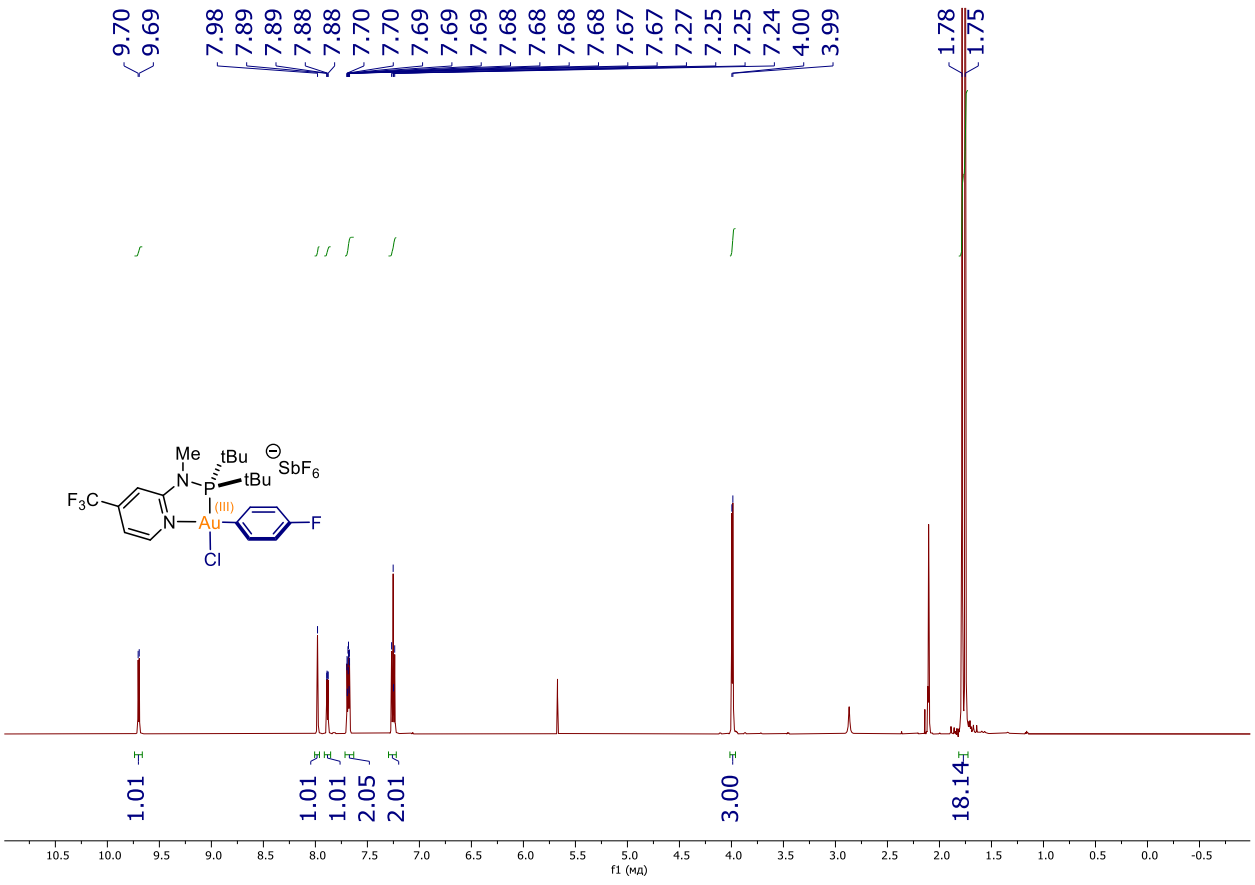

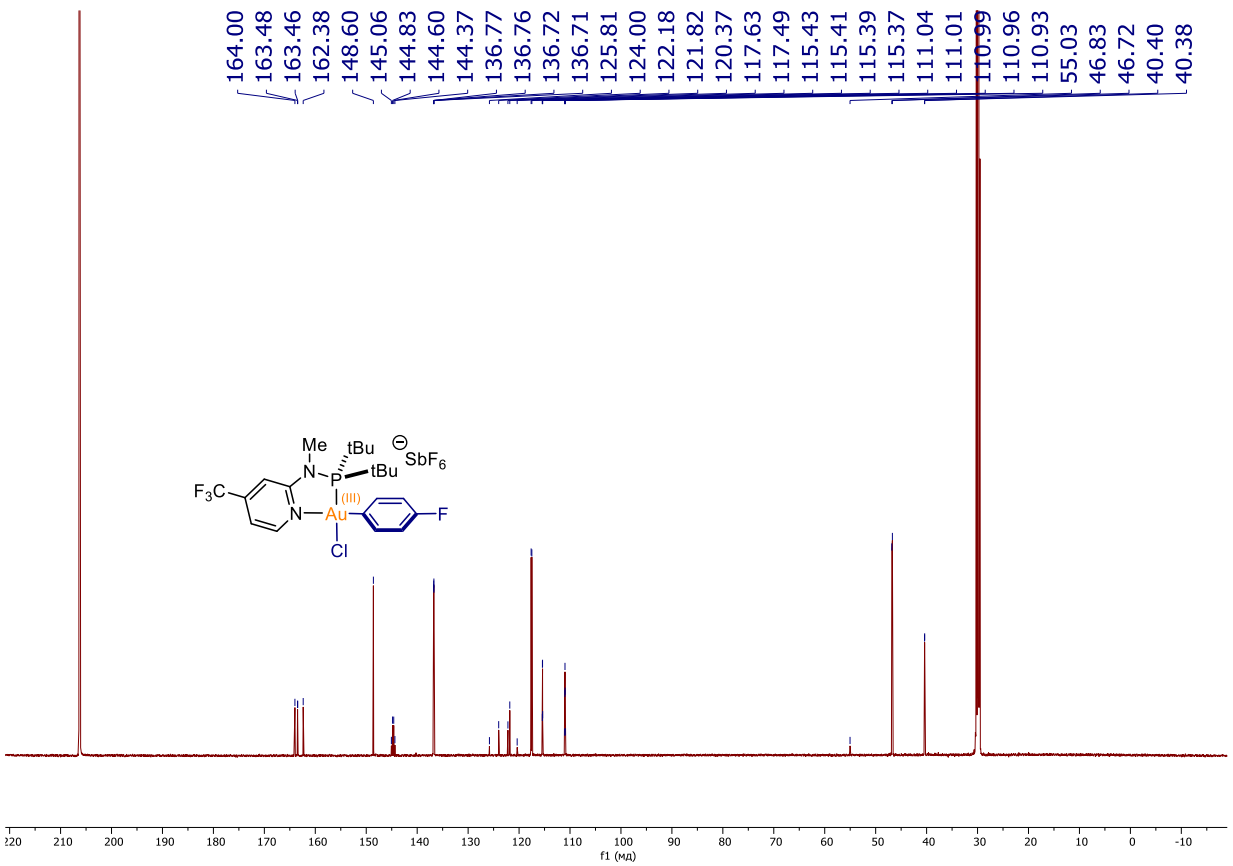
164.00
163.48
163.46
162.38
148.60
145.06
144.83
144.60
144.37
136.77
136.76
136.72
136.71
125.81
124.00
122.18
121.82
120.37
117.63
117.49
115.43
115.41
115.39
115.37
111.04
111.01
110.99
110.96
110.93
55.03
46.83
46.72
40.40
40.38
Me
tBu
tBu
SbF6
F3C
N
P
(III)
Au
F
Cl
f1 (мд)

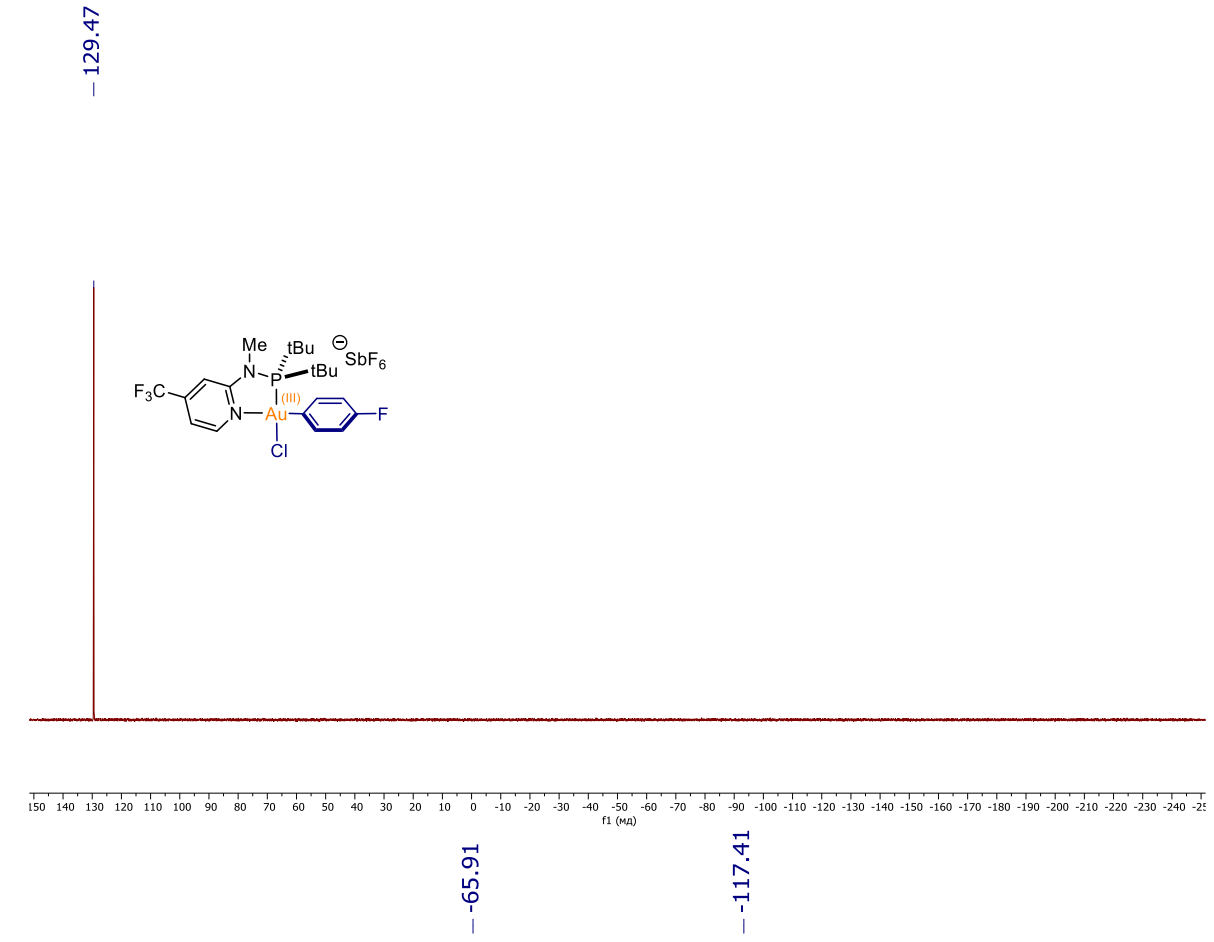

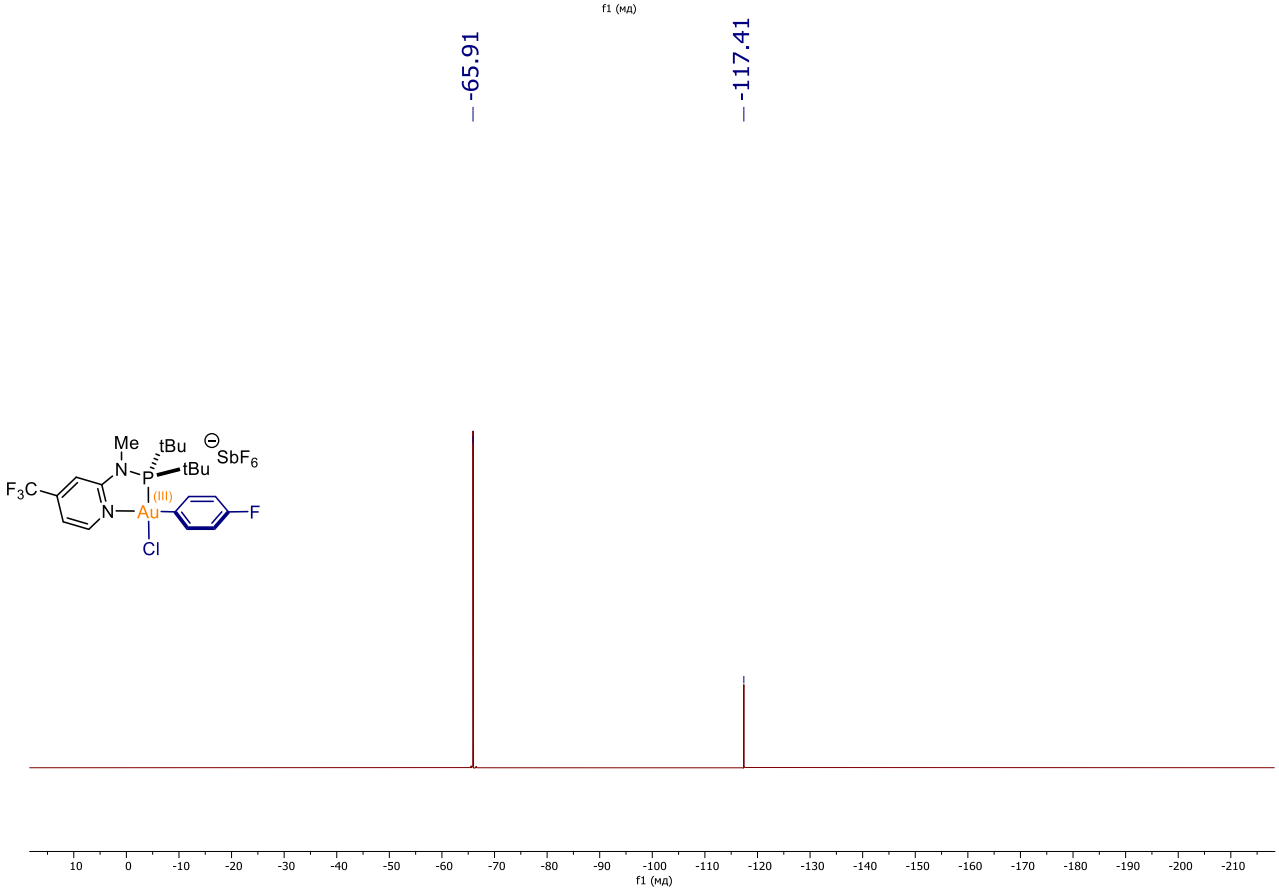

Gold (III) complex 3.3-13$_H$

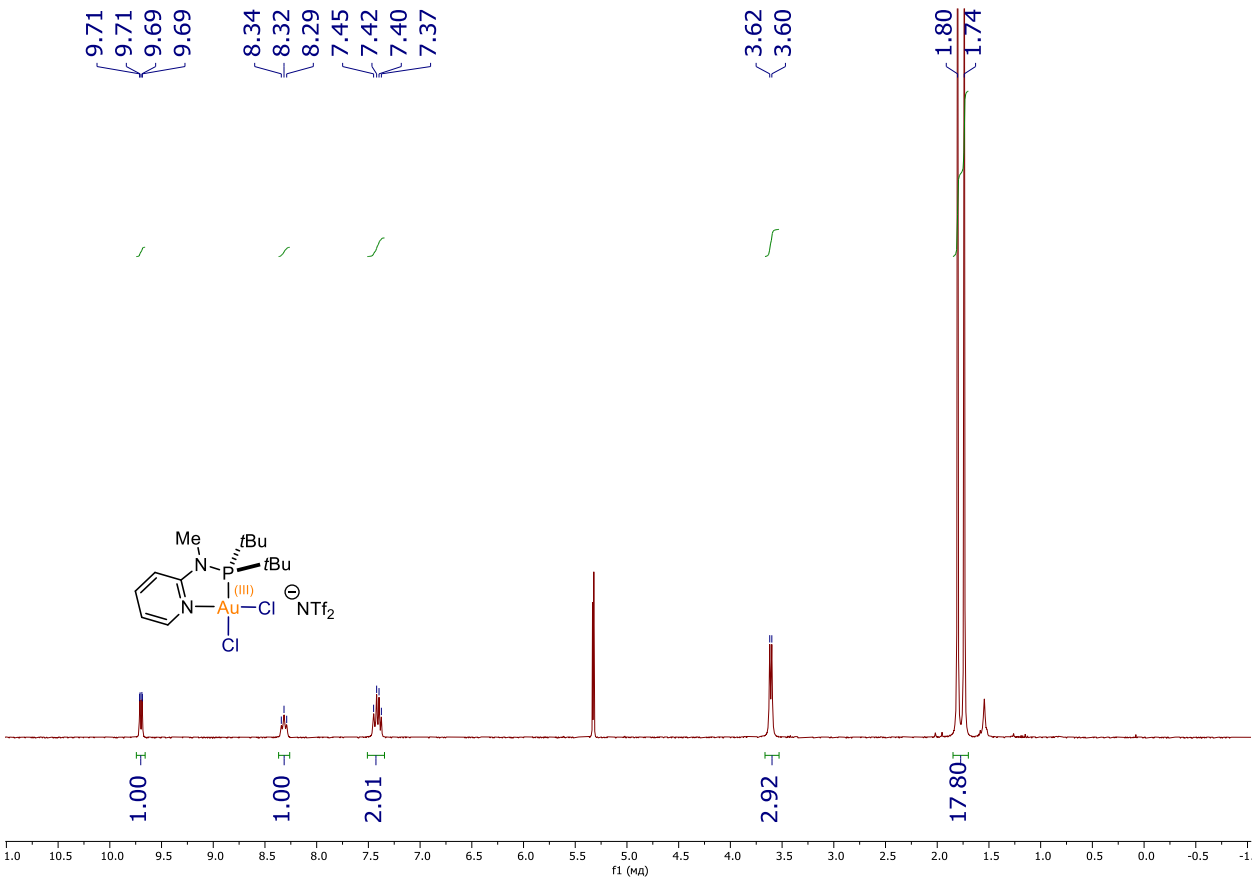
9.71
9.71
9.69
9.69
8.34
8.32
8.29
7.45
7.42
7.40
7.37
3.62
3.60
1.80
1.74
Me
tBu
tBu
N
P
(III)
N
Au
Cl
Cl
NTf2
1.00
1.00
2.01
2.92
17.80
f1 (мд)

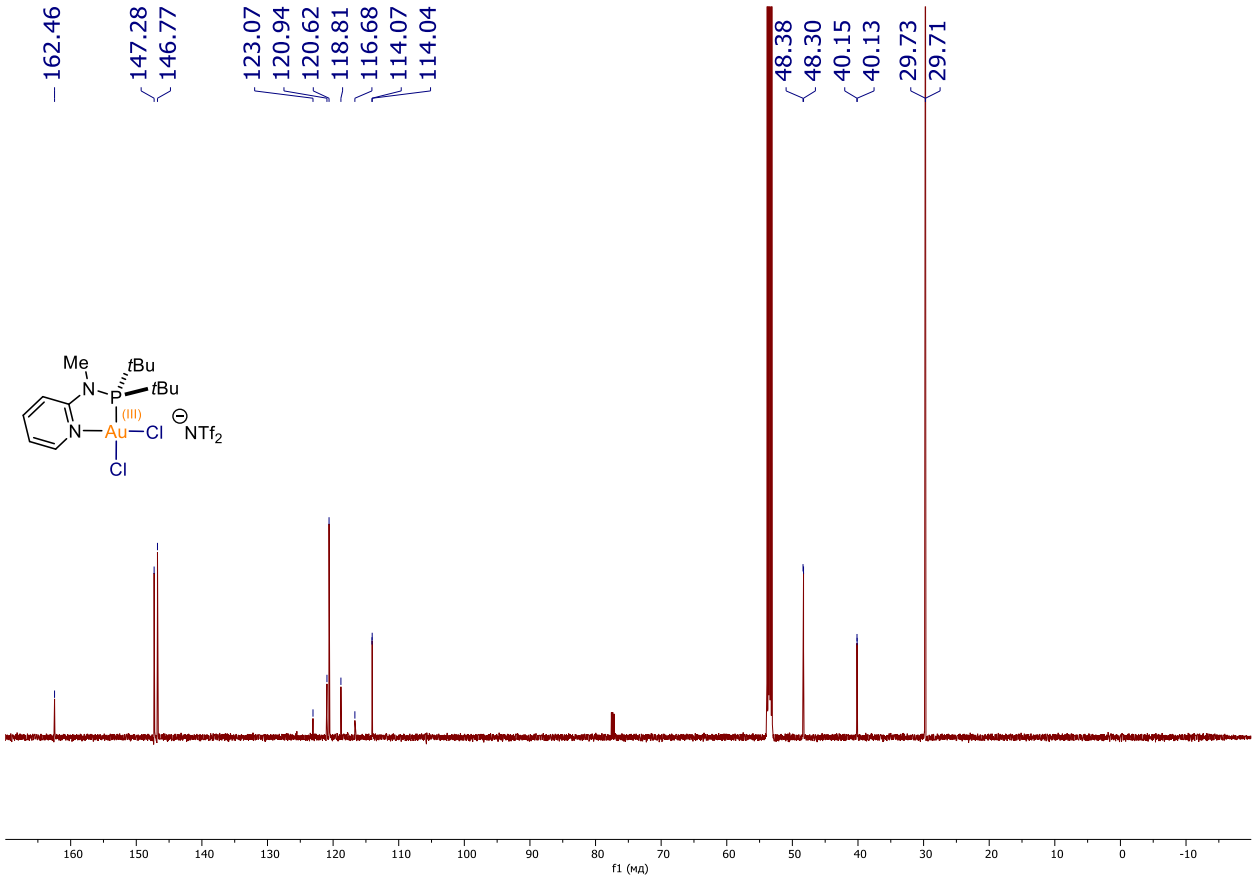

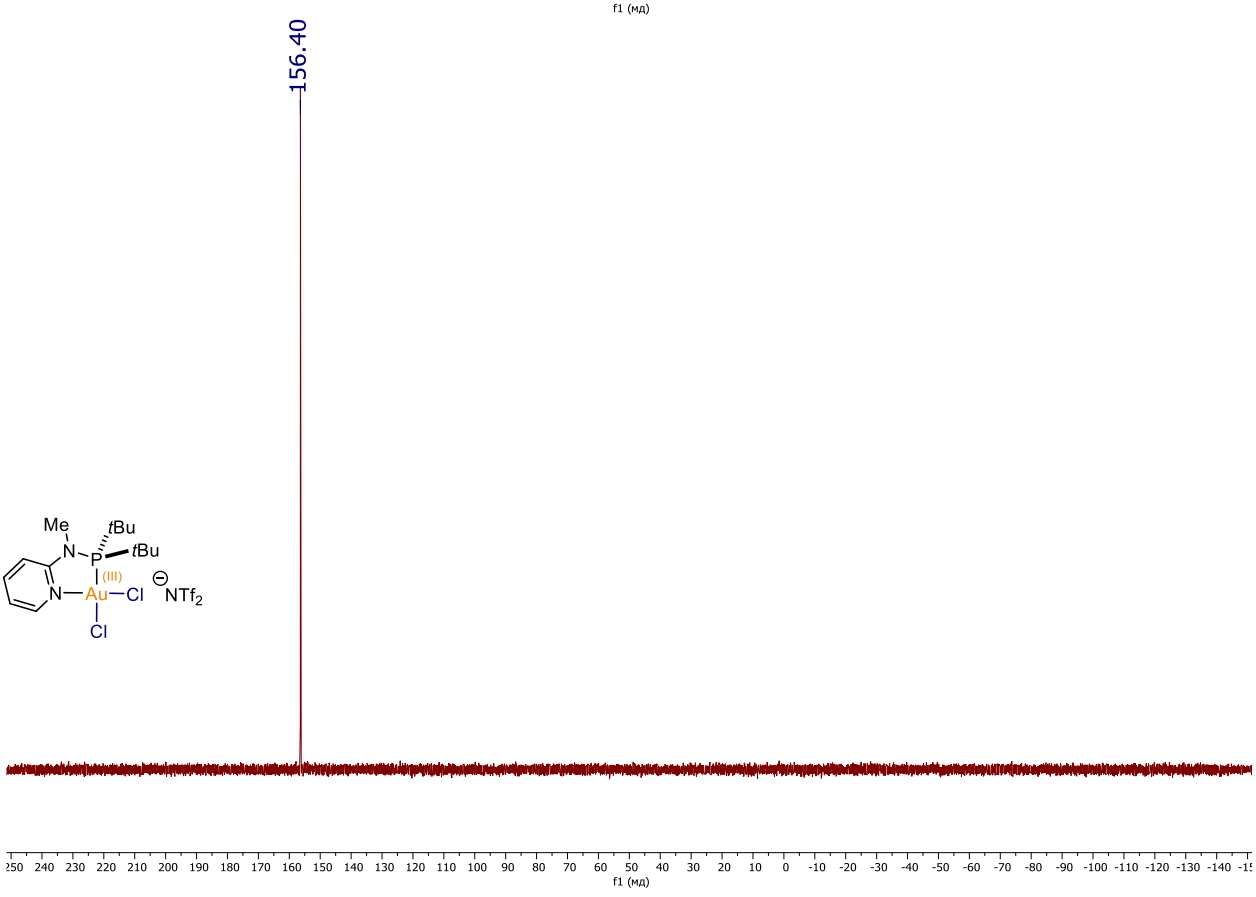

Gold (III) complex 3.3-13$_{OMe}$

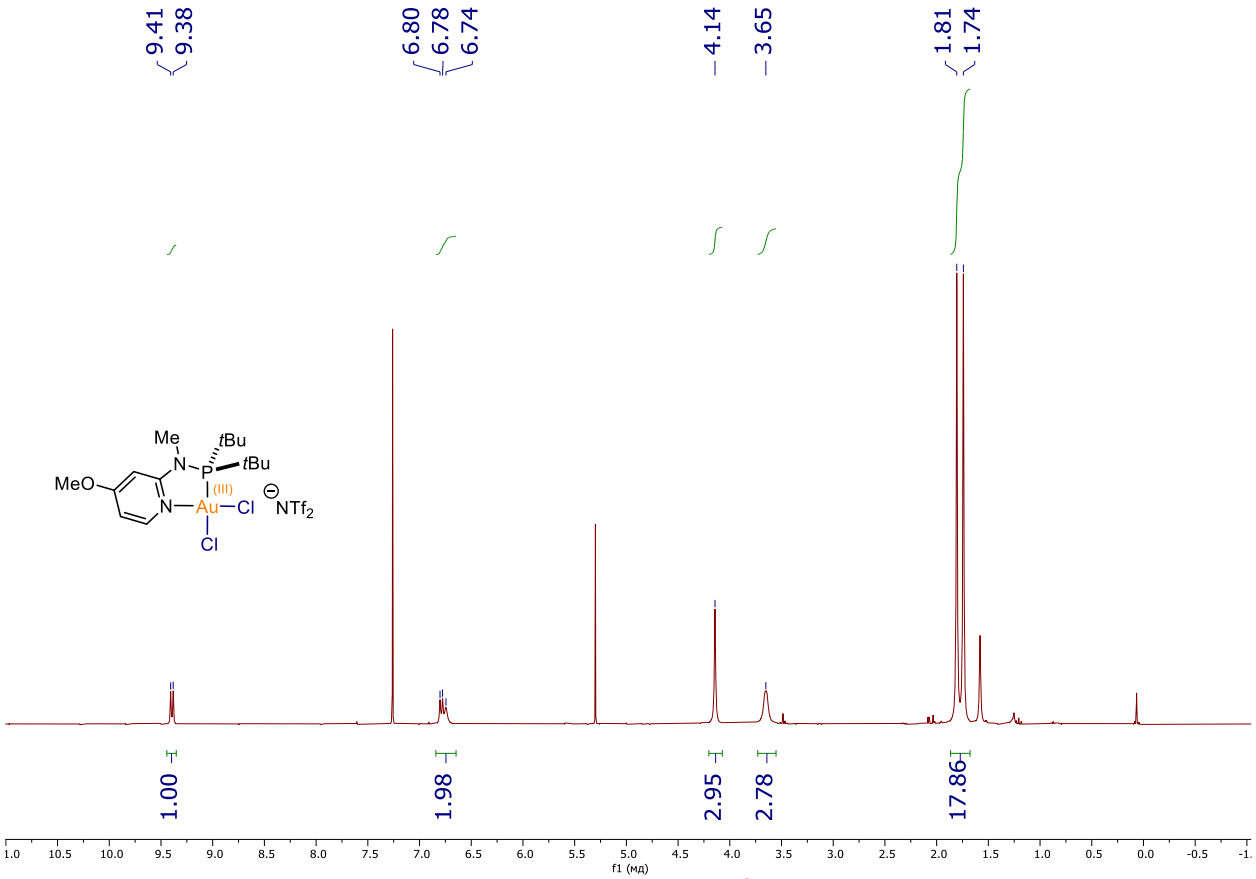
9.41
9.38
6.80
6.78
6.74
4.14
3.65
1.81
1.74
Me
tBu
tBu
MeO
(III)
Au
Cl
Cl
NTf2
1.00
1.98
2.95
2.78
17.86
f1 (мд)

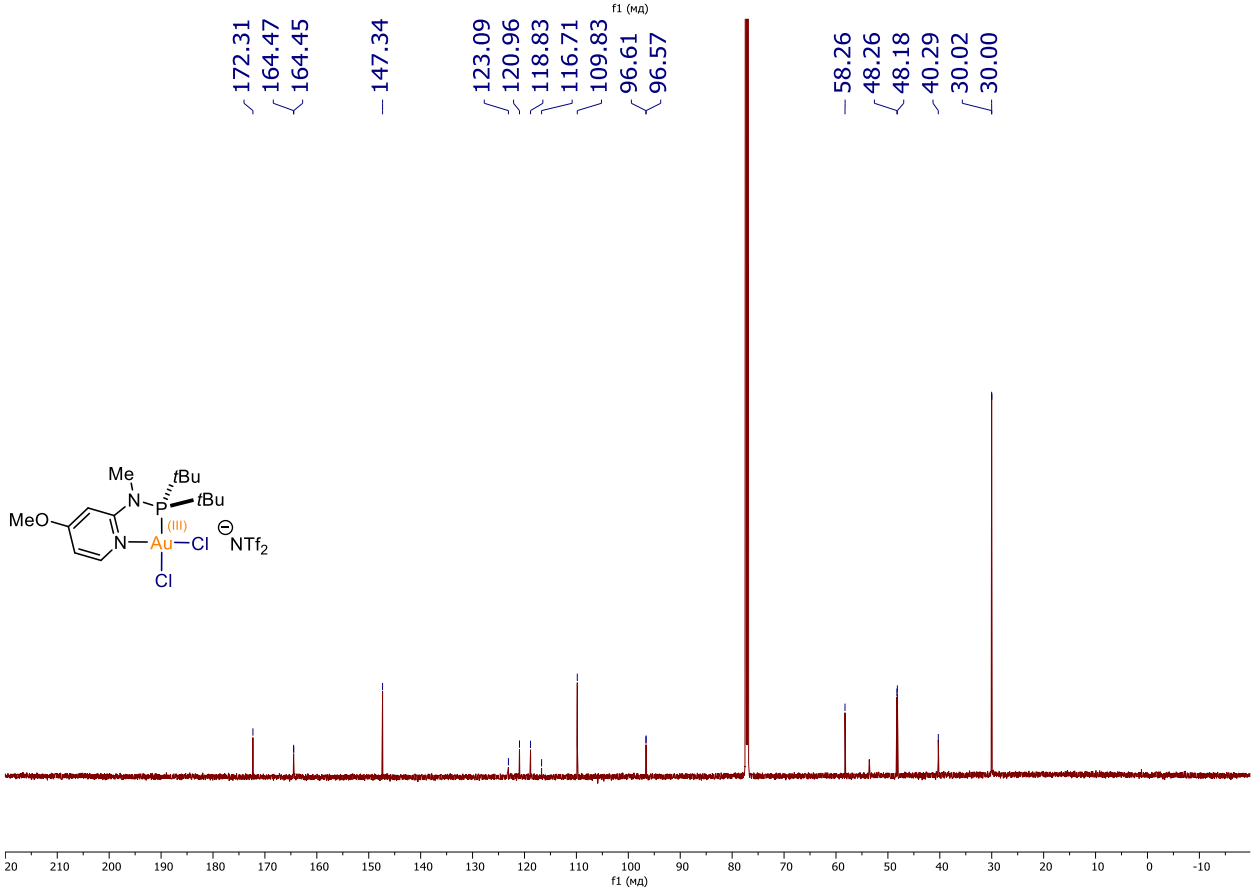
172.31
164.47
164.45
147.34
123.09
120.96
118.83
116.71
109.83
96.61
96.57
58.26
48.26
48.18
40.29
30.02
30.00
Me
tBu
tBu
MeO
(III)
Au
Cl
Cl
NTf2
f1 (мд)

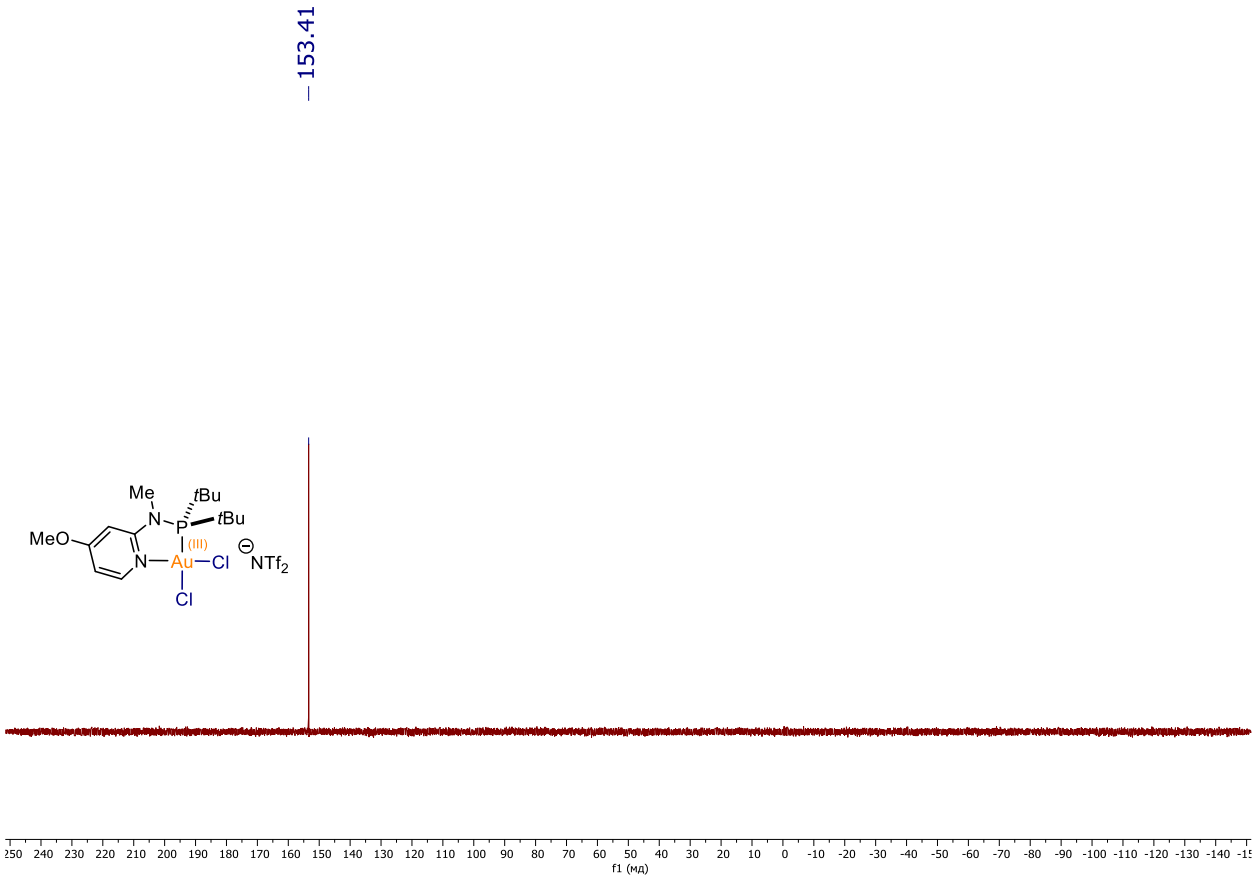

Gold (III) complex 3.3-13$_{CF3}$

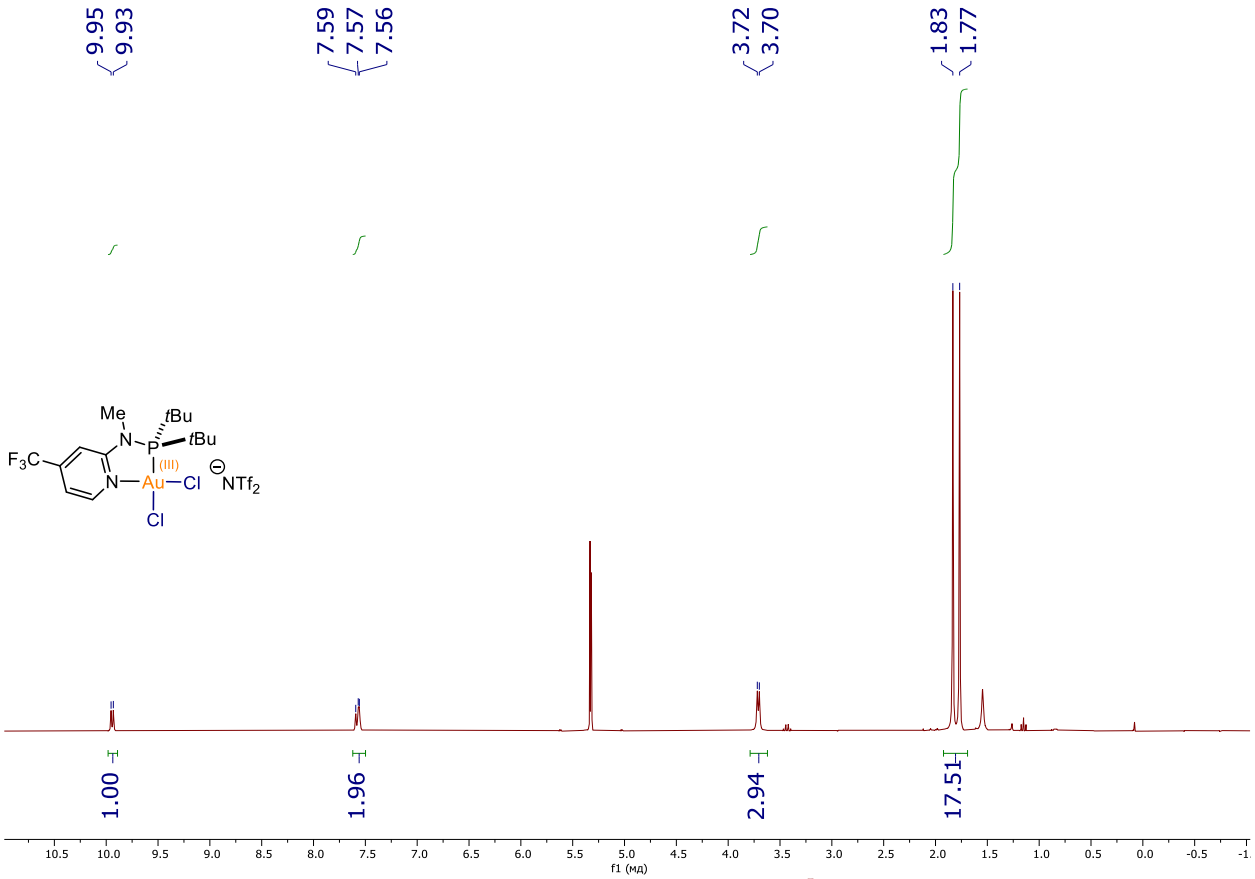
9.95
9.93
7.59
7.57
7.56
3.72
3.70
1.83
1.77
Me
tBu
tBu
F3C
N
P
(III)
Au
Cl
NTf2
1.00
1.96
2.94
17.51
f1 (мд)

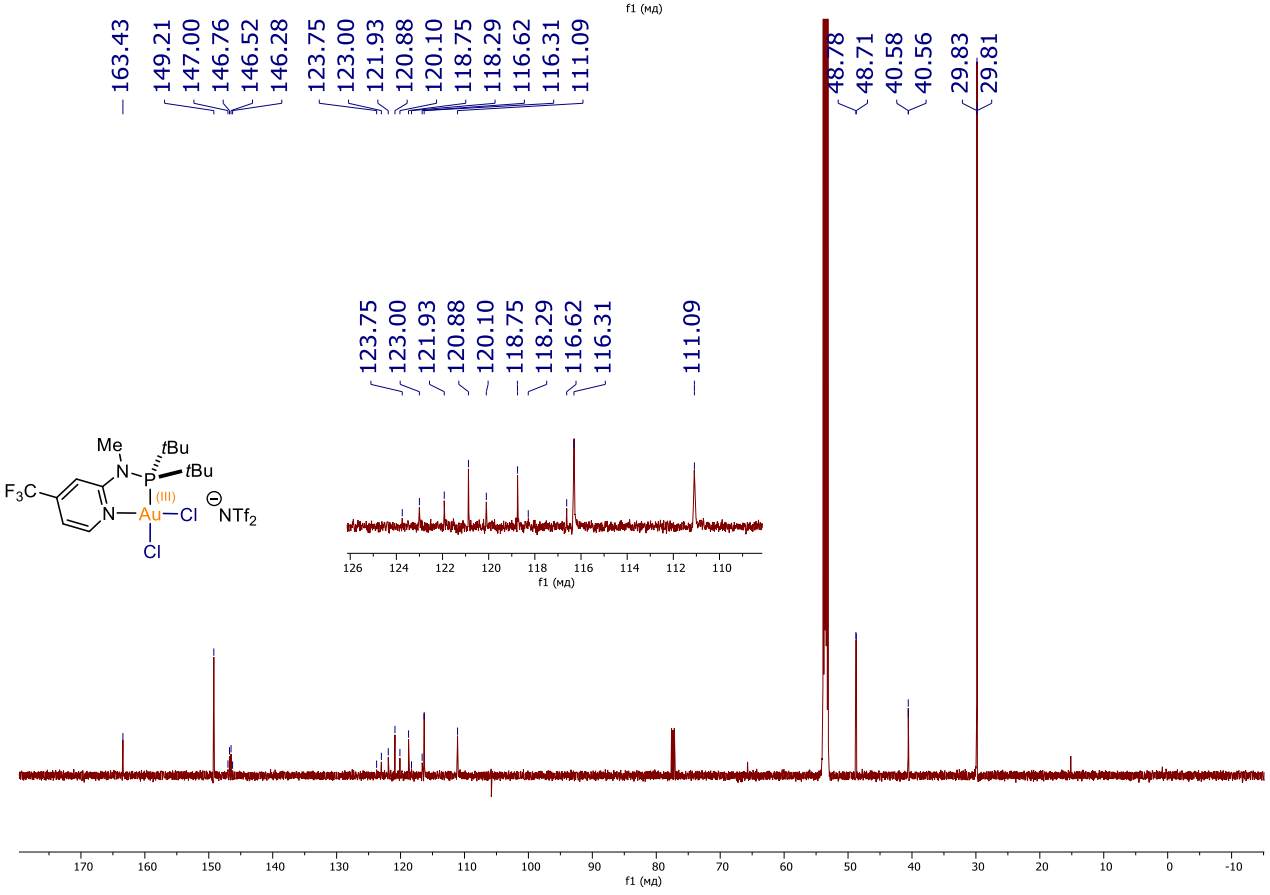
163.43
149.21
147.00
146.76
146.52
146.28
123.75
123.00
121.93
120.88
120.10
118.75
118.29
116.62
116.31
111.09
48.78
48.71
40.58
40.56
29.83
29.81
Me
tBu
tBu
F3C
N
P
(III)
Au
Cl
NTf2
f1 (мд)

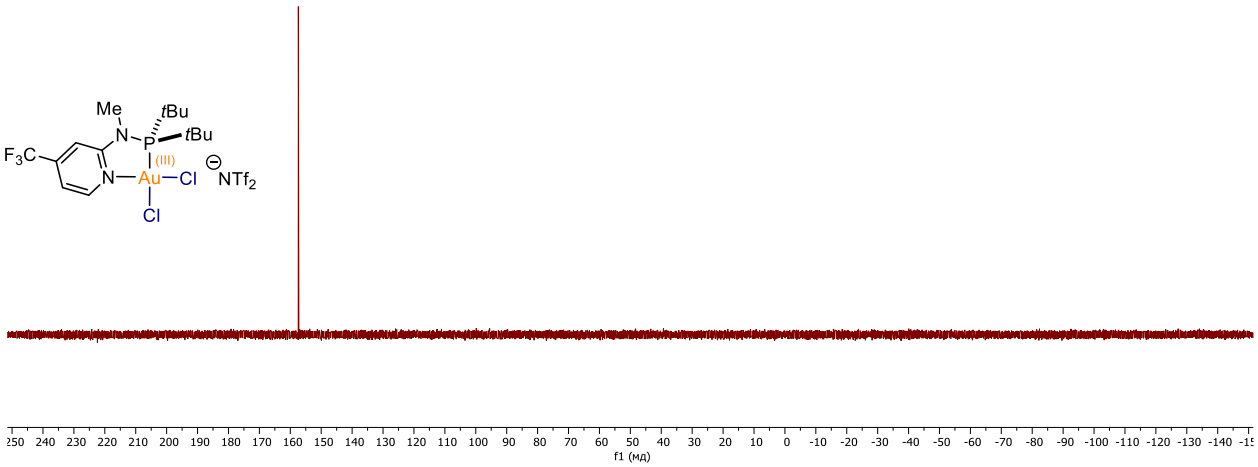

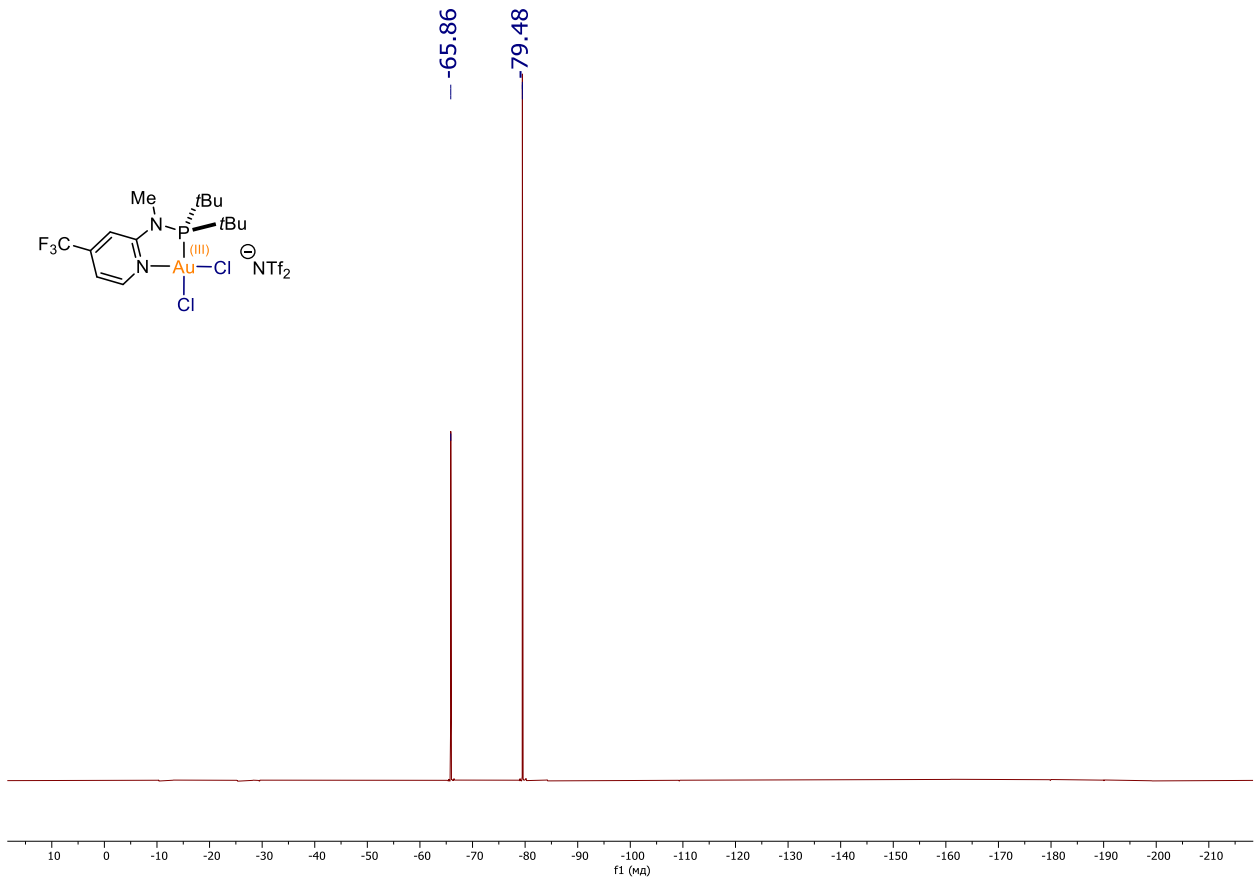

Gold (I) complex 3.3-31$_{STs-Cl}$

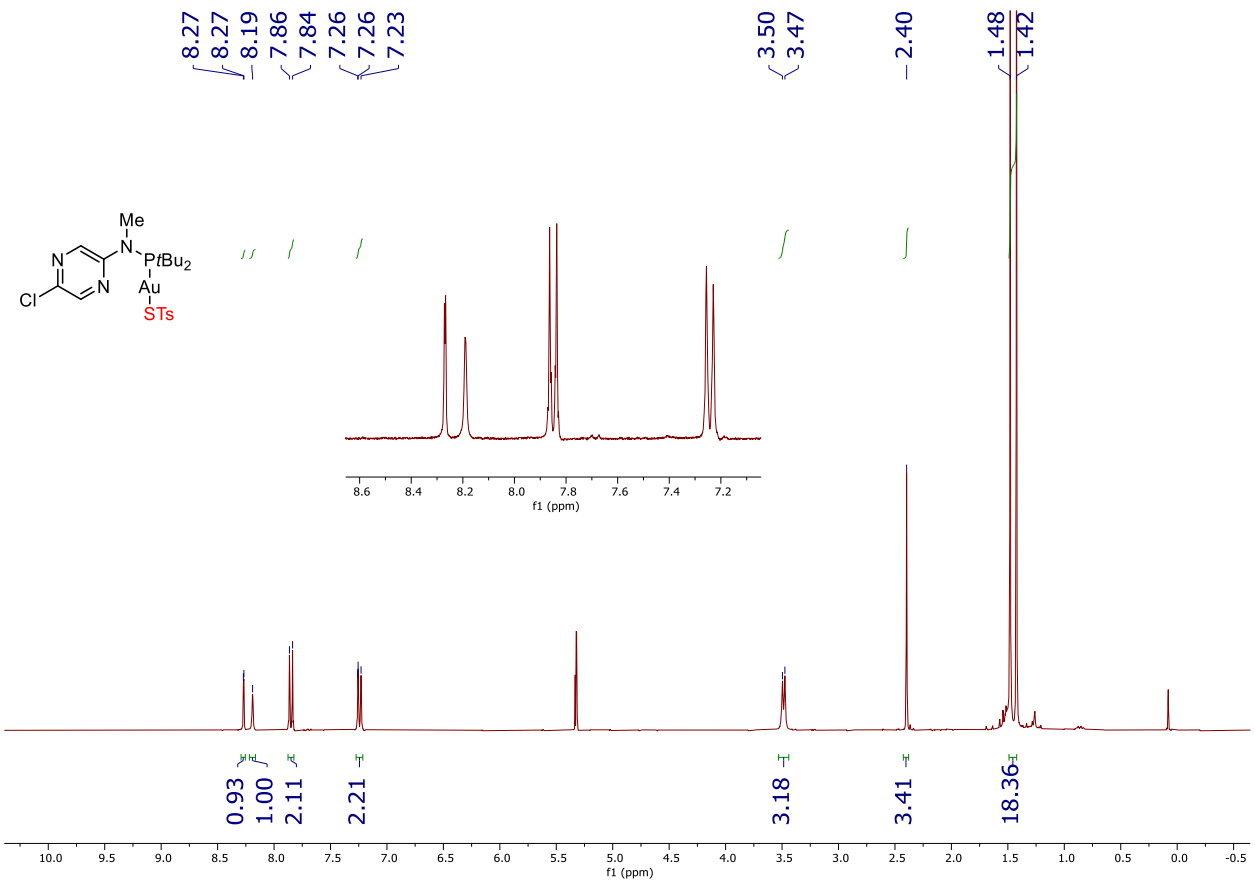
8.27
8.27
8.19
7.86
7.84
7.26
7.26
7.23
3.50
3.47
2.40
1.48
1.42
Me
N
PtBu2
Au
STs
Cl
N
N
0.93
1.00
2.11
2.21
3.18
3.41
18.36
f1 (ppm)

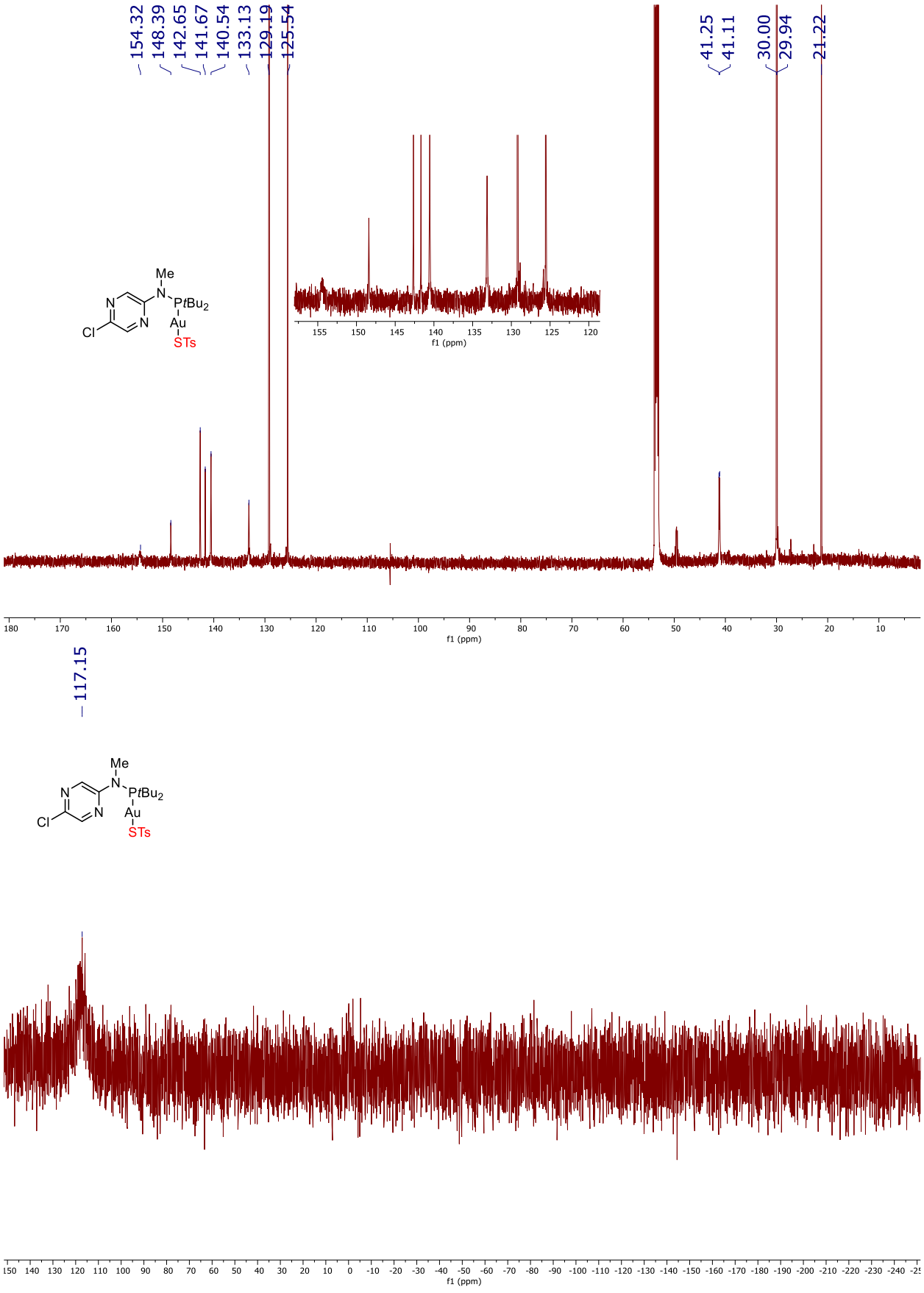

S-([1,1'-biphenyl]-4-yl) 4-methylbenzenesulfonothioate 3.3-43c

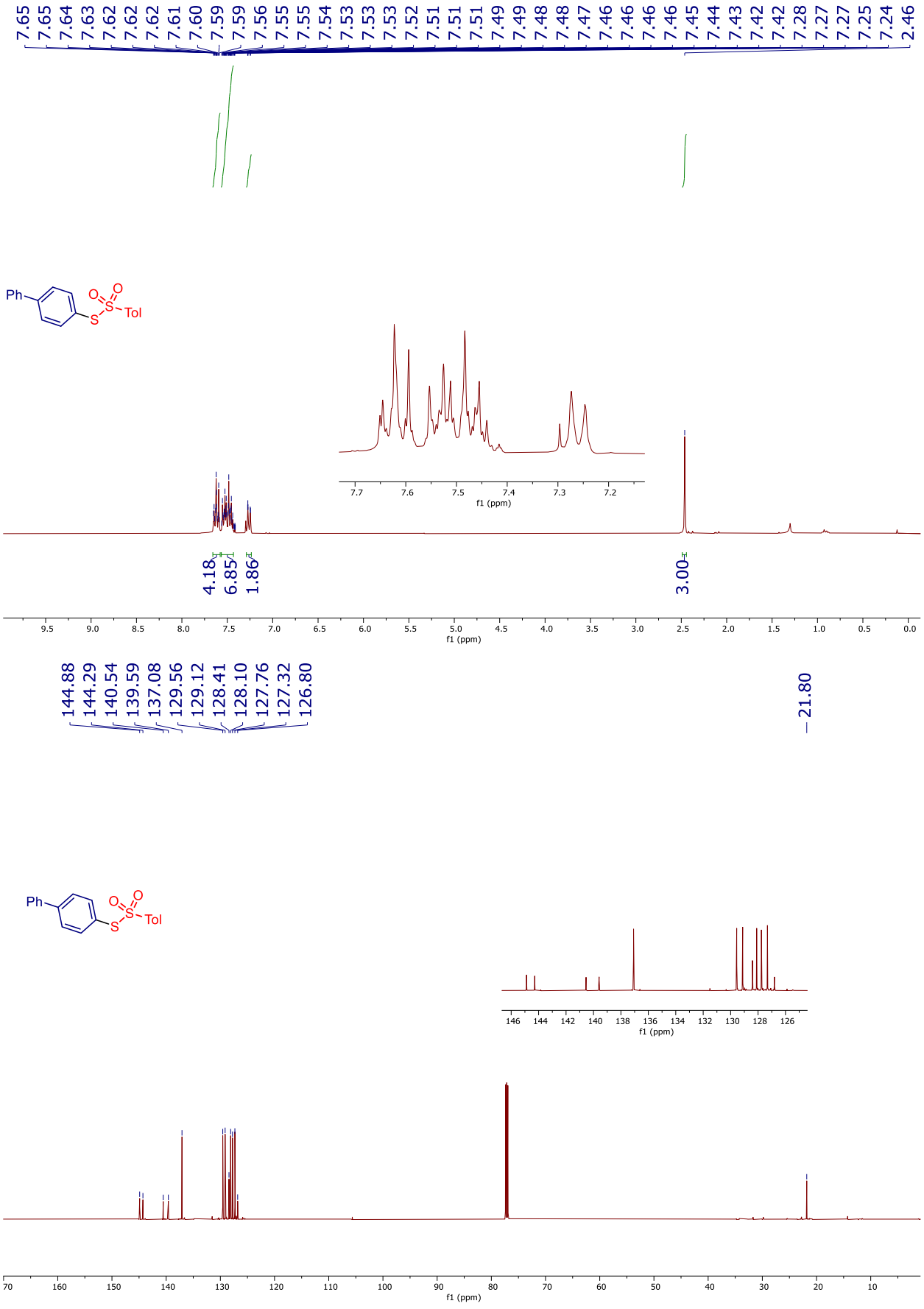

S-(2-ethylphenyl) 4-methylbenzenesulfonothioate 3.3-43e

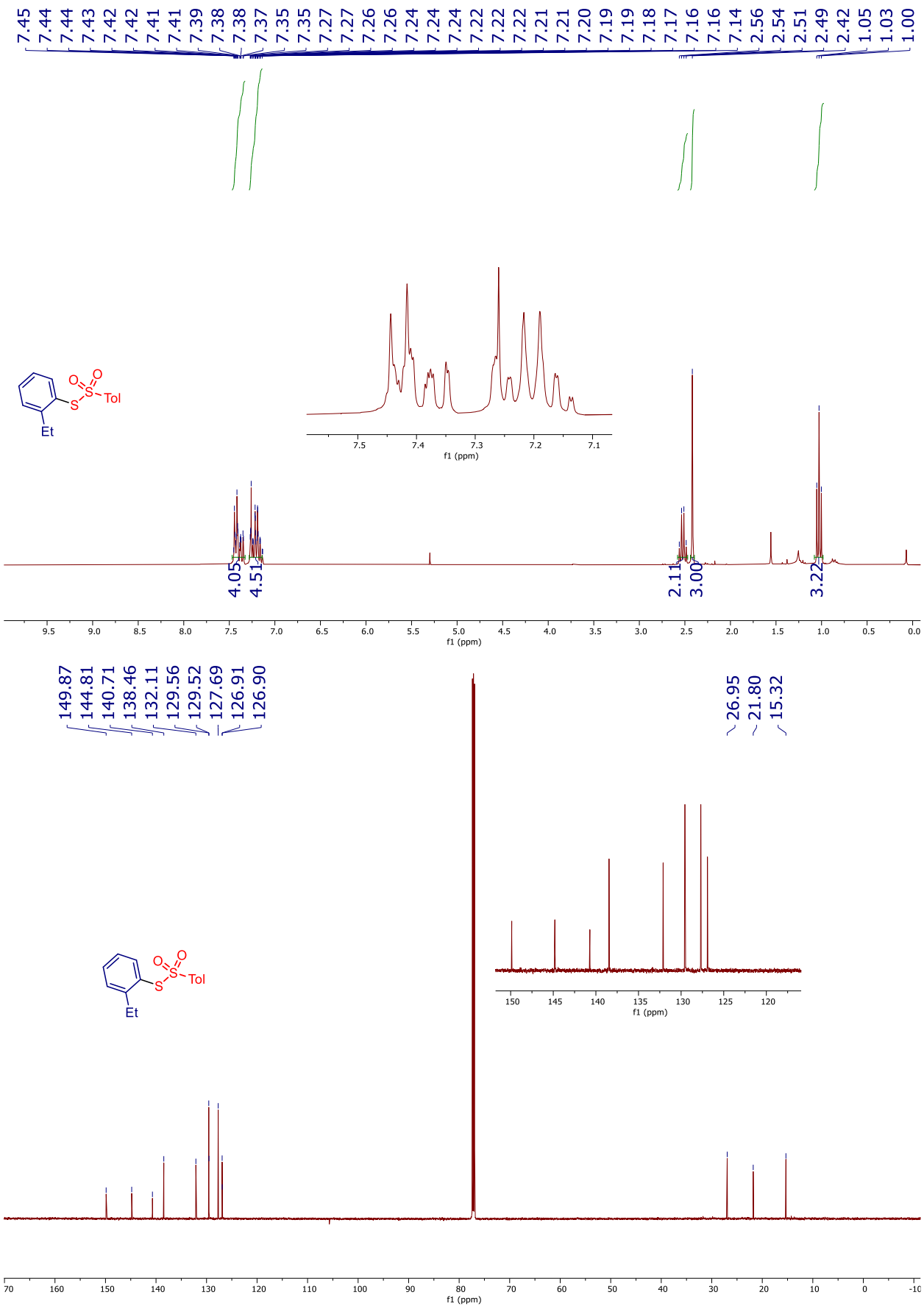

S-(4-isopropylphenyl) 4-methylbenzenesulfonothioate 3.3-43h

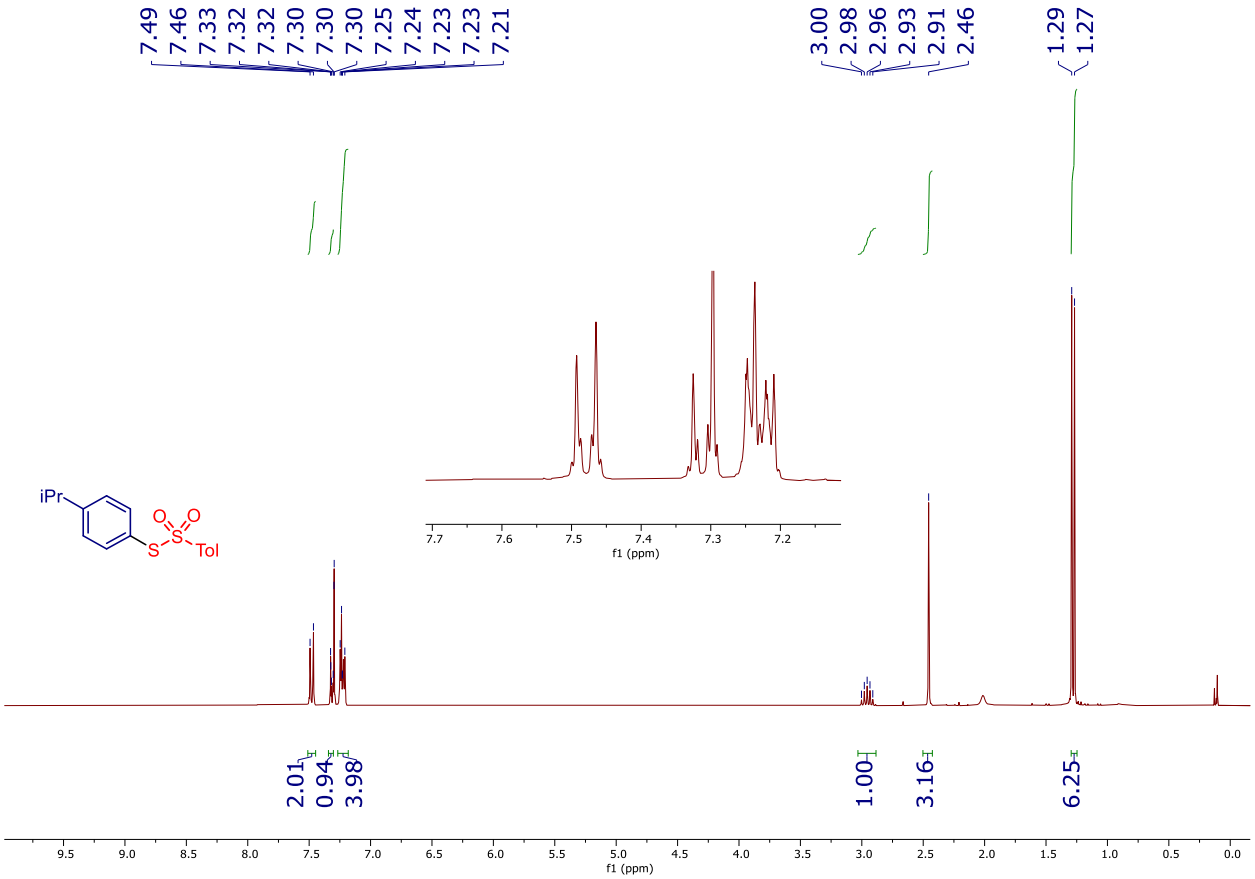

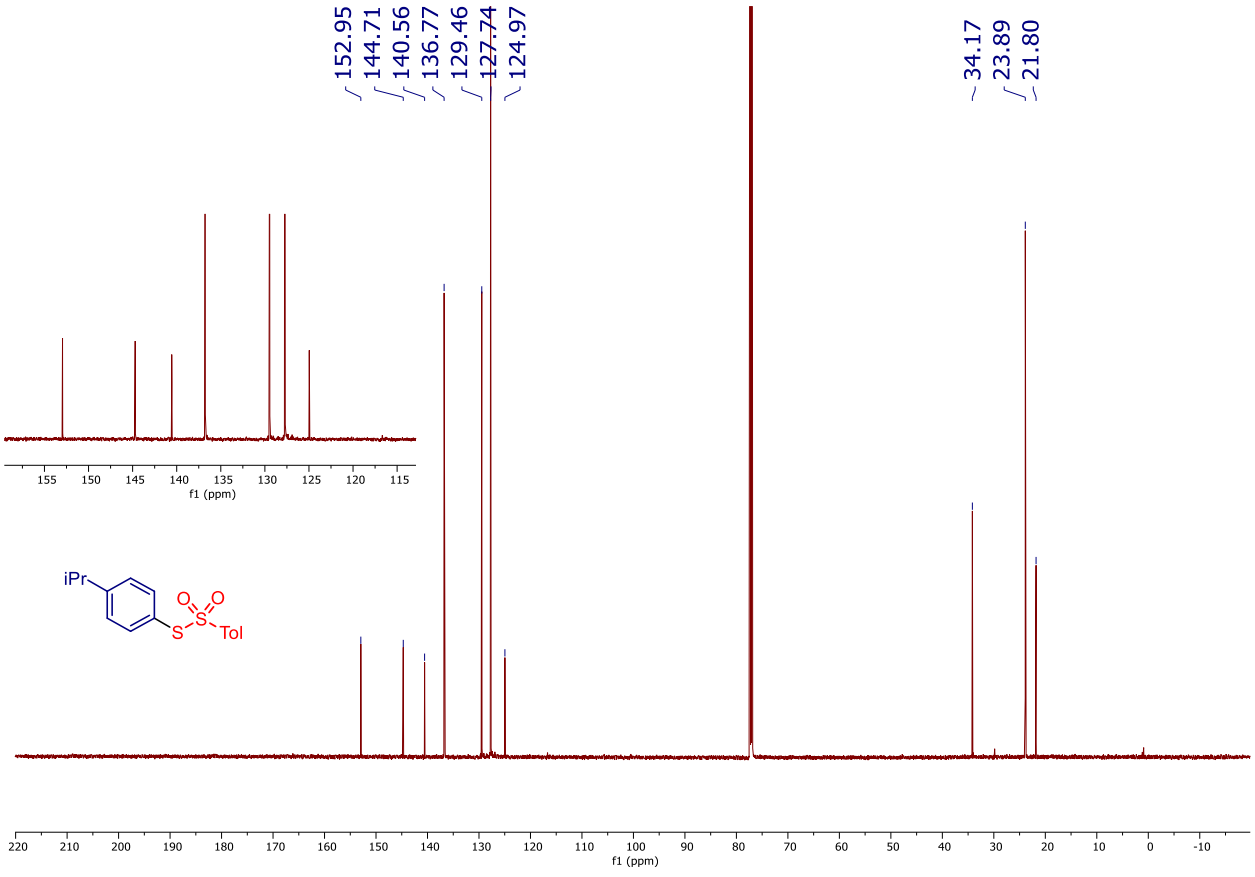

S-(3,5-dimethylphenyl) 4-methylbenzenesulfonothioate 3.3-43j

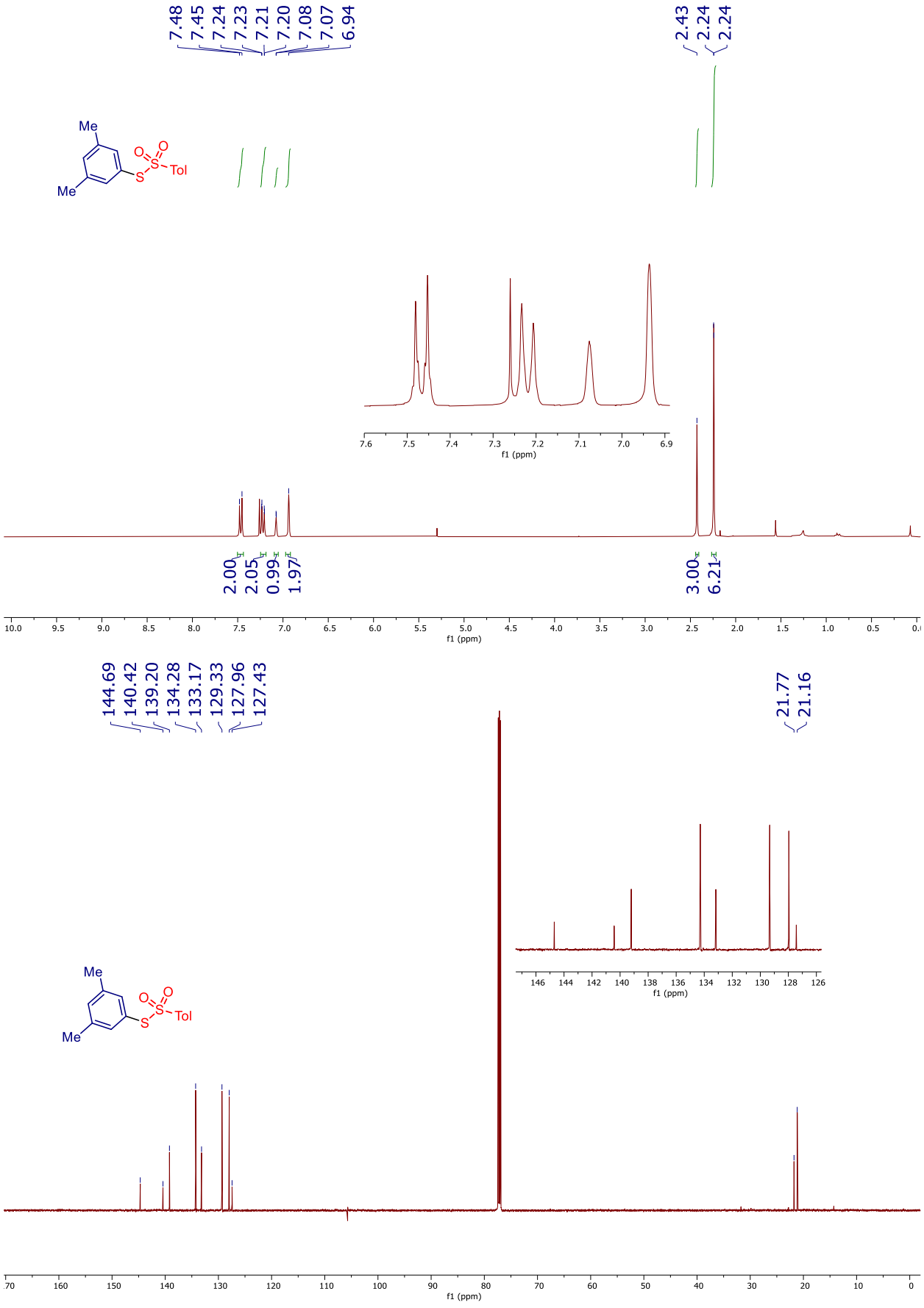

S-(9H-fluoren-2-yl) 4-methylbenzenesulfonothioate 3.3-43l

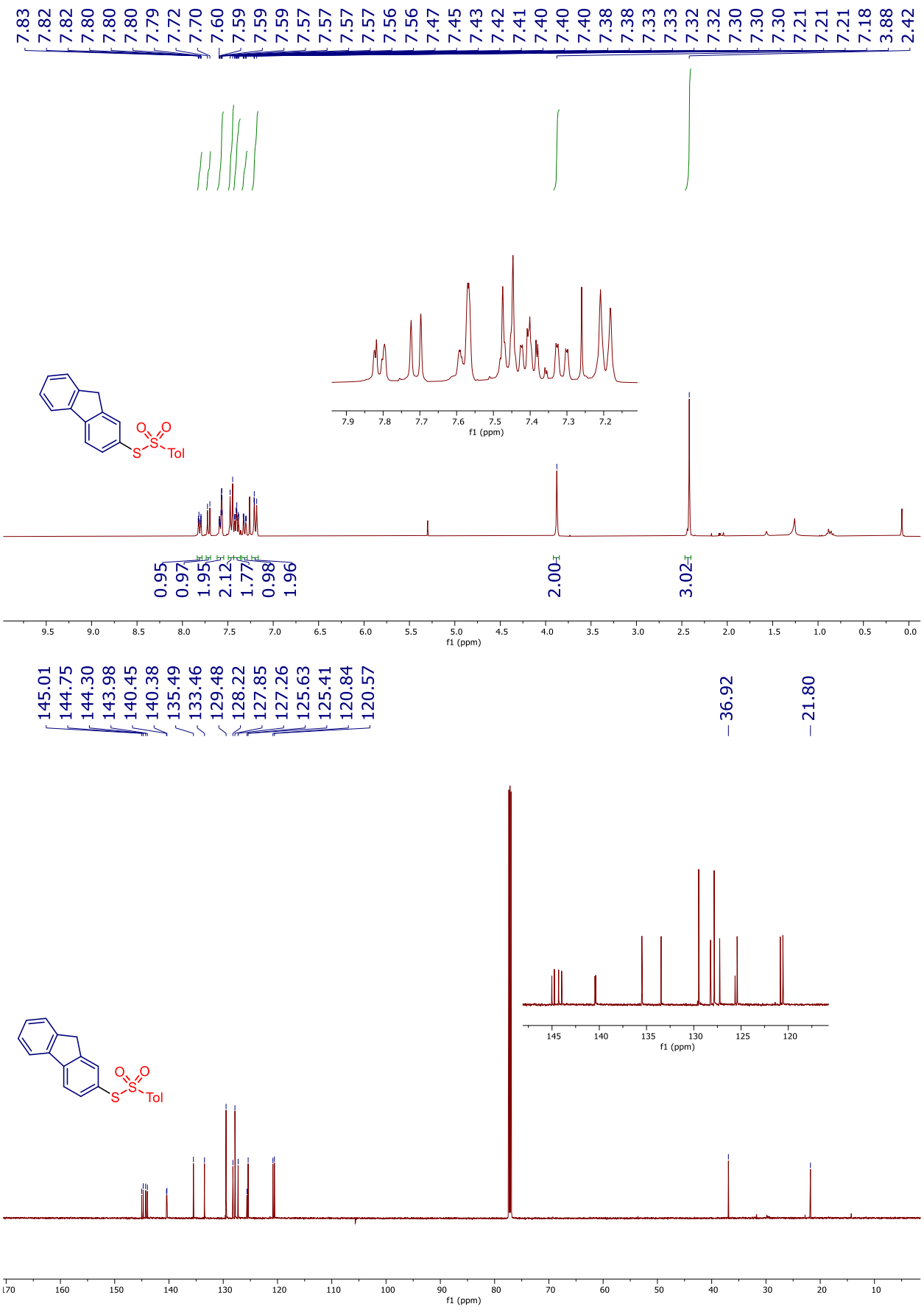

S-(naphthalen-1-yl) 4-methylbenzenesulfonothioate 3.3-43m

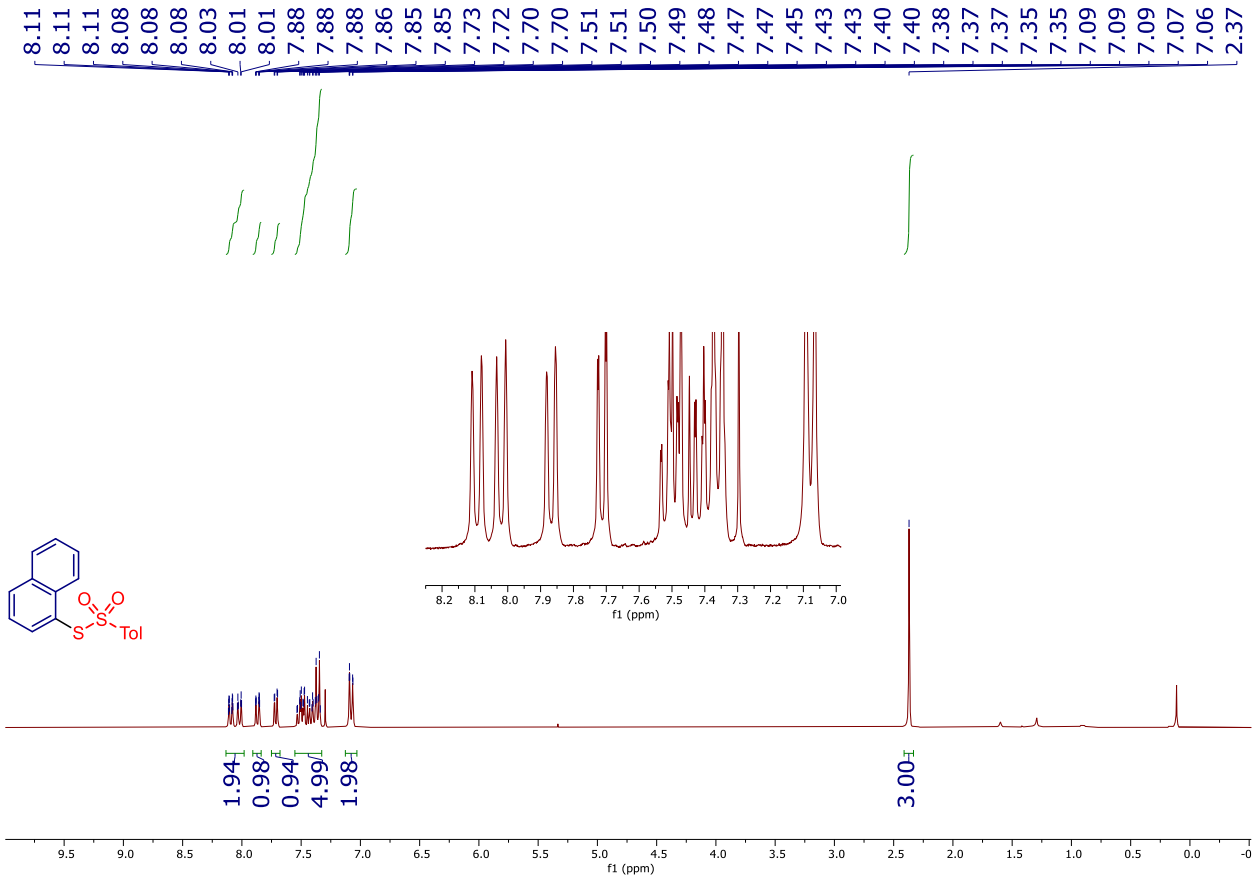

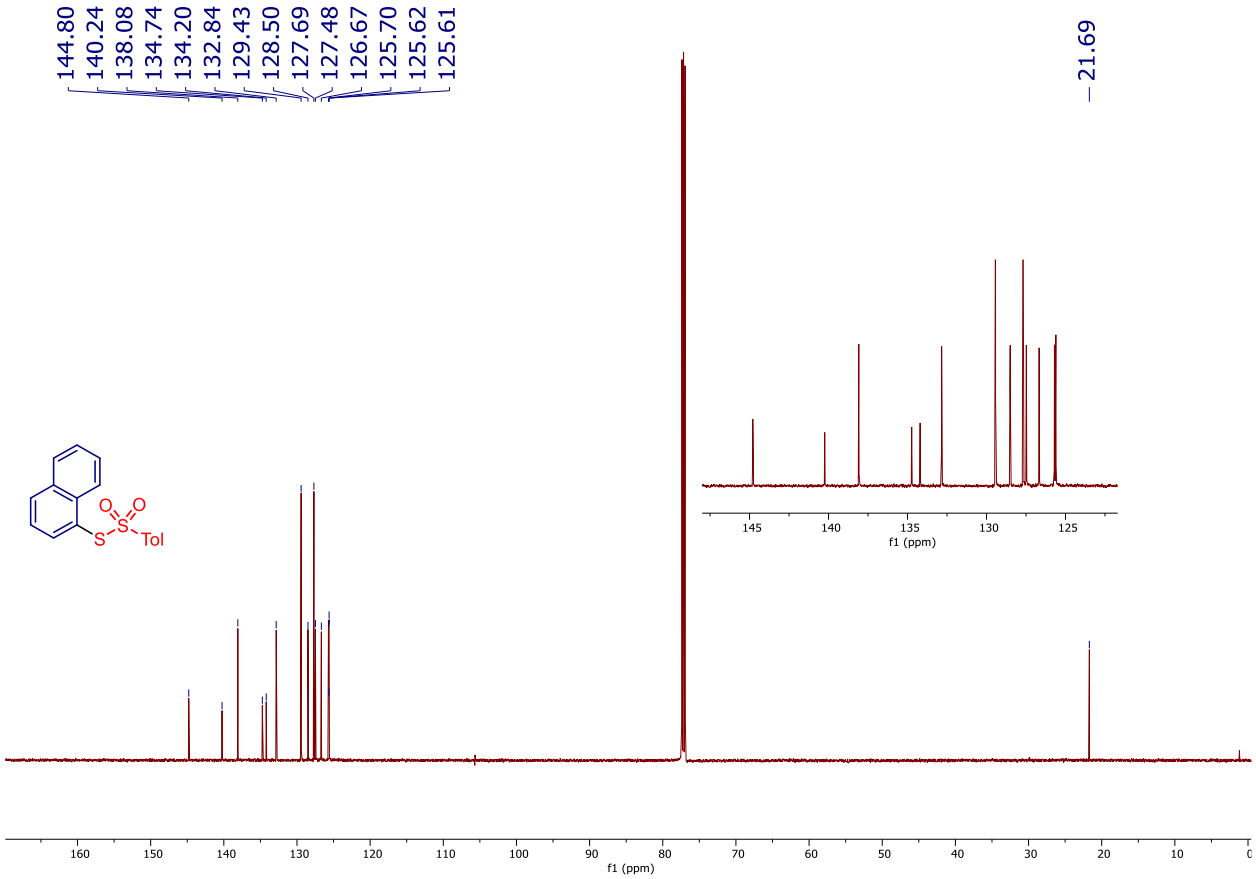

S,S'-(1,4-phenylene) bis(4-methylbenzenesulfonothioate) 3.3-43n

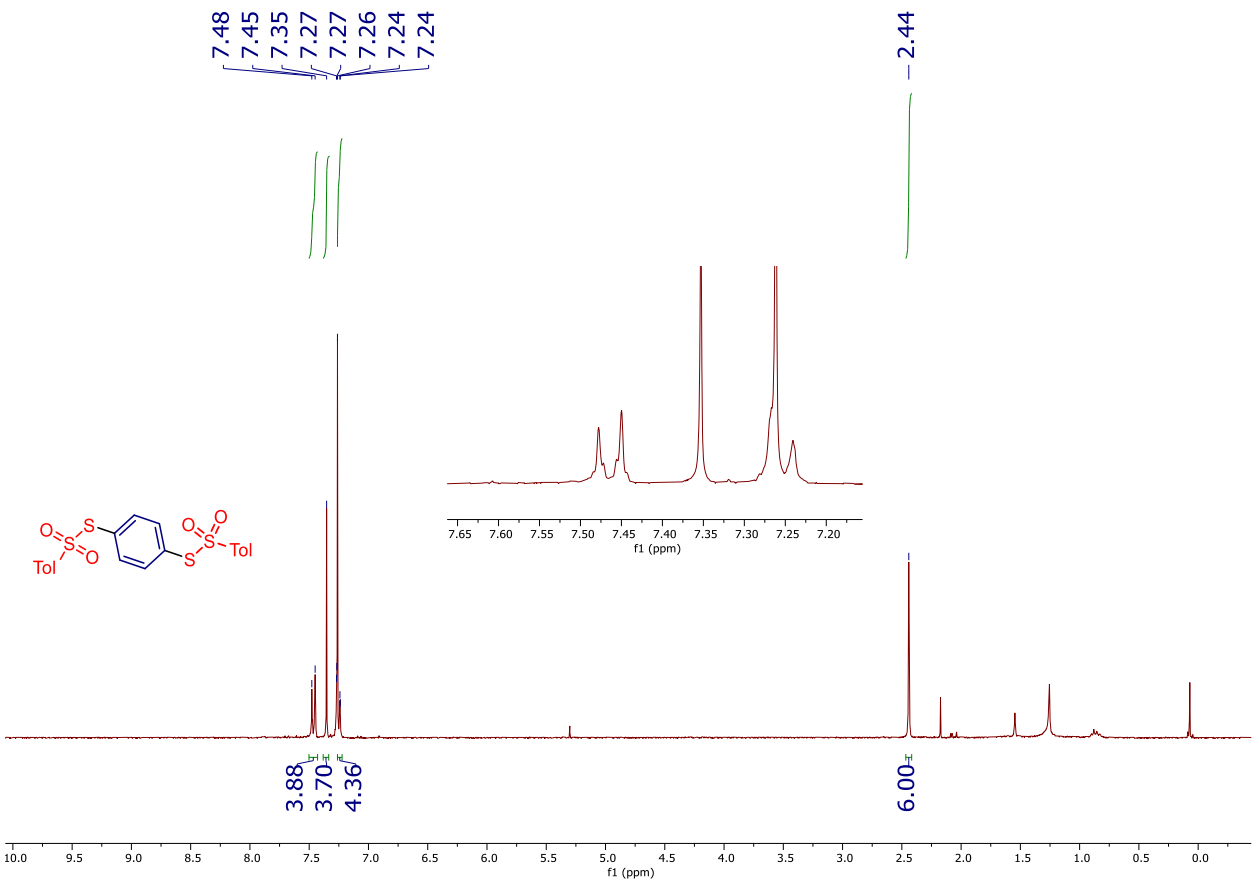

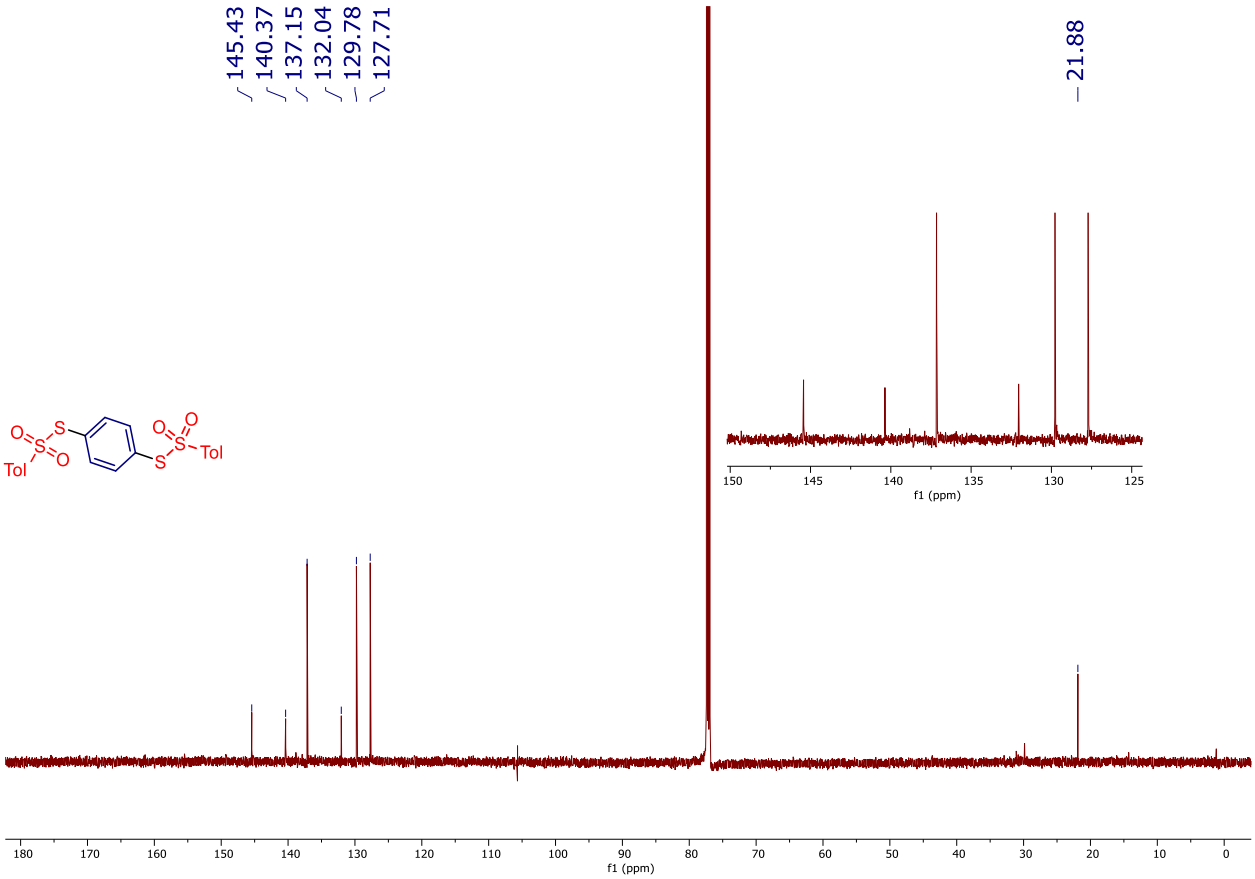

S-(4-ethoxyphenyl) 4-methylbenzenesulfonothioate 3.3-43r

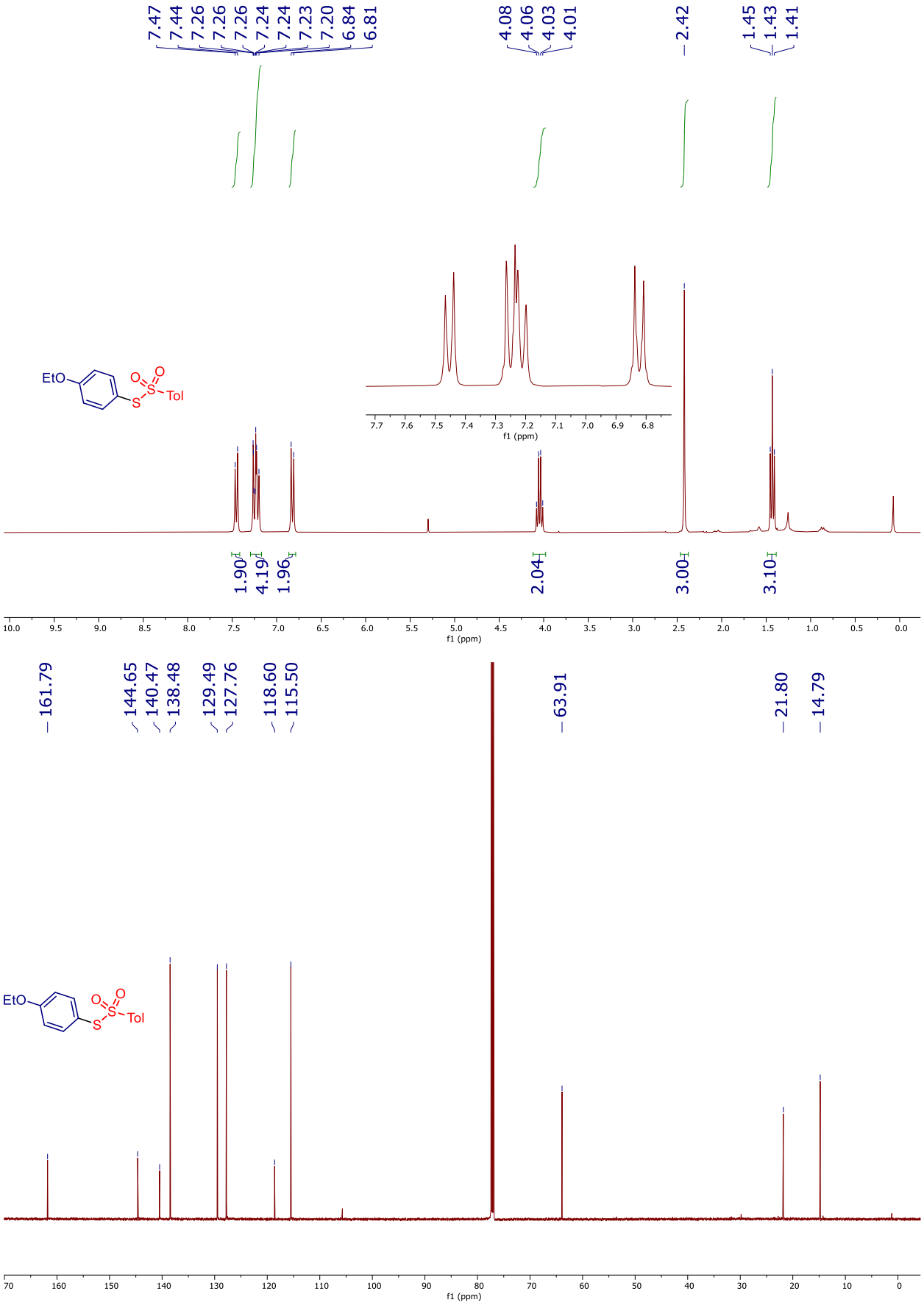

S-(4-acetamidophenyl) 4-methylbenzenesulfonothioate 3.3-43s

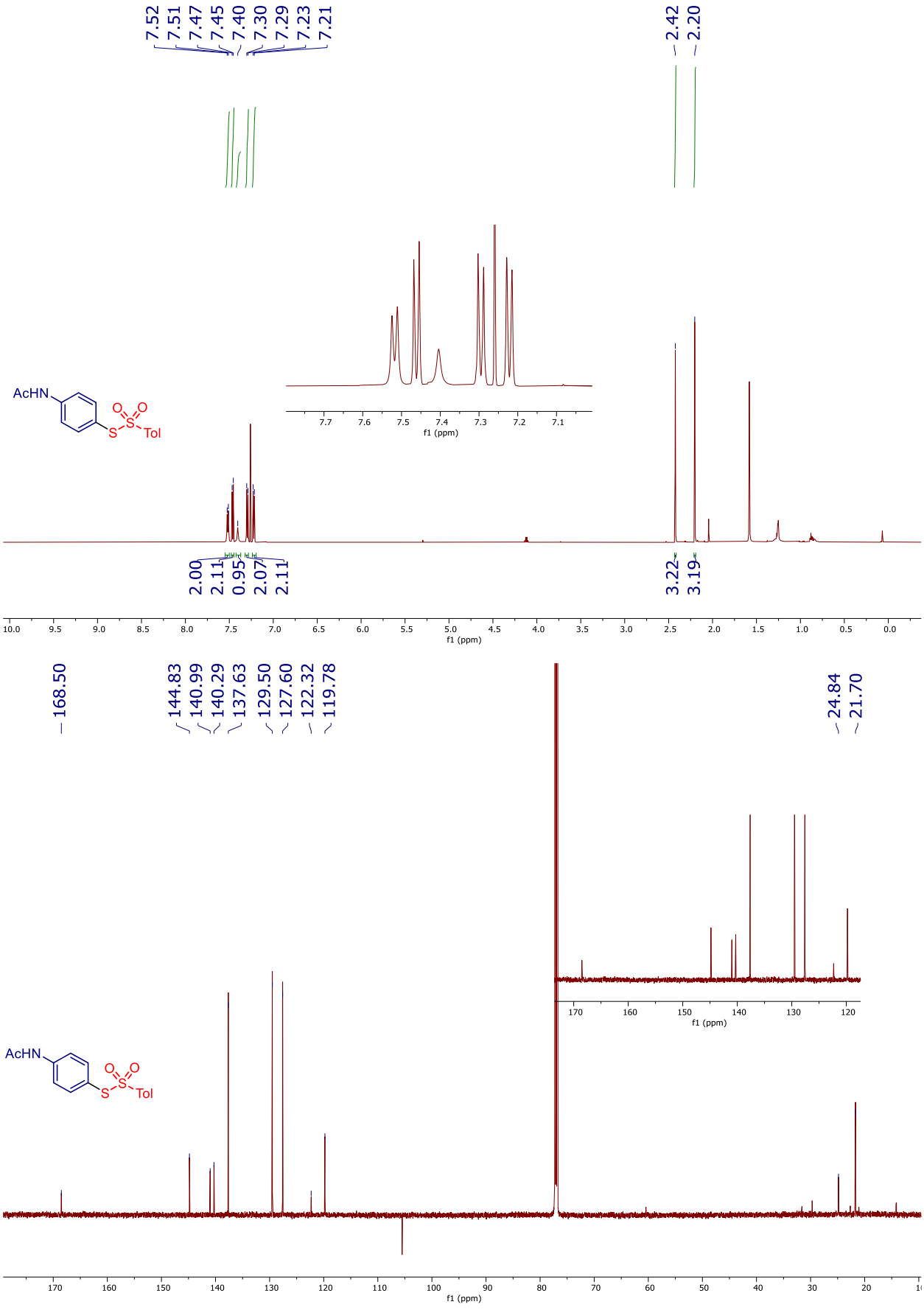

S-(benzo[d][1,3]dioxol-5-yl) 4-methylbenzenesulfonothioate 3.3-43t

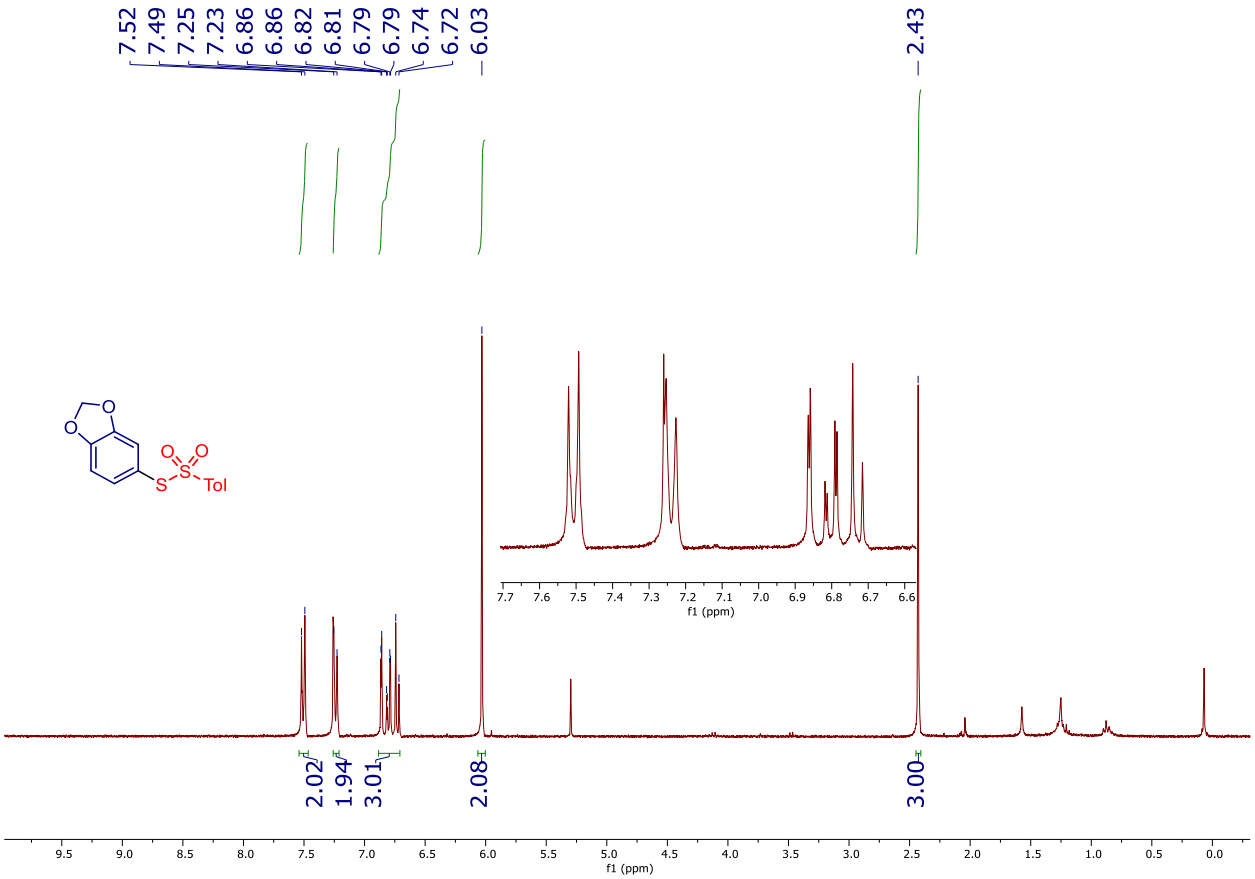

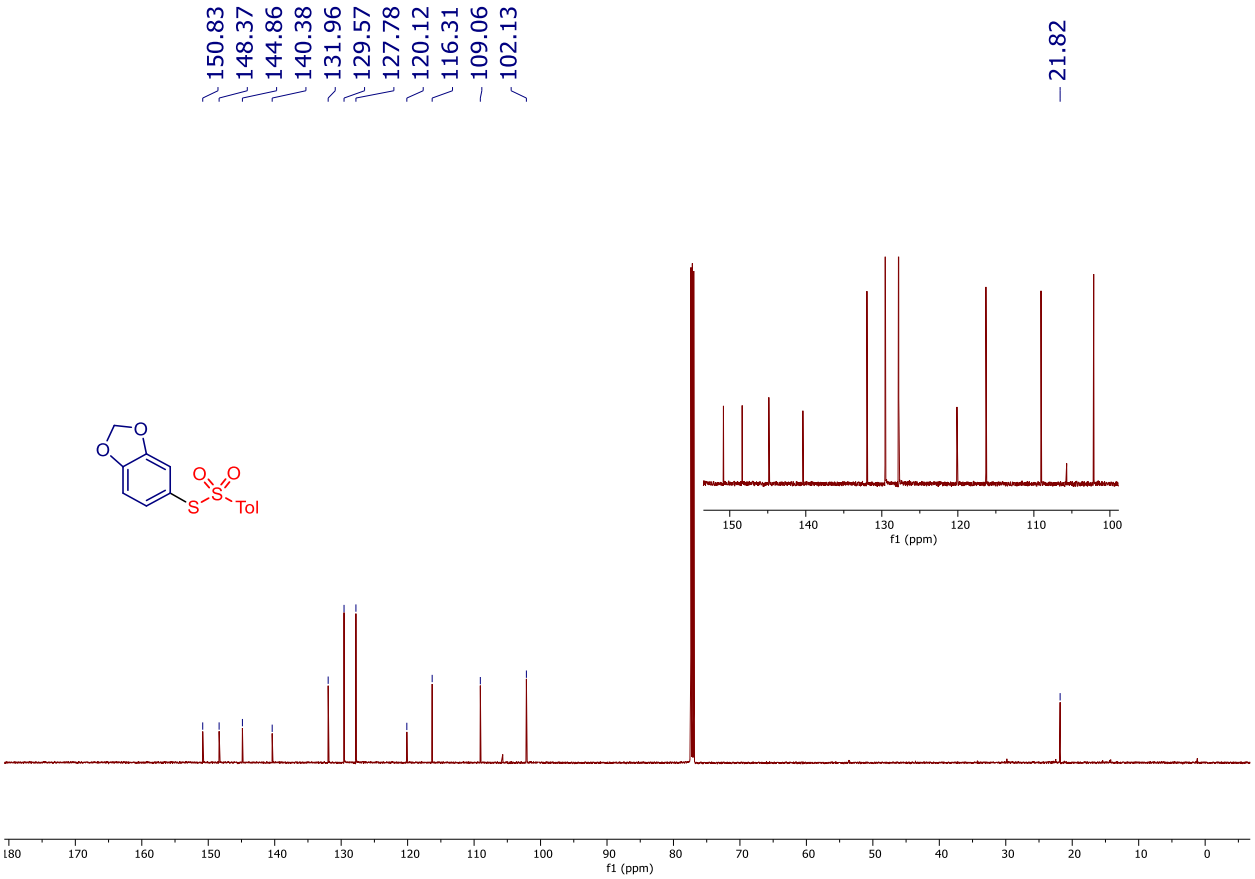

S-(2,6-difluorophenyl) 4-methylbenzenesulfonothioate 3.3-43y

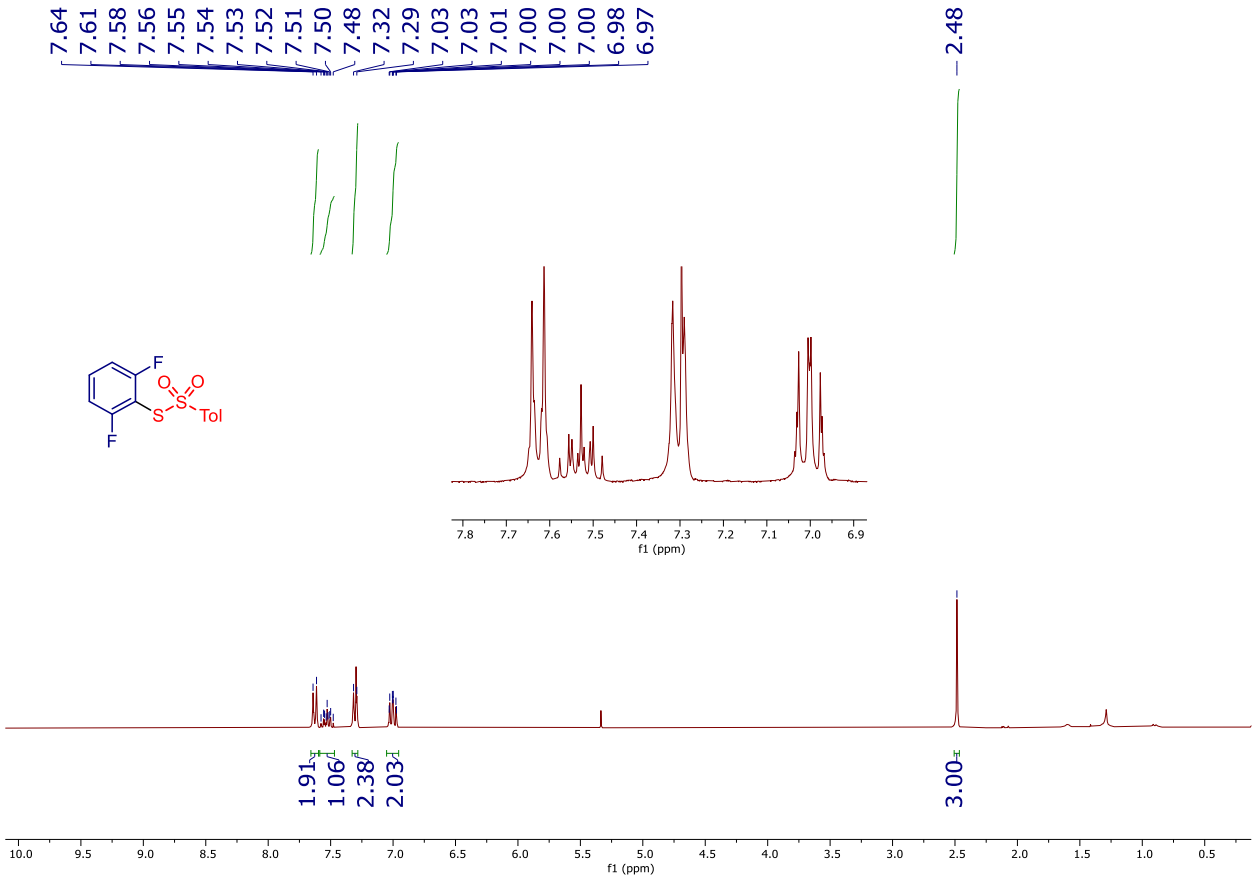
7.64
7.61
7.58
7.56
7.55
7.54
7.53
7.52
7.51
7.50
7.48
7.32
7.29
7.03
7.03
7.01
7.00
7.00
7.00
6.98
6.97
2.48
F
O
O
S
S
Tol
F
7.8 7.7 7.6 7.5 7.4 7.3 7.2 7.1 7.0 6.9
f1 (ppm)
1.91
1.06
2.38
2.03
3.00
10.0 9.5 9.0 8.5 8.0 7.5 7.0 6.5 6.0 5.5 5.0 4.5 4.0 3.5 3.0 2.5 2.0 1.5 1.0 0.5
f1 (ppm)

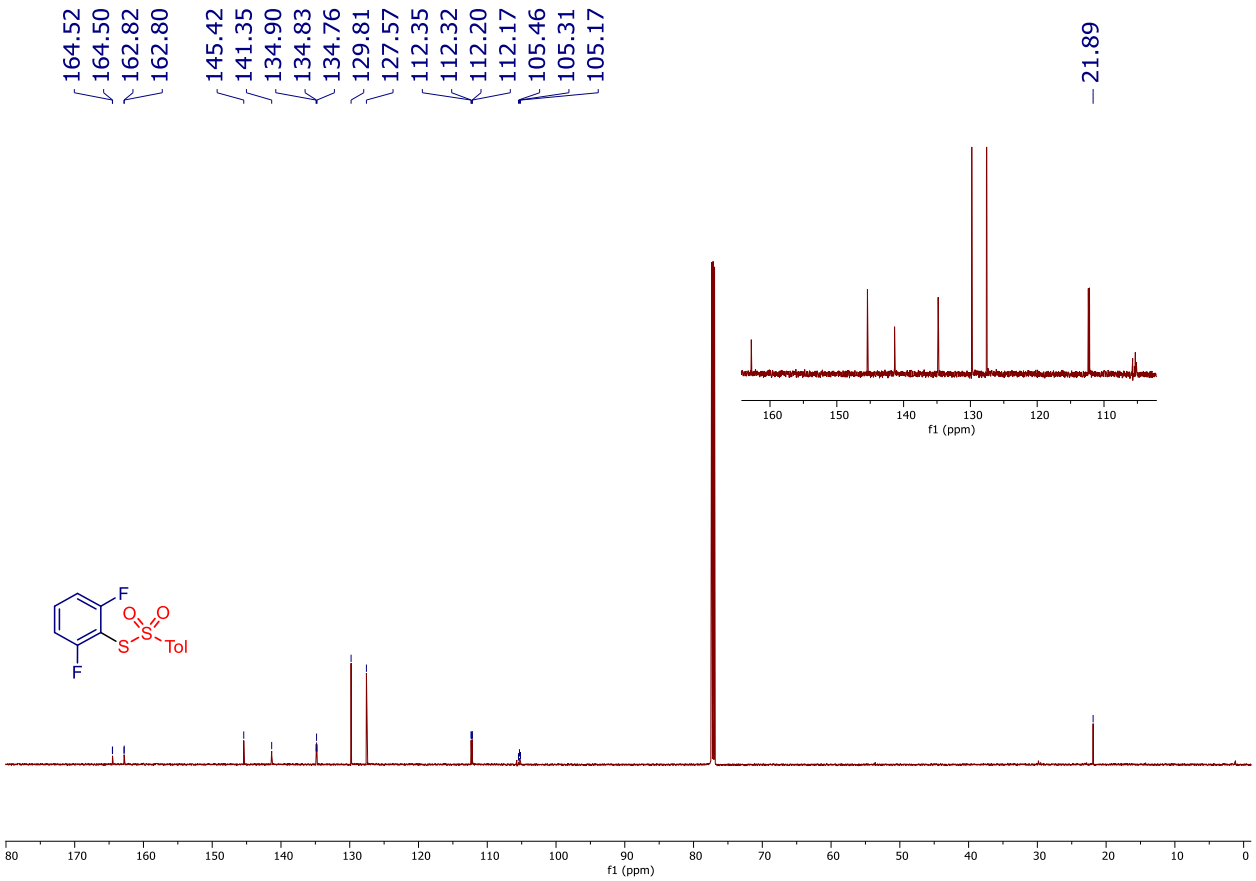
164.52
164.50
162.82
162.80
145.42
141.35
134.90
134.83
134.76
129.81
127.57
112.35
112.32
112.20
112.17
105.46
105.31
105.17
21.89
160 150 140 130 120 110
f1 (ppm)
F
O
O
S
S
Tol
F
80 170 160 150 140 130 120 110 100 90 80 70 60 50 40 30 20 10 0
f1 (ppm)

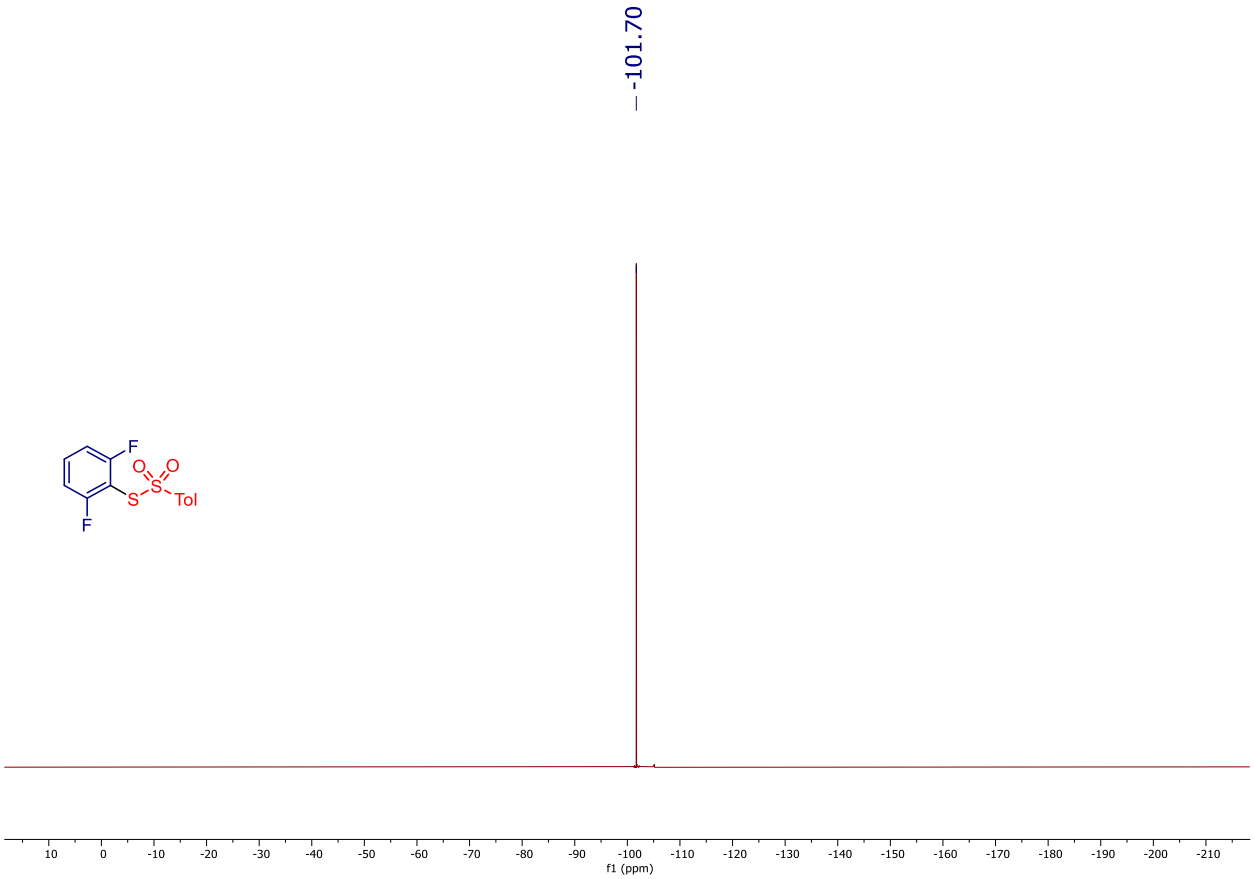

S-(3-bromo-5-chlorophenyl) 4-methylbenzenesulfonothioate 3.3-43aa

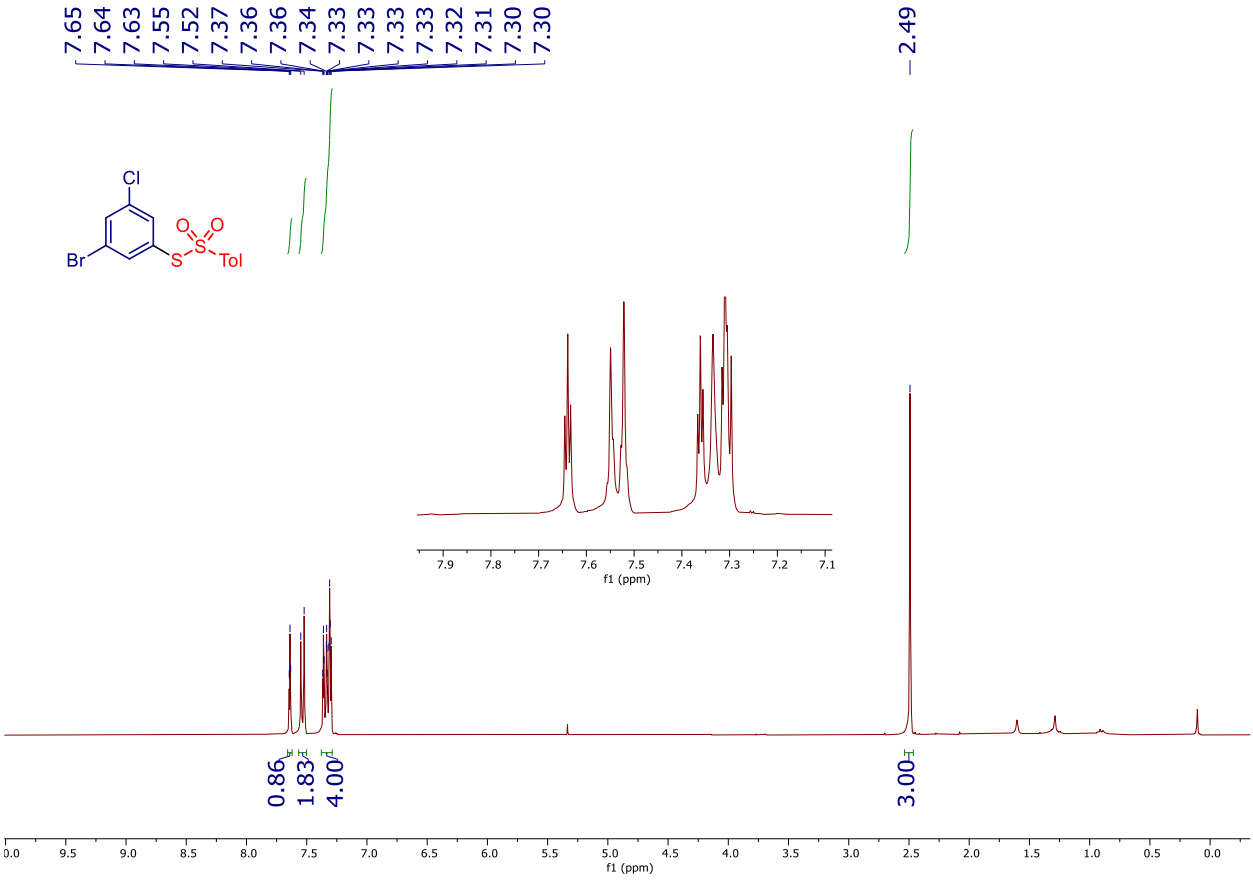

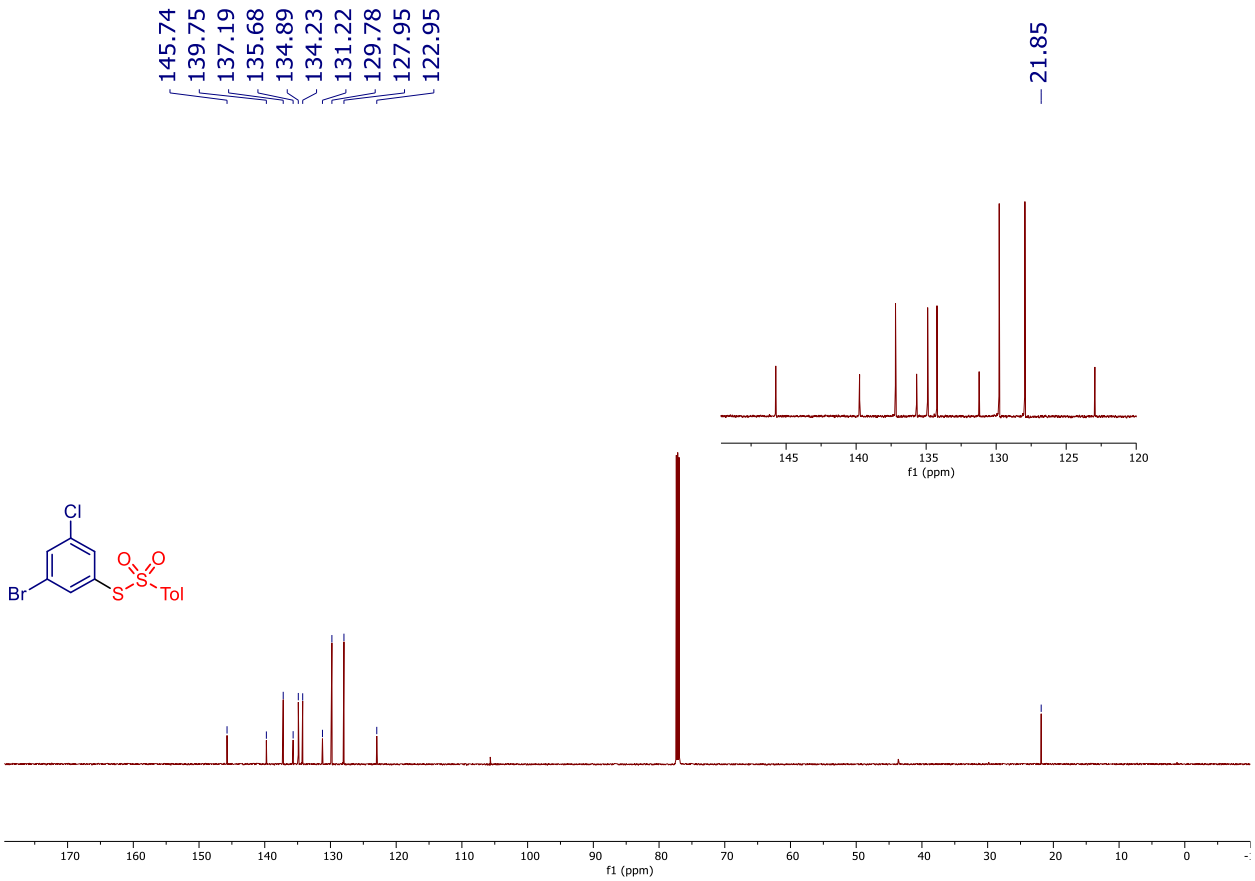

S-(4-bromo-3-chloro-2-fluorophenyl) 4-methylbenzenesulfonothioate 3.3-43ab

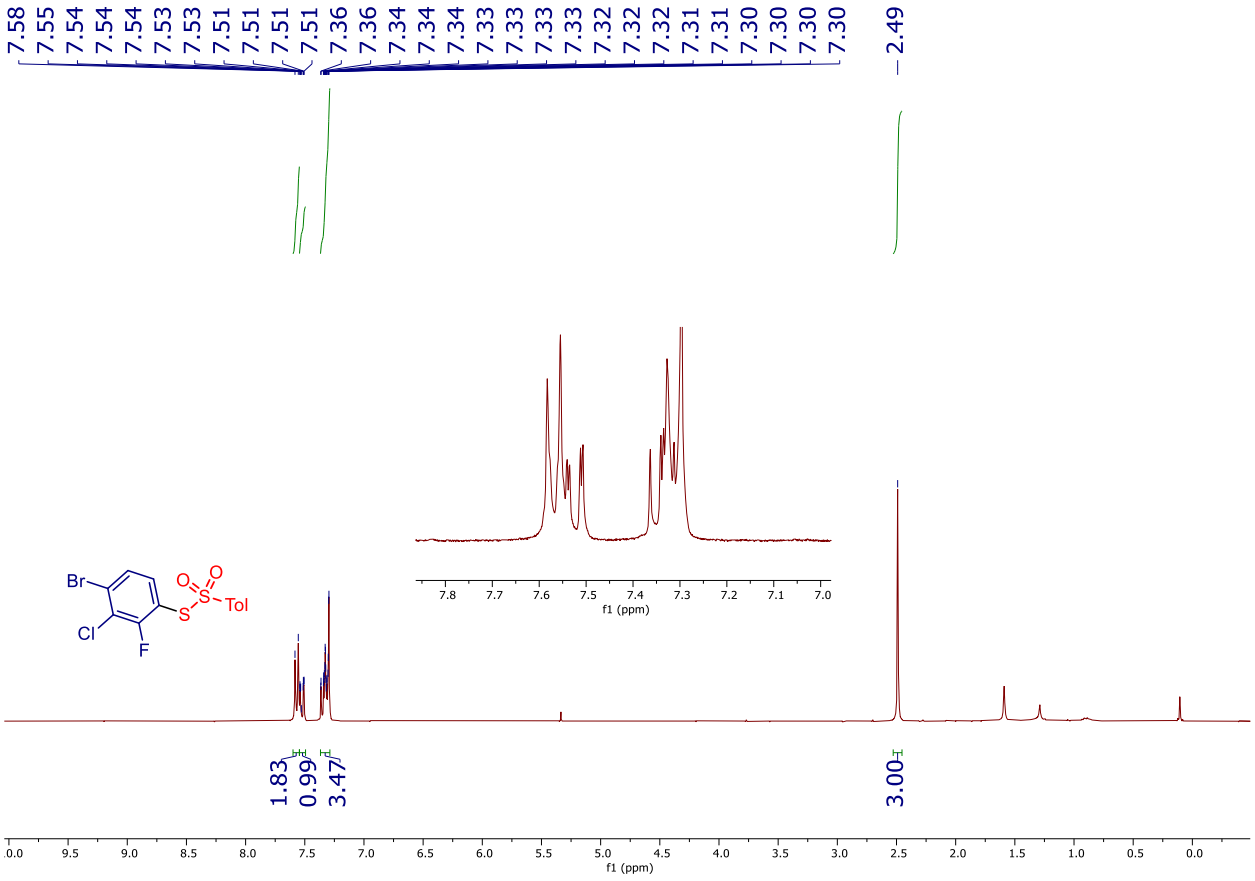

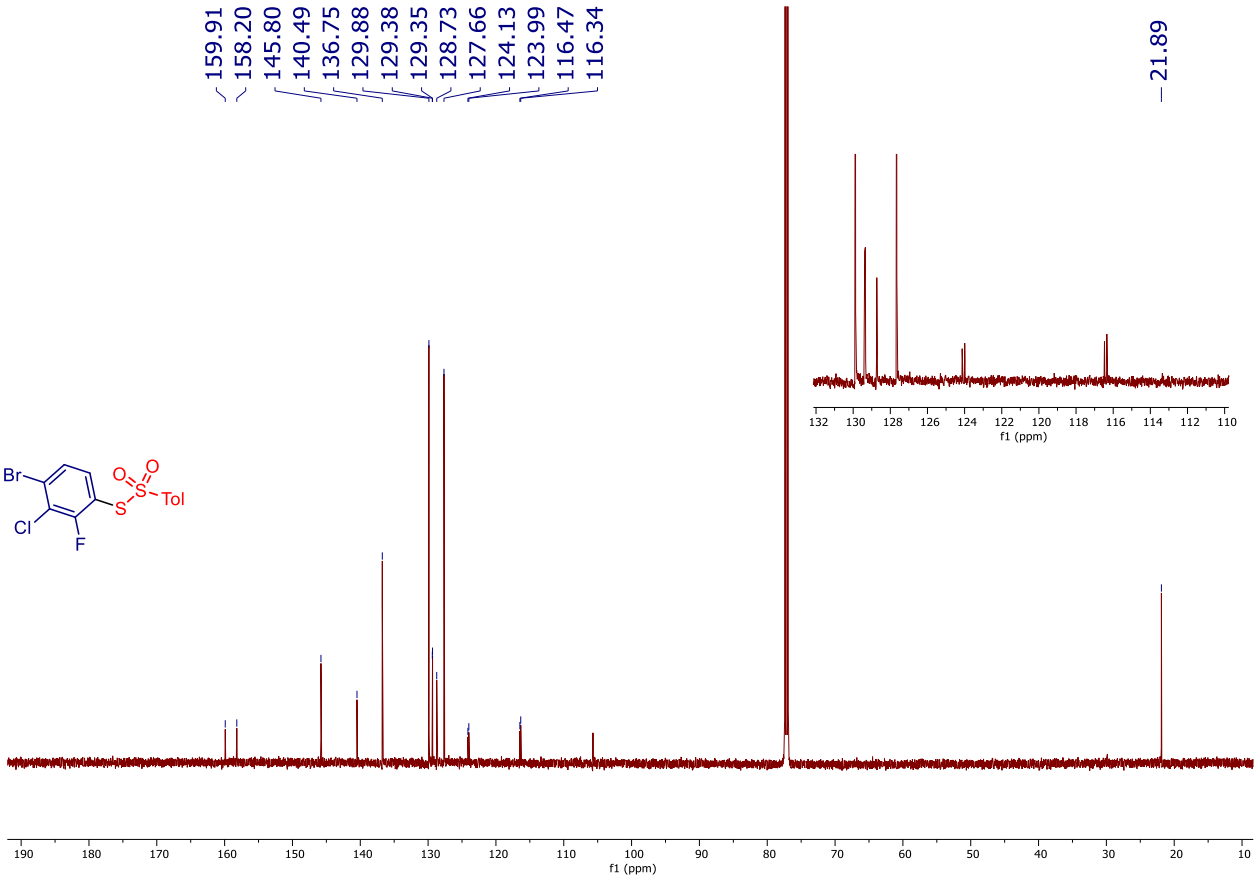

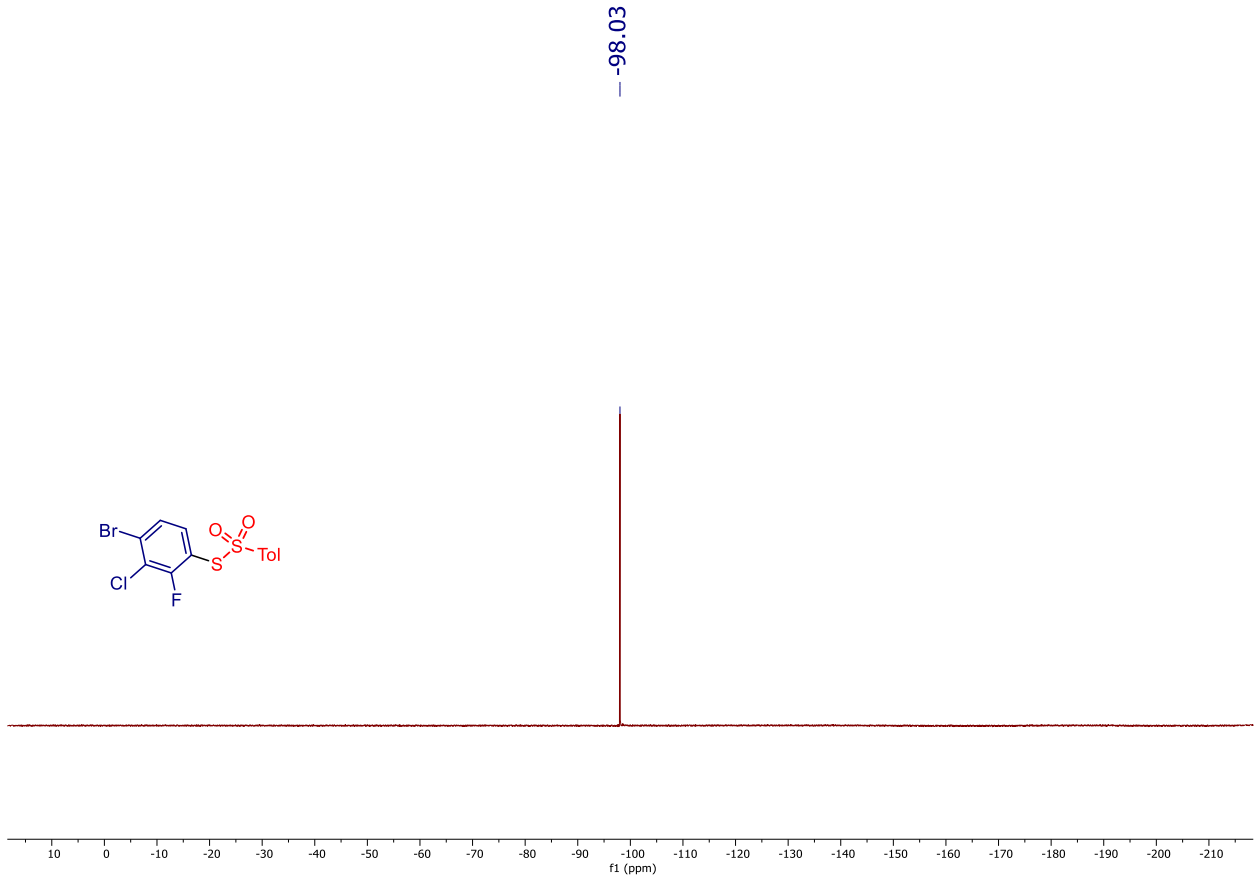

S-(3,4-dichlorophenyl) 4-methylbenzenesulfonothioate 3.3-43ac

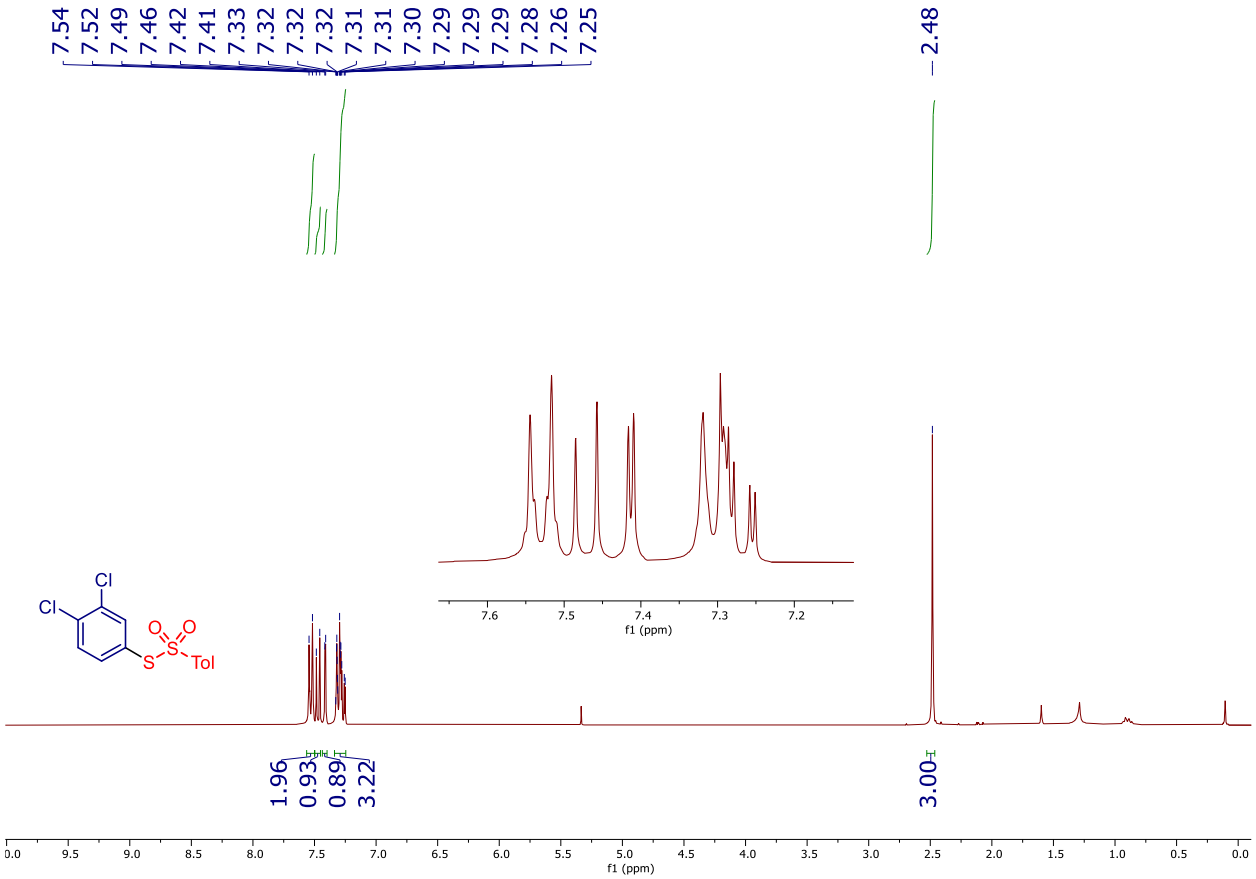

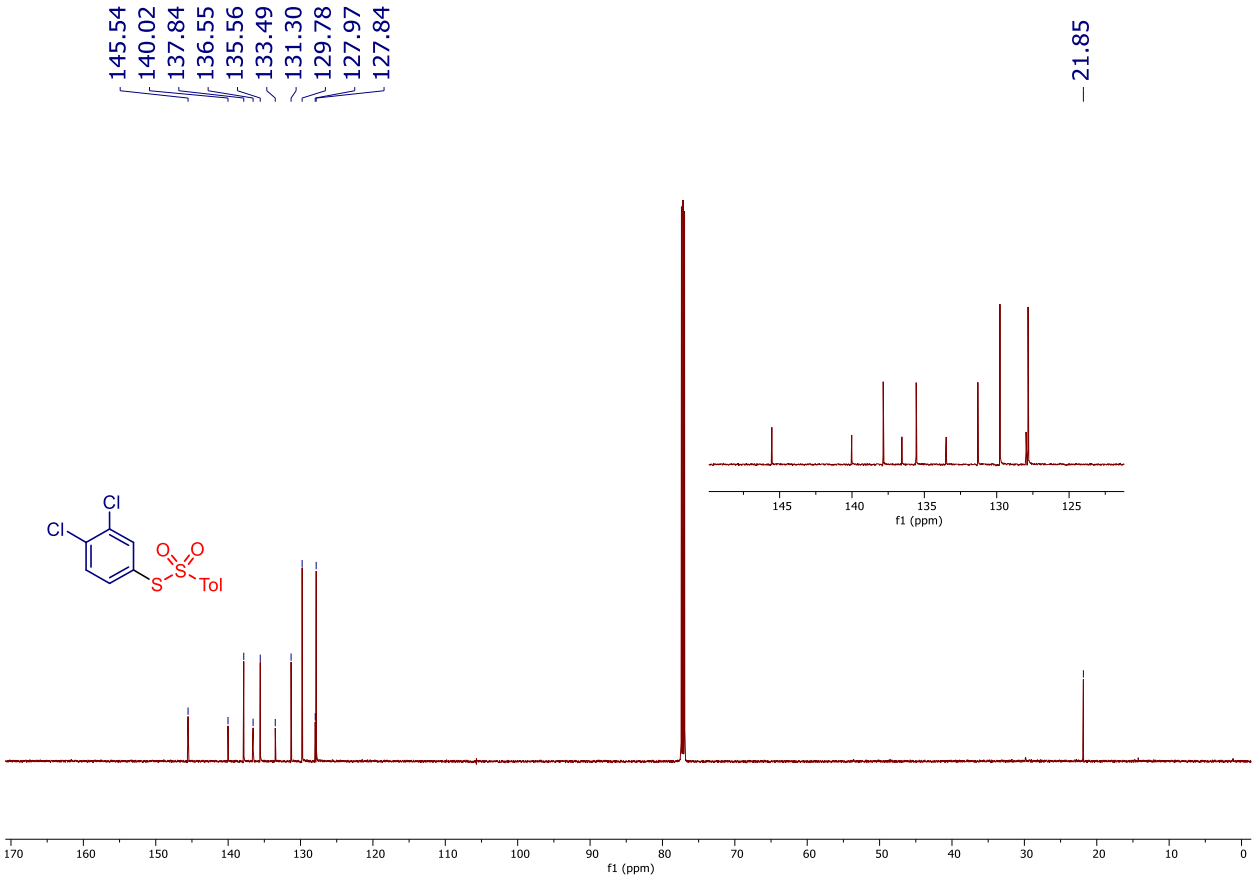

S-(4-formylphenyl) 4-methylbenzenesulfonothioate 3.3-43ad

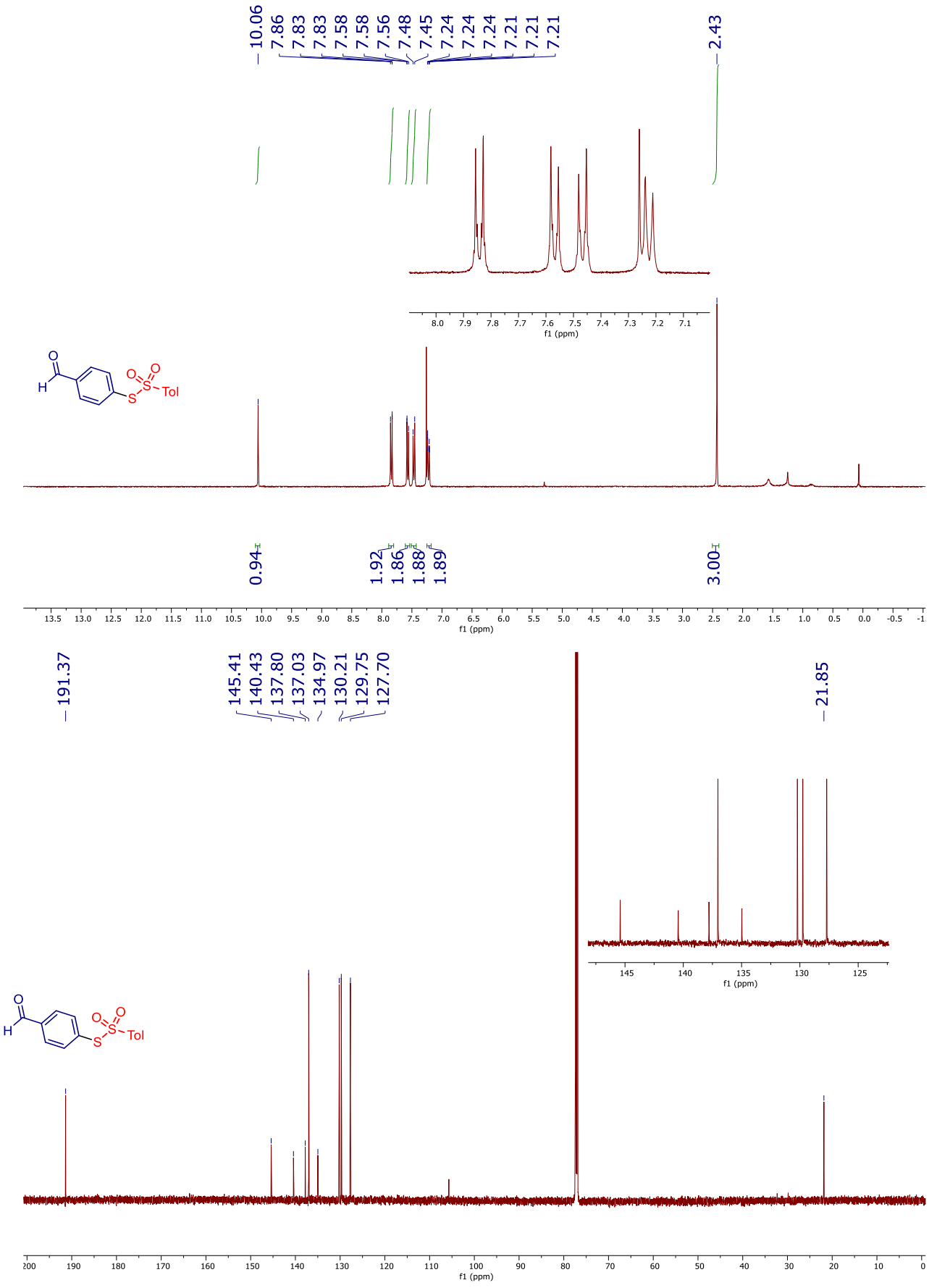

S-(2-formyl-4-methoxyphenyl) 4-methylbenzenesulfonothioate 3.3-43ae

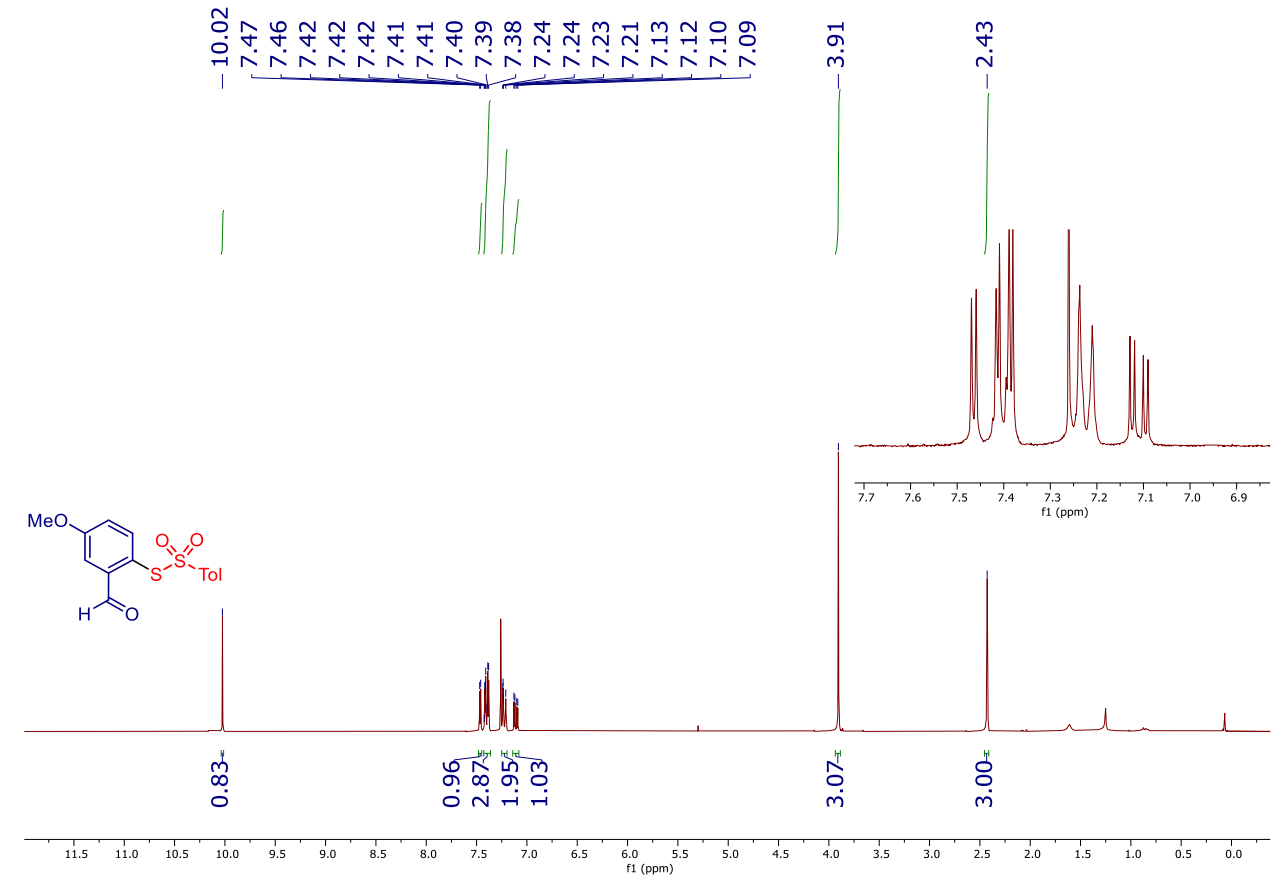

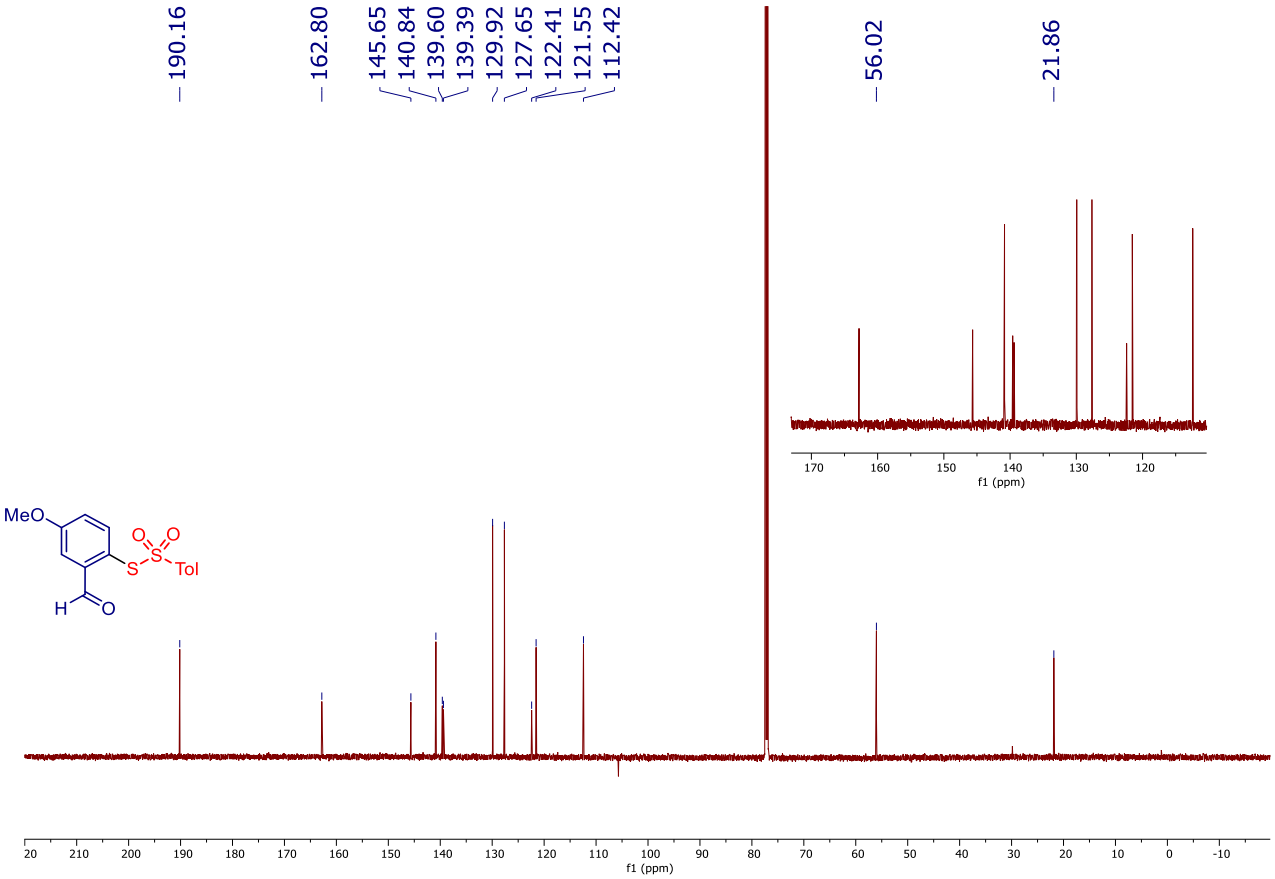

S-(4-acetylphenyl) 4-methylbenzenesulfonothioate 3.3-43af

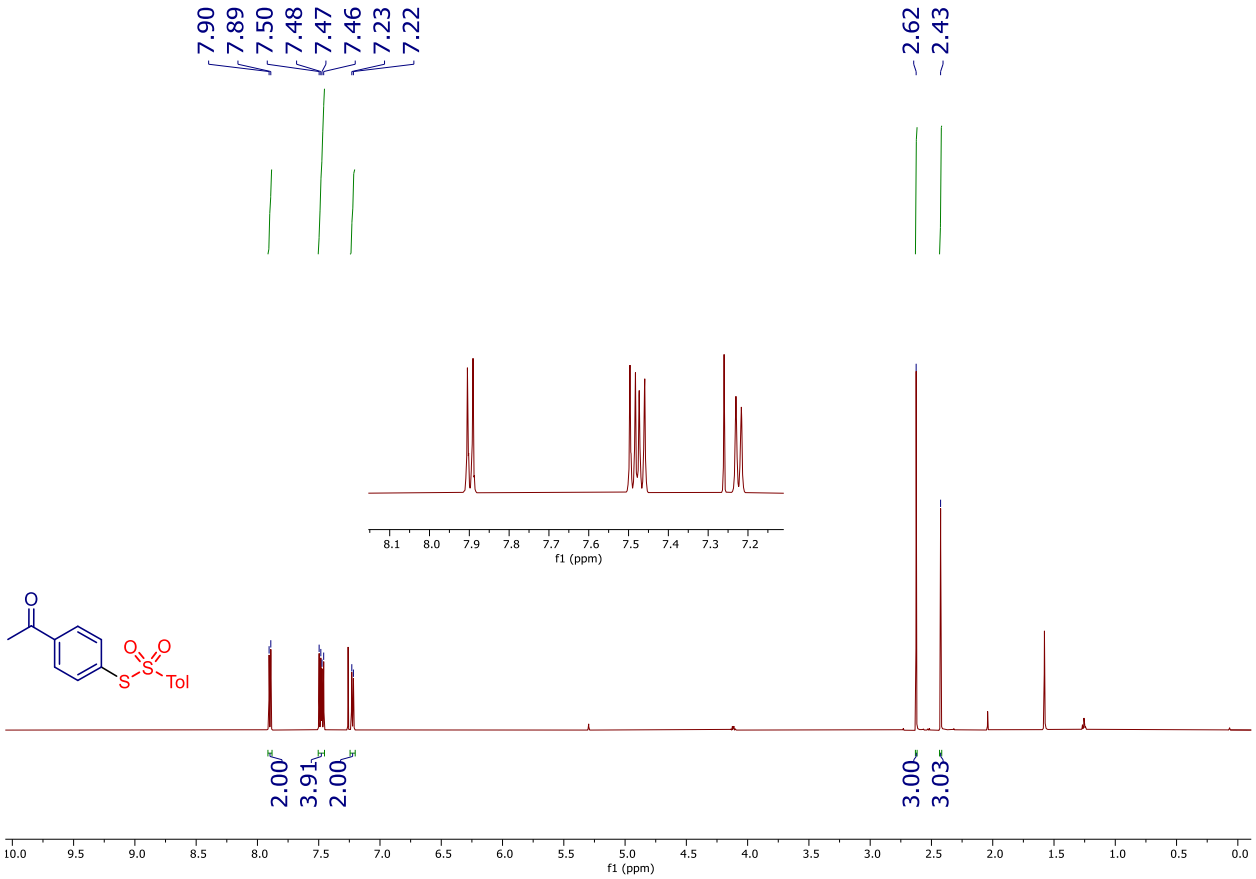

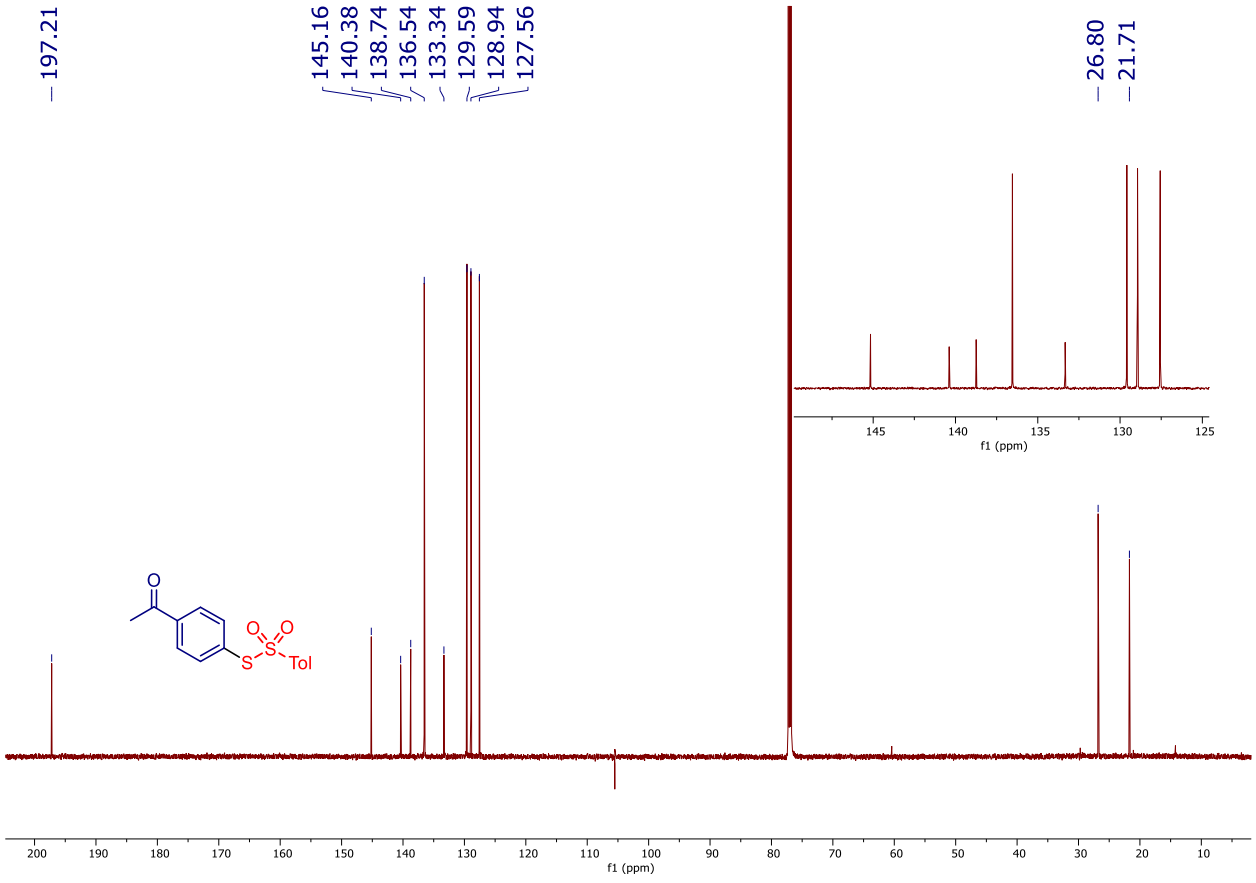

S-(2-cyanophenyl) 4-methylbenzenesulfonothioate 3.3-43ai

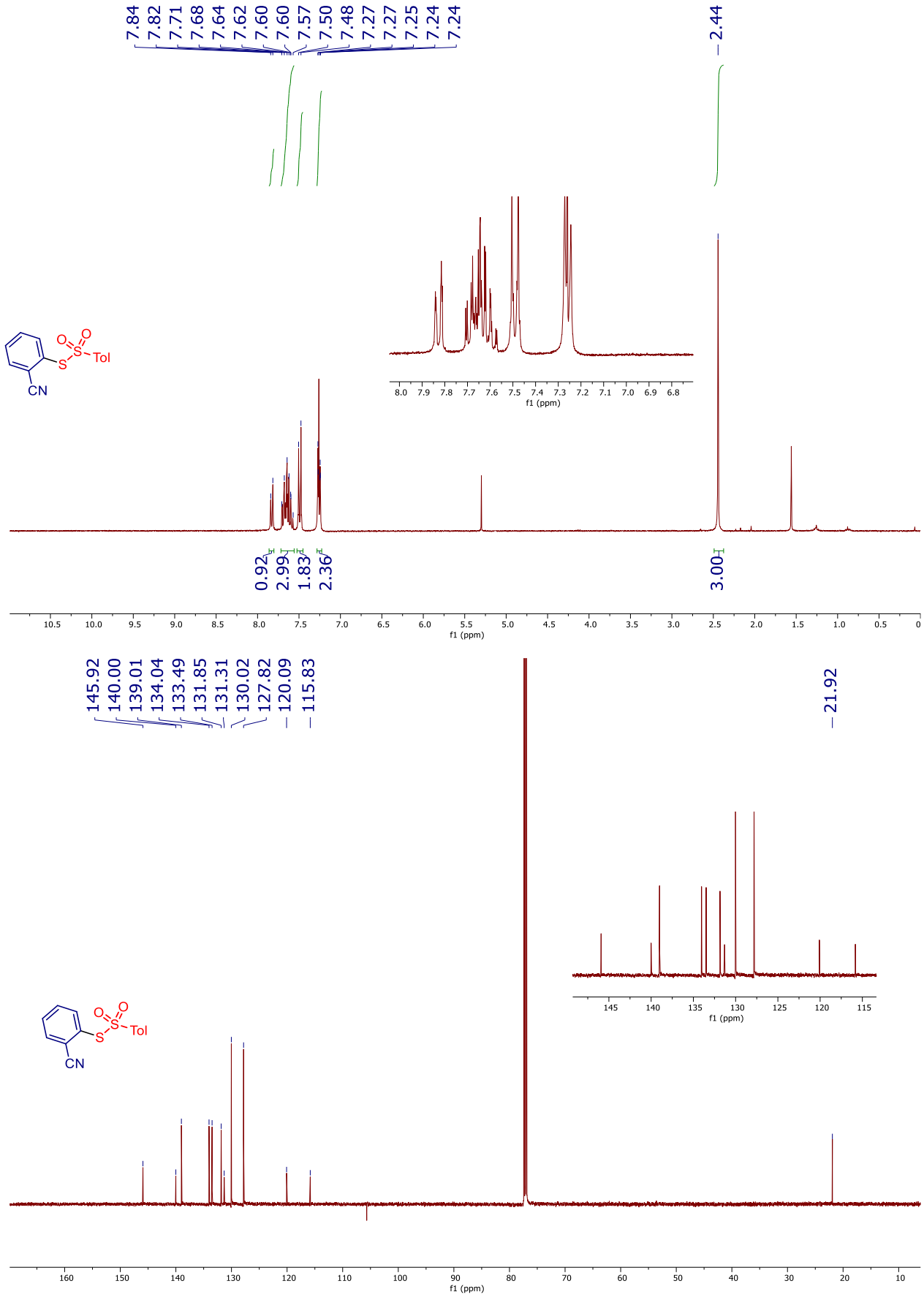

S-(4-cyanophenyl) 4-methylbenzenesulfonothioate 3.3-43aj

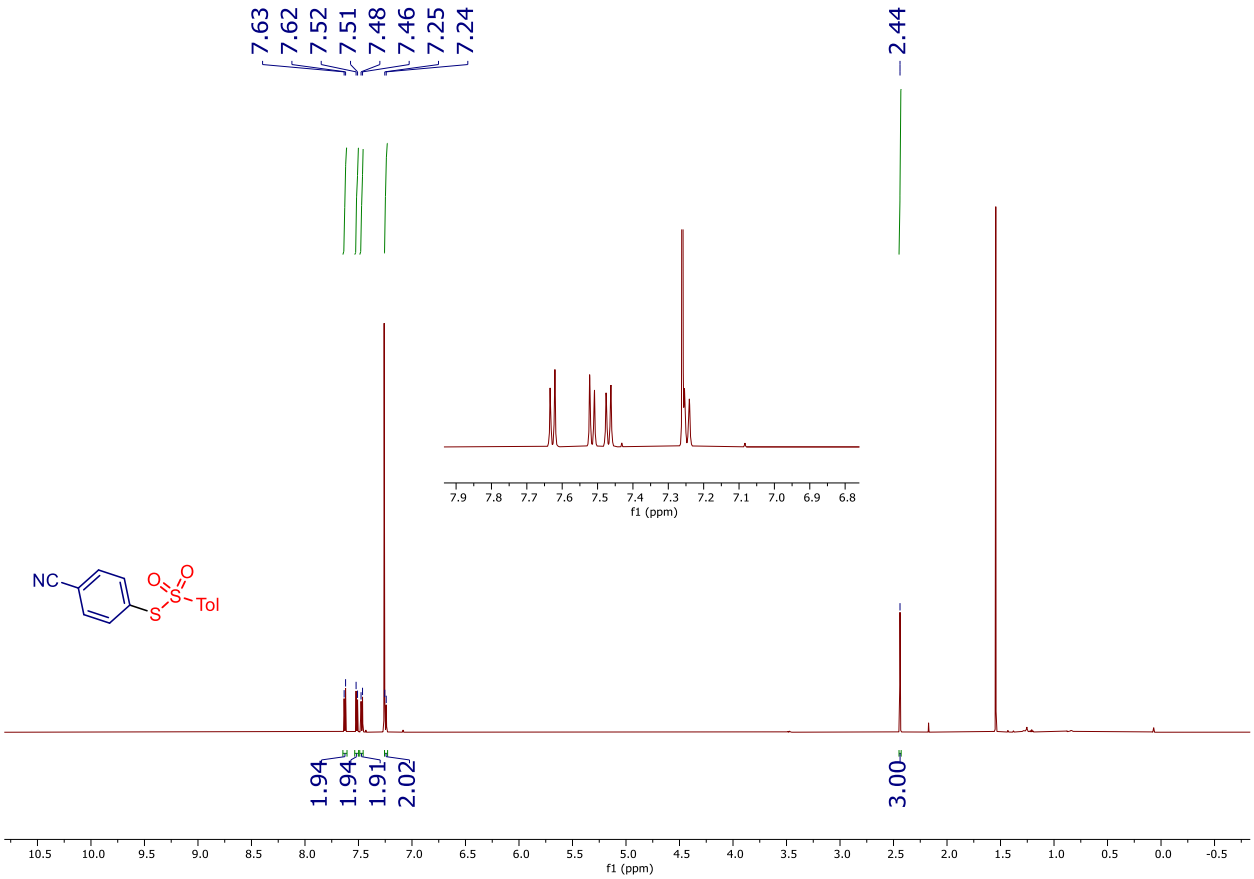

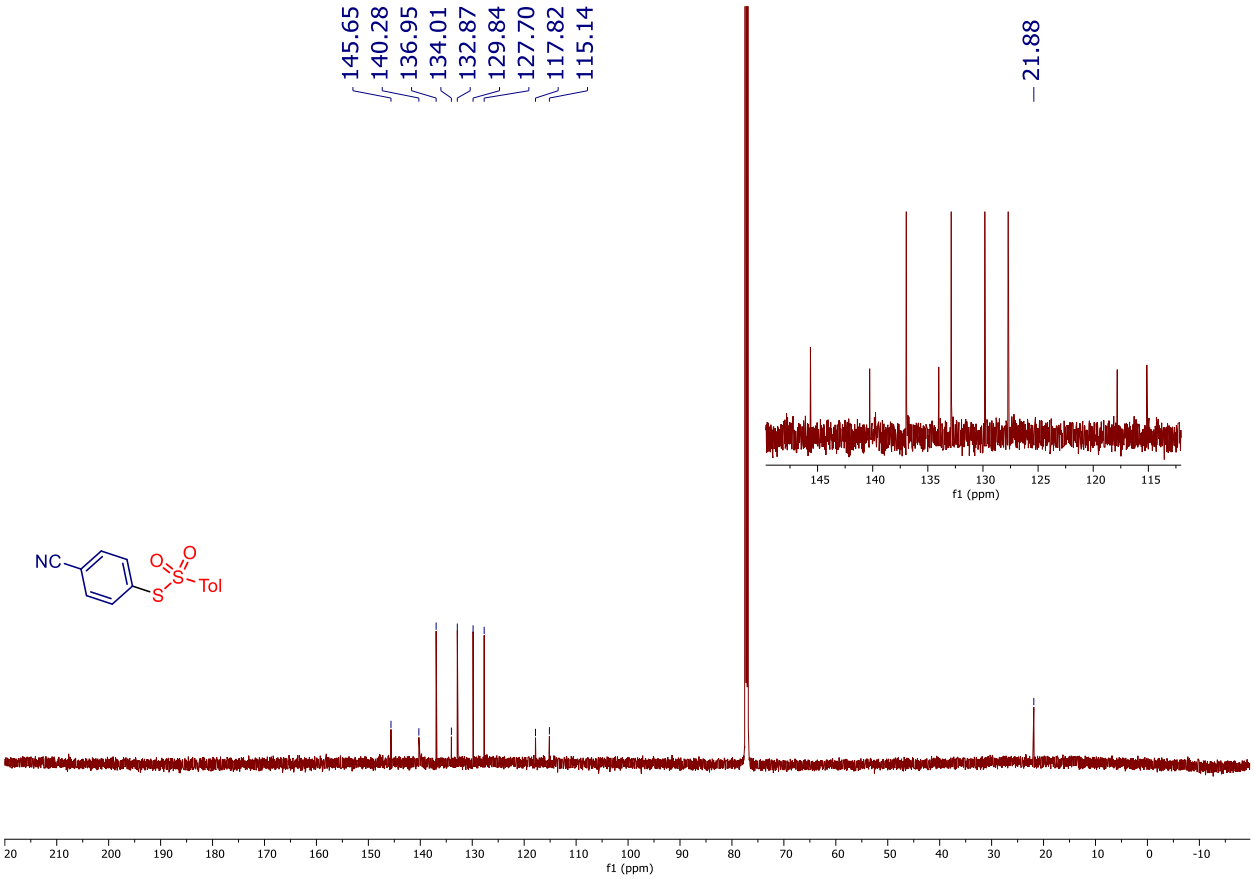

S-(3-(trifluoromethyl)phenyl) 4-methylbenzenesulfonothioate 3.3-43al

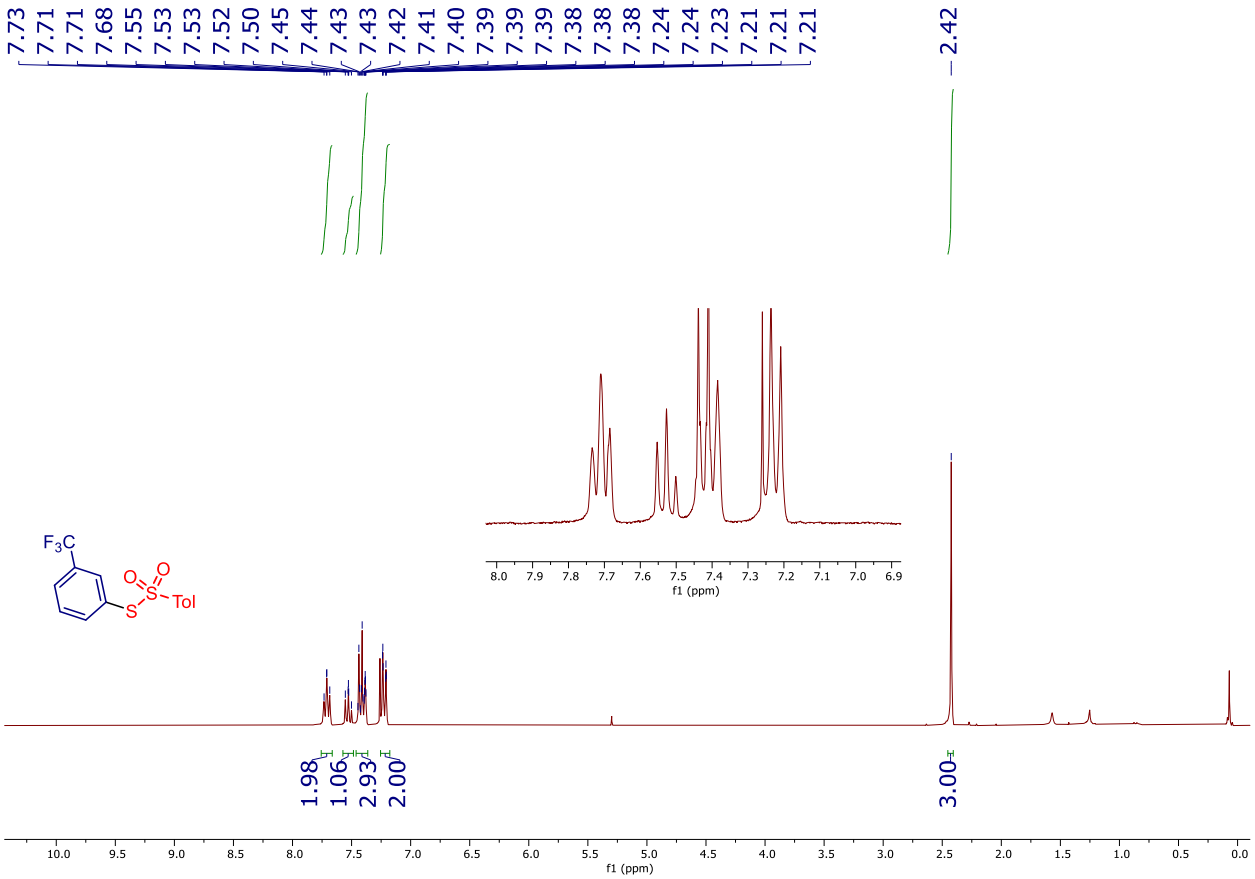
7.73
7.71
7.71
7.68
7.55
7.53
7.53
7.52
7.50
7.45
7.44
7.43
7.43
7.42
7.41
7.40
7.39
7.39
7.39
7.38
7.38
7.38
7.24
7.24
7.23
7.21
7.21
7.21
2.42
F3C
O
O
S
S
Tol
1.98
1.06
2.93
2.00
3.00
f1 (ppm)

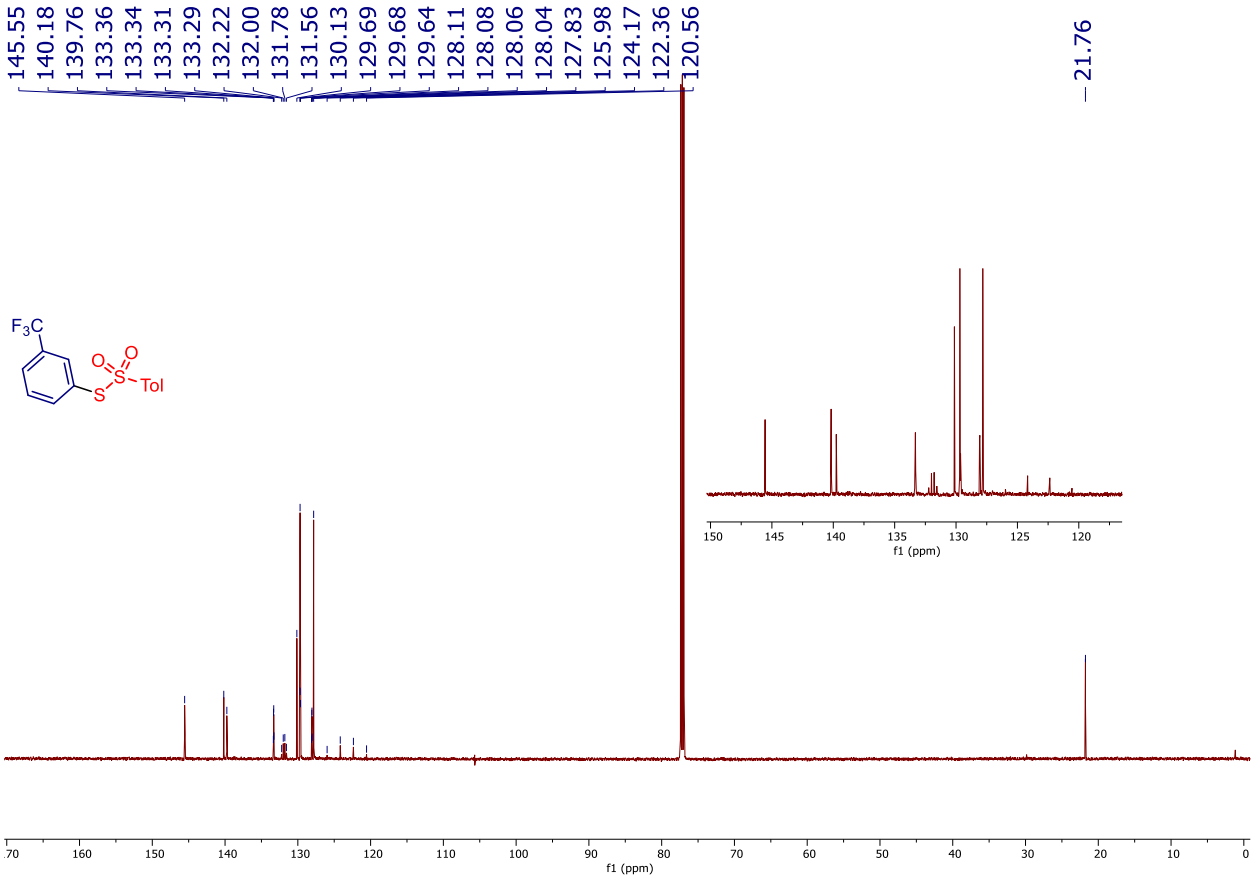
145.55
140.18
139.76
133.36
133.34
133.31
133.29
132.22
132.00
131.78
131.56
130.13
129.69
129.68
129.64
128.11
128.08
128.06
128.04
127.83
125.98
124.17
122.36
120.56
21.76
F3C
O
O
S
S
Tol
f1 (ppm)

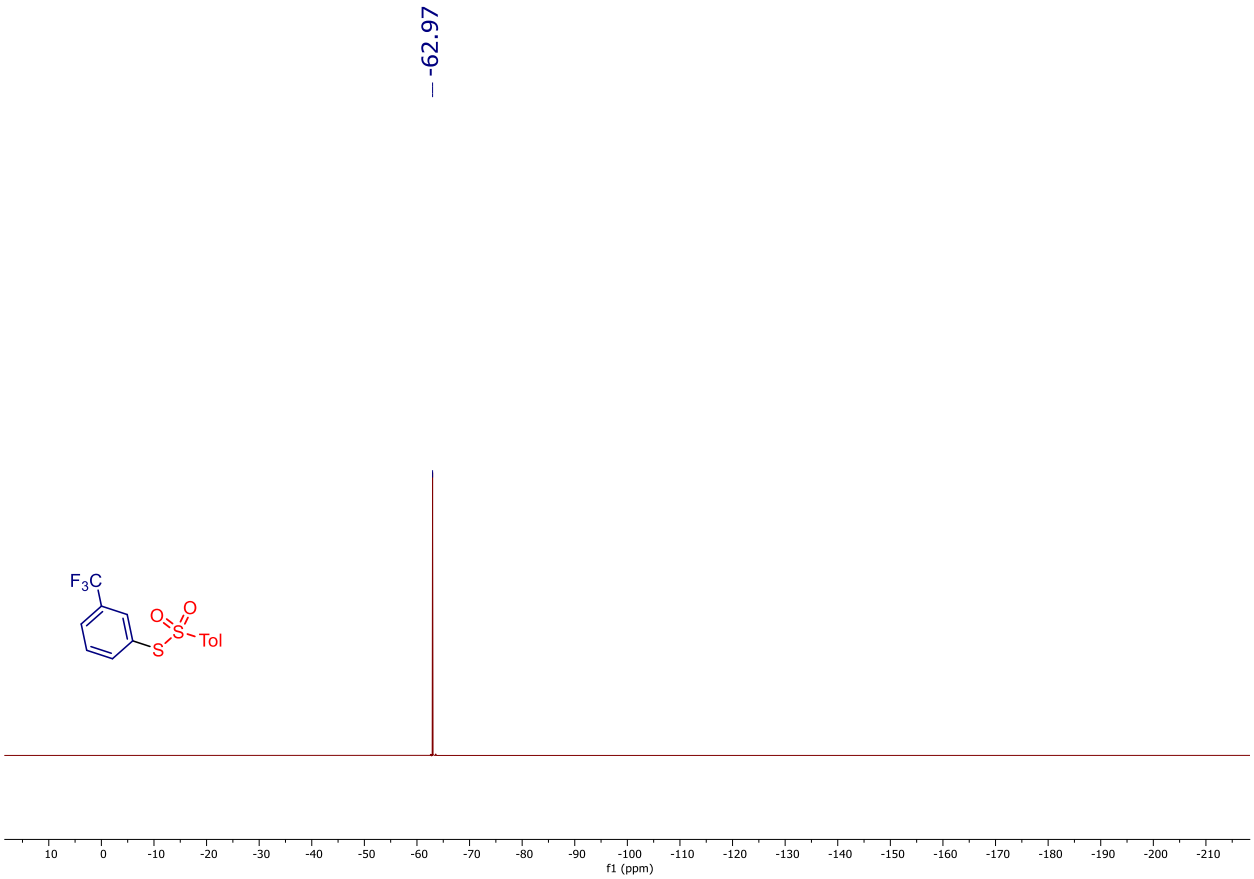

S-(3,5-bis(trifluoromethyl)phenyl) 4-methylbenzenesulfonothioate 3.3-43an

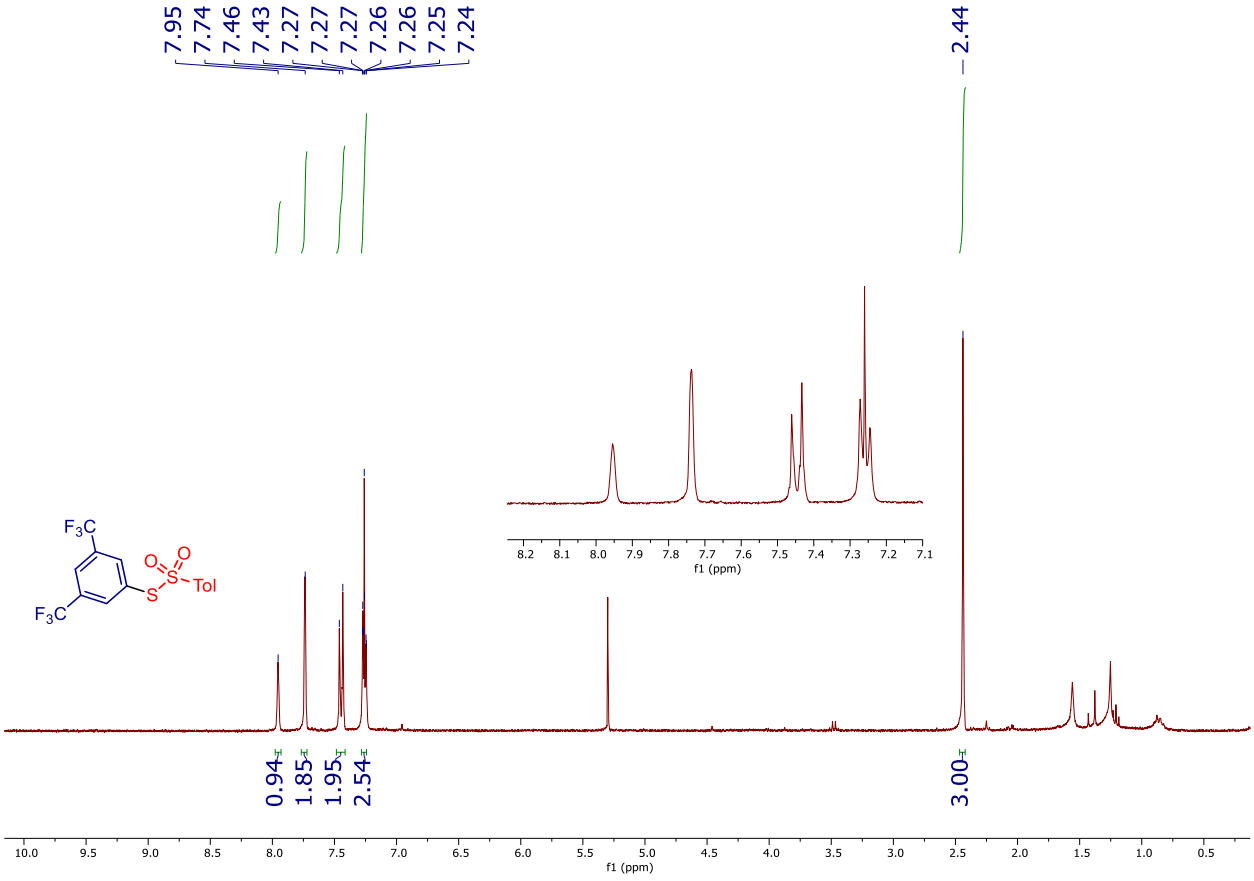

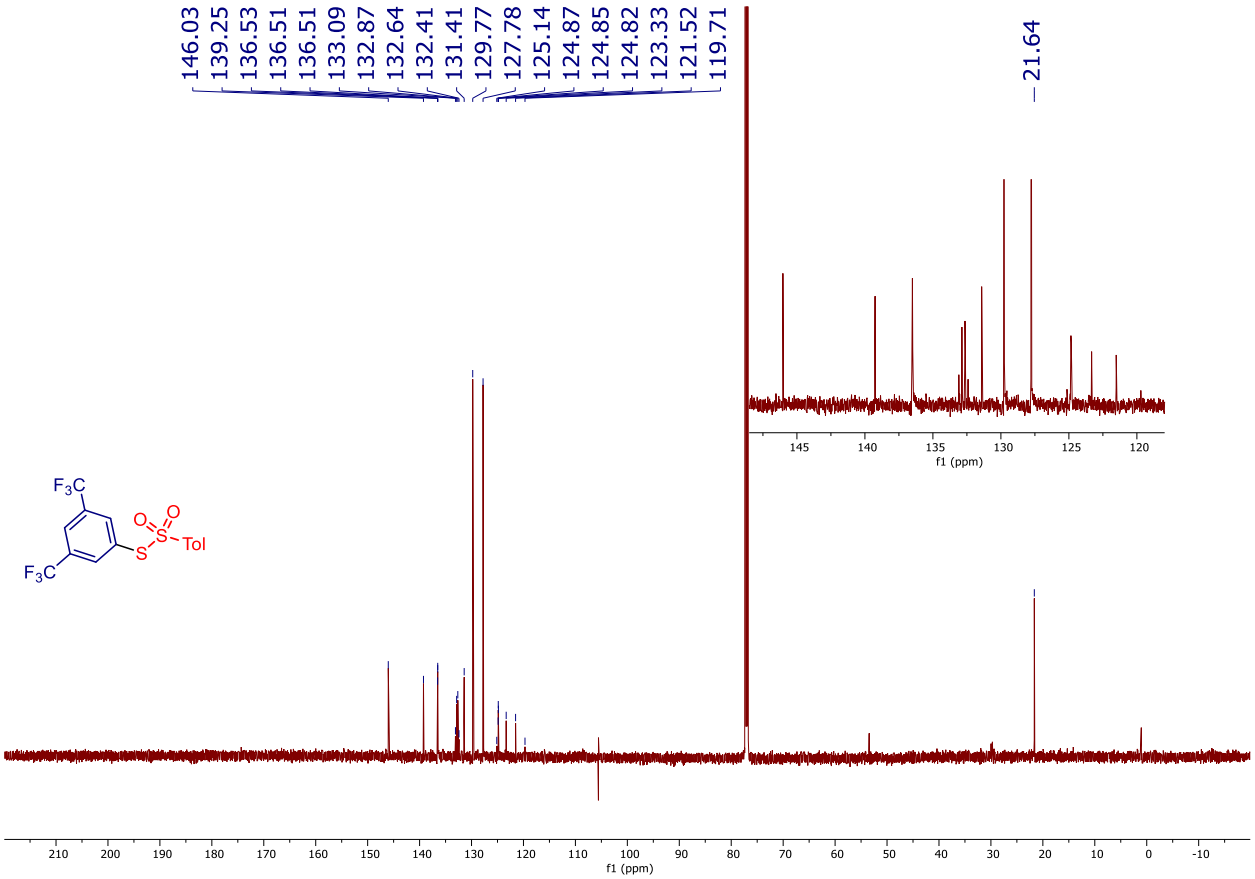

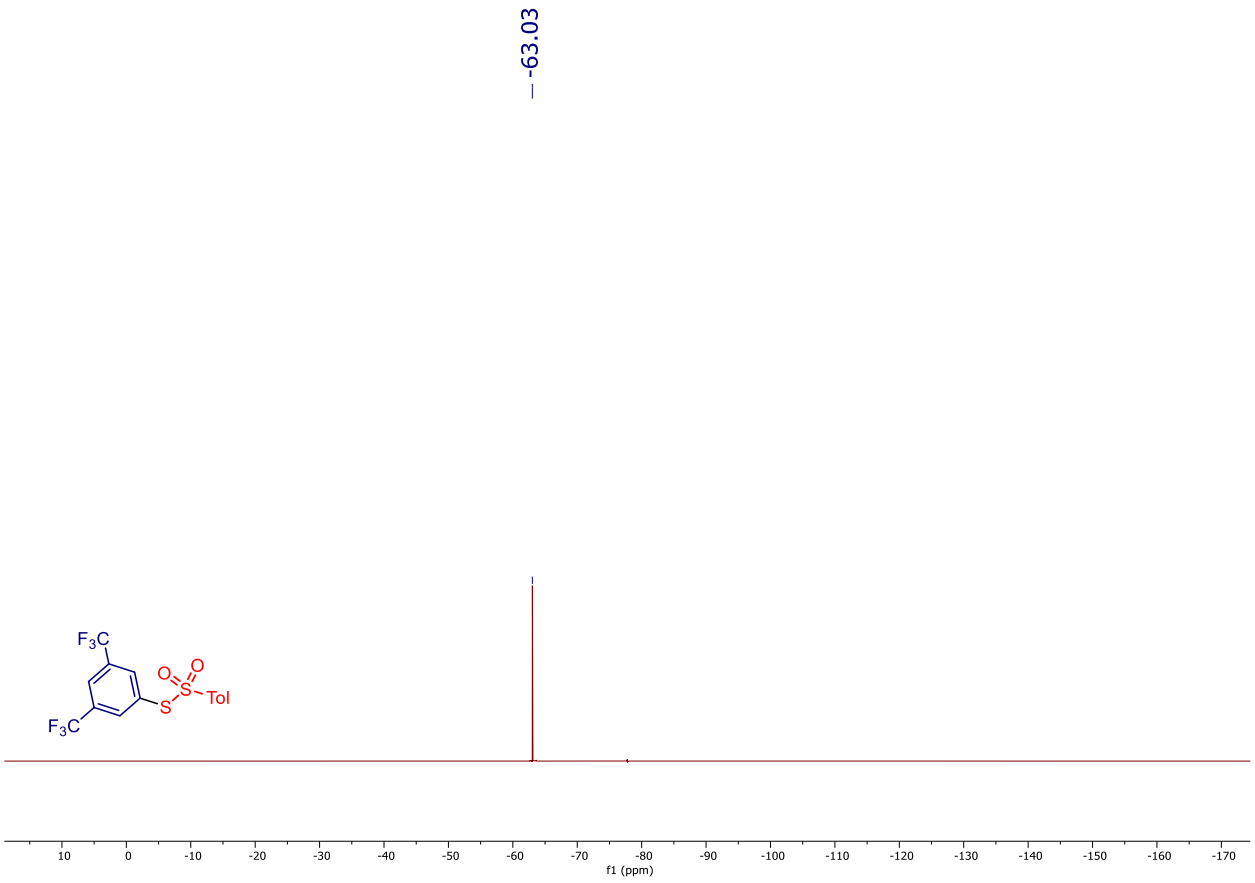

dimethyl 5-(tosylthio)isophthalate 3.3-43ao

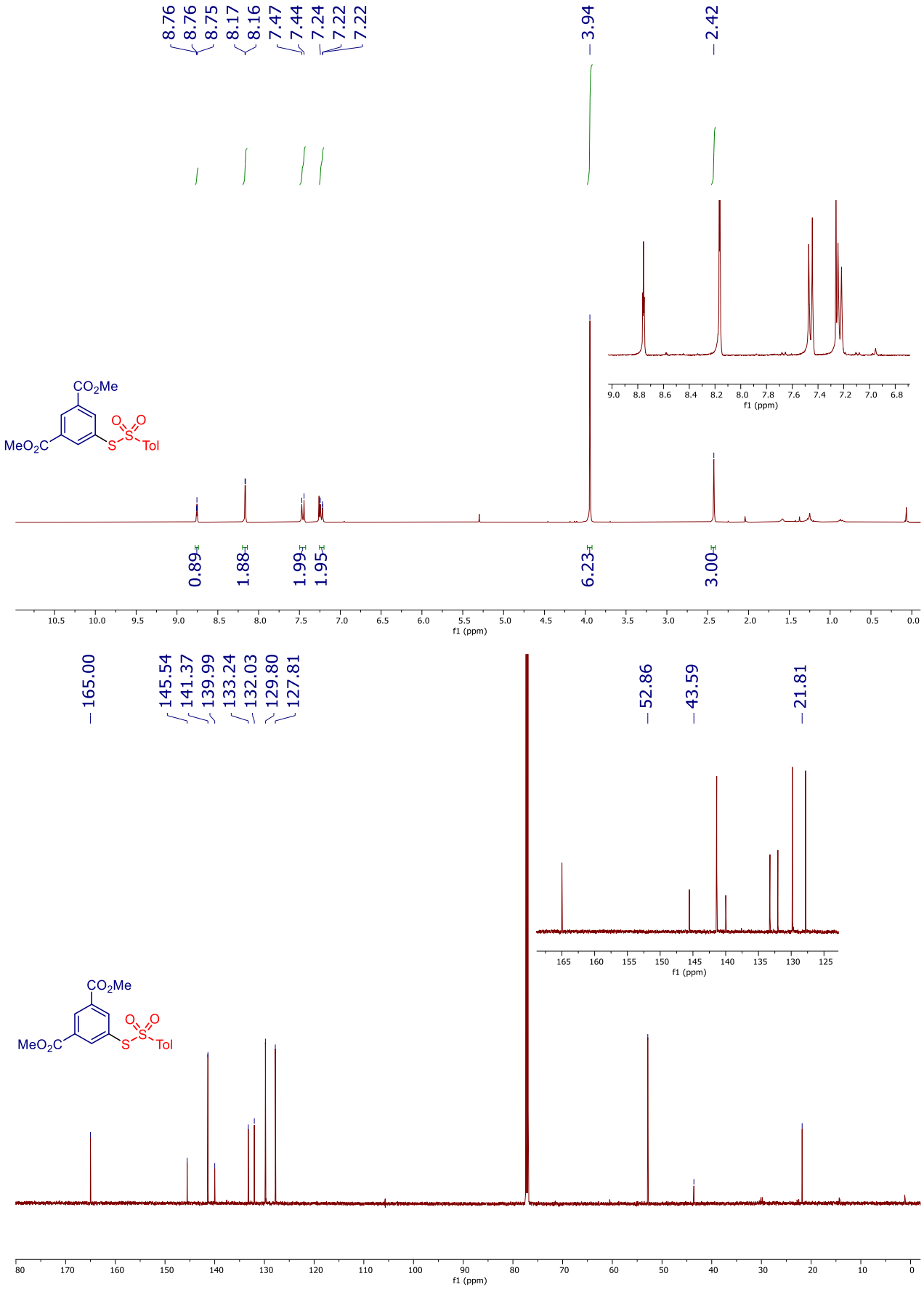

(S,S'-(thiophene-2,5-diyl) bis(4-methylbenzenesulfonothioate 3.3-43aq

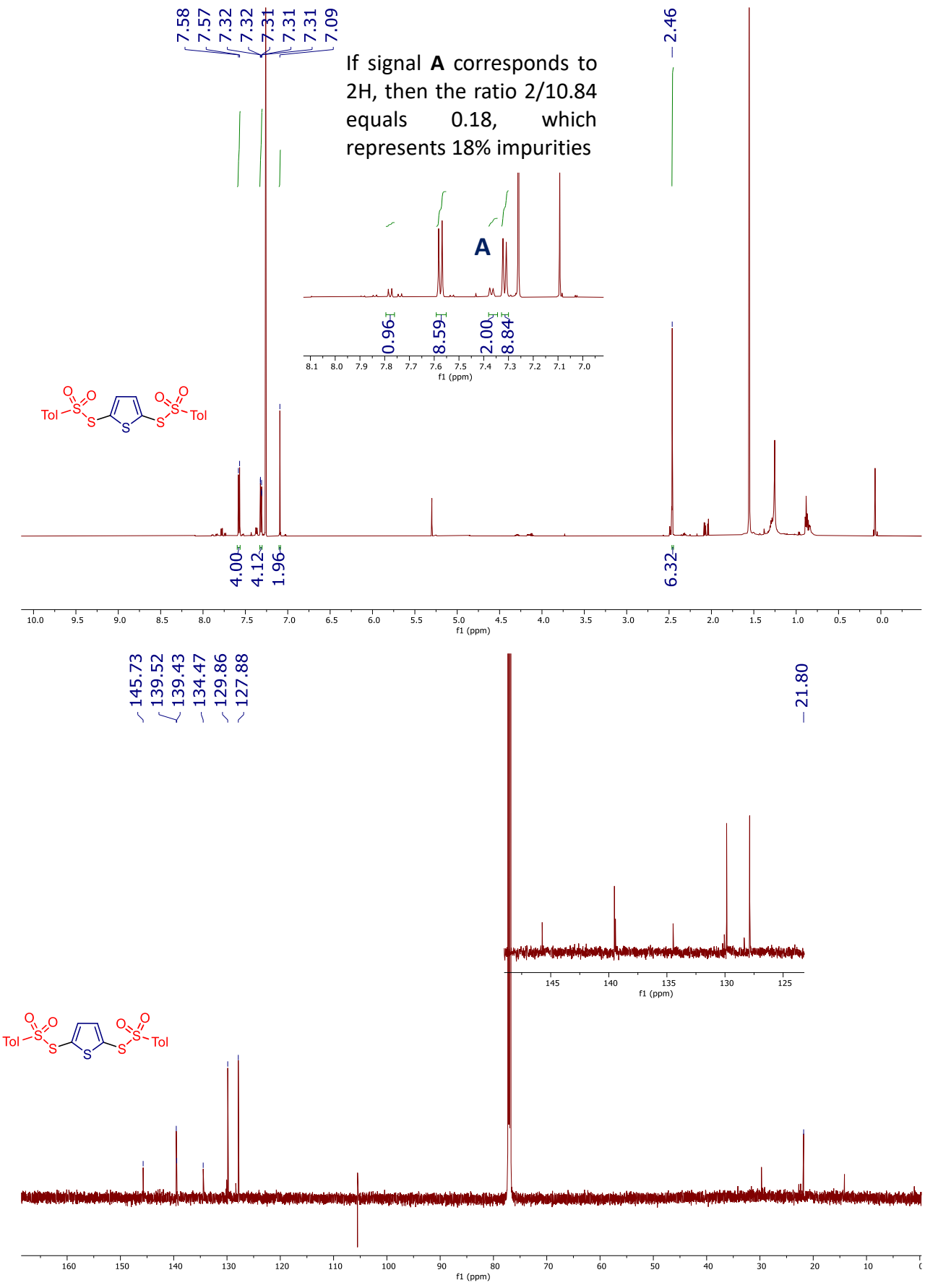

(*E*)-S-styryl 4-methylbenzenesulfonothioate 3.3-43at

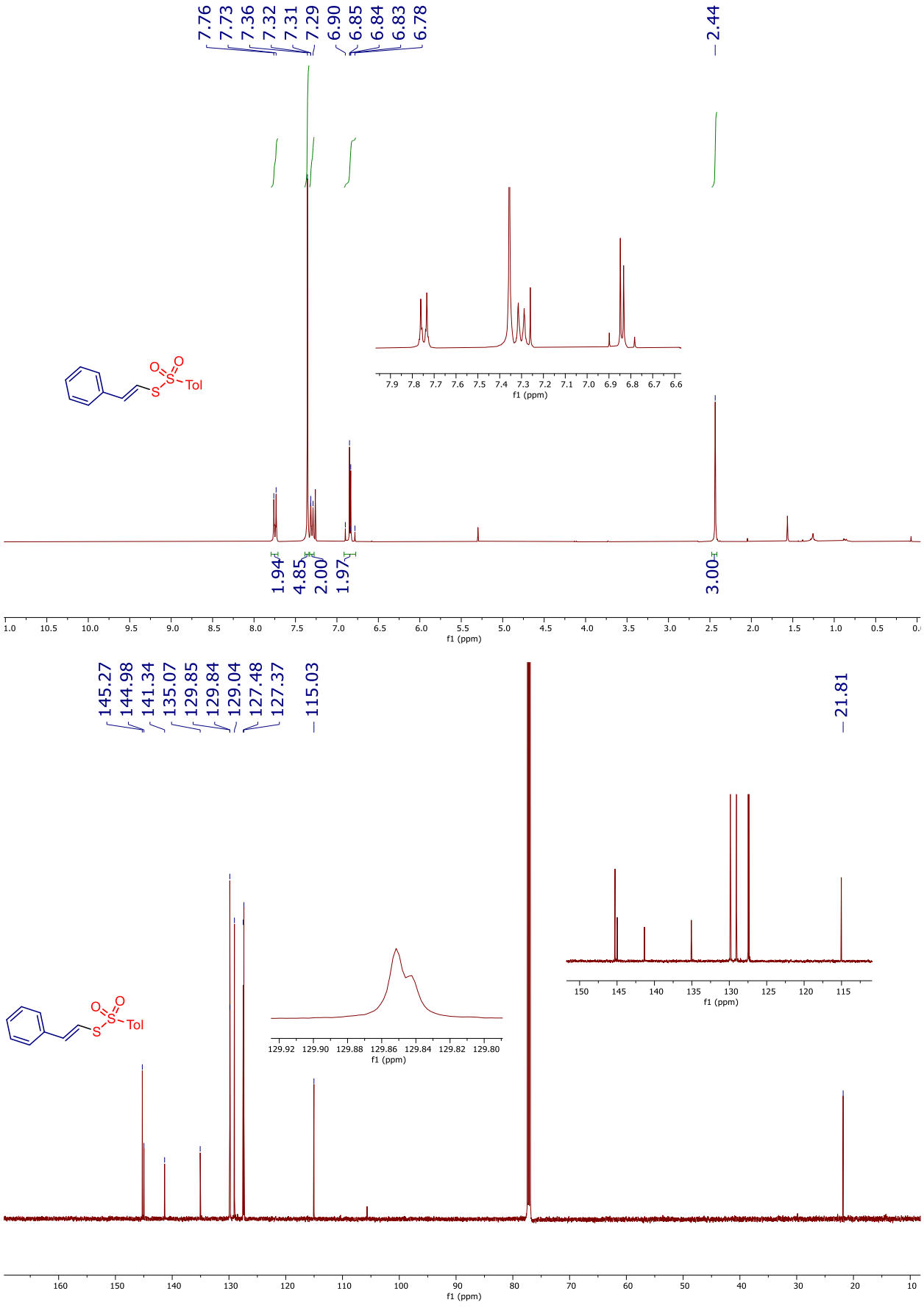

2-(tosylthio)phenyl 4-methylbenzenesulfonate 3.3-43au

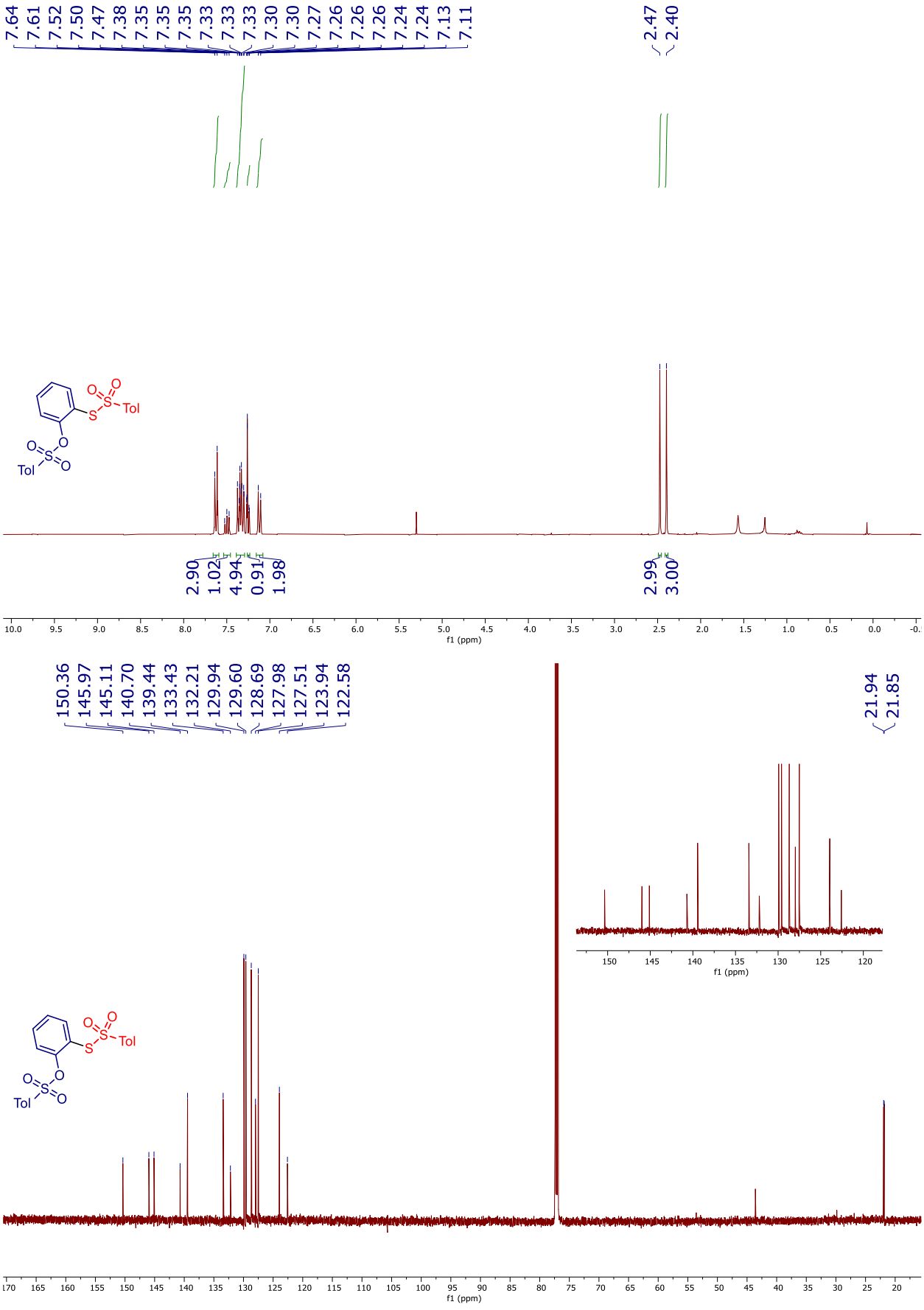

(*E*)-S-(oct-1-en-1-yl) 4-methylbenzenesulfonothioate 3.3-43-av

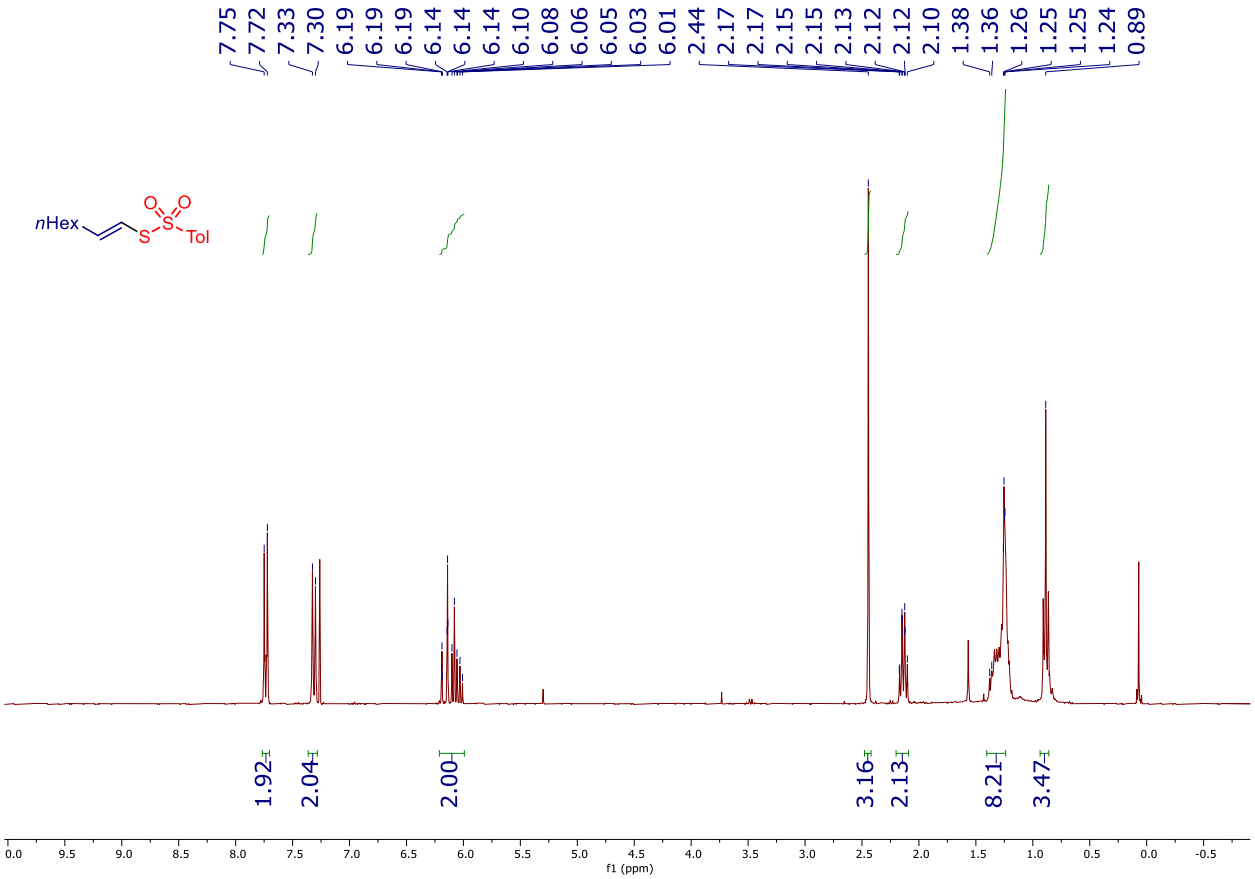
7.75
7.72
7.33
7.30
6.19
6.19
6.19
6.14
6.14
6.14
6.10
6.08
6.06
6.05
6.03
6.01
2.44
2.17
2.17
2.15
2.15
2.13
2.12
2.12
2.10
1.38
1.36
1.26
1.25
1.25
1.24
0.89
nHex
S
O
O
S
Tol
1.92
2.04
2.00
3.16
2.13
8.21
3.47
f1 (ppm)

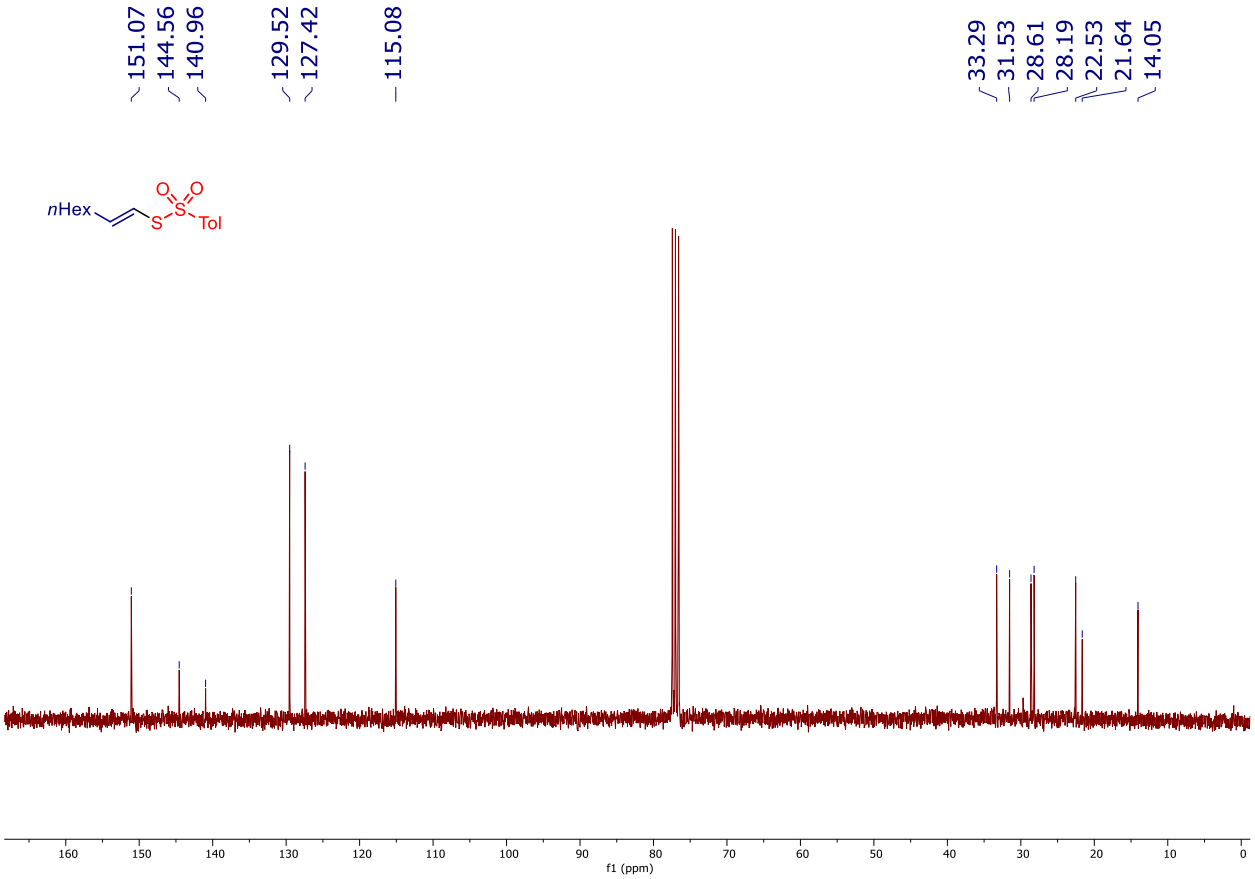
151.07
144.56
140.96
129.52
127.42
115.08
33.29
31.53
28.61
28.19
22.53
21.64
14.05
nHex
S
O
O
S
Tol
f1 (ppm)